Slovak University of Technology
Faculty of Chemical and Food Technology

Polymer Institute
Slovak Academy of Sciences

in cooperation with

INCHEBA EXPO BRATISLAVA

5th International Conference
Polymeric Materials in Automotive
PMA 2013
&
21th Slovak Rubber Conference
SRC 2013

23 - 25 April, 2013

Conference Center of hotel Bonbon

Bratislava,
Slovak Republic

In May 2005, the first International Conference on Polymeric Materials in Automotive was organized in Bratislava. followed by the second PMA in 2007. The events reflected steeply rising importance of automotive industry in Slovakia, derived from the presence of dominant investors in Slovakia, namely Volkswagen, PSA and Kia including a number of other companies – suppliers of plastics and rubber parts being a significant part of them – building up their new facilities in the country. Almost 350 participants from 25 countries attended the two conferences which were ranked as successful and interesting. The appreciated feature consisted in a fact that, although targeted to polymeric materials used in automotive industry, the scope of the conference was kept highly scientific. Thus, new ideas have been presented, many of these being far away from industrial application, still contributing significantly to a progress in the area.

Similar to the PMA 2005, PMA 2007, PMA 2009 and PMA 2011 the upcoming conference PMA 2013 is targeted on various aspects related to plastics and rubber in the automotive industry, with the aim to exchange the innovative approaches towards new polymer products increasingly having a decisive influence on the design and appearance of new generation of cars. Developing goals such as aesthetic appeal and comfort, safety and lightweight construction, as well as quality and cost are affected directly by the material concept and the corresponding processing and product technology.

International scientific conference on rubber, Slovak Rubber Conference, was organized every year by the Rubber Research Institute of Matador Púchov. From 2005 this traditional event was organized as a part of the International Conference on Polymeric Materials in Automotive and in 2013 the 21th Slovak Rubber Conference will be held.

In this year the International Conference Polymeric Materials in Automotive PMA 2013 & Slovak Rubber Conference SRC 2013 will be connected the 23th International Car Show AUTOSALON which ranks among significant motoring events in Central Europe.

Prof. Ivan Hudec
Chairman of the Organizing Committee

Prof. Ivan Chodák, DSc.
Chairman of the Program Committee

MAIN LECTURES

ML-01
AGING PROCESSES – MECHANISMS AND QUANTITATIVE CHARACTERIZATION CONCERNING POLYMER STRUCTURE, ANTIOXIDANTS AND CROSSLINKING

ULRICH GIESE*, I. HOMEIER, Y. NAVARRO TORRÉJON, and S. KAUTZ

Deutsches Institut für Kautschuktechnologie e. V., Eupener Str. 33, 30519 Hannover / Germany
Ulrich.Giese@DIKautschuk.de

1. Introduction

The exposure of elastomer components during service against environmental influences like oxygene, temperature, static and dynamic mechanical load or UV-light effects aging processes. Especially chemical changes caused by those influences are responsible for irreversible changes in properties[1]. Depending on the polymer type, on the used crosslinking system and on processing the aging mechanisms lead macroscopically to increasing stiffness and hardness or stickiness[2]. Failures in function of the component are the consequence. Alongside the selection of polymers, the aging process is determined mainly by the use of anti-aging agents – e.g. p-phenylenediamines or by substituted phenols[3,5–8]. This work focuses specifically on temperature dependency, kinetic aspects of thermal-oxidative aging, on the influence of polymer structure, crosslinking density and crosslink structures and on the consumption and mechanistic aspects of antioxidants. The knowledge about kinetics and of the most efficient processes should be used for simulation models in future.

2. Theoretical aspects of thermal-oxidative aging

The chemical aging of polymers in presence of temperature and oxygene is determined by means of a three-phase radical mechanism[9–14]. The chain reaction is terminated by recombination reactions with the formation of stable compounds, such as, for instance, the constitution of C-C or C -O-C bonds from two macroradicals, tantamount to an increase in crosslinking density. An embrittlement of the material is the macroscopic consequence. On the polymer, there is also formation of polar oxygenic side groups, which likewise have a stiffening effect due to inter- and intramolecular interactions. Especially at higher termperatures for some polymers like NR, chain scission can also be observed as a dominant effect, accompanied by elastomer viscosity. The two reaction channels compete with one another, with the polymer configuration (double bonds of the main chain, side groups) playing a more significant role like the nitrile group in the case of NBR[19,20]. The formation of sulfones, sulfonates and sulfates is described for reactions in the area of the sulfur network[21,22].

Antioxidants are usually used to avoid aging processes. The antioxidants have different effectiveness in dependency on their molecular structure, chemical reactivity and diffusion behavior. Considering chemical reaction mechanism in the subject of thermal-oxidative aging two groups of antioxidants are exists, the primary (chain breaking) and secondary antioxidants[10,23–25]

3. Methods and materials

Systematic investigations were performed on the aging stability of uncrosslinked, crosslinked NBR`s (varied in acrylonitrile content) and SBR´s (varied in vinyl content).

Measurements were carried out by means of rheometry, chemiluminescence (CL)[17], ATR-FT-IR spectroscopy, in combination with CL and NMR-relaxation. The characterization of changes in physical properties during aging stress-strain measurements and determination of hardness were used in dependency on aging in ventilated air cabinets up to 1000 h at different temperatures in the range of 80 to 140 °C.

Furthermore the consumption, diffusion and effectiveness of *p*-phenylenediamines as antioxidants were investigated by means of ATR-FT-spectroscopy using a sandwich arrangement of a reservoir for the diffusing substance and a thin layer of the matrix. The calculation of diffusion coefficients bases on the Fick`sch law and the time lag method.

4. Results

4.1. Investigations on uncrosslinked NBRs

The thermal oxidation aging of polydienes is significantly influenced by the double bond concentration in the main chain (1,4 units)[17,18], which is reduced with increasing concentration of the acrylonitrile side groups. So the oxidative stability of the pure polymers after extraction of the stabilizers added by the polymer producers should result in decreasing oxygene induction times (OIT values) in chemiluminescence (CL) measurements. The influence of the ACN-content of extracted NBR's on OIT is shown in scheme 1.

The values in scheme 1 show clearly, that up to 28 % ACN- content the OIT values are increasing against to a limit at 34 % ACN . Depending on the ACN-content the aging resistance is increased by factor appr. 3. This is more or less in line with the expectation, that the OIT is depending on the C=C-double bond concentration in the main chain. Unclear is the situation for the extreme high ACN-content of 34 % and especially of 39 %. May be that reactions of the ACN-groups are responsible. This aspect has to be proven by further investigations by means of FT-IR spectroscopy and model substances, which can be analysed by chromatographic methods.

The temperature dependent investigations of oxidative aging on NBR`s results in decreasing times OIT values with

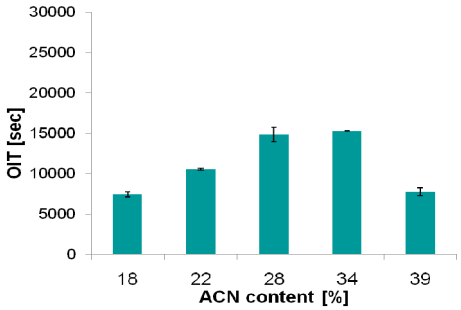

Scheme 1. **OIT-values as function of ACN-content for extracted uncrosslinked NBR`s at 100 °C**

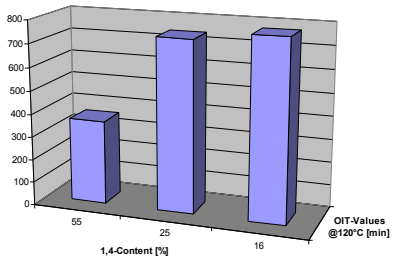

Scheme 3. **OIT-values at 120 °C as function of 1,4 butadiene-content for cured SBR`s with similar crosslinked densities**

increasing temperature in CL measurements as it is shown in the following scheme 2.

The evaluation using the normalized slopes of the first part of the curves[26] and the Arrhenius principle results in activation energies describing the temperature dependency of the aging process are between 37 and 73 kJ mol^{-1}. The values show an increasing tendence with the ACN-content.

4.2. Investigations on crosslinked SBR-rubbers

SBR`with varied vinyl content between 16 % and 55 % were sulfur crosslinked using a unique SEV-system. Fillers were not used. The characterization of the vulcanizates by means of CL results in CL-curves with two maxima, where the first one is considered for the evaluation. The OIT-values result from the cross-section of the tangent with the x-axis by extrapolation from the rising part of the CL-curves. The OIT-values of the SBR`s with different microstructure but with a constant crosslink system at 120 °C are shown in scheme 3.

The OIT-values are increasing with a lower content of C=C-double bonds as it is to be expected considering the reaction mechanism. The reactive part is the hydrogene atom at the allyl-position. This is explained by the inductive effect of the double bond in the chain on the allylic C-H-bond. The bonding energy is lowered in comparison to the C-H-bond in the vinyl-group, so that the abstraction is favoured in this position. An uncertainty of the values is given by the situation, that the material was not extracted and that the crosslink densities are not exactly the same. The variation of the temperature for the aging process in the CL results in decreasing OIT-values with increasing temperature due to the accelerating effect of the temperature for the reaction speed.

In the case of a high C=C-double bond content of the main chain in SBR 1 the activation energy of the reaction controlled by CL is the lowest one. This is in line with the low OIT values for this type of rubber. For SBR 2 and 3 the values are more than double, that means, that a change in temperature has a very high influence on the reaction speed.

4.3. Influence of crosslinking

The OIT values of SBR 2 vulcanizates with low, medium and high crosslink densities are in the range of appr. 400 min at 130 °C, the differences are in the range of the standard deviation of the CL-method, which is in ideal cases appr. 6 %rel. (ref. [27]). The influence of crosslink densities on the thermal oxidative aging was investigated by means of CL, NMR relaxation and physical testing. The OIT values of SBR 2 vulcanizates with low, medium and high crosslink densities (S/CBS 0.5/0.5; 1.5/1.5; 2.5/,2.5) are in the range of appr. 400 min at 130 °C, the differences are in the range of the standard deviation of the CL-method, which is in ideal cases appr. 6 % rel. (ref.[27]). So the crosslink density play a minor role in comparison to the structure of the polymer. The effect of temperature on the aging process in dependency on the crosslink density was characterized by means of the determination of the activation energies using NMR, CL and elongation at break-measurements (scheme 4).

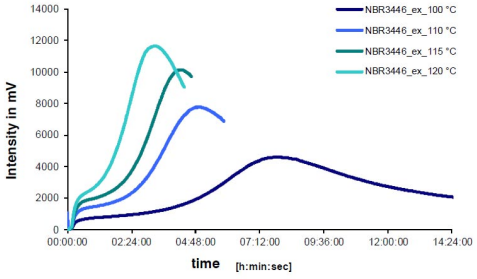

Scheme 2. **OIT-values as function of temperature for extracted uncrosslinked NBR** (ACN-content 28 %)

Table I
Activation energies from CL of the SBR-vulcanizates

Vulcanisate[a]	E_A [kJ mol^{-1}]
SBR 1(15 S, 30 V)	65
SBR 2 (25 S, 63 V)	157
SBR 3 (20 S, 55 V)	135

[a] Crosslinked: 1.5 phr S, 1.5 phr CBS, S = styrene content in %, V = vinyl content in %

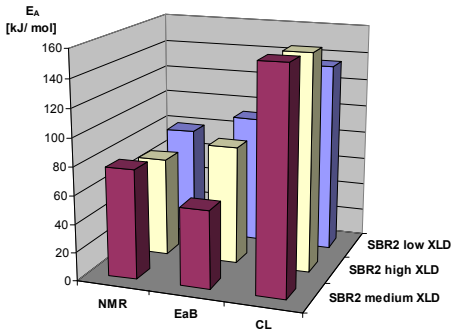

Scheme 4. **Activation energies in dependency of crosslink density for SBR 2 vulcanizates, measured with NMR, EaB = elongation at break and CL**

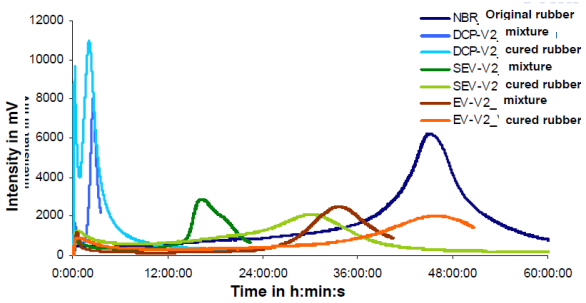

Scheme 5. **CL-curves at 130 °C as function of crosslink structures (EV, SEV and DCP system) at constant XLD for NBR (28 % ACN), uncured NBR compound and original NBR**

In principle the results in scheme 4 are showing, that the values for E_A are depending extremely on the used method measuring different processes. Overall the differences internal of one method are very small. So it is to conclude, that the influence of crosslink density is small in comparison to the effect of the polymer structure and that the different methods show different parts of the oxidation reaction.

The investigations on the influence of crosslink density (XLD) and crosslink structure for NBR (28 % ACN-content) were performed using EV- and SEV systems on two levels (high = V1 and low = V2) with the same XLD per each pair. For comparison a peroxide crosslinked system (Dicumylperoxide = DCP) was used with the same XLDs on the 2 levels as they were prepared for the sulfur systems. The crosslink densities were adjusted by rheometry. The CL-curves at 130 °C for the lower level of XLD with varied crosslink structures incl. the peroxide crosslinked systems shown in scheme 5.

It is obvious, that the mixing process and the vulcanization affect a reduction in the thermal oxidative stability. The maximum of the curve of the original NBR without any treatment is at much higher times than all the others. The reason is, that during processing the material is pre-aged, whereas it is to note, that the antioxidant system added by the manufacturer is consumed during processing. Furthermore the sulfur systems especially the EV-system is much more stable than the DCP-system, which shows, that residual peroxide is a initiator in aging.

4.4. Consumption and effectiveness of antioxidants

The efficiencies of DPPD, 6PPD and 77PD as antioxidants (3 phr per each) were determined using CL with determination of the OIT values of SBR-compounds with different vinyl content of the polymer and of an IR-compound. The highest efficiency calculated from the slope of the graph OIT as f(concentration) shows in all cases the DPPD followed by 6PPD and 77PD. The diffusion coefficients of the antioxidants measured by time lag method and FT-IR spectroscopy are in the range of 4.3 to 0.16 $*10^{-6}$ for all systems, where the values are the lowest one for DPPD and overall they correlate with the chain flexibility of the polymer. So the diffusion is in line with the efficiency, which is depending on the reactivity and on the availability in the system limited by the diffusion speed.

The authors deeply acknowledge the Deutsche Kautschuk Gesellschaft (DKG e.V.) and the Arbeitsgemeinschaft industrieller Forschungsvereinigungen e. V. (AiF) for the support of this work.

REFERENCES

1. DIN 50035 (1972).
2. IUPAC Recommend.-Definitions of Terms Relating to Degrad. Ageing and Rel. Chem. Transf. of Polymers (1996).
3. H. W. Engels, H. Hammer, D. Brück, W. Redetzky: Rubber Chem. Technol. *62*, 609 (1989).
4. J. Sampers: Polym. Deg. Stab. *76*, 455 (2002).
5. D. F. Parra, M. T. De, A. Freire, M.-A. De Paoli: J. Polym. Sci. *75*, 670 (2000).
6. J. C. Ambelang, et al.: Rubber Chem. Technol. *36*, 1497 (1963).
7. J. Boxhammer: Material Test. Prod. Tech. News (Atlas Sun SP) *30*, 1 (2000).
8. R. H. Krüger et al.: Food Additives and Contaminants *22*, 968 (2005).
9. G. Scott: Chemistry and Industry *16*, 271 (1963).
10. G. Scott: *Mechanismen of Polymer Degradation and Stabilisation*, Elsevier Appl. Science, pp. 170, 1990.
11. A. Hoff, S. Jacobsson: J. Appl. Sci. *27*, 2539 (1982).
12. G. Scott: Developments in Polymer Stabilisation, Appl. Science Publishers LTD, pp. 145, 1981.
13. E. A. Snijders, A. Boersma, B. van Baarle, J. Noordermeer: Polymer Degrad. Stab. *89*, 200 (2005).
14. J. L. Bolland: Trans. Faraday Soc. p. 669, 1949.
15. R. W. Keller: Rubber Chem. Technol. *58*, 637 (1985).
16. P. M. Norling, T. C. P. Lee, A. V. Tobolsky: Rubber Chem. Technol. *38*, 1198 (1985).
17. M. Santoso, U. Giese, R. H. Schuster: Rubber Chem. Technol. *81*, 762 (2007).
18. M. Santoso, U. Giese, R. H. Schuster: KGK, Kautsch. Gummi Kunstst. 60, 192 (2007).

19. H. Bender, E. Campomizzi: KGK, Kautsch. Gummi Kunstst. *54*, 14 (2001).
20. S. Bhattacharjee, A. K. Bhowmick, B. N. Avasthi: Polym. Degradation and Stability 31 (1991).
21. G. Scott: Rubber Chem. Technol. *58*, 269 (1985).
22. H. Modrow, R. Zimmer, F. Visel, J. Hormes: KGK, Kautsch. Gummi Kunstst. *53*, 328 (2000).
23. A.G. Ferradino: Rubber Chem. Technol. *76*, 694 (2003).
24. H.-W. Engels: KGK, Kautsch. Gummi Kunstst. *47*, 12 (1994).
25. D. Brück, H.-W. Engels: KGK, Kautsch. Gummi Kunstst. *44*, 1014 (1991).
26. L. Zlatkevich: *Chemiluminescence in Evaluating Thermal Oxidative Stability in Luminescence Techniques in Solid State Polymer Research.* Marcel Dekker, New York 1989.
27. U. Giese, M. Santoso, R. H. Schuster: Lecture: International Rubber Conference (IRC) Nuernberg, July 2009.

ML-02
NANOSCALE STRUCTURE AND PHYSICAL PROPERTIES CHARACTERIZATION FOR SUPER FUEL-EFFICIENT TIRES

TOSHIO NISHI[a] and KEIZO AKUTAGAWA[b]*

[a] *Tokyo Institute of Technology, 2-12-1 Ookayama, Meguro-ku, Tokyo 152-8550, JAPAN,* [b] *Bridgestone Corporation, 3-1-1 Ogawahigashi-cho, Kodaira-shi, Tokyo 187-8531, JAPAN*
akutag-k@bridgestone.co.jp, tnishi@polymer.titech.ac.jp

NEDO has carried out a new program with industries and academia to develop super fuel-efficient tire materials between 2009–2011. The program focuses on the design of tire compound with three-dimensional nano-hierarchial architecture optimized for super fuel-efficient tires. It aims not only to reduce rolling resistance but also to solve the trade -off between rolling resistance and wear performance. Computational science and imaging techniques were extensively used to design and control the nano-architecture of the tire compound. The virtual simulation of the nano-architecture gives us ideas that have never been realized in compound design[1].

For this project we have proposed new characterization methods for three-dimensional nano-scale hierarchical architecture, which can be divided into three different scale ranges: 10nm with crosslinks, 100nm with filler dispersion and 1000nm with polymer blends. The 3D-TEM and AFM were developed to derive the 3D image of actual nano-hierarchial architecture and the distribution of mechanical properties in nano-scale, respectively. These techniques were developed working together with special members organized under the NEDO program. These methods can enable us to visualize the mechanical behavior of the compound under deformation with stress concentration in nano-scale[2].

The technology can be applied not only to complex elastomeric materials but also to polymer alloys, blends, and composites. In this invited lecture we will introduce some of the main concepts and results of the project since it is very complex and there are many members from industry and academia.

Visualization of crosslink network structure

The crosslink network in 3D was visualized with combination of 3D-TEM and the Shi-ibashi method, which is a technique of special pretreatment for the visualization of the crosslinks of cured rubbers[3]. The specimen was prepared with the crosslinked rubber swollen with styrene monomer which was polymerized after swelling. The crosslinked rubber chain was stained and visualized by 3D-TEM. The 3D structural image of crosslink network is shown in Fig. 1, which was processed with the thinning image software. The reconstructed image in 3D was divided into cubical cells and calculated the volume fraction of rubber at each cell. The crosslink density of each cell was calculated using Flory-Rehner equation and the modulus were calculated. The histogram of the modulus is also shown in Fig. 1, where it is found that the modulus in nano-scale are widely distributed[2].

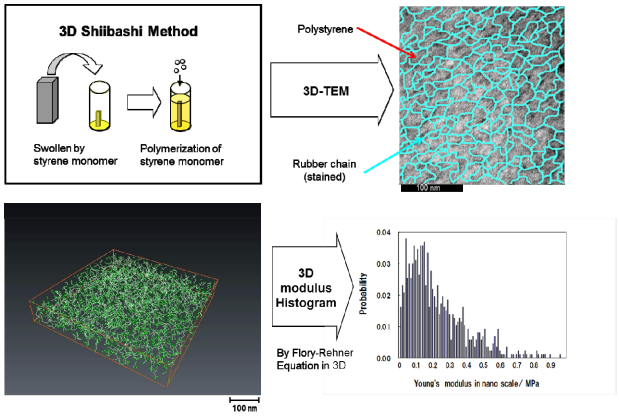

Fig. 1. **Visualization of 3D crosslink network using Shi-ibashi method[2]**

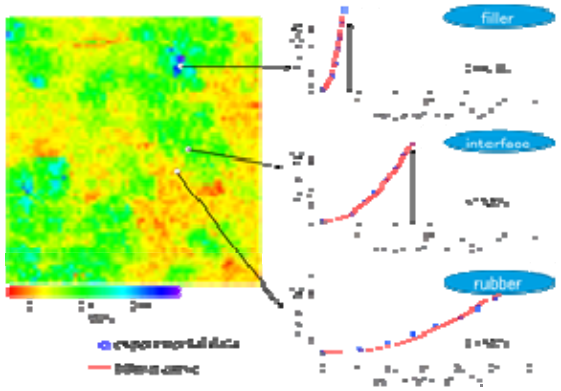

Fig. 2. **Young's modulus distribution of filled rubber using nano-mechanical mapping technology[4]**

Young's modulus mapping of filled rubber

Atomic force microscopy (AFM) was applied to visualize topographic and mechanical properties in nano-sscale. Young's modulus can be derived with nano-scale resolution by means of analyzing the force-distance curve with Hertz theory. Young's modulus distribution of filled rubber with this method are shown in Fig. 2. It can be recognized that the magnitude of modulus can be divied into three regions; rubber, carbon black (or bound rubber) and interfacial regions[4].

3D distribution of fillers

The filler network structure in nano-scale was visualized by 3D-TEM (ref.[5]). The advantage of this method is direct observation of filler network without any pretreatment such as etching of the filled rubber. The complicated structure of filler network can be seen and was combined with voxel method to construct the 3D finite element model in nano-scale[6]. The reconstructed filler network image and its digitized sheet were shown in Fig. 3.

Finite element analysis in mesoscopic scale and nano-mechanical simulation

The model is transferred into finite element analysis software and stretched in uni-axial direction up to 15 % strain. In each strain step, the stress and strain energy density are calculated for each voxel. Overall stress and strain energy density are calculated by sum of all voxels data. From strain energy data, Young's modulus is calculated and this data is compared with experimental data as shown in Fig. 5. To the first approximation, Young's modulus calculated from FEM shows a good agreement with the experimental data, and the magnitude is 4 times higher than that of unfilled rubber. This gap is thought to be a Payne effect and volume effect by filler incorporation in rubber. Also shown in the sliced images of Fig. 5, color graduation represents the strain distribution in rubber under strain. Dark blue colored pixel represents zero deformation and red colored pixel represents strain over

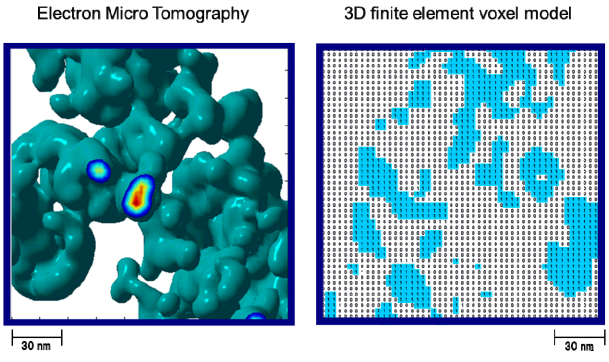

Fig. 3. **Visualization of filler network using 3D electron micronto-mography and its digitized image for 3D finite element voxel model[6]**

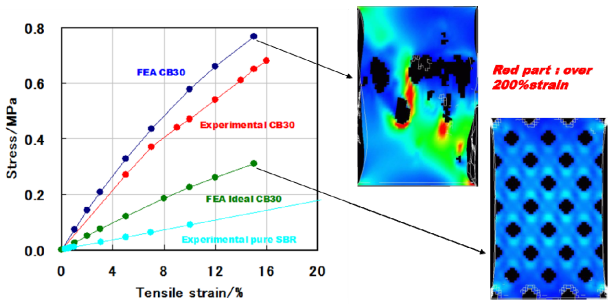

Fig. 4. **Stress-strain curves of calculated and measured results with sliced images. FEA CB30:actual rubber, FEA Ideal CB30:virtual rubber and Experimental CB30:measured**

100 %. Strain distribution is not uniform and even if overall strain is 15 %, red colored position which shows over 200 % of strain can be seen.

Nano hierarchical structure control for super fuel-efficient tire rubber

The finite element method in nano-scale was used to determine the ideal nano-hierarchical architecture to solve the trade-off between rolling resistance and wear performance as described in Fig. 5. For A-B polymer blend architecture the phase A with high wear toughness and the phase B with low energy loss should be placed together in nano-scale. For filler architecture the filler particle should be placed in highly dispersed state. For cross-link network architecture the cross-link points should be distributed uniformly. Three steps of nano-architecture control technologies were applied to satisfy these preconditions of the ideal nano-hierarchical architecture. The optimization of polymer blend improved wear with 60 %, the improvement of filler dispersion reduced the energy loss with 52 % and the optimization of the crosslink network gave additional improvement in energy loss with 12 %. As a result the compound optimized in nano-hierarchical architecture was able to satisfy the target performances of balance between energy loss and wear.

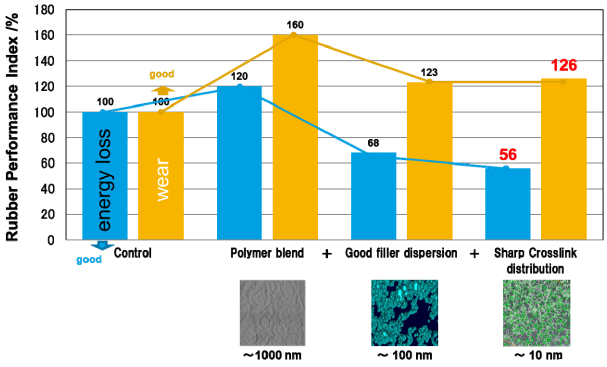

Fig. 5. **Nano-architecture design steps to solve trading-off between energy loss and wear properties of tread compounds[2]**

Conclusion

1. Nano-structure visualization methods were developed by collaboration between industry and academia with a project supported by NEDO.
2. Nano-hierarchical structure controls such as good dispersion of filler and sharp distribution of crosslink density can give lower energy loss, which is necessary for fuel-efficient tires.
3. Nano visualization technologies are found to be useful to design the nano-architecture, especially for the development of the super fuel-efficient and better wear tires.

We are grateful for the support of New Energy and Industrial Technology Development Organization NEDO. We also would like to thank Bridgestone Corporation, WPI-AIMR Tohoku University (Prof. Ken Nakajima), IMCE Kyushu University (Prof. Hiroshi Jinnai), AIST (Dr. Hiroshi Morita), and JSR Corporation (Mr. Takuo Sone) for their cooperation.

REFERENCES

1. Akutagawa K.: *Tire Technology EXPO Conference Program,* Day 1, Feb. 5, 2013, Koeln Messe, Germany.
2. Nishi T.: *Tire Technology EXPO Conference Program,* Day 1, Feb. 5, 2013, Koeln Messe, Germany.
3. Shi-ibashi T., Hirose K., Tagata N.: Kobunshi Ronbunshu *46*, 473 (1989).
4. Nishi T., Nukaga H., Fujinami S., Nakajima K.: Chinese J. Polymer Sci. *25*, 1 (2007).
5. Jinnai H., Shinbori Y., Kitaoka T., Akutagawa K., Mashita N., Nishi T.: Macromolecules *40*, 6758 (2007).
6. Akutagawa K., Yamaguchi K., Yamamoto A., Heguri H., Jinnai H., Shinbori Y.: Rubber Chem. Technol. *81*, 182 (2008).

ML-03
POLYMER BLENDS AND NANOCOMPOSITES FOR AUTOMOTIVE APPLICATIONS

Appropriately formulated blends of polypropylene (PP) with ethylene-octene elastomers (EOR), organoclays based on montmorillonite (MMT) clays and a maleated PPcan lead to Thermoplastic Olefin (TPO) materials with better toughness and stiffness that are suitable for many automotive applications.

RAJKIRAN TIWARI and DONALD R. PAUL*

University of Texas at Austin, Department of Chemical Engineering, Austin, Texas 78712 USA

Elastomer particle size has a significant effect on the impact strength of rubber-toughened thermoplastics. We have shown that the size of ethylene-co-octene elastomer, EOR, particles are significantly reduced by the addition of organoclay based on montmorillonite, MMT, and as the molecular weight of the polypropylene, PP, matrix is increased . The high shear stress exerted by the PP matrix and the inhibition of coalescence of elastomer particles caused by the MMT facilitate this decrease in the elastomer particle size .In addition, the elastomer particle size is also affected by the elastomer rheology, i.e., melt flow index, MFI, and octene content of the elastomer. The EOR particles are mostly elongated in shape due to deformation during the injection molding process .

The matrix molecular weight is known to influence the mechanical properties and toughness of rubber-toughened blends; this is related to the inherent ductility of the matrix and its response to toughening for different elastomers. However, little is known in particular for extruder-made TPO

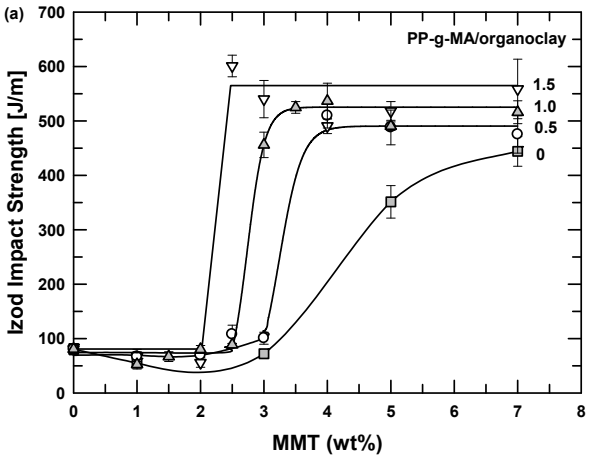

Fig. 1. **Effect of MMT and PP-g-MA on the room temperature Izod impact strength of a PP/EOR blend**

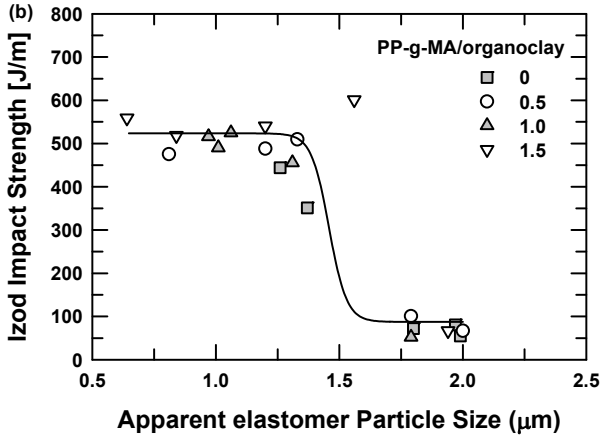

Fig. 2. **The combined effects of MMT and PP-g-MA content translate into an effect of EOR particle size which controls the Izod impact strength**

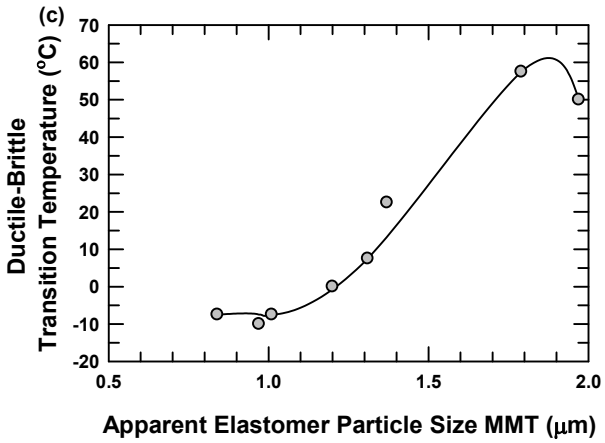

Fig. 3. **The reduction in EOR elastomer particle size by addition of MMT and controlling the PP-gMA content reduces the ductile-brittle transition temperature of PP/EOR blends**

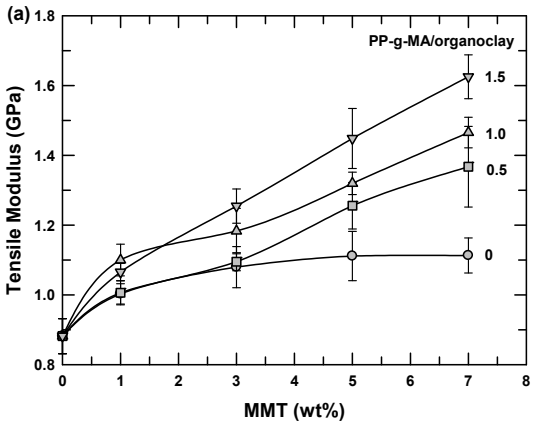

Fig. 4. **Addition of MMT increases the modulus of the PP/EOR blends as does increasing the PP-g-MA content**

nanocomposites about how the PP molecular weight, elastomer type, and MMT content affect the elastomer particle size and toughness. This is important since nanocomposites with a good balance of toughness and stiffness have many potential applications. Extruder-made TPO blends from low MFI PP (< 1g/10 min @ 190 °C) have shown toughness > 600 J m^{-1}; however, applications of such blends are limited due to processibility issues arising from high matrix viscosity; on the other hand, controlling elastomer particle size using MMT provides a unique combination of toughness and stiffness even for low molecular weight PP useful for injection molding[24].

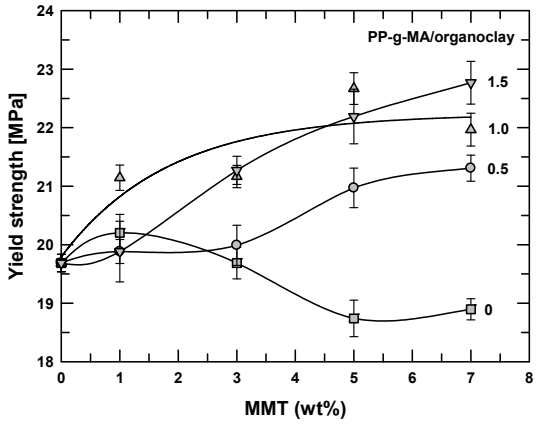

Fig. 5. **Increasing the MMT and PP-g-MA content increases the yield strength of the PP/EOR blend**

This paper explores the combined effects of elastomer particle size along with the molecular weight of PP, elastomer MFI, elastomer octene content and MMT content on the toughness of extruder-made PP/PP-g-MA/MMT/EOR nanocomposites. The room temperature Izod impact strength is examined to separate out effects of each parameter on the toughness of the PP/PP-g-MA/MMT/EOR nanocomposites. The effects of elastomer particle size and PP molecular weight on impact strength are reported. The tensile modulus and yield strength are shown to increase with MMT content. The extruder-made TPO nanocomposite provides a favorable balance of properties relative to a commercial reactor-made TPO nanocomposite. The results from this study should be useful for developing formulations of extruder-made TPOs in terms of elastomer particle size control and toughness, based on end-use applications.

The property enhancements that are possible by this strategy are illustrated in Figures 1–5.

Further details about this investigation can be found in the following references[1–5].

REFERENCES

1. Tiwari R.R., Paul D.R.: Polymer. *52*, 4955 (2011).
2. Tiwari R.R., Paul D.R.: Polymer. *52*, 5595 (2011).
3. Tiwari R.R., Paul D.R.: Polymer. *53*, 823 (2012).
4. Tiwari R.R., Paul D.R.: J. Polym. Sci., Part B: Polym. Phys. *50*, 1577 (2012).
5. Tiwari R.R., Paul D.R.: J. Polym. Sci., Part B: Polym. Phys. In press.

ML-04
NANOTECHNOLOGY AND CARBON FIBRE IN GREEN COMPOSITES

MOHINI MOHAN SAIN

Centre for Biocomposites and Biomaterials Processing, University of Toronto, 33 Willcocks Street, Toronto, Canada
m.sain@Utoronto.ca

ML-05
CNT-RUBBER INTERACTION – A BASE FOR INNOVATIVE RUBBER MATERIALS

ROBERT H. SCHUSTER *, H. CHOGULE, and H. WITTEK

Deutsches Institut f. Kautschuktechnologie, Eupener Str. 33, 30519 Hannover
Robert.Schuster@DIKautschuk.de

Over the last decade carbon nanotubes (CNTs) have been the subject of intense investigations in both fundamental and applied science[1]. Due to outstanding mechanical strength, sur-face specific area, aspect ratio and electrical properties CNTs are promising candidates to produce polymeric nano-compo-sites with outstanding mechanical properties and high electrical conductivity. The challenge in achieving the desired goals is to find suitable processing strategies for efficient CNT dispersion in the polymer matrix[2]. In many studies CNTs are incorporated into the polymer via suspensions in fluids and sonication followed by solvent evaporation[3].

The contribution aims to investigate application oriented strategies for CNT dispersion by mechanical mixing and latex compounding into rubbers with different but defined chemical constitution (NR, NBR, HNBR, EVA, EPDM, Q and FKM). The experimental series have been carried out using four different types of Multiwalled Carbon Nanotubes (MWCNT): Nanocyl (NC) NC7000, NC3100 and Baytubes (BT) C150HP and C70P.

The focus is to emphasize the effect of CNT dispersion on polymer chain dynamics, transport phenomena, mechanical reinforcement and ultimate properties. In addition the impact of CNTs on rubbers mixes filled with high loadings of well dispersed carbon black and/or silica was investigated (hybrid systems) as an option for short term applications of CNTs in elastomeric products.

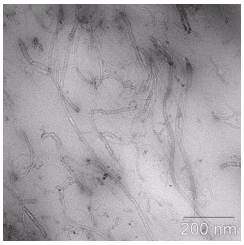

Fig. 1. **CNT dispersion**

Master batches with up to 5 vol.% CNT were prepared by (i) dry melt mixing using a laboratory internal mixer at variable rotor speed and mixing time, (ii) subsequent mixing on a two-roll mill, (iii) extrusion through a special die and (iv) latex compounding.

By dry melt mixing a good dispersion and random distribution of MWCNTs is observed. High shear rates and prolonged mixing on the two roll-mill lead to a better homogeneity but also to a break-down of the tube length and a lower aspect ratio. By the technique of latex compounding good dispersion was obtained.

It is shown that the electrical percolation threshold is influenced (i) by the chemical nature of the polymer, (ii) the type of the CNT and the process parameters that control the dispersion. For constant mixing conditions in the internal mixer (20 min.) the following sequence of electrical percolation thresholds (in vol.% CNTs) was established:

NR (1.0)< FKM(1.3)<Q(1.5)<NBR(1.5)<HNBR(1.8)

Keeping the mixing conditions at constant it was observed that the electrical percolation threshold decreases with the polarity of the polymer indicating specific interactions. The percolation threshold increases with the tube diameter and the entangle-ment density of the CNTs. Furthermore the saturation conductivity systematically higher for polymers with lower percolation limits and reach conductivity values up to 1S/cm.

Crosslinked CNT/Rubber nanocomposites demonstrate similar dynamic-mechanical properties as CB filled elastomers but at far less volume fraction of the filler. Due to the strong polymer-CNT interaction and the high degree of dispersion the “Payne-Effect” is less pronounced than in CB filled elastomers. Consequently the nanocomposites demonstrate lower hystere-sis and higher elasticity at the same hardness or stiffnes of the systems.

The reinforcement by CNTs is clearly seen in the increase of the stress in the strain region up to 300 % as well as in the non -linear increase of the tensile strength as a function of the CNTs content This level of reinforcement cannot be achieved by CB or silica. For CNTs with a small tube diameter the reinforcing effects are considerably higher than for ones with large tube diameter. The effect is attributed to the higher polymer-filler contact surface per unit volume and to the higher surface activity due to more pyramidalization[4].

If the normalized stress at a given elongation is considered as a criteria for reinforcement the plotted curves

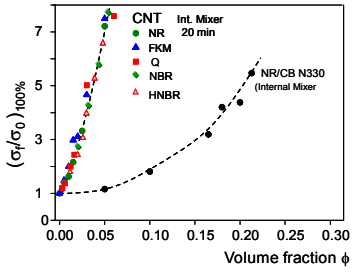

Fig. 2. **Reinforcing factor for CNT- and CB-systems**

for all the systems under investigation demonstrates that the intrinsic reinforcing mechanism depends primarily on the CNTs and their state of dispersion (Fig. 2).

Remarkable improvements of the mechanical properties were observed for hybrid nanocomposites. The addition of small con-centrations of CNTs to CB filled compounds increases the Young's modulus, stress values, tear energy and dyna-mical cut growth resistance significantly.

The authors acknowledge the support given by the BMBF within the InnoCNT Allianz.

REFERENCES

1. S. B. Sinnot, R. Andrews: Crit. Rev. Solid State Mater. Sci. *26*, 145 (2001).
2. M. M. J. Treacy, T. W. Ebbesen: Nature *382*, 678 (1996).
3. L. Bokobza, M. Rahmani: KGK, Kautsch. Gummi Kunstst. *62*, 112 (2009).
4. X. Lu, Zh. Chen: Chem. Rev. *105*, 3643(2005).

KEY LECTURES

KL-01
CHAIN STRETCHING AND RHEOLOGICAL BEHAVIOUR OF CIS-BR: ROLE OF MOLECULAR ARCHITECTURE FOR TYRE APPLICATION

FABIO BACCHELLI and SALVATORE COPPOLA

versalis spa, ENI Group, Research Centre, via Baiona 107, 48123 Ravenna, Italy
fabio.bacchelli@versalis.eni.com

Introduction

Rheology is the science of deformation and flow of matter, whose investigation tools essentially result from continuum mechanics considerations.

If elastomers are to be processed under optimum conditions, knowledge of rheological properties proves essential. Processing of rubber compounds involves the application of rapid and large deformations in both shear and elongation. This indicates that transient flow and a large degree of stretching are actually prevalent. Nevertheless, the analysis of unit operations is usually performed on the basis of the rheological response to steady state, mild shear flow.

Commercial rubbers possess more complex structures with respect to model polymers and the non-linear rheology of a compound is strongly affected by changes in the relaxation time spectrum of its polymer matrix as a consequence of variations in molar mass distribution or branching patterns.

In the last decade, following the requirements of Kyoto environmental treaty, polymer producers are facing the challenge of producing materials with different molecular structures to reach the targets set by the new regulations. Indeed, because of the recent restrictions in terms of carbon dioxide emissions into the atmosphere, the tires producers are focusing their attention on the reduction of rolling resistance while keeping constant or even improving all the other mechanical performances and also the processability.

The mixing process of two partially miscible polymers, such as high-cis polybutadiene and natural rubber, is indeed strongly influenced by the rheological properties of the pure components. Moreover, the final mechanical properties of the blends strongly depend on the characteristics of the pure components. In the linear regime, the polymers have been characterized performing small angle oscillatory shear and creep tests. Using the Time Temperature Superposition technique, the dynamic mechanical spectrum has been determined in a wide range of frequencies and the corresponding relaxation spectrum has been calculated.

The rheological properties of two blends, obtained mixing natural rubber with two different high-cis-BR grades characterized by different molecular architecture (molecular weight distribution and degree of branching), were analyzed in a wide temperature range (30–110 °C). Moreover the curing kinetics of these blends were investigated as a function of polymer structure, temperature (140–180 °C), and frequency (0.1–10 Hz). The morphology of the vulcanized mixtures was studied by AFM. A rolling resistance prediction was determined in the frame of Futamura's methodology[1] for tire evaluation. Eventually, cyclic extensions up to large deformation were used to characterize the vulcanized blends in terms of hysteresis. The high-cis polybutadiene with narrower molecular weight distribution and a lower degree of branching is promising not only in the perspective of an easier mixing process, but also in terms of a reduced rolling resistance of the cured compound.

Experimental

Two high-cis-BR (97 % cis content) of comparable Mooney Torque /ASTM D1646) were used in the present work, namely a commercial grade (versalis spa, named BR BROAD MWD) and a model polymer (versalis spa, BR NARROW MWD). NR/BR rubber blends (50/50) were obtained using a 350 cc Brabender laboratory mixer. Characteristics are reported in Table I. Pure polymers were mixed together with curing agents. Mixtures were vulcanized at 140 °C and 180 °C.

Dynamic rheological measurements were performed with a rotational rheometer SR5000 (Rheometrics) using a parallel plates configuration (D = 25 mm) in the temperature range 30–110 C° for pure components, uncured blends and vulcanizates.

The curing kinetics of the blends were investigated as a function of polymer structure, temperature (140–180 °C), and frequency (0.1–10 Hz). The morphology of the samples vulcanized at T = 150 °C and 1 Hz were analysed with a AFM Veeco Nanoscope III in tapping mode.

Cyclic extension and retraction were applied to vulcanized films with a rotational rheometer Anton Paar Physica-MCR501 equipped with a SER Extensionale Platform. The tests were performed at T = 25 °C at two Hencky strain rates: 0.01 s-1 and 0.1 s-1. Each specimen was extended and retracted until completion of 4 cycles.

Results and discussion

The linear viscoelastic response of pure BR, pure NR and related unvulcanized blends is reported in Fig. 1a and 1b. BR BROAD is characterized by a broader spectrum of relaxation times and a higher elasticity at low frequency, due to a higher degree of branching. Mixtures based on different BR grades show a comparable viscoelastic response,

Table I
Characteristics of investigated BR grades

High-cis-BR	ML 1+4@100 °C MU	Mw g mol^{-1}	Mw/Mn –
BR BROAD	42	460000	4.4
BR NARROW	40	330000	2.5

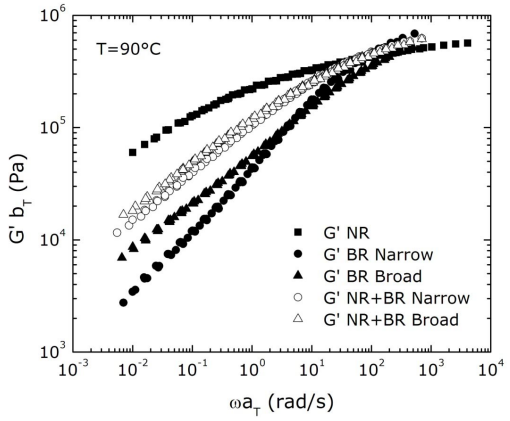

Fig. 1a. **Storage modulus vs frequency for pure components and uncured mixtures**

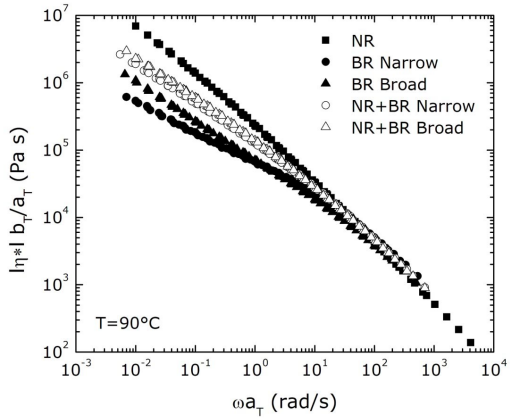

Fig. 1b. **Complex viscosity vs frequency for pure components and uncured mixtures**

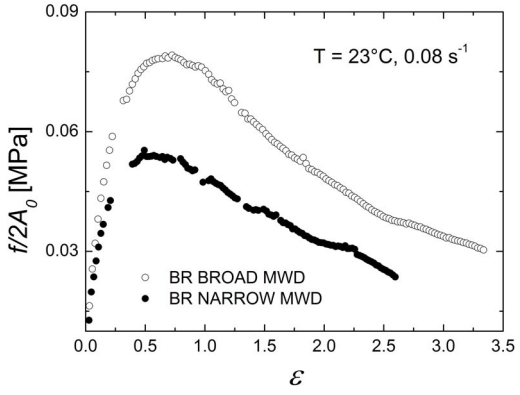

Fig. 2. **Extensional response of pure componentsat constant Hencky strain rate**

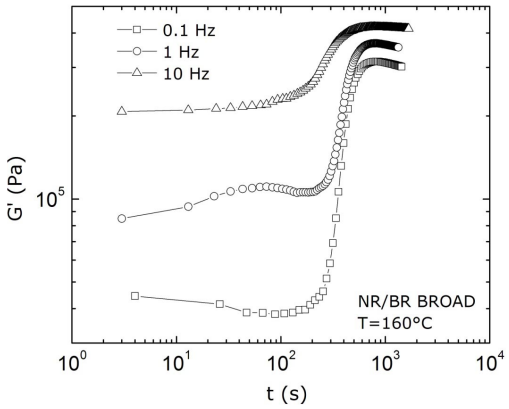

Fig. 3. **Cure kinetics of the NR/BR BROAD blend at 160 °C and various frequencies**

intermediate between pure BR and pure NR. BR NARROW shows a lower complex viscosity, accounting for a better processability.

Differences related to the high molecular weight fraction are clearly observed in extensional flow, as reported in Fig. 2. The different position of maximum stress is related to different chain stretching in the transient flow behaviour.

Vulcanization kinetics of the NR/BR BROAD mixture are depicted in Fig. 3 at T = 160 °C and at various frequencies. The increase of elastic modulus vs time is related to the network formation.

A weak effect of frequency is observed, while temperature plays a major role (Fig. 4). Comparable results are obtained with the NR/BR NARROW blend.

A kinetic constant of vulcanization has been calculated as follow:

$$\alpha(t) = \frac{G'(t) - G'_0}{G'_\infty - G'_0} \qquad (1)$$

$$K_{0.5} = \frac{1}{t_{(\alpha=0.5)}} \qquad (2)$$

The elastic modulus of NR/BR mixtures vulcanized at T = 140 °C and 1 Hz has been determined at 30 °C and 110 ° C. As already pointed out, rheological properties weakly depend on frequency, accounting for a good vulcanization network. A smaller decrease of elastic modulus vs temperature is observed for the NR/BR NARROW mixture, related to a reduced number of network defects (Fig. 5). The G"/G' ratio is also reported in Fig. 5. A lower value is observed in the case of the blend containing BR NARROW. These results may be related to a better rolling resistance in the frame of tire traction predictors, following the approach of Futamura[1].

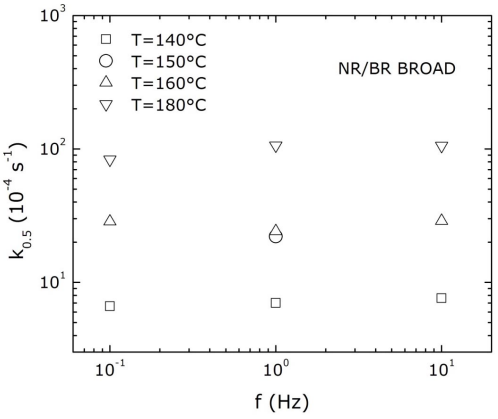

Fig. 4. **Vulcanization constant for the NR/BR BROAD blend at various curing temperatures**

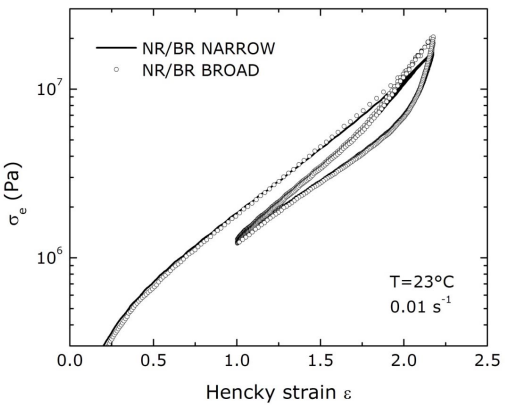

Fig. 7. **Softening effect in uniaxial elongation for NR/BR mixtures**

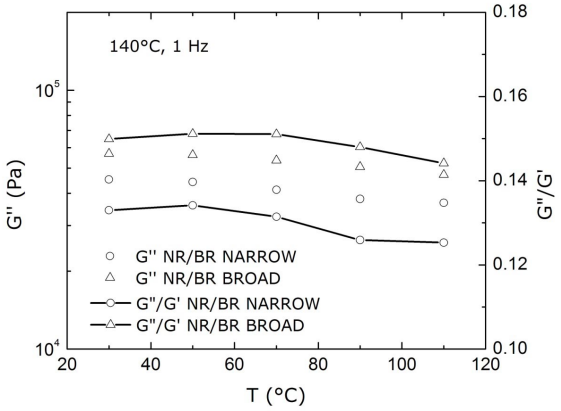

Fig. 5. **Viscoelastic parameters of cured NR/BR mixtures at 140 °C**

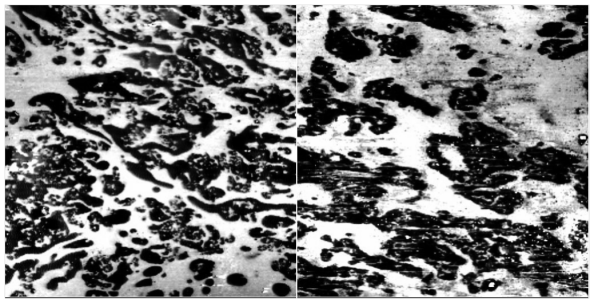

Fig. 6. **AFM images (tapping mode) of cured NR/BR mixtures. NR/BR BROAD left, NR/BR NARROW right**

NR/BR blends represent immiscible systems[2]. Both mixtures show a co-continuous morphology, as depicted in Fig. 6 (AFM images). The observed differences are related to the phase dispersion during mixing, as a function of the rheological response of the investigated BR grades.

The uniaxial elongation of cured specimens (Fig. 7) was performed through repeated extension and retraction cycles representing a sort of Mullins[3] effect of the unfilled system. An evident softening behaviour is observed for both samples. The differences between the two blends under cyclic extensional deformation are almost undetectable. The behaviour is therefore dominated by the common polymer (NR). Comparable mechanical properties at large strain are, then, expected.

Conclusions

A high-cis polybutadiene with low polydispersity and a lower degree of branching is promising not only in the perspective of an easier mixing process, but also in terms of a reduced rolling resistance of the final cured compound.

Versalis spa is gratefully acknowledged for the permission to publish this work.

REFERENCES

1. Futamura S.: Rubber Chem. Technol. *64*, 57 (1991).
2. Hess W. M., Herd C. R., Vegvari P. C.: Rubber Chem. Technol. *66*, 329 (1993).
3. Mullins L.: Rubber Chem. Technol. *42*, 339 (1969).

KL-02
CURE KINETICS AND VARIABLE TEMPERATURE ANALYSIS METHODOLOGIES FOR SOLVING FACTORY PROBLEMS

JOHN S. DICK and EDWARD NORTON

Alpha Technologies, 3030 Gilchrist Road, Akron, OH, USA
john.dick@dynisco.com

Abstract

Some major quality problems observed in the rubber industry are traced to poor control of rubber compound cure characteristics, which results in high internal and external failure costs in rubber fabrication processes. A more effective way to detect and investigate these problems is through the use of cure kinetics studies and variable temperature analysis (VTA) with the Rubber Process Analyzer (ASTM D6204 Part C test method).

This Paper provides a review of reaction cure kinetics and variable temperature analysis which can be used together to investigate potential rubber compound problems. Several laboratory design of experiments with selected rubber compound variations were conducted to compare the effectiveness of both cure kinetics and VTA.

Cure Kinetics

The Reaction Kinetics Module can be accessed through the Eclipse® software package. It enables the calculation of additional parameters such as reaction order, reaction rate constant, and activation energy.

Up to ten cure points can be used to determine the reaction rate constant. Changing these values will allow the user to concentrate on and/or ignore particular parts of the curve. Enabling the activation energy calculation will allow the user to include up to eight tests in determining the activation energy of the compound. These tests should be run at various temperatures so that the Arrhenius equation can be applied.

In the Reaction Kinetics Module, there are other tabs that enable the user to view the curves and results of the tests. Under the conversion variable tab, the torque curve is normalized by subtracting the minimum from each point and then dividing by (maximum-minimum). This allows the curve to be plotted in a range of 0.0 to 1.0 where each value corresponds to a cure point. For example a value of 0.9 would represent the cure point tc90. Example conversion variable curves can be seen in the figure below.

As one can see, these equations match the functions used for the scaling on the conversion curves. In the figure below, an example conversion curves plot is shown representing four tests run at different temperatures on the same compound. If a plot of ln(k) versus 1/T is made, the slope of the linear regression line will be $-E_a/R$ and the intercept will be ln(A).

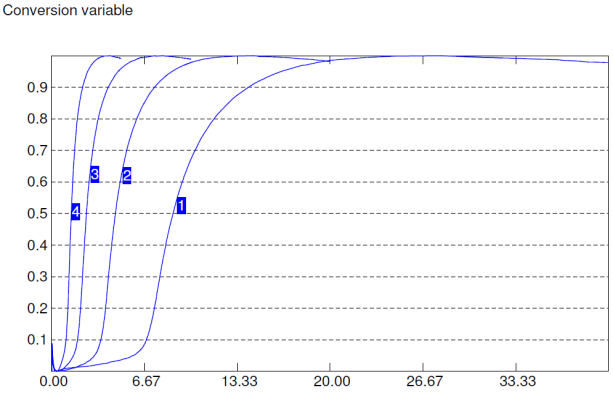

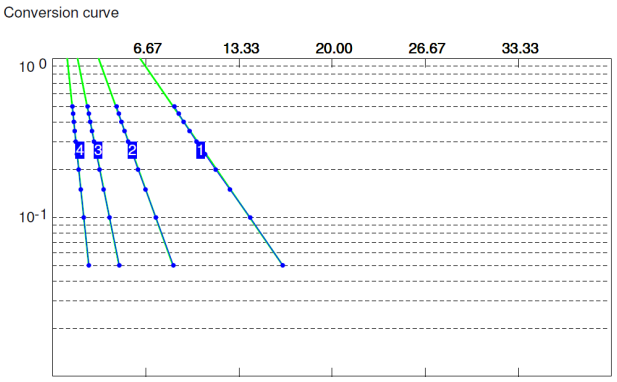

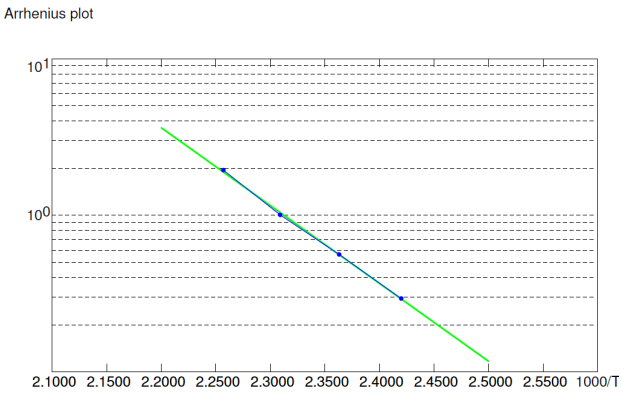

Variable Temperature Analysis

Variable Temperature Analysis or VTA was available originally on the RPA in 1993. This use of digital technology for the first time allowed the RPA to replace the older analog "Cure Simulator", which was used in the tire industry in the 1980s. Through the VTA feature, an RPA could now be programmed to follow exactly a time-temperature profile from a thermocouple tire cure study just as the earlier cure simulators did. However this VTA program could also be set up on the RPA to implement a precisely controlled linear, thermal ramp from a processability temperature, such as 100 °C, up to a high cure temperature, such as 190 °C. Figures below demonstrate how this linear thermal ramp is 50 % more sensitive to differences in scorch time than a corresponding isothermal cure test.

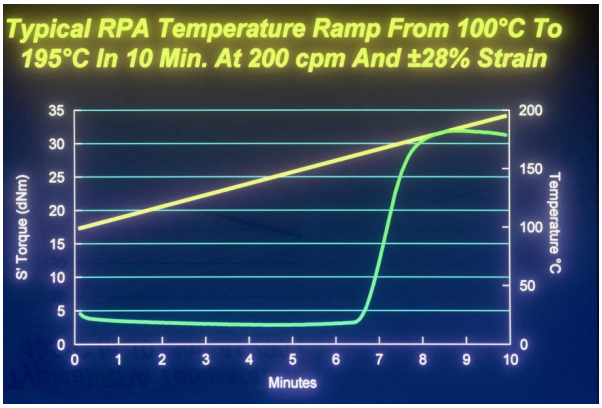

Because of this improvement in statistical test sensitivity, a new Part C was added to the ASTM D6204 method for using the RPA as a processability tester. Because this technique is commonly used in rubber technology today, it was felt that such a VTA configuration should also be used with our cure kinetics software to study the effects of deliberate changes in cure packages on curing properties.

Experimental

A series of mixed stocks with controlled variations in curatives were completed with a BR laboratory banbury and blend mill. Model formulations based on sulfur cures for SBR and NR based compounds were used in this study as well as comparisons of different peroxide / promoter curatives in EPDM, CM, CR, and FEPM.

Identification of coagents

Coagent Abbreviation	Chemical Name	Trade Name
TMA	Trifunctional (meth) acrylate ester	Santomer Saret®SR517
HVPBD	High vinyl poly (butadiene)	Sartomer Ricon®154
PBDDA	Poly(butadiene) di-acrylate	Sartomer SR307
PDM	N,N'-m-phenylene dimaleimide	Sartomer SR525
TAC	Triallyl Cyanurate	Sartomer SR507

An RPA 2000 Rubber Process analyzer was used for establishing this data base.

Forty-three rubber compounds were included in these experiments.

Results

From the testing of 42 different rubber compounds, many comparisons of EA and order of reaction were made as shown below in two examples.

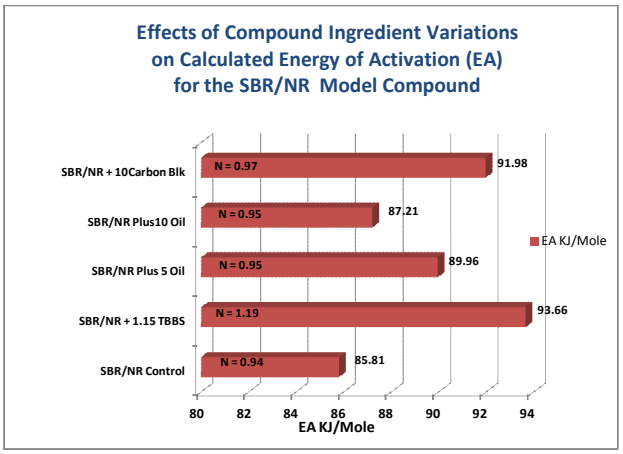

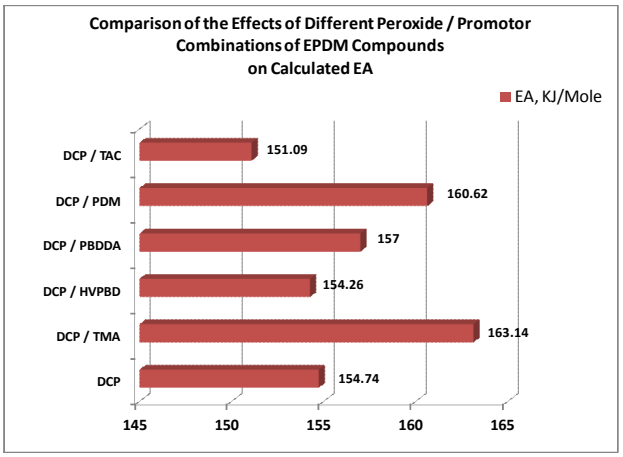

Also direct VTA vs. isothermal cure comparisons were made for sulfur and peroxide cures as illustrated below for EPDM.

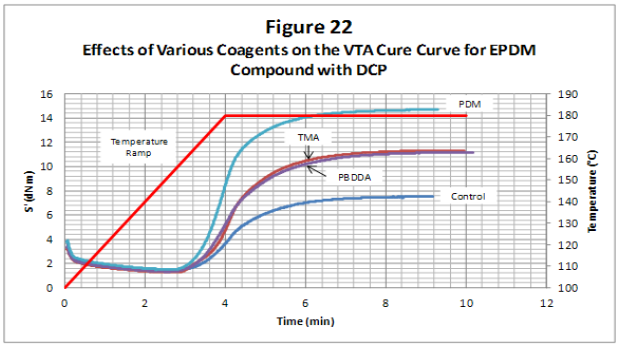

Figure 23
Effects of Various Coagents on the Isothermal 150°C Cure Curve for EPDM Compound with DCP

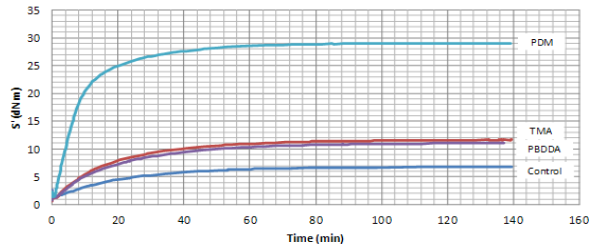

Also comparisons were made by VTA vs. isothermal cures for CPE based compounds.

Figure 24
Effects of Various Coagents on the VTA Cure Curve for CPE Compound with DCP

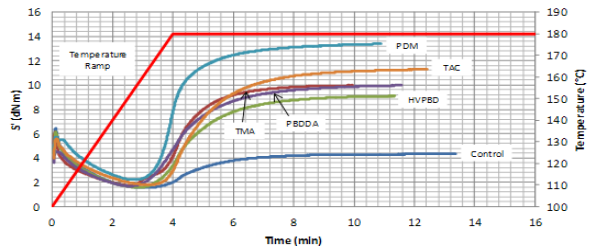

Figure 25
Effects of Various Coagents on the Isothermal 150°C Cure Curve for CPE Compound with DCP

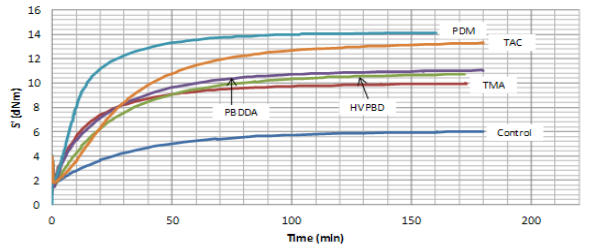

Conclusion

1. The Reaction Kinetics Module of Eclipse® Software is very effective at measuring order of reaction (N) and energy of activation (E_a) for the 42 rubber compounds used in this study.
2. Repeatability of these cure kinetics measurements, such as E_a and N, were very good, with a coefficient of variation of 1.6 % for the E_a.
3. Typically conventional sulfur cures will be between 65 and 140 KJ/Mole while peroxide cures will be between 140 and 165 KJ/Mole for E_a.
4. Typically conventional sulfur cures can deviate greatly from a first order reaction where many non-CPE peroxide cures can have an order of reaction (N) very close to unity.
5. With conventional sulfur cures, increases in carbon black or oil can sometimes elevate the calculated E_a of the compound.
6. Increasing accelerator loading or changing to an ultra accelerator for sulfur cures can increase the energy of activation (E_a).
7. Adding a coagent to a peroxide cure can also increase the E_a.
8. VTA can give better information (such as scorch times) during the early stages (onset) of cure.
9. VTA can provide a better compromise in test lapse time for measuring changes that are occurring at the onset of cure vs. the ultimate state of cure
10. VTA is more sensitive to changes that occur at the onset of cure, especially with the peroxide cured halogenated elastomers (such as CPE and FEPM) in that not only the scorch time can be measured, but the VTA scorch temperature as well. "Scorch temperature" might be more sensitive to real differences with halogenated elastomer compounds than "scorch time"

KL-03
AUTOMOTIVE APPLICATIONS OF THERMOPLASTIC ELASTOMERS –WHAT'S NEW

JIŘÍ G DROBNÝ

Drobny Polymer Associates, 11 Quails Way, Merrimack, NH 03054 USA
jdrobny@drobnypolymer.com

Thermoplastic elastomers (TPEs) are rubbery materials with fabrication characteristics of conventional thermoplastics and many performance properties of thermoset (vulcanized) rubber. Most of them are block and graft copolymers[1], although current commercial products include combinations of hard polymer/and elastomer, ionomers and polymers with core/shell morphologies[2]. Considering such variety of materials, it is clear that their properties will be within a wide range, from soft rubbery, even gel-like to hard and tough at which point they approach the ill-defined borderline between elastomers and thermoplastics. TPEs can be processed by the same methods as most thermoplastic materials, such as polyethylene, polypropylene, and polyvinyl chloride. On the other hand, their basic properties are very similar to those of conventional rubber materials, such as natural rubber, SBR, EPDM, NBR, polyurethanes, and polychloroprene. Thermoplastic elastomers offer a variety of practical advantages over vulcanized rubber, such as simple processing with fewer steps, shorter fabrication times, and the possibility of recycling of production and post-consumer scrap. Current developments include TPEs resisting to media, such as oils, greases, fuels, cooling liquids as well as temperatures of 150 °C or higher[3].

These and other advantages are the main reasons why TPEs are being used in many industrial applications and their consumption has been growing at constantly increasing rate during the past two decades. This growth of thermoplastic elastomers market in the United States and elsewhere is gradually attaining commodity status, leading to a slew of

changes in terms of price and profit margins[4]. Their excellent performance capabilities and the environment-friendly nature of TPE continue to drive their market growth. Worldwide demand for thermoplastic elastomers is estimated at 4.1 million metric tons with annual growth rate averaging 6.3 % (ref.[5]).

Automotive applications represent currently nearly 30 % of the total worldwide demand for TPEs (ref.[5]). Recent technological developments include new types with improved resistance to elevated temperatures, in some cases coupled with increased resistance to oils, fuels, cooling fluids and other chemicals. This opened greater potential for their under-the-hood applications. This may include seals, hoses, tubes and different injection molded parts.

Additional improvements include new materials and designs for the exterior, such as door seals, window seals, and glass encapsulation[6]. Moreover, TPEs are finding increasing use in the automotive interiors replacing many traditional materials. This contribution focuses on the most recent developments in materials and applications of the TPEs in the automotive industry.

Traditional uses of TPEs in automotive sector include: styrenic wire and cable applications, styrenic bumper rub strips, grommets, holders and plugs, TPU sight shields, filler panels and bumper systems; TPU blow-molded bellows; olefinic wire harnesses, bumper covers, air dams, and air ducting; and copolyester gasoline tank caps, seat belt locking devices, and door latch covers.

In general, TPEs offer several advantages: short manufacturing cycles, very low amount of production scrap, recyclability of the scrap and of post-consumer waste. Another advantageous process is overmolding, i.e. molding a thermoplastic elastomer material over another substrate, such as a hard plastic. This technology has developed developing rapidly over the past several years.

Recent developments include new and/or improved materials, new and/or improved technologies as well as new applications. Examples of new or improved materials are: Specialty TPOs for vehicle exteriors and interiors[7], high melt strength SEBS copolymers[8,9], high performance TPVs (s-TPVs)[3,10,11], high flow (low viscosity SEBS)[4], bio-based TPEs, based on castor oil, polyols from corn, compounds with starch, monomers from biomass[4], and monomers from sugar cane[12]. New and/or improved or modified technologies include blow molding or blow molding combined with sequential coextrusion[13] as well as rotational molding[14].

New applications are driven by the following requirements:

– Reduced weight of parts affecting the gasoline consumption
– Environmental issues, such as lowering VOC, low odor, the use of sustainable materials
– Oil and fuel resistance, heat resistance (often by replacing parts made from conventional vulcanized rubber, such as hoses, under the hood seals and window encapsulation, body glazing seals. Typical new applications are shown in Fig. 1 (ref.[15]).

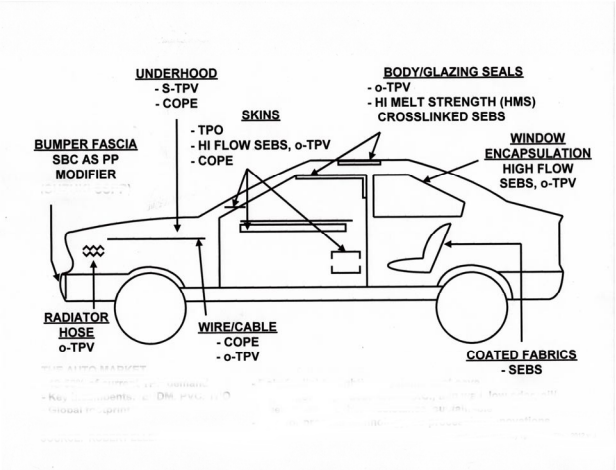

Fig. 1. **Automotive applications for thermoplastic elastomers (Courtesy Robert Eller Associates LLC)**

REFERENCES

1. Holden G., Kricheldorf H. R., Quirk R. P.: *Thermoplastic Elastomers,* 3rd Edition, Chapt. 1, p. 1, Hanser Publishers, Munich 2004.
2. Drobny J. G.: *Handbook of Thermoplastic Elastomers,* p. 5, William Andrew Publishing, Norwich, NY 2007.
3. Osen E., Klingshirn C., Eckrig D.: paper presented at TPE Forum, DKT 2012, Nuremberg, Germany, July 3–4, 2012. In German.
4. Eller R.: paper presented at TPE 2012 Conference, Smithers RAPRA, Berlin, Germany, November 13–14, 2012.
5. *World Thermoplastic Elastomers, Study #2551, Sept. 2011*, Freedonia Group, Cleveland, OH.
6. Vroomen G. L.: paper presented at TPE 2012 Conference, Smithers RAPRA, Berlin, Germany, November 13–14, 2012.
7. *Specialty Elastomers for Automotive TPO Compounds,* Dow Chemical Co., November 2006, Form No.777-00401-1106 AMS.
8. Tasaka M., Tamura A.: U.S. Patent 8,071,680, (December 20110 to Ricen Technos Corporation.
9. Sonnier R., Taguet A., Rouif S.:in *Functional Polymer Blends* (Mittal, V., Ed.), CRC Press, Boca Raton 2012.
10. Magg H.: paper presented at TPE Forum, DKT 2012 Conference, German Rubber Society, Nurnberg, July 2–5, 2012.
11. Geissinger M.: paper presented at TPE 2012, Conference, Smithers RAPRA, Berlin, Germany, November 13–14, 2012.
12. Taylor D.: paper presented at TPE 2012 Conference, Smithers RAPRA, Berlin, Germany, November 13–14, 2012.
13. Recht U., Hoppman C., Neuß A., Wunderle J.: paper presented at TPE 2012 Conference, Smithers RAPRA, Berlin, Germany, November 13–14, 2012.
14. von Falkenhayn D., Quian G., Mayer G., Venkatasvamy K.: paper presented at TPE 2012 Conference, Smithers

RAPRA, Berlin, Germany, November 13–14, 2012.
15. Eller R.: paper presented at the Thermoplastic Elastomers 10thTopCon 2012 Conference, Society of Plastics Engineers, Akron, OH, USA, September 10–12, 2012.

KL-04
A SUPER IMPACT-ABSORBING NYLON ALLOY

TAKASHI INOUE*

Department of Polymer Science and Engineering, Yamagata University, 4-3-16 Jonan, Yonezawa, 992-8510 Japan
tinoue@yz.yamagata-u.ac.jp

Nylon 6 (PA) was reactively blended with poly(ethylene -co-glycidylmethacrylate) (EGMA) at 70/30(PA/EGMA) wt. ratio. The reactive blending yielded a nano-salami morphology of the sub-μm EGMA particles in which 20 nm PA micelles are occluded by the pull-in of *in situ*-formed graft copolymer, as schematically shown in Fig. 1.

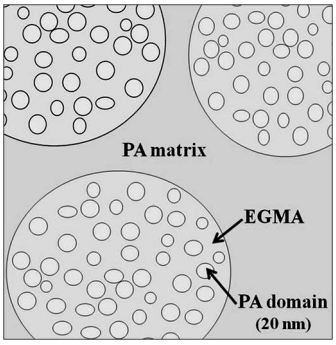

Fig. 1. **Nano-salami morphology**

The alloy showed a strange tensile behavior; the tensile modulus decreased as the elongation speed increased[1]. Then, we adapted a nickname of NOVA (non-viscoelastic alloy) for this alloy. NOVA was a rigid plastics, however, the necking was not observed during the tensile test but it deformed uniformly. It was apparently similar to the crosslinked rubber. It was so even for ultra-high speed tensile test of 36 km/h.

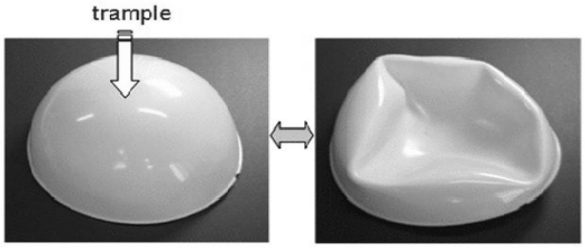

Fig. 2. **Injection-molded hemispherical body (1 mm thick, 130 mm diameter): as molded (left), trampled (right), and recovered (left)**

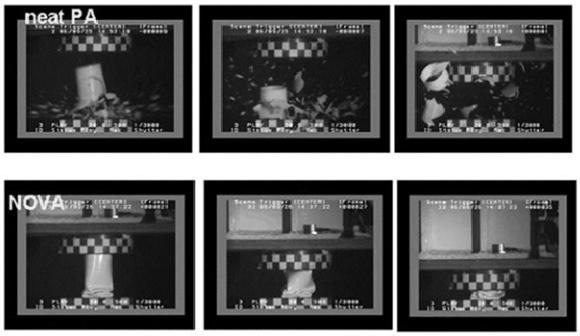

Fig. 3. **Video images during the falling weight impact test for pipe samples (50 mm diameter, 150 mm height, 2 mm thick); for neat PA (above) and NOVA (below)**

NOVA was nicely injection-molded as shown in Fig. 2, suggesting the good melt-processability. The mold was for a hemispherical lamp cover. The hemispherical body was placed on floor and trampled very quickly (at the highest speed for ordinary man) by heel. It plastically deformed as shown by the right picture in Fig. 2. Even at the highly deformed state, there was not the whitened region which is commonly observed for the plastics. Surprisingly, the trampled body was completely recovered to the original shape by pushing back with hand. Memory of the large deformation did not remain.

The results of high-speed falling weight impact test are shown in Fig. 3. A 193 kg weight fell from 0.5 m height (impact speed = 11.2 km h^{-1}) on pipe sample. Neat PA crashed to tiny fragments immediately after the weight hit the pipe sample. The impact condition was so severe that a typical engineering plastics, PA, broke in the very brittle manner. Even for such severe impact test, NOVA did not break but it just deformed. It looks like rubber hose and steel can.

The unique ductile deformation mechanism seems to be caused by the percolation of the dilation stress fields in PA matrix around the EGMA particles in which negative pressure

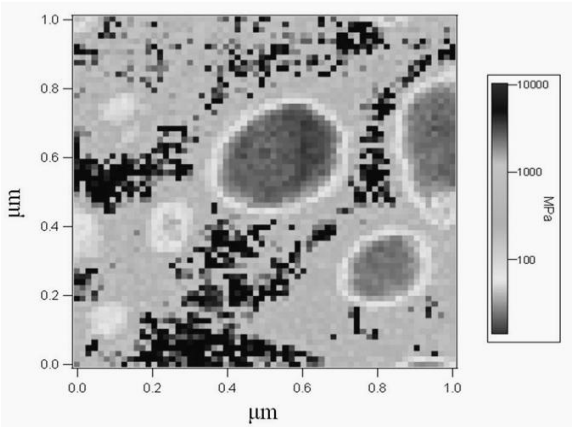

Fig. 4. **Local modulus mapping of NOVA by AFM analysis**

is evolved by thermal shrinkage mismatch[2] between PA matrix and EGMA particles upon cooling from the liquid state. It is supported by an AFM analysis of local modulus (Fig. 4).

REFERENCES

1. Sato D., Kadowaki Y., Kobayashi S., Inoue T.: e-J. Soft Mater. *3*, 9 (2007).
2. Inoue T., Ogata S., Kakimoto M., Imai Y.: Macromolecules *17*, 1417 (1984).

KL-05
PYROLYSIS AND GASIFICATION OF USED TYRES

C. G. JUNG*[a] and J.-P. BOUYSSET[b]

[a] Université Libre de Bruxelles, Polytechnic School, 4MAT, Av. F.D. Roosevelt, 50, B-1050 Brussels, [b] ETRA, av. de Tervueren, 16 B3, B-1040 Brussels
cgjung@ulb.ac.be

Alternative used tyres treatments to incineration are gasification and pyrolysis. Gasification is a thermal conversion process in default of air, while pyrolysis occurs in absence of oxygen.

Used tyres pyrolysis is a well-known process, using different technologies since the 70'th. Pyrolysis is performed in batch[1] or continuous processes[2], either at atmospheric pressure or under vacuum[3,4]. The more sophisticated processes were involving the reprocessing of used tyres into secondary raw material, gaseous, liquid or solid carbon products. Presently, given the market of raw materials and energy, the by-products valorization issued from used tyres thermal treatments did not find economically profitable outlets.

Until very recently, tyre recovery treatments focused on benefiting from either the material or the energy outputs. However, today, due to recent technological advances coupled with a reconceptualization of how best to exploit both the material and the energy capacities of tyres, new generation of technologies, treatments and materials have evolved.

Technologies available today at industrial scale for used tyres pyrolysis and gasification and their issued products will be presented. Depending on the valorisation paths after tyre pyrolysis or gasification, various end-products can be produced (scheme 1).

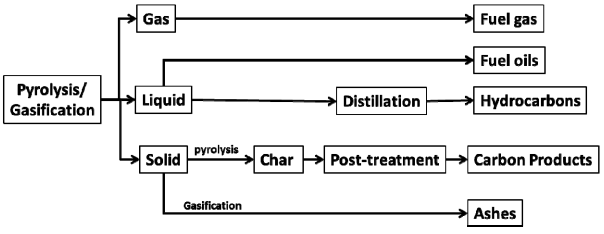

Scheme 1. **Thermal treatment valorization paths and products**

Research is performed to upgrade the char to ensure specific physical and chemical properties of the issued carbon products[5]. This valorisation path could be coupled with the use of the energy produced by the combustion of gas and oils produced during the process.

REFERENCES

1. Williams P. T., Besler S., Taylor D. T.: Proc. Instn. Mech. Engrs. *207*, 55 (1993).
2. Cyprès R.: *Proceedings 1st Int. Conf. on Tyre Recycling, Brussels*, 113–122 (1994).
3. Roy Ch., Labrecque B., de Caumia B.: Ressources, Conservation and Recycling *4*, 203 (1990).
4. Kraus T., Buděšínský M., Závada J.: Carbohydr. Res. *304*, 81 (1997).
5. Jung, C. G., Bouysset J.-P.: Proceedings, *Brussels ETRA 18th annual Conference* (2010 and 2011).

KL-06
BEHAVIOR OF SEISMIC-PROTECTION ELASTOMERIC ISOLATORS AT THE REALLY BIG EARTHQUAKES

TOSHIO NISHI[a] and NOBUO MUROTA*[b]

[a] Tokyo Institute of Technology, 2-12-1 Ookayama, Meguro-ku, Tokyo 152-8550, [b] Bridgestone Corporation, 1, Kashio-cyo, Totsuka-ku, Yokohama, 244-8510, Japan
tnishi@polymer.titech.ac.jp, murota-n@bridgestone.co.jp

In Japan, there are more than 2,800 buildings using elastomeric-seismic protection isolators since the first introduction of this kind in 1983. The number increased dramatically after the Hyogoken Nambu Earthquake in 1995 because of the excellent performance of that system.

At The East Japan Giant Earthquake on March 11, 2011 with magnitude 9.0 which was the fourth biggest earthquake in the world record in the history, there were more than 1,500 buildings with this system in the east Japan area. We could get very important data on the behavior of elastomeric-seismic protection isolators at the real big earthquake.

On the other hand, as a convener (TN) and a secretary (NM) of ISO/TC45/SC4/WG9 (Elastomeric Isolators) and Chairman country (Japan), we could issue ISO 22762 (Part 1~3) for elastomeric-seismic protection isolators on July 15, 2005 and revised them on November 1, 2010 due to the technological progress in these field[1]. Based on ISO 22762, we could issue Japanese Industrial Standard(JIS) JISK6410 (Part 1 and 2) for elastomeric isolators for buildings on August 22, 2011 and for bridges (JISK6411) on March 21, 2012 although they were issued after the giant earthquake. Anyway, these standards will contribute to protect buildings and bridges from big earthquakes in the future not only in Japan but also in the world. We will give short introduction on the science and technology of elastomeric isolators and show the performance of them under the giant earthquake. Then, we will present future problems for the elastomeric isolators for more important application.

Seismic isolation and seismic-protection isolators

Seismic isolation (hereafter SI) is an aseismic design concept to reduce the seismic force transmitted to the structure by supporting with a flexible element – elastomeric isolators – at the base or sometimes middle story of the buildings, to elongate the natural period of the structure and thereby decouples it from the ground (Fig. 1)[2]. Basically, SI systems provide functions of restoring force and energy dissipation. SI has gained popularity in the recent decade as a counter measure for seismic protection of structures. This is especially true in Japan, where over 2800 seismically isolated buildings have been constructed or are under construction. Fig. 2 shows the growth of the number of SI buildings in Japan. It is obviously observed that the number has drastically increased after the 1995 Hyogoken Nambu (Kobe) earthquake. Since 1995, there occurred 7 major earthquakes, whose moment magnitude was more than 6.0, in Japan until the 2011 East Japan Giant Earthquake. The SI technology has been applied to many types of buildings as shown in Fig. 3. Apartment has the largest number of application, followed by office buildings, and hospitals. In these earthquakes, SI buildings verified its effectiveness by its performance during earthquakes.

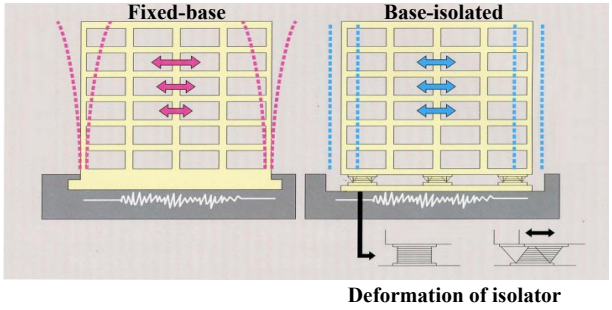

Fig. 1. **Principle of seismic isolation**

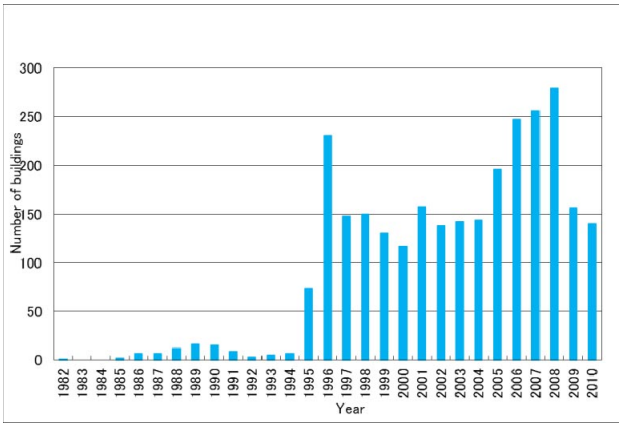

Fig. 2. **Growth of the number of SI building (Courtesy of Japan Society of Seismic Isolation**

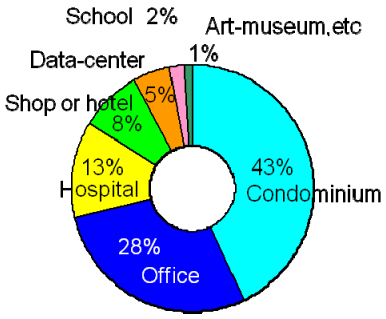

Fig. 3. **Various application of seismic isolation**

The principal requirements for elastomeric isolators are listed below;

1. Rigid stiffness to sustain vertical load for long term
2. Flexible stiffness to shift natural period of structures
3. Large deformation capability to absorb displacement of buildings during earthquake
4. Durability for long term use

The elastomeric isolator, made up with layers of alternating rubber and steel plates, as shown in Figure 4, is the most popular device to satisfy above requirements. The two components of the elastomeric isolators, rubber and steel plates, are bonded to each other by strong adhesion materials. The function of the steel plates is confinement of the rubber layers to support vertical loads with low horizontal stiffness. Generally, the ratio of the vertical and horizontal stiffness is over 1000. Generally, the elongation of the rubber used for isolators reaches over 600%. The large deformation supposed at design level earthquake is typically around 400mm, and isolators are designed to have shear strain of around 200% at that displacement.

Behavior at the east japan giant earthquake

The main earthquake occurred on March 11, 2011 but there have been so many aftershocks since then. (Fig. 5) There were 7 major earthquakes larger than M7 and more than 200 times medium scale earthquakes with shaking degree stronger than level 4 by the end of 2011 and it is still continuing in less degree even now.

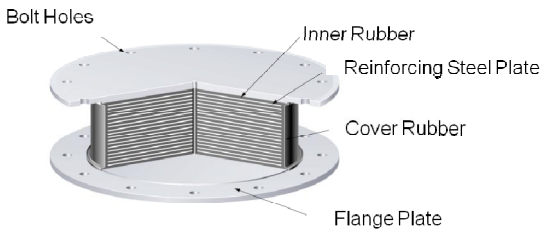

Fig. 4. **Basic construction of elastomeric isolators**

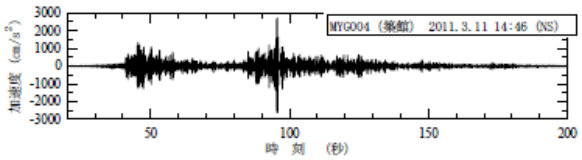

Fig. 5. **Time history of ground accerelation recorded in Tsukidate -city, Miyagi-prefecture (from K-NET Tsukidate)**

There are 236 seismically isolated buildings in Tohoku area, and basically they showed excellent performance during earthquake. Figure 6 shows the response acceleration of SI buildings at several sites. All of them promote significant reduction, 1/2 to 1/3, in response acceleration from the peak ground acceleration (PGA) whereas 2 to 3 times amplification is observed in fixed-base buildings. And, no damage in isolators were reported, and no replacement or repair of isolators were conducted. The largest displacement of elastomeric isolators was 41.5 cm in Sendai, and still the residual deformation was only 1.5 cm or smaller[3].

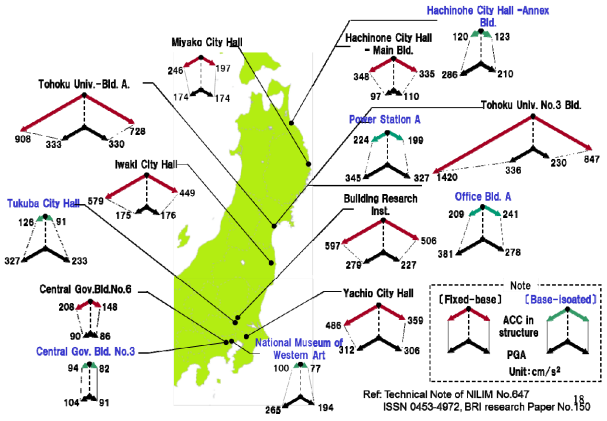

Fig. 6. **Examples of response acceleration of SI buildings comparing with fixed-base buildings**

This kind of report will never be possible without cooperation from many organizations like Government ministries, Japan Rubber Manufacturers Association(JRMA), and ISO/TC45, Japan Seismic Structure Institute(JSSI) and so on.

REFERENCES

1. Nobuo Murota, James M. Kelly, Keith Fuller, Fu Lin Zhou, Toshio Nishi et al.: "New International Standard for Elastomeric Seismic-Protection Isolators", *5th National Seismic Conference on Bridges and Highways, 2006, San Francisco*, CA.
2. F. Naeim, J. M. Kelly: *Design of seismic isolated structures: from theory to practice*, J. Wiley and Sons, 1999.
3. *Summary of the Field Survey and Research on "The 2011 off the Pacific coast of Tohoku Earthquake"* (the Great East Japan Earthquake), National Institute for Land and Infrastructure Management (NILIM), Ministry of Land, Infrastructure, Transport and Tourism, Japan. Building Research Institute (BRI), Technical Note of NILIM No.647,ISSN 0453-4972 BRI Research Paper No.150.

KL-07
CURRENT TRENDS IN POLYPROPYLENE DEVELOPMENT TOWARDS AUTOMOTIVE INDUSTRY

MARTIN OBADAL[a] and KAI FEHLING[b]

[a] *Borealis s.r.o., Nad Ovčírnou 3685, Zlín, Czech Republic,*
[b] *Borealis, Autovision WOB, SE-Zentrum, SE 1, Büro 372, D-38442 Wolfsburg, Germany*
martin.obadal@borealisgroup.com

The word mobility is unavoidably connected with the verbs, change, travel, flow, fly, migrate or move – consequently it is not therefore surprising that its importance in the global megatrends is very high though whole human historical genesis. The megatrends have been continuously changing as a reflection of the actual society development; currently these can be summarized into three main streams: urbanization, rising world population and aging population in mature markets. Additional factor to be considered is the oil consumption and its remaining reserves. Turning them into the mobility context, in particular to its automotive part – producers are focusing strongly on car efficiency, driving experience and handling, and safety/accident-free driving.

Polymeric materials give here several opportunities; in particular polymer composites have become already inevitable automotive materials and are increasingly used in several applications. Apparently, the key matrix material is the isotactic polypropylene and its copolymers – today, each passenger car contains more than 70 kg of PP based polymers being with approx. 40 % part of total plastics weight the predominant polymeric material in the car. PP already as a homopolymer possesses favourable mechanical properties, however for some already demanding applications in automotive the impact strength or stiffness are not sufficiently enough. However also here polypropylene offers variety of opportunities through its phase morphology variation and modification via fillers[1,2]. As a result the material can vary from soft material to the material with very high stiffness reaching easily the modulus of 10 GPa. Here the knowledge and availability of the multistep polymerization facilities (eg. Borstar®) and high compounding and compatibilisation competence is a key factor for production of advanced compounds (namely Daplen™, Nepol™, Xmod™)[3,4]. The materials can be then tailored to specific demands allowing an increase of the passenger and pedestrian safety, increasing the driving and travelling comfort, allowing the weight reduction and subsequent fuel consumption and reduction of the emissions, etc.

Current expectation, needs and motivation to use reinforced polypropylene in the automotive industry will be

Fig. 1. **Dashboard carrier made of 20% long-glass fibre PP compound Nepol™ GB215HP (*left*); the relevant dashboard of BMW 7 series (*right*)**[5]

presented from both market and technical perspectives. Special attention is paid to explain the need not only for traditional mechanical property interrelations (stiffness vs. toughness) but also for the other characteristics like aesthetical and haptic properties, emissions and odour, lightweight environmental requirements. Polypropylene compounds thanks to their versatility gives here several opportunities to fulfill such market needs.

Fig. 2. **Some structural PP application: VW Golf VII dashboard carrier made of expanded 20% short-glass fibre PP compound Xmod™ GE277AI (*upper)*; air intake manifold - 35% short glass fiber PP Xmod™ GB306SAF (*bottom left*); pedal carrier made of 30% short glass fibre PP compound Xmod™ GD301FE (*bottom right*). *The figures are not in scale***

REFERENCES

1. Obadal M., Čermák R., Baran N., Stoklasa K., Šimoník J.: Int. Polym. Proc. *19*, 35 (2004).
2. Gahleitner M., Hauer A., Bernreitner K., Ingolic E.: Int. Polym. Proc. *17*, 318 (2002).
3. www.reinforcedplastics.com/view/11141/volkswagen-switches-to-polypropylene-composite-for-air-intake-manifolds/
4. http://www.borealisgroup.com/industry-solutions/mobility/lightweight-vehicles/
5. http://www.reinforcedplastics.com/view/8113/bmw-selects-glass-reinforced-polypropylene-for-dashboard-carrier/

KL-08
REPROCESSING OF TECHNOLOGICAL AND POSTCONSUMER WASTE FROM AUTOMOTIVE PRODUCTION

LÁSZLO PADANYI

Ereme Enginnering Recycling maschinen und anlagen ges.m.n.h. Unterfeldstrasse 3, 4052 Ansfelden-Linz, Austria
s.hochreiter@erena.at

KL-09
OPTIMIZING MECHANICAL PERFORMANCE OF NANOSTRUCTURED POLYURETHANE ELASTOMERS AND FILMS

CRISTINA. PRISACARIU* and SERGIU COSERI

Institute of Macromolecular Chemistry "Petru Poni", Aleea Grigore Ghica Voda, Nr. 41 A. 700487, Iasi, Romania
crispris@icmpp.ro

The present work represents a new approach towards gaining insight into novel systems of copolyurethane elastomers (PUs) derived from complex dibenzyl hard segmentS, which are characterized by different packing structures in the PU hard domains[1–5]. A study has been made of inelastic effects in the deformation of PUs, where there is potential for formation of a two-phase microstructure (hard reinforcing particles embedded in an elastomeric matrix), but where the nature of the hard phase and the degree of phase separation can be controlled via the chemical structure and preparation conditions. The role of the hard segment structure was investigated. Two hard segments were compared, based on the diisocyanates: 4,4'-methylene bis(phenyl isocyanate) (MDI) and 4,4'-dibenzyl diisocyanate (DBDI), (Fig. 1 and 2).

The conformational mobility of the flexible diisocyanate DBDI causes an unusually wide range of mechanical, physical and chemical properties, associated with the

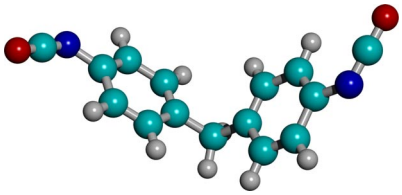

Fig. 1. **Extended conformation of 4,4'-methylene bis(phenyl isocyanate) (MDI)**

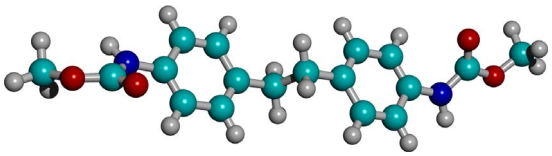

Fig. 2. **Extended conformation of 4,4'-dibenzyl diisocyanate (DBDI)**

possibility of pronounced phase separation into a domain – matrix morphology, and with a higher tendency to crystallization and self-association by hydrogen bonding, which is not available with the conventional MDI in melt-cast polyurethanes.

Thus, new polymers were achieved, with a controlled ordering of copolymer hard segment blocks on the macromolecular chain[2–5].

A study has been made of a family of PUs, in which the chemical components were chosen as shown in Fig. 3. The materials were all synthesized by the authors in the Romanian laboratory. They were all three-component systems combined in stoichiometric proportions, and consisting of: (1) a diisocyanate (DI) generating hard segment (HS) (MDI or DBDI); (2) a soft segment macrodiol (MD) – poly(ethylene adipate) PEA, polytetrahydrofuran PTHF, or poly (caprolactone) glycol PCD; and (3) a small molecule diol as chain extender (CE) – anhydrous ethylene glycol EG, or diethylene glycol DEG. The macrodiols were all of molar mass M_w = 2000 ± 50 g mol^{-1}. The three components were always mixed in the proportions HS:CE:MD = 4:3:1, giving hard segment mass fractions in the region of 30%, and isocyanic index I =100. The synthesis procedures followed was the pre-polymer route described previously by Prisacariu et al.[1–3].

The PUs mechanical responses were measured. Particular attention was paid to characterising the inelastic features – hysteresis, strain energy input and stress relaxation – and their variations between the materials. The same materials were also investigated by wide-angle X-ray scattering (WAXS and SAXS) to determine levels of crystallinity and phase segregation[2,5].

Stress-strain curves showed systematic differences. As seen in Fig. 4, the PU based on DBDI was observed to have a higher flow stress than its corresponding material based on the conventional diisocyanate MDI.

The results shown here are for materials with PTHF as soft segment and EG as a chain extender.

The same pattern was observed in polymers where the adopted macrodiol was PEA[2].

To obtain the true stress at break, tensile strength values were multiplied by the extension ratio $\lambda(= l/l_0)$, where l and l_0 are the extended and original PU sample lengths and the true strain true λ elongation at break, ε ($\varepsilon = \lambda + 1$).

Strain cycles such as those in Fig. 5 showed large differences in hysteresis between the materials, on the first load-unload cycle to each value of deformation (e_{max}). The DBDI polymers systematically showed higher first cycle hysteresis than those based on MDI, and this was enhanced by crystallisation of the hard segments.

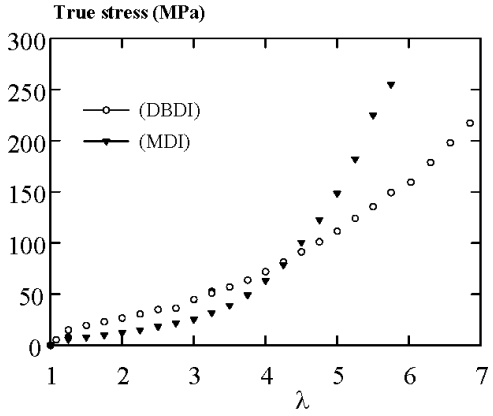

Fig. 4. **Comparison between the stress-strain data of two PUs with similar structures, based on DBDI and MDI respectively, at nominal strain-rate = 0.0042/s**

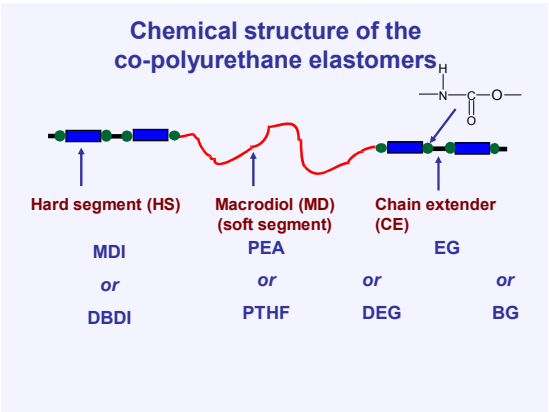

Fig. 3. **Chemical structures of the PUs studied in this work**

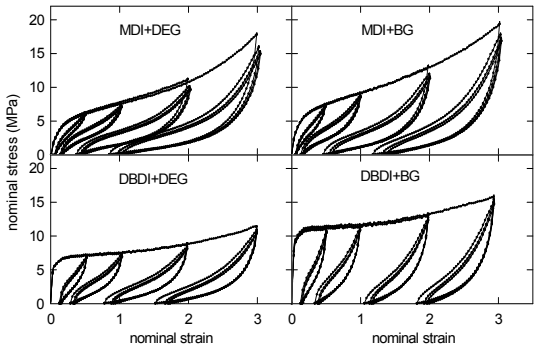

Fig. 5. **Examples of cyclic deformation for selected PUs from Fig. 3 after extension to various maximum nominal strains e_{max} (ref.[6])**

The presence of DBDI hard segments instead of the conventional MDI hard segments led systematically to increases in: the input strain energy to a given elongation, hysteresis and residual strain under cyclic loading, and stress relaxation.

The primary differences between the polymers in Fig. 4 and 5 arise solely from the higher flow stress of pure DBDI hard phase, resulting from its crystallinity. As shown elsewhere, optimum response was obtained by us with mixed MDI and DBDI hard segments[1,5].

The strengthening process in segmented PUs and filled elastomers in general, depends on the properties of the matrix and the dispersed phase hard domains (or fillers). Hard domains are primarily responsible for high strength, the matrix playing a subordinate role.

The strengthening process is also influenced by the PUs hard segment content. The flexible soft domains influence the PUs elasticity, making important contributions towards the hardness and modulus of the material, while the hard domains mostly affect modulus, and also determine the upper use temperature by their ability to remain associated at elevated temperatures[5].

The influence of the increasing the hard segment percent from 20 % to 100 %, on the mechanical properties was followed. The study of the stress– strain response included load-unload cycles to a nominal strain of 3, at constant rate of extension, with measurement of hysteresis and strain recovery, as shown in Fig. 6 and 7.

Increasing the hard segment percent led systematically to increases in the input strain energy elongation. With increasing the hard segment percent, polymers based on DBDI hard segments, displayed higher stiffness and strength than the conventional MDI-based PUs. Both features of the response were attributed to differences in hard phase plastic flow stress, resulting from crystallinity in the DBDI phase. With increasing the hard segment percent from 20 % to 100 %, lower strain recovery and strain energy recovery on cycling were observed in the case of PUs derived from dibenzyl structures. Inelasticity (residual strain, hysteresis) increased with increasing the hard-phase percent and was

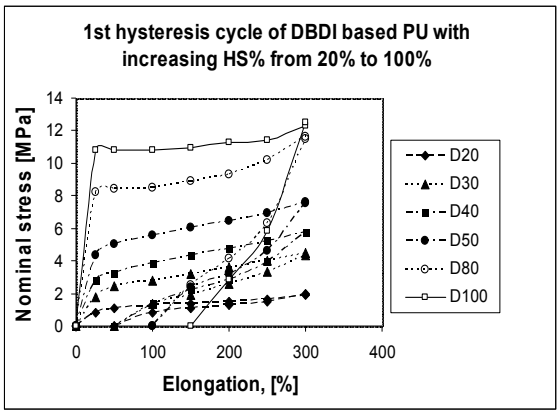

Fig. 6. **Tensile load/unload cycles for a thermoplastic material based on DBDI: (EG-PTHF-DBDI,I = 100), at strain rate 0.03 s-, with increasing the hard segment percent from 20 % to 100 %**

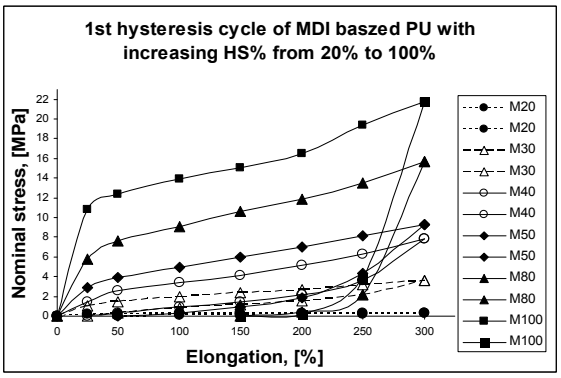

Fig. 7. **Tensile load/unload cycles for a thermoplastic material based on MDI: (EG-PTHF-MDI,I = 100), at strain rate 0.03 s-, with increasing the hard segment percent from 20 % to 100 %**

greater for DBDI hard segment than for MDI. Young modulus values increased proportionally with increasing the isocyanate content and were higher in the case of materials with DBDI.

In all cases the more mobile DBDI structure led to hard segments with a higher tendency to self associate evidenced by higher melting points and crystallization tendency which was visible even when such structures were included in the polyurethane soft segment matrix. The X-ray diffraction patterns of Fig. 8 show that crystallizability of DBDI based PU largely remains even after of inclusion of soft segments. The crystallinity was however, considerably reduced with the incorporation of MDI[1,5].

The dominant results from this work were the differences between polymers based on the two hard segments DBDI and MDI. Hard domain hydrogen bonding and crystallinity exerted strong influences on inelasticity of PU elastomers. The hard domains did not act simply as rigid crosslinks for the soft domain

The results were interpreted in terms of a physically-based constitutive model framework previously proposed[2,5]. This revealed that the observed effects of varying hard segment could all be explained by the hard domains having a

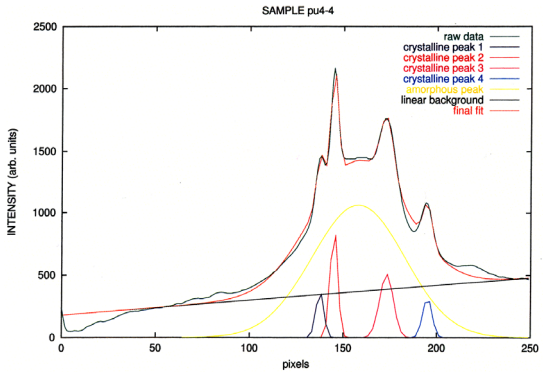

Fig. 8. **WAXS patterns of a PU based on the flexible diisocyanate DBDI**

higher flow stress in the presence of DBDI relative to MDI, associated with increased hydrogen bonding in DBDI-based polymers, which is enhanced in some cases by hard segment crystallinity.

Results of the mechanical tests were interpreted in terms of a physical model in which the stress was separated objectively into two distinct contributions: an elastic-viscoplastic stress σ^b rising from bond-stretching in the hard phase, and a hyperelastic stress σ^c,[2,5]. The response σ^b was elastic-viscoplastic, so during steady-state flow $\sigma^c(\lambda) = \frac{1}{2}[\sigma(+\dot{\lambda},\lambda) + \sigma(-\dot{\lambda},\lambda)]$, and stress-strain data for load/unload cycles were processed to determine separately the bond-stretch and conformational contributions to the stress. This separation has been carried out in the case of the EG-PEA combination and varying DBDI content[2]. The primary effect of the presence of DBDI hard segments was shown to be a substantial increase in σ^b, for any given elongation, as a result of the closer self-association of hard segments by hydrogen bonding. This single effect of the DBDI has been sufficient to explain most of the DBDI-induced differences in the observed mechanical response, across the range of materials studied.

This revealed that the observed effects of varying hard segment could all be explained by the hard domains having a higher flow stress in the presence of DBDI relative to MDI, associated with increased hydrogen bonding in DBDI-based polymers, which is enhanced by hard segment crystallinity

The measured constitutive response showed characteristic features of a two-network material, where, at any instant, the free energy of deformation had two contributions. These arised from simultaneous stretch of a hyperelastic network and, of another elastic network where thermally activated viscoplastic flow allowed relaxation of stress. A plausible speculation was that these two contributions arised from the soft segments without and with constraint from incorporation of their end blocks in hard phase, respectively. The validity of such a model for the present case was evidenced by the consistency of its predictions with physical reality. In terms of the model, the higher stresses and lower recovery of strain and strain energy observed with the DBDI based polymers all resulted from the higher flow stress of pure DBDI hard phase, resulting from its crystallinity. Regardless the type of the diisocyanate (MDI or DBDI), the apparent hyperelastic network contributions in all the studied polymers, were observed to be closely similar, consistent with the fact that they all had the same soft phase structure[2,5].

The results from this study provide new insight into the physical origin of inelastic effects in reinforced elastomers, to assist with the development of physically-based constitutive models.

This work is dedicated to Professor Adrian Caraculacu, formerly Professor at Institute of Macromolecular Chemistry Petru Poni, Iasi, Romania.

REFERENCES

1. Prisacariu C., Olley R. H., Caraculacu A., Bassett D. C., Martin C. M.: Polymer *44*, 5407 (2003).
2. Prisacariu C., Buckley C. P., Caraculacu A.: Polymer *46*, 3884 (2005).
3. Buckley C. P., Prisacariu C., Martin C.: Polymer *51*, 3213 (2010).
4. Prisacariu C., Scortanu E.: Int. J. Polym. Anal. Charact. *15*, 277 (2010).
5. Prisacariu C.: *Polyurethane Elastomers*, Springer-Verlag (2011).
6. Buckley C. P., Martin C. M., Prisacariu C.: DYFP 2012, *13th International Conference on Deformation, Yield and Fracture of Polymers, Conf. Proceedings*, p. 246–254 (2012).

KL-10
CHEMICAL SIDE AND RECOMBINATION REACTIONS OF NON-INTENTIONALLY AND INTENTIONALLY ADDED CHEMICAL SUBSTANCES IN RUBBERS AND POLYMERS AND THEIR IMPACT ON THE FINAL PRODUCT PROPERTIES REGARDING THE CAR INDOOR ENVIRONMENT

FRANKY PUYPE and JIRI SAMSONEK

Institute for Testing and Certification – Zlín, analytical division – separation science, Třida Tomáše Bati 299, 764 21 Zlín-Louky, Czech Republic
fpuype@itczlin.cz

Introduction

The automotive market is flooded with basic chemicals and additives for the production of rubber and polymeric materials. All added chemicals have their function in the polymer system and are due to their presence influencing the final material properties. However, many of the presented substances are still reactive and their quality is appearing differently on the market causing specific defects. In many cases when giving analytical support on defect analysis or emission properties, it is crucial to define if the detected chemical is an external contaminant or not. Surprisingly, many defects are caused by a side reaction from a basic additive or monomer in the rubber or polymer itself.

For such a group of chemicals there exists already an abbreviation concerning safety assessment and food contamination by polymers. The European commission defined the term ``non-intentionally added chemical substances`` (NIAS) in Regulation (EU) No 10/2011 on Plastic Materials and Articles Intended to Come into Contact with Food[1]. Substances used in the manufacture of plastic materials or articles may contain impurities or degradation products originating from their manufacturing or extraction process. These impurities are non-intentionally added together with the substance in the manufacture of the plastic material.

The definition of NIAS can be expanded to the term ``intentionally added chemical substances`` (IAS) when it comes to study the presence of original products in rubbers and plastics. During the investigation of defects and contaminants related to polymer and rubber mixtures, the abbreviations IAS and NIAS can be taken over from the food contact scientific community. The IAS is added with

a particular function in the rubber or polymer while the NIAS is added as a side product or appearing as a reaction/ recombination product. The term IAS or NIAS exclude by their definition any contamination from external sources.

Concerning the car interior environment, visual and health aspects are very important for the customers. For the producers of car interior compounds the choice of an appropriate IAS is important due to the risk of many defects (smell, fogging, discoloring, blooming, migration, degradation, cracking, etc.). It is recommended to foresee unwanted reactions and presence of NIAS in the polymer with eye on the risk assessment and external influences during the product lifetime. Generally, if the IAS creates a too much problematic NIAS, it is recommended to replace the IAS in the rubber or polymeric application for a less ``risky`` one.

From the analytical perspective, many defects or mechanisms can be explained by using mass spectral methods like direct inlet mass spectrometry (DI-MS), thermal desorption-gas chromatography-mass spectrometry (TD-GC-MS) or pyrolysis-gas chromatography-mass spectrometry (PY-GC-MS). Especially when it comes to target and non-target screening of trace analytes for the study of defects like discoloring, fogging or odor these methods are very helpful.

Intentionally added chemical substances (IAS)

Rubber or polymeric systems are based on a combination of engineered chemicals which all have their specific function. Their function can be necessary for the polymerization or stabilization process but in the final product they can harm the requested properties concerning the marked requirements. Problems with IAS are more related to their concentration in the polymer or rubber mixture. Such an example is the use of triethylene diamine (TEDA) in polyurethane sealing or foam. TEDA is a very effective amine catalyst during the foaming reactions of polyurethane but might create problems with fogging on other colder car parts when this polyurethane is used as a car seat or sealing. Moreover, the use of amine catalysts in polyurethanes should be dosed properly due to their high influence on the smell properties of the final product.

An aliphatic brominated flame retardant like hexabromocyclododecane (HBCD) is an effective flame retardant used in car interior parts and one of the key IAS concerning consumers` safety. Due to the fact that this brominated flame retardant is not covalently bounded with the polymer there is a potential risk that this rather insoluble compound is migrating on the surface of the product resulting in white blooming defects (Fig. 1). Therefore the dosage of HBCD should be done very precise.

An important IAS are chemicals used for surface treatment of polymers. Paints and varnishes based on acrylates contain residual solvents. Such types of varnish dry immediately after solvent evaporation. But when applying the varnish on a polymer surface the solvents gets solved into the polymer and after a time trapped between the dried acrylate layer and the polymer. Another observed problem with such products is the stacking and storing of such products, where the residual solvent vapors are getting stuck between 2 finished products. Traces of residual solvents (e.g. ketones or alcohols) migrate slowly through the coating surface and influence highly the smell properties of the final product.

Fig. 1. **Textile from a car door panel used with white HBCD blooming defect**

Many rubber applications use octasulfur, accelerators and oil as main key additives. Despite the fact that they are crucial for the vulcanization and protection of the final product, they are the most frequent IAS detected in rubber blooming defects due to the fact that a fraction remains un-reacted and migrate quickly toward the surface. Concerning the oils in rubbers, TD-GC-MS as an analytical tool has the advantage to compare oil distributions (Fig. 2). The comparative method between a defect and reference sample can distinguish the use of wrong processed oil as IAS. Both oil distributions in the chromatogram are different. Beside the hydrocarbon distributions also the identity of the oil can be distinguished by mass spectrometry (aromatic oil, aliphatic oil, fatty acid based or silicone oil).

Non-intentionally added chemical substances (NIAS) from the polymer

A majority of defects in rubbers and polymers for car interior applications are caused by NIAS as side reaction products from the major IAS compounds. Starting from the

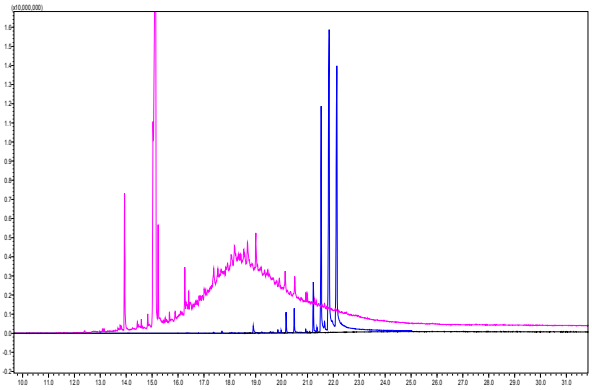

Fig. 2. **Comparison of chromatograms after TD-GC-MS analysis showing a comparative analysis of 2 rubber sealing samples** (reference sample-more left side/aliphatic and a defect-more right side/fatty acid)

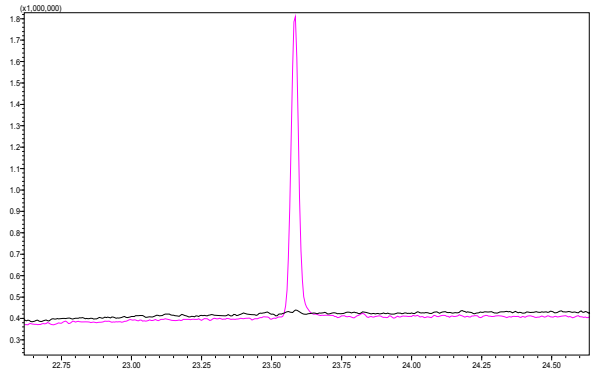

Fig. 3. **Chromatogram after TD-GC-MS analysis showing the peak of a cyclic ester of terephtalate-butanediol-terephtalate-butanediol from polyester based polyurethane found in a fog layer on car glass**

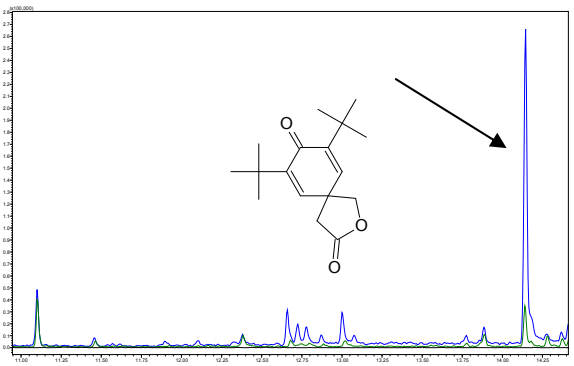

Fig. 4. **Chromatogram after TD-GC-MS analysis showing a peak of 7,9-di-tert-butyl-1-oxaspiro(4,5)deca-6,9-diene-2,8-dione from a car part with discoloring/blooming defects**

polymer itself, each polymer contains a fraction of oligomers which are remaining un-reacted in the polymer. Due to their volatility their presence might cause some smell defects, increase emissions properties or blooming.

In case of acrylonitrile-(butadiene)-styrene (ABS) the monomers from SAN are during the polymerization recombining by a Diels-Alder cyclo-addition reaction. The ever presence of Diels-Alder trimers in ABS increase the FOG value measurement according to VDA 278 with 0,5-20 ug g^{-1} *n*-hexadecane equivalent[1]. Blooming on car interior parts consisting of ABS by these NIAS has already been observed.

Polyurethane sealing based on polyester polyol release cyclic polyesters which cause fogging defects. On colder car parts there was condensation of vapors observed from the cyclic ester of terephtalate-butanediol-terephtalate-butanediol (Fig. 3).

Non-intentionally added chemical substances (NIAS) from additives in polymers

Polymer additives like antioxidants should establish stability in the polymer and avoid degradation of the polymer during the processing and lifetime. During the ageing of the polymer the antioxidant should sacrifice its availability to the polymer. Irgafos 168 is a common antioxidant used in polymers. Initially this one is presented in its phosphite form, as IAS. When oxidizing, the phosphate form is remaining, as NIAS. By TD-GC-MS polymers can be evaluated on their additive composition and so the ratio between the irgafos 168 as phosphite and phosphate can be screened. Irgafos 168 is initially designed to oxidize and hydrolyze forming free steric hindered alkylphenol, However, the presence of the phosphate form of irgafos 168 is an indication of the additive quality. The higher the phosphate form the more the additive (and probably the polymer) was exposed to oxidation.

Steric hindered phenolic antioxidants like butylated hydroxytoluene (BHT) and BHT releasing antioxidants like irganox 3114 are in many cases subject for discussion due to the fact that the BHT from irganox 3114 is seen a NIAS. BHT is able to get yellow under certain pH conditions or to get red after nitration with the environment. Therefore there should be paid attention on the usage of acid scavengers in PP and residual Ziegler-Natta catalysts and their influence on the pH in the polymer.

The use of bigger additives, like pentaerythritol diphosphite based hindered phenolic stabilizers, are an important part from the molecular architecture of the polymer due to the non-blooming properties. However such type of additives are easily hydrolyzing and the phenolic hydrolyzates are reacting further resulting under certain conditions into discoloring defects. Big phenolic anitioxidants based on 3,5-bis(1,1-dimethylethyl)-4-hydroxy-benzenepropanoic acid like irganox 1010 and irganox 1076 can undergo a backbiting reaction making a phenolic cyclic product which results in discoloring of the final product and blooming (Fig. 4 and 5).

Ester based plasticizers in polymers added as IAS can easily hydrolyze and release free alcohols. These free alcohols like iso-nonylalcohols (hydrolyzed or residual) from di-isononylphtalate have a strong influence on the smell properties of the final product (Fig. 6) and create a significant increase on the VOC and FOG value according to VDA 278.

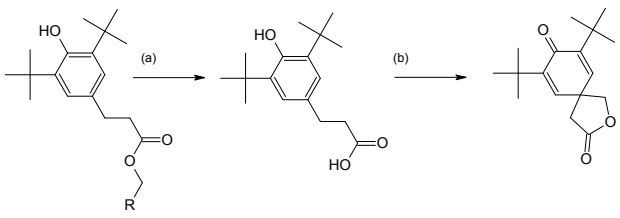

Fig. 5. **(a) Hydrolysis reaction of 3,5-bis(1,1-dimethylethyl)-4-hydroxy-benzenepropanoic acid ester (like irganox 1010 or irganox 1076) (b) backbiting reaction resulting in 7,9-di-tert-butyl-1-oxaspiro(4,5)deca-6,9-diene-2,8-dione**

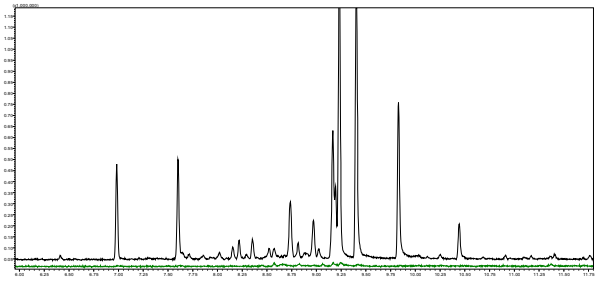

Fig. 6. **Comparison between 2 samples a smelling PVC sample containing free aliphatic alcohols (upper signal, defect) and a PVC sample giving no smell and no emissions (lower signal, reference)**

Non-intentionally added chemical substances (NIAS) from additives in rubbers

An essential NIAS influencing the smell and fogging properties are the degradation products from accelerators. Chemicals like benzothiazole, sulphenamines, alkylthiurams and thiocarbamates are breaking down and causing volatiles which are found as emissions in emission tests like VDA 278 or PV 3341 (ref.[2]). Thiuram disulfide based accelerators as an example gives high emissions of carbondisulfide. Mercaptobenzthiazole based accelerators gives carbondisulfide and aniline emissions.

Conclusion

Many defects in polymers are caused by side-reactions coming from the main components like monomers, antioxidants which are defined as IAS. These side-reactions result in degradation products called NIAS which are responsible for several specific defects like blooming, smelling, cracking, fogging and coloring. Both of them (IAS and NIAS) are influencing directly the car interior properties by their overall composition. Minor influence from the external environment has been observed.

REFERENCES

1. VDA 278 Thermal Desorption Analysis of Organic Emissions for the Characterization of Non-Metallic Materials for Automobiles.
2. VDA 277 / VW PV 3341. total carbon TVOC.

KL-11
PLASTIC IN AUTOMOTIVE

JAN RODA

Institute of Chemical Technology, Faculty of Chemical Technology, Department of Polymers, Technická 3, 166 28 Prague 6, Czech Republic
jan.roda@vscht.cz

Permanently growing consumption of plastics and rubbers in automotive industry accompanies development and production of all types of cars during their whole history. A wide variety of plastic materials, their composites, sandwich structures etc. are used, modified and developed for a greater comfort, safety and lower fuel consumption. Polymers are highly appreciated compared to metals with respect to their low density, simple processing of very complicated product shapes, application comfort and ecological aspects of their application. Some examples of basic plastics with their fundamental characterization will be presented – above all polypropylene, polyethylene, acrylonitrile-butadiene-styrene copolymers (ABS), poly (butyleneterephtalate), polycarbonate and polyamides.

Five families of materials can be distinguished – metals, ceramics, glasses, polymers and composites (combinations of two or more materials – above all combination of polymer matrix and filler, etc.). All these materials are used in car construction.

Synthetic polymers are the "youngest" materials family known approx. only 100 years and play now an irreplaceable role in car production. Application of polymers was tightly connected with development of automotive industry – in 2010 around 9 % of world polymer production was consumed in automotive. The first production of cars was for many years bound with cellulosics (cellulose nitrate), modified cassein and late with phenolics. The great revolution began with the large scale production of thermoplastics in 60ties of 20th century– mainly polyolefins, later by the development of engineering thermoplastics and reactoplastics.

Nowadays plastics form 8–9 per cent of car weight (but the volume fraction is due to valuated low specific gravity higher) – except the plastics we have to include to the polymer consumption also rubbers, coatings and textiles – together polymers form around 15 % of car weight.

Plastics play a fundamental role in construction of modern cars and improve the comfort of usage and influence positively many ecological aspects. Consumption of plastics has increased every year in automotive industry because of their relatively low cost, ease in manufacture and design, flexibility, chemical resistance. Choice of polymeric material depends basically on mechanical and physical properties but also on ageing, degradation characteristics, surface properties, styling requirements, visual appearance etc. Weight of polymers (plastics) influences the engine efficiency, which means the overall fuel economy (plus emissions).

Twenty eight per cent of plastics consumption in typical mid-size vehicles is formed by polyolefins. The most widened commodity polymer polyethylene (PE) does not play so important role in automotive as polypropylene (PP). PP frequently modified or filled is applied in interior (instrument

panels) or also in exterior (bumpers) of cars. A low glass temperature of PE is appreciated for preparation of different car components above all for production of multilayer fuel tanks and fluid reservoirs.

Consumption of both aliphatic-aromatic polyesters and polyurethanes has exceeded ten percent in automotive industry. Poly(ethylene terephthalate) (PET) is used as fibre forming material in car interior – carpetings, seat coverings, floor mats. Structurally close poly(butylenes terephthalate) (PBT) serves as irreplaceble material for electric systems, connectors, fuse boxes etc. and other underhood application. Both polyesters are semicrystalline but differ in the rate of crystallization.

Next special polyester – polycarbonate (PC) – is amorphous with excellent optical properties and acts preferably as material for head-lights and spot-lights. Highly regarded toughness can be additionally improved by blending with PBT.

Another amorphous material – terpolymer of acrylonitrile – butadiene-styrene (ABS) – in fact forms two phase system with excellent balance of properties for different interior and exterior car components.

Only a part of polyurethane (PUR) family behaves as plastics but different combination of chemical substances can form crosslinked structures – hence reactoplastics, foams and elastomers. The diversity in PUR structures determines the miscellaneous application areas in automotive – dampers, gaskets, seats, cushionings (seats), foams for sound, noise and vibration reduction.

Polyamide (PA) engineering plastics continually replace metals in underhood application. Two basic aliphatic polyamides – PA6 and PA66 (filled frequently with glass fibres) constitute more than 90 % of polyamide consumption. Well known applications are in air and cooling systems (air intake manifold, fans, shrouds, air bags).

Various polymers are used in over 1000 different parts of all shapes and sizes in cars, from instrument panels and interior trim to bumpers and radiator grilles, fuel tanks and engine parts. The material selection for a particular application will depend primarily on the ability to meet the required specification and also on polymer price and total systems cost. The total systems cost includes the polymer, processing and tooling and assembly, and is a prime consideration for cost-conscious car manufacturers.

Commodity polymers, engineering polymers and high performance plastics are used to manufacture more demanding applications in the car. The most valued properties of engineering plastics for automotive applications are their high heat resistance, dimensional stability, strength and resistance to a range of chemicals. These properties have led to the replacement of traditional materials such as metals and reactoplastics in motor vehicles.

KL-12
AKROMID RM – POLYMER BLENDS BASED ON PA6 WITH REDUCED MOISTURE ABSORPTION FOR DIMENSIONALLY STABLE APPLICATIONS

STEPHAN SCHNELL

K. D. Feddersen CEE GmbH Member oft he Feddersen Group Fachgasse 35-37, A-1150, Vienna, Austria

KL-13
SHARK® – EXTRUDER GEAR PUMP SYSTEM WITH SIDE FEEDER FOR CONTINUOUS COMPOUND BLENDING, INJECTION OF RE-WORK MATERIAL AND FINAL MIXING

JOZEF SMEJKAL

SUBTER PLUS s.r.o., Jarošovská 1162/II, Jindřichův Hradec 37701, Czech Republic
info@subterplus.cz

Shark® extruder gear pump system consists of a Transfermix single screw extruder in conjunction with a gear pump (see also Fig. 1). The latest development includes a second extruder gear pump System (Combex) for side feeding as schematically depicted in Fig. 1. Gear pump #1 as used for the Shark® provides total output control of the setup with a high precision.

Output control of the Combex side feeder is given by gear pump #2 (see Fig. 1). Thanks to gear pump technology compound B, re-work material or high concentration chemical batch can be injected by the side feeder into the Shark® for continuous compound blending and mixing.

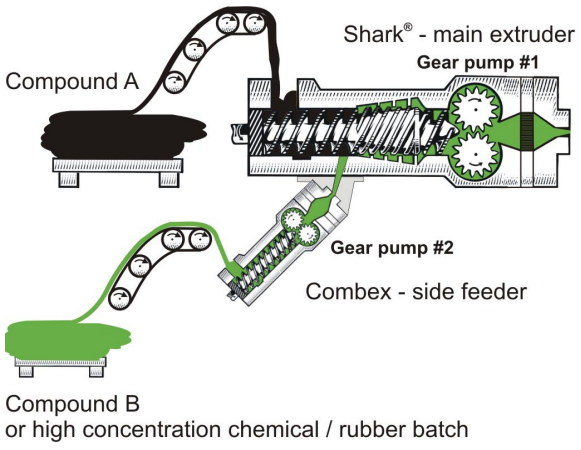

Fig. 1. **Typical schematic of the Shark® extruder gear pump system with Combex side feeder**

In case of continuous compound blending up to 50 % compound B can be injected by the side feeder. Inside the Shark® the Transfermix zone ensures sufficient mixing of the two compounds A and B. VMI's unique Transfermix single screw extruder design features an exchangeable Transfermix section.

In case of different mixing requirements the Transfermix barrel can be exchanged to provide the right mixing efficiency.

Additionally, the Transfermix extruder can be equipped with a Vacuum zone for degassing of moisture or other substances to ensure profile extrusion without porosity.

Both machines, the Shark® main extruder as well as the Combex side feeder, are fed with continuous rubber strips.

Besides compound blending the side feeder allows injection of pre-dispersed, polymer bound chemicals for continuous final mixing during extrusion.

A further application is for precise injection of re-work material such as uncured rubber profiles (for example: side wall, tread…). Due to the Shark® technology with Combex side feeder the injected amount of re-work material can be exactly maintained.

Furthermore, it is possible to mount a cutting unit to the outlet of the Shark® for integrated production of rubber preforms.

VMI offers Shark® extruder gear pump systems with side feeder for an output range starting with 150 kg/up to 4.000 kg/h. A typical production machine design is represented in Fig. 2. This machine consists of a Shark® 90 main extruder with a Combex 90 side feeder for continuous compound blending including production of preforms in just one process step. Optionally the head mounted to the Shark® provides space for a strainer plate to offer integrated compound straining if required.

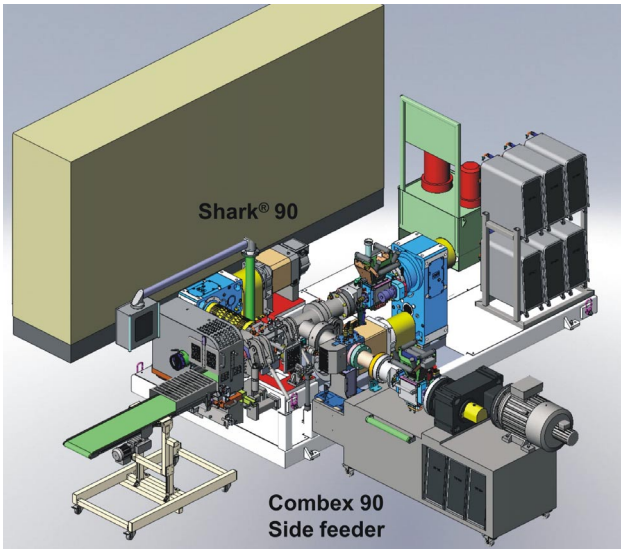

Fig. 2. **Layout of Shark® 90 with Combex 90 side feeder including cutting unit for integrated preform production**

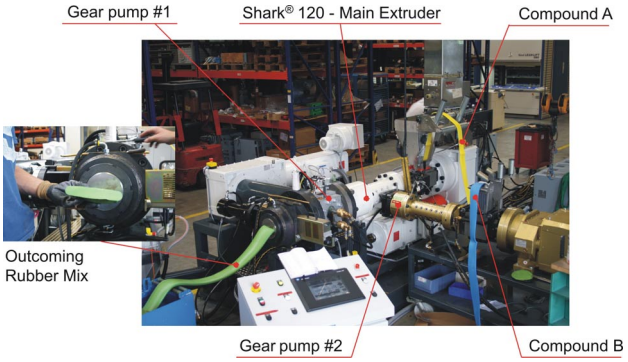

Fig. 3. **Test setup for compound blending with Shark® 120 and side feeder at VMI-AZ Extrusion in Running, Germany**

At VMI-AZ Extrusion in Running (Germany) a test machine is available for customer testing. This particular setup consists of a Shark® 120 with a 75 mm side feeder including rapid screen changer for optionally straining and a cutting unit in case of integrated preform production.

Montech rubber testing instruments

MonTech rubber testing instruments, Buchen, Germany is specialized in development, production as well as service and calibration of rubber testing instrument. With over 15 years experience MonTech is today one of the leading manufacturers of rheological testing equipment for rubber and polymers.

MonTech products include the fully automated Moving Die Rheometer Series MDR 3000 Basic in various versions – these totally new entry level testing instruments with Basic features include full automation capabilities to a very attractive price.

Also the new laboratory platen press series LP 3000 as well as a new bale cutter for laboratory usage, CP 3000 have been recently added to the MonTech product portfolio

Besides this MonTech also offer software systems for quality control, laboratory workflow management, recipe development as well as international laboratory link systems.

This systems make it possible to set-up a global quality control network within a company or also with an integration of customers and suppliers – this means all quality relevant data can be accessed from any workstation in any lab which finally leads to a more consistent and stringent quality control process.

Another new type of instrument is a density testing instrument for uncured rubber RD 3000 – the first bulk density testing instrument which works fully automated and can optionally be equipped with sample storage and feeding systems.

Subter plus s.r.o.
Jarošovská 1162, 377 01 Jindřichův Hradec
www.subterplus.cz , info@subterplus.cz

KL-14
PP-BASED NATURAL FIBER COMPOSITES – SUBSTITUTION POTENTIAL, CHALLENGES AND CHANCES

LUKAS SOBCZAK[a]*, REINHOLD W. LANG[b], ANDREAS HAIDER[a], and HERMANN BRAUN[c]

[a] *Competence Centre for Wood Composites and Wood Chemistry (Wood K plus), Altenberger Straße 69, 4040 Linz,* [b] *Johannes Kepler University Linz, Institute for Polymer Materials and Testing, Altenberger Straße 69, 4040 Linz,* [c] *Borealis Polyolefine GmbH, St. Peter-Straße 25, 4020 Linz, Austria*
Hermann.Braun@borealisgroup.com, l.sobczak@kplus-wood.at, reinhold.lang@jku.at

Introduction

Natural fibers and wood (= lignocellulosics) have become of interest to reinforce thermoplastics like PP, producing novel natural fiber composites (NFC) and wood polymer composites (WPC)[1–3]. Along with cost saving aspects and expected ecological benefits, the main motivation driving these developments is related to the mechanical property profiles of natural fibers and wood. Combined with their low density, NFCs and WPCs may result in lighter weight structures when compared to conventional PP composites (like PP-talc or PP-glass)[4–6].

Despite high industrial interest in NFCs and WPCs[7–10], and significant scientific efforts, the actual market penetration of such materials is still rather limited, at least in injection molding applications. The question remains if this is because those materials do simply not fulfill the requirements for potential applications, or if the industry just hesitates from implementation because of the challenges and uncertainties still associated with those rather novel compounds. Thus, a prime objective for this work is to find out what WPCs and NFCs are really capable of at the moment, and to identify the most straightforward ways to improve their properties (by modification of the fiber/matrix interface). Furthermore, the impact performance, a weak point of WPCs, has been investigated in more detail. Finally, the optimization of compounding processes, and methods for determining wood and moisture contents are discussed.

Substitution potential

When this work was started, no comprehensive overview existed on the mechanical property profiles of NFCs and WPCs. Thus we attempted to compile such an overview, and also a comparison with commercial composites based on mineral, glass and carbon fiber reinforcements[10]. Furthermore, commercially available NFC and WPC compounds were compared with the mechanical property data taken from the scientific literature, to find out to which extent new developments are implemented in industrial products.

All of the data presented here is taken from scientific literature or material data sheets provided by the suppliers. To ensure a sufficient comparability of the material property values, only data generated utilizing injection molded specimens and applying equivalent test procedures and conditions has been included.

The *"Ashby plot"* was chosen as means of presentation. In terms of relevant properties, Ashby plots were generated as tensile strength vs. tensile modulus for the reinforcement constituents, and as tensile strength vs. tensile modulus, and impact strength (Charpy unnotched) vs. tensile modulus for PP and its composites.

Looking at commercially available composites, it is obvious that WPCs fulfill expectations based on the data published in scientific papers. Thus, they are superior to PP-talc for tensile properties (Fig. 1), but inferior for impact properties (Fig. 2). As to the commercial NFCs, the situation is more complex. The fact that tensile property data published in the scientific literature are superior to that of the available composites means that there is probably still room for improvement of the latter. On the other hand, progress has been made in improving NFC impact performance, with the highest performance achieved by employing Tencel® and Kraft pulp fibers as reinforcements. Interestingly, commercial compounds show higher values than those published in the scientific literature.

Overall, the substitution potential of WPCs and NFCs can be summarized as follows: NFCs can largely compete with PP-glass fiber composites (PP-gf) for stiffness and impact properties, but not for strength. PP-gf still provides the best balance of stiffness and fracture toughness, limiting the substitution potential of the more novel composites. WPCs can exceed PP-talc for tensile properties. The relatively low impact strength remains the weak point of the partly natural composites, but more recent developments show some improvement. Finally, it has to be said that there has been a

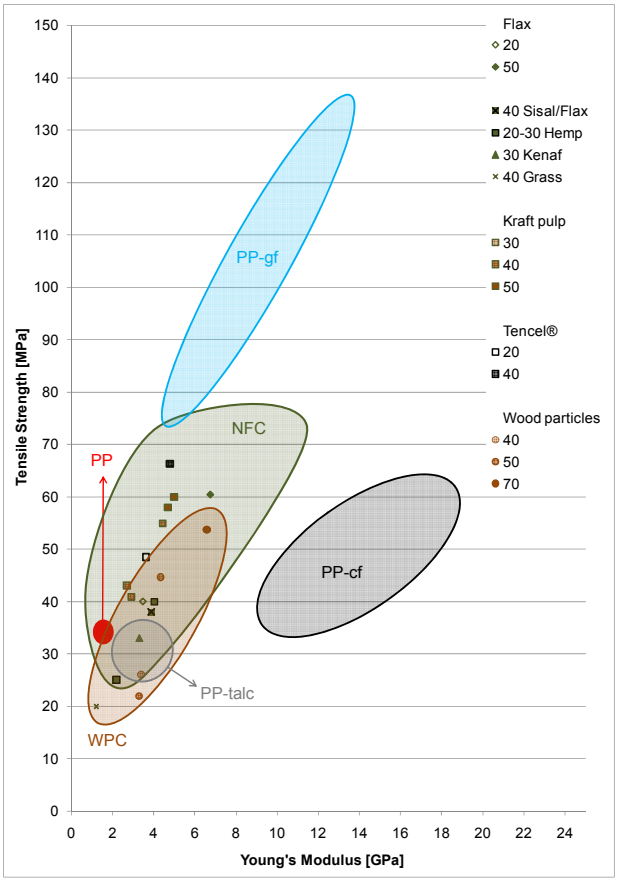

Fig. 1. **Tensile properties of commercially available NFCs and WPCs (represented by single symbols) as compared to the property areas of neat PP, PP-talc, PP-gf and PP-cf. The property areas shown for NFCs and WPCs represent data taken from the scientific literature. The numbers in the legend give the gravimetric fiber content (e.g. 20-30 Hemp means PP with 20–30 % hemp fibers)**

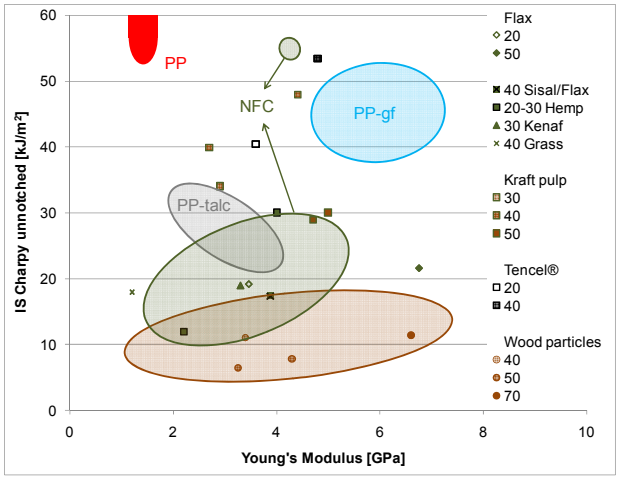

Fig. 2. **Impact strength vs. tensile modulus of commercial WPCs and NFCs (represented by single symbols) in comparison with property areas of neat PP, PP-talc, PP-gf and PP-cf. The property areas shown for NFCs and WPCs represent data taken from the scientific literature. The numbers in the legend give the gravimetric fiber content (e.g. 20-30 Hemp means PP with 20–30 % hemp fibers)**

tendency to overestimate the substitution potential of NFCs and WPCs in recent years. Over-optimistic prognoses regarding the replacement of glass fiber reinforced composites are, at least from the mechanical performance point of view, simply unrealistic.

Interface modification

The chemical incompatibility between hydrophilic lignocellulosic or cellulosic fibers or particles and hydrophobic matrix polymers like polyolefins is an inherent downside of NFCs and WPCs alike. Numerous strategies to overcome this weakness have been investigated, with varying success. Basically, these approaches can be classified into two categories: Fiber- and matrix-based strategies, respectively. While the former require a pretreatment of the fiber, the latter rely on additives which are deployed in the compounding process[11].

Several reviews on fiber/matrix interaction in NFCs and WPCs are available, however, none of them focuses on polyolefinic composites and compares modification strategies based on quantitative material data. Thus, we have considered only papers in which the effects of a compatibilization strategy on composite mechanical properties or water absorption are given. To allow for comparability of the effects reported, we have focused on PE and PP-based short fiber or particle reinforced compounds, with specimens prepared by either compression or injection molding.

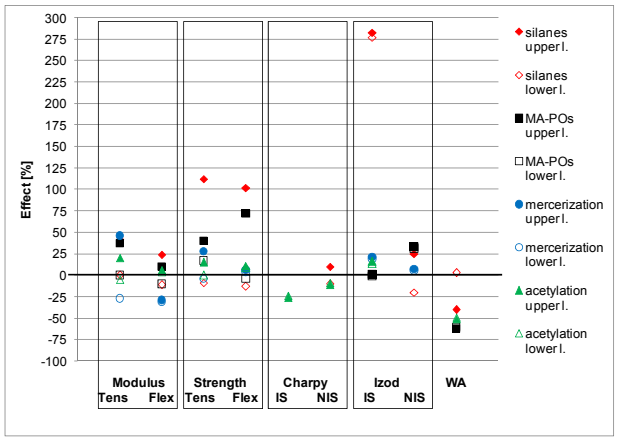

Fig. 3. **Effects of various fiber-based modification treatments on the properties of NFCs and WPCs. For each strategy, full symbols represent the upper limit, and open symbols the lower limit as found in the literature**

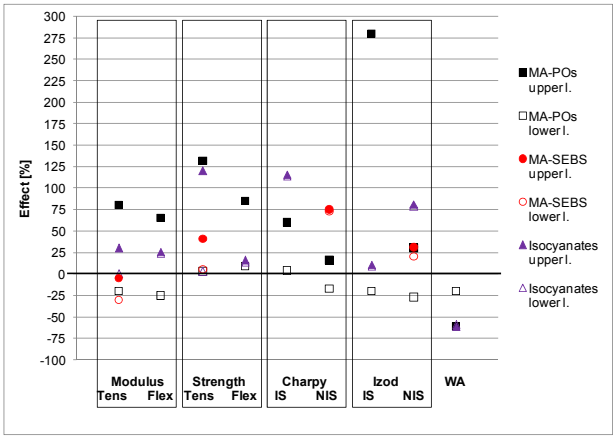

Fig. 4. **Effects of various matrix-based modification approaches on the properties of NFCs and WPCs. For each strategy, full symbols represent the upper limit, and open symbols the lower limit as found in the literature**

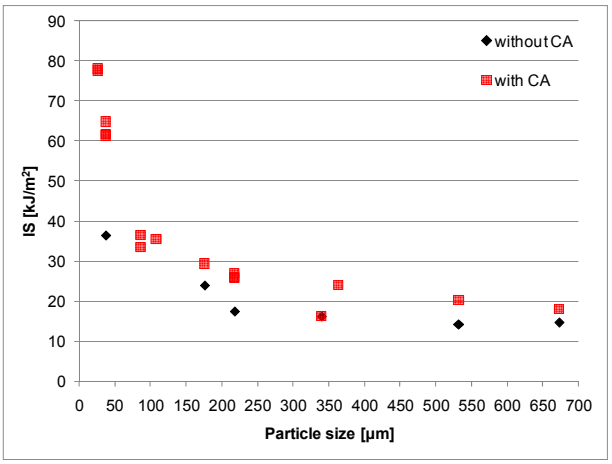

Fig. 5. **IS as a function of lignocellulosic filler particle size. All compounds are based on the same PP impact copolymer, and contain 20 % filler per weight**

Summarizing the data presented in Fig. 3 and Fig. 4, it can be said that approaches based on maleic anhydride grafted polyolefins (MA-POs; as applied as matrix additive) and silanes (as applied to the fiber) are most thoroughly investigated, and also most promising for NFC and WPC interface modification. Considering that MA-POs are commercially available in a broad variety, very easy to apply, and allow similar improvements in compounds as silane pretreatments, they can be deemed as the best coupling agents available to date.

Impact performance

In studies conducted together with our partner Borealis Polyolefine GmbH, WPCs with low filler content for injection molding applications were focused on. To at least partly overcome the impact strength deficiency of this material class, a highly impact modified PP copolymer was employed. On the basis of this matrix type, compounds with various wood and natural fiber types were prepared and tested. A very fine-grained talc type was used as reference filler.

Surprisingly, when increasing the filler content, notched Charpy impact strength (NIS) saw a drastic decline in the case of wood particles, while it remained more or less unchanged in the case of talc. The most straightforward explanation for this phenomenon is probably related to the difference in mean particle size. While the talc type used is in the range of 5 µm, wood particles typically employed in WPCs are usually between 200–1000 µm in size. However, when employing lower mean particle size lignocellulosic fillers, unnotched Charpy impact strength (IS) did increase (Fig. 5), while NIS was only minimally affected (data not shown).

In this context, it is interesting to note that coupling or interface modification can have quite different effects on IS and NIS, respectively (Fig. 3 and Fig. 4). While IS usually benefits from improved compatibility, NIS is often increased to a lesser degree or even reduced. This is probably related to the contribution of two different fracture mechanisms: In IS testing, the total fracture energy is dominated by crack initiation, which is facilitated by low adhesion at the fiber/filler-matrix interface. In NIS testing, on the other hand, fiber/filler pull-out is an important mechanism increasing the energy for crack propagation. The latter, however, can be impeded by improved fiber/filler-matrix compatibility. Obviously, impact performance is an issue which deserves further scientific efforts.

Processing and Quality Control

The compounding of wood and natural fiber reinforced composites is demanding, mostly due to the thermal sensitivity and hydrophilicity of such reinforcements. However, on parallel co-rotating twin screw extruders, as the most relevant compounding systems, an optimized screw configuration and temperature profile facilitate the production of high quality compounds. In this context, it can only be highlighted that the removal of volatiles, like water vapor, is the single most important factor in NFC and WPC compounding. Efficient degassing improves homogeneity and process stability, and reduces the required energy input.

When it comes to commercial production, quality control methods for filler and moisture content determination are required. In contrast to mineral fillers and glass fibers, simple incineration of a compound is not sufficient for content determination in the case of lignocellulosics. However, offline rheometric and thermogravimetric methods, respectively, and online near infrared based methods (NIR) can be employed for this task. Compound moisture content determination is very important for further processing, particularly by injection molding. Simple heating balance methods might not be reliable for low filler content materials. For such compounds, also the abovementioned NIR methods represent an interesting alternative which can be implemented online in production.

Conclusion

Despite not quite fulfilling expectations as to their substitution potential, polyolefin-based NFCs and WPCs are promising lightweight, low cost composites. Additivation with MA-POs is the method of choice for achieving optimal properties. The impact behavior, the most significant drawback of these composites, is complex and as yet not fully understood. Processing problems associated with lignocellulosic fillers can largely be avoided by careful design of the compounding process, and the implementation of adapted quality control methods.

REFERENCES

1. Mohanty A. K., Misra M., Drzal L. T.: *In: Natural Fibers, Biopolymers, and Biocomposites*; Taylor & Francis. 2005
2. Vogt D., Carus M., Ortmann S.: Wood plastic composites (WPC)-Studie, report. Nova Institut (2005).
3. Klyosov A. A.: *In:Wood-Plastic Composites,* p. 698; J. Wiley 2007.
4. Mohanty A. K., Misra M., Hinrichsen G.: Macromol. Mater. Eng. *276/277*, (2000).
5. Maya J. J., Anandjiwala R. D.: Polym.Compos. *29*, 187 (2007).
6. Zampaloni M., Pourboghrat F., Yankovich S. A., Rodgers B. N.: and others Composites: Part A *38*, 1569 (2007).
7. Otremba F., Baur E., Huber T., Müssig J.: Plastverarbeiter 07/2008, 50 (2008).
8. Ford Motor Company: K-Berater 43, 43 (2011).
9. Huber T.: Kunststoffe 7/2008, 97 (2008).
10. Sobczak L., Lang R. W., Haider A.: Compos. Sci. Technol. *72*, 550 (2012).
11. Sobczak L., Brüggemann O., Putz R. F.: J. Appl. Polym. Sci. *127*, 1 (2013).

KL-15
UNIVERSAL RHEOMETRICAL TOOLS TO BRIDGE THE GAP OF ELASTOMERS CHARACTERISATION AND THEIR PROCESSING

AXEL GOETTFERT and JOACHIM SUNDER*

Goettfert GmbH, Germany
axel@goettfert.de, joachim.sunder@goettfert.de

Abstract

Rheology has become a powerful method to characterize structure and especially processing rubber polymers and compound. In practical application often only standard rheometers are used operating far from processing. This paper introduces three possibilities in area of material research and quality control to bridge the gap between test and process deformation and allows predicting material processing.

Especially tests for analysis of structure and predicting processing in the area of compression molding and simple extrusion can be performed by the dynamic rheometer Visco-Elastograph in the frequency range of 0.01–50 Hz and at strain rates up to 1200 %. Data of frequency sweeps displaying the flow behavior are presented and correlated to other methods. The right selection of fillers for certain application can be assisted by amplitude sweeps showing the reinforcing effect of different fillers on polymer-filler networks (Payne effect). Detection of loss angle of the vulcanized compound at different frequencies can predict damping behavior of the final part.

The major part of processing is done by extrusion and injection molding were capillary rheometry is the most similar test method also for rubber compounds. Data of wall slip behavior show different processing behavior only to be seen in testing by capillary rheometry. A new tool to analyze flow instabilities is presented. Here flow instabilities for different rubber compounds occurring in the process can be displayed in a small scale before processing. The high selectivity of this powerful tool is shown by an example of EPDM extrusion compound. Further the option pVT (pressureVolumeTemperature) can measure shrinkage behavior after vulcanization and can be used for mould design and the behavior at low temperatures for sealing materials.

The QC test device for testing under extrusion and injection molding conditions RCR (rubber capillary remoter) is introduced. Some comparison between MDR testing with no selectivity and high selectivity of RCR to processing is presented. Further a method to estimate viscosity data under curing conditions is presented for injection molding simulation of thermo sets.

Concluding three interesting test methods are presented, which give much more detailed and useful information than the conventional testing of Mooney and only cure behaviour.

Introduction

Rheometry in rubber industry is mainly performed using Mooney rheometer and MDR rheometers, measuring far from the range of processing deformation. Because of the non linear behavior of the materials a prediction of processing behavior is often not possible because of missing selectivity or is even wrong. Rubber materials contain waxes and plasticizer, which lead to slip behavior in processing. Conventional rubber testing instruments cannot detect this effect while capillary rheometry can give nice predictions of difficult processing areas. Flow instabilities are only detected by manual observation of extrudates; while using the option shark skin for capillary rheometers and extruders can easily separate between different extradite qualities.

Wrong processing behavior often is recognized after starting production. This leads to a waste in production time.

Experimental

Dynamic testing

Dynamic testing is performed on Visco-Elastograph (see Fig. 1). Visco-Elastograph is a dynamic rheometer with closed and sealed chamber for rubber and thermoplastics and quasiclosed paste chamber if also liquids should be tested. Deformation frequencies in the range of 0.01 to 50 Hz and

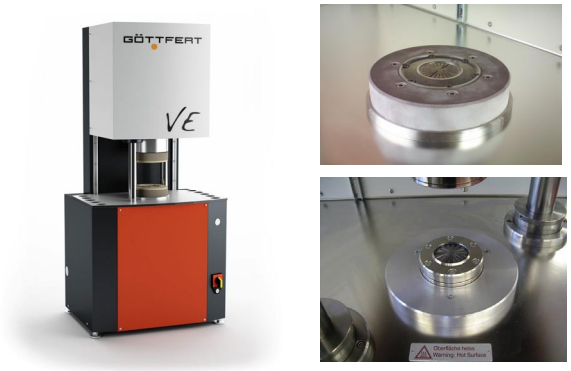

Fig. 1. **Visco-Elastograph with closed chamber (top) and quasi closed chamber (bottom)**

deformation amplitudes in the range of 0.01–90° (app. 1250 % max. strain) can be set for test conditions.

The device is equipped by a high resolution servo drive. The operation methods are:

– frequency and amplitude sweeps under pre or post cure conditions,
– vulcanization isothermal or non-isothermal,
– ramp relaxation.

Flow curves are obtained by frequency sweeps in the range of 0,1–50 Hz. The Payne effect is studied by amplitude sweeps in the range of 0,1–50° oscillation angle.

Capillary rheometry

Tests of capillary rheometry are performed on a Rheograph 75 twin bore 15 mm barrel with 75 kN piston force with PVT option isothermal isobar (See Fig. 2).

Correction of entrance pressure loss is performed by a simultaneous measurement of a long die L/D 20 and a zero length die.

Wall slip velocity, a very important material property especially in rubber processing, is obtained by the model of Mooney using dies of the same L/D ratio but different

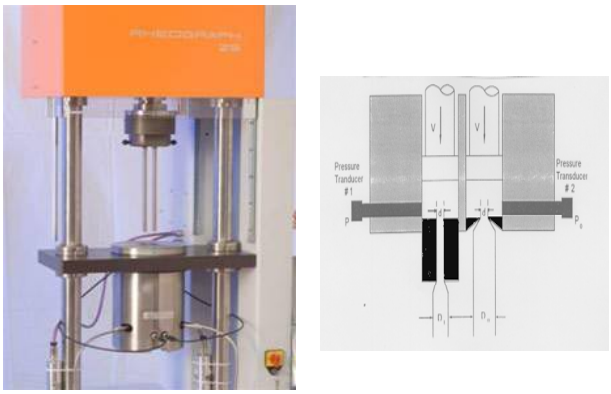

Fig. 2. **Goettfert Twin bore capillary rheometer and principle of measurement**

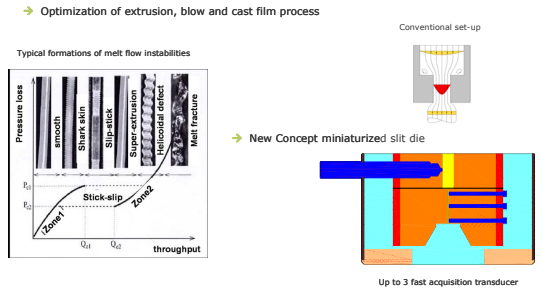

Fig. 3. **Option shark skin to detect flow instabilities**

diameter (e.g. 20/1 mm and 40/2 mm length/diameter). Before performing Mooney correction, the data are Bagley corrected. Slip velocity is calculated only from differences in the flow curves dies of different diameters. Therefore a measurement with high accuracy is needed. Sensitivity and reproducibility of pressure measurement of the series Rheograph 20–120 is improved by more than one decade which aids the precise and selective determination of wall slip velocity.

Especially in extrusion flow instabilities can occur which are detected by the option Shark Skin.

Here high acquisition pressure transducers are located inside a slit die (Fig. 3), which can detected the high frequency oscillation when instabilities occur were conventional transducers do not detect or show only part of the pressure signal.

A comparison of the pressure signal detected by a conventional pressure transducer before the die and a fast acquisition transducer inside the die is given in Fig. 4.

Measured pressure oscillations are analyzed by the software in regard of frequency and amplitude. Pressure oscillations correlate to surface defects, which is analysed and proved in ref.[2].

Beside rheological and flow behaviour shrinkage behaviour is one of the most important parameters. This is measured using the option pVT for capillary rheometers. PVT option for Goettfert capillary rheometers (see Fig. 5) is the only available capillary rheometer option, which can measure isothermal (at step of constant temperature and changing pressure) or isobaric (at constant pressure applying a certain cooling rate).

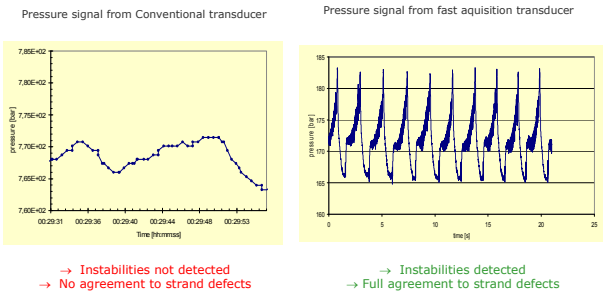

Fig. 4. **Pressure signal comparison conventional versus fast acquisition transducer**

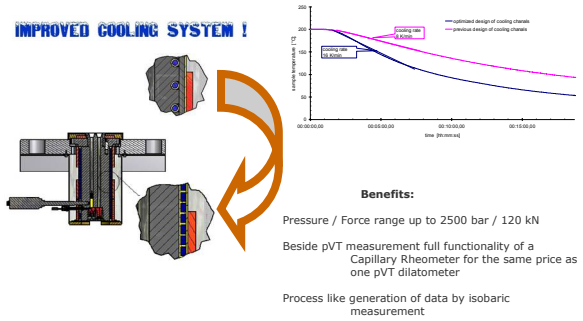

Fig. 5. **Goettfert pVT option with cooling mantel for isobaric / isothermal pVT measurement**

For the test the material is filled and a sample of a height of 10–20 mm is generated where different pressures are applied by a sealed piston under different thermal conditions.

Processability test with new test possibilities

To generate a processability test for injection mould and extrusion the RCR[1] was generated with basic functions of the Rheovukameter and gives excellent correlation especially to extrusion and injection molding. The device (Fig. 6) now is been upgraded with a servo electric drive so beside pressure controlled operation also speed controlled operation is possible according injection molding processing.

For rubber testing the device is equipped with a piston, a test chamber (short barrel) with die and mould. In the mode "open mould" an extrusion test similar to a capillary test is possible. The new RCR allow running 3 speed or pressure steps within one test, thus a three point flow curve can be obtained in less than 5 minutes including cleaning. In the mode "closed mould" an injection molding test can be performed. Heat insulation between Chamber and mould allows to set different temperatures in the plasticizing area of the chamber and mould similar to the cold runner injection molding principle.

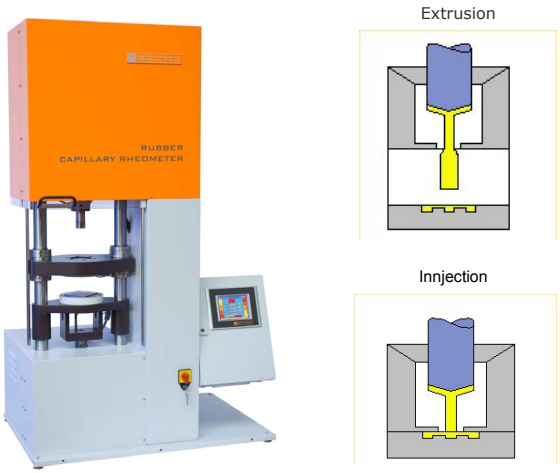

Fig. 6. **RCR with principle of operation mode**

Results and discussion

Dynamic testing

Flow curves of different NBR compounds of the same recipe measured by frequency sweep using the Visco-Eastograph are shown in Fig. 7. By repeating sample B a clear and selective difference of the compounds can be seen showing higher viscosity in the hole measured shear rate range predicting also higher pressure in processing for sample A. Shear rates of the measurement are in the range of compression molding and compounding.

The stability of a filler network of different strains as they occur in processing or use of the vulcanized rubber can be analyzed by a strain sweep. G´and G´´ are calculated from measured torque and loss angle. A silica based compound measured shows in Fig. 8 a constant storage modulus G´ over a wide range of strains before the filler network collapses and the in this case the storage modulus drops even below the loss modulus. This example shows a stable level up to app. 50 % strain, which indicates the operation area for the final part.

Capillary rheometry

Different processing behavior of two samples of a fluorelastomer compound cannot be explained by corrected shear and extensional viscosity. Therefore also Mooney correction is applied on a corrected flow curve of a die 20/1 and 40/2. Fig. 9 shows the corrected flow curves measured by these two different die lengths. On the left side for the batch

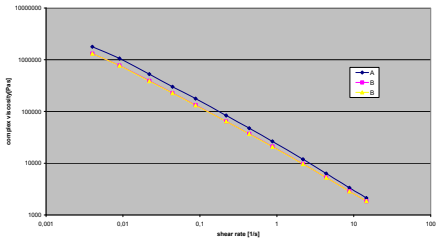

Fig. 7. **Complex viscosity of tow NBR compounds with the same recipe but different raw polymers**

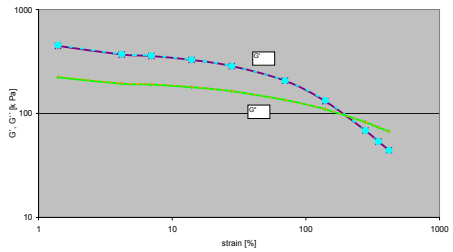

Fig. 8. **Strain sweep for a silica based compound showing Payne effect**

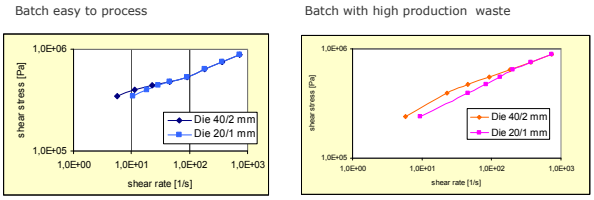

Fig. 9. **Stress versus shear rate of two fluorelastomer compounds with different slip behaviour**

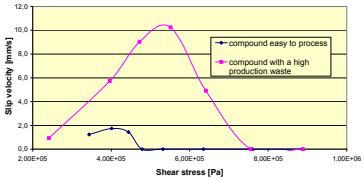

Fig. 10. **Different wall slip velocities calculated using Mooney correction**

easy to process both curves nearly overlap and show only slight differences. The curves of the sample with high production waste on the right side of Fig. 9 are different over a wide range.

On the previous data Mooney correction is applied and slip velocity is plotted versus shear stress, as process parameter. Slip velocity from Mooney correction in Fig. 10 shows a big difference between the batch easy to process, were slip velocity is nearly zero, and the batch of high production waste, where slip velocity is high in a wide range of shear stress.

Materials are processed by injection moulding. The analyses of the stress level in processing shows that the main peak of slip velocity for the material with high production waste occur in the area of the stress level in the plasticizing unit. Therefore poor plasticizing of the compound is generated causing high production waste.

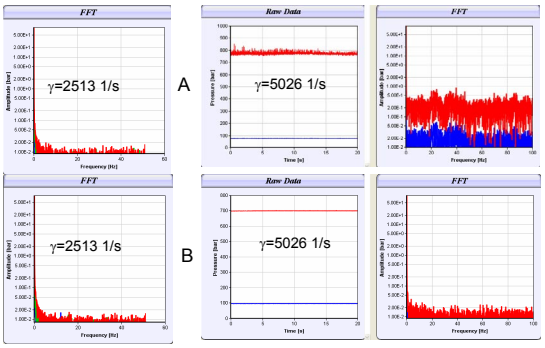

Fig. 11. **Pressure oscillations detected on two EPDM compounds – top rough, bottom smooth surface**

Two EPDM extrusion compounds with similar rheological behaviour show different extrusion quality at a shear rate of app. 5000 1/s. One was smooth and the other showed a rough surface. Both materials are analysed by the Option shark skin for capillary rheometers. Fig. 11 shows for both compounds pressure peak as a function of frequency from pressure oscillation at two shear rates. Both compounds show smooth signal at shear rate 2513 1/s. Compound A with rough surface shows pressure oscillations of 1 decade higher pressures than smooth signal while compound B also a shows smooth pressure signal. Thus an effective test of the behaviour in production can be performed in small scale by this capillary rheometer option.

Shrinkage behavior of a HNBR compound is analyzed using PVT option in the temperature range from –20–180 °C. The pVT diagram (spec. volume versus temperature for different isobaric lines) in Fig. 12 shows begin of transition region from 0–20 °C depending on pressure and for the highest pressures the glass transition point below –15 °C. These PVT data can be used for design of sealings in low temperature application, were sealings loose their sealing force due to shrinkage. Further pVT volume measurement (three dimensions) is more related to practical application than single dimension thermal expansion measurement.

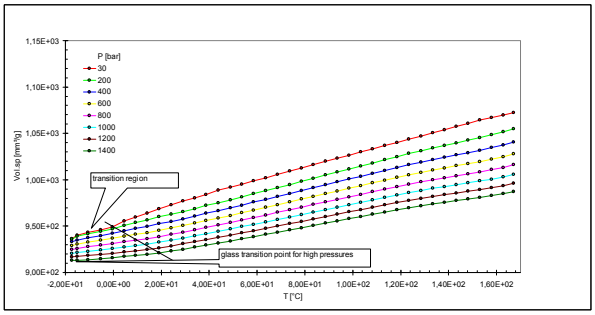

Fig. 12. **PVT diagram of a HNBR compound**

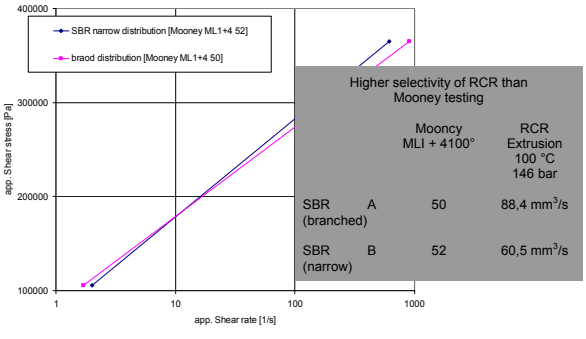

Fig. 13. **RCR measurement in extrusion mode on SBR grades**

Processibility test using RCR with new test possibilities

Viscosity test is performed in extrusion mode in a two step mode of different pressure using RCR for different SBR raw polymers and compared to Mooney viscosity data. Fig. 13 shows a 30 % difference at high pressure generating high shear rates while Mooney measurement shows less than 4 % difference which is near the area of Mooney measurement selectivity but also in a reversed order. For the low pressure step at the RCR, the difference between the materials is lower and in the same order as the Mooney test.

Measurement in injection mode is performed on two batches SBR compounds of different processability and compared to conventional vulcanization measurement in Fig. 14. Vulcanization measurement (left) shows only slight difference in loss angle and the increase of torque while the volume curve gives about 30 % differences indicating the problems of processing.

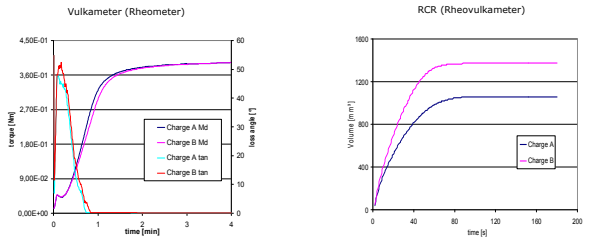

Fig. 14. **Comparison of different batches between Vulkameter and RCR**

Conclusions

Three different measurement devices with various test methods are presented. Dynamic testing by Visco-Elastograph gives more detailed information of structure and processing in the area of compression molding and extrusion. Capillary rheometry with several options allows predicting processing behavior and is an effective tool for the analysis of problems in processing. The processability test with the upgraded RCR is a fast and effective QC test.

The option shark skin for capillary rheometers is developed in collaboration with Prof. Wilhlem KIT Karlsruhe, Germany. We thank Prof. Wilhelm and his team for the effective collaboration on this project.

REFERENCES

1. J. Sunder, A. Goettfert in *4th Pacific Rim Conference on Rheology*, 2005, CD.
2. H. Plaza, S. Filipe, I.F.C. Naue, M. Wilhelm: Polymer *51*, 522 (2010).

CONTRIBUTED LECTURES

CL-01
THE INFLUENCE OF THE PROCESSING CONDITIONS ON THE STRUCTURE OF THE PP/GLASS FIBER COMPOSITES

JACEK ANDRZEJEWSKI, MAREK SZOSTAK, DANUTA CHMIELEWSKA, and TOMASZ STERZYŃSKI

Poznan University of Technology, Institute of Materials Technology, Piotrowo street 3,61-138 Poznan, Poland
jacek.andrzejewski@put.poznan.pl

Introduction

The glass fiber reinforcement (GF), in particular study utilized to strengthen the polypropylene (PP) matrix, is used mainly as mechanical properties improving filler. Stiffness, strength, heat deflection temperature, and the beneficial to weight properties allows to apply the glass fiber reinforced polypropylene composites (GFPP) as a metal replacing material. Since several years the polypropylene based reinforcement composites are replacing the automotive parts, up to now made from polyamide. For example the air-intake systems are now made from GFPP. The other trend observed in the car industry composite materials is the wide range of applications of long glass fiber composites. These automotive applications, where the elevated temperature conditions are standard, requires the best quality material which are normally fulfilled by long glass fiber reinforced polypropylene composites (LGFPP). The basic mechanical properties of long fiber composites are generally twice better, comparing with the short fiber composites.

The benefits resulting from the application of LGFPP composites manifest themselves through the more functional products and shorter manufacturing cycle. Other advantage is the material and weight saving ability, achieved through wall thinning and the lowest density that PA or PC resins.

In this work the results of the comparison of two types of polypropylene based composites reinforced with long and short glass fiber reinforcement are presented. Particularly, the influence of processing conditions on the properties of injection molded samples were investigated

Fig. 1. **Underbody shield made from LGFPP** (provided by Styron)

Experimental

Two types of glass fiber reinforced PP composites were used for these studies. First one filled with 45 wt.% of short glass fiber, second one filled with 60 wt. % of long glass fiber. As a reference material neat polypropylene matrix has been applied. Injection molding machine ENGEL ES80/20 HLS, has been used for samples preparation, the screw diameter was 22 mm and L/D =18. The nozzle diameter was 2 mm, the injection temperature was 225 °C for both materials, and the screw rotation speed was equal to 80 rpm.

The "dog bone" samples (according to ISO 527), produced by injection molding were analyzed in terms of the structure and mechanical properties. Mechanical properties were determined by means of static tension test, at normal and elevated temperatures. The DMTA test were performed using variable frequencies.

The investigated fibers were recovered from incineration of composite samples (according to DIN EN 60). The samples of raw pellets, and molded parts were kept 2 hours at 650 °C in a muffle furnace, after that the PP matrix was removed. The fiber length observations were performed using the NIKON Eclipse microscope. The length of selected fibers was measured, thus the fiber length distribution could be estimated.

Results and discussion

The results of the mechanical tests are presented in Table I. The measurements were carried out at ambient temperature, and at the operating temperature of the car engine compartment, which is equal to 80 °C. The recycling process, consisting of parts milling, should have a significant influence on the properties of recycled molded parts. Nevertheless, the relatively low decrease in mechanical properties of recycled LGFPP composites have been observed.

Table I
Results of mechanical tests at normal conditions (20 °C) and at elevated temperatures * (80 °C)

Type of material	R_m [MPa]	E modulus [GPa]	Strain at peak [%]	Strain at break [%]
pure PP	26,5 (12,1)*	1,8 (0,52)*	3,7 (6,8)*	24,5 (>100)*
PP+longGF	102 (62)*	5.5 (2,65)*	2,4 (2,9)*	2,6 (3,2)*
PP+longGF (recycled)	92,5 (45,2)*	3,7 (2,3)*	3,3 (3,5)*	3,3 (3,8)*
PP+shortGF	81 (38,4)*	4,6 (1,83)*	4,5 (6,4)*	4,6 (7,9)*
PP+short GF (recycled)	68,5 (31,5)*	2,65 (1,6)*	5,4 (6,1)*	5,6 (8,4)*

The results obtained from the DMTA test, such as storage modulus E' and tangent δ as a function of temperature are presented in Fig. 2 and 3. The values of storage modulus at 80 °C of the LGFPP is 2 times higher than GFPP, and several times for neat PP resin. It is interesting that changes of material properties after second injection molding process were observed only for one type of composites. The significant decrease of E' modulus have been noticed only for long fiber reinforced materials, where the average decrease was 25 %, for short fiber it was only 15 %. Nevertheless, the 40 % higher values of E' modulus for recycled LGFPP than for raw GFPP composite have been observed. The analysis of the T_g from the tangent δ curve did not show any significant changes in that area. The reduction in length of the glass fiber leads to an increase of the damping factor, which can be explained by lower energy dissipation for stronger fiber/ matrix interface.

Microscopic examination were conducted in order to estimate the length of the glass fibers before and after processing. The pictures on Fig. 4 present the glass fibers obtained directly from the pellets. The length of the short fibers was in average about 300 μm, where for long type GF it was about 11 mm. The diameter of both fiber types was the same, 12 μm. The microphotographs on Fig. 5 illustrate the influence of injection molding on the short and long fibers length and distribution. As it may be seen most often the breakage occurs not in the middle but at the end of the fiber. Thus, the mechanical properties of the long glass fiber reinforced composite after two stage injection molding are not decreasing rapidly. Shortening the fibers ends result in the appearance of a significant amount of glass fiber sections with a maximum length 30 μm, and a larger distribution of this fraction occurs in long fiber composite.

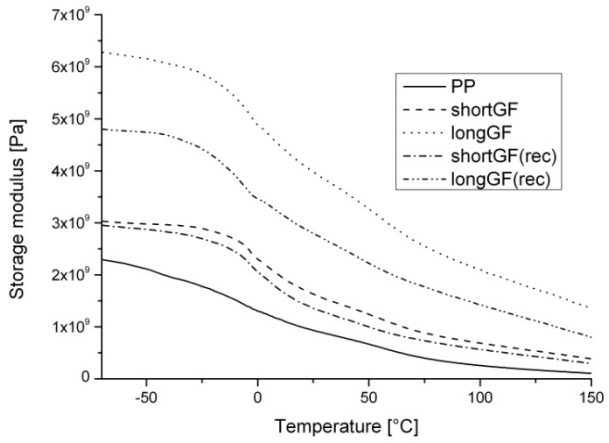

Fig. 2. **The DMTA storage modulus as a function of temperature**

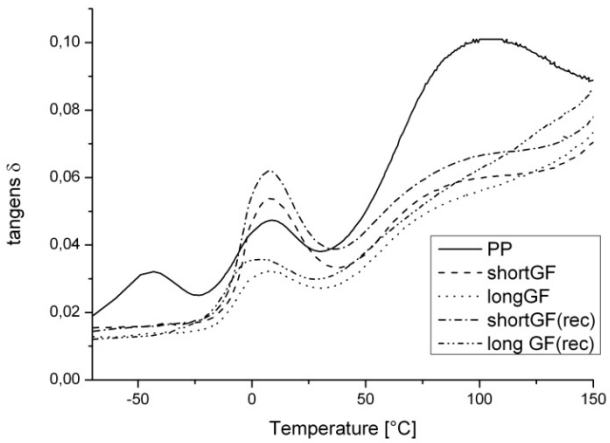

Fig. 3. **The DMTA tangent δ as a function of temperature**

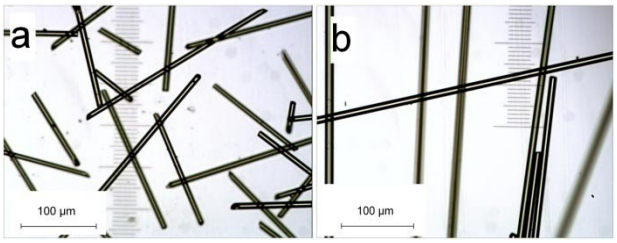

Fig. 4. **Microphotographs of a) short and b) long fibers obtained directly from raw pellets**

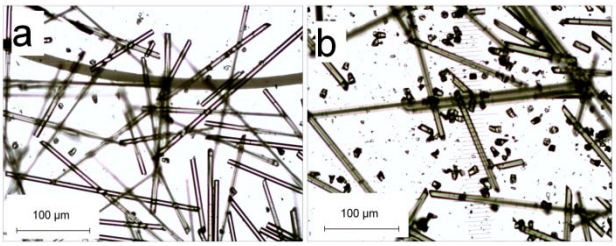

Fig. 5. **Microphotographs of a) short and b) long fibers obtained after injection molding**

Conclusion

The results of the study allowed to draw several conclusions. A significant difference in mechanical properties remains after the recycling process. Fiber breaking process takes place mainly at its ends, which finally doesn't result in dramatic decrease in the length of the reinforcement. The use of long fibers leads to superior mechanical properties, even after several processing cycles. This knowledge may be important if the recycled materials should be applied. The properties of LGFPP composites are significantly better, than of conventional GFPP materials. Therefore by application of recycled LGFPP, its good quality properties and possibility to use as a full value material for car industry parts should be taken into account.

REFERENCES

1. Markarian J.: Plastics Engeneering 8, 22 (2011).
2. Lafranche E., Krawczak P., Ciolczyk J. P., Maugey J.: eXPRESS Polym. Lett. *1*, 456 (2007).
3. Inceoglu F., Ville J., Ghamri N., Pradel J. L., Durin A., Valette R., Vergnes B.: Polym. Compos. *32*, 1842 (2011).
4. Kwiatkowski D., Gnatowski A., Nabiałek J.: Composites: Practice and Theory *11*, 294 (2011).
5. Gnatowski A., Kwiatkowski D., Nabiałek J.: Composites: Practice and Theory 9, 128 (2009).
6. Shon K., White J. L.: Polym. Eng. Sci. *39*, 1757 (1999).
7. Kuciel S., Kuźniar P., Liber-Kneć A.: Polimery *57*, 627 (2012).
8. Gądek A., Kuciel S., Wojnar L., Dziadur W.: Polimery 51, 206 (2006).

CL-02
THE METHOD OF VIBROACOUSTICAL PROPERTIES DETERMINATION OF THE INTERNAL CAR DOOR PANELS

ROMAN BARCZEWSKI*[a], MATEUSZ BARCZEWSKI[b], and MAREK SZOSTAK[b]

[a] *Poznan University of Technology, Institute of Applied Mechanics, Piotrowo Street 3, 61-138 Poznań,* [b] *Poznan University of Technology, Institute of Materials Technology, Piotrowo Street 3, 61-138 Poznań, Poland*
roman.barczewski@put.poznan.pl

This paper describes an application of a laser vibrometry technique in order to determine the vibroacoustical properties of interior car door panel. The testing procedure was based on non-contact vibration measurements executed by a laser beam scanning the surface of a car door element in several representative points after acoustic excitation of specimens. A methodology and a description of measuring procedure were also presented.

Introduction

Dynamic, technical and economical development observed in the automotive industry is accompanied with a permanent increase of the amount of polymeric materials used in production. Most of all used polymeric materials are thermoplastics such as polyolefins, polycarbonate, polyamide and thermoplastic elastomers. Due to relatively low cost of isotactic polypropylene and its good processability during injection moulding, it is often applied as a material proper for large and unloaded elements. Usually polymeric matrix is modified or filled accordingly to technical and economical requirements which must be fulfilled[1–3].

Most of measuring techniques used for determination of polymer's properties require a preparation of a specific sample for each test. In case of determination of damping behavior or sound/vibration attenuation it is important not only to observe the specific parameters occurring during standardized test but also to evaluate behavior of a complete part. The application of non-contact tests results in a possibility of properties' investigation of used polymeric material but also allows to examine the influence of shape and manufacturing process on the behavior of ready-to-assembly parts. Several methods of mechanical and damping properties determination of thin walled parts were described in many papers. Differences between them are caused by the way of excitation (modal hammer, sound excitation) and also by the measuring method (piezoelectric accelerometer, laser vibrometer)[4–10].

In presented case studies the laser vibrometry technique was applied in order to determine vibroacoustical properties of indoor car door panel made of isotactic polypropylene under acoustic excitation.

Experimental

The experiments were performed by means of a specially designed measuring system which consists of a tested object (internal car door panel), a laser vibrometer (Polytec OFV-505), a special loudspeaker (omnidirectional sound source), a free-field microphone, and a signal acquisition and analysis system. To reduce the effect of boundary conditions on the test results the indoor car door

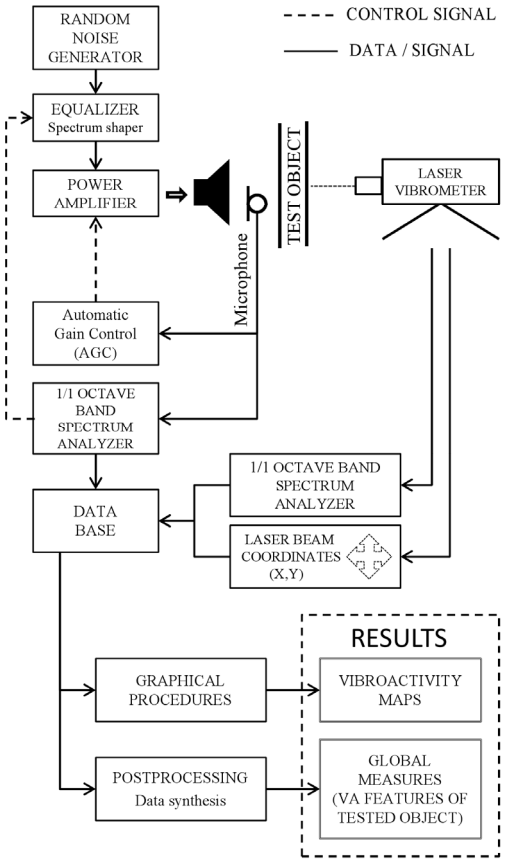

Fig. 1. **Connections diagram and procedures of the digital signal processing system**

panel was hanged by four mounting holes. Connections diagram, the system elements and digital signal processing procedures are presented in Fig. 1.

The pink noise was used as a signal of an acoustic excitation. During the test procedure the sound pressure levels (SPL) close to specimen's surface (in a distance of 10 cm) in the octave bands (center frequencies from 125 Hz to 8 kHz) were stabilized on the level of 80 dB. Due to acoustic source used type and loudspeaker's characteristics it was problematic to achieve the nominal of 80 dB SPL in the octave bands below 125 Hz and above 8 kHz. However, when only acoustic properties are evaluated the analyzed frequency band can be limited to the frequency band of best noise perception of human ear.

Results and discussion

Internal car door panel with a measuring grid used to positioning of the laser beam is presented in Fig. 2.

The results of investigations carried out according to a proposed testing procedure could be presented in a form of:

vibroactivity maps (VA maps) obtained in the octave band (Fig. 3) or in the wide frequency range (Lin),

global measures – an average of vibration levels determined for the whole tested surface (by VA maps postprocessing) in octave bands and wide frequency range, respectively (Fig. 4).

An example of the vibroactivity map presented in Fig. 3 indicates the regions of the highest vibrations levels for 250 Hz octave. Representative measuring points, useful in further fast industrial testing procedures, can be determined on the base of this type of graphical results presentation. The global measures can be applied in order to determine and evaluate the vibroacoustical properties or to proceed overall quality control of internal car door panels (Fig. 4).

Conclusion

Results obtained from presented test method can be applied to:

an optimization of the vibroacoustical thin walled polymer car parts (e.g. the effect of incorporation of different additional damping materials in the regions of the highest vibroactivity, based on VA maps),

a manufacturing quality control procedure, by a comparison of VA maps (e.g. differential maps) or advanced pattern recognizing techniques. In this case local failures of polymer parts caused by improper injection moulding parameters or differences in used material damping behavior can be detected,

a fast final product qualification (intact/wrong) based on global measures by comparison to experimentally determined criteria or limit values of intact products.

In comparison to a typical modal analysis the proposed test method does not provide detailed information about the modal/dynamic properties of tested elements. Obtained data are rather characterized as a general. However, this type of results is more suitable and useful for direct application in the industrial systems of products' automatic quality control.

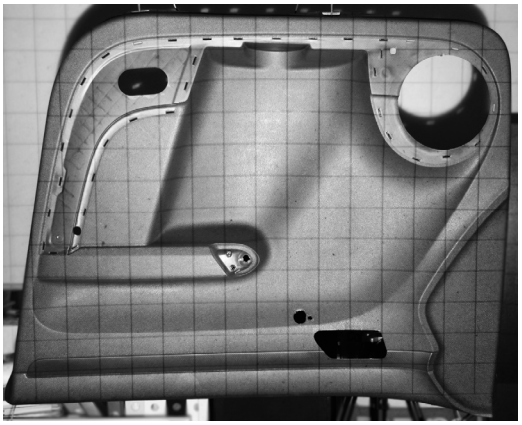

Fig. 2. **Measurement grid on the tested object (5 × 5 cm) used for laser beam scanning**

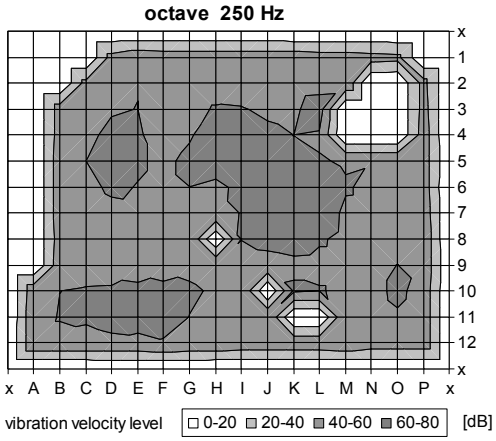

Fig. 3. **An example of vibroactivity map for an octave of 250 Hz** (excitation - pink noise, 80 dB in each octave band)

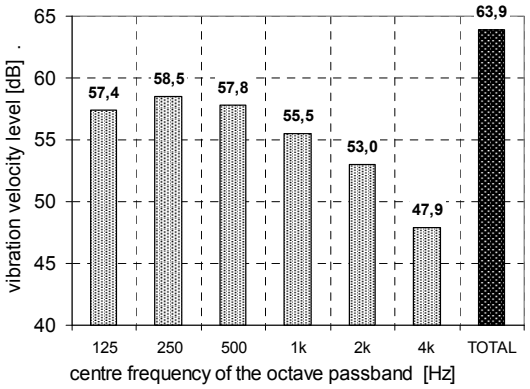

Fig. 4. **Vibration velocity level in the octave band and total vibration level** (averaged on the surface of tested object; excitation - pink noise, 80 dB in each octave band)

REFERENCES

1. Correnti A., Bocchino M., Filippi S., Magagnini P. L., Polacco G., La Mantia F. P.: J. Appl. Polym. Sci. *96*, 1716 (2005).
2. Szostak M.: Chem. Listy 105, s307 (2011).
3. Jakubowska P., Sterzyński T., Królikowski B.: , J. Appl. Polym. Sci. *109*, 1993 (2008).
4. Barczewski R., Jakubek B.: Vibrations in Physical Systems *25*, 59 (2012).
5. Barczewski R., Kabała A.: Vibrations in Physical Systems *25*, 65 (2012).
6. Shorter P. J.: J. Acoust. Soc. Am. *115*,1917 (2004).
7. Wang F., Mechefske C. K.: Journal of Sound and Vibration 311, 554 (2008).
8. Gibson R. F.: Compos. Sci. Technol. *60*, 2769 (2000).
9. Markiewicz E., Borysiak S., Paukszta D.: Polimery *54*, 430 (2009).
10. Fernandez-Grande E., Jacobsen F., Leclère Q.: J. Acoust. Soc. Am. *132*, 3818 (2012).

CL-03

MORPHOLOGY AND MECHANICAL PROPERTIES OF PVC/ POLY (MMA)-*b*-POLY (*N*-BUTYL ACRYLATE)-*b*-POLY (MMA) TRIBLOCK COPOLYMER BLENDS

SAMIR H. BOTROS[a], NEHAD N. ROZEIK[a], IVAN CHODAK[b], and AHMED F. MOUSTAFA[a]*

[a] *National Research Center, Polymers Department, Dokki-12311, Giza, Egypt,* [b] *Institute of polymers, Bratislava, Slovak Republic*
amoustafa1971@gmail.com

Abstract

Homogeneity of solution cast films of the PVC/triblock copolymer blends was examined with scanning electron microscopy (SEM) and dynamic mechanical thermal analysis (DMTA). The micrographs revealed that the blends are compatible for all blend ratios examined. The mechanical properties of the blend films were determined. Blending of the triblock copolymers with PVC improved the elasticity of PVC but reduced the tensile strength. The elongation at break, % and the tensile strength values show straight line behavior versus the triblock copolymer content in the blend, indicating the homogeneity of those blends.

Introduction

The blends of PVC and acrylic copolymers[1–3] are still of great interest due to their diverse mechanical properties, in addition to the contradictory results about the system compatibility[4–6]. Acrylic/PVC products have been used for construction purposes such as siding, window profiles and decking[2]. In the present research commercial triblock acrylic copolymers based on poly (MMA)-*b*-poly(*n*-butylacrylate)-*b*-poly(MMA), were blended separately with PVC of 67 k value, in different blend ratios. Homogeneity of these blends was investigated with SEM, DMTA and mechanical properties.

Experimental

Triblock copolymes (LA 1401, LA 2140 and LA 2250) of various MMA ratios (15 %, 23 % and 32.5 %) and with weight average molecular weights 85000, 80000 and 75000, respectively, are gifts from Kurary America INC. USA). PVC/triblock copolymer blend films were prepared by casting the mixed solutions (in tetrahydrofuran) at different blend ratios (100/0, 75/25, 50/50, 25/75, and 0/100 wt.%) on glass plates, and were left to dry at room temperature.

Results and discussion

The morphology of PVC/ triblock copolymer blend films (50/50 by weight) was examined by scanning electron microscope at magnification M = 500×. The SEM micrographs of PVC and its blends with the triblock copolymers of different PMMA ratios are illustrated in Fig. 1 (a–d). Fig. 1a illustrates the PVC phase. Fig. 1(b–d) shows one phase for the PVC/ triblock copolymer blend films (50/50) and illustrates no phase separation taking place. The PVC agglomerates spread through the triblock copolymer phase. The morphology revealed homogeneity of the PVC/ triblock copolymer blends for the blend ratio investigated. This can be explained as a result of the hydrogen bonding interaction between the acidic hydrogen atoms of PVC with the carbonyl groups of acrylic moiety of the triblock copolymer, this in turn results in decreasing the surface tension of the two phases, leading to improvement in the blend homogeneity.

Dynamic mechanical thermal analysis (DMTA)

The DMTA tg ∂ peaks for all the blends are shown in Table I. In some cases only one peak appeared, in others, either two peaks or shoulders were observed. The DMTA record for PVC shows Tg to be 62 °C which corresponds to PVC with 10 ppp (parts per polymer) of DOP plasticizer.

Tg data of the two triblock copolymers, namely LA 1401 and LA 2250 (both with 10 ppp of DOP) are identical being –34 °C and much lower than Tg of PVC/DOP. When

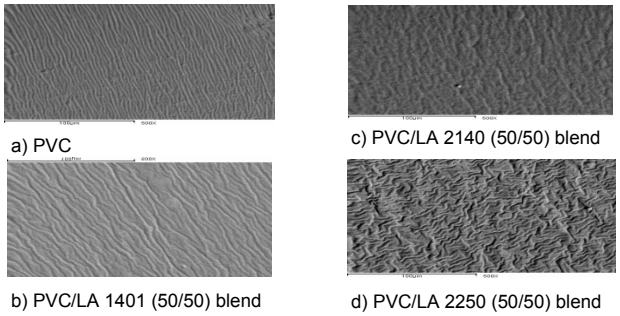

Fig. 1. **SEM micrographs of PVC and its blends with triblock copolymers of different PMMA ratios**

Table I
Composition of prepared blends and temperatures of t_g ∂ maxima of peaks for each blend

PVC	Triblock	LA 1401		LA 2250	
		1st.	2nd.	1st.	2nd.
10	0	62.2		62.2	
7.5	2.5	87.4		75.2	35 sh
5	5	78	5.7	72	7 sh
2.5	7.5		–5.7	91.6	–2.9
0	10		–34.2		–34.5

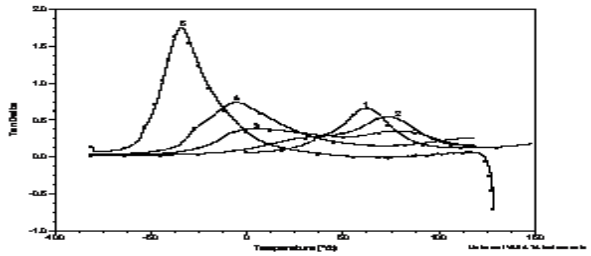

Fig. 2. **Curves of loss angle tan ∂ measured by DMTA for PVC(1), triblock LA 1401 (5) and blends PVC/LA 75/25 (2), 50/50 (3) and 25/75 (4)**

discussing the blends of these two copolymers with PVC, the trends are quite obvious and understandable. For both polymeric components of the blend in virgin state one peak is only appearing. In blends of PVC/LA 1401, two peaks are

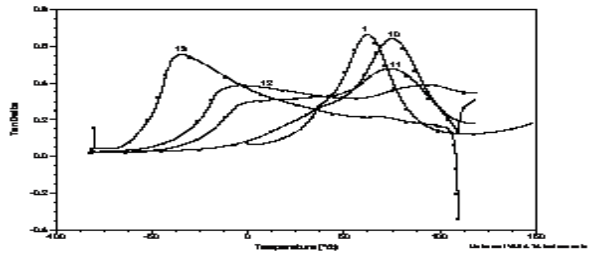

Fig. 3. **Curves of loss angle tan ∂ measured by DMTA for PVC(1), triblock LA 1401(13) and blends PVC/LA 75/25 (10), 50/50 (11) and 25/75(12)**

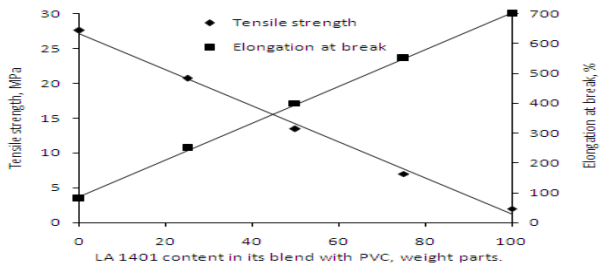

Fig. 4. **Tensile strength and elongation % of PVC/LA 1401 blends**

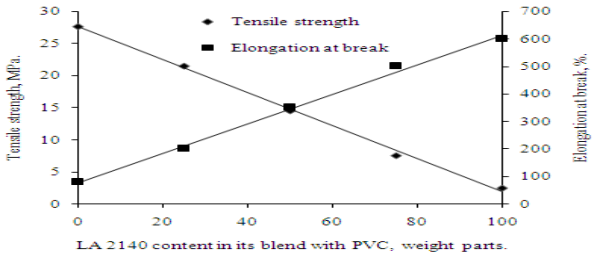

Fig. 5. **Tensile strength and elongation % of PVC/LA 2140 blends**

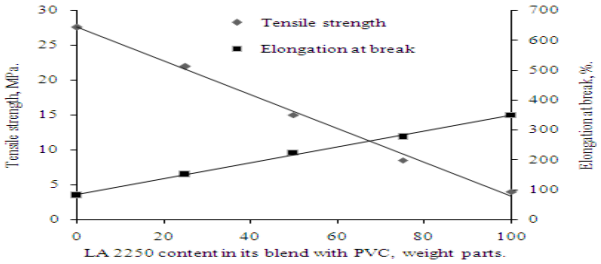

Fig. 6. **Tensile strength and elongation % of PVC/ LA 2250 blends**

clearly seen at composition 50/50, for all other compositions, only one peak is observed corresponding to PVC for lower LA 1401 content and to LA 1401 at higher triblock content. Similar situation occurs also for blend of LA 2250 triblock with PVC, just some shoulders are visible also for blend 75/25 and two peaks appear at composition 25/75. The DMTA records showing the thermal dependence of loss angle are shown in Figs. 2 and 3, demonstrating the facts described above. It is also clear that Tg values corresponding to the individual blend components are not constant. This means that the two-phase morphology should be present in the blends, depending on the content of the components. On the other hand, the blends seem to be partially miscible since Tg of both components is changing with changes of the blend composition. The latter conclusion should be discussed in more details. The peculiar aspect consists in the fact that the addition of the triblock copolymer leads to an increase of the temperature corresponding to the PVC peak although Tg of the triblock is much lower compared to PVC. On the other hand, Tg of the both triblocks is decreasing with a decrease of PVC content that corresponds to the Fox equation based on additivity of blend components regarding the effect on Tg changes in the blend of two thermodynamically miscible polymers. This inconsistency can be explained by proposing that the two polymers (PVC and triblock copolymer) are partially miscible up to certain content of triblock in the blend.

Mechanical properties

Mechanical properties of PVC/triblock copolymer (of different PMMA ratios) blend films of different blend ratios namely (100/0, 75/25, 50/50, 25/75, and 0/100 wt.%), were

measured and illustrated in Figs. 4–6. It was found that, as the triblock copolymer content in its blend with PVC increases, the elongation at break% increases; due to the elasticity of the triblock copolymer because of the butylacrylate portion. However the tensile strength at rupture increases as the PVC content in the blend increases because of the rigidity and crystalinity of PVC. Also, as the PMMA ratio increases (or the butylacrylate ratio decreases) in the triblock copolymer, the elongation at break% decreases. This can be attributed to the crystalinity of PMMA portion. It is obvious that the elongation at break increases linearly, whereas tensile strengths at rupture decreases linearly as the triblock copolymer amount increases in the blend. The linear behavior of mechanical properties vs the triblock copolymer content indicates homogeneity of PVC/ triblock copolymer blend.

Conclusions

SEM micrographs revealed no phase separation in PVC/ triblock copolymers blends and showed that these blends are homogeneous. Blending of PVC with PMMA-b-PBA-b-PMMA tribock copolymers is advantageous because enhancement of the elasticity of PVC and improvement of the tensile strength of the triblock copolymers. DMTA indicated that PVC/triblock copolymer blends seem to be partially miscible.

REFERENCES

1. Tong J. D., Leclere Ph., Rasmont A., Bredas J. L., Lazzaroni R., Jerome R.: Mol. Chem. Phys. *201*, 1250 (2000).
2. Haba Y., Narkis M.: Polym. Adv. Technol. *16*, 495 (2005).
3. Haba Y., Shach-Caplan M., Cohen Y., Narkis M., Bianco-Peled H.: Polym. Adv. Technol. *16*, 451 (2005).
4. Karlou K., Schneider H. A.: J. Therm. Anal. Calorim. *59*, 59 (2000).
5. Tong J. D., Jerome R.: Polymer *41*, 2499 (2000).
6. Tong J. D., Leclere Ph., Doneux C., Bredas J. L., Lazzaroni R., Jerome R.: Polymer *42*, 3503 (2001).

CL-04
PLASMAPLUS® COATINGS FOR HYBRID POLYMER-METAL PARTS IN AUTOMOTIVE INDUSTRY

ARTUR GRISHIN*, ALEXANDER KNOSPE, and CHRISTIAN BUSKE

Plasmatreat GmbH, Bisamweg 10, 33803 Steinhagen, Germany
artur.grishin@plasmatreat.de

Polymers and metals are the key materials in automotive manufacturing industry. Combining of both material classes in polymer-metal hybrid structures is the way to create components with unique functionalities, exactly tailored for any specific requirement. Such hybrid structures are replacing more and more one-material solutions in all automotive production segments. Rubber-metal, plastic-metal or composite-metal structures are currently used in tires, carrossery, motor, interior and exterior parts. Although a great variety of techniques available for joining of polymers and metals together, there is a big interest in new technologies due to design, economical and environmental concerns.

PlasmaPlus® technology (combination of plasma cleaning and plasma deposition of thin coatings at atmospheric pressure) have been applied for deposition of adhesion promoting coatings for direct bonding of polymers on metals. Solutions for rubber to metal vulcanizing, injection molding of fibre reinforced thermoplastics on metals, and welding of plastic with metals are offered. Proposed technology provide promising alternative to common joining technologies or can be used in combination with them in order to reduce number of production steps and consumption of VOC-based chemicals, minimize the amount of waste created, and, as a result, significantly reduce environmental impacts and whole process costs. Slightly modified industrial PlasmaPlus® equipment, used in these experiments, can be easily integrated in exiting production lines or applied as stand-alone solution.

CL-05
THERMAL DECOMPOSITION OF AUTOMOBILE SHREDDER RESIDUE (ASR)

JUMA HAYDARY and DALIBOR SUSA

Institute of Chemical and Environmental Engineering, Faculty of Chemical and Food Technology, Slovak University of Technology, Radlinského 9, 812 37 Bratislava, Slovakia
juma.haydary@stuba.sk

The product of a usual EU automobile shredder contains approximately 70 wt.% of metals separated by magnetic separators. Other 5–6 wt.% represent non ferrous metals. After the separation of metals, the remaining part is a complex mixture of materials including plastics, foam, textiles, rubber, glass and others. This waste, which creates approx. 20–25 wt.% of the original vehicle's mass, is called Automobile Shredder residue (ASR) or auto fluff. In the European Union, about 2–2,5 million tons of this waste are produced every year[1,2]. At the present time, ASR is usually landfilled but the European draft Directive 2000/53/CE forces the development of alternative solutions requiring 95 % of ELV to be reused / recovered and 85 % to be reused / recycled by 1.1.2015.

Feedstock recycling methods such as pyrolysis and gasification represent an economically and ecologically acceptable solution for the disposal of this waste[3,4]. The ASR is a heterogeneous mixture of all materials found in cars and the composition of ASR varies depending on the producer, type of shredded vehicles, used shredding technology, fractionation of the shredded cars and many other factors. However, the design of a thermal process (incineration, gasification or pyrolysis) requires the knowledge of the characteristics of the raw materials.

In this work, thermogravimetric (TG) analyses of individual components and of the representative samples of ASR were provided by a simultaneous TG/DSC analyzer. The aim was to describe the thermal decomposition characteristics

of ASR based on the behavior of thermal decomposition of its individual components.

Materials and methods

The samples used in this work were obtained from a light fraction of ASR. The basic organic component of ASR was identified as rubber, plastics, foam, textile and other organic materials.

Table I shows the mass fraction of individual material categories in ASR and also their proximate and elemental composition.

Simultaneous thermogravimetric (TG) / differential scanning calorimetric (DSC) measurements using a simultaneous thermal analyzer (Netzsch STA 409 PC Luxx, selb, Germany) was applied in the thermal analysis of ASR. Experimental conditions were met at the linear heating rates of 10 °C min^{-1} in the nitrogen flow of 60 ml h^{-1}. The samples were heated from 20 to 800 °C and they were kept at this temperature for round 30 minutes, then, they were combusted by oxygen supplied to the system. Samples of individual categories of ASR and of the mixed ASR with the mass of around 20 mg were used in the TG/DSC measurements. For these measurements, the plastic fraction was divided into three different subcategories (rigged plastics, semi-rigged plastics and soft plastics). In addition, a mixed sample of ASR with the composition shown in Table I was prepared. Data obtained from thermogravimetric experiments were used for the determination of kinetic parameters of thermal decomposition.

Results and discussion

Non-isothermal thermogravimetric analyses of individual material categories of ASR were used for the determination of kinetic parameters of thermal decomposition. The measured behavior of TG curves is shown in Fig. 1. Except for textile and plastic1, other components showed two degradation regions.

For a multi-step thermal decomposition, the total decomposition rate can be calculated as a sum of individual decomposition reactions:

$$\frac{d\alpha}{dt} = \sum_{i=1}^{n} A_i \exp\left(-\frac{E_i}{RT}\right)(1-\alpha_i)^{n_i} \qquad (1)$$

Table I
Proximate and elemental analysis of individual components of ASR

Category	w_i [kg/kg]	Moisture [wt. %]	Volatile matter [wt. %]	Fixed carbon [wt. %]	Ash [wt. %]	N [%]	C [%]	H [%]	S [%]	O [%]	Ash [%]
Rubber	0,455	0,4	46,8	15,6	37,3	0,31	48,16	4,79	1,67	7,73	37,3
Foam	0,018	1,4	91,4	5,8	1,4	6,47	62,61	8,40	0,20	20,91	1,40
Plastics	0,474	0,3	91,9	4,0	3,3	2,39	69,65	8,74	0,26	15,66	3,30
Textile	0,023	0,9	83,2	10,0	6,0	0,99	58,22	4,33	0,20	30,31	6,00
Other OM	0,03	6,0	73,6	13,1	7,8	0,03	49,61	5,94	0,36	36,29	7,80

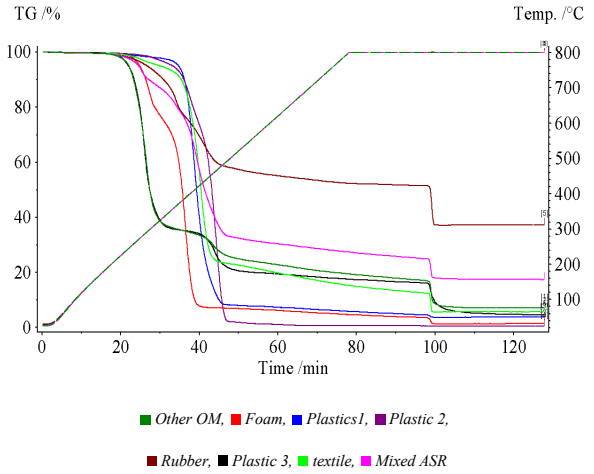

Fig. 1. **Behavior of thermal decomposition of individual components of ASR and mixed sample of ASR**

where A is the apparent pre-exponential factor, E is the apparent activation energy, T is the temperature, n is the reaction order, t is the time and R is the gas constant. Conversion, α, was calculated according to Equation (*2*):

$$\alpha = \frac{m_0 - m}{m_0 - m_{final}} \qquad (2)$$

where m_0, m, and m_{final} correspond to the initial, actual, and final sample mass, respectively.

Parameters A, E and n for each decomposition step were obtained from a set of kinetic experiments on the dependence of the reaction rate *vs*. temperature by fitting the calculated and experimental data (Fig. 2). The used objective function was:

$$f = \sum_{i=1}^{k}\left(\frac{d\alpha_{\exp}}{dt} - \frac{d\alpha_{cal}}{dt}\right)^2 \qquad (3)$$

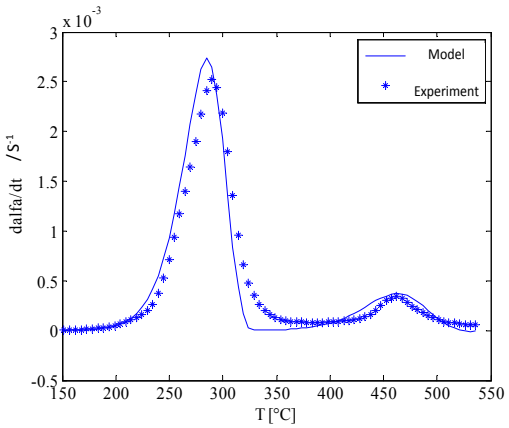

Fig. 2. **Fitting of DTG curves for the determination of kinetic parameters**

The estimated kinetic parameters for all material categories are presented in Table II.

The total decomposition rate of mixed ASR can be calculated additively using the rate of thermal decomposition of individual material categories as follows:

$$\frac{d\alpha_{ASR}}{dt} = \sum_j w_j \frac{d\alpha_j}{dt} = \sum_j w_j \left(\sum_{i=1}^{n} A_i \exp\left(-\frac{E_i}{RT} \right) \left(1-\alpha_i\right)^{n_i} \right)_j \qquad (4)$$

Using Equation (*4*), the rate of thermal decomposition of a mixed ASR was calculated and compared with the experimentally determined rate of reaction of a mixed ASR sample. The coherence between conversion calculated based on Equation (*4*) and the experimentally determined data is clear from Fig. 3.

Table II
Kinetic parameters of thermal decomposition of ASR components and a mixed ASR

Sample	A_1 [s^{-1}]	E_1 [J mol^{-1}]	n_1	A_2 [s^{-1}]	E_2 [J mol^{-1}]	n_2
Rubber	$2{,}50.10^{11}$	$1{,}70.10^{5}$	1,70	$2{,}88.10^{11}$	$1{,}83.10^{5}$	1,01
Foam	$1{,}00.10^{12}$	$1{,}63.10^{5}$	1,10	$3{,}48.10^{14}$	$2{,}10.10^{5}$	1,00
Plastic 1	$1{,}53.10^{13}$	$2{,}04.10^{5}$	1,00	-	-	-
Plastic 2	$3{,}96.10^{7}$	$1{,}38.10^{5}$	1,07	$4{,}20.10^{11}$	$1{,}95.10^{5}$	1,08
Plastic 3	$3{,}59.10^{13}$	$1{,}71.10^{5}$	1,00	$9{,}34.10^{11}$	$2{,}01.10^{5}$	1,00
Textile	$3{,}61.10^{14}$	$2{,}22.10^{5}$	1,00	-	-	-
Other OM	$1{,}86.10^{10}$	$1{,}33.10^{5}$	1,05	$1{,}04.10^{11}$	$1{,}86.10^{5}$	1,06
Mixed ASR	$9{,}20.10^{10}$	$1{,}47.10^{5}$	2,02	$8{,}61.10^{10}$	$1{,}79.10^{5}$	1,00

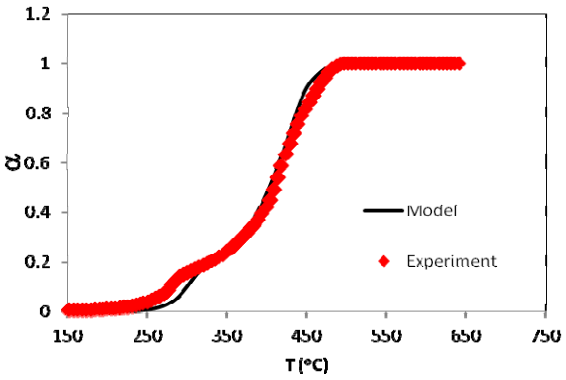

Fig. 3. **Conversion of ASR, determined by model and experiment**

This work was supported by the Grant VEGA No. 1/0753/13 from the Slovak Scientific Grant Agency.

REFERENCES

1. Antonis A. Zorpas, Vassilis J. Inglezakis: Technology in Society *34*, 55 (2012).
2. Fiore S., Ruffino B., Zanetti M.C.: Waste Management *32*, 1548 (2012)
3. Horii M., Iida S.: JSAE Rev. *22*, 63 (2001).
4. Day M., Cooney J. D., Shen Z.: J. Anal. Appl. Pyrol. *37*, 49 (1996).

CL-06
CHARACTERISTICS OF FUNCTIONAL GROUPS ON CURED NBR MATERIAL SURFACES

HIDETOSHI HIRAHARA, JING SANG, SUMIO AISAWA, KATSUHITO MORI, TAKAHIRO KUDO, EIICHI NARITA, YOSHIYUKI OISHI and KUNIO MORI

The Graduate School of Engineering, IWATE University, 4-3-5 Ueda, Morioka IWATE 020-8551, Japan
hiraha@iwate-u.ac.jp

Key Words: NBR, Peroxide Curing, Surface, Functional Structure, XPS, AFM

1. Introduction

Properties of materials are a summation of surface and bulk functions. Their functions are easily estimated to affect the types, processing methods of materials and the amount and types of additives to materials, but its actual situation is always not clear. For example, unsaturated rubber is widely known to be cured in the presence of peroxides[1–4]. However, it is not clear whether curing structure in the surface and bulk of rubbers is same or not so, and whether the curing level is same or not so. So far, in the case that peroxide-cured unsaturated rubbers indicate surface adhesiveness, surface properties have being improved as the formation of hydro peroxides is inhibited by carrying the curing out in vacuum. Peroxide curing systems do not contain the subject matters for surface properties while there are issues for capital cost due to vacuum press machine is present. However, in the peroxide curing systems, the difference of curing reaction and chemical structure in the surfaces and insides of peroxide-cured must be clearly caught, on the standpoint of making use of the positively surface function of acrylonitrile-butadiene rubber (NBR) cured, chemical structure was investigated by X-ray photoelectron spectroscopy (XPS) surface analysis in the surfaces and cut-surfaces of DCP-cured NBR.

On the other hand, it is widely known that surface structure in the molding processing of polymer materials is different from surroundings to contact[5–8]. The surface structure of NBR cured by peroxides is predicted to causes chemical changes due to the contact surroundings and curing conditions during processing. The interesting subject matter and information such as the formation of functional groups on

the NBR surfaces obtained by peroxide curing and the chemical change and diffusion of functional groups is contained a lot[9]. In this work, for the purpose to obtain fundamental information for making effective use of the surface function of cured NBR, it is investigated using XPS analysis that the types and amount of functional groups in the surfaces and bulk (inner) are influenced by curing conditions. In addition, chemical and physical properties on the cured NBR surfaces are also investigated.

2. Experimentals

2.1. Materials and reagents

The rubber used here is acrylonitrile-butadiene rubber (NBR, AN: 35 %, N230S, JSR Co.), and base compounds and curing systems for NBR are NBR rubber (100 phr), carbon black (50 phr), stearic acid (1 phr) and stabilizer ZnO (5 phr). Additives were prepared by company. The curing agent, bis (α,α-dimethyl benzyl) peroxide (dicumyl peroxide: DCP, reagent grade) as an accelerator was added to the base compounds.

2.2. Compounding and Curing

The uncured NBR compound sheets were obtained after mixed of NBR polymers, filler, stearic acid and ZnO by banbury mixer and then adding DCP to the NBR master batch on the two roll mill. After the blending, the uncured NBR compound sheets were molded being folded between two 6-nylon (PA6: UBEPA6, 100 μm, heat softening temperature; 180 °C/451 kPa) films into a rheometer cabinat 140 °C, 150 °C, 160 °C, 170 °C, and 180 °C for 30 min. The cured NBR samples were immediately removed from the rheometer molds. The surfaces and cut-surfaces of cured NBR rubbers for Analytical samples of cured NBR rubbers were prepared as cured NBR (2 × 2 × 10 × mm) with six surfaces which are obtained by cutting, after peeling out PA6 firms from NBR cured at first and used after 24 hr keeping in vacuum; one surface is the surface (outside) obtained by curing and others are cut-surfaces (inside) obtained by cutting and means chemical structure of balk in cured NBR.

2.3. Measurement

The surfaces and cut-surfaces of cured NBR rubbers were analyzed XPS (PHI QUANTERA ESCA system) with the Multi Technique spectrometer, the focusing monochromator (ULVAC-PHI inc.) and Al Kα X-ray source which has 100 μm×100 μm spot for surface analysis. Pass energies of the analyzer were 69 eV for high-resolution scans at 300 W. The angle resolved measurements were made at an electron take-off angle of θ = 45°(θ is the angle between the sample surface and the direction of the analysis photoelectrons). And the electron flood gun was used for charge neutralization were used and the analysis chamber remained at 3.0×10^{-6} Pa in the process of the whole XPS measurement. The XPS spectra were subjected to Shirley background subtraction formalism and the data was using the saturated C 1s peak at 284.8 eV and which were used in chemical-bonding-state assignments. The full width at half maximum (FWHM) of C-C/C-H component was left to vary freely then the other components were fixed to adopt this value. During all the fitting curve treatments, Gaussian-Lorentzian lines of variable proportion were used and the XPS experimental curve fitting process were taken by Mutipak software.

Surface morphologies were measured by automatic atomic force microscope (AFM, SIMAZU SPM-9600) with the tapping mold. The scan speed used with 1.0 kHz, and scan area is 1×1 μm^2.

3. Results and discussion

3.1. Analysis of surfaces and cut-surfaces in DCP-cured NBR

Elemental component ratios calculated from the recipe in Table I are C: 93.6 %, N: 6.2, and O: 0.16 %.

Fig. 1 shows the elemental component ratios of surfaces and cut-surfaces which are obtained from XPS analysis of DCP-cured NBR at various temperatures. The founded value for O atom is larger than the calculated value.

N atoms arise from nitrile (-CN) groups and O atoms come from DCP and oxidation during curing process. The differences of element quantities between surfaces and cut-surfaces are due to that the reaction on surface and at the bulk are different during curing process. It can be easy to understand that the quantity of oxygen to react with NBR on the surface curing reaction is much more than the cut-surface one. Therefore, it can explain that the oxidation reacted on the surfaces is much more than that on the cut-surface at the temperature from 140 °C to 180 °C.

The relationships of curing temperature and N and O atomic concentrations are also showed in Fig. 1. From the figures, it can be found that on the cured NBR surface the tendency of the concentrations of N concentration is decreasing and the O concentration is increasing with the curing temperature growing. While, on the cut-surface of cured NBR there is no obvious change with the raise of curing temperature. When the curing temperature up to 160 °C, N start to be going down and O start to be going up on the surface of curing NBR. And when curing temperature is up to 180 °C, N atomic concentrate is down to 3.0 at.% and O concentrate is up to 5.9 at. %.

To clear the chemical structure on the surface and cut-surface of cured NBR high-resolution XPS analysis be employed. The differences of functional groups on the NBR surfaces cured at 140 °C and 180 °C are shown in Fig. 1a and 1b. As shown in Fig. 1, functional groups consisting of carbon, oxygen and nitrogen atoms, using the wave separation techniques of C1s peaks obtained from XPS analysis are investigated to know functional groups oxygen and nitrogen compounds in NBR cured at 140 °C. Carbon and carbon hydride in cured NBR appear as a main peak at the 284.7 eV of binding energy. Carbone hydride (CH_2) of adjacent nitrile groups (*CH_2CH(CN)*CH_2, *;corresponding carbon) are recognized at 285.4 eV as binding energy. Functional groups such as *CH(CN) groups and *C- OH groups which are linked directly to nitrile groups are predicted to be present overlapping at 286.6 eV as binding energy[10–13]. Both carbonyl (>*C=O) and carboxyl (-*COOH) groups are not recognized

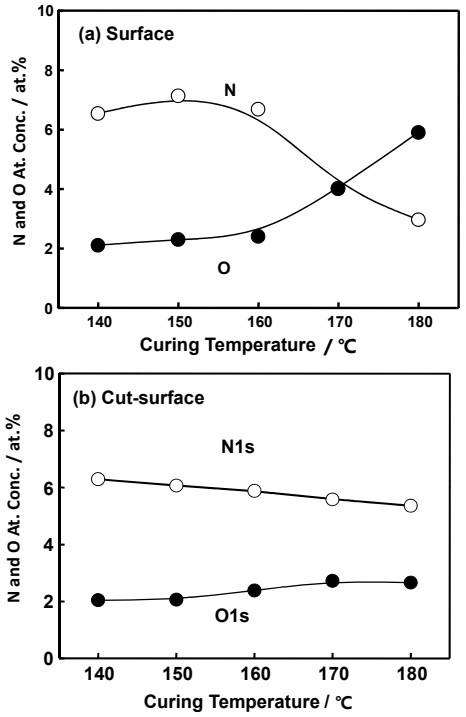

Fig. 1. **Effect of curing temperature on the N and O atomic concentration on DCP-cured NBR (a) surfacec (b) cut-surface**

in the case of 140 °C curing temperature, but carbonyl groups are recognized on the NBR surface cured at 180 °C.

Table I shows functional groups for C1s and component ratios of DCP-cured NBR surrounding the carbon atomics after different temperature (140 ºC, 150 ºC, 160 ºC, 170 ºC, 180 ºC,) curing processing. For the DCP-cured NBR at 140 ° C, the component ratios of >*CHOH groups on the surfaces are over that on the cut surface, while the component ratios of >*CHOH groups on the surfaces and cut-surfaces are roughly the same. With the curing temperature increasing, the atomic number of >*CN on the surface of NBR is decreasing which is consistent with the changes in the atomic ratios in Fig. 1.

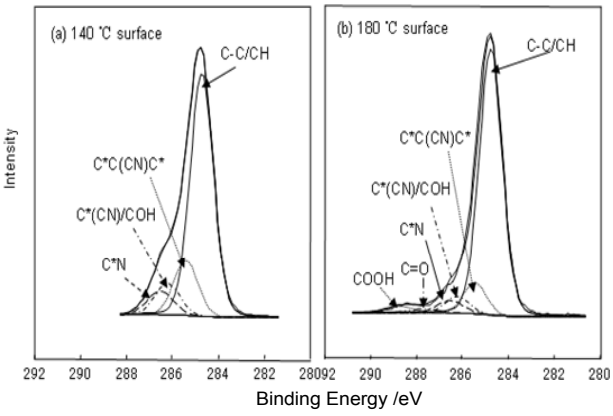

Fig. 2. **High-resolution XPS spectra of C 1s a) NBR surface cured at 140 °C, b) NBR surface cured at 180 °C**

Table I
Cls component in the surface of DCP-cured NBR at various temperatures

NBR	Curing Temp. / ℃	C1s component / at.%			
		>*CN	>*CHOH	>C=O	—COOH
		286.6 eV	286.3 eV	287.3 eV	288.8 eV
surface	140	6.9	2.6	0	0
	150	7	2.3	0	0
	160	6	2.5	0.1	0
	170	4.6	1.5	0.7	1
	180	4	0.8	1.4	2.2
Cut-surface	140	6.8	1.7	0.7	0
	180	6.5	1.8	0.9	0

And it is considered that with the curing temperature going up, >*CN groups returned from surface to the bulk. The quantity of chemical structure of >*CHOH is decreasing trend with the curing temperature up. This can indicated that >*CHOH was reacted into >C=O and -COOH.

Moreover, in the Table I it can be observed that at the curing temperature of 140 °C and 150 °C. There are no the chemical bond of >C=O and -COOH because it is difficult to performance under the low temperature. However, when the temperature up to 160 °C the reactions to form >C=O and -COOH started. And with the temperature increasing >C=O and -COOH is increasing. When the curing temperature up to 180 °C, >C=O and -COOH increased to 1.3 % and 2.2 %. While, the concentration of chemical structure of cut surface almost have no change with curing temperature and the -COOH groups are not recognized on the cured NBR cut-surface even in the curing temperature at 180 °C.

3.2. Curing temperature and AFM images

AFM has now become a relatively common tool, which is widely used in the study of materials. It is a powerful technique for distinguishing surface properties such as visco elasticity, stiffness, friction and adhesion of materials[14,15]. Formulti-component polymers, the differences in these properties for different regions of the surface can be translated into morphology especially from phase imaging AFM. AFM phase images of these blends in tapping mode displayed islands in the sea morphology or matrix-dispersed structures[16]. By using such a concept, AFM has been applied to the study of NBR to investigate the morphologies of NBR surfaces and cut-surface which cured at different temperatures. And the results are showed in Fig. 3.

From the topographic image of NBR cured at different temperature, it cannot be found obvious differences so it can be considered that the morphology of NBR surfaces cured at different temperatures are almost similar. However, according to the phase images the obvious different from 140 °C to 180 °C was observed. With the temperature going up, the black and white stripes come forth. While, they are not found in the topographic images. And these phase differences stand for the different hardness and different physics property on NBR surfaces cured at different temperatures. In the phase image of cured NBR at 140 °C, it shows the homogeneous surface, while at 180 °C white stripe can be considered as

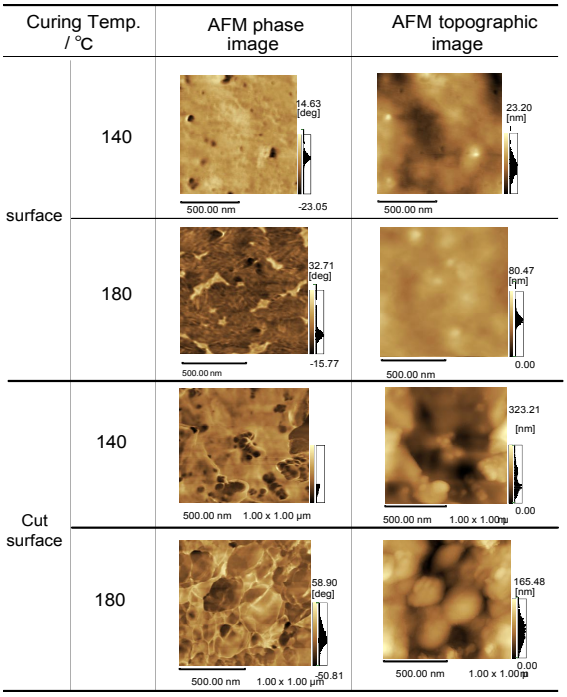

Fig. 3. **AFM images of NBR surface cured at different curing temperatures**

butadiene group and black stripe as acrylonitrile. At the high curing temperature as 180 °C butadiene phase are shown on the surface, acrylonitrile phase return from surface to the bulk. Therefore, the N concentration of NBR surface cured at 180 °C is smallest. And this result is also corresponding to the XPS result.

Further to research the phase image of inner NBR cured different temperatures, at 180 °C it shows the cured NBR polymeric agglomerate structures like a big polymer block, whereas, there are no obvious agglomerate structures on the NBR cut-surface. Because at 140 and 180 °C have different curing rate, and which is not sufficient after 30 min curing process at 140 °C.

4. Conclusion

XPS result showed that NBR surface compositions are different with curing temperature change. With the temperature increasing, the O concentration of DCP-cured NBR surface is increasing, while the N concentration has the reverse tendency.

AFM height images and phase images displayed the different morphology with islands in the sea morphology or polymeric agglomerate structures.

NBR with DCP, curing reaction and sub-reaction on the surfaces and cut-surface as well as chemical and physical properties are different.

REFERENCES

1. Matsukura K.: Nippon Gomu Kyokaishi. *393*, 44 (1971) (Japanese).
2. Kaneko H.: Polymer No Tomo, *672*, 11 (1980) (Japanese).
3. Dierkes W., Tiwari M., Guo R., Datta R., Talma A., Noordermeer J., Ooij W. V.: Rubber Chem. Technol., in press.
4. Khaled F., El N.: Materials & Design *3361*, 32 (2011).
5. Mori K., OishiY., Hirahara H., Iwabuchi A. J.: Polym. Sci. Technol. *629*, 50 (1993) (Japanese).
6. Mori K., Oishi Y., Hirahara H., Iwabuchi A.: Rubber Chem. Technol. *797*, 67 (1994).
7. Mori K., Oishi Y., Hirahara H.: Nippon Kagaku Kaishi. *281*, (2000).
8. Mori K.: Journal of Japanese Society of Tribologists *85*, 54 (2009).
9. Sang J., Hirahara H., Mori K., MastunoY., Kudo T., Aisawa S., Narita E., Oishi Y., Mori K.: Journal of The Society of Rubber Industry, Japan. *75*, 85 (2012) (Japanese).
10. Loan L. D.: Pure Appl. Chem. *175*, 30 (1972).
11. Baldwin F. P., Borzel P., Cohen C. A., Vander C.: Rubber Chem. Technol. *522*, 43 (1970).
12. Moore C. G., Mullins L., Mclswift P.: J. Appl. Polym. Sci. *293*, 5 (1964).
13. Farmer E. H.: J. Polym. Sci. *293*, 1 (1946).
14. Jeon I. H., Kim H., Kim S. G.: Rubber Chem. Technol. *1*, 76 (2003).
15. Mclean R. S., Sauer B. B.: Macromolecules *8314*, 30 (1997).
16. Urska S., Jozsef K. K., Matjaz K., Ralf T.: J. Appl. Polym. Sci. *E41*, 125 (2012).

CL-07
SURFACE CHARACTERISTICS OF POLYAMIDE 6 FILLED WITH CALCIUM CARBONATE AFTER FINISH TURNING

TADEUSZ CHWALCZUK, DAMIAN PRZESTACKI, and DANUTA CHMIELEWSKA

Institute of Mechanical Technology, Poznan University of Technology, ul. Piotrowo 3,60-965 Poznan, Poland
tadeusz.chwalczuk@put.poznan.pl

The machinability of Polyamide 6 (PA6) composite is presented. Samples of PA6 filled with calcium carbonate in different amount of mineral filler (5–20 wt.%) were mixed by means of twin screw extruder and compression moulded in form of rollers.

2D and 3D surface measurements were made after longitudinal turning with cemented carbide and PCBN inserts. The influence of process parameters like feed rate (f) and cutting speed (v_c) on surface roughness parameters was investigated. The analysis of *Ra*, *Rz*, *RSm*, *Rsk*, *Rku* parameters and bearing area ratio was presented. Assumptions about future surface functionality according to surface roughness parameter were made.

The results show that turning parameters have great influence on surface roughness parameters. The range of cutting parameters (f, v_c) and tool geometry has been determined to give proper surface topography. The analysis of power spectrum density (PSD) roughness profile proved that all machined geometrical structure had the cutting edge kinematics representation.

CL-08
NON-FLUID JUNCTION TECHNIQUE OF PEROXIDE CURED NBR

HIDETOSHI HIRAHARA, JING SANG, SUMIO AISAWA, KATSUHITO MORI, TAKAHIRO KUDO, EIICHI NARITA, YOSHIYUKI OISHI, and KUNIO MORI

The Graduate School of Engineering, IWATE University, 4-3-5 Ueda, Morioka IWATE 020-8551, Japan
hiraha@iwate-u.ac.jp

Key Words: NBR, Functional Structure, Adhere, Non-fluid Junction, Surface, XPS

1. Introduction

Over the last decade, with continuously growing demands for greater operating performance, the growth in the use of adhesives, especially in ever more technically demanding applications, has been rapid and many major developments in the technology of adhesion and adhesive have been reported[1,2]. Moreover, adhesion technology plays a decisive role in the field of basic material manufacture technology and the synthetic adhesive have great progress with the development of polymer. However, there are many defects during the process of adhesion using the adhesive, for instance, the burrs, boundary stress, strength, persistent and material dependence problems[3,4].

To resolve these traditional adhesive problems a method called molecule adhesion technology which can successfully adhere to different materials and has the advantages such as material independence and strong adhesion strength without any adhesive agent. The authors' research group have developed this method which succeed joined the different materials such as polymers, rubbers and by molecular adhesion of 6-triethoxysilylpropylamino-2,5-dithiol-1,3,5-triazine (TES)[5,6]. All materials (Polymer Material A) have functional groups on the surfaces through special discharge treatment[7,8] which can react with the molecular adhesion TES. According to this reaction the polymer link TES and form chemical bonds on material surfaces (Material A). Then adhesion between Material A and Material B are performed under optimum conditions which make TES and Material B react with each other on the interface. Adhesion occurs and exhibits strong adhesion strength when TES linked on Materials A reacts with Materials B (a kind of rubber or other polymer materials) for the formation chemical bonds on the interface[9–11].

The adhesion technology also have been aided greatly by the development of the tools, for example, specific surface analytical techniques, such as X-ray photoelectron spectroscopy (XPS) and secondary-ion mass spectroscopy (SIMS) which can put to good use in furthering our understanding of the science of adhesion[12]. In this work, acrylonitrile butadiene rubber (NBR) rheological processing was carried out at different temperatures and treated with TES. Cured NBR surfaces and after treated by TES were analyzed by XPS. The molecule adhesion used in the adhesion between the cured NBR are investigated.

2. Experimentals

Acrylonitrile-butadiene rubber (NBR, AN: 35%, N230S, JSR Co.) was used here, and base compounds and curing systems for NBR are NBR rubber (100 phr), carbon black (50 phr), stearic acid (1 phr) and stabilizer ZnO (5 phr). Those additives above were prepared by company. Then, the curing agent, dicumyl peroxide (DCP, reagent grade) was added to the base compounds by two-roll mixer. 6-Triethoxy-silylpropyl amino-2,5-dithiol-1,3,5-triazine (TES) was prepared by the reaction of triethoxysilylpropylamine, cyanuric chloride and NaSH in ethanol. 1H-NMR (400MHz, $CDCl_3$, ppm); 0.55 (t,2H, J=8.5Hz, CH_2Si,), 1.15 (t,9H,J=7.0Hz, CH_3), 1.48~1.56 (m,2H, $CH_2CH_2CH_2$), 3.20~3.25 (m,2H,CH_2N), 3.75(t,6H, J=7.0, CH_2O), and 7.33 (t,1H, J=5.5,NH). 13C-NMR (100MHz, $CDCl_3$, ppm); 7.14, 18.16, 22.47, 42.72, 57.67, 155.56, 177.64, and 182.36.

After blending the curing agent DCP, uncured NBR compound sheets which were folded between two 6-nylon (PA6: UBEPA6, 100 μm, heat softening temperature; 180 °C / 451 kPa) films and was employed the molding process with the hotpress condition at 140~180 °C for 30 min. PA6 films were peeled out from cured NBR at first after molding process, then the cured NBR samples were kept in vacuum for 24 hr as the analyze samples.

Cured NBR samples were immersed into 0.1% alcohol solution of TES at a room temperature for 10 min and after drying in an air, heated at 120 °C for 10 min to make TES-bond on NBR sheets. Obtained NBR samples are used as the samples for analysis and adhesion. The two TES-bond NBR sheets are superposed upon each other and pressed at 140 °C for 30 min to take adhesion process between cured NBR.

The surfaces and cut-surfaces of cured NBR rubbers were analyzed by XPS (PHI QUANTERA ESCA system) with the Multi Technique spectrometer, the focusing monochromator (ULVAC-PHI inc.) and Al Kα X-ray source which has 100 μm×100 μm spot for surface analysis. Pass energies of the analyzer were 69 eV for high-resolution scans at 300 W. The angle resolved measurements were made at an electron take-off angle of θ = 45° (θ is a angle between sample surface and direction of analysis photoelectrons). During the measurement process, the electron flood gun was used for charge neutralization and the analysis chamber remained at 3.0×10^{-6} Pa. The XPS spectra were subjected to Shirley background subtraction formalism and the data was using the saturated C 1s peak at 284.8 eV and which were used in chemical-bonding-state assignments. The full width at half maximum (FWHM) of C-C/C-H component was left to vary freely and the other components were fixed to adopt this value. All the XPS experimental curves were fitted to Gaussian-Lorentzian lines of variable proportion using

Mutipak software.

NBR adhesion products were evaluated with peeling tests for adhesion properties between TES-bond-NBR's interface. The peeling test was carried out following tensile machine (JIS K-6854-4) according to the 180 ° type peeling test at a crosshead speed of 100 mm min^{-1} and 25 °C room temperature.

3. Results and discussion

3.1. Analysis of surfaces of DCP-cured NBR at different curing temperatures

Chemical structures of DCP-cured NBR surfaces were investigated by XPS. The High-resolution XPS spectra of C1s peaks of NBR surface cured at different temperature are shown in Fig. 1. From Fig. 1 it reveals (*CH(CN), *;corresponding carbon) and *C-OH group peak overlapped at 286.6 eV on the surfaces of NBR cured at the temperature from 140 °C to 180 °C. In addition, at the binding energy of 288.8 eV carboxyl (-*COOH) group peak obviously be obserbed in the spectra of NBR surface cured at 180 °C (ref.[13,14]). As can be seen from the spectrum, at the curing temperature is 140 °C the (-*COOH) peak was not observed, and with the curing temperature is going to be higher up to 170 °C, (-*COOH) peak come out and with the curing temperature raising the intensity of (-*COOH) peak is going stronger than the spectra of NBR cured at low curing temperature. Therefore, it was indicated that the oxide functional group (-*COOH) reacted during the curing processing by DCP. It can be said that the NBR surface is easier oxidized at high curing temperature than at low curing temperature. Moreover, (*CH(CN), *; corresponding carbon) and *C-OH group peak is going weaker with the curing temperature going up. It also can be considered that the functional groups which reacted on the surfaces at different curing temperatures are different.

3.2. Reaction of cured NBR with TES

After curing process, cured NBR surface treated by the molecular adhesive (6-triethoxysilylpropylamino-1,3,5-triazine-2,4-ditiols, TES) has been investigated to clarify the reaction mechanism between NBR and TES. The Chemical structures of cured rubber surfaces treated by TES were also investigated by X-ray photoelectron spectroscopy.

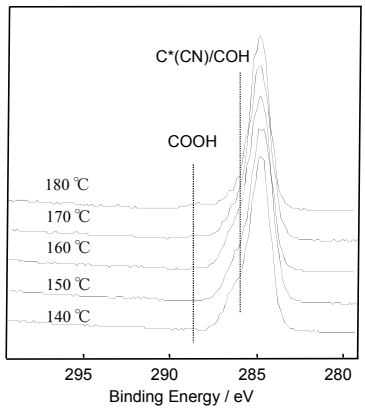

Fig. 1. **High-resolution XPS spectra of C 1s peaks of NBR surface cured at different curing temperature**

Fig. 2 shows the high-resolution XPS spectra of the C 1s photoelectrons of TES treated NBR surfaces, which cured at different curing temperatures. The results showed that the peak of COOH disappeared for the NBR surfaces treated at over 160 °C after the treatment by TES, which is indicating that COOH functional groups were reacted in with TES. It is considered the oxidation compounds getting from the curing process can have reactions with TES after the immersion and heating treatments. As can be seen from the spectra, S2p, be observed on the surfaces of NBR cured at all the temperatures which elements belong to TES. This indicated that TES can react with the functional group on cured NBR surfaces at the curing temperature from 140 °C to180 °C.

S2p core level spectra of TES treated NBR surfaces, which cured at different curing temperatures, were showed in Fig. 2b. The high-resolution XPS spectra are deconvoluted into three component peaks revealing two $2p_{3/2}$ and $2p_{1/2}$ peaks at 162.08 eV and 164.0 eV, 167.0 eV respectively as expected from the spin splitting of the 2p electrons of S2p, which shows that composition of the chemical structures are C=S, S-S / SH and SOx for TES treated NBR surfaces[15,16]. Table I shows a summary of the chemical structure bond results about S2p after curve fitting. From the Table I, it can figure out that the quantity of C=S of the NBR surface cured at 140 °C treated after TES is the most than other NBR surfaces cured at 150 °C to 180 °C, whereas, the S-S group concentration is the fewest than any other surfaces.

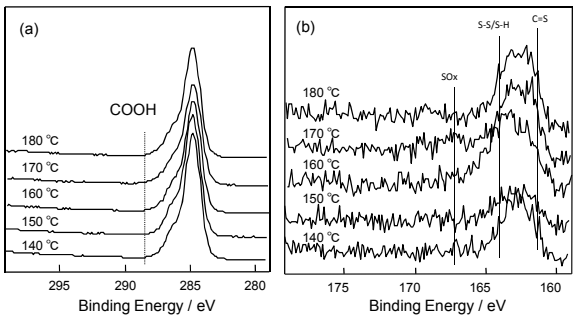

Fig. 2. **XPS spectra at different curing temperature after TES surface treatment (a) C1s (b) S2p**

Table I
Functional groups for S2p components on DCP surfaces at different curing temperature after treated by TES

Curing temp.	140℃	150℃	160℃	170℃	180℃
C=S (162.08 eV)	62.0	43.2	31.5	36.5	38.0
S-S/S-H(164.0)	28.3	47.4	44.2	52.4	46.3
SOx (167.0eV)	9.7	9.4	24.3	11.1	15.7

3.3. Non-fluid adhesion between NBR treated by TES

Direct adhesion between the same NBR treated by TES without any adhesive were employed by hot-press at 140 °C and under the adhesion pressure of 1.1×10^{-5} kN m^{-2}. After Peel the curing temperature of NBR influenced strength in the adherents. The interfacial surface microstructure between the adhered NBR after the peel measurement has been investigated by scanning electron microscopy (SEM).

The results of non-fluid adhesion between the same treated NBR of curing and TES treatment by the peel measurement is shown in Fig. 3. The NBR cured at 140 °C showed strongest peel strength (10.1 N cm^{-1}) than other cured temperatures. While when the curing temperature at 150 °C, the peel strength is 7.1 N cm^{-1}, fracture phenomenon occurred during the peel tests. However, when the curing temperature at over 160 °C, the peel strength of NBR are getting lower as 3.6 N cm^{-1}, 2.7 N cm^{-1}, 3.1 N cm^{-1}, respectively. All of the three couples NBR sheets had peeled off from each other. This can explain that adhesion between the same NBR were directly adhered result to the reaction between SH which was proved by the XPS results that on the NBR surface curing at 140 °C. According to the result of XPS S-S bonds can be not produced that much on the NBR cured at 140 °C during the reaction with TES, which is shown in Table I. After the TES treatment, when the group of S-S much more reacted, there are no much enough functional groups on the surface to react with the same treatment surface each other during the adhesion process. Moreover, It is possible that during TES treatment, -*COOH structures on the NBR surfaces cured at the temperature over 160 °C were dissolved in the solvent of ethanol. Afterwards, the quantity of chemical structures is getting fewer to react to each other during the adhesion process.

The results of Photos of rubber breaking and the interface SEM after non-fluid adhesion between the same treated NBR of curing and TES treatment by the peel measurement are shown in Fig. 4. When the curing temperature is over 160 °C, although NBR did not show strong peel strength during the peel test, the surface after peel

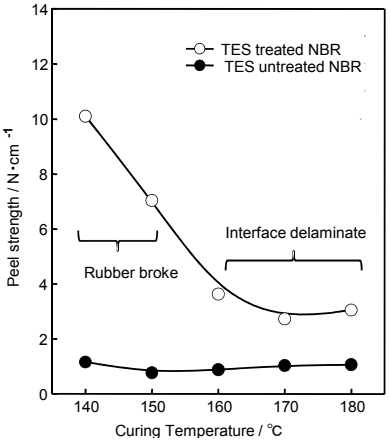

Fig. 3. **Effect of curing temprature on the peel strength of adherents between NBR using molecular adhesives** (TES 0.1 wt. %)

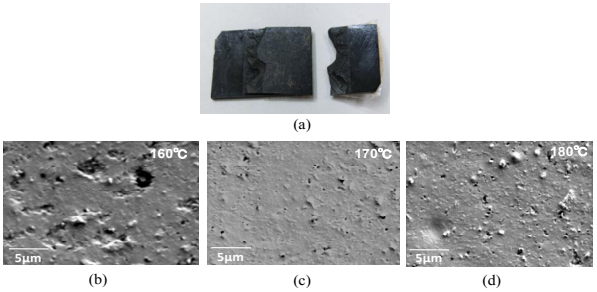

Fig. 4. **Photos of rubber breaking and the interface SEM microstructure of NBR after peel measurement, Curing temperature (a) 140 °C and 150 °C (b) 160 °C (c) 170 °C (d) 180 °C**

test are characterized delamination traces. It can be explain that NBR cured over 160 °C after treated by TES adhered under pressure at 140 °C can also react with each other.

4. Conclusion

From the XPS result, it is cleared that the functional structures formed on the NBR surfaces cured at different curing temperatures are different.

TES can be successfully reacted on the cured NBR surface after TES treatment. And adhesion products fabricated during hot-press adhered process between the same treatment NBR sheets which were cured at 140 °C and 150 °C showed the high peel strengths and fractured during the peel test. Adhesion between the same NBR were directly adhered result to the reaction between SH which was proved by the XPS results.

Cured NBR surface treated by the molecular adhesive can be successfully non-fluid adhered to each other by molecules adhere technology.

REFERENCES

1. Kinloch A. J.: J. Mater. Sci. *2141*, 15 (1980).
2. Kang B. U., Jho J. Y., Kim J. K., Lee S. S., Park M., Lim S., Choe C. R.: J. Appl. Polym. Sci. *38*, 79 (2001).
3. Kaelble D. H.: J. Adhes. *205*, 37 (1992).
4. Marshall S. J., Bayne S. C., Baier R., Tomsia A. P., Marshall G. W.: Dental Mater. *e11*, 26 (2010).
5. Hirahara H., Aisawa S., Mori K., Narita E., Oishi Y.: Surf. Interface Anal. *953*, 35 (2003).
6. Mori K., Shi X., Hirahara H., Oishi Y.: Rubber Chem. Technol. *1019*, 76 (2003).
7. Reilly B.: Rubber World *26*, 246 (2012).
8. Zaldivar R. J., Steckel G. L., Morgan B. A., Nokes J. P., Kim H. I.: J. Adhes. Sci. Technol. *381*, 26 (2012).
9. Hachisuka S., Nakayama J., Mori K., Hirahara H., Oishi Y.: J. Adhesion Sci. Technol. *725*, 17 (2003).
10. Martineza L., lvareza L., Huttela Y., Mendeza J., Romana E., Vanhulselb A., Verheydeb B., Jacobs R.: Vacuum *1489*, 81 (2007).
11. Mitra S., Ghanbari-Siahkali A., Kingshott, P., Rehmeier H. K., Abildgaard H., Almdal K.: Polym. Degrad. Stabil. *81*, 91 (2006).

12. Jin J., Cassell R. A., Pacholski M. L.: Tech. Meet Rubber Div. Am. Chem. Soc. *1558*, 178th. 3 (2010).
13. Mousa A., Heinrich G., Simon F., Wagenknecht U., Stochelhuber K. W., Dweiri R.: Mater. Res. *671*, 15 (2012).
14. Huang G. B., Chen S. Q., Tang S. W., Gao J. R.: Mater. Chem. Phys. *938*, 135 (2012).
15. Mohamed M. N., Hamdani S.: Appl. Surf. Sci. *3073*, 252 (2006).
16. Kang Z X.; Lai X. M., Sang J., Li Y. Y.: Thin Solid Films *800*, 520 (2011).

CL-09
RUBBER COMPOUNDS WITH INCORPORATED CRUMB RUBBER

JÁN KRUŽELÁK[a]*, VALÉRIA HAMADOVÁ[b], ALENA KŇAZEOVÁ[b], and IVAN HUDEC[a]

[a] Slovak University of Technology in Bratislava, Faculty of Chemical and Food Technology, Institute of Polymer Materials, Department of Plastics and Rubber, Radlinského 9, 812 37 Bratislava, [b] Vegum, a.s.,Gumárenská 337, Dolné Vestenice, Slovakia
jan.kruzelak@stuba.sk

The aim of the work was the study of preparation and properties of rubber compounds based on styrene-butadiene and butadiene rubber with applied crumb rubber. The crumb rubber based on styrene-butadiene rubber, with different granulometry, was used as a substitution of the part of rubber in the rubber compounds. The rubber crumb was applied in original and modified forms in various concentrations. The study was focused on the preparation of rubber compounds and evaluation of the rubber crumb influence on the curing characteristics, cross-link density and physical-mechanical properties of prepared materials. The influence of thermo-oxidative ageing on the evaluated properties was also investigated.

The commercial compound based on styrene-butadiene rubber SBR (DSSK 2560 M27) and butadiene rubber BR (NEOCIS BR 40) provided by VEGUM a.s., Dolné Vestenice, Slovak Republic was used. Besides rubbers and carbon black as a filler, the rubber compounds contained components of curing system, antidegradants, plasticizers and other processing additives. The content of filler (79 phr) and other additives (81 phr) was kept constant in all experiments. The crumb rubber with granulometry 0.2 mm and 0.4 mm in unmodified form, and also after its subsequent surface modification (only crumb rubber with granulometry 0.2 mm, in the work specified as 0.2 mm M) was dosed to the rubber compounds as a substitution of the part of styrene-butadiene rubber, not as a filler. The amount of crumb rubber in rubber compounds changed from 0 to 40 phr. The detailed characterization of applied crumb rubber is mentioned in Table I.

The modification of crumb rubber was carried out by means of chemical accelerators, generally used in rubber industry, in the laboratory mixer BANBURY. The total time of mixing was 7 min. The crumb rubber was fist mixed at 60 °C for 2 min. The modificative reagents were then added and temperature increased up to 90 °C. The mixing process continued for next 5 min.

Table I
Characteristics of crumb rubber

Characteristics	0.2 mm	0.4 mm
Specific surface area [m^2/g]	8.43	9.71
Total porosity [%]	13.44	8.92
Specific volume of pores [cm^3/g]	7.7×10^{-3}	7.89×10^{-3}
Density [g/cm^3]	1.11	1.14
Average radius of pores [nm]	4892	3923

The rubber compounds were prepared in the laboratory mixer WERNER-PFLEIDERER GT 2ST in two mixing steps. The curing process was performed at 160 °C for the optimum cure time under a pressure of 20 MPa. The physical-mechanical properties were determined in accordance with the valid technical standards. The Flory-Rehner equation modified by Krause for filled vulcanizates was introduced to determine the cross-link density of prepared materials. For ageing test (70 °C, 168 h) the Geer method was used.

From Fig. 1 it is obvious that by incorporation of 5 phr of crumb rubber into the original sample, the optimum cure time t_{C90} was found to decrease (from about 6.5 min to approximately 2.5 min). With next increasing of crumb rubber content, the optimum cure time did not change significantly and ranged from 2.5 to 3 min, independently on the amount of crumb rubber incorporated.

The rubber compounds filled with modified crumb rubber required the shortest time essential for their curing process.

The cross-link density n_{ch} of prepared vulcanizates first decreased when 5 phr of unmodified crumb rubber was incorporated into rubber compounds, but with the next increasing of crumb rubber content, the cross-link density tends to slightly increase (Fig. 2). The cross-link density of vulcanizates with 30 and 40 phr unmodified crumb rubber (0.2 mm) achieved approximately the same values in

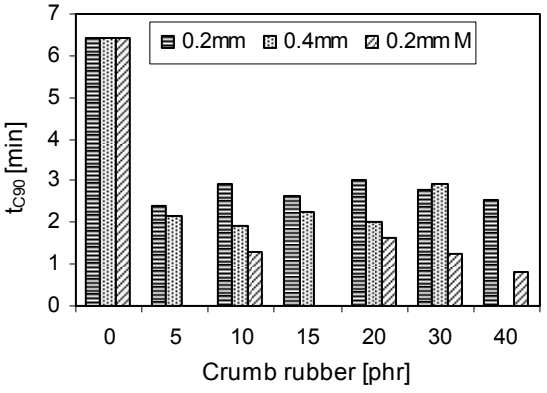

Fig. 1. **Influence of crumb rubber content on optimum cure time t_{C90} of rubber compounds**

comparison with the cross-link density of the reference. As seen in Fig. 2 the highest values of cross-link density were spotted in case of vulcanizates with modified crumb rubber.

The differences in the values of n_{ch} of tested materials with modified and unmodified crumb rubber are attributed to the surface modification of crumb rubber, during which the active centers on its surface are formed. This leads to the higher interactions and adhesion between the rubber matrix and the particles of crumb rubber and it is estimated that sulphur cross-links are not formed only between the macromolecules of the rubber matrix, but also between the rubber matrix and the particles of crumb rubber.

As a consequence of thermo-oxidative ageing, the values of cross-link density of test samples with unmodified crumb rubber increased in comparison with corresponding values n_{ch} of vulcanizates before ageing (Fig. 2). The increase of the cross-link density during thermo-oxidative ageing can be attributed to the additional cross-linking of the rubber. This presumption is also supported by the change of physical-mechanical properties of vulcanizates, mainly by increasing values of moduli and decreasing values of elongation at break of examined vulcanizates after thermo-oxidative exposure in comparison with the original values before ageing. In case of vulcanizates with modified crumb rubber (besides the sample with 40 phr of crumb rubber), there was recorded the decrease of cross-link density after thermo-oxidative ageing.

The influence of crumb rubber content and thermo-oxidative ageing on physical-mechanical properties of prepared materials is illustrated in Fig. 3, 4. As seen in Fig. 3, the elongation at break exhibits the decreasing trend with increasing content of crumb rubber. Compared to the reference, there was possible to observe more than 40 % decrease of elongation at break of the sample with maximum 0.2 mm unmodified crumb rubber. In case of vulcanizates with 0.4 mm crumb rubber, the 40 % decrease of elongation at break was achieved by applying of 30 phr crumb rubber. The most significant decrease of elongation at break was shown by incorporation of modified crumb rubber. The

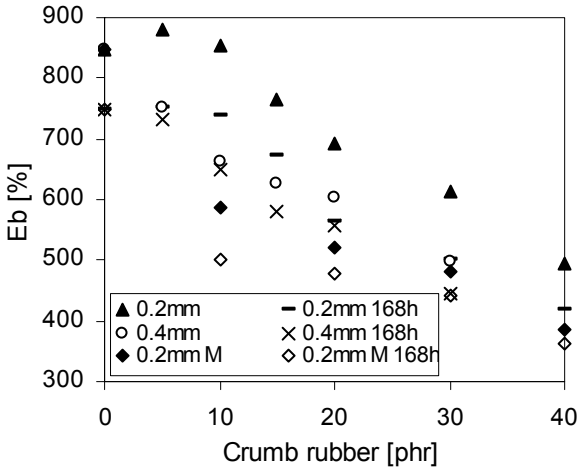

Fig. 3. **Influence of crumb rubber content and thermo-oxidative ageing on elongation at break Eb of vulcanizates**

tensile strength at break of prepared vulcanizates as a function of crumb rubber content was also examined as shown in Fig. 4. It becomes obvious that the tensile strength at break decreased in ranged from 2 to 3 MPa when 5 phr of crumb rubber was incorporated in rubber compounds. Then, the values of tensile strength fluctuated in the low range, almost independently on the amount of crumb rubber. From Fig. 4 it is possible to observe that higher values of tensile strength at break were obtained by applying of crumb rubber with granulometry 0.2 mm (modified and also unmodified).

Based upon the results obtained by the study of influence of thermo-oxidative ageing, it can be stated, that this process affects the evaluated properties in various ways. But almost all evaluated properties of vulcanizates after ageing remained character of their variations depending on

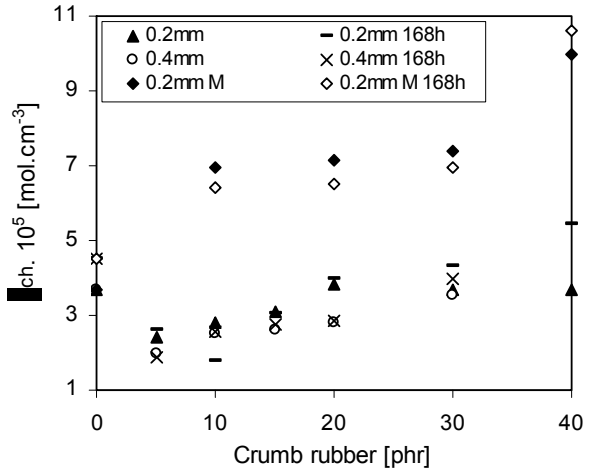

Fig. 2. **Influence of crumb rubber content and thermo-oxidative ageing on cross-link density n_{ch} of vulcanizates**

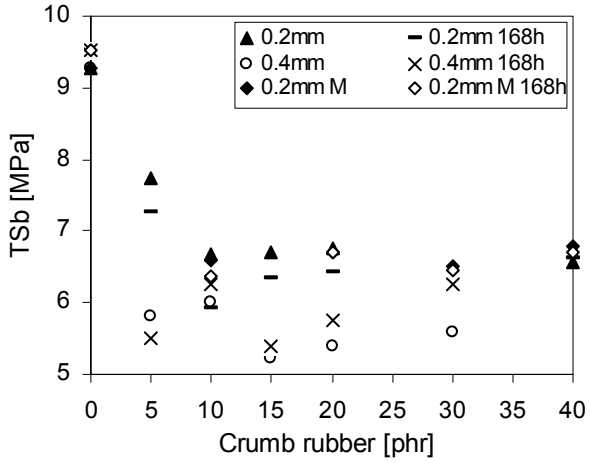

Fig. 4. **Influence of crumb rubber content and thermo-oxidative ageing on tensile strength at break TSb of vulcanizates**

the content of crumb rubber incorporated The values of physical-mechanical properties of vulcanizates after ageing are higher or lower in comparison with corresponding values of vulcanizates before thermo-oxidative degradation.

The achieved results point out the possibilities of preparation of rubber materials with applied crumb rubber by the processes used in rubber technologies. Seeing that the incorporation of examined type of crumb rubber into the rubber compounds leads mainly to the decrease of tensile strength at break of equivalent vulcanizates, the efficient methods of crumb rubber modifications should be developed, in order to improve the compatibility and adhesion between the rubber matrix and the particles of crumb rubber.

The authors like to thank to Vegum, a.s., Dolné Vestenice for supporting this work.

CL-10
STABILIZING EFFECT OF LIGNIN IN RUBBER BLENDS

JANKA KUBAČKOVÁ*[a], JOZEF FERANC [a], IVAN HUDEC[a], ŠTEFAN ŠUTÝ[a], and JOZEF PREŤO[b]

[a] Slovak University of Technology in Bratislava, Faculty of Chemical and Food Technology, Institute of Polymer Materials, Radlinského 9, 812 37 Bratislava, [b] VIPO, a.s., Partizánske, Slovakia

Introduction

Lignin has been long time viewed as a waste material with limited utilization as a fuel. However, in the recent years there has been an explosion of research of lignin-based products. Development of lignin value-added products has several economic and environmental benefits. Lignin can be used to substitute fossil based materials in wide range of products, from plastics to individual chemical products and carbon fiber and contribute to higher usage of raw materials from renewable resources.

Lignin is one of the main constituents of wood and is available in large amounts. Chemically, lignin is a crosslinked macromolecular polyphenolic material which arises from copolymerization of three phenylpropanoid monomers – coniferyl, sinapyl and *p*-coumaryl alcohols. Lignin is a highly branched, three-dimensional polymer with a wide variety of functional groups providing active centers for chemical and biological interactions. In wood, the lignin is primarily a structural material to add strength and rigidity to cell walls and its content generally ranges from 19 to 35 %. Except of mechanical function, lignin is noted for its protective function in plants. In comparison with cellulose, lignin is more resistant to biological attack and moreover increases plants stability to sunlight and frost. Lignin shows antimicrobial and antifungal activity, acts as antioxidant, exhibit flame-retardant properties and serve to adhesion of the cellulose fibers. In addition, there are many factors which promote industrial utilization of lignin, such as availability in huge amounts, reasonable price, a number of reactive points in the structure, good compatibility with several chemicals, good rheological and viscoelastic properties etc. On the other side, many difficulties complicate its application in industrial products. Low purity, heterogeneity, odour and color of lignin-based product are problems, which should be overcome[1–3].

In our previous works, the basic exploration of lignin application in model as well as in real rubber blends was reported[4,5]. It was shown that commercial calcium lignosulfonate significantly improves tensile properties of NR vulcanizates and affects the vulcanization process. In the next work, it was proved that lignin can be used as a replacement of carbon black in quite wide range of concentrations without changing the evaluated properties, which could lead to the cheaper rubber blends. In the present work, we tested lignin as a stabilizer in carbon black filled NR/SBR blends. The prepared blends were submitted to accelerating thermo-oxidative aging. The physical-mechanical properties as well as crosslink density of vulcanizates before and after aging were measured. Efficiency of lignin stabilizing properties was compared with synthetic antioxidant.

Experimental

Materials

The batch of natural rubber SMR 5, styrene-butadiene rubber Kralex 1502 and carbon black N550 was used. Calcium lignosulfonate CA 120 in the form of brown powder and IPPD (*N*-phenyl-*N*-isopropyl-*p*-phenylene diamine) were added as stabilizers. The semi-EV vulcanization system was composed of sulphur and sulphenamide accelerator CBS (*N*-cyclohexyl-2-benzothiazyl sulphenamide).

Methods

The components for rubber blends are given in Table 1. Mixing of batch and other ingredients except of curing additives was carried out in chamber of Plasticorder Brabender at mixing temperature 80 °C and a rotor speed of 70 rpm. Prepared blends were vulcanized in hydraulic press at 150 °C, pressure 20 MPa and time corresponding to optimum cure time (t_{c90}). Cure characteristics of the rubber blends were examined using RPA 2000 at 150 °C. Mechanical properties of vulcanizates (tensile strength and elongation at break) were measured using Zwick Roell at crosshead speed of 500 mm min^{-1}. Tested dumbbell shaped specimens for tensile tests were cut from the 2 mm thick molded slabs. Crosslink density of prepared vulcanizates was determined on specimens with dimensions 10 × 10 × 2 mm, immersed in 1% solution of IPPD in xylene at room temperature to reach swelling equilibrium. The crosslink density was calculated using Flory-Rehner equation. Accelerating thermo-oxidative aging was carried out on dumbbell specimens in an air-circulating oven for 72 and 168 hours at 70 °C. Tensile properties and crosslink density were measured before and after aging.

Table I
Composition of rubber blends

	B1	B2	B3	B4	B5
NR	80	80	80	80	80
SBR	20	20	20	20	20
N550	40	40	40	40	40
CA120	0	0	1	2	1
IPPD	0	1	0	0	1
ZnO	5	5	5	5	5
Stearin	2	2	2	2	2
Sul-phur	2	2	2	2	2
CBS	2	2	2	2	2

Content of all ingredients in Table I is expressed in phr.

Results and discussion

Antioxidant activity of commercial stabilizers consists in limiting or retarding of oxygen and heat effects. A wide variety of chemicals have been found that exhibit antioxidant activity in elastomers. Typical antioxidants include substituted phenols and amine materials which are more effective. Lignin is hindered phenolic polymer which can act as stabilizer of reaction induced by oxygen and its radical species[6,7]. FTIR spectrum of the tested lignin (Fig. 1) has a wide band between 3500–3100 cm^{-1} assigned to OH stretching vibrations. This band is caused by presence of alcoholic and phenolic hydroxyl groups. Especially, phenolic hydroxyl groups may have significant influence on the stabilization of rubber blends. The phenolic content and compatibility between the additive and rubber matrix are important factors for the antioxidant activity of lignin.

The influence of IPPD and lignin on the obtained vulcanization characteristics of carbon black filled rubber blends are shown in Table II. The effect of used stabilizers isn't significant, but there are some differences in the behavior of blends with content of lignin and blends with content of IPPD. The scorch time $\mathbf{t_{s1}}$ of blends containing IPPD is slightly lower in comparison with standard blend without stabilizer (B1) and also in comparison with blend containing lignin. Moreover, addition of IPPD causes slight decrease of optimum cure time $\mathbf{t_{c90}}$. Vice versa, the lignin increases scorch time as well as optimum cure time.

Table II
Vulcanization characteristics

	t_{s1}	t_{c90}
B1	6,10	10,44
B2	5,49	9,65
B3	6,38	11,99
B4	6,22	10,77
B5	5,51	10,37

In order to investigate stabilization effect of lignin in NR/SBR blends, the prepared vulcanizates were exposed to thermo-oxidative aging at 70°C for different time period (3 and 7 days). The mechanical properties of tested aged specimens were determined relative to original values (Figs. 2-4). Tensile strength and elongation at break of non-stabilized vulcanizates significantly decreased with extending aging time probably due to degradation processes. On the other hand, samples stabilized with lignin or IPPD were more stable towards accelerating aging. Vulcanizates with lignin content 1 or 2 phr exhibited better retention of tensile properties than that with addition of IPPD or mixture of IPPD and lignin after 3 days of aging. Samples with addition of lignin had even more than 100% retention of elongation at break. The best retention of evaluated properties after 168 hours of thermo-oxidative aging had samples with IPPD in amount of 1 phr, but almost the same retention of tensile characteristics was displayed in case of samples stabilized with 1 phr of lignin. Hardness of prepared vulcanizates slightly increased in all specimens during aging. Based on the obtained results, lignin doesn't increase stabilization effect of commercial antioxidant IPPD.

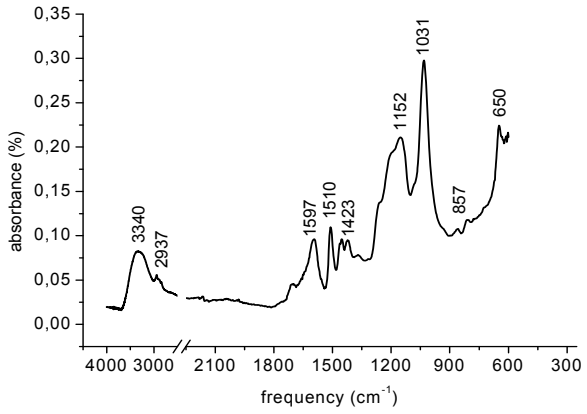

Fig. 1. **FTIR spectrum of tested lignin**

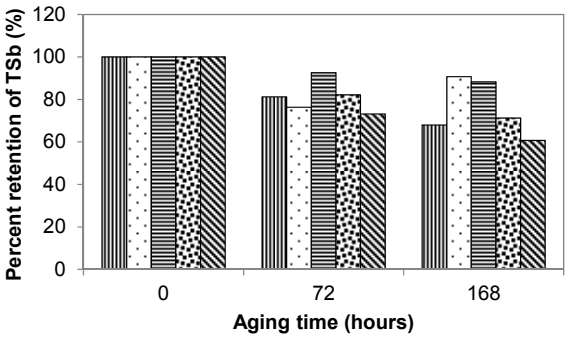

Fig. 2. **Plot of percent retention of tensile strength at break vs. aging time of NR/SBR vulcanizates;**
without stabilizer 1phr IPPD 1 phr lignin
2 phr lignin 1 phr IPPD + 1 phr lignin

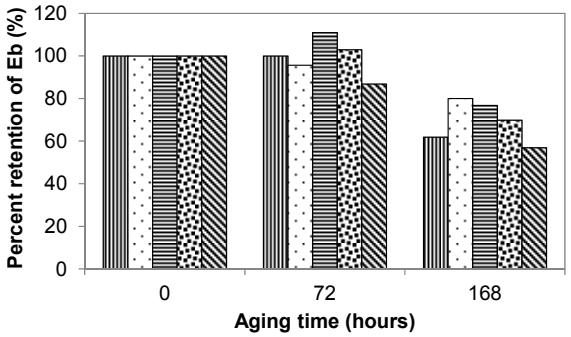

Fig. 3. **Plot of percent retention of elongation at break vs. aging time of NR/SBR vulcanizates;**
without stabilizer 1phr IPPD 1 phr lignin
2 phr lignin 1 phr IPPD + 1 phr lignin

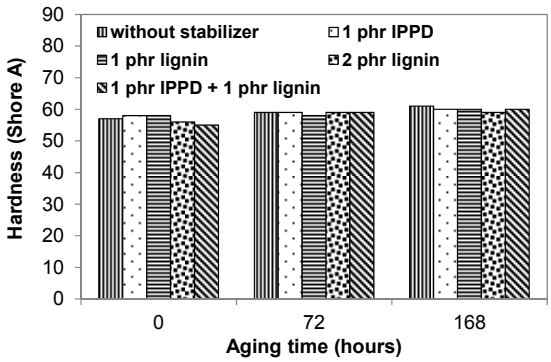

Fig. 4. **Hardness vs. aging time of NR/SBR vulcanizates**

Fig. 5 shows the influence of aging time on the crosslink density of prepared vulcanizates stabilized with IPPD, lignin or with the mixture of 1 phr IPPD and 1 phr lignin. It is seen, that aging caused increasing of crosslink density in all studied samples probably because of dominant crosslinking reactions during aging.

Conclusion

The obtained results showed that tested lignin powder has a potential to be used as an antioxidant in carbon black filled NR/SBR blends. Lignin in amount of 1 phr acted as stabilizer and its stabilizing effect was comparable with commercial rubber antioxidant IPPD. These results indicate the possibility of lignin to substitute commercial product IPPD.

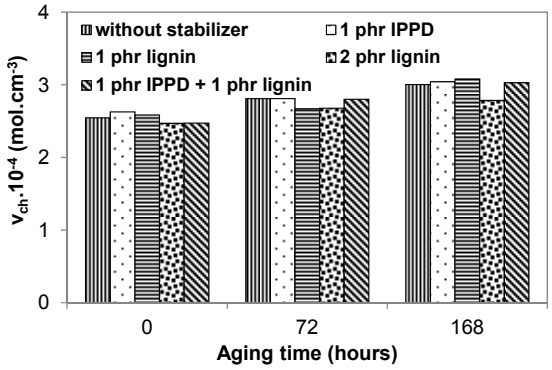

Fig. 5. **Crosslink density vs. aging time of NR/SBR vulcanizates**

This work was supported by Ministry of Education of Slovak Republic project No.26220220091 by the Research & Development Operational Program funded by the ERDF.

REFERENCES

1. Mancera C., et al.: Biomass and Bioenergy *35*, 2072 (2011).
2. Doherty W. O. S., Mousavioun P., Fellows F. M.: Industrial Crops and Products *33*, 259 (2011).
3. Thielemans W., Can E., Morye S. S., Wool R. P.: J. Appl. Polym. Sci. *83*, 323 (2002).
4. Kubačková J., Hudec I., Feranc J.: Chem. Lett. *105*, 352 (2011).
5. Kubačková J., Hudec I., Feranc J.: Elastomery *16*, 5 (2012).
6. Pouteau C., et al.: Polymer Degrad. Stab. *81*, 9 (2003).
7. Gregorová A., Košíková B., Moravčík R.: Polymer Degrad. Stab. *91*, 229 (2006).

CL-11
TEMPERATURE INFLUENCE OF RUBBER TESTING SAMPLES DURING ITS PREPARATION

KAMIL KYAS, VLADIMIR PATA, MICHAL STANĚK, MARTIN BEDNAŘÍK, ALEŠ MIZERA, and JAN NAVRÁTIL

Tomas Bata University in Zlin, Department of Production Engineering, Nam. T.G.Masaryka 275,762 72 Zlin, Czech Republic
kyas@ft.utb.cz

Abstract

Injection molding is one of the most widespread technologies in polymer process. Advantages of this technology were found in rubber industry too. But each product of every technology has to be tested for receiving its properties. By making a testing samples by cutting the sample can be influenced by temperature or pressure and it can lost

original properties. This poster shows laboratory device which was constructed for preparing rubber samples. It is checked by thermal camera Flir and proves that sample isn't influenced by using this device.

1. Introduction

Rubber injection molding of rubber began in the early 1940s. Today, the process is used for manufacturing a wide range of industrial products. Injection molding of rubber is a process whereby a rubber mix is injected into a closed mold where the material is shaped to the desired geometry. When the cavity is filled, temperature gradients persist in the rubber. With having completely filled the cavity rubber mix is vulcanized.

Infrared light or thermography is the use of an infrared imaging and measurement camera to "see" and "measure" thermal energy emitted from an object. Thermal, or infrared energy, is light that is not visible because its wavelength is too long to be detected by the human eye; it's the part of the electromagnetic spectrum that we perceive as heat. Unlike visible light, in the infrared world, everything with a temperature above absolute zero emits heat. Even very cold objects, like ice cubes, emit infrared.

The higher the object's temperature, the greater the IR radiation emitted. Infrared allows us to see what our eyes cannot. Infrared thermography cameras produce images of invisible infrared or "heat" radiation and provide precise non-contact temperature measurement capabilities. Nearly everything gets hot before it fails, making infrared cameras extremely cost-effective, valuable diagnostic tools in many diverse applications. And as industry strives to improve manufacturing efficiencies, manage energy, improve product quality, and enhance worker safety, new applications for infrared cameras continually emerge.

The most important feature of a surface that affects the amount of energy radiating from it in stationary thermal conditions is its emissivity. If a surface whose temperature is to be measured had the properties of a black body, the radiant exitance for fixed temperature and wavelength could be determined from Planck's law. However, under real conditions Planck's law determines only a limiting (maximum) estimate of the thermal flux density. This is a consequence of the fact that all physical bodies have limited absorbing capacity; that is, they do not satisfy Planck's postulate referring to a black body.

Therefore, it is necessary to introduce a parameter determining the absorbing capacity of a body's surface.

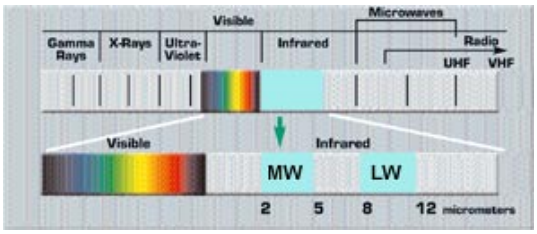

Fig. 1. **IR spectrum**

The emissivity ε of a body over the full radiation range, called the total emissivity, is the ratio of full-range radiant exitance M(T) of that body to full-range radiant exitance Mb (T) of a black body at the same temperature.

$$\varepsilon(\lambda) = \frac{M(T)}{Mb(T)}$$

2. Experiment

In this part of research amount of temperature influence was verified. The part was a cube with dimension 30 × 30 × 30 mm. It was prepared by injection molding technology and it is prepared for testing tensile strength and shore A. For testing in each layer of products, it has to be divided. These layers must have identical cross section in whole length and it mustn't be influenced by temperature in cutting process.

It had to be invited laboratory device for dividing rubber and softened materials.

This device consists of tool, special vice and propulsion mechanism. The cutting tool consists of two parts. The first is a toothless rotary disc with a defined edge of tool steel. The second part is used to clamp the chuck which is called the tool body and is made of ordinary structural steel. One of the biggest advantages is the versatility; the tool can be clamped to any chuck. During the process of division is important to

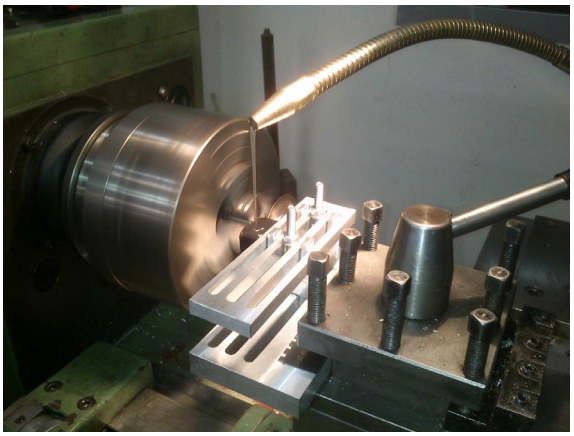

Fig. 2. **Laboratory device for dividing rubber material**

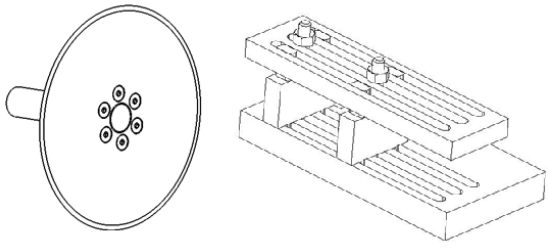

Fig. 3. **Left – Tool (rotary disc); Right – special vice for softened material**

Table I
Setting of Thermal camera

Emissivity – Object	0,950	
Distance – Object	1.5	m
Reflected temperature	23.0	˚C
Optic's temperature	20	˚C
Optic's transmission	1	s
Atmospheric temperature	18	°C
Relative humidity	75	%
Computed transmission	0,99	

Fig. 4. **Scanning device by TC Flir 660**

use a cooling medium. If cutting parameters are optimized layers smaller than 1mm can be easily split. This device is mental protected by no. PUV2012-26920.

Cutting process was recorded by thermal camera FLIR SC660. Its parameters are: IR resolution 640 × 480 pixels, thermal sensitivity 30 mK at 30 °C, spectral range 7.5–13 µm, temperature range –40 °C to +1500 °C and others. Camera was set according to Tab. I.

3. Results and discusion

As it was told, cut product was very intensively cooled by emulsion. In lathe there was set 560 rpm. Secondary movement by vice which was fastened in tool head was done manually.

Recorded video took 38 minutes. It started to record 10 second before cutting a stopped 10 second after. From this video it could be taken plenty of results which were evaluated in software ThermoCAM Researcher Professional 2.10. It is important to say that emissivity was set for rubber cube therefore results was observed there. In this cover of cube there were created three horizontal sections for measuring in software. In the beginning of measuring temperature of sample was the same as atmospheric temperature. In Fig. 5 is sample of evaluation of measuring in 10 s. There can be seen

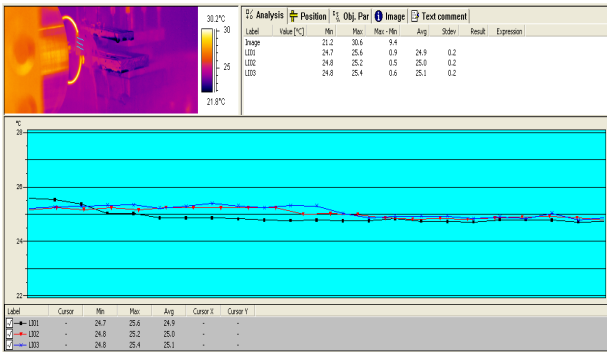

Fig. 5. **Results from software in 10 sec**

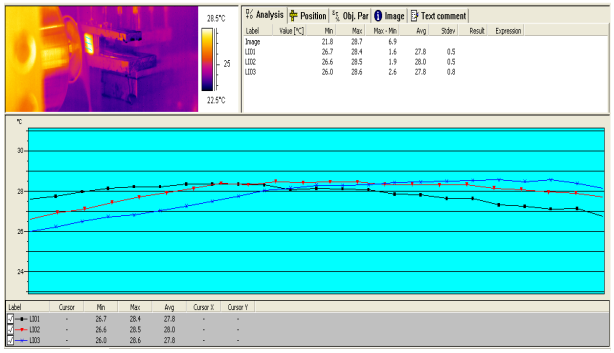

Fig. 6. **The highest temperature in product**

that temperature is almost same in whole section. In Fig. 6, there can be seen the highest temperature of all measuring. It was situated in the center of cube and it was 28,5 °C.

4. Conclusion

This laboratory device is ready to use for dividing rubber and softened material. As it was proved; product and each cut layers aren't affected by high temperature. Cooling emulsion is sufficient for conducting away heat which is caused by friction in cutting process.

This paper is supported by the internal grant of TBU in Zlin No. IGA/FT/2013/020 funded from the resources of specific university research and by the European Regional Development Fund under the project CEBIA-Tech No. CZ.1.05/2.1.00/03.0089.

REFERENCES

1. Manas D., Manas M., Stanek M., Danek M.: Arch. Mater. Sci. Eng. *32*, 69 (2008).
2. Kyas K., Stanek M., Manas M., Stanek M., Krumal M., Holik Z.: Chem. Listy *105*, s354 (2011).
3. Manas D. et al.: Thin Solid Films *530*, 49 (2013).

CL-12
MICROHARDNESS OF POLYMERS POLY(BUTYLENE TEREPHTHALATE) PBT

DAVID MANAS, MIROSLAV MANAS, MICHAL STANEK, MARTIN OVSIK, PETR KRATKY, JAKUB JAVORIK, and MARTIN BEDNARIK

Tomas Bata University in Zlin, Faculty of technology, Department of Production Engineering, nam. T.G. Masaryka 275, 762 72 Zlin, Czech Republic
dmanas@ft.utb.cz

Abstract

Hard surface layers of polymer materials, especially polypropylene, can be formed by chemical or physical process. One of the physical methods modifying the surface layer is radiation cross-linking. Radiation doses used were 0, 30, 45, 60 and 99, 132, 165, 198 kGy for unfilled Poly (butylene terephthalate), PBT with the 5% cross-linking agent (triallyl isocyanurate). Individual radiation doses caused structural and micromechanical changes which have a significant effect on the final properties of the PBT tested The improvement of micromechanical properties was measured by an instrumented microhardness test.

Introduction

Poly (butylene terephthalate), PBT, is a commercially important engineering polymer with a wide range of applications such as injection molding and extrusion. As a member of the polyester family, it is also often used as the matrix material in glass fiber reinforced composites, having attractive mechanical properties, good moldability and fast crystallization rate. PBT has some processing advantages over its chemical relative, poly (ethylene terephthalate), PET[1–4]. The melting temperature of PBT is about 230 °C, which is lower than PET, (ca. 270 °C), allowing PBT to be processed at lower temperatures. In addition, PBT has a lower glass transition temperature, a faster crystallization rate.

The irradiation cross-linking of thermoplastic materials via electron beam or cobalt 60 (gamma rays) proceeds is proceeding separately after the processing. The cross-linking level can be adjusted by the irradiation dosage and often by means of a cross-linking booster[1–4].

The main deference between β- and γ -rays is in their different abilities of penetrating the irradiated material. γ-rays have a high penetration capacity (Fig. 1). The penetration capacity of electron rays depends on the energy of the accelerated electrons.

The thermoplastics which are used for production of various types of products have very different properties. Standard polymers which are easy obtainable with favourable price conditions belong to the main class. The disadvantage of standard polymers is limited both by mechanical and thermal properties. The group of standard polymers is the most considerable one and its share in the production of all polymers is as high as 90 %.

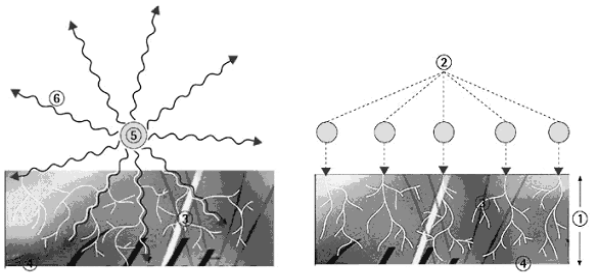

a b

Fig. 1. **Design of Gamma rays (a) and Electron rays (b);** a) 3 – secondary electrons, 4 – irradiated material, 5 – encapsulated Co – 60 radiation source, 6 – Gamma rays, b) 1 – penetration depth of electron, 2 – primary electron, 3 – secondary electron, 4 – irradiated material

The engineering polymers are a very important group of polymers which offer much better properties in comparison to those of standard polymers. Both mechanical and thermal properties are much better than in case of standard polymers. The production of these types of polymers takes less than 1 % of all polymers[1–4].

High performance polymers have the best mechanical and thermal properties but the share in production and use of all polymers is less than 1 %.

Common PBT, when exposed to the effect of the radiation cross-linking, degrades and its mechanical properties deteriorate. Using cross-linking agent TAIC (triallyl isocyanurate) produces a cross-linking reaction inside the PBT structure. The utility properties of PBT improve when the noncrystalline part of PBT is cross-linked.

The present work deals with the influence of morphology on the microhardness of irradiated crosslinked PBT.

Experimental part

For this experiment poly (ethylene terephthalate) V-PTS -CREATEC-B3HZC * M800/25 nature; PTS Plastics Technologie Service, Germany (unfilled, PBT+TAIC, MFR – 230 °C /2.16 kg – 7 g/10 min) was used. The material already contained a special cross-linking agent TAIC – triallylisocyanurate (5 volume %), which should enable subsequent cross-linking by ionizing β-radiation. The prepared specimens were irradiated with doses of 33, 66, 99, 132, 165 and 198 kGy at BGS Beta-Gamma Service GmbH & Co. KG, Germany[1–4].

The samples were made using the injection molding technology on the injection molding machine Arburg Allrounder 420C. Processing temperature 240–260 °C, mold temperature 75 °C, injection pressure 80 MPa, injection rate 65 mm s^{-1}.

Instrumented microhardness tests were done using a Micro Combi Tester, CSM Instruments (Switzerland) according to the CSN EN ISO 6507-1. Load and unload speed was 2 N min^{-1}. After a holding time of 90 s at maximum load 1 N the specimens were unloaded. The indentation hardness

H_{IT} was calculated as maximum load to the projected area of the hardness impression according to:

$$H_{IT} = \frac{F_{max}}{A_p} \quad \text{with} \quad h_c = h_{max} - \varepsilon \frac{F_{max}}{S} \qquad (1)$$

Where h_{max} is the indentation depth at F_{max}, h_c is contact depth. In this study the Oliver and Pharr method was used calculate the initial stiffness (S), contact depth (h_c). The specimens were glued on metallic sample holders [1–5].

Results and discussion

The values measured during the microhardness test showed that the lowest values of indentation microhardness and microhardness Vickers were found for the irradiated PBT by dose of 33 kGy. On the contrary, the highest values of indentation hardness were obtained for PBT irradiated by a dose of 165 kGy (by 15 % higher in comparison with the irradiated PBT by dose 33 kGy), as can be seen at Fig. 2.

According to the results of measurements of microhardness, it was found that the highest values of indentation modulus of elasticity were achieved at the PBT irradiated with dose of 165 kGy (by 9 % higher than compared with non-irradiated PBT). On the contrary, the lowest values of the indentation modulus of elasticity were found for irradiated PBT by dose 198 kGy as is seen at Fig. 3.

Material deformation in time under constant stress (indentation creep) measured by instrumented test of microhardness showed (Fig. 4) that the highest creep values were measured on non-irradiated PBT (8,2 %), while the lowest creep value was found in PBT irradiated by 198 kGy dose (5,6 %). The creep dropped by 31 % as a result of radiation, which represents a considerable increase of surface layer resistance.

Conclusion

Very interesting results were obtained for irradiation modified PBT. When comparing the irradiated and non-irradiated (irradiated by dose 33 kGy) PBT it was apparent that the values of indentation microhardness, Vickers microhardness and the indentation modulus considerably increased, in some cases even by 15 % at the irradiation dose of 165 kGy.

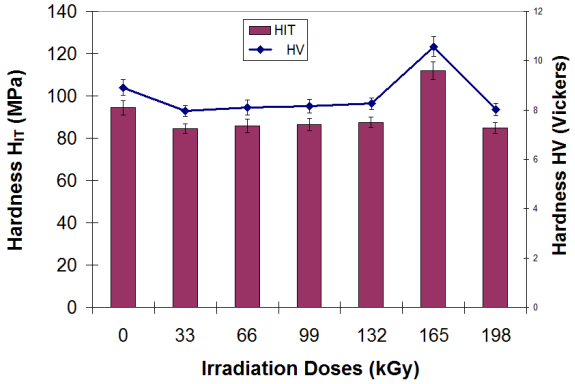

Fig. 2. **Indentation and Viskers microhardness of PBT**

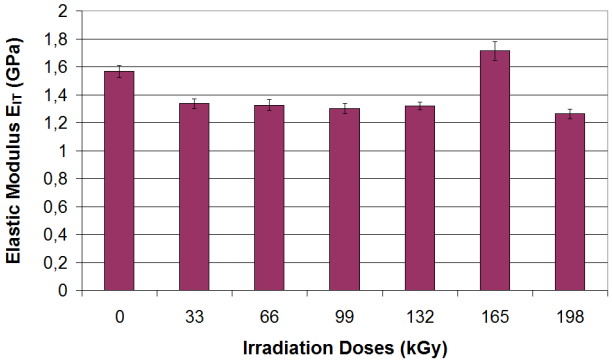

Fig. 3. **Elastic indentation modulus of PBT**

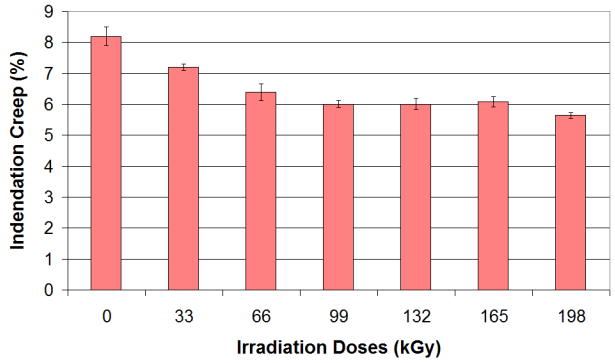

Fig. 4. **Indentation creep of PBT**

This paper is supported by the internal grant of TBU in Zlin No. IGA/FT/2013/020 funded from the resources of specific university research and by the European Regional Development Fund under the project CEBIA-Tech No. CZ.1.05/2.1.00/03.0089.

REFERENCES

1. Manas D., Manas M., Stanek M., Danek M.: Arch. Mater. Sci. Eng. *32*, 69 (2008).
2. Oliver W. C., Pharr G. M.: J. Mater. Res. *7*, 1564 (1992).
3. Chvatalova L., Navratilova J., Cermak R., Raab M., Obadal M.: Macromolecules *42*, 7413 (2009).
4. Manas D., et al.: Thin Solid Films *530*, 49 (2013).
5. Gilbert M., Hybart F.: J. Polymer *13*, 327 (1972).

CL-13
A COMPARISON OF MATERIAL PROPERTIES FOR MAGNETORHEOLOGICAL AND CONVENTIONAL ELASTOMERS

JENNIFER MCINTYRE[a,b] and STEPHEN JERRAMS[b]

[a] German Institute for Rubber Technology (DIK), Eupener Straße 33. D-30519 Hannover, Germany, [b] Dublin Institute of Technology, Focas Research Institute, Dublin 8, Ireland
Jennifer.mcintyre@dikautschuk.de

Abstract

A magnetorheological elastomer (MRE) compound was tested and compared to a reference material. An anisotropic specimen of the material exhibited an increase in shear storage modulus, G' of approximately 50 %, which corresponded to 1 MPa for this material. Isotropic specimens of the composite showed a reduced tensile strength and increased elongation at break compared to the reference material. These differences were attributed to variations in the hardness and zero-field modulus of the materials as a result of alterations in their recipes. The MRE material experienced lower values of maximum stress.

Introduction

Anisotropic magnetorheological elastomers (MREs) are adaptive composite materials consisting of chains of magnetic particles in an elastomer matrix. These particles are added to the matrix during the compounding stage prior to curing in the presence of an external magnetic field so that the particles are aligned into chains along the magnetic field lines (see Fig. 1). Components fabricated from these smart materials respond to changes in magnetic flux density. The magnetic interactions between the particles resist external forces applied to the material thereby raising the shear modulus and hence increasing the stiffness of the composite material. These properties can be controlled by increasing the magnetic flux density of an external magnetic field. One potential advantage of such a material is in damping of vibrations in automotive applications where the stiffness and thus the damping ability of the material, could be tuned to suit the vibrations encountered in service.

In order to be suitable for industrial applications, product engineers must be confident that the materials will withstand dynamic stresses and strains that can be anticipated in their normal use.

Materials

The MREs investigated consisted of an optimised recipe containing a 25 % volume fraction of carbonyl iron particles (CIP), Grade SW-S from BASF. Some plasticizer was added to soften the mixture and a small amount of retardant was added to increase the incubation time of the material's vulcameter curve, allowing more time for the alignment of the magnetic particles. The reference material contained no magnetic powder but had a much higher quantity (50 phr) of carbon black. No plasticizer was added to this reference material. The MRE material had a hardness of approximately Sh A 40 and the reference material had a hardness of Sh A 65.

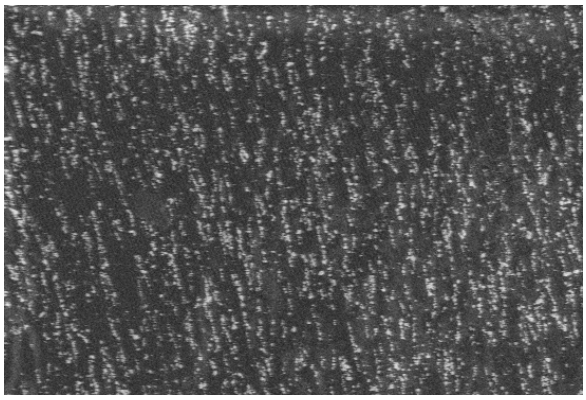

Fig. 1. **SEM image of an MRE (200 phr CIP)**

Two samples of the same MRE mixture were vulcanised, the first placed in a press that had been heated to 45 °C before the magnetic field was switched on. The press was heated to 160 °C and the mixture vulcanised for a period of $7^1/_2$ m.

The second sample was placed in a press at 60 °C and a magnetic field of 600 mT was applied. The material was allowed to heat very slowly for approximately 30 m until the temperature within the mould reached 130 °C. At this point the heating was increased to the maximum set-point and the temperature rose rapidly to 160 °C. This resulted in an extended period where there the magnetic particles were free to move and to align before cross-linking occurred. The material was allowed to vulcanise for $7^1/_2$ m.

Results and discussion

Uniaxial Testing

A Zwick 1445 universal test machine was employed to conduct a tensile test on three isotropic specimens (containing homogenously dispersed CIP) to determine the ultimate tensile stress (UTS) and elongation at break of the MRE material. The MRE material was found to have a tensile strength of 9 MPa, approximately a third of that of the reference material (30 MPa). The results of the uniaxial testing are summarised in Table I. At almost 650 % the elongation at break was higher for the MRE material than that of the reference material (480 %). This makes sense because the hardness of the MRE material is much lower than that of the reference material.

Many researchers have observed a decrease in tensile strength when magnetic particles are added to a rubber compound[1,2]. However, it should be noted that the higher quantity of carbon black increased the tensile strength in the reference material and that the addition of softener (plasticizer) increased the elongation at break in the MRE material. As with all filled rubbers, dispersion of filler plays a significant role in the properties of the material. Similar MRE recipes with higher tensile strengths are possible and recipes can be adjusted to suit the required application[3].

Table I
Summary of uniaxial test programme

Tensile testing	MRE (NR-400 SW-S)	Ref (D4)
UTS (MPa)	9.1	29.9
Elongation at break (%)	648.8	480.8
Multi-hysteresis	Max. stress (MPa)	Max. stress (MPa)
30 % strain	0.5	1.5
70 % strain	0.6	2.6
120 % strain	0.9	5.2

Quasi-static cyclic testing was conducted on two specimens of the MRE material that were cycled at strains of 30 %, 70 % and 120 % for a total of three cycles at each strain. The same tests were carried out with a reference material: five specimens to determine UTS and three specimens for the quasi-static cycling. The maximum stresses experienced by the MRE material were much lower than those experienced by the reference material. Although testing was not continued until failure, it is reasonable to assume that the MRE material would have a longer lifetime than the reference material.

Preliminary crack growth investigations have shown that the addition of micro-sized magnetic particles is not initially harmful to the rubber mixture[4]. However, oxidation of iron particles may reduce the lifetime of MRE materials[5].

Rheometric testing

Anisotropic specimens of both materials were sheared in an Anton Paar Physica MCR 501 plate-plate rheometer, which contains a magnetic coil. The magnetic field was switched on and off every 20 s and the magnetic flux density increased in steps of 200 mT up to a maximum value of 1 T. The samples were 2 mm thick. Plots of change in shear modulus as the magnetic flux density was raised are shown in Fig. 2 and 3 and the results are summarised in Table II. The two MRE specimens show clear increases in G' in the presence of a magnetic field while the reference material shows a negligible change.

Conclusions

It has been suggested that in order to obtain MREs with a high magnetorheological effect, the matrix viscosity must be quite low[6,2]. This could limit MREs to soft materials of low zero-field modulus which would in turn limit the applications of such materials. The research described here suggests that this is not necessarily the case. Although the matrix viscosity does hinder the alignment of magnetic particles, it is possible to produce composites with reasonably high mechanical properties which exhibit a significant MR effect.

As the particle diameters of commercial CIPs tend to be quite small (approximately 2–10 μm), they are unlikely to act as stress raisers and so cause problems in filled materials provided they are well-dispersed. Reductions in material properties are more likely to occur when particles agglomerate or as a result of increased chemical activity which would accelerate ageing[5].

Table II
Summary of rheometric results

Sample	CIP [phr]	G_0 [MPa]	G_1 [MPa]	ΔG [MPa]	$\Delta G/G_0$ [%]
SW-S	400	2.30	3.24	0.94	41
SW-S slow heating	400	2.15	3.30	1.15	54
Reference material	0	0.79	0.80	0.01	1

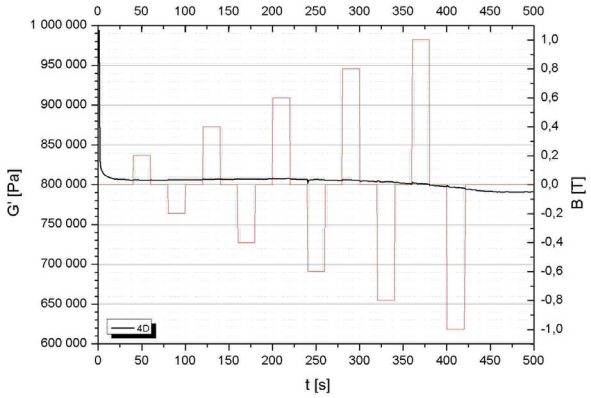

Fig. 2. **Rheometric plot of reference material**

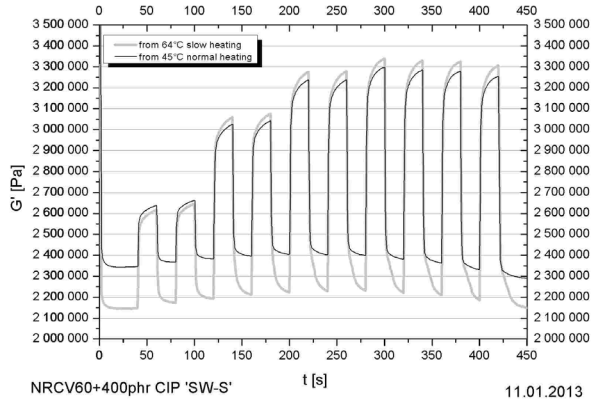

Fig. 3. **Rheometric plot of MRE material**

REFERENCES

1. Chen L., Gong X. L., Li W. H.: Polym. Test. *27*, 340 (2008).
2. Chen L., Gong X. L., Jiang W. Q., Yao J. J., Deng W. H, Li W. H.: J. Mater. Sci. *42*, 5483 (2007).
3. McIntyre J.: "Development of magnetorheological elastomers for automotive applications." *Tire Technology*

Expo 2013 Cologne, February 2013. Retrieved from ukintepress website: http://www.ukintpress-conferences.com/uploads/SPTTX13/ d3_s1_p5_jennifer_mcIntyre.pdfKlippen.
4. McIntyre J., Jerrams S., Steinke T., Maslak A., Wagner P., Möwes M., Alshuth T., Schuster R.: in *7th European Conference on Constitutive models for Rubber* (ECCMR) p.313. CRC Press/Balkema Press 2011.
5. Lokander M., Reitberger T., Stenberg B.: Polym. Degrad. Stabil. *86*, 467 (2004).
6. Boczkowska A., Awietjan S. F.: J. Mater. Sci. *44*, 4104 (2009).

CL-14
PRE-TREATMENT OF BEECH WOOD BY RADIO-FREQUENCY DISCHARGE PLASMA

IGOR NOVÁK[a], ANTON POPELKA[a], IVAN CHODÁK[a], JÁN SEDLIAČIK[b], VLADIMÍR VANKO[c], and ANGELA KLEINOVÁ[a]

[a] Polymer Institute, Slovak Academy of Sciences, Dúbravská cesta 9, 845 41 Bratislava 45, [b] Faculty of Wood Sciences and Technology, Technical University in Zvolen, Department of Furniture and Wood Products, T. G. Masaryka 24, 960 53 Zvolen, [c] VIPO, a.s., Partizánske, Slovakia
igor.novak@savba.sk

Abstract

The low-temperature discharge plasma has been used to improve the wetting and adhesion properties of wood. The pre-treatment of wood surface using discharge plasma is attractive for various wood applications mainly because of their lower cost. However, we have identified a significant increase of polar component of wood surface energy after modification by low-temperature plasma. Polar component of surface energy is associated with the presence of acid-base forces (electron donor–acceptor bonds). The treatment of wood exhibited a substantial aging effect, but the modified surface never recovers to its initial hydrophobic state. The enhancement of wood wettability is a necessary condition to promote a better adhesion with a water-based adhesives and coatings, which is currently being studied.

Introduction

The bonding of wood after discharge plasma surface modification is of considerable interest with the respect to construction of the strongest wood adhesive joints (1-6). Great efforts have been made in developing various kinds of furniture using wood or plastics veneers in adhesive joints wood-adhesive-veneer. The radio-frequency (RF) discharge plasma at reduced pressure is currently an efficient method for modificatuion of surface and adhesive properties of wood, and is considered as the 'green' ecologically friendly method (4, 7). For a common industrial wood application various woods have to possess a large set of various surface characteristics, including polarity (hydrophobicity or hydrophilicity), dyability, scratch resistance, tailored adhesive properties, antibacterial resistance etc. Nanoscale changes to the surface of wood materials enable the changes in materials surface, while maintaining the desirable bulk material properties.

In experimental work we have been focused to study of surface and adhesive properties of beech (Fagus sylvatica) wood modified by RF discharge plasma.

Experimental

Materials

Beech wood plates with dimensions 50 × 15 × 5 mm (TU in Zvolen, Slovakia), ChS Epoxy 510, Telalit T 410 (Spolchemie, Czech Republic), set of 5 testing liquids (water, ethylene glycol, formamide, diiodmethane, 1-bromo-naphthalene), dichlorometane.

Modification method

In this paper the beech wood surface was pre-treated by RF discharge plasma. There are two reasons why in the case of wood to apply discharge plasma modification. Firstly, discharge plasma in air itself significantly increases hydrophilicity of the wood, because of formation various polar groups (e.g. hydroxyl, carbonyl, carboxyl, etc), and, the wood macromolecules are also cross-links (up to a few microns) what leads to the increase in scratch resistance and to the improvement in barrier properties of the wood material. Second reason for the plasma use is an increase of adhesion in adhesive joint between wood substrate, that is important for industrial applications due to growth of wood wettability.

The modification of wood by the capacitively coupled RF (CCRF) plasma was performed in a laboratory CCRF plasma reactor (Scheme 1) working at reduced pressure 80 Pa consists of two 240-mm brass parallel circular electrodes with symmetrical arrangement, 10 mm thick, between which CCRF plasma was created.

The electrodes of CCRF plasma reactor are placed in a locked-up stainless steel vacuum cylinder. The one is powered and the other one is grounded together with steel cylinder. The voltage of CCRF plasma reactor is 2 kV, frequency 13.56 MHz, current intensity was 0.6 mA, and the

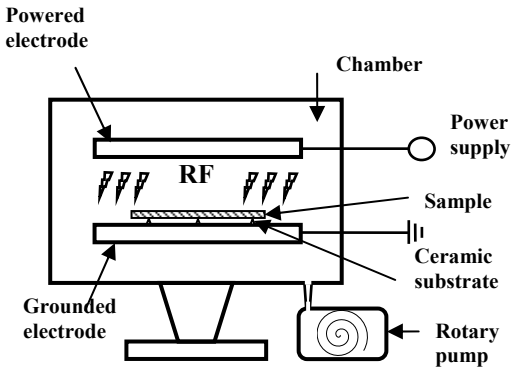

Scheme 1. **Scheme of CCRF plasma source**

max. power of the CCRF plasma source is 1200 W. The wood samples were modified by CCRF plasma at the power 300 W.

The improvement of hydrophilicity and/or hydrophobicity of the wood, its surface properties, the improvement of strength of adhesive joint of wood/wood composites with epoxy adhesive were studied for the determination of the appropriate structure of the plasma modified wood surfaces.

The surface energy of beech wood was determined using contact angles measurements with selected testing liquids set using SEE (Surface Energy Evaluation) device completed with a web camera (Advex, Czech Republic), and necessary PC software.

The drop of the testing liquid (V = 20 μl) was placed with a micropipette (Biohit, Finland) on the polymer surface, and a contact angle of the testing liquid was measured. The contact angle of testing liquid drop on the wood surface was measured instantly after its placing. The surface energies of wood were evaluated by Owens-Wendt-Rabel-Kaelble (OWRK) equation (7).

Results and discussion

The contact angle of water drop on the beech wood surface was measured immediately after drop deposition. The contact angles of water decreased with time of the activation by CCRF plasma. The contact angles of water showed a steep decrease from 66° (pristine sample) to 40° after 120 s activation of wood by CCRF plasma in air. The decrease of the contact angles of polar testing liquid (water) can be explained by an increase of the hydrophilicity of beech wood surface due to the treatment by CCRF plasma in air. The hydrophilicity of the surface depends on the formation of polar oxygenic functional groups on wood surface during the plasma modification in air. After saturation of the polymer surface with polar groups the hydrophilicity was stabilized.

The surface energy and its polar component of beech wood increased with time of plasma activation. The surface energy of beech wood treated 120 s by CCRF plasma in air increased from 66 (pristine sample) to 78 mJ m^{-2}, and the polar component of the surface energy increased from 17.4 (pristine sample) to 27.2 mJ m^{-2} (120 s). If the longer activation time was applied the changes od surface energy and its polar component were very small. This fact relates to saturation of wood surface with oxygen-containing functional groups due to modification by CCRF plasma.

The shear strength of adhesive joint beech wood modified by CCRF plasma in air – epoxy adhesive vs. activation time increased non-linearly from 5.2 MPa (pristine wood) up to 7.8 MPa (120 s activation by CCRF plasma).

Conclusions

The contact angles of water deposited on beech wood surface showed a steep decrease after activation by CCRF plasma in air. The surface energy and its polar component of beech wood increased with time of activation by plasma. The surface energy of beech wood treated by CCRF plasma in air increased from 66 (pristine sample) to 78 mJ m^{-2}, and the polar component of the surface energy increased from 17.4 to 27.2 mJ m^{-2}. The shear strength of adhesive joint of beech wood using epoxy adhesive increases non-linearly with activation time from 5.2 to 7.8 MPa.

Authors are grateful to financial supports by the Ministry of Education of the Slovak Republic project No. 26220220091 by Research & Development Operational Program funded by ERDF, as well as the project „Application of Knowledge-based Methods in Designing Manufacturing Systems and Materials“ the project No. MESRSSR 3933/2010-11,and project of the Slovak Academy of Sciences (Grant VEGA 2/0185/10).

REFERENCES

1. Kiguchi M.: *Surface modification and activation of wood*. In: Hon D. N. (Ed.) S. chemical modification of lignocellulosic materials, pp. 197–227. Marcel Dekker, New York 1996.
2. Kamdem D. P., Pizzi A., Triboulot M. C.: Holz-Roh-Werkstoffe *58*, 253 (2000).
3. Wolkenhauer A., Avramidis G., Hauswald E., Militz H., Viol W.: Int. J. Adhes. Adhes. *29*, 18 (2009).
4. Denes R., Tshabalala A., Rowell R., Denes F., Young A.: Holzforschung *53*, 318 (1999).
5. Acda M. N., Devera E. E., Cabangon R. J., Ramos H. J.: Int. J. Adhes. Adhes. *32*, 70 (2012).
6. Moghadamzadeh H., Rahimi H., Asadollazadeh M., Hemmati A. R.: Int. J. Adhes. Adhes. *31*, 816 (2011).
7. Frihart C. R.: *Handbook od wood chemistry and wood composites*, Rowell R. M. (Ed.), Chapter 9: Wood Adhesion and Adhesives, p. 216–277. CRC Press, London 2005.
8. Novák I., Popelka A., Krupa I., Chodák I., Janigová I., Nedelčev T., Špírková M., Kleinová A.: Vacuum *86*, 2089 (2012).

CL-15
AKROMID LITE AND XTRALITE – THE LIGHWEIGTH POLYAMID FOR TECHNICAL PARTS

ONDREJ OSTROLUCKÝ

K. D. Feddersen CEE GmbH Member oft he Feddersen Group Fachgasse 35-37, A-1150, Vienna, Austria
Ondrej.Ostrolucky@kdfeddersen.com

CL-16

EFFECT OF BETA LOW IRRADIATION DOSES ON THE INDENTATION HARDNESS OF GLASS FIBER-FILLED POLYPROPYLENE

MARTIN OVSIK* , DAVID MANAS, MIROSLAV MANAS, MICHAL STANEK, MARTIN BEDNARIK, and PETR KRAKTY

Tomas Bata University in Zlin, Faculty of Technology, Department of Production Engineering, TGM 5555, 760 01 Zlin, Czech Republic
Ovsik@ft.utb.cz

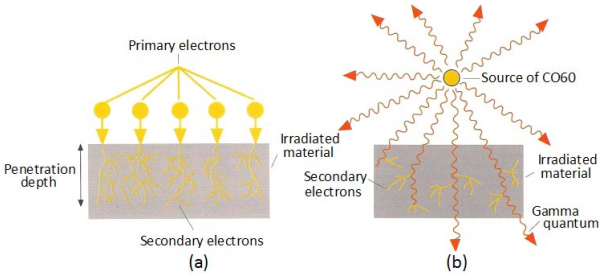

Fig. 1. **Scheme of radiation crosslinking by electrons (a) and gamma rays (b)**

Abstract

This study examines micro-mechanical properties of glass fiber-filled polypropylene, that is a modified by low β-radiation doses. The specimens were made using the injection molding technology and subsequently irradiated by β-radiation. Micro-mechanical properties were studied by method DSI – Depth Sensing Indentation on the Micro hardness tester by CSM. This paper examines effect of β-radiation on the micro-mechanical properties (indentation hardness and indentation modulus) of glass fiber-filled PP, which were measured using DSI.

Keywords: polypropylene, glass fiber, microhardness, crosslinking, β-radiation, DSI – Depth Sensing Indentation

1. Introduction

Polypropylene (PP) is a stereospecific polymer prepared by polymerization using an organometallic catalyst system. Commercial PP have up to 95 % isotactic content, which means that pendant methyl groups are almost all on the same side of the chain. When polypropylene is exposed to ionizing radiation, free radicals are formed and these cause chemical changes. Since PP is highly crystalline, these radicals are relatively immobile, and consequently may not be available for reaction for long periods of time. As with other polyolefins, upon irradiation the free radicals are formed along with evolution of hydrogen gas. If the radical is formed on the pendant methyl, the resulting reaction is cross-linking. However, if the radical is formed in the main chain, the chain end may react with hydrogen, thus causing an irreversible scission. Although the processes of chain scission and cross-linking occur simultaneously, and even though the net effect is crosslinking, the overall effect is the loss of mechanical strength[1,2,4].

Crosslinking is a process in which polymer chains are associated through chemical bonds. Crosslinking is carried out by chemical reactions or radiation and in most cases the process is irreversible. Ionizing radiation includes high-energy electrons (electron beam), γ-rays, and x-rays. These not only are capable of converting monomeric and oligomeric liquids into solids, but also can produce major changes in properties of solid polymers. Also, in comparison to UV and visible radiation, they can penetrate considerably deeper into the material[2,3,5].

Electron beams (β-rays) generated by accelerators are monoenergetic and the absorbed dose is greatest just below the surface of the irradiated material and falls rapidly at greater depths in the material (Fig. 1a). The energy range of electron beams used in radiation processing is from 0.15 to 10 MeV. Compared with gamma irradiation, electron accelerators have advantages of higher power and directional beams. The time of irradiation by β-rays is in seconds. The limited penetrating power of electron beams means that they are mainly used for irradiating relatively thin objects like wires and cable insulation[4,6].

Gamma radiation has a high penetration capability at relatively low dose intensity as shown. The most used source of gamma rays (Fig. 1b) is cobalt-60 (Co60). The energy of emitted gamma rays is about 1.3 MeV. Conversely the electron accelerators, source of gamma rays cannot be turned off. Therefore the rays are sheltered, in most cases by water tank. Time of irradiation depends on dose intensity and reaches up to several hours. The gamma radiation is mainly used for radiation sterilization[2,4–6].

2. Experimental

For this experiment polypropylene PP PTS -Crealen EP-865HS-M0083 filled by 25% glass fiber, that were supplied by PTS Plastics Technologie Service, Germany was used. The material already contained the special cross-linking agent TAIC – triallyl isocyanurate (5 volume %), which should enable subsequent cross-linking by ionizing β-radiation. The prepared PP specimens were modified by radiation with β-radiation doses of 15 and 30 kGy at BGS Beta-Gamma Service GmbH & Co. KG, Germany.

The samples were made using the injection molding technology on an injection moulding machine Arburg Allrounder 420C. Processing temperature 220 °C, mold temperature 55 °C, injection pressure 90 MPa, injection rate 50 mm s^{-1}.

Instrumented microhardness tests were done using a Micro Combi Tester, CSM Instruments (Switzerland) according to the CSN EN ISO 6507-1. Load and unload speed was 2 N min^{-1}. After a holding time of 90 s at maximum load 1 N the specimens were unloaded. The measurements were provided at room temperature.

The indentation hardness H_{IT} was calculated as maximum load to the projected area of the hardness impression according to:

$$H_{IT} = \frac{F_{max}}{A_p} \quad \text{with} \quad h_c = h_{max} - \varepsilon \frac{F_{max}}{S} \tag{1}$$

where h_{max} is the indentation depth at F_{max}, h_c is contact depth. In this study the Oliver and Pharr method was used calculate the initial stiffness (S), contact depth (h_c). The specimens were glued on metallic sample holders.

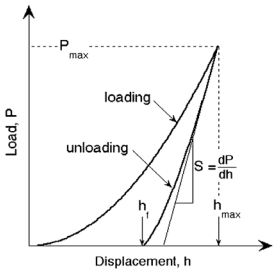

Fig. 2. **Schematic illustration of indentation curve (a) and unloading process (b)**

The indentation modulus is calculated from the Plane Strain modulus using an estimated sample Poisson's ratio:

$$E_{IT} = E^* \cdot (1 - \nu_s^2) \tag{2}$$

The reduced modulus and Plane Strain Modulus E^* is calculated from the following equation:

$$E_r = \frac{\sqrt{\pi} \cdot S}{2 \cdot \beta \cdot \sqrt{A_p(h_c)}} \quad \text{and} \quad E^* = \frac{1}{\frac{1}{E_r} - \frac{1 - \nu_i^2}{E_i}} \tag{3}$$

Where E_i is the Elastic modulus of the indenter, E_r is the Reduced modulus of the indentation contact, n_i is the Poisson´s ratio of the indenter.

3. Results and discussion

Indentation characteristics determined by DSI method are depicted in Fig. 3. They characterize course of loading force in dependence on indentor penetration depth, which gives an idea about course of instantaneous values of observed micro-mechanical properties.

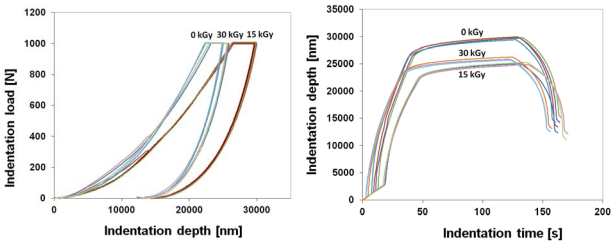

Fig. 3. **Indentation characteristic of PP**

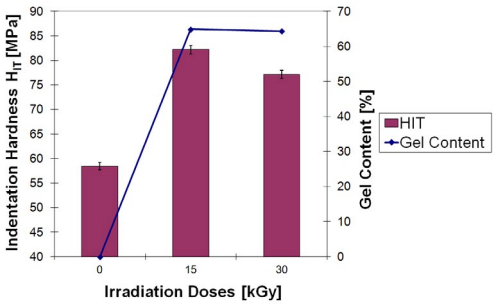

Fig. 4. **Indentation hardness H_{IT} vs. irradiation doses**

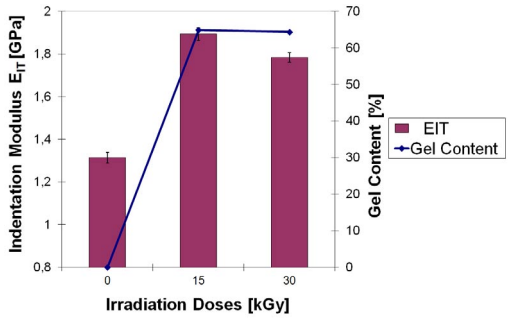

Fig. 5. **Indentation modulus E_{IT} vs. irradiation doses**

With increased dose of β-radiation caused improvement value of gel content which is apparent in Fig. 4, 5.

When comparing the irradiated and non-irradiated specimens of PP, it was apparent that the values of indentation hardness (Fig. 4) a indentation modulus (Fig. 5) considerably increased. The values measured during the indentation test showed that the lowest values of indentation hardness (58 MPa) and indentation modulus (1,31 GPa) were found for the non-irradiated PP. On the contrary, the highest values of indentation hardness (82 MPa) and indentation modulus (1,89 GPa) were obtained for PP irradiated by a dose of 15 kGy, as can be seen at Fig. 4, 5. The highest radiation doses are used, micro-mechanical properties decreases which can be caused by radiation induced degradation of the material.

4. Conclusion

Irradiation of glass fiber-filled polypropylene with a β-radiation influences the micro-mechanical properties in the following way:

- Radiation of specimens caused improvement values of indentation hardness and indentation modulus.
- The highest values of indentation hardness and indentation modulus were achieved at the PP irradiated with dose of 15 kGy.
- Higher radiation dose does not influence the indentation hardness and indentation modulus significantly.

– Values of indentation hardness and indentation modulus correspond to the gel content.

This paper is supported by the internal grant of TBU in Zlin No. IGA/FT/2013/020 funded from the resources of specific university research and by the European Regional Development Fund under the project CEBIA-Tech No. CZ.1.05/2.1.00/03.0089.

REFERENCES

1. W. C. Oliver, G. M. Pharr: J. Mater. Res. *19*, 3 (2004).
2. D. Manas, M. Hribova, M. Manas, M. Ovsik, M. Stanek, D. Samek: Thin Solid Films *530*, 49 (2013).
3. W. C. Oliver, G. M. Pharr: J. Mater. Res. *7*, 1564 (1992).
4. M. Ovsik, D. Manas, M. Manas, M. Stanek, M. Hribova, K. Kocman, D. Samek: Chem. Listy *106*, 507 (2012).
5. G. Zamfirova, V. Gaydarov, T. Zaharescu, L. G. Silva: Chem. Listy *104*, 283 (2010).
6. M. Manas, M. Stanek, D. Manas, M. Danek, Z. Holik: Chem. Listy *103*, 24 (2009).

CL-17
A MATERIAL MODEL FOR POROUS ELASTOMERS WITH STRESS SOFTENING PHENOMENON

RATHAN RAGHUNATH and DANIEL JUHRE*

Deutsches Institut für Kautschuktechnologie e.V. (DIK), 30519-Hannover, Germany
daniel.juhre@DIKautschuk.de

Abstract

This paper presents a new prospect of investigating the mechanical behaviour of cellular rubber using a porous hyperelastic material model within the framework of homogenisation method to consider pore volume fraction. There are number of hyperelastic material models to describe the behaviour of homogeneous elastomer, but very few to characterise the complex properties of cellular rubber. The analysis of dependence of material behaviour on pore density using the new material model is supported with experiments to characterise the actual material behaviour. The finite element simulations are then followed by compression load tests to validate the material model.

1. Introduction

A cellular rubber is a mixed cell structured porous elastomer with high flexibility, good resilience, high compressibility and very good damping properties. It is widely used in industrial applications as gaskets or sealings due to its leak proof characteristics ranging from accoustics to chemicals. In the event of the heterogeneous cellular rubber, in contrast to conventional materials, there are no suitable tools for general material characterisation.

The porosity in elastomers may arise during the manufacturing process due to the defects or by deliberately introducing the porosity in order to get a high-density foam. When compared to the homogeneous elastomer, even low levels of porosity alters the mechanical properties of the material such as change in the elasticity modulus, decrease in shear and bulk modulus and the common assumption of incompressibility breaks down. A new material model for porous elastomers by Danielsson et al.[1] decouples the influence of porosity from the mechanical properties of the solid material by introducing volume fraction of the pores as an explicit scalar variable and it can be directly implemented into the finite element software packages where it can be used to simulate arbitrary geometries under various loading conditions.

The scalar value that determines the density of pores in the material is characterised by a method called Micro-CT (Computer Tomography) scanning. In addition to pores, the stress softening phenomenon[3] (Mullin's effect) has been considered in the model with necessary inputs from multi-hysteresis quasi static experiments. These experiments are then accompanied by finite element simulations of a car door sealing and is validated against the test results of compression -load tests to check the accuracy of the new material model.

2. A model for cellular rubber at finite deformations

The material with non-uniformly distributed pores is first homogenised into a pore-containing matrix with a thick walled sphere considered to represent the undeformed porous material subjected to external loading (Fig. 1a). The initial material, whose matrix is taken to be pointwise incompressible, is characterised by an initial void volume fraction $f_0 = (A/B)^3$, where A and B are the inner and outer radii of the sphere, respectively. When subjected to the principal macroscopic stretch state $(\bar{\lambda}_1, \bar{\lambda}_2, \bar{\lambda}_3)$, the outer surface of the sphere transforms into an ellipsoid (Fig. 1b,c).

The kinematic relationship of the deformation field subjected to macroscopic stretches together with the boundary conditions is given by

$$x_i = \frac{\bar{\lambda}_i}{\bar{J}^{1/3}}\left(1+\frac{B^3(\bar{J}-1)}{R^3}\right)^{1/3} X_i \quad , \quad \bar{J} \equiv detF = \bar{\lambda}_1\bar{\lambda}_2\bar{\lambda}_3 = 1 \qquad (1)$$

The components of the microscopic/pointwise deformation gradient, **F**, at every point in the matrix is

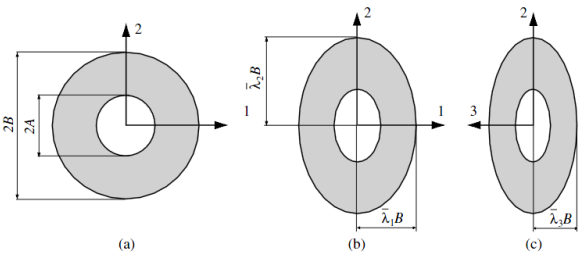

Fig. 1. **The spherical volume element: (a) undeformed configuration, (b and c) deformed configuration**[1]

$$[F]_{ij} = \frac{\bar{\lambda}_i}{\bar{J}^{2/3}}\left(\frac{(1-\bar{J})}{\phi^2 R^2}\frac{B^3}{R^3}X_i X_j + \phi\delta_{ij}\right), \quad (2)$$

$$\phi = (1+(\bar{J}-1)(B/R)^3)^{1/3}$$

The pointwise strain energy density function for an incompressible isotropic hyperelastic material determined at every point of sphere can be expressed in terms of the stretch invariants I_1 and I_1 as

$$W = \hat{W}(I_1, I_2; f_0) \quad (3)$$

The homogenised strain energy density of the sphere, $\bar{W}$ is

$$\bar{W} = \frac{1}{V_0}\int_{Bf_0^{\frac{1}{3}}}^{B}\int_0^{2\pi}\int_0^{\pi}\hat{W}(I_1, I_2; f_0)R^2 \sin\Theta\, d\Theta\, d\Phi\, dR \quad (4)$$

where, B is the outer radius of the sphere (Fig.1), the reference volume is given by $V_0 = 4\pi B^3/3$. $0 \le \Theta \le \pi$ and $0 \le \Phi \le 2\pi$ are standard spherical angles, measured in the reference configuration used to define the components of position vector **X** in spherical coordinate-system.

The strain energy density function of the Yeoh model for solid materials is defined by

$$W_Y = C_{10}(I_1^{iso} - 3) + C_{20}(I_1^{iso} - 3)^2 + C_{30}(I_1^{iso} - 3)^3 + W^{vol} \quad (5)$$

yields the resulting energy function for the porous material

$$\bar{W}_Y = \sum_{i=1}^{3} C_{i0}\left[I_1\left(2 - \frac{1}{J} - \frac{f_0 + 2(J-1)}{J^{\frac{2}{3}}\eta^{\frac{1}{3}}}\right) - 3(1-f_0)\right]^i, \quad (6)$$

$$\eta = \left(1 + \frac{J-1}{f_0}\right)$$

Considering the stress softening phenomenon in material parameters[4], C_{i0} can be rewritten as

$$C_{i0} = C_{i0_v} + b_i \quad e^{c_i(I_{1max}-3)} \quad (7)$$

where C_{i0_v} is the parameter for virgin loading and b_i, c_i are for stress softened loading. The second Piola-Kirchhoff stress then can be derived using the general relation

$$\mathbf{S} = 2\frac{\partial W}{\partial I_1}\mathbf{1} + J\frac{\partial W}{\partial J}\mathbf{C}^{-1} \quad (8)$$

3. Experiments and model fitting

For hyperelastic material characterisation and to determine stress softening phenomenon, simple deformation tests (uniaxial tension, equibiaxial tension and pure shear) are conducted. The experiments are not directly conducted on cellular rubber, due to the presence of pores in the material which lead to an inelastic and inhomogeneous deformation. The Fig. 2 shows multi-cyclic experiments conducted on solid

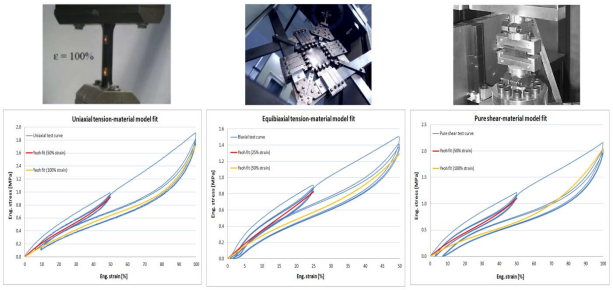

Fig. 2. **Multi-hysteresis experiments for hyperelastic material characterisation**

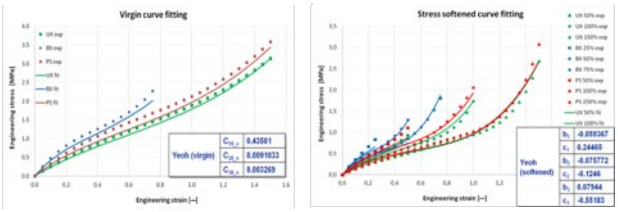

Fig. 3. **Yeoh hyperelastic material model fit: (a) virgin curves and (b) stress-softened curves**

filled elastomer (EPDM-50Shr) while the pores are explicitly introduced into the mathematical model as the scalar value f_0.

The moderate strain amplitude curves from each of the experiments are prepared for Yeoh hyperelastic material model fitting considering stress softened phenomenon is shown in Fig. 3a, b. The scalar value f_0 determines the density of pore in the material and is measured by a method called Micro-CT scanning (a non-destructive method to reproduce three-dimensional images of components including internal in -homogeneities). Here, the Micro-CT Nanotom (GE Phoenix/ X-Ray) has been used to scan the car door sealing (made up of solid elastomer as a base for supporting cellular rubber over it). The material density in the scanned 3D image of car door sealing is then calibrated to determine the range of void volume fraction f_0. The range of f_0 was between 0.55 to 0.6 and for further simulations $f_0 = 0.6$ has been considered.

4. Validation

To validate the material model, the deformation behaviour of car door sealing has been compared with the results of compression load test. During the experiment, the load is applied on sealing using a metal cell placed over it, which simulates a displacement driven closure process. The tilting base-metal on which the sealing was glued has given an opportunity to investigate the change in deformation behaviour at different angles.

The actual deformed shape during compression load test has been compared with the simulated shape in Fig. 4a. The force-displacement curves in Fig. 4b show a good correlation between the experimental and simulated results. The growth of simulated curve is smoother compared to the test curve,

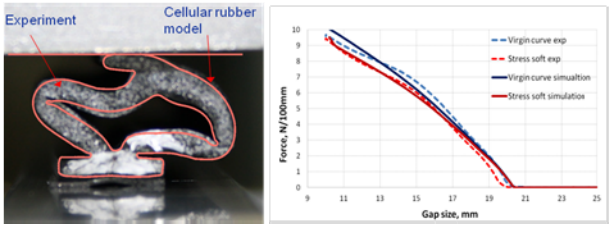

Fig. 4. **(a) Deformed shapes of experiment and simulation, (b) force-displacement curves**

and able to capture the real behaviour at initial and later stages.

5. Summary

The results have shown the capability of the new model to predict the deformation behaviour of cellular rubber in a wide deformation range. At present, the energy functions of new model depends on I_1 and can be extended easily to an additional I_2 dependence. The advantage of the model's structure is the sufficient use of standard homogeneous tests on the solid rubber for fitting the material parameters. The material parameter f_0 is physically motivated and is effective enough to describe the influence of the pore volume on the material behaviour. The validation of the cellular rubber model using FE simulations show a good accordance with the experiments thereby predicting the reasonable behaviour of actual material.

The authors would like to acknowledge the financial support by METZELER APS GmbH.

REFERENCES

1. M. Danielsson, D. M. Parks, M. C. Boyce: Mech. Mater. *36*, 347 (2004).
2. H. Hou, R. Abeyaratne: J. Mech. Phys. Solids *40*, 571 (1992).
3. J. Diani, B. Fayolle, P. Gilormini: Eur. Polym. J. *45*, 601 (2008).
4. J. Meier, J. McNamara, F. Hüls: *8th Rubber Fall Colloquium, 2008.*

CL-18

THE INFLUENCE OF SOFT MAGNETIC FILLERS ON THE PROPERTIES OF THE MAGNETOPOLYMER COMPOSITE

JANA REKOŠOVÁ*[a], MARIANA UŠÁKOVÁ[b], ELEMÍR UŠÁK[b], RASTISLAV DOSOUDIL[b], and IVAN HUDEC[a]

[a] Slovak University of Technology in Bratislava, Faculty of Chemical and Food Technology, Department of Plastic and Rubber, Radlinského 9, 812 37, Bratislava, [b] Slovak University of Technology in Bratislava, Faculty of Electrical Engineering and Information Technology, Institute of Electrical Engineering, Ilkovičova 3, 812 19 Bratislava, Slovak Republic
jana.rekosova@stuba.sk

In recent years, the area of application of radio-absorbing materials (RAMs) has been substantially extended. In addition to traditional directions (radio masking, electromagnetic compatibility, etc.), the direction related to environmental safety and protection of people from the action of electromagnetic fields has arisen[1]. Polymers integrated into composites with soft magnetic materials are recently attracting the interest in industrial and scientific branch for their beneficial properties[2]. In this paper, the influence of soft magnetic ferrites on physical-mechanical, rheological and magnetic properties of magneto-polymer composites based on natural rubber SMR 20 are studied. The laboratory prepared NiZn and commercially available MnZn ferrites were used as magnetic filler with concentrations 100, 200, 400 and 600 phr. The preparation of ferrite fillers as well as composite samples was described in paper[3].

The structural properties of the soft magnetic fillers were investigated by scanning electron microscope. The size and shape of NiZn and MnZn ferrite particles are shown in Fig. 1. The SEM micrographs of both ferrite samples illustrate to present of heterogeneous particles of polyhedral shape aggregated to clusters.

The physical-mechanical properties of prepared composites are plotted in Fig. 2. The tensile strength at break rapidly decreased in dependence of filler content, for the NiZn ferrite filled composites from 14.20 to 3.30 MPa (79 %) and

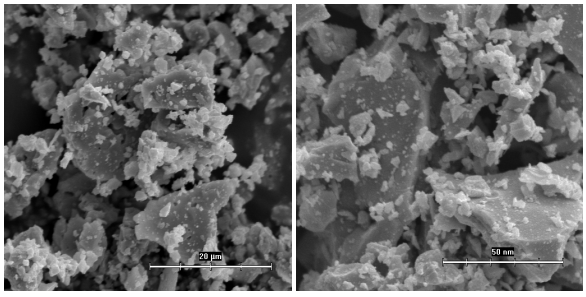

a b

Fig. 1. **SEM micrographs of a) NiZn and b) MnZn ferrite fillers**

for the MnZn composites it firstly rises up slightly from 15.60 to 16.50 and then decreased to 3.40 MPa (78 %). The hardness of composites for both types of ferrite fillers increased approximately by 103 % for NiZn and 79 % for MnZn ferrite filled samples. The influence of ferrite fillers in the natural rubber matrix expressed by means of Payne effect suggests higher affinity of NiZn ferrite filler to rubber than in the case of MnZn ferrite filler (Fig. 3). The slope of the lines expressing the activity coefficient of both filler materials is given in this figure (see the legend) as well.

The measured frequency dependencies of the complex permeability $\mu = \mu' - j\mu''$ for synthesised composite materials was measured in the frequency range from 1 to 3000 MHz by means of two vector network analyzers and a coaxial holder can be found in Figs. 4 and 5. In these figures, the parameter of curves is the ferrite particle concentration in phr. It can be seen that the values of μ' and the peak values of $\mu''(f)$ dependencies (at the resonant frequency f_r) get higher with increasing ferrite particle concentration. On the other hand, the resonant frequency shifts towards lower values (see also Fig. 6). One can state that the complex permeability of composite materials is strongly dependent on ferrite particle concentration and frequency. As can be seen from the presented figures, also the choice of ferrite filler material significantly affects resulting dynamic magnetic properties represented by the complex permeability (see the differences between Figs. 4 and 5 – both vertical scales are kept the same). Since pure MnZn ferrite material exhibits in general larger value of initial permeability than NiZn one, the composites with MnZn ferrite filler in general reach higher values of the complex permeability components for the same filler concentration than those with NiZn filler. Note that the differences in quasi-static initial permeability (measured at $f = 50$ Hz) of both materials are relatively small (Fig. 6). As the ferrite concentration grows up, the influence of ferrite filler becomes more important and the differences boost as well. Observed facts are in a good agreement with our previous investigations[3–5]. An important role in $\mu(f)$ dependencies plays the demagnetising field H_d which is created in filler particles embedded in the non-magnetic polymer matrix due to the presence of magnetic poles on the opposite sides of particles[4]. H_d is antiparallel to applied high-frequency magnetic field and increases with the decrease of ferrite particle concentration due to the reduction of induced magnetic moment in particles. Therefore, μ' at low frequencies apparently decreases and f_r increase with the drop of filler concentration.

The results achieved in this study confirmed considerable influence of the soft magnetic filler on the physical-mechanical, rheological and magnetic properties of magneto-polymer composites with matrix based on natural rubber. The use of various magnetic filler materials with various concentrations enables to prepare magneto-polymer composite materials of required properties for a wide range of applications, such as EM-wave absorbers, wireless radio communication systems, EMF shielding, sensors, etc.

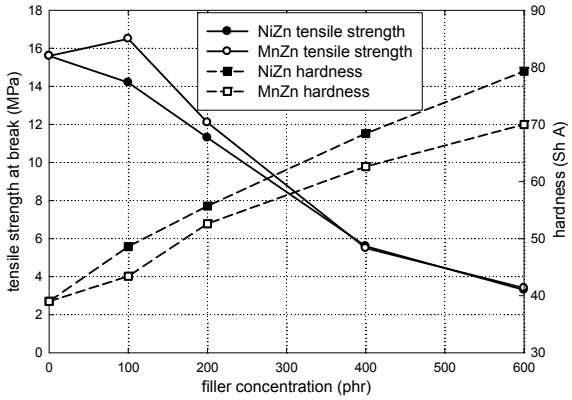

Fig. 2. **Influence of NiZn and MnZn ferrite contents on tensile strength at break and hardness of composite samples**

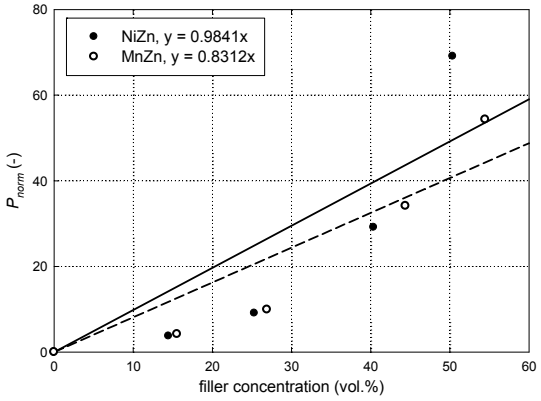

Fig. 3. **Influence of NiZn and MnZn ferrite fillers on the normalised parameter P_{norm} of natural rubber composites**

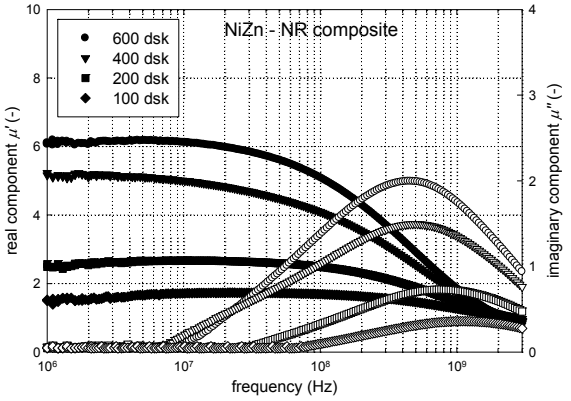

Fig. 4. **Frequency dependencies of the real (solid symbols) and imaginary (open symbols) component of complex permeability for NiZn - NR composites with various filler contents**

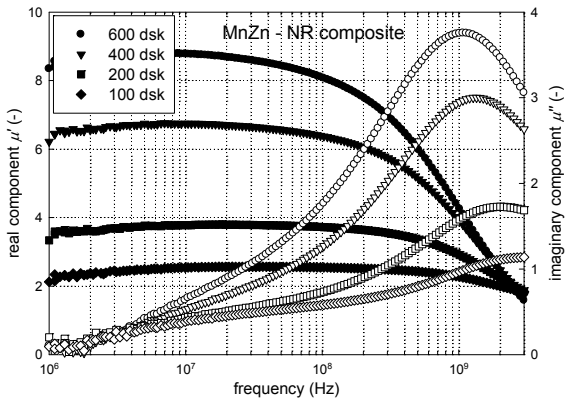

Fig. 5. **Frequency dependencies of the real (solid symbols) and imaginary (open symbols) component of complex permeability for MnZn - NR composites with various filler contents**

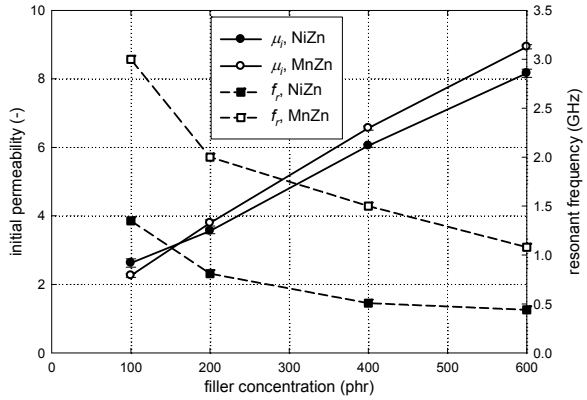

Fig. 6. **Dependence of initial permeability μ_i and resonant frequency f_r on ferrite filler contents of composite samples**

This work was supported by the Slovak Research and Development Agency under the contract No. APVV-0062-11 and by the Scientific Grant Agency of the Ministry of Education, Science, Research and Sport of the Slovak Republic and the Slovak Academy of Sciences (VEGA), projects No. VG-1/1163/12 and VG-1/1325/12.

REFERENCES

1. Lopatin A. V., Kazantseva N. E., Kazanstev Yu. N., D'yakonova O. A, Vilčáková J. Sáha P.: J. Commun. Technol. Electron. *53*, 487 (2008).
2. Weidenfeller B., Anhalt M., Riehemann W.: J. Magn. Magn. Mater. *320*, 362 (2008).
3. Rekošová J., Dosoudil R., Ušáková M., Ušák E., Hudec I.: IEEE Trans. Magn. *49*, 38 (2013).
4. Dosoudil R., Franek J., Sláma J., Ušáková M., Grusková A.: IEEE Trans. Magn. *48*, 1524 (2012).
5. Dosoudil R., Ušáková M., Franek J., Sláma J., Grusková A.: IEEE Trans. Magn. *46*, 436 (2010).

CL-19
INFLUENCE OF CARBON BLACK TYPE ON ELECTRICAL CONDUCTIVITY OF FRC IN AUTOMOTIVE

LADISLAV FOJTL[a], SOŇA RUSNÁKOVÁ[a], VLADIMÍR LABAŠ[b], ONDREJ BOŠÁK[b], EMIL SELIGA[b], MARIAN KUBLIHA[b], and MILAN ŽALUDEK[a]

[a] Department of Production Engineering, Faculty of Technology, Tomas Bata University in Zlín, Nad Stráněmi 4511, 760 05 Zlín, Czech Republic, [b] Department of Physics, Institute of Materials Science, Faculty of Material Science and Technology, Slovak University of Technology, Paulínska 16, 917 24 Trnava, Slovak Republic
fojtl@ft.utb.cz

1. Abstract

Polymer composites allow creation of specific materials depending on trends in research and development due to large-scale combinations of individual components. Polymeric materials in consideration of their electrical conductivity belong to the insulators and their specific electrical conductivity is less than 10^{-12} S cm^{-1}.

The conductivity of those materials can be increased by the addition of the electro-conductive fillers into the polymer matrix. This research paper presents some results about electrical conductivity of polyester composites with carbon reinforcement consisting carbon black fillers.

2. Introduction

The electrical conductivity belongs to the physical quantities describing the conduction of the electric charge in specific material. Polymer materials are normally electrically non-conductive. To transform those materials to electrically conductive, the electrical conductive substances have to be added[1].

The electrical conductivity of dielectrics is divided by electric charge carriers to ionic or electron conductivity[1].

The ionic conductivity ensures the transfer of electric charge by ions, which can be the part of the material, or may come from impurities. The electron conductivity ensures the transfer of electric charge through the free electrons. Most of dielectrics have an absence of such electrons, therefore the conductivity manifests only at high intensities of electric field[1].

The electrical conductivity is also divided by the movement of charges on the inner and surface electrical conductivity. The inner electrical conductivity depends on the composition of the substances and on the intensity of the acting electric field. Furthermore, conductivity can be divided into ion and electron according to the character of the charge

carriers. The ion conductivity occurs at the insulator in the solid phase at low or medium intensities of the electric field. On the other hand, the inner conductivity of insulators depends on the temperature, due to the temperature changes of the concentration of charge carriers. The electrical conductivity of insulators and semiconductors grows with increasing temperature. The surface conductivity depends on the moisture content of the material and their ability to repel water[1].

Possible charge carries in polymers are ion, electrons and holes. The electrical conductivity in polymers has hopping character and the move of electrons is driven by tunneling mechanism[2,3].

3. Materials and methods

The samples were prepared from carbon fabric reinforcement (bidiagonal 420 g m^{-2}, 45/45°, 5 plies) impregnated by polyester resin with two types of electro-conductive carbon black with mass percentage 0 %, 2,5 % and 5 % (Tab. I).

Electric and dielectric parameters were measured on LCR meter HIOKI 3522-50. Totally, eighty frequencies in the range from 0,1 Hz to 100 kHz were used for measuring in alternating electric field (AC). The measuring apparatus for experiments was adapted for monitoring of the changes in the polymer systems, possibly to other materials with low electrical conductivity[4,5,6].

The measurements on the samples (Tab. I) were conducted in a single measuring cycle sequentially at temperatures from 30 °C to 150 °C gradually by 10 °C . The samples were conditioned for measuring temperature of 1200 s before each measurement. The measurements were carried out in a continuous cycle without interruption (removing from the electrode system). Samples were prepared in the quadrate shape with the flat base of 15 × 15 mm without application of the graphite layer.

4. Results

The frequency dependence of the AC conductivity and loss factor of prepared composite samples measured at 100 °C are shown in Fig. 1 and Fig. 2.

Table I
The description of the prepared samples

Polyester Aropol G 105E	Carbon Black A Cabot XC72R [%]	Carbon Black B VXC605 [%]	Description of the samples in the figures
1	5	–	Polyester 1 500 A
2	2,5	–	Polyester 2 250 A
3	–	5	Polyester 3 500 B
4	–	2,5	Polyester 4 250 B
5	0	0	Polyester 5

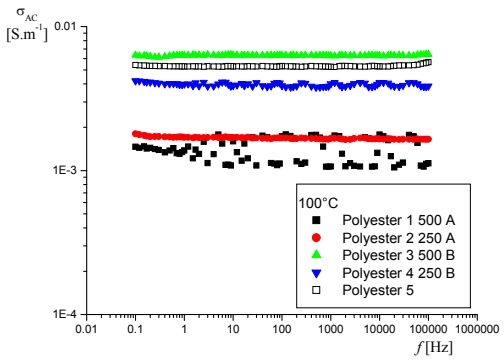

Fig. 1. **The frequency dependence of the AC conductivity (samples Tab. I) with various concentration and kind of carbon blacks measured at 100 °C**

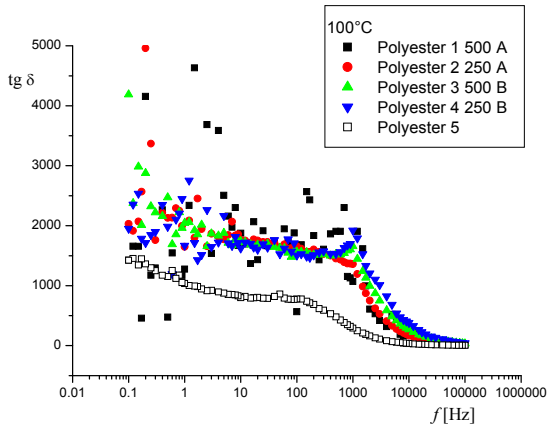

Fig. 2. **The frequency dependence of the loss factor (samples Tab. I) with various concentration and kind of carbon blacks measured at 100 °C**

The values of AC conductivity are relatively high. Those high values of conductivity are apparently influenced by the dominant carbon fabric at the sample. The effect of carbon black on the loss factor is shown in Fig. 2, where 2,5% mass percent of carbon black represents a full saturation of the material.

The courses of the temperature-dependent electrical conductivity for individual samples are shown in Fig. 3. The different course of conductivity in Polyester 5 can be described by two possible changes in the material. Firstly, the release of the conductive filler probably water. This effect, however, should occur at least in part on other samples. Second possible change could be the release of the gas in volume of the sample.

5. Conclusion

The presented results show that contrary to the expectation, the addition of carbon black increased the electrical conductivity only above the temperature of 100 °C. We suggest that this result is caused by the inappropriate

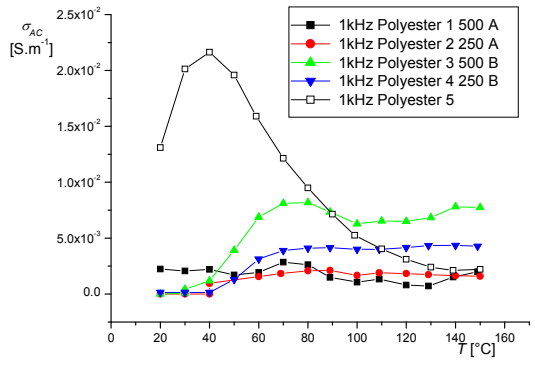

Fig. 3. **Temperature dependence of the AC conductivity (samples Tab. I) with various concentration and kind of carbon blacks measured for 1 kHz**

dispersion of carbon black into the matrix of the composite, which was suitable and verified for dispersion of other electro conductive fillers. Carbon black VXC 605 XC did not increase the conductivity as much as VXC 605. Furthermore, this type of carbon black showed a decreased of conductivity with higher mass percentage.

This work was supported by the Ministry of Education and Youth of the Czech Republic under project APVV CZ–0168-11,7AMB12SK109 and by Slovak National Science Foundation under grant VEGA No. 1/0356/13 and by internal grant of TBU in Zlín No.IGA/FT/2013/022 funded from the resources of specific university research.

REFERENCES

1. Chodák I., Omastová M., Pionteck J.: J. Appl. Polym. Sci. *8*, 1903 (2001).
2. Ehrenstein G. W.: *Polymerní kompozitní materiály*. 1. vydání, p. 351, Scientia, Praha 2009.
3. Meisner B., Zilvar V.: *Fyzika Polymerů. Struktura a vlastnosti polymerních material.* 1. vydání. Státní nakladatelství technické literatury, Praha 1987.
4. Kubliha M.: *Investigating structural changes and defects of non-metallic materials via electrical methods*. 1 st ed., p. 74. Forschungszentrum Dresden, Rossendorf, Dresden 2009.
5. Bošák O., Kalužný J., Preto J., Vacval J. Kubliha M., Hronkovič J.: Polym. Adv. Technol. *18*, 141 2007.
6. Minárik S., Kubliha M., Labaš V., Kalužný J.: J. Optoelectron. Adv. Mater. 8, 1524 (2006).

CL-20

ARTIFICIAL NEURAL NETWORKS PREDICTION OF CHOSEN RUBBER BLENDS PHYSICAL AND MECHANICAL PROPERTIES

IVAN RUŽIAK[a], JANKA JURČIOVÁ[c], MILADA GAJTANSKÁ[a], ĽUBOŠ KRIŠŤÁK[a], PAVEL HUSA[a], PAVEL KOŠTIAL[b], ZORA JANČÍKOVÁ[b], and VLADIMÍR RUSNÁK[b]

[a] Technical University of Zvolen, Faculty of Wood Sciences and Technology, T. G. Masaryka 24, 960 53 Zvolen, Slovak Republic, [b] VŠB – Technical university of Ostrava, Faculty of metallurgy and material engineering, 17. listopadu 15/2172, 708 33 Ostrava, [c] Saar Gummi Slovakia s.r.o, Gumárenská 397/21, 97223 Dolné Vestenice, Slovak Republic

Abstract

In our work we have studied influence of different types of plasticizers on mechanical properties of rubber blend mixtures. We have used Oleic acid as a plasticizer. Reference sample was mixed with plasticizers containing 1 DSK and 3 DSK of ETOXON 2, 4, 6, 8, 10, 20, 30 wt.%. Mechanical properties such as tensile strength, ductility, moduluses M100, M200, M300 have been measured. All measured mechanical properties change with chemical composition.

Artificial neural networks (ANN) have been used for prediction of mechanical properties with respect to rheological properties and chemical composition. ANN application was controlled by statistical functions RMSE_rel and R^2 which value for all predicted values was higher than 0.93.

Key Words: rubber blend, artificial neural networks, physical – mechanical properties, prediction

1. Introduction

Rubber blends are mixtures of rubber with fillers such as carbon black, activators, plasticizers, accelerators. To their unique properties belong super elasticity, small thermal conductivity, relatively low thermal expansion coefficient, low electrical conductivity and relatively low density. Due to their properties variation with composition they are frequently used in various applications.

Carbon black is active filler which raise electrical and thermal properties because of his strong interactions with natural rubber. This interaction causes Payne's effect responsible for the elastic modulus decrease under static and dynamic load of rubber blends[2].

This article deals with the usage of artificial neural networks (ANN) for characterization of rubber blend mixtures with different plasticizers.

Rubber blends belong to elastomers which have high ductility *A* between 100% and 1000%. Basic properties of rubber mixtures – Young´s modulus of elasticity *E*, tensile strength R_m and density ρ are shown in Table I.

Table I
Basic properties of chosen polymeric materials

Material	E [MPa]	R_m [MPa]	ρ [MPa]
Rubber blends [1]	1–100	10 – 25	1000–1200
PMMA [3]	2243–3243	48–72	1170–1200
PC [4]	2381	63–72	1200–1220

Essential ingredient for the manufacture of rubber compounds is plasticizer, which affects the workability of mixtures (mixing, rolling, extrusion ...), reduction of stiffness as well as the final properties of vulcanizates. The positive effect of plasticizer is in a favourable influence of processing characteristics, physical and mechanical properties as well as dynamic – mechanical properties of mixtures[5].

Artificial neural networks (ANN) are used for materials properties prediction when analytical physical approximation cannot be found. From this very robust mathematical tool, material properties can be predicted. Some of the examples are:

- mechanical properties of *PS* rubber blends composites prediction[6],
- mechanical properties of *LLDPE* rubber blends composites prediction[7],
- location of acoustic emission source prediction in *CFR* plastic composites[8] and many others.

ANN usage is tested by statistical parameters *REL_RMSE* and R^2 which are defined by following equations

$$REL\_RMSE = \sqrt{\frac{\sum_{i=1}^{n}(y_i - o_i)^2}{n.(n-1)}} \qquad R^2 = \left(\frac{E(y).E(o)}{E(y.o)}\right)^2 ,$$

Where:

y_i – measured values

o_i – predicted values

n – number of input values

$E(y)$ – statistical mean value of inputs

$E(o)$ – statistical mean value of predicted values

$E(y.o)$ – mean value of multiplification of predicted and input values

From publications[6–8] is good to see, that *ANN* prediction is very useful tool for technology especially in cases of preparation of large amount of samples.

2. Experimental procedures

2.1. Samples

In our experiments we used as reference rubber mixture of composition in *DSK* shown in Table II.

2.2. Experimental procedure

We have measured physical and mechanical properties of oleic acid mixtures with oleic acid content *1 DSK* and *3 DSK*. Measured values of tensile strength R_m, ductility A, moduluses *M100*, *M200*, *M300* of samples with *1 DSK* oleic acid are shown in Table III.

Measured values of tensile strength R_m, ductility A, moduluses *M100*, *M200*, *M300* of samples with *3 DSK* oleic acid are shown in Tab. IV.

Table II
Chemical composition of reference rubber mixture

Ingredient	DSK content
SMR	100
Sulphur	2
ZnO	5
Stearine	2
Sulfenax	2
N339 CB	50
Gumodex	10

2.3. Ann prediction

In Fig. 1 is shown function of predicted tensile strength R_m versus measured tensile strength R_m. In Fig. 2 is shown

Table III
Measured values of 1 DSK oleic acid mixtures

Etoxon wt%	R_m [MPa]	A [MPa]	M100 [MPa]	M200 [MPa]	M300 [MPa]
0%	17	474	3,60	7,20	10,80
2%	18,01	473	3,80	7,60	11,40
4%	18,71	458	4,10	8,20	12,30
6%	19	455	4,20	8,40	12,50
8%	19,28	447	4,30	8,60	12,90
10%	19,83	428	4,60	9,30	13,90
20%	20,50	404	5,10	10,10	15,20
30%	21,90	399	5,50	10,90	16,50

Table IV
Measured values of 3 DSK oleic acid mixtures

Etoxon wt%	R_m [MPa]	A [MPa]	M100 [MPa]	M200 [MPa]	M300 [MPa]
0%	18,50	465	3,90	7,90	11,90
2%	18,72	456	4,10	8,20	12,30
4%	18,90	455	4,20	8,30	12,50
6%	19,16	450	4,30	8,50	12,80
8%	19,85	423	4,70	9,40	14,10
10%	20,50	403	5,10	10,20	15,30
20%	21,42	399	5,40	10,70	16,10
30%	22,49	393	5,70	11,40	17,20

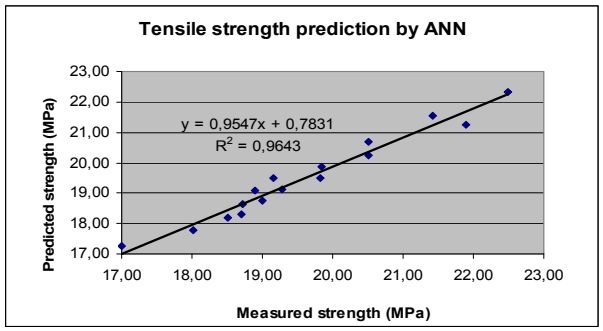

Fig. 1. **Predicted versus measured values of R_m for oleic acid mixtures before ageing process**

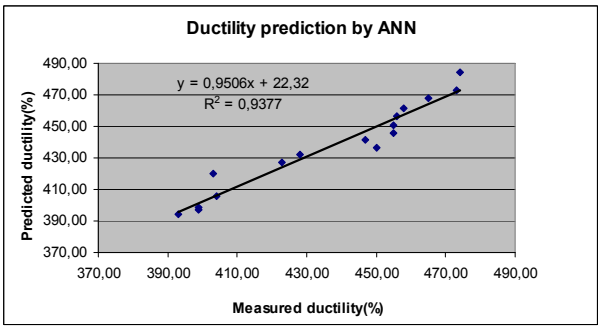

Fig. 2. **Predicted versus measured values of *A* for oleic acid mixtures before ageing process**

function of predicted ductility *A* versus measured ductility *A*.

3. Conclusions

From presented results of *ANN* prediction is good to see, that *ANN* can predict mechanical properties of rubber mixtures as a function of different plasticizers and *ETOXON* tenside.

REFERENCES

1. Ibrahim S.: *Superior compatibilizer of rubber blend. Novel rubber blends for ultra oil resistance applications,* p. 136. Lamber Academic Publishing, 2012.
2. Le Ilisch S., Kasaliwal G. R., Radusch H.-J.: Gel. Rubber Chem. Technol. *81*, 767 (2008).
3. Acrylic. Material properties dostupné na http://www.efunda.com/materials/polymers/properties/polymer_datasheet.cfm?MajorID=acrylic&MinorID=4.
4. Polycarbonate. Material properties dostupné na http://www.efunda.com/materials/polymers/properties/polymer_datasheet.cfm?MajorID=PC&MinorID=2.
5. Ďurfinová J., et al.: Chem. Listy *105*, s327 (2011).
6. Sresungsuwan N., Hansupalak N.: J. Appl. Polym. Sci. *127*, 356 (2013).
7. Suresh A., Sureshkumar M. S., Kargupta K., Ganguly S., Naskar K., Nando G. B.: Plast., Rubber Compos. *38*, 173 (2009).
8. Caprino G., Lopresto V., Leone C., Papa I.: J. Appl. Polym. Sci. *122*, 3506 (2011).

CL-21
A UNIQUE APPROACH TO MODELLING OF COMPOSITE MATERIALS AND STRUCTURES

ZDENĚK RŮŽIČKA[a], JAN SEYFARTH[b], and ROGER ASSAKER[b]

[a] SimulPlast s.r.o. (CZ), Bratrská 1114, 751 31 Lipník nad Bečvou, Česká republika,[b] e-Xstream engineering (L), Z. I. Bommelscheuer, L-4940 Bascharage, Luxembourg
simulplast@simulplast.cz

Abstract

Even though a notable rise in the practical use of composite materials can be observed in the Automotive industry, the simulation of composite structures still poses a challenge. The combination of the softwares Moldex3D and DIGIMAT offers a unique approach to stand up to this challenge.

Composites in Automotive Industry

The complexity of structural design in the automotive industry rises. One of the challenges is the need to develop greener vehicles with a minimal CO_2 footprint while improving safety, quality and performance. The reduction in CO_2 emissions can be achieved via different technologies, but all combined with light-weight structures. For the design of light-weight vehicles, the optimal use of high performance composite materials is the key enabler.

Composites cover a large variety of materials where a matrix phase is reinforced by one or more inclusion phases like fibers and/or other fillers. Most commonly composites based on thermoplastic or epoxy matrices are combined with short, long or continuous fibers. Depending on the type of material automotive parts are processed via injection molding, draping or other technologies.

From this situation real complexity arises. The material microstructure is directly influenced by the processing conditions. This change in microstructure influences the physical properties of the material and thus the final performance of the composite part.

The Simulation Challenge

For the simulation engineer this complexity poses a special challenge. Only a good solution to the question of how to best describe these parts in computations the assured design of automotive parts can be guaranteed. Computer Aided Engineering (CAE) has been used for many years to reduce the time and cost of vehicle design and manufacturing. However, the majority of the CAE processes, tools and even

engineering mindset have been optimized and mainly targeted toward anisotropic materials which are homogeneous like steel.

There is a lack of sufficient description of heterogeneous composite materials on the simulation market. For them, all different kinds of performance must be tackled, among them mechanical stiffness, thermal as well as strain rate dependency and failure.

The Composite Solution

A predictive solution that shows excellent correlation with the experimental response is based on multi-scale modeling techniques taking into account the influence of material microstructure on the material and part response. This technology has been implemented in the DIGIMAT software. On the base of micromechanics a new type of material model is offered to the simulation engineers. These models are able to read in the local microstructure information coming from some processing simulation – for instance simulation software for injection molding Moldex3D. This software is unique among the available softwares for injection molding by its precision of the 3D fiber orientation changing through the wall thickness thanks to hybrid 3D volumetric mesh composed from different types of volumetric elements with more detailed description in the surface layers (see Fig. 1).

After reading the information about the material structure Digimat calculates the correct nonlinear, strain rate and/or temperature dependent material response and communicate this to the FEA solver (see Fig. 2).

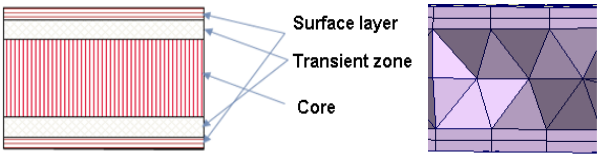

Fig. 1. **Layers with different orientation of short fibers in injection molded parts (cut through the wall thickness) vs. unique hybrid 3D volumetric mesh in the simulation software for injection molding Moldex3D, which is enabling precise fiber orientation**

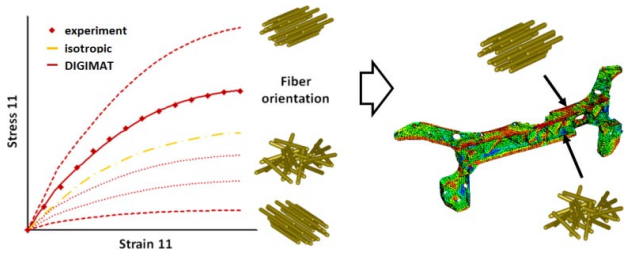

Fig. 2. **Micromechanical based material models are sensitive to the fiber orientation. On the foundation of injection molding simulation this can be used to predict the local stiffness on the part.** (Courtesy of Renault)

Today, these models cover all of the above described material performances and are used to describe static as well dynamic testing of automotive parts.

Applications

The usage of micromechanical material models proves highly advantageous. Compared to the classical isotropic approach vast differences can be seen in the prediction of the performance of the part.

A typical injection molded plastic part like an air intake manifold must be able to withstand a high pressure peak resulting from piston backfire (see Fig. 3). In simulation two different time points during this dynamic event have been investigated (see Fig. 4). A complete and qualitative difference in the performance could be observed with the classical isotropic and the state-of-the-art micromechanical approach. The classical method fails completely to predict correctly the stress distribution not only over the part, but also

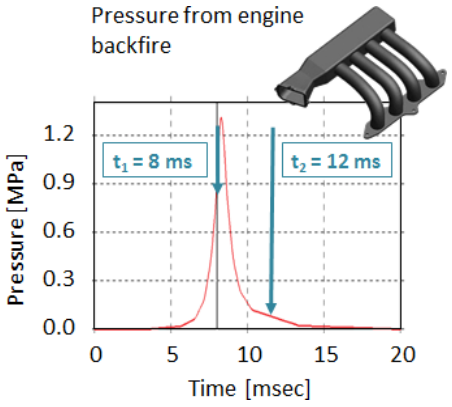

Fig. 3. **An intake manifold is prone to dynamic pressure loads caused by engine piston backfire.** (Courtesy of JSOL Corporation)

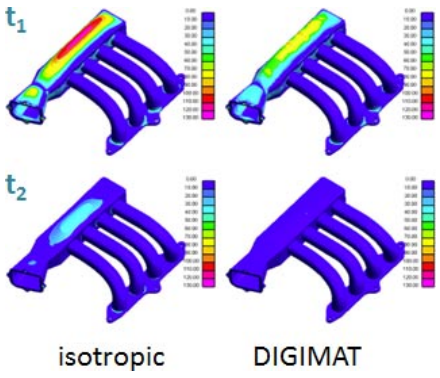

Fig. 4. **Two different time points in this dynamic event have been investigated for isotropic homogeneous and anisotropic inhomogeneous material.** (Courtesy of JSOL Corporation)

in time domain whereas the DIGIMAT modeling gives a realistic picture.

To improve on this well-known limitation of isotropic models usually some scaling factor is introduced to describe an average of the material properties as varying over the part. However, this procedure is not predictive as no unique scaling factor can be derived from any rule of thumb. As a consequence, even though experimental curves might be fitted via this approach, the simulation itself is not predictive.

This fact shows well on a plastic part in a sunroof system where two cases, one global and one local loading, have been investigated (see Fig. 5). To fit the experimental curves for both cases vastly different scaling factors had to be used (see Fig. 6). In contrary, re-running the analyses with one unique DIGIMAT material directly gave excellent correlation with the experiment.

Future in material modelling

In a similar manner all kind of performances of composites have been investigated so far using the DIGIMAT approach. For precise description of the material microstructure (especially the change of the fiber orientation) for injection molded parts Moldex3D simulation software with unique 3D hybrid volumetric mesh can be used.

Thanks to the excellent correlation of the simulation with reality this technique today is developing a new standard on the market. Engineers correctly predict static or dynamic scenarios including the failure behavior of the part. Most recently temperature dependency has been included to be able to tackle all kind of under-the-hood applications. The same as today with injection molding and short fibers, draping as a processing technology for continuous fiber composites will enter the stage soon. But also new material models are in preparation which will be able to describe the dependency of local fatigue properties on the material microstructure. The final goal is to go for a full life time prediction of composite parts.

More information at www.e-Xstream.com, www.moldex3d.com, www.simulplast.com

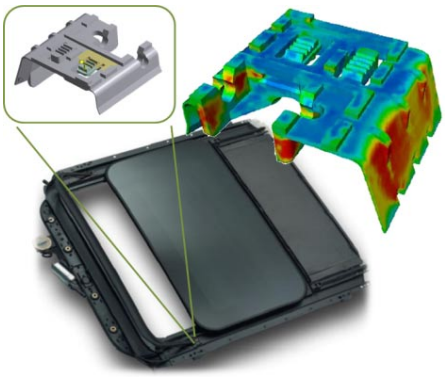

Fig. 5. **Injection molded part with varying fiber orientation in a sunroof system.** (Courtesy of Ticona and ArvinMeritor)

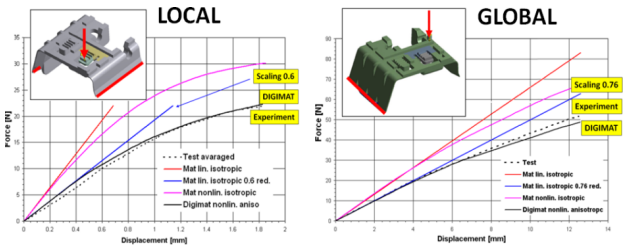

Fig. 6. **Comparison between isotropic and anisotropic approach for two load cases.** The DIGIMAT approach correlates excellently with the experiment. (Courtesy of Ticona and ArvinMeritor)

CL-22
MOLDABILITY OF HIGHLY FILLED POLYMERS

DANIEL SANETRNIK[a,b], and BERENIKA HAUSNEROVA[a,b]

[a] Dept. of Production Engineering, Faculty of Technology, Tomas Bata University in Zlín, nám. T.G.Masaryka 5555, 760 01 Zlín, [b] Centre of Polymer Systems, University Institute, Tomas Bata University in Zlín, Nad Ovčírnou 3685, 760 01 Zlín, Czech Republic
dsanetrnik@ft.utb.cz, hausnerova@ft.utb.cz

Injection molding of ceramic and metal powders is relatively new technology applied in automotive, medicine, electronic or military industries. Small and complex-shape parts can be generated with this technology, and material wastage and ecological load are less than in traditional metallurgy.

Feedstocks contain two components: polymer binder and metal or ceramic powder. The main quality factor of the process is the uniform dispersion of a powder within a binder. Since polymer binder is removed after injection molding (prior sintering) a nonuniform powder-binder distribution can cause defects on a final part.

Mixing is the first step to control the powder-binder uniform distribution, where a minimal material segregation and absence of agglomerations as well as voids are desirable. Any weakness ocurring during mixing causes problems in the following steps[1,2].

Even if a fairly uniform powder and binder distribution is attained after mixing (as evident from SEM micrograph, Fig. 1) of the sample of the commercially available feedstock prepared by pressing (2 minutes preheating at 200 °C, 3 minutes pressing at 200 °C and 5 minutes cooling), the dispersion of the powder within a polymer binder may dramatically change during high shear processing as injection molding. Thus, moldability of highly filled compounds is the main concern of this paper.

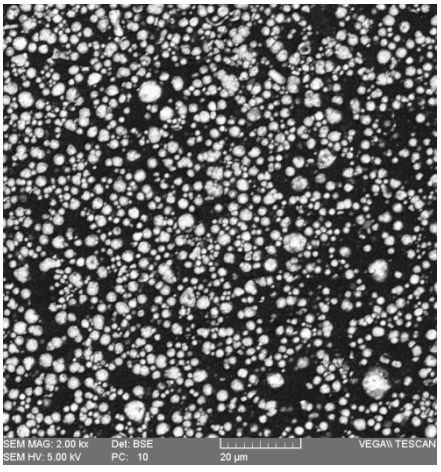

Fig. 1. **SEM of commercially available highly filled (60 vol.%) feedstock**

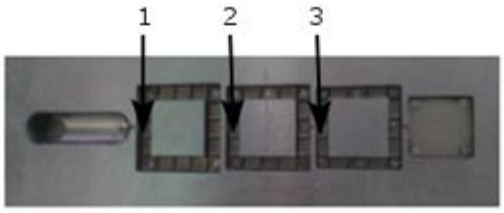

Fig. 2. **Mold for testing moldability of highly filled polymers**

Shear rate and corresponding shear stress during injection molding generate local gradients resulting in the nonuniform powder-binder distribution. The critical geometrical elements of a molded part are mostly inner and outer corners, radical thickness changes including gates, weld-lines and thin films or flashes.

Thus, a mold for testing moldability of highly filled polymers was developed at the Polymer Centre, TBU in Zlín (in cooperation with Fraunhofer IFAM, Bremen)[3], which includes the critical geometrical elements mentioned (Fig. 2). The length of the inert walls of the first three elements is 10 mm. Width of the elements wall is gradually decreased from 3 mm to 2.5 mm and 2 mm. Length of the gates between elements is 1 mm with 0.5 mm diameter.

Three commercially available feedstocks (abbreviated C, P and E) were tested; their flow properties are demonstrated in Fig. 3.

Injection molding machine Arburg Allrounder 370S (EUROMAP size 700-100) with a special surface treatment of the screw for highly filled materials was used. Screw diameter was 20 mm with an effective screw length (L/D) of 16.7.

While injection molding of the feedstocks C and P was optimized successfully, the feedstock E, which has demonstrated a high tendency toward the slip during rheological testing, was molded with the following difficulties. The first problem was that the material was entrapped in the feed hopper. After mechanical enhancement, the pellets went through the feed hopper, but sticked just above a screw creating the solid plug and preventing the flow of the rest of the pellets along the screw towards the melting and terminal zones.

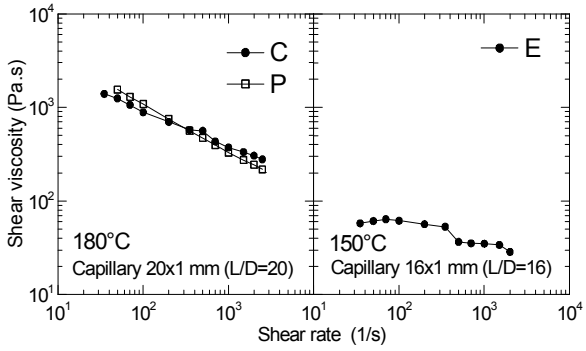

Fig. 3. **Shear viscosity as function of shear rate for feedstock C, P and E**

After a thorough preheating of the material (50 °C) and setting up rather low speed of a screw (not to exceeding 60 mm s^{-1}) this issue was solved.

Plasticity and enhanced adhesion of the feedstock E caused next problem in a sprue bush. Opening of the mold caused a break of the runner system (Fig. 4). A part of the runner system remained in a fixed half of the mold. Removing of this part from the sprue bush was rather complicated. This problem prevented effective injection molding. Thus, various conditions of a molding cycle were tested – nozzle temperature varied from 140 °C to 160 °C, mold temperature from laboratory temperature to 70 °C, injection pressure (900 bar to 2000 bar), holding pressure (900 bar to 1500 bar), injection speed (from 25 mm s^{-1} to 150 mm s^{-1}). In all cases the problem was observed.

The solution was the reduction of the sprue bush length from the originally 74 mm to 50 mm. It should be noted that after such reduction the nozzle must run inside the mold.

Further, the mold had ejectors located only in the corners of each square element. The molded samples of feedstock E were destroyed by ejectors in B and C square elements. Thus, additional ejectors to B and C square elements were implemented to the mold.

The optimized molding conditions for the particular feedstocks are summarized in Table I.

Nevertheless, all three tested materials exhibit a non-uniform powder distribution after injection molding into a testing mold. The critical changes in powder distribution

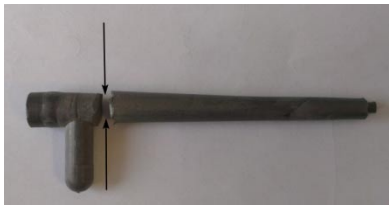

Fig. 4. **The crack of the runner system detected for the feedstock E**

Table I
Optimized molding conditions for tested feedstocks

Material	P	C	E
Zone 1 temperature (°C)	160	160	100
Zone 2 temperature (°C)	185	170	110
Zone 3 temperature (°C)	190	180	120
Zone 4 temperature (°C)	195	190	130
Nozzle temperature (°C)	200	200	150
Mold temperature (°C)	85	85	50
Injection speed (mm/s)	220	188	150
Injection pressure (bar)	2000	2000	1000
Injection time (s)	0.19	0.19	0.19
Hold pressure (bar)	2100	2100	800
Hold pressure time (s)	4.0	4.0	4.0

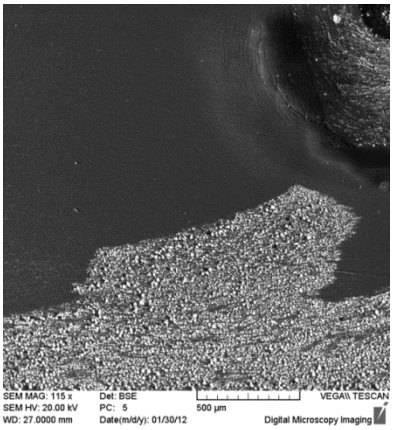

Fig. 5. **SEM of the molded feedstock C at the critical element 3 of the testing sample** (see Fig. 2).

were detected behind the gates 1, 2 and 3. The segregation of the material components can attain a considerable effect as evident from SEM in Fig. 5, where the completely separated areas (dark areas without a powder) causing warpage of a product structure during sintering can be seen.

The quantification of the powder/binder segregation is provided via combined SEM/EDX analysis followed by an analytical approach developed at present[4].

Operational Program Research and Development for Innovations co-funded by the ERDF and national budget of Czech Republic, within the framework of project Centre of Polymer Systems (reg. number: CZ.1.05/2.1.00/03.0111) and Operational Program Education for Competitiveness co-funded by the European Social Fund (ESF) and national budget of Czech Republic, within the framework of project Advanced Theoretical and Experimental Studies of Polymer Systems (reg. number: CZ.1.07/2.3.00/20.0104) are acknowledged. IPG Milotice na Becvou, Czech Republic is acknowledged for the valuable consultation and technical support.

REFERENCES

1. German R. M, Bose A.: Injection Molding of Metals and Ceramics, Metal Poder Industry, 413 p. ISBN 978-1878954619 (1997).
2. Jenny M., Zauner R., Stampfl J.: Measurement Methods for Powder Binder Separation in PIM Components. In *EURO PM 2009: Proceedings Vol 2*. Copenhagen : European Powder Metallurgy Association, 2009. pp. 141 -146. ISBN 978-1899072071.
3. Jiranek L., Hausnerova B., Hartwig T.: Community Design 001704974, Office for Harmonization in the Internal Market, Alicante (6 May, 2010).
4. Hausnerova B., Sanetrnik D., Ponizil P.: Surface Structure Analysis of Injection Molded Highly Filled Polymer Melts, Polymer Composites, submited December 2012.

CL-23
THE EFFECT OF ORGANOPHILIC CLAY ON TRIBOLOGICAL PROPERTIES OF GRAPHITE/EPOXY COMPOSITES

VIERA KHUNOVÁ

The Slovak University of Technology, Faculty of Chemical and Food Technology, Institute of Polymer Materials, Radlinského 9, 812 37 Bratislava, Slovakia

Introduction

Due to remarkable improvement in a wide range of physical and engineering properties polymer nanocomposites are progressively replacing traditional structural materials in the automotive and aerospace industry. Polymer nanocomposite properties are primarily a function of nanofillers particle size, surface properties, distribution in polymer matrix and interactions on filler/matrix interface.

Recently it was found that polymer nanocomposites are also of high importance in applications where low friction of materials is required[1–5]. Furthermore, a very effective approach how to increase tribological properties of polymers is combination nanofillers with conventional micro sized fillers[6]. Thus, proper selection of nanofillers together with compounding equipment and mixing conditions play a key role in polymer nanocomposite end use properties.

This work highlights the effect of organophilic clay on tribological properties of graphite/epoxy composites. To evaluate the role of compounding parameters on structure and properties composites have been prepared by mixing in high shear (10.000 rpm) as well as standard (500 rpm) mixing equipment.

Materials

As a polymer matrix has been used a resin Bisphenol-A-Epichlorohydrin epoxy resin and a Hardener type Ancamine from Air Products GmbH 3-Aminoethyl-3,5,5-trimethyl-cyclohexylamin (Ancamine 3473), Bisphenol-A diglycidyl ether (BADGE) (Ancarez RZ 4020).

Natural micro crystal structure graphite EPDM 90/91 with the average particle size was 20 µm, product of German company Kropfmühl AG, has been used.

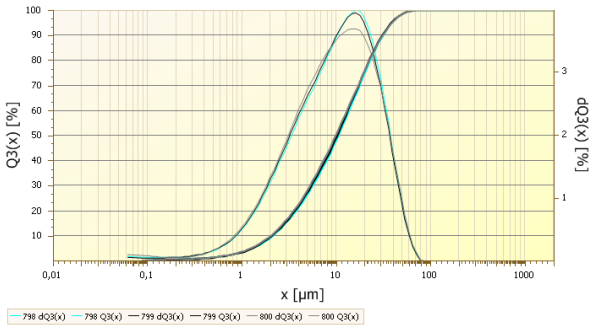

Fig. 1. **Organophilic clay Nanomer I.30E size distribution**

Organophilic clay Nanomer I.30E, modified by 27 %wt. octadecylamine, was obtained from Nanocor Inc. Original Nanomer I.30E particle size 10 µm (Fig. 1) was determined by Laser Particle Sizer (ANALYSETTE 22).

Composites preparation

Composites have been prepared in two stages by mixing in low speed and high speed mixing equipments:

– high shear mixer (Ultraturrax 50 E) from IKA
– standard mixer a four paddle-stirrer

Graphite/epoxy and clay/epoxy were prepared by mixing Bisphenol-A-Epichlorohydrin resin and hardener with clay and/or graphite.

Hybrid graphite/clay/epoxy composites have been prepared by mixing in two phases:

1. the organophilic clay (Nanomer I30.E) was mixed in the ER (Ancarez RZ 4020) in high shear and/or standard mixer.
2. graphite and the hardening agent was mixed with ER/ I30.E composite in a conventional mixer with a four-paddle-stirrer.

Composition of studied composites and corresponding mixing conditions are presented in Table I.

Tribological analyses

The characterization of the frictional and wear behavior was carried out in accordance with the standard test method for ranking resistance of plastics to sliding wear in block-on-ring wear test (cumulative wear method, DIN ISO 7148-2 respective). The tribological properties were determined on a part-test bench (Universalprüfstand Fa. Krauss) as follows:

– abrasive wear (at 1 MPA, 60 °C, 6,6 m s^{-1})
– static coefficient of friction (at 1 MPA, 60 °C, 6,6 m s^{-1})
– sliding coefficient of friction (at 1 MPA, 60 °C, 6,6 m s^{-1})

Results and discussion

In order to eliminate potential mutual effect of the other components (e.g. fibers, lubricants, etc.) and to evaluate solely the effect of clay on tribological performance epoxy/ graphite composites, the number of additional components was reduced to epoxy resin, graphite and clay. The clay and graphite content was kept constant on 5 wt.%.

As a polymer matrix has been used epoxy resins due to outstanding tribological and favourable mechanical, thermal, mixing and curing properties. Nanomer I.30E was applied

Table I
Composite compositions and mixing conditions

Composite composition	Epoxy	Epoxy/clay	Epoxy/clay/ graphite
Nanomer I.30E	0	5 wt %	5 wt %
Graphite	0	0	5 wt %
Mixing equipment	Shear mixer 10.000 rpm 30 min		
	Four paddle stirrer 500 rpm 10 min		

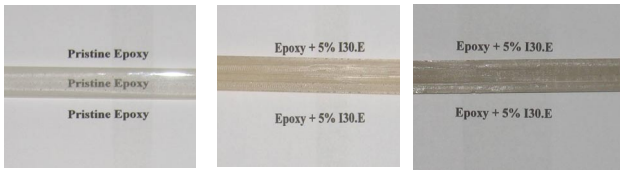

a b c

Fig. 2. **The effect of clay (I30.E) on transparency of epoxy resin: a) neat epoxy resin, b) clay/epoxy composites prepared by standard mixing, c) clay/epoxy composites prepared by high speed shear mixing**

since (as a result of catalytic function of the acidic primary onion ions that facilitate epoxy rings) in this type of organophilic clay the highest level of exfoliation (compared with e.g. Nanomer I.28E, Cloisite C 10, C 15A, C 20A) was achieved[7].

To evaluate the effect of compounding on structure and properties composites have been prepared by mixing in high shear (10.000 rpm) as well as standard (500 rpm) mixing equipment.

As it is evident from the Fig. 1, original particle size of Nanomer I.30E was 10 µm. Extensive reduction of transparency of clay/epoxy composites (Fig. 2) indicate, that during both, standard and high speed mixing, the major part

a b

Fig. 3. **Structure of epoxy/clay (I30.E) composites prepared by a) standard mixing; b) high speed shear mixing**

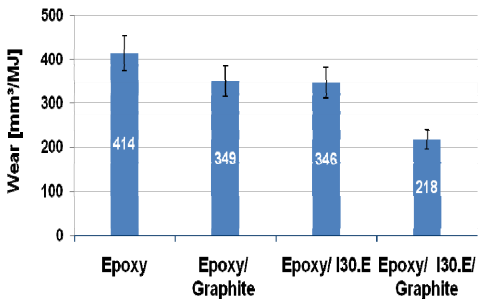

Fig. 4. **Influence of graphite and clay (I30.E) on the wear of epoxy composites prepared by standard mixing**

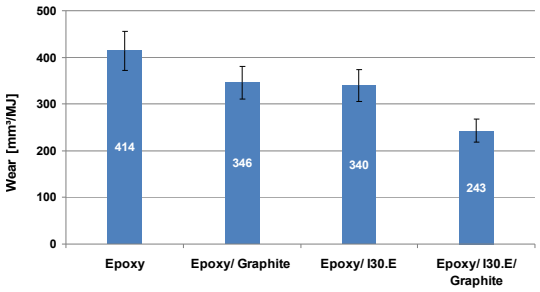

Fig. 4. **Influence of graphite and clay (I30.E) on the wear of epoxy composites prepared by shear mixing**

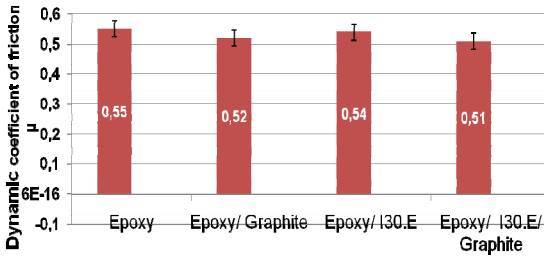

Fig. 5. **Influence of graphite and clay (I30.E) on dynamic coefficient of friction of epoxy composites prepared by shear mixing**

of clay particles did not reach nanostructure level. Although the microscopic analyse (resolution microscope 1000×) of clay/epoxy composite structure confirmed significant reduction of clay particle size (up to 0,5 / 1,0 µm), the number of exfoliated particles, if any, was negligible (Fig. 3).

Whilst in both, clay and graphite based epoxy composites by adding of 5 wt.% of single fillers only negligible (16 %) reduction of wear compared to neat epoxy resin was observed, the effect of hybrid clay/graphite fillers was much more significant (Fig. 4). The highest, 48 % wear reduction, was observed in clay/graphite/epoxy composites prepared by standard mixing.

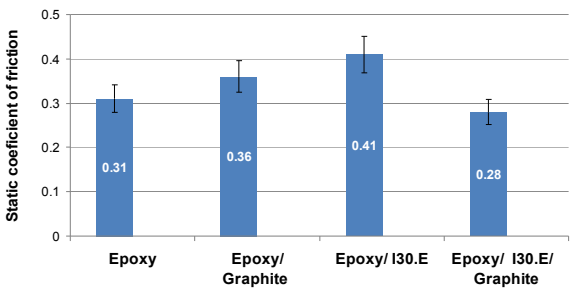

Fig. 6. **Influence of graphite and clay (I30.E on static coefficient of friction of epoxy composites prepared by standard mixing**

Similar, 41 % reduction of wear was observed in clay/ graphite/composites prepared by high speed shear mixing (Fig. 5). Unlike wear, there was observed negligible only effect of mixing conditions as well as single and also hybrid clay/graphite fillers on the dynamic (Fig. 5) and static coefficient of friction (Fig. 6).

Conclusions

In the paper the effect of organophilic clay Nanomer I.30E on tribological performance of graphite/epoxy composites has been studied. It was found that addition of clay lead to comparable wear reduction as in graphite/epoxide composites. However, the most significant improvement of tribological behaviour was observed in hybrid clay/graphite/ epoxide composites. In this case important 50 % reduction of wear was achieved by addition just 5 wt.% of clay and 5 wt.% of graphite. There was not observed synergistic effect of hybrid fillers on static and dynamic coefficient of friction.

REFERENCES

1. Q.-H. Wang, J. Xu, W. Shen, Q. Xue: Wear *209*, 316 (1997).
2. F. Li, K. A. Hu, J.-L. Li , B.Y. Zhao: Wear *249*, 877 (2002).
3. A. Srinath, R. Gnanamoorthy: J. Mater. Sci. *40*, 2897 (2005).
4. B. Wetzela, F. Hauperta, M. Q. Zhangbgood: Compos. Sci. Technol. *63*, 2055 (2003).
5. Wetzel B., Haupert F., Friedrich K., Zhang M. Q., Rong M. Z: Polym. Eng. Sci. *42*, 1919 (2002).
6. G. Shi, M. Q. Zhang, M. Z. Rong, B. Wetzel, K. Friedrich: Wear *254*, 784 (2003).
7. Chen B.-K., Liu J., Chen H., Wu J.: Chem. Mater. *16*, 4864 (2004).

CL-24
POLYMER FLUIDITY INFLUENCED BY THE FILLER

MICHAL STANEK*, DAVID MANAS, MIROSLAV MANAS, VOJTECH SENKERIK, and ADAM SKROBAK

Tomas Bata University in Zlin, nam. T. G. Masaryka 5555, 760 01 Zlin, Czech Republic
stanek@ft.tub.cz

Abstract

This paper shows the influence of cavity surface roughness and on the flow length of filled polymers by talc into mold cavity. Application of the measurement results may have significant influence on the production of shaping parts of the injection molds especially in changing the so far used processes and substituting them by less costly production processes which might increase the competitiveness of the tool producers and shorten the time between product plan and its implementation.

1. Introduction

Injection molding is one of the most extended polymer processing technologies. It enables the manufacture of final products, which do not require any further operations. The tools used for their production – the injection molds – are very complicated assemblies that are made using several technologies and materials. Working of shaping cavities is the major problem involving not only the cavity of the mold itself, giving the shape and dimensions of the future product, but also the flow pathway (runners) leading the polymer melt to the separate cavities. The runner may be very complex and in most cases takes up to 50 % volume of the product itself (cavity). In practice, high quality of runner surface is still very often required. Hence surface polishing for perfect conditions for melt flow is demanded. The stated finishing operations are very time and money consuming leading to high costs of the tool production.

Delivery of polymer melts into the mold cavity is the most important stage of the injection molding process. This paper shows the influence of cavity surface roughness and technological parameters on the flow length of polymer melt into mold cavity. The fluidity of polymers is affected by many parameters (mold design, melt temperature, injection rate and pressures) and by the flow properties of polymers. Results of the experiments carried out with polypropylene contained different amount of filler proved a minimal influence of surface roughness of the runners on the polymer melt flow. This considers excluding (if the conditions allow it) the very complex and expensive finishing operations from the technological process as the influence of the surface roughness on the flow characteristics does not seem to play as important role as was previously thought.

2. Injection molding

The injection mold for was designed for the easiest possible manipulation both with the mold itself and during injection while changing the testing plates, size of the mold gate etc. The injection mold is inserted into a universal frame (Fig. 2) which was designed for use with many different injection molds that fit the size of the frame. This makes the change of the separate injection molds easier, because the frame remains clamped to the injection molding machine and only the shaping and ejection parts of the molds are changed. Attaching right and left sides of the frame to fixed and moving plates of the injection machine is done using four clamps on each side.

The shaping part of the injection mold is composed of right and left sides, see Fig. 2. The most important parts of the injection mold concerning the measurements are: testing plate, cavity plate and a special sprue puller insert.

The cavity (Fig. 2 – right) of injection mold for is in a shape of a spiral with the length of 2000 mm and dimensions of channel cross-section: 6x1 mm. The cavity is created when the injection mold is closed, i.e. when shaping plate seals the testing plate.

Injection mold can operate with 5 exchangeable testing plates (Fig. 2 – left) with different surface roughness.

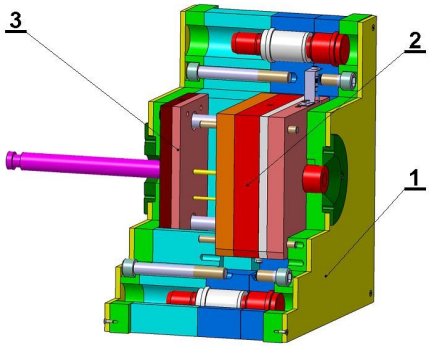

testing sample

Fig. 1. **Assembly of injection mold;** 1 – frame, 2 – injection mold, 3 – ejection system

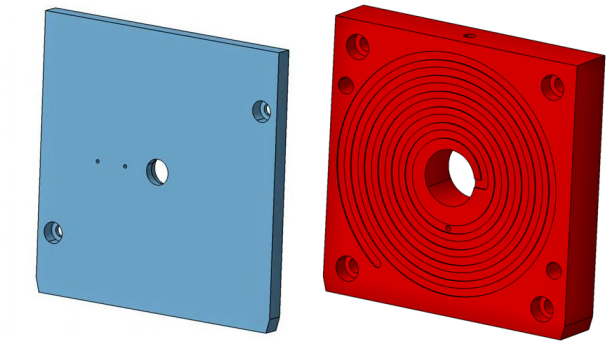

Fig. 2. **Cavity plates** (left – testing plate, right – shaping plate)

The surface of the plates was machined by four different technologies, which are most commonly used to work down the cavities of molds and runners. These technologies are polishing, grinding, milling and electro-spark erosion. The testing plates are used for changing the surface of the mold cavity.

3. Results

Natural polypropylene and polypropylene with different amount of filler – talc (10 %, 20 %, 30 %, 40 % of talc) has been used for the experiment.

The aim of the measurements was to find out the influence of separate parameters, especially the quality of the injection mold cavity surface and filler amount, on the flow length. The main results are given on the Fig. 3–6.

Table I
Surfaces of testing plates

Polished plate	Ground plate	Electro – spark machined plate (fine design)	Milled plate	Electro – spark machined plate (rough design)
R_a [μm]	R_a [μm]	R_a [μm]	R_a [μm]	R_a [μm]
0,102	0,172	4,055	4,499	9,566

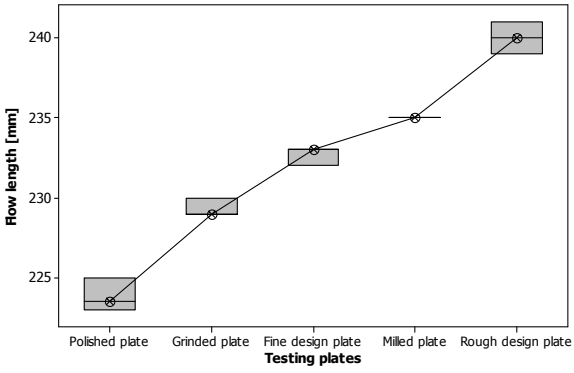

Fig. 3. **Dependence of the flow length on surface quality (0 % talc)**

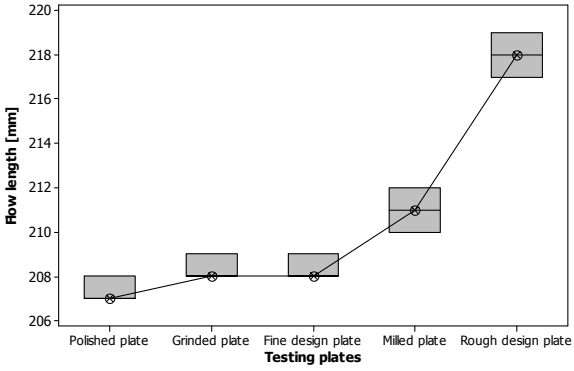

Fig. 4. **Dependence of the flow length on surface quality (20 % talc)**

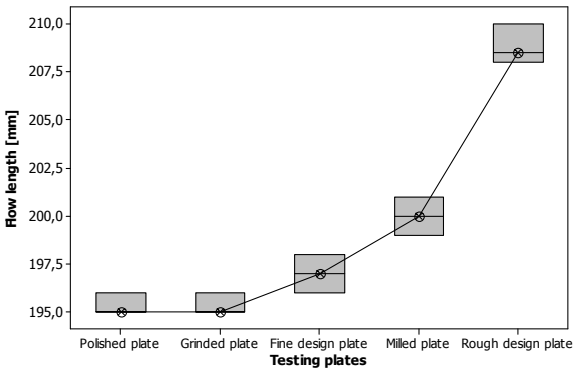

Fig. 5. **Dependence of the flow length on surface quality (40 % talc)**

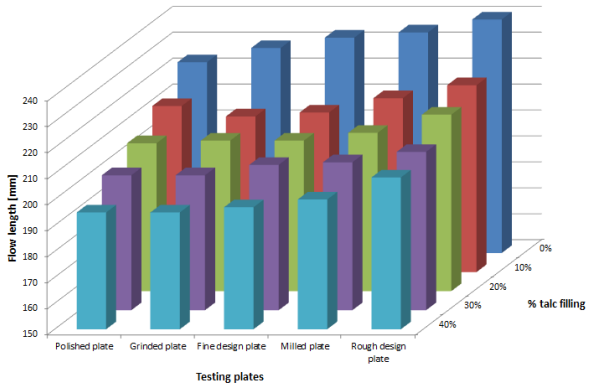

Fig. 6. **Dependence of the flow length on surface quality and filler amount**

4. Conclusion

This research looked into the influence of technological parameters on filling of the injection mold cavity and the flow length respectively. The differences in flow lengths at the testing cavity plates with different surface roughness were very small, rather higher in case of rougher surfaces. But the there is demonstrable difference of worse flow properties on each testing plate with increasing percentage of filler (talc). The measurement shows that surface roughness of the injection mold cavity or runners have no substantial influence on the length of flow. This can be directly put into practice. It also suggests that final working and machining (e.g. grinding and polishing) of some parts of the mold, especially the flowing pathways, are not necessary.

This paper is supported by the internal grant of TBU in Zlin No. IGA/FT/2013/020 funded from the resources of specific university research and by the European Regional Development Fund under the project CEBIA-Tech No. CZ.1.05/2.1.00/03.0089.

REFERENCES

1. Manas D., Manas M., Stanek M., Danek M.: Arch. Mater. Sci. Eng. *32*, 69 (2008).
2. K. Kyas, M. Stanek, Manas, M. Stanek, M. Krumal, Z. Holik: Chem. Listy *105*, s354 (2011).
3. D. Manas et al.: Thin Solid Films *530*, 49 (2013).
4. Ovsik M., Manas D., Manas M., Stanek M., Hribova M., Kocman K., Samek D.: Chem. Listy *106*, 507 (2012).
5. Mizera A., Manas M., Holik Z., Manas D., Stanek M., Cerny J., Bednarik M., Ovsik M.: Int. J. Math. Comput. Simulation *6*, 592 (2012).

CL-25
FUTURE TRENDS IN TYRE CHARACTERIZATION

RADEK STOČEK*[a,b], REINHOLD KIPSCHOLL[c], ROMAN ČERMÁK[d], and GERT HEINRICH[f]

[a] PRL Polymer Research Lab., Nad Ovčírnou 3685, 760 01 Zlín, Czech Republic, [b] Centre of Polymer Systems, University Institute, Tomas Bata University in Zlín, Nad Ovčírnou 3685, 760 01 Zlín, Czech Republic, [c] Coesfeld GmbH & Co. KG, Tronjestr.8, 44319 Dortmund, Germany, [d] Department of Polymer Engineering, Faculty of Technology, Tomas Bata University in Zlín, Czech Republic, [e] Leibniz-Institut für Polymerforschung Dresden e.V., Hohe Str. 6, 01069 Dresden, Germany
radek.stocek@prl-z.com

Abstract

The understanding of dynamic behavior as well as fracture behavior of rubber-like materials is of great practical importance for the prediction of rubber-like product's life time. The aim of this work is concentrated (i) to the description of mechanisms leading to rubber failure with respect to real loading conditions of the products and (ii) to a proposal resp. discussion of future trends in practical rubber characterization. We firstly demonstrate a relationship between Fatigue Crack Growth (FCG) behaviors under different loading conditions. Concluding we introduce a closed characterization method of dynamic rubber behavior with respect to tyre tread wear including the specific role of the FCG behavior of the rubber materials.

Introduction

The most important high dynamically loaded technique rubber parts are especially tyres, which are very important parts for the live-safety in the daily usage. The mechanical behaviour of tyre can be observed from two different views, because of the anatomy and functionality of tyre. The design of tyre consists from the in- and outside parts, which are exposing different conditions as loading, ozone concentration, temperature etc. The most affected part in tyre is the tread, because of the contact with the roughness of the road, high dynamic loading conditions, variation of fatigue dynamic and quasi-static loading, impact, influence of high temperature fluctuation, ozone concentration, solar radiation, influence of fluid medium etc. The composition of the compound has a highly important influence on the mechanical behavior of the tread. The standard used rubber types by compounding of tread are also depend on anatomy of tyre and consist of SBR (styrene-butadiene rubber), NR (natural rubber) and/or BR (Polybutadiene rubber). Whereas the other important technical rubber products are mostly based on EPDM (ethylene propylene diene monomer)

It is well known that the extreme requirements for the high dynamic loading conditions, composition of tyre compound as well as the design of tyre tread have an effect on the fatigue and failure of tyres. These processes lead to the

degradation of the mechanical behaviour of rubber matrix. The initiation of local instability in tyre tread due to failure is particularly caused by micro-crack initiation. Its propagation could have fatal consequences because of the resulting global tyre's instability and thus danger caused due to car's accident. The understanding of the relationship between the crack initiations caused by impact, fatigue or combination of both and its propagation is a subject of high scientific interest, therefore its description will improve the safety, a higher durability and life service of the tyre as well. The tests and determination of tyre failure are time and money consuming and thus the effective testing method in laboratory condition is highly appreciated.

The exact description of the real dynamic behaviour and failure of tyre tread in the laboratory depends on many conditions, which are listed in the previous paragraphs and therefore the realisation of the analysis is very complicated. The main important question from the tyre producers is: *"Which methods could lead to the exact prediction and quantitative characterization of tyre tread behaviours while the tyre development process?"*. According to the character of cyclic loading of tyre (s. Scheme 1) only dynamical loading test conditions can lead to a proper description of mechanical behavior and investigation of tyre failure. Thus the efficient approach for the exact characterization of tyre tread behaviour is defined as follows: "*The development of new methods or utilization of the systems and equipment for physical material testing of polymeric materials has to be performed under the application of real loading conditions"*.

What are the reasons for the crack initiation, its propagation and what are the influences of the initiation time, FCG velocity and FCG orientation? These are the local and main important subjects of scientific research for investigating of fracture mechanics of tyre tread under the real loading conditions. Most efforts in this field are based on the fundamental work of Rivlin and Thomas[1].

The Scheme 1 represents the tyre rolling with the visualization of real dynamic loading, denoted as pulse loading and detail of the contact between tyre tread and road surface. The real dynamic loading condition is defined due to proceeding of loading at the orange denoted region (correspond to the tyre footprint) in the timing range of milliseconds, after that the contact is enable and the zone in the tyre tread relaxes until the next contact (revolution of tyre) proceeds. A tyre does not make perfect contact with the road over the whole footprint area (s. Scheme 1). The asperity of the contact regions causes, that the tyre rubber–road contact area is just a few per cent of the nominal footprint contact area[2]. The dissipated energy increase in the smallest asperity contact regions and the material forces as crack driving forces are applied. Thus the fracture processes with the micro-crack initiation of the tyre tread have been started!

The micro-crack initiation proceeding during frictional sliding of a hard blade abrader on the rolling rubber surface is termed a stick-slip motion[3]. This fracture process is caused due more different mechanisms regarding to the real rolling of tyre. Generally the process could start with the dynamic impact of the strange object (profile of the road surface asperity), which has a considerable higher E-modulus in comparison with the impacted tyre tread. The impactor stresses the tread in the direction of loading and currently

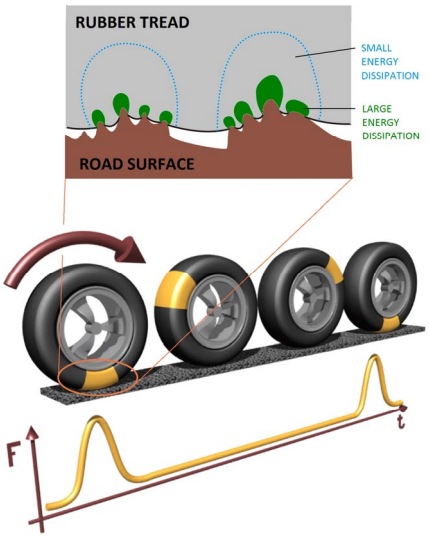

Scheme 1. **The tyre rolling with the visualization of real dynamic loading and detail of the contact between tyre tread and road surface**

influences the stress at the contact zone with the frictionally sliding. After the proceeding of loading in the timing range of milliseconds the contact is enable and the zone in the tire tread relaxes. This mechanism repeats in the frequency of rolling and depends on road surface, because of its fractal 3D structure. The micro-crack can be initiated and proceeds in the phase of the impact or the initiation can start in the phase of sliding, whereas the both processes are characterized due to unreproducible high dynamics change of stress and energy dissipation in the material between relaxed and stressed conditions. The first measurements of rubber abrasion at steady state started Liang et al.[6] and the method demonstrating the Chip & Cut effect introduced Maňas et al.[7].

As tyre undergoes millions of fatigue cycles, these initiated micro-cracks propagate continuously and lead to catastrophic failure. The observation of rubber resistance against the FCG is necessary to characterize. The tearing energy criterion is commonly used for the fatigue dynamic fracture analysis. There is only one commonly used test equipment for the quantitatively description of dynamic crack propagation working under the real loading conditions. This is the Tear Analyzer made by Co. Coesfeld GmbH & Co. KG[4].

Materials and experimental details

Three different rubber compounds firstly based on 50/50 SBR/NR (denoted: S-NR-N) and secondarily on 50/50 SBR/EPDM (denoted: S-E-N) blends were filled with 60 phr of normal carbon black N234. The third compound, also based on 50/50 SBR/EPDM (denoted: S-E-M), was filled with carbon black N234 in the masterbatch form. The additional typical curatives corresponding to the composition of the real tyre compound were added. The rubber compounds were prepared using a laboratory internal mixture. The test specimens were cured in a compression mould according to

the determined rheometric properties.

The experimental analysis were performed according to the real rolling condition of tyre 215/70 R16 at a speed of 8 Kmph corresponding to the pulse loading frequency 1 Hz whereas the loaded tyre footprint consists of 35° segment of the whole tyre. Thus the pulse width was determined on 100 ms.

FCG measurements were carried out using Tear Analyzer under pulse as well as sinusoidal loading conditions for the comparison of the real and unrealistic simulation of tyre rolling. The frequency for the pulse loading was set on 1 Hz, while the sinusoidal loading was carried out at frequency
10 Hz, to measure under the identical impact duration while 100 ms. The strain was varied between 5 % and 25 %. The analysis was performed at room temperature. In this study, two double notched and one not-notched pure shear test specimens were simultaneously analysed, whereas the un-notched test specimen was used for determination of tearing energy[1]. The standard pure shear test specimen with the geometry ratio L_0 (length)/Q (width) = 1:8 was used[5]. Each of the pure shear test specimen was notched with notch length a_0 = 21 mm in the both side of test specimen calculated from the definition of minimal notch length a_{0min} in dependence on geometry ratio[6] L_0/Q.

The analysis of the frictional sliding of a hard blade abrader on the rolling rubber test specimen has been performed using the test equipment developed by Maňas et al.[7]. The standard cylindrical test specimens with the diameter 55 mm were used and the testing conditions were set according to the above denoted tyre rolling. The energy E = 2,77 J impacted the revolving test specimen in frequency 1 Hz.

Results and discussion

In Scheme 2, the influence of the real (pulse) and unrealistic (sinusoidal) loading conditions simulation of impact to the rolling tyre as well as the different types of compounds on FCG rate becomes apparent. It was found that the FCG rate at a given tearing energy as well as the FCG trend increase significantly under the pulse in comparison to the sinusoidal loading conditions independent on type of analysed compound. Therefore, the real pulse loading represents a more critical condition for the fracture behaviour of tyre! The reason for this behaviour is the effect of stress relaxation in the test specimen occurred in the un-loaded phase of tyre rolling. When the deformation forces are removed, the rubber network adopts a state, that is different from the initial state and the rubber relaxes[9]. The again dynamically applied stress, after the relaxation, the fracture and recombination of crosslinks take place. The comparison of pulse and sinusoidal loading conditions also shows different trends in the FCG resistances. The FCG resistance for the compounds analysed under sinusoidal loading conditions were determined in the following order: S-E-N < S-E-M < S-NR-N, whereas under pulse loading the different trend is shown: S-E-M < S-E-N < S-NR-N. As expected, the blend based on SBR/NR shows the highest FCG resistence due to the strain induced crystallinity in NR.

The relationship between the FCG rate and tearing

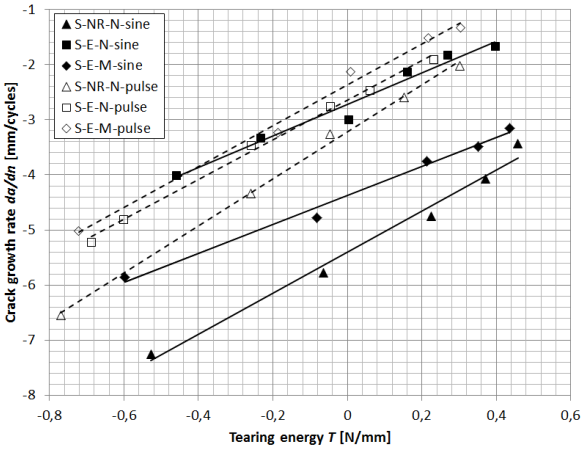

Scheme 2. **Influence of sinusoidal and pulse loading conditions on FCG**

energy is compared to the independently measured rate of wear. In the Scheme 3 the wear resistance of the compounds were determined in the following order: S-E-M < S-E-N < S-NR-N, whereas the compound based on SBR/NR shows the highest wear resistance. A significantly decrease in the wear resistance measured in the remaining compounds is caused due to EPDM basis. The trend of wear resistance diverges with the FCG resistance determined under sinusoidal loading, while the trend corresponds with the FCG resistance of the compound analysed under the pulse loading. The simulation of near to similar testing conditions between the FCG rate and Chip & Cut measurement provides the identical trends of mechanical behaviours.

The future trends for the characterization of the relationship between the structure of rubber matrix and fracture mechanical behaviors are conditioned with the development of new measuring system for simulation of frictional sliding of a hard blade abrader on rubber test specimen corresponding to the real loading of a rolling tyre. The measuring method and equipment based on real pulse simulation in dependence of tyre dimension is objective of the common research of Co. PRL Polymer Research Lab. The future measuring system takes in to account the on-line

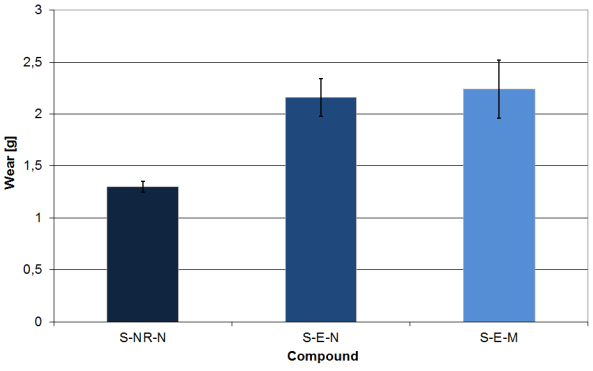

Scheme 3. **Comparison of the mass loss respectively wear rate**

controlling of the time and depth as well as the impact frequency of abrader sliding on the rubber test specimen during the complete analysis. The process of analysis is electronically controlled with force respectively energy of sliding or with defined depth of sliding abrader in test specimen. Thus the real testing condition of rolled tyre can be simulated and the energy dissipation during the sliding of hard abrader can be firstly exact determined.

Conclusion

The work deals with description of influence of the real (pulse) and unrealistic (sinusoidal) loading conditions corresponding to the rolling tyre on FCG rate. It was demonstrated, that the real pulse loading represents a more critical condition for the fracture behaviour of tyre. This fact together with the diverse relationship between the evaluated wear and determined FCG resistance under sinusoidal loading pointed out the relevance of the analysis under the real loading conditions. As future trends for the exact characterization of the relationship between the structure of rubber matrix and fracture mechanical behaviors caused due to the frictional sliding of a hard blade abrader on rubber according to the tyre rolling conditions a new measuring method and system has been introduced.

This contribution was written with support of Operational Program Education for Competitiveness co-funded by the European Social Fund (ESF) and national budget of Czech Republic, within the framework of project Advanced Theoretical and Experimental Studies of Polymer Systems (reg. number: CZ.1.07/2.3.00/20.0104).

REFERENCES

1. Rivlin R.S., Thomas A.G.: J. Polym. Sci. *10*, 291 (1953).
2. 2. Persson B., Albohr O., Tartaglino U., Volokitin A.I., Tosatti E.: J. Phys.: Condens. Matter *17*, R1-R62 (2005).
3. Fukahori Y., Liang H., Busfield J.J.C.: Wear 265, 387 (2008).
4. Eisele U., Kelbch S.A., Engels H.-W.: KGK, Kautsch. Gummi Kunstst. *45*, 1064 (1992).
5. Stoček R., Heinrich G., Gehde M., Kipscholl R.: KGK, Kautsch. Gummi Kunstst. *65*, 49 (2012).
6. Stoček R., Heinrich G., Gehde M., Rauschenbach A.: J. Plast. Technol. *01*, 2 (2012).
7. Liang H., Fukahori Y., Thomas A.G., Busfield J.J.C.: Wear *266*, 288 (2009).
8. Manas D., Manas M.: JAMME *37*, (2009).
9. Rivlin R.S., Thomas A.G.: Eng. Fract. Mech. *18*, 389 (1983).

CL-26
COMPOSITION OF TIRE PYROLYSIS PRODUCTS

DALIBOR SUSA and JUMA HAYDARY*

Institute of Chemical and Environmental Engineering, Faculty of Chemical and Food Technology, Slovak University of Technology in Bratislava, Radlinského 9, 812 37, Bratislava, Slovakia
juma.haydary@stuba.sk

1. Introduction

This contribution deals with pyrolysis of waste tires and the influence of various process parameters on product distribution and composition. Waste tires are composed of more than 100 substances, the main of them being: rubber (50 wt.%), fillers like carbon or silica gel (25 wt.%), steel cords (10 wt.%), sulphur (1 wt.%) zinc oxide (1 wt.%) and many other additional substances such as processing oil, plasticizer, anti-degradants and vulcanization accelerators. Due to their high heating value, carbon and volatile matter content, waste tires are a valuable material for energy recovery.

Pyrolysis experiments were carried out in a laboratory screw type reactor, under different conditions, by varying temperature and residence time. The effect of above mentioned parameters was investigated with regard to composition of process gas and mass yields. Liquid and solid products were analysed by elemental analysis and gas compositions were determined by gas chromatography.

It was found that the liquid fraction decrease with higher temperature and increase with longer residence time. The gas fraction consisted mainly of hydrogen, methane and light hydrocarbons. The formation of hydrogen and methane was preferred at higher temperature and shorten residence time, opposite to the light hydrocarbons formation.

2. Experimental

Shredded steel-less tire sample was used for the experiments. In order to quantify the amount of volatile and non-volatile components thermogravimetric and elemental analysis of raw sample was performed. The volatile fraction was determined to be 63.5 mass% and the non-volatile one was 36.5 mass%. Elemental composition of tire sample is shown in Table I.

The pyrolysis experiments were carried out in a laboratory pyrolysis reaction unit in a nitrogen atmosphere. The pyrolysis unit consisted of a continual screw type reactor, a cooling system and a gas analyser. The flow reactor was working under isothermal conditions and the residence time of the solid particles was controlled by a frequency circle of rotating metal screw. The pyrolysis experiments were performed over the range of temperatures of 600–750 °C and at residence times Rt1 (135.4 s), Rt2 (99.4 s) and Rt3 (75.5 s). A detailed description of the apparatus is provided in ref.[1]. Solid and liquid fractions were analysed using an elemental analyser Vario Macro Cube (Elementar Analysensysteme, Hanau, Germany). The analysis of gaseous phase was done on a Micro Box III (SLS MICRO TECHNOLOGY, Hamburg,

Table I
Elemental composition of raw tire sample

Component	N	C	H	S	O[a]	Residue[b]
Content / mass %	0.4	80.4	7.4	1.6	2.7	7.5

[a] Calculated from the difference to 100 %, [b] residue: non-combustible matter

Germany) gas chromatograph with a thermal conductivity detector TCD.

3. Results and discussion

Solid and liquid pyrolysis yields were determined in each experiment by weighing the obtained amount and calculating the corresponding percentage. The gas yields were determined by difference and, therefore, include all the experimental errors and inaccuracies. Product yields of solid, gaseous and liquid (tar) fraction at various temperatures and residence times are shown in Fig. 1. An increase in the amount of gases and a consequent decrease in the amount of liquids can be seen. This decline in the liquid fraction and increase in the gaseous yields was also observed by other authors and it can be explained by the stronger thermal cracking processes taking place at higher temperatures[2]. Concerning residence time, there was a slight increase in liquid yields with temperature as a result of shorter time for decomposition to take place.

Tire pyrolysis gases were mainly composed of light hydrocarbons (ethane, ethene etc.), hydrogen and methane together with some CO, CO_2 and H_2S.

The results for the composition of the gases are shown in Fig. 2, where it is to be observed that the higher the pyrolysis temperature is, the more methane and hydrogen is present in the gas, while the remaining hydrocarbons decrease. This drop in the light hydrocarbon chains and the

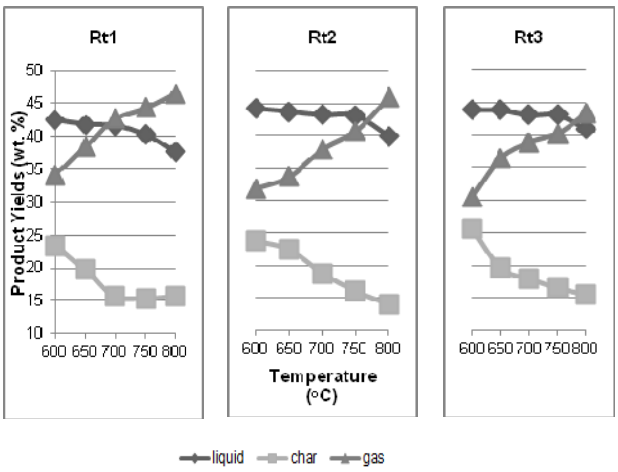

Fig. 1. **Product yields as a function of temperature and residence time**

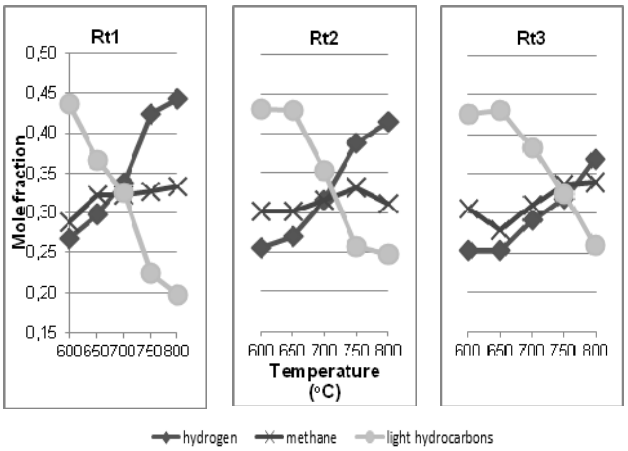

Fig. 2. **Composition of key gas components**

rise in the methane and hydrogen with temperature is due to the mechanism of the pyrolysis process itself. As temperature rises, the heavier hydrocarbons are cracked, giving rise to lighter ones, methane and hydrogen[3]. Consequently, the gas samples become enriched with the lighter hydrocarbons as the temperature increases. Furthermore, the higher the final temperature of pyrolysis is, the less CO_2 is produced, while CO increases, probably because of the secondary reactions taking place during the pyrolysis process. In this last step CO is formed from reactions in the gas phase between CO_2 and hydrocarbons or from other cracking reactions.

Pyrolysis liquid is a very complex mixture of organic compounds of 5–20 carbons and with a great proportion of aromatics and aliphatic. The elemental analysis results are shown in Table II. There can be seen a decrease in carbon fraction at higher temperature, possibly due an increase of aliphatic, nitrogenated and benzothiazol compounds. It may be concluded that in the low temperature pyrolysis, there are more free aliphatic compounds, while in the higher-temperature liquid, many of such aliphatic are linked to aromatic structures. Similar results concerning the increase of aromatics with temperature have been observed at other residence times.

The increase in oxygen could be caused due to the production of oxygenated compounds at higher temperatures.

Table II
Elemental composition of liquid at Rt1

T [°C]	N	C	H	S	O+others[a]
600	1,24	89,91	7,53	1,15	0,17
650	2,03	85,91	7,67	1,17	3,22
700	2,13	85,31	7,64	1,15	3,77
750	1,14	83,12	7,71	1,14	6,89
800	1,21	82,56	7,37	1,12	7,74

[a] Calculated from the difference to 100 %

Table III
Elemental composition of solid at Rt1

T [°C]	N	C	H	S	Ash[a]	O+others[b]
600	0,05	86,48	0,86	2,56	9,50	0,54
650	0,00	86,98	0,76	2,52	9,60	0,14
700	0,00	86,35	0,82	2,38	9,90	0,55
750	0,00	85,48	0,63	2,50	10,30	1,09
800	0,00	86,39	0,54	2,51	9,50	1,06

[a] Determined by thermogravimetry, [b] calculated from the difference to 100 %

These compounds have been identified by several authors[4]. The presence of these compounds can be explained as a result of the thermal degradation of oxygenated compounds of tires, such as stearic acid, extender oils, etc.

Pyrolysis char is composed mainly of carbon black and ash. The elemental composition of the solid obtained at every temperature and residence time is presented in Table III. The ash contained in the pyrolytic residues come from the inorganic fillers of the original tire. It can be seen that there is almost no effect of pyrolysis temperature on the elemental composition of the chars. This is logical since the main polymeric component of automotive tires is styrene–butadiene rubber and temperature above 600 °C is sufficient for release of all volatiles. Similar results have been observed at other residence times Rt2 and Rt3.

4. Conclusions

Yields of solid, liquid, and gas obtained from isothermal pyrolysis of waste tire have been calculated. The studied parameters were: temperature and residence time. Increasing the temperature resulted in an increase of gas fraction and a decrease of liquid and solid fraction. The influences of residence time on the product distribution is negligible compared to the influence of temperature.

The gas fraction was a mixture of hydrocarbons of low molecular weight (ethane, ethene) methane and hydrogen. The composition of this gas fraction depends on the final temperature of pyrolysis. High temperatures favour the presence of hydrogen and methane, while low ones mean a higher proportion of light hydrocarbons.

This work was supported by the Grant VEGA No. 1/0753/13 from the Slovak Scientific Grant Agency.

REFERENCES

1. Haydary J., Jelemenský Ľ., Markoš, J., Annus, J.: KGK, Kautsch. Gummi Kunstst. 661–665 (2009).
2. Font R., Fullana A., Conesa J.: J. Anal. Appl. Pyrolysis *74*, 429 (2005).
3. Dai X.,W., Yin X., L., Wu C., Z., Zhang W., N., Chen Y.: Energy *26*, 385 (2001).
4. Laresgoiti M. F., Caballero B. M., De Marco I., Torres A., Cabrero M. A., Chomon M. J.: J. Anal. Appl. Pyrolysis *71*, 917 (2004).

CL-27
INFLUENCE OF PA6 GF25 REGRINDS CONTENTS ON THE MECHANICAL PROPERTIES OF THE OIL FILTER CORE

MAREK SZOSTAK and JACEK ANDRZEJEWSKI

Poznan University of Technology, Institute of Materials Technology, Piotrowo street 3, 61-138 Poznan, Poland
marek.szostak@put.poznan.pl

Filters for internal combustion engine vehicles appeared shortly after the construction of the first vehicles of this type of drive. Currently, each vehicle equipped with elements for removing impurities from the oil, fuel, air supplied to the engine and the passenger compartment. The continuous development of engine components increases the demands on the filter, the more strained and finely crafted units must be better protected from pollution. In addition to the technical requirements of the growing ecological requirements. The objective is to design the filter to minimize the negative impact on the environment[1–3]. At the same time customers demand the best performance at the lowest price. For several years popularity of EKO filter, in which plastic parts replace metal details is growing. This solution lowers the cost of production and facilitates the recycling of used filters. Manufacture of large quantities of plastic parts leads to the formation of waste products that must be exploited. Transformation of plastics by injection makes it possible to re-use material by grinding and recycling in injection molding technology. Reprocessing of materials may change its properties, which in some, especially high loaded elements disqualifies its use[1–3].

The aim of this study was to determine the maximum content of PA6 GF25 regrind in the oil filter core C-2073 by examining the influence of regrind on the mechanical properties of that part.

EKO-type oil filters are mounted in demountable enclosures, which are an integral part of the engine. His filter cartridge consists of filter paper fused in upper and lower bottom. The oil supplied from the oil pan through the oil pump is purified by flow through the filter medium in the direction of the filter interior. OE673 oil filter is one of the most popular filter installed in many modern cars such as: Citroen C2, C3, C4, Ford Focus, Kuga, Peugeot 207, 308, 407, both gasoline and diesel engines[4].

The material used for the oil filter bottoms is polyamide 6 with talc, which as filler lowers the cost and makes it easier to fusion barrier filter into the bottom. Cores are produced from polyamide 6 reinforced with glass fiber, which improves its mechanical properties. The core in EKO type oil filter prevents the paper collapse into the filter, in some of the solutions have also some other functions. The OE673 oil filter core has a cross (Fig. 1), whose task is to close the oil drain into the oil pan. At the time of the filter changing after unscrewing the housing nut, the trigger is opened and the oil can flow from the filter housing. In the case of the cross cracks in the core, the oil from filter housing drains into the sump, which caused the reducing the pressure in the oil system. The loss of oil pressure in the lubrication system may result in damage to the engine; therefore, it is very important

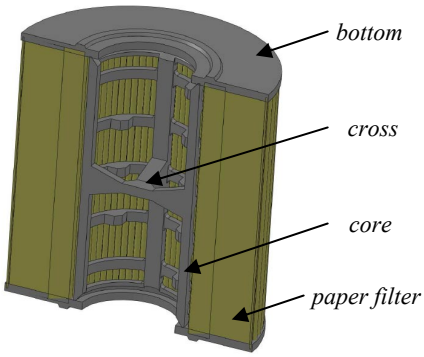

Fig. 1. **Construction of the oil filter type OE673 (ref.[4])**

to provide adequate mechanical properties of the core.

Core C-2073 is produced from polyamide 6 with 25 % glass fibers (Tarnamid T-27 GF25) on the injection molding machine MARS 1600 from HAITIAN Company. The parameters of the injection molding process are as follows: melt temperature 260–280 °C, mold temperature 65 °C, drying temperature 110 °C, injection pressure 65 MPa, injection speed 40–65 mm s^{-1}, holding pressure 40 MPa, holding time 2 s, cooling time 8 s.

To carry out the test, samples containing regrind from 0 to 50 % weight contents were prepared. In addition, the cores made from 100 % regrind have been prepared too. The regrind has been obtained from production wastes by grinding them in the mill. The regrind has two times bigger size (around 5 mm) to compare with original polyamide 6 granulates (grains about 2.5 mm). From each samples with different regrind content, 20 cores has been obtained by injection molding from which 6 was selected for further study. Selected cores were measured before conducting the tests. The results of dimension measurement are presented in the Table I and II. The cores strength tests has been preceded on the Zwick testing machine and consisted of pushing the special rod into the core cross. An attempt was to simulate the operation of the core in the filter housing. In order to check the strength of the internal core cross, the axial load was applied (Fig. 2 and 3). The results of mechanical tests are shown in Table I.

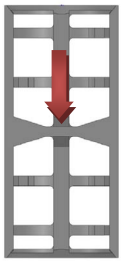

Fig. 2. **The point of force application to the core**

Fig. 3. **The view of testing stand**

Table I
The results of force [N] required to destroy the core in dependence on the regrind content

Test no.	0%	10%	20%	25%	40%	50%	100%
1.	783	741	728	769	772	714	726
2.	787	759	720	747	767	729	757
3.	719	763	776	737	751	782	758
4.	781	718	781	732	742	779	775
5.	766	775	762	782	738	753	765
6.	719	782	771	741	759	774	752
Average	**759**	**756**	**756**	**751**	**754**	**755**	**756**

The mminimum reference force is 650 N which has been determined on the basis of strength tests of the OE filter cores, which are regarded as a model. Differences in the strength results can be partly due to the lack of perfect eccentricity during conducting the tests. As shown in Table II, the increase of the regrind contents does not change the force required to destroy the sample. Therefore, the use of regrind not adversely affects the mechanical properties of the C-2073 core.

As it is seen from the Tables II and III, with increasing of regrind content in the input material, the core diameter decreases gradually, obtaining a dimension smaller of

Table II
Results of core diameter [mm] measurements in dependence on the regrind content. Nominal diameter 29 (+/-0,2)mm

Test no.	0%	10%	20%	25%	40%	50%	100%
1.	29,11	29,05	29,09	29,07	29,02	28,98	28,94
2.	29,15	29,04	29,12	29,06	29,04	28,97	28,90
3.	29,12	29,03	29,13	29,06	29,01	28,98	28,93
4.	29,09	29,05	29,11	29,05	29,01	28,99	28,94
5.	29,11	29,04	29,09	29,06	29,02	28,96	28,95
6.	29,08	29,05	29,06	29,07	29,03	28,95	28,92
Average	**29,11**	**29,04**	**29,10**	**29,06**	**29,02**	**28,97**	**28,93**

Table III
Results of core height [mm] measurements in dependence on the regrind content. Nominal height 64 (+0,3/–0,1)mm

Test no.	0%	10%	20%	25%	40%	50%	100%
1.	64,15	64,15	64,19	64,19	64,22	64,25	64,29
2.	64,16	64,19	64,20	64,18	64,21	64,27	64,30
3.	64,15	64,17	64,18	64,19	64,21	64,25	64,29
4.	64,14	64,18	64,18	64,18	64,23	64,27	64,31
5.	64,14	64,14	64,19	64,19	64,19	64,28	64,30
6.	64,16	64,15	64,19	64,21	64,21	64,27	64,29
Average	**64,15**	**64,16**	**64,19**	**64,19**	**64,21**	**64,27**	**64,30**

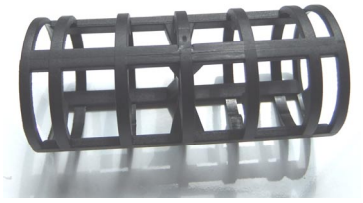

Fig. 4. **The injection point on the C-2073 core**

0.19 mm. In that same time the height of the core is increasing of 0.15 mm.

The location of the injection point (Fig. 4) causes the problem of an accurate determination of the various types of contractions in different areas of the analyzed part.

We suppose that grinding in the sieve mill can causes a degradation of polymer, which may have a direct effect on the processing shrinkage. Longitudinal shrinkage, most noticeable to the core height, seems to be smaller. That dimension for core obtained from 100 % regrind material achieved the upper tolerance limit – 64,30 mm. For the outer core diameter, it is very difficult to determine clearly which type of shrinkage predominated and what their size is. The nominal outer core diameter is 29,00 +/– 0,2 mm and with increasing the regrind content it decreases but remain within the established tolerances.

- The research has shown that adding the polyamide regrind does not affect the mechanical properties of the oil filter core C-2073.
- Dimension analysis of the molded part has shown that the optimal content of the PA6 regrind material is 25 %, due to assurance of the tolerance field for the molded C-2073 core.
- It is possible to use the regrind from production PA6 wastes for manufacturing the new elements with good mechanical properties and suitable dimensional tolerance.

REFERENCES

1. *Recykling odpadów polimerowych z elektroniki i pojazdow*, Kozłowski M., Rydarowski H., Wydawnictwo Naukowe Instytutu Technologii Eksploatacji, Radom (2012).
2. *Plastics Recycling in Europe*, Kozłowski M. Wydawnictwo Politechniki Wroclawskiej, Wroclaw (2006).
3. *Kunststoff im Automobil*, Einsatz und Verwertung, VKE, Frankfurt/Mainz (2008).
4. Wix Filtron – producer data (2011).

CL-28
DEVELOPMENT OF MODULAR FLOOD BARRIER CONCEPT MADE FROM RECYCLED PLASTIC

ĽUBOMÍR ŠOOŠ[a], JURAJ ONDRUŠKA[a], PETER BIATH[a], and PAVEL KOVÁČ[b]

[a] Faculty of mechanical engineering STU in Bratislava, Nám. Slobody 17, 812 31 Bratislava,Slovakia, [b] TU Noví Sad, Serbia
lubomir.soos@stuba.sk

Key words: recycled plastic, ant flooding, Watergates

This contribution describes developments in the area of plastic recycling aimed at the reuse of waste materials for the manufacture of a useful product. Throughout development of the concept “modular flood barrier structure”, the recovery of plastic materials was assessed, primarily, plastic waste from automobiles and industry. For the modular design of the structure a utility model was prepared[2]. In terms of the type and composition of source material, polypropylene (PP) and polyethylene (PE) were the materials chosen. When designing the geometry and constructing the barrier, the first stage was to design the structure based on the shape of unified blocks made from PP and PE. These unified blocks were designed in Slovakia at Chemosvit Environchem, a.s. but are also available internationally. In cooperation with Chemosvit, the focus was to produce blocks made from recycled materials and their subsequent application for beneficial use. The present need for flood protection inspired its production from these recycled materials. The suitable shape and strength characteristics of the plastic blocks provided sufficient grounds for the development of the flood barrier. In the first phase, different structural shapes were assessed in terms of their stability to determine their suitability for the given application. The results of these efforts were the initial design of the whole structure and its parts. Following this, the structure was revised and a prototype was constructed. The structure underwent numerous optimization processes including finite element analysis (FEA) and internal/external stability analysis. Production documentation, prototypes, and field tests were also performed. Currently, changes to the design are being performed in order to prepare it for mass production.

Development

The Slovak university of technology in Bratislava is currently involved in the project “research of progressive technologies for the recovery of waste from scrap automobiles” in harmony with the priorities of the Slovak

ministry of environment (SME). The principal coordinator of the project is the faculty of mechanical engineering, and the project is financed by the recycling fund in Slovakia. SME has stated in a press release that: "foremost, the effective protection against flooding, and the reduction of environmental burdens in sensitive and national park zones remain a priority". Ing. Peter Žiga, PhD., press release minister of Environment SR, (SME,1.7.2012 and HN, 28.2.2013)."

The primary objective of the project is to increase the effectiveness and sustainability of developing ecological security in the collection and processing of scrap automobiles and solving problems in their recycling. To meet the goals of the project, specific objectives were set, whose integrated results satisfy the main goal. The specific goals of the project can be divided into four parts:

1) Prediction, determining optimal technologies, methods and logistics in processing automobiles.
2) Proposal of optimal structure and function from research centers in collaboration with the automotive industry in the Slovak republic and processors of scrap vehicles.
3) Specification in the areas of research and development of new technologies and specific machine nodes on the basis of waste and secondary materials.
4) Research of new products which increase the recovery of recycled materials and ensure its demand in the synergy of waste processes.

The key requirement of the project results are that the results of the research were not tied to one processor but rather to be implemented in all processors of scrap vehicles in the SR under the auspices of the Slovak automotive industry. In terms of the current state of scrap vehicle processing, three consecutive and chronological stages with two main branches (analytic and scientific research) are proposed. In order to ensure the highest quality of the results, individual parts of the project are solved in cooperation with qualified external organizations with unique or otherwise appropriate specializations.

The first stage of the project was performed from May 2011 to June 2012.

The major challenges that emerged from the analysis are "Research of technology for the effective processing of car bodies" and "research of technologies for the recycling of difficult to recover waste, proposal of new products which increase the usage of recovered materials" – and applying this to successfully develop a needed product "flood barriers".

Modular structure of mobile flood barrier concept manufactured from recycled plastic

Integrating the outputs of cooperating groups, the investigators began to explore possibilities in applying plastic waste from scraped vehicles as recycled material in the production of new products. Many types of flood barriers exist internationally. During the implementation of the project's first phase (May 2011 to June 2012) problems in mobile flood barrier concepts were explored. The structure, shape, material and operation of a wide range of flood barrier products were analyzed with the intention of identifying strong and weak points of each individual design and applying the knowledge obtained in the research of a new concept. This new concept was based on the integration of existing systems, using their benefits to design a new flood barrier. The basic requirements for the new barrier were that it would be: produced from recycled materials, self-anchoring but not permanently anchored to the ground, could be used on firm and soft ground, allow for convex and concave configurations, can copy rough terrain, can be easily deployed and removed, and can adjust the barriers height. The investigators filed a utility model application no. SK 5847 Y12 entitled "Modular flood barrier structure". This utility model serves as a basis for more detailed solution of flood barriers. The proposed design structure theoretically allows, from one system, to create two similar configurations and arrangements from the modular flood barrier structure.

The first modular flood barrier structure has a vertical wall constructed of braced, L-shaped structures seen in Fig. 1. The water enters the barrier from the inside and the braces are loaded in tension. The stability of the barrier (in terms of shifting and tipping) is guaranteed by the force action of hydrostatic pressure in the vertical direction.

The second modular structure consists of an angled and horizontal part (Fig. 2). In this design, the water acts on the barrier from the outside were the connecting braces are loaded in compression. The hydrostatic pressure of the water on the sloped surface ensures adequate anchorage to prevent its movement.

If the barriers are installed on firm ground, then a rubber seal is placed below the horizontal parts of both water barriers. In the case that the barriers are located on uneven or soft ground, then anchoring pikes are used on the horizontal

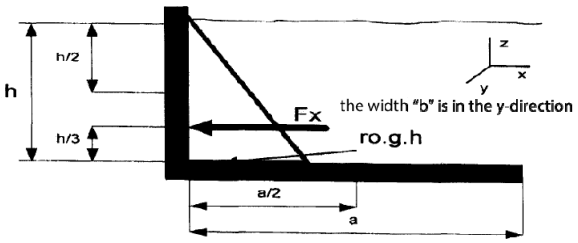

Fig. 1 **Flood barrier with vertical wall, 1-base, 2-vertical wall, 4-brace**

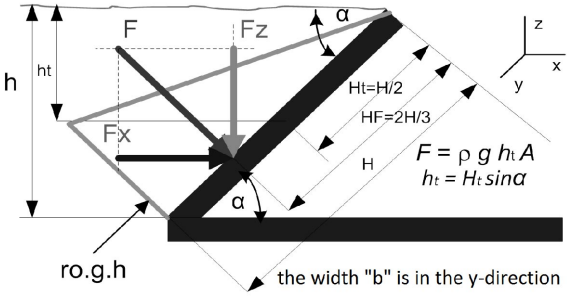

Fig. 2 **Flood barrier with sloping wall**

parts. Connecting the vertical parts is done by using attachment bars. To obtain greater stability, the vertical parts are mounted to each other in a pattern (long to short to long etc…) and are connected with bars. The structure, to a certain extent, allows for a curved barrier. For a convex shape (Fig. 3a) the horizontal parts are not necessary to connect. For concave shape (Fig. 3b) it is only necessary to connect every other horizontal part. The modular structure of the flood barrier also allows for deployment over uneven terrain (Fig. 3c). In this configuration, the horizontal bars are not necessary.

The most practical realization indicated a sloped configuration. The main reason for this was the undesirable effect of submerged functional parts in the L configuration. The sloped barrier consists of a system of horizontal parts and sloped parts. The angle of the sloped part is adjustable by the length of the braces and the position of their attachment point. The modular structure allows for the change in length of the sloped parts. The technical advantages of the modular structure are evident in the effects induced externally.

Calculation of the barriers under static loading was performed through two independent methods. The results from the faculty of mechanical engineering STU (SjF STU, Table I) in Bratislava and the results from external experts at the faculty of civil engineering at STU (SvF STU, Table I) in Bratislava where compared for different angles of the barrier under given loading conditions (Table I).

An important part of the development process was the constant assessment of the structure by experts in the area of FEA and statics (Fig. 4). The initial, relatively simple, simulation indicated that the system can become unstable and therefore it was necessary to perform a more complex analysis of the assembly which included all important interactions so that the simulated state best represented real conditions.

In the next phase, the construction was optimized, mainly with respect to satisfy the manufacturing processes for the test model. A parametric simulation model was constructed with variable geometry in order to obtain the most suitable shape of the structure. The simulation consists of the load F1=17720 N, pressure acting on the walls at a water level of 1.6 m, water pressure on the flap p1= 0,016 MPa, and the assumption of terrain between the base and the surface f=0,55. All of which resulted in the stress spectrum and deformation of a system which best represents the real conditions, states, and reactions in important nodes of the device (Fig. 5).

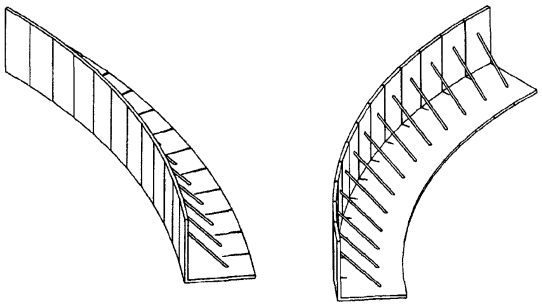

a) Convex shape b) Concave shape

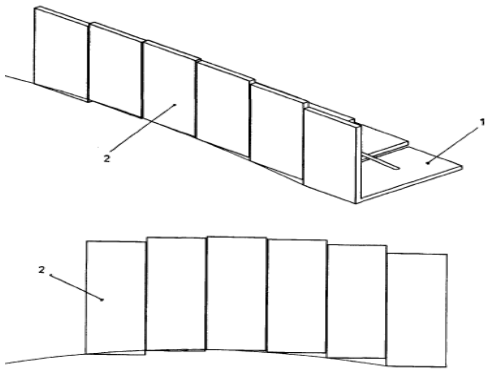

c) Following uneven terrain

Fig. 3. **Modular flood barrier structure**

Table I
Forces acting on the wall segment with a width of 1.12m at different angles and water depths

Angle alpha[°]	h[m]	H[m]	F[kN] SjF STU	F[kN] SvF STU	Fx[kN] SjF STU	Fx[kN] SvF STU	Fx[kN] SjF STU	Fz[kN] SvF STU
90	2,05	2,052	23,132	-	23,132	-	0	-
60	1,78	2,052	20,033	20,033	17,349	17,349	10,016	10,016
55	1,68	2,052	18,948	18,949	15,522	15,522	10,868	10,868
50	1,57	2,052	17,72	17,72	13,574	13,574	11,39	11,39
45	1,45	2,052	16,357	16,357	11,566	11,566	11,566	11,566
40	1,32	2,052	14,869	14,869	9,557	9,558	11,39	11,39
35	1,18	2,052	13,268	-	7,61	-	10,868	-
30	1,03	2,052	11,566	-	5,783	-	10,016	-

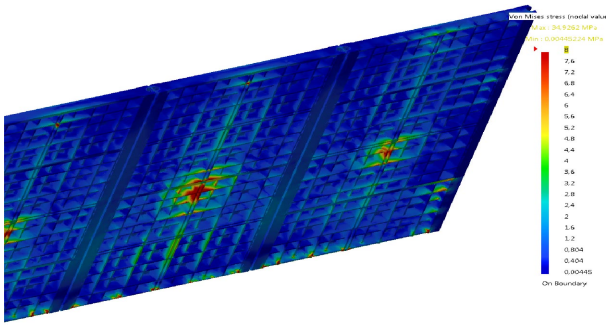

Fig. 4. **MKP analysis of a system of blocks, Von Mises stress assessment [MPa]**

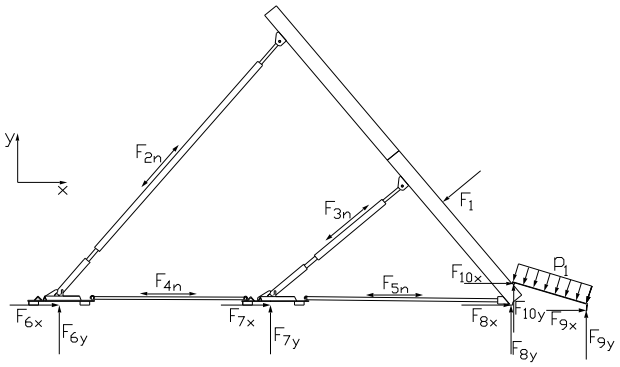

Force	[N]	Force	[N]	Force	[N]
F1	17720	F6x	1443,5	F8y	11018,6
F2n	5288	F6y	3996,8	F9x	7922
F3n	1118	F7x	64,9	F9y	1720
F4n	2017	F7y	762,8	F10x	-6111
F5n	2782	F8x	5934	F10y	-4388

Fig. 5. **Graphical interpretation of the complex FEA simulation, reaction values**

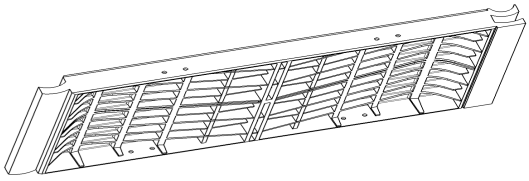

Fig. 6. **Weight savings of the plastic blocks with clip connections**

variant a)

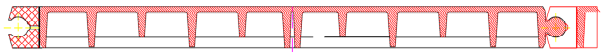

variant b)

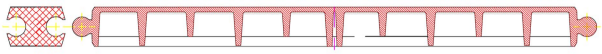

variant c)

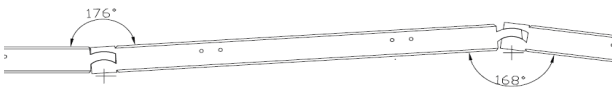

Fig. 7. **Possibilities of connector modules and blocks**

Ambition and direction of further research

In terms of the optimization of the structure, the investigators will focus on factors affecting the mass production of the flood barrier and its effectiveness, Fig. 6. Another goal is to determine a simpler construction for less demanding operational conditions, Fig. 7. The optimal manner for production seems to be injection. However, to this point, there have not yet been any producers capable or willing to realize such a process. Despite this, the proposed design has been considered very successful so far.

This contribution was made by realization of the project Development of progressive technology of compacting biomass and manufacture of prototypes and highly-productive tools (ITMS code of the project: 26240220017), based on the support of operational system of program Study and development financed from European fond of regional improvement.

REFERENCES

1. Šooš Ľubomír a kol: Research of progressive waste recovery technologies for scrap vehicles, Project Recycling fund, April 2011.
2. Šooš Ľubomír, Prikkel Karol, Ondruška Juraj, Olekšák Ján: Modular structure of flood barrier. 2011, 16 s.: No. Utility model: 5847 SK , Effective as of: 19.8. 2011
3. Šooš Ľubomír, Ondruška Juraj, Čačko Viliam, Biath, Peter: Modular structure of mobile flood barrier concept. In: Waste – Luhačovice 2012 : 20. IC,- ISBN 978-80-904356-6-7. - Pp. 49–58
4. Radonjić S., Kovač P., Slavković R., Dučić N., Baralić J.: Experimental determination of chip compression ratio during counterboring, Tehnics tehnologies education management, 2012, Vol. 7, No 2, pp. 539–543, ISSN 1840-1503

CL-29
BIODEGRADABLE POLYMER BLENDS FROM RENEWABLE RESOURCES

KATARÍNA TOMANOVÁ, PAVOL ALEXY, MIROSLAVA MIKUŠOVÁ, MICHAL MIHALÍK, RODERIK PLAVEC, JÁN BOČKAJ, and ZUZANA VANOVČANOVÁ

Institute of Polymer Materials, Faculty of Chemical and Food Technology, Slovak University of Technology, Radlinského 9, 812 37 Bratislava, Slovak Republic
katarina_tomanova@stuba.sk

Abstract

In this work, attention was focused on study of polylactid acid (PLA) and thermoplastic starch (TPS) blends modified with modifier M. In these blends, the content of each component was gradually changing and influence of modifier on mechanical properties was studied.

Introduction

Biodegradable polymeric packaging materials, especially polymers from renewable resources, represent a new generation of packaging materials. Their main advantage is a fact, that their whole life cycle is oriented to protecting environment and human healthy. But these polymers have some disadvantages like sensibility on water and air moisture, they have worse thermal stability, worse some mechanical and barrier properties. The solution of these problems lies in finding appropriate modification techniques, either by adjusting the processing conditions, a suitable composition of polymer blend, or combination of both.

Polylactic acid (PLA) is semi-crystalline, linear, thermoplastic polyester with good processability, biocompatibility and biodegradability as well. PLA is the front runner in the emerging bioplastics market. PLA can be produced by condensation polymerization directly from its basic building block lactic acid or by conversion of lactide—the cyclic dimer of lactic acid—to PLA via ring-opening polymerization[1]. PLA exists in two enantiomeric forms – L-lactic acid and D-lactic acid. It has similar mechanical properties like polystyrene (PS), with elastic modulus of 3000–4000 MPa, tensile strength of 50–70 MPa, glass transition temperature of about 60–70 °C and elongation at break of 2–10 %. It is a versatile polymer, with high transparency, high molecular weight, good processability and water solubility resistance. Its usage is oriented in packaging, biomedicine, electronics, automobile and other consumer applications like blown bottles, extruded cast and oriented films, and melt-spun fibers for nonwovens, textiles and carpets.

Starch is a renewable and widely available raw material, being the end product of photosynthesis. It is the storage polysaccharide of cereals, legumes and tubers. Starch is composed of a mixture of two substances, an essentially linear polysaccharide-amylose and a highly branched polysaccharide-amylopectin[2]. The size, shape, and morphology of the starch granules are characteristic of the particular botanical source. The glass transition temperature of the dry starch is in the range of 240–250 ºC (ref.[2]). Native starch is a nonplasticized material because of the intra- and intermolecular hydrogen bonds between hydroxyl groups of starch molecules. In order to process thermoplastic starch, it is necessary to disrupt its crystalline structure. The physical properties of the thermoplastic starch (TPS) are greatly influenced by the amount of plasticizer present. Mostly, polyols are usually used as plasticizers, of which glycerol in combination with water is the major one. Main application areas of TPS or starch based materials include foams for the loose-fill foam market, films for agriculture, shopping bags and mouldable products like pots, cutlery or fast food packaging.

Experimental

Materials

- Polylactic acid – PLA 4042D from NatureWorks, LLC, USA
- Starch – Meritena 100 from Amylum Slovakia, SR
- Glycerol – GL from H.C.I. Slovakia, SR as starch plasticizer
- Water – as auxiliary starch plasticizer
- Modifier M as blend modifier

TPS preparation

Thermoplastic starch (TPS) was prepared directly in proces of PLA/TPS blending by means of twin-screw extruder using glycerol and water as starch plasticizers.

PLA/TPS blends preparation

PLA/TPS blends were prepared using twin-screw extruder at thermal profile 140 – 150 – 160 – 160 – 160 – 160 – 160 – 160 – 160 – 160°C. Extruded material was chilled with air on the belt loop and granulated into small pellets.

PLA/TPS films preparation

Granulated material was used to PLA/TPS films preparation on single-screw extruder at thermal profile 160 – 165 – 170 – 180 °C, where flat die and chill-roll technology were used.

Measurement of mechanical properties of prepared blends

Yield strength (σ_y), tensile strength at break (σ_b) and the elongation at break (ε_b) were done according to ISO 527 standard using Zwick machine at cross-head speed 1 mm/min in the deformation range of 0–3 % and after this value of elongation the speed increased up to 50 mm min^{-1}. These properties were determined based on recorded tensile curves.

Results and discussion

At first, an influence of modifier M on mechanical and rheological properties was studied. Modifier content in PLA/TPS blends varied from 0 to 1 %wt., and content of TPS, PLA, GL and water was constant. Figures 1–2 show dependencies of chosen properties: tensile strength at yield and elongation at break on modifier content in PLA/TPS

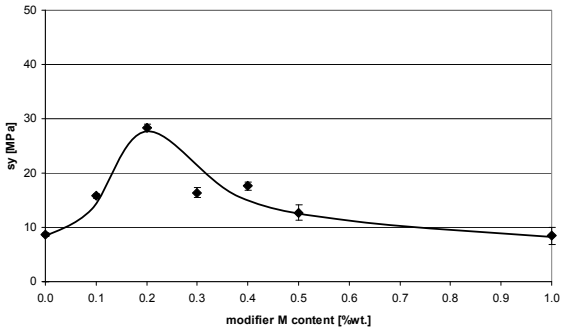

Fig. 1. **Dependence of tensile strength at yield on** modifier M content in PLA/TPS blends

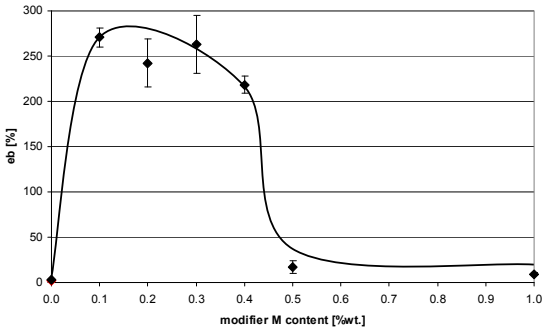

Fig. 2. **Dependence of elongation at break on modifier M content in PLA/TPS blends**

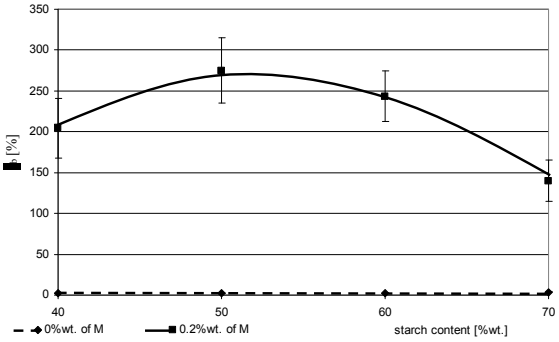

Fig. 4. **Dependence of elongation at break on starch content in PLA/TPS blends prepared with and without modifier M**

blends.

Fig. 1 shows that tensile strength at yield (σ_y) has its maximum at modifier content of 0,2 %wt. Above this concentration, tensile strength at yield was decreased. Modifier M has positive influence on elongation at break of prepared blends. A small addition of modifier (0,1 %wt.) caused an increase of e_b from 0 % to 250 %. Prepared blends have value of elongation at break above 200 % up to modifier content of 0,4 %wt. Above this concentration of modifier, elongation at break was decreased to almost zero value.

On the next figure, there is a dependency of chosen mechanical property of prepared biodegradable blends PLA/TPS on starch content. Content of GL and water was constant, it was varied the content of starch in blends, from 40 %wt. up to 70 %wt. It was studied an influence of starch content on properties of PLA/TPS blends prepared with and without modifier M at its one concentration.

Tensile strength at yield (Fig. 3) of studied blends PLA/TPS was decreased with increasing content of starch. Blends prepared without modifier M have 2 times lower values of studied property than those prepared with modifier M.

Blends prepared without modifier M have almost zero value of elongation at break (Fig. 4). But blends with modifier have value of this property from 150 up to 300 %, maximum was reached at starch content of 50 %wt.

Besides changing modifier and starch content in PLA/TPS blends, content of GL and water was gradually varied as well. After research of basic properties of modified PLA/TPS blends, Design of experiment (DoE) method was used and

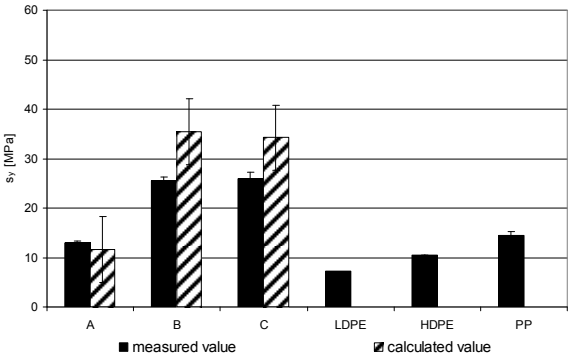

Fig. 5. **Tensile strength at yield of optimized modified PLA/TPS blends with various composition**

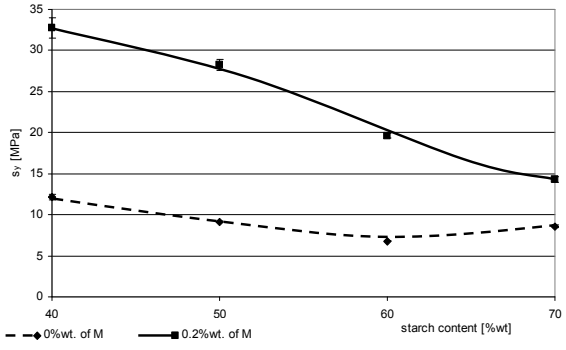

Fig. 3. **Dependence of tensile strength at yield on** starch content in PLA/TPS blends prepared with and without modifier M

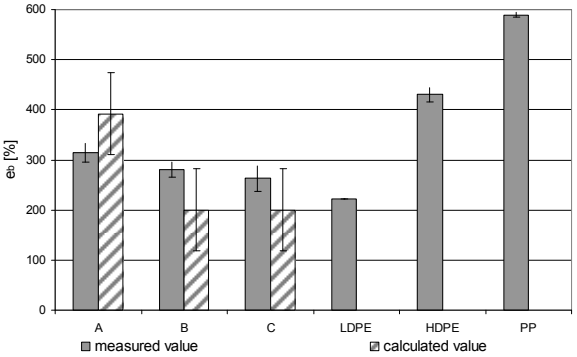

Fig. 6. **Elongation at break of optimized modified PLA/TPS blends with various composition**

after evaluating of DoE, optimization of blend composition followed. Blends were optimized according to 3 criteria: A, B, C. Fig. 5 and 6 show results of measurement of chosen mechanical properties.

Obtained results presented on Fig. 5 shows, that values of tensile strength at yield of optimized modified blends are higher than values of σ_y of standard polyolefins like LDPE, HDPE or PP. In the case of elongation at break (Fig. 6) of optimized blends PLA/TPS, it can be concluded that all 3 optimized blends have similar or higher ε_b than LDPE, its value is approximately 300 %.

Conclusion

Based on reached results it can be concluded that it is possible to set up composition of modified PLA/TPS blends with required properties which are comparable with properties of polyolefins usually used in packaging applications. Presented material has high potential for its practical usage.

REFERENCES

1. Rudnik E., in: *Compostable Polymer Materials*, Chap. 2, p. 14, Elsevier 2008.
2. Rudnik E., in: *Compostable Polymer Materials*, Chap. 2, p. 21, Elsevier 2008.
3. Edgar K.J., Buchanan C.M., Debenham J.S., Rundquist P.A., Seiler B.D., Shelton M.C., Tindall D.: Prog. Polym. Sci. *26*, 1605 (2001).

CL-30
RECYCLING OF USED TIRES AND REUSE OF RUBBER GRANULATE

RASTISLAV ZAHORANSKÝ

V.O.D.S., a.s., Jarmočná 2, 040 01 Košice, Slovakia
rastislav.zahoransky@avesk.sk

There are several methods of material recovery of used tires like: mechanical recovery, pyrolysis recovery, cryogenic recovery or ozone recovery. The most popular method in the world is mechanical recovery which is also used in our company.

Mechanical recovery

The actual process of recovery could be described in a simple form as a continuous multi-stage mechanical crushing of tires into rubber granules of the desired fractions, during the process the metal and textile components of the tire are separated.

The first step is chopping used tires to size approximately 25 × 25 cm (tire shreds) in to a machine Super chopper. The process continues by cutting tire shreds in Heavy rasper to tire chips with size app. 2 × 2 cm, process of crushing continues to 1st Granulator which makes 0–10 mm granules, then granules enter the 2nd Granulator and the output is rubber granules, fraction 0–4 mm. During the process the metal and textile components of the tire are separated. Last machinery in line is Aspirator. Aspirator sorts the resulting rubber granulate (0–4 mm) into required fractions (for example: 0,0–0,5 mm / 0,5–1,0 mm / 1,0–3,0 mm).

Reuse of rubber granulate

The main final product material of material recycling is rubber granulate, which is used in many areas. For example: filling for artificial turf (grass surfaces), safe children playground surfaces, rubber tiles for animal housing, replacement of concrete and ceramic tiles, noise protection walls and barriers, rubber plates to absorb underground vibrations, rubber side-way panels for the rails, sorbents, modified asphalt, rubber mixtures (compounds) that are used in the rubber industry. The waste is then converted into a finished product, thereby closing the recycling circle.

POSTERS

P-01
SINGLE POLYMER COMPOSITES AS REPLACEMENT FOR GLASS FIBER REINFORCEMENT

JACEK ANDRZEJEWSKI, MONIKA DOBRZYŃSKA-MIZERA, TOMASZ STERZYŃSKI, and MATEUSZ BARCZEWSKI

Poznan University of Technology, Institute of Materials Technology, Piotrowo street 3, 61-138 Poznan, Poland
jacek.andrzejewski@put.poznan.pl

Introduction

The reinforced plastic composites are promising alternative to metal parts, although comparing with composites the recycling of raw materials is much easier. Despite the possibility of re-processing of glass fiber-reinforced composites, applicability of the recovered materials have their limitations due to high content of reinforcing fibers. Generally, it is possible to use this kind of waste as a cheaper alternative to raw composite, but still frequently the combustion is used as the method of utilization. Recycling problems do not restrict the rapidly growing use of fiber reinforced composites. The replacement of metal parts by polymeric composites, for high performance plastic composites, resulted in car parts weight reduction, low number of components and of the processing operations. All these benefits lead also to cost reduction.

The interesting alternative to glass fiber-reinforced composites are single polymer composites. The idea of SPC (single polymer composite) is the use as reinforcement and composite's matrix polymers from the same group, or even of the same type. The polymers used as fibers are characterized usually by properties different from the matrix, such as molecular weight, density, chain branching and macromolecular structure. However the chemical structure is usually the same. The main advantages of SPC are similar to glass reinforced composites, however problems with recycling of glass fibers and its high density are eliminated. The use of the same polymer as a matrix and a filler results in an easy re-processing which is the biggest profit. During the reprocessing, fibers are melted together with the matrix and form a homogeneous mixture.

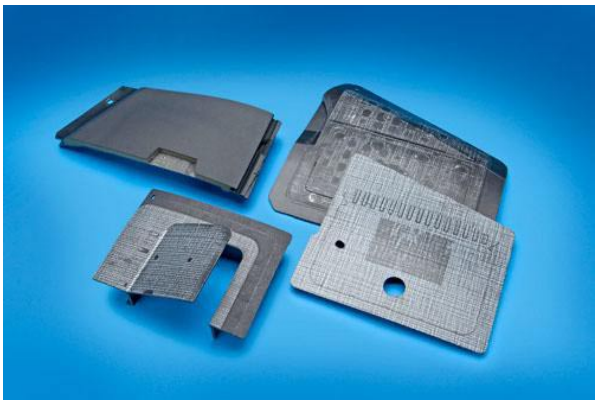

Fig. 1. **The SPC door airbag system** (Van Buren Township)

Previous studies focused mainly on SPC materials made of polyamides and polyolefins. The research presented in this paper are focused on polyesters, poly(ethylene terephthalate) (PET) and its copolymer (LPET). The commonly used name for this type of composites is srPET, states from self-reinforced poly(ethylene terephthalate).

Experimental

The presented results concern to two types of SPC materials where both were supplied by the Comfil ApS. As a reference materials, semi-finished products in a form of sheets for thermoforming were used, and the reinforcing fibers contain of 50 %. The investigated material was in a form of pellets suitable for injection molding, with a PET fibers content of 33 %. The samples used for mechanical tests were cut from SRC sheets. The samples from SPC pellets were prepared by injection molding, acc. to ISO 527 standard. The conditions of injection molding correspond to the manufacturers recommendations, with maximum temperature limited to 220 °C, to prevent the melting of reinforcing fibers. The reference sample was formed in the processing temperature of 270 °C where the PET fibers are melted and the material acquires properties of the matrix.

The mechanical properties of the samples were determined by means of static tension tests using INSTRON 4481 universal testing machine and DMTA Anton Paar analysis. The structure observations were carried out using the NIKON Eclipse microscope, and the material in a form of film produced by compression molding by 200 °C.

Results and discussion

The mechanical tests were conducted by the tensile rate of 10 mm/min, at ambient temperature. The results are presented in Table I. For samples obtained by injection molding low values of elastic modulus were observed, where the E value and the tensile strength R_m values are higher for entirely melted composition. The average value of E modulus, which may be found for standard commercial PET resin, is about 3 GPa, and the stiffness of both investigated samples produced by injection molding is somewhat lower. This effect may be explained by inferior mechanical properties of PET copolymer used a matrix polymer, and by irreversible changes of the fiber orientation due to relatively high processing temperature.

Mechanical tests of srPET sheets were realized under the same condition as other samples. In this case the tensile strength is more than twice higher, comparing to pure PET resin, which proves the reinforcing effect of highly oriented macromolecules in the PET fibers. Only a slight increase of the E modulus for this type of SRC's may be a result of an ab-

Table I
Results of mechanical tests at an ambient temperature

Type of material	R_m [MPa]	E modulus [GPa]	Strain at peak [%]	Strain at break [%]
srPET (melted)	72,5	2,74	4	4,2
srPET (unmelted)	54	2,4	3,1	3,4
srPET (sheet)	152	3,3	23	24

sence of a draw orientation of fibers at the initial stage of deformation. First during the tensile deformation the fibers structure is elongated at the main tensile direction, and the fibers are fully charged along its intrinsic macromolecular orientation.

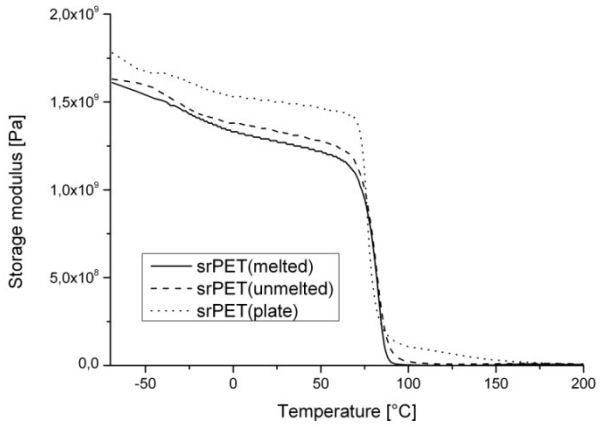

Fig. 2. **The DMTA storage modulus as a function of temperature**

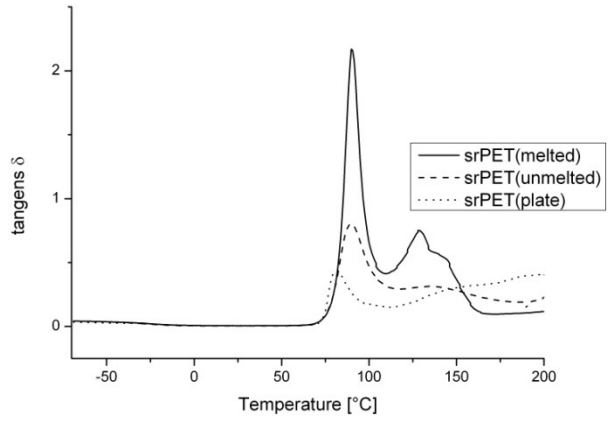

Fig. 3. **The DMTA tangens δ *vs.* temperature**

The thermo-mechanical tests were conducted by means of DMTA measurements, using rectangular samples in rotational mode with deformation of 0,01 %, and frequency of 1 Hz. The heating rate was 2 °C min^{-1}, and the temperature range was −70 °C to 200 °C. The results of these measurements are presented in a form of thermograms in the Fig. 2 and 3.

The course of the storage modulus and tangens δ peaks show a decrease of mechanical properties at softening temperature of about 80 °C, for all three examined compositions. Thus, the use of srPET composites inside the car engine compartment is not recommended.

The microphotographs of the srPET samples are presented in Fig. 4. The form of the fiber's structure is different before and after injection molding. The processing by injection molding results in a decrease of mechanical properties, due to thermal relaxation of fiber orientation. This process is influenced mainly by the temperature and shear forces existing in the plasticizing unit of the injection molding press.

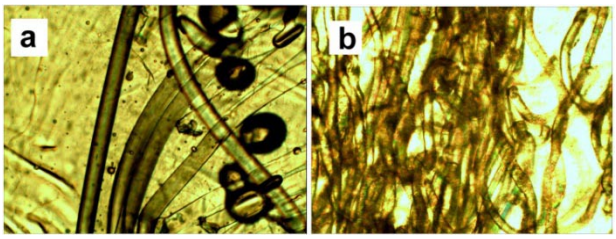

Fig. 4. **The PET fibers a) SPC pellets, b) after injection molding**

Conclusions

The results of srPET investigations did not confirm the possibility of using them as a full alternative to glass fiber composites in a car industry. The main reason is the lowering of mechanical properties of the polyester fibers, especially during processing by injection molding. The mechanical strength of PET fiber reinforced composite is comparable to the pure polyester matrix. Promising results were obtained for srPET sheets. The possibility of using this material for thermoforming applications is very broad, considering the fact of excellent correlation of strength, weight and cost in comparison with pressed metal parts. The replacing of steel and aluminium parts by SPC materials is very realistic prospect.

REFERENCES

1. Hine P. J., Ward I. M.: J. Appl. Polym. Sci. *91*, 2223 (2004).
2. P. Rojanapitayakorn P., Mather P. T., Goldberg A. J., Weiss R. A.: Polymer *46*, 761 (2005).
3. Evstatiev M., Fakirov S., Krasteva B., Friedrich K., Covas J. A., Cunha M.: Polym. Eng. Sci. *42*, 826 (2002).
4. Sterzyński T., Śledź I.: Polimery *52*, 443 (2007).
5. Szostak M.: Mol. Cryst. Liq. Cryst. *416*, 465 (2004).
6. Saujanya C., Radhakrishnan S.: Polymer *42*, 4537 (2001).
7. Kmetty A., Tábi T., Kovács J.G., Bárány T.: eXPRESS

Polym. Lett. *7*, 134 (2013).
8. Mondadori N. M. L., Nunes R. C. R., Zattera A. J., Oliveira R. V. B., Canto L. B.: J. Appl. Polym. Sci. *109*, 3266 (2008).
9. Błędzki A. K., Gorący K., Urbaniak M.: Polimery *57*, 620 (2012).
10. Żakowska H.: Polimery *57*, 613 (2012).
11. Makomaski G., Ciesińska W., Zieliński J.: Polimery *57*, 635 (2012).

P-02
STRENGTH OF BONDED JOINTS OF LDPE AFTER SURFACE TREATMENT BETA RADIATION

MARTIN BEDNAŘÍK, DAVID MAŇAS, MIROSLAV MAŇAS, JAN NAVRÁTIL, MARTIN OVSÍK, KAMIL KYAS, and ALEŠ MIZERA

Tomas Bata University in Zlin, nam. T. G. Masaryka 275, 762 72 Zlin, Czech Republic
mbednarik@ft.utb.cz

Abstract

Joining materials by bonding joints has spread into almost all sectors of practice and it would be very difficult to find an industry in which there is not a need to use this technology. This article describes the effect of beta radiation on the contact angle of wetting, on the surface energy and on the final strength of bonded joints of LDPE.

Introduction

In comparison with conventional joining methods (riveting, welding and screwing) bonding provides a new combination of options and it allows obtaining special shapes and properties which cannot be created by conventional methods of coupling. Joining materials using an adhesive offers several benefits over mechanical joints[2,4]:

1. Bonding allows connecting the same or dissimilar materials, irrespective of their thickness.
2. It is possible to prepare water – tight and gas – tight joints and the profile of bonded file is not disturbed.
3. Joints are more resistant to flexural, fatigue, and vibrational stresses.
4. Bonding does not grow weight of bonded file and dampens vibrations in construction.
5. Bonding is often less expensive and faster than mechanical joining[2].

For the formation of quality bonded joints it is important to wet the adhesive bonding surface well. Wettability is characterized by the contact angle of wetting. The liquid must have a lower surface tension than the solid in order to be able to wetting the solid substance[2,5].

Experimental

Materials

For this experiment Low Density Polyethylene LDPE DOW – LDPE 780E, DOW – Chemical company, USA were used. LDPE material has a non-polar character and due to a low surface energy it is difficult to bond. For the formation of quality joint is necessary to activate the surface of bonded material[3,6].

The samples were made using the injection molding technology on the injection molding machine Arburg Allrounder 420C. Processing temperature was 190–220 °C, mold temperature 40 °C, injection pressure 80 MPa, injection rate 50 mm s^{-1}. The samples had the shape and dimensions according to the CSN EN ISO 527-2 (ref.[3]).

Surface treatment by beta radiation

For bonding LDPE is necessary to modify surfaces which will be bonded. Surface modification improves its wettability and surface energy. The ionization beta radiation is a very effective tool[1,3].

Before bonding surfaces of samples ionization beta radiation were irradiated with doses of 0, 33, 66, 99 and 132 kGy at Beta – Gamma Service GmbH & Co. KG, Germany[6].

Wetting contact angle measurements

To measure the contact angle of wetting the sessile drop method was used and surface energy was determined by WORK method (Owens – Wendt – Rabel – Kaeble method). The distilled water, glycerol and ethylene glycol with known γ^p (polar component) and γ^d (dispersive component) were used for the calculating of the surface energy of LDPE[2,4].

Testing the strength of bonded joints

After irradiation of samples and measuring the contact angles of wetting surface energy were calculated. Then the samples were bonded and their strength was measured. For testing the strength of bonded joints there was used a tensile test on the test machine Zwick 1456. Test conditions were according to the CSN EN ISO 527-1 and CSN EN ISO 527-2. Speed was 10 mm min^{-1} and evaluation software was Test/Expert Standard[6].

Table I
Surface energy (γ_1) and its dispersive component (γ_1^d) and polar component (γ_1^p) of used liquids

Liquid	γ_1 [mJ m^{-2}]	γ_1^d [mJ m^{-2}]	γ_1^p [mJ m^{-2}]
Distilled water	72,8	21,8	51,0
Glycerol	64,0	34,0	30,0
Ethylene glycol	48,0	29,0	19,0

Results and discussion

Contact angle and surface energy

The measurement results of contact angle of LDPE for different doses of radiation and for different test liquids are shown in Fig. 1. Results show that the contact angle is the highest in the untreated surface and its size is 89.2°, 79.2°, and 67.9° for distilled water, glycerol, and ethylene glycol, respectively. After irradiation dose of 132 kGy the contact angles considerably reduced to values 66.4°, 62.1°, and 50.5° for distilled water, glycerol, and ethylene glycol, respectively.

The following figure (referring to: Fig. 2) shows a plot of surface energy from the measured contact angles on the surface of the LDPE. It shows that surface energy of untreated surface is 24.1 mJ m^{-2} and 23.2 mJ m^{-2} for water + glycol and water + ethylene glycol, respectively.

Similar trend was observed for the polar component (referring to: Fig. 3). The properties such as wettability, adhesion strongly depend upon the surface energy.

Beta radiation increases the surface energy. The surface energy values considerably increased after irradiation by a dose of 132 kGy shifting them to higher values 35.8 mJ m^{-2} and 35.7 mJ m^{-2} for water + glycol and water + ethylene glycol, respectively.

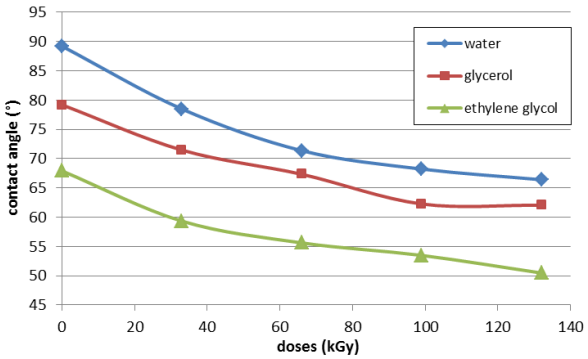

Fig. 1. **Variation of contact angle with respect to radiation dose**

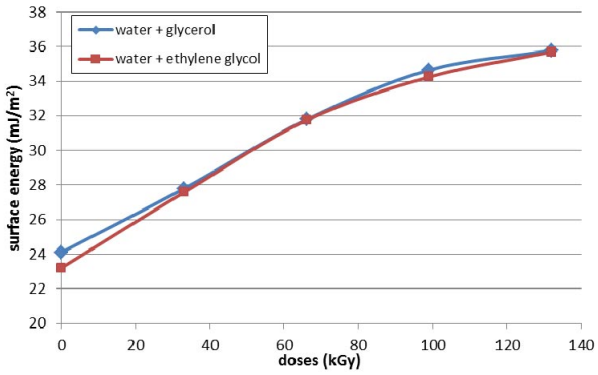

Fig. 2. **Variation of surface energy with respect to radiation dose**

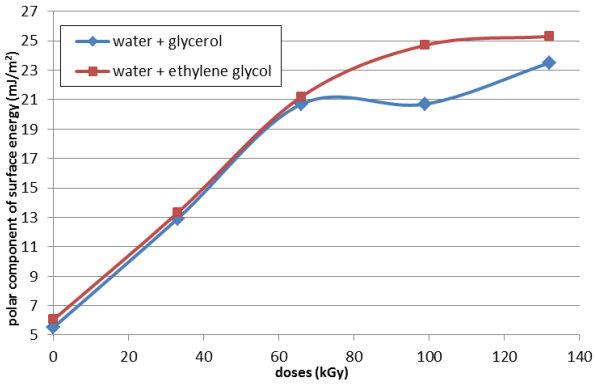

Fig. 3. **Variation of polar component with respect to radiation dose**

Strength of bonded joins

Strength of bonded joints is characterized by the maximum burdensome force which endured bonded sample. For bonding of LDPE two types of cyanoacrylate adhesives of companies Cyberbond were used (Cyberbond 1008 and Cyberbond 2028).

The highest strength of bonded joints samples have those which were irradiated by a dose of 132 kGy. After the irradiation by a dose of 132 kGy strength is increased by more than 100 % for both adhesives.

Conclusion

This article describes the effect of beta radiation on the contact angle of wetting, on the surface energy and on the final strength of bonded joints of LDPE. Beta radiation increases the strength of bonded joints of LDPE and improves its adhesion properties. The best results were achieved by irra-

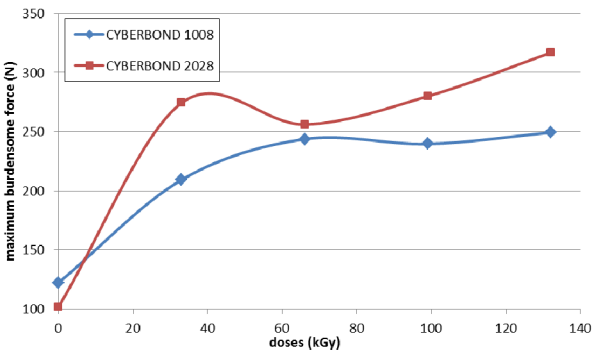

Fig. 4. **Variation of strength of bonded joints with respect to radiation dose**

diation at a dose of 132 kGy by which the highest surface energy and the highest strength of bonded joints of LDPE were achieved.

This paper is supported by the internal grand of TBU in Zlin No. IGA/FT/2013/020 founded from the resources of specific university research and by the European Regional Development Found under the project CEBIA–Tech No. CZ.1.05/2.1.00/03.0089.

REFERENCES

1. M. Manas et al.: Chem. Listy *103*, s24 (2009).
2. Lapčíková B., Lapčík L., Smolka P., Dlabaja R., Hui D.: J. Appl. Polym. Sci. *102*, 1827 (2006).
3. D. Maňas, M. Maňas, M. Stanek, T. Drga: Chem. Listy *101*, s27 (2007).
4. M. Lehocký, H. Drnovská, B. Lapčíková, A. M Barros-Timmons, T. Trindade, M. Zembala, L. Lapčík Jr.: Colloids Surf. *222*, 125 (2003).
5. D. Manas et al.: Thin Solid Films *530*, 49 (2013).
6. A. Mizera, et al.: Int. J. Mathematics and Computers in Simulation *6*, 584 (2012).

P-03
BIODEGRADABLE POLYMER BLENDS PET/PLA

FRANTIŠEK BENOVIČ , MIROSLAVA MIKUŠOVÁ, PETER VITKOVSKÝ, KATARÍNA TOMANOVÁ, and PAVOL ALEXY

Ústav polymérnych materiálov, Fakulta chemickej a potravinárskej technológie, Slovenská technická univerzita, Radlinského 9, 812 37 Bratislava, Slovak Republic
frantisek_benovic@stuba.sk

Introduction

Polyethylene terephthalate (PET) is a very important polymer for industrial applications; particularly, bottles have experienced a rapid growth since the 1970s when the technique of blow moulding was introduced[1]. Plastics such as PET are strong, inexpensive, easily to process and durable. This kind of materials is resistant to biological degradation because their carbon components cannot be broken down by the enzymes of microorganisms and also their hydrophobic character inhibits enzyme activity[2]. Furthermore, consumers are demanding food packaging materials that are potentially biodegradable, for this reason there is an urgent need to develop renewable source based biopolymers able to degrade via a natural composting process.

Poly (lactic acid) (PLA) is an interesting biodegradable polymer, which is obtained from renewable agricultural resources[3]. Polylactic acid (PLA) is a rigid thermoplastic polymer that can be semicrystalline or totally amorphous, depending on the stereopurity of the polymer backbone. L(_)-lactic acid (2-hydroxy propionic acid) is the natural and most common form of the acid, but D(_)-lactic acid can also be produced by microorganisms or through racemization and this "impurity" acts much like comonomers in other polymers. PLA possesses good mechanical properties, with elastic modulus and tensile strength in the range of 3.2–3.7 GPa and 55–60 MPa, respectively. PLA is a partially crystalline polymer with a glass transition temperature (*Tg*) in the range of 65–70 °C and a melting temperature (*Tm*) around 160–170 °C. However, PLA has not good barrier properties and has relatively high cost. And therefore its usage in packing industries (especially in production of bottles) is still limited[4].

This article is focused on study of possibility of preparation of binary blends polylactic acid (PLA)/polyethylene terephthalate (PET). The basic description of influence of blend composition on properties of blends was done. Based on the results obtained in the present work conclusions and recommendations were done for designing of PET/PLA blends exhibit improved biodegradibility.

Experimental

Materials

- Polylactic acid – PLA 4042D from NatureWorks, LLC, USA,
- Polyethylene terephthalate (PET),
- Catalysts of type A, B, C and D from Kenrich Petrochemicals, USA,
- Triacetine as PLA plasticizer.

PET/PLA blends preparation

Both polymers PET and PLA were dried 120 minutes at the temperature of 80 °C in hot-air oven and then blends were prepared using twin-screw extruder. PLA content in the blends gradually changed from 0 % to 100 % wt. Thermal profile of extrusion in the direction from feeder to die was set on 250 – 260 – 260 – 260 – 260 – 260 – 255 – 250 – 245 – 240 °C and extrusion speed was 80 rpm. Extruded material was chilled with cold water and then it was granulated into small parts.

PET/PLA monofils preparation

Granulated material was dried again 120 minutes at the temperature of 80 °C in hot-air chamber. Dried granules were used to PET/PLA monofilaments preparation using. Temperature profile of monofils extrusion in the direction from feeder to die was set on 240 – 250 – 270 – 260 °C and extrusion speed was 10 rpm.

Measurement of physical-mechanical properties of prepared blends

Yield strength (σy), tensile strength (σb) and the elongation at break (εb) were measured with Zwick machine at cross-head speed 1 mm min^{-1} in the deformation range of 0–3 % and after this value of elongation the speed increased up to 50 mm min^{-1}. These properties were determined based on recorded tensile curves.

Results and discussion

In first part of our work we focused on basic research of effect of PLA content in the binary blends PET/PLA. Fig. 1 and 2 show dependence of tensile strength at yield, tensile strength at break and elongation at break on PLA content in PET/PLA blends.

Fig. 1 shows that tensile strength at yield (σy) hardly decreased at the PLA content in blends of 20 % and at the higher content of PLA was σy slightly increased. Tensile strength at break (σb) of PET/PLA blends was decreased with an addition of PLA nearly to the half of initil value.

Fig. 2 shows dependency of elongation at break (εb) on PLA content in PET/PLA blends. Effect of PLA content in blends has already been achieved in its content of 5 %. The value of εb decreased from 920 % to 3 %. This tendency corresponded with property of pure PLA. Therefore the plasticiser (PLA) was used in the next step with aim to improve elongation at break (εb).

We prepared mixtures of PET/PLA in ratio 80:20; with four concentrations of TAC in the PLA (5, 10, 15 and 20 %. To measure the mechanical properties, we found that the addition of 15 % of the TAC increase σb and does not increase σy, and also significantly increase the Eb, as it is shown in Fig. 3 and 4.

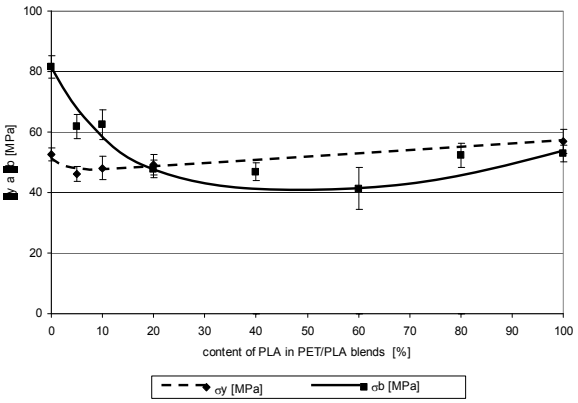

Fig. 1. **Dependence of tensile strength at yield and tensile strength at break on PLA content in PET/PLA blends**

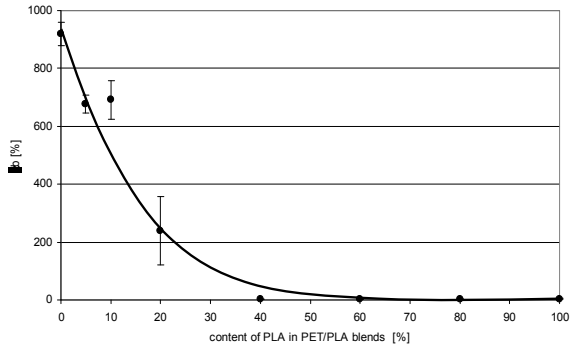

Fig. 2. **Dependence of elongation at break on PLA content in PET/PLA blends**

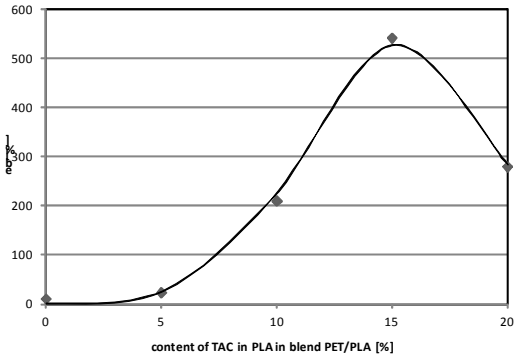

Fig. 3. **Dependence of elongation at break on TAC content in PLA in PET/PLA blends**

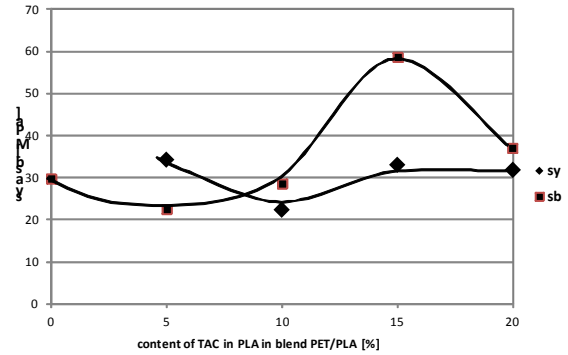

Fig. 4. **Dependence of tensile strength at yield and tensile strength at break on TAC content in PLA in PET/PLA blends**

Positive effect of TAC is originated probably in the effect of similar viscosity of PLA and PET. Finer dispersion of PLA is probably resulting of it and tensile strength is improved. The presence of plasticizers also logically improves the relative elongation at break.

Conclusion

Based on obtained results it can be concluded that the concentration of PLA in the PET/PLA blends has significant influence on physico-mechanical properties. We found that at 20 % of the PLA in mixtures can be achieved comparable yield strength as for pure PET. However, PLA significantly reduced the value of elongation at break. Applying 15 % TAC causes gives sufficient strength values as well as relative elongation at break.

REFERENCES

1. L. Shen et al.: Resour., Conserv. Recycl. *55*, 34 (2010).
2. C. Bastioli: *Handbook of Biodegradable Polymers,* 1a. ed., p. 183. UK: Rapra Technology Limited, 2005.
3. M. A. del Nobile et al.: J. Food Eng. *93*, 1 (2009).
4. Lee J. K., Lee K. H., Jin B. S.: Eur. Polym. J. *37*, 907 (2001).

P-04
MODIFICATION OF PROCESSING AND MECHANICAL PROPERTIES OF STARCH/ POLYHYDROXYBUTYRATE BLENDS

JÁN BOČKAJ, KATARÍNA TOMANOVÁ, MICHAL MIHÁLIK, RODERIK PLAVEC, MIRKA MIKUŠOVÁ ZUZANA VANOVČANOVÁ, and PAVOL ALEXY

Institute of Polymer Materials, Faculty of Chemical and Food Technology, Slovak University of Technology, Radlinského 9, 812 37 Bratislava, Slovak Republic
jan.bockaj@stuba.sk

Introduction

Plastic packages based on nonbiodegredable material (polyethylene, terephalate) cause increasing of their accumulation in the environment. These materials are difficult to recycle or reuse due to mixed levels of contamination and complex composites[1]. The current trend predict that in the next couple of years, many plastic material as packages or bottles will be replaced by biodegradable materials that could be compostable.

The compostability attribute is very important for biopolymer materials because while recycling is energy expensive, composting allows disposal of packages in the soil. By biological degradation it produced only water, carbon dioxide, biomass and inorganic compounds' without toxic residues[2]

In our work PHB/Starch/Glycerol/water/Modifier blends were studied. The aim of our work was study of influence of modifier and plasticizer on rheological and mechanical properties of PLA/PHB blends.

Materials and methods

PHB from Biomer, Germany was used as polyhydroxybutyrate, Starch from Amylum Slovakia, Glycerine (GL) was used as plasticizer.

Preparation of blends

The blends of polyhydroxybutyrate/starch with content of polyhydroxybutyrate 60 %wt. were prepared using twin screw extruder with screw diameter 16 mm, L/D = 40 with three kneading zones. The content of glycerol was 40, 50, 60 %wt., content of water was 20 %wt. These blends were modified by addition of specific modifier (0/ 0,2/0,4/0,6/0,8/1/1,5/3 %wt.) as well.

Rheological measurements

Rheological parameters of blends were measured using oscillation rheometer RPA 2000 from Alpha Technologies. Two types of tests were used in our work – strain sweep and timed test. Frequency was set up to 50 cpm during the strain sweep, while angle of strain varied from 0–60°. Timed test was done at constant angle of strain 30° and constant frequency 60 cpm. Time period of test was 20 min. Temperature of measurement for all prepared blends was 200 °C.

Mechanical properties measurement

For tensile test according to ISO 527 the Zwick machine was used at cross-head speed 1 mm min^{-1} while deformation range was of 0–3 % and after this value of deformation the speed increased up to 50 mm min^{-1}. The tensile strength of break (σb), elongation at break (εb) and tensile strength at yield (σy) were determined based on recorded tensile curves.

Results and discussion

The dependencies of mechanical properties on modifier content in the blends of PHB/starch/Glycerol/water/modifier are shown in Fig. 1–3.

At first, we prepared and analyzed mixtures with maximum content of modifier 1 %wt. Fig. 1 and Fig. 2 show that tensile strength and elongation at break had minimal increase

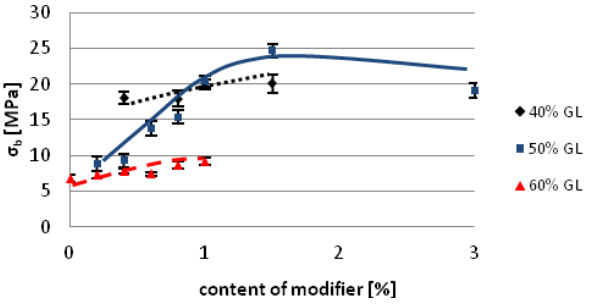

Fig. 1. **The dependency of tensile strength at break on modifier content**

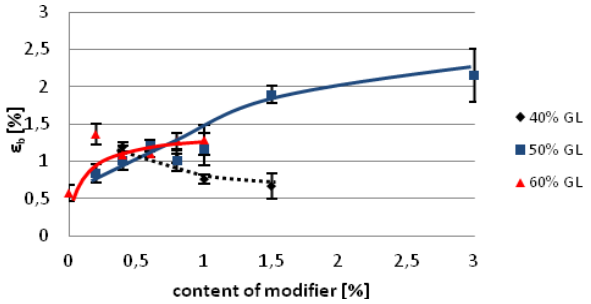

Fig. 2. **The dependency of elongation at break on modifier content**

at GL concentration at 40 and 60 %wt. However at 50 %wt. concentration of GL, significant increase of both characteristics is visible with increasing amount of modifier. Based on this results were decided to increase the amount of modifier to 3 %wt. for samples which contains 50 %wt. of GL. Based on these results we determined that optimal amount of modifier which is 1.5 %wt. in samples contain 50 %wt. of GL.

In terms of elongation at break the results show increasing values with increasing amount of modifier, however the absolute values of elongation at break are too low – maximum 2.5 %.

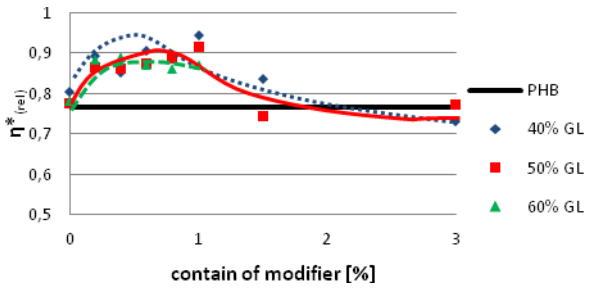

For illustration, dependence of $\eta^*_{(rel)}$ on concentration of modifier ( ) at 40, 50 and 60 %wt. of GL content was constructed. The viscosity after 4th minute of test was taken in account (Fig. 3). The results show that more stable mixtures are obtained in concentration range from 0.2 to 1.5 %wt. of modifier compared to PHB aloneAddition of modifier shows significant influence on viscosity in mixtures. The biggest influence is observed in mixtures with 40 % amount of GL as plasticizer.

Based on obtained results it can be concluded that such mixtures are more stable during processing in the melt state as pure PHB.

Dependences of complex viscosity (η*) on modifier at 2 different shear rate for 40, 50, 60 %wt. of plasticizer are shown in Fig. 4. All curves show maximum. Based on these results, we determined the optimal mixture, which contain 0.2 %wt. of modifier and 40 to 50 %wt. of GL.

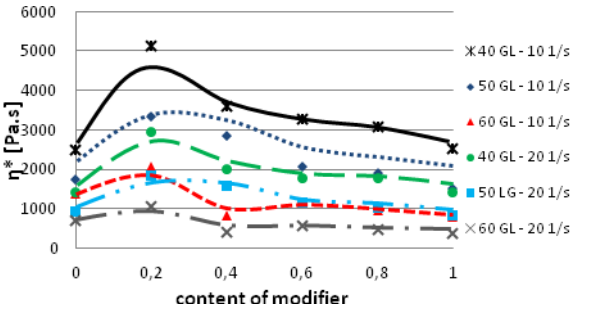

Fig. 4. **The dependency of complex viscosity (η*) on modifier content with 2 different shear rate**

Conclusion

Tested specific modifier effectively decreases viscosity of thermoplastic starch and increase viscosity of PHB. The modifier significantly reduces high sensitivity of PHB during thermal processing as well. The results show that individual components of mixtures are able to change processing and mechanical properties. Effect of individual components (modifier, plasticizer) does not have synergic effect, but in the studied system significant interactions were observed. By addition of modifier to the mixture with suitable concentration of plasticizers it is possible to obtain mixture with better processing and mechanical properties compared to the PHB alone.

REFERENCES

1. G. Davis, J. Song: Industrial Crops and Products *23*, 147 (2006).
2. V. Siracusa, P. Rocculi, S. Romani, M. Dalla Rosa: Trends in Food Science & Technology *19*, 634 (2008).

P-05
SURFACE MODIFICATION OF NONWOVENS FROM BIODEGRADABLE POLYMERS

MONIKA BOTOŠOVÁ, ĽUDMILA ČERNÁKOVÁ, and MAGDALÉNA WOLFOVÁ

Slovak University of Technology in Bratislava, Faculty of Chemical and food technology, Institute of Polymer Materials, Department of Plastics and Rubber, Radlinského 9, 812 37 Bratislava, Slovakia
monika.botosova@gmail.com

Introduction

In recent years, a growing interest in the use of bio-based materials or materials from renewable resources has been detected. This interest has also reached the technical industries because of increasing environmental concerns, potential biodegradability and the use of overall eco-friendly materials[1].

Since last few years biodegradable nonwoven industry has grown abruptly and apart from its application in geotextiles, nappies, filters, bags, etc. have now started to find its application in textile and automotive industry. Automotive textiles are the growing markets in terms of quantity, quality and product variety.

Flexible nonwoven structures can be used as thermal and/or acoustic insulating materials in interior automotive parts. These can provide interesting properties as lining materials because of their ease of handling and shape adaptability[2]. The use of nonwovens is also being generalized as filtering media and new substrates based on natural fibers are being developed[3]. Nonwovens have been increasingly used in car interiors for noise reduction. Most of these nonwovens are subjected to thermal treatments to give the nonwovens their

final three-dimensional forms. According to present need, nonwovens have been modified which opens a wide variety of new applications[5].

This work is focused on surface modification of nonwoven from poly (lactic acid) with cyclodextrins (CD). Cyclodextrins contain a hydrophobic internal cavity that can act as a host for various, generally lipophilic, guest molecules. Therefore, molecules such as fragnances, drugs and textile dyestuffs can be complexed by CDs.

As pretreatment method before coating, plasma activation by Diffuse coplanar surface barrier discharge (DCSBD) has been used[5]. The possible aims of this are improved wettability and adhesion of coatings.

Experimental

The poly (lactic acid) nonwoven (PLANW) was activated by atmospheric-pressure plasma treatment in ambient air or nitrogen. Based on our previous result, the times of activation was 2 seconds on one side. The activated samples were immersed in solution of β-cyclodextrins/chitosan. The concentration of cyclodextrins were 6, 12, 18 g l^{-1}. The drying process for PLA sample was realized in the air at laboratory temperature or in drying chamber at temperature 120 °C.

Surface modification was confirmed gravimetrically and using SEM and ATR-FTIR spectroscopy.

Results and discussion

At first, the PLANW samples without plasma activation were coated with solution of β-CD/chitosan and after drying the modified samples were washed in distilled water. It was found by gravimetric analysis, that about 82 % from all coated amount of modifying β-CD layer was removed.

Because of that fact, it was chosen the possibility to modify the PLANW by β-CD in combination with chitosan after plasma activation in air or nitrogen atmosphere. DCSBD have been used to incorporate new functionalities at the surface of PLANW. The type of functionalization of PLA imparted by plasma varied by selection of plasma gas and operating parameters. Air plasma has been used to incorporate oxygen containing functional groups to PLA surface and nitrogen plasma has been used to impart also amine group to the surface.

Three parameters were studied, working atmosphere during plasma activation, the concentration of CD solution and adhesion of modified layer on PLANW.

Fig. 1 indicated that the amount of β-CD/chitosan adhered to the PLA fibers without plasma activation increases to the concentration of β-cyclodextrin in solution and varied from 4,5 wt.% to 7 wt.%. After washing almost the all content of β-CD/chitosan layer was washed out.

On the contrary, plasma activated PLANW samples in air or nitrogen atmosphere (Fig. 2, Fig. 3) have two times higher content of modifying β-CD/chitosan layer on PLA fibers after coating and also after washing. The content of permanently fixed CD layer was about 2 wt.% independently of type of plasma activation in air or nitrogen. The best results from the point of view of permanently fixed CD layer were obtained after plasma activation in nitrogen and using for coating CD solution in concentration of 18 g l^{-1}.

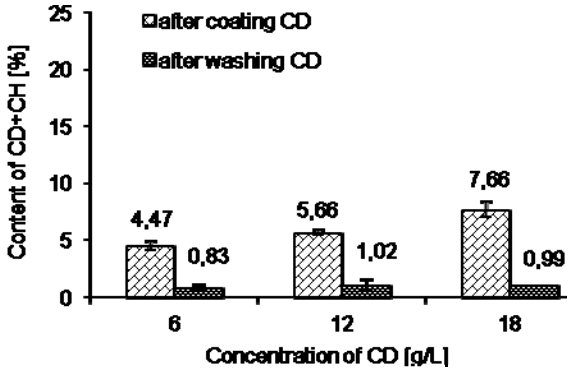

Fig. 1. **The content of CD+CH layer on concentration of CD solution, without plasma activation**

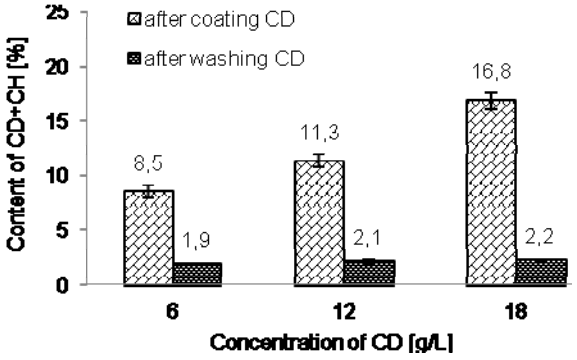

Fig. 2. **The content of CD+CH layer on concentration of CD solution, plasma activated in air atmosphere**

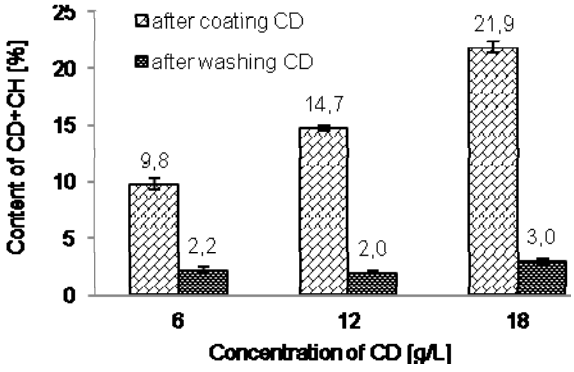

Fig. 3. **The content of β-CD/chitosan layer on concentration of CD solution, plasma activated in nitrogen atmosphere**

The modification of PLANW by β-CD was analyzed by scanning electron microscopy (Fig. 4).

A B

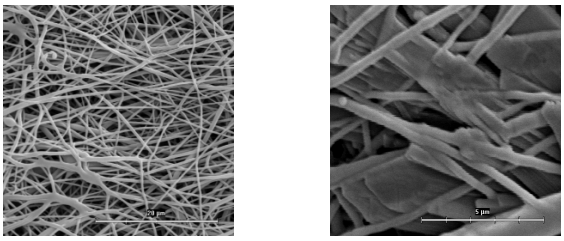

Fig. 4. **SEM pictures of A) PLANW and B) plasma activated PLANW coated by β-CD/chitosan**

A B

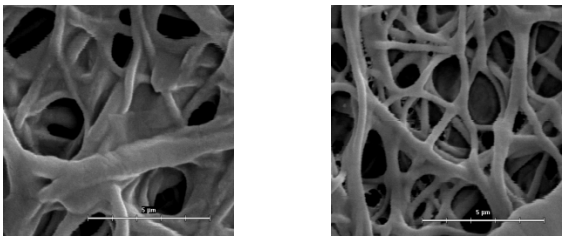

Fig. 5. **SEM pictures of PLANW coated with CD /chitosan, A) before washing B) after washing**

As can be seen in SEM pictures (Fig. 4) β-cyclodextrine layer effectively coated not only PLANW fibres, but is situated also in the space between fibers. The adhesion of modifying CD layer to the fibre was tested by washing in distilled water. Fig. 5 illustrates that first of all the CD layer situated in inter fibre space was washed out. The fibres were coated with CD layer also after washing, as it is evident from the picture Fig. 5B.

Conclusion

In this work the effect of plasma pretreatment of poly (lactic acid) nonwoven before modifying with cyclodextrins has been studied. It was found that non-thermal plasmas as Diffuse coplanar surface barrier discharge are suited to apply to the poly (lactic acid) nonwoven activation.

The adhesion between modifying β-CD/chitosan layer and fiber surface of PLA was improved and the content of permanently fixed CD/chitosan layer on PLA was two times higher in comparison with samples whithout plasma pretreatment.

This work was supported by the Scientific Grant Agency of the Ministry of Education, Science, Research and Sport of the Slovak Republic and the Slovak Academy of Sciences (VEGA), projects No.1/0818/13.

REFERENCES

1. Chen J. J., Guo Z.: Adv. Mater. Res. *194–196*, 471 (2011).
2. El Hajj N., Mboumba-Mamboundou B., Dheilly R. M., et al.: Ind. Crop. Prod. *34*, 921 (2011).
3. Fages E., Cano M. A., Gironés S., Boronat T., Fenollar O., Balart R.: Textile Res. J. *0(00)*, 1 (2012).
4. Yilmaz N. D., Powell N. B. , Banks-Lee P., Michielsen S.: J. Ind. Textiles *0(00)*, 1 (2012).
5. Černák M., Černáková Ľ., Hudec I., Kováčik D., Zahoranová A.: Eur. Phys. J. Appl. Phys. *47*, 22806 (2009).

P-06
THE INFLUENCE OF MOISTURE ON VULCANIZATION CHARACTERISTICS OF NATURAL RUBBER MIXTURES WITH DIFFERENT TYPES OF ACCELERATORS

DRAHOMÍR ČADEK*, ANTONÍN KUTA, JAKUB BAREŠ, and EVA KOVÁŘŮ

Institute of Chemical Technology, Faculty of Chemical Technology, Department of Polymers, Technická 5, Prague 6, 166 28, Czech Republic
drahomir.cadek@vscht.cz

Abstract

Improper storage, transportation and other manipulation of raw natural rubber can lead to introduction of moisture into rubber. Moisture can be introduced into a rubber mixture also with additives especially with fillers. Improper storage conditions of rubber mixtures can affect their moisture content as well. The influence of moisture on four types of rubber mixtures with different accelerators was studied. Moisture incorporated by rubber influenced vulcanization characteristics, like scorch time or modulus. Sensitivity of accelerators and their mixtures to moisture content is different.

Introduction

Absorption of water relates to many types of rubber products and this way their various properties can be changed. For example electrical properties of cables and insulating materials, or mechanical properties (adhesion, rolling resistance, abrasion, creep, stress relaxation) of tyres, hosepipes, sealing, etc.[1] Moisture and water have influence on processes that take place during production (rubber processing, vulcanization, storage) or product testing.

Two types of moisture are distinguished in rubber. The first one can be removed by drying at room temperature with usage of drying agent (e.g. sulphuric acid). The second one, residual moisture, can be removed by drying at temperatures higher than 100 °C only[2]. The rate of moisture absorption and

the amount of absorbed water by rubber depends on air relative humidity and temperature. At relative humidity of 75 %, the amount of water absorbed by natural rubber (NR) (less than 0.5 %) is constant after 10 hours. When relative humidity increases to 85 %, the constant amount of absorbed water (0.8 %) is reached also after 10 hours. When relative humidity is getting closer to 100 % the rubber (after the exposure of 50 hours) absorbs 2.5 % of water. All these measurements were done at room temperature[3].

Nonrubber constituencies (proteins, saccharides, esters of fatty acids …) in NR are responsible for difficulties with the prediction of rubber behaviour during processing[4–9]. They have some influence on moisture content as well. For example, residual moisture content decreases with the increasing amount of proteins in the rubber[2].

NR with moisture can be attacked by a mould. The rubber, thanks to many nonrubber constituencies, is source of nutrition for microorganisms. If the moisture content in rubber is higher than 0.7 %, then the growth of mould is possible. Nuclei of mould could be introduced to the rubber in the latex stadium or during its converting to raw "dry" rubber, but also during transportation and storage[10]. But the influence of the mould on rubber properties is slightly disputable. There are articles, where the role of the mould is downplayed, in others is significant.

Moisture can be introduced into a rubber mixture also with additives especially with fillers. Moisture can cause chemical changes of some additives, what can lead to changes of rubber mixture properties. Authors[1] studied the influence of moisture on the behaviour of sulphur vulcanization accelerator (*N*-morpholylbenzothiazole-2-sulfenamide, MBS). Present moisture hydrolyzed nitrogen – sulphur bond, what led to change of MBS to 2-merkaptobenzothiazol (MBT). This change influenced the vulcanization reaction; vulcanization was faster due to MBT.

Improper storage conditions of rubber mixtures can affect their moisture content as well. Subsequent chemical changes of rubber additives in the mixture can influence final mechanical properties of vulcanisates – adhesion, rolling resistance, abrasion …[1]

Experimental

The influence of moisture on four types of rubber mixtures with four types of accelerators was studied. The mixtures were prepared according to ASTM ACS I recipe – natural rubber SIR 10 (100 phr), zinc oxide 6 phr, stearic acid 0.5 phr, sulphur 3.5 and an accelerator 0.5 phr (ref.[11]). Rubber mixture was prepared on two roll mill. Accelerators which were used have different vulcanization activity: mercaptobenzothiazole (MBT), *N*-cyclohexyl-2-benzothiazole (CBS), tetramethylthiuram disulfide (TMTD) and zinc dimethyldithiocarbamate (ZDMDC).

One part of prepared mixtures was put in the desiccator with relative humidity of 100 % and the second part was put in the desiccator with relative humidity approaching 0 %.

Samples of rubber mixtures from both desiccators were measured on RPA instrument in specified intervals. Vulcanization characteristics of rubber mixtures from 0 % and 100 % relative humidity environments were measured and compared.

Results and discussion

Mixtures with MBT accelerator which contained higher content of moisture had vulcanised faster than mixtures without moisture and also than mixtures with lower moisture content. Values of storage modulus were shifted to the lower values with increasing moisture content.

TMTD mixtures with higher content of moisture were faster as well. Mixtures after 50 days of moisture treatment (2.5 weight percent) had no scorch time.Mixtures with higher moisture content had storage modulus at vulcanization maximum by 6 units lower than "drier" mixtures.

At ZDMDC mixtures there was very similar trend to TMTD with higher difference of storage modulus.

Mixtures of CBS accelerator exhibit trend similar to MBT mixtures.

Rubber mixtures which were in desiccator with 0 % relative humidity environment were also measured on RPA. Gained values were used for correction of vulcanization characteristics of moist mixtures. Correction eliminated the influence of aging of rubber mixtures.

Conclusion

Vulcanization characteristics (e. g. scorch time, time of vulcanization maximum, storage modulus) of all mixtures have been influenced by moisture content. The extent of the influence increased with absorbed moisture. The influence on cured characteristics of mixtures depends also on used accelerator.

This work has been carried out with the financial support from the specific university research grant: MSMT - A1_FCHT_2013_001.

REFERENCES

1. Butler J., Freakley P. K.: Rubber Chem. Technol. *65*, 374 (1992).
2. Skinner S. J., Drakeley T. J.: Rubber Chem. Technol. *5*, 222 (1932).
3. Daynes H. A.: Rubber Chem. Technol. *6*, 24 (1933).
4. Sakdapipanich J. T., Chanmanit A., Suchiva K.: KGK *60*, 380 (2007).
5. Eng A. H., Chang C. F., Kahawara S.: J. Rubb. Res. *5*, 199 (2002).
6. Ngolemasango F., Ehabé E., Aymard C., Sainte-Beuve J., Nkouonkam B., Bonfils F.: Polym. Int. *52*, 1365 (2003).
7. Bonfils F., Flori A., Sainte-Beuve J.: J. Appl. Pol. Sci. *74*, 3078 (1999).
8. Bonfils F., Doumbia A., Char C., Sainte-Beuve J.: J. Appl. Pol. Sci. *97*, 903 (2005).
9. Amnuaypornsri S., Nimpaiboon A., Sakdapipanich J. T.: KGK *62*, 88 (2009).
10. Tillekeratne L. M. K., Vimalasari T.: J. Chem. Tech. Biotech., B *35*, 117 (1985).
11. Roth F. L., Bullman G. W., Wood L. A.: J. Res. Nbs. A Phys. Ch. *69A*, 347 (1965).

P-07
HIGH-FREQUENCY NOISE REDUCTION IN AUTOMOTIVE ELECTRONICS USING HYBRID FERRITE-POLYMER COMPOSITE MATERIALS

RASTISLAV DOSOUDIL and MARIANA UŠÁKOVÁ

Institute of Electrical Engineering, Faculty of Electrical Engineering and Information Technology, Ilkovičova 3, 812 19 Bratislava, Slovakia
rastislav.dosoudil@stuba.sk

The development of soft magnetic composites is an exciting topic both from fundamental and application points of view. Their fundamental electromagnetic properties, complex permeability and permittivity may be modified by filler particle size, shape and concentration in the composite structure. From an application point of view, automotive systems require more and more electronics and computer technology to be incorporated into the automobile[1]. To function properly they should not be affected by electromagnetic radiation. Nor should automobiles cause emissions that pollute the electromagnetic environment. Soft magnetic composite materials consisting of magnetic powder filler with defined granulometry and morphology, embedded in a non-magnetic polymeric matrix are capable to behave as electromagnetic interference (EMI) suppressors (i.e. electromagnetic wave absorbers) or shielding materials. Ferrite-polymer composites are a good choice for solving EMI problems. Hybrid composites are relatively a new class of materials possessing electromagnetic properties that could be better tuned compared to composites with only one kind of filler[2,3].

The aim of this investigation is to develop the hybrid ferrite-polymer composite materials with two kinds of soft magnetic filler (manganese-zinc ferrite and lithium-zinc ferrite) embedded in a non-magnetic polymeric (polyvinylchloride) matrix. The selected electromagnetic property, namely frequency dispersion of complex permeability has been measured and analyzed. The obtained permeability spectra for prepared composites were used to calculate the monolayer electromagnetic wave (EM-wave) absorbing parameters, such as return loss, matching thickness, matching frequency and bandwidth. Based on achieved results, the best candidate from composites for high-frequency EMI noise suppression in automobile electronic devices and circuits has been chosen.

Hybrid ferrite-polymer composite materials were fabricated by mixing a commercially available polyvinylchloride (PVC) with two different spinel ferrites: MnZn ferrite of composition $Mn_{0.52}Zn_{0.43}Fe_{2.05}O_4$ purchased from Pramet Šumperk Co., Czech Republic and LiZn ferrite of composition $Li_{0.525}Zn_{0.30}Ti_{0.35}Fe_{1.825}O_4$ synthesized by a standard ceramic process at 1050 °C/3.5 h in air. The mixtures were then thermally processed at a temperature of 145 °C and a pressure of 5 MPa into the toroidal shape (with an outer diameter of 7.9 mm, an inner diameter of 3.2 mm and a thickness of less than 2.5 mm). The concentration and particle size of the hybrid MnZn/LiZn ferrite filler were constant: 60 vol.% and 0–250 μm, respectively. The morphology and granulometry of ferrite fillers were confirmed by scanning electron microscopy (SEM), Fig. 1. We adjusted the volume fraction ratios of MnZn:LiZn filler to: 1:0, 0.7:0.3, 0.5:0.5, 0.3:0.7, and 0:1.

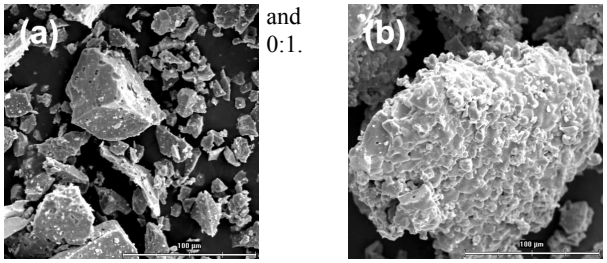

Fig. 1. **SEM photographs of a) MnZn and b) LiZn powder fillers**

Frequency dispersion of complex permeability $\mu = \mu' - j\mu''$ for fabricated sintered ferrites and hybrid composites was measured by means of a coaxial transmission line method using three vector analyzers (Hioki 3522-50, Agilent E4982A and Agilent E5071C) over the frequency interval 10 kHz – 6.5 GHz (ref.[4,5]). EM-wave absorption parameters of composites such as return loss RL, matching thickness d_m, matching frequency f_m, and the bandwidth Δf for RL ≤ –15 dB were evaluated by computer simulations.

Frequency variation of complex permeability $\mu = \mu' - j\mu''$ for sintered MnZn and LiZn ferrites is depicted in Fig. 2a. At the testing frequency interval, the permeability is dispersive for both ferrites. As can be seen from the inset of Fig. 2, the μ' of MnZn ferrite is constant with frequency at first and reached the value of 5130, then exhibited a small peak at a frequency

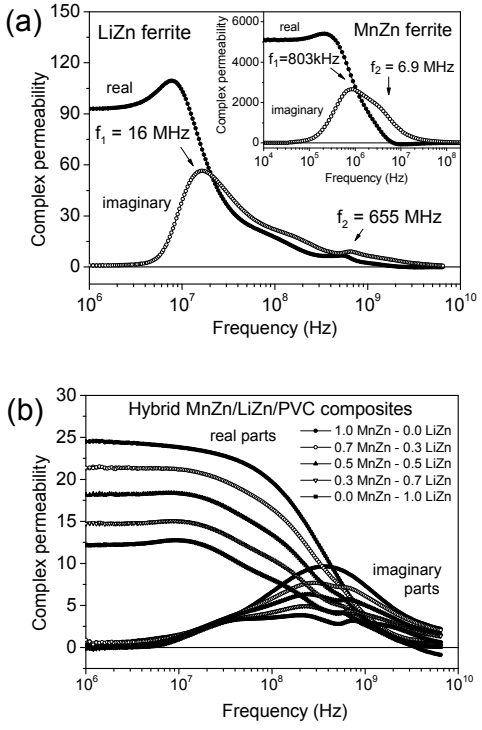

Fig. 2. **Complex permeability as a function of frequency for (a) sintered ferrites and (b) hybrid composites**

of 250 kHz followed by an abrupt drop to a zero value at $f_2 = 6.9$ MHz. The μ″ rises with frequency and achieved the maximum value 2655 at $f_1 = 803$ kHz. In case of LiZn ferrite μ′ starts with the constant value of 92 followed by two peaks at 7.9 MHz and 603 MHz, respectively. The μ″ obtained two maximum values: the first is 55 at $f_1 = 16$ MHz and the second is 9 at $f_2 = 655$ MHz. The measured frequency variation of μ for both ferrites confirmed the resonance type of permeability dispersion which is attributed to two basic kinds of resonance phenomena, namely the Bloch wall resonance and the natural ferromagnetic resonance[2,3]. The former is brought about by vibrations of walls at lower resonance frequencies (denoted f_1) and the latter is caused by spin precessions in magnetic domains at microwave resonance frequencies (denoted f_2).

Fig. 2b illustrates the frequency dispersion of complex permeability for synthesized MnZn/LiZn/PVC composites. One may say that the μ and its dispersion varied fluently with the alternation of hybrid filler fraction ratio in composite structure. It is interesting that the type of dispersion changed from relaxation one observed in MnZn/PVC sample to resonance one achieved in LiZn/PVC composite. The former is confirmed by our previous works[2,3] while the latter is a rare event. At low frequency (≈ 1 MHz), the μ′ fell off from 24.5 for MnZn/PVC composite to 12.2 for LiZn/PVC one. The MnZn/PVC sample exhibited only one dispersion range with a single resonance frequency (347 MHz). By contrast, samples with the fraction ratios of MnZn:LiZn filler 0.7:0.3, 0.5:0.5 and 0.3:0.7 exhibited two dispersion regions (the f_1 had the values between 230 and 260 MHz and the f_2 culminated around 690 MHz). The LiZn/PVC sample reached three dispersion ranges: the first one at 36 MHz (near the f_1 of sintered LiZn ferrite), the second one at 268 MHz, and the third one at 697 MHz (close to f_2 in LiZn ferrite). The achieved behaviour in μ–f dependences (f stands for frequency) of composites can be adjudged to the formation of demagnetization field H_d in filler particles isolated by polymeric matrix. In contrary to sintered ferrites, μ′ decreased and resonance frequencies f_1,f_2 shifted higher due to the contribution of H_d. In addition, the variation of fraction ratio in composites had the direct influence on the change of magnetocrystalline anisotropy and hence also the values of μ′ and f_1,f_2.

The measured frequency dependences of permeability for composites were used to the numerical computation of return (or reflection) loss, RL. Fig. 3a plots the RL as a function of frequency. The computation of RL was carried out on the condition that the thickness d of the monolayer absorber backed by a perfect conductor is small enough in comparison with the wavelength l of the incident plane transversal EM-wave: $RL = 20 \log |(Z_{in}–Z_o)/(Z_{in}+Z_o)|$, where $Z_{in} \approx jZ_o(2\pi/\lambda)$ μd is the input wave impedance at the air-composite interface and Z_o is the wave impedance of air. The impedance-matching condition representing the perfectly absorbing properties ($Z_{in} = Z_o$) is satisfied at a particular matching thickness (d_m) and a matching frequency (f_m), where minimum return loss occurs[2,3].

The plots of d_m, f_m and the bandwidth Δf for RL ≤ –15 dB as a function of volume fraction of LiZn ferrite filler in composites are shown in Fig. 3b. As the fraction ratio of hybrid MnZn:LiZn filler in composite changed from 1:0 to 0:1, the

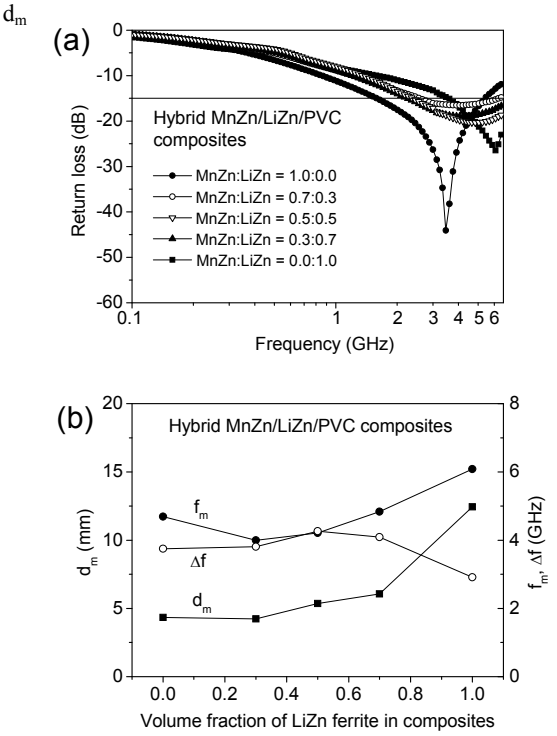

Fig. 3. **(a) Return loss as a function of frequency for hybrid composites and (b) selected absorption parameters as a function of volume fraction of LiZn ferrite in composites**

rose from 4.3 to 12.4 mm, the f_m increased from 4.7 to 6.1 GHz and Δf changed from 3.7 to 2.9 GHz with the maximum value of 4.3 GHz for the sample with MnZn:LiZn = 0.5:0.5 filler. Thus, the composite with the fraction ratio of filler MnZn:LiZn = 0.5:0.5 had the highest bandwidth of high-frequency absorption and thus is considered to be the best candidate for EMI suppression purposes in automotive electronic systems especially those dedicated to wireless communication.

This work was supported by Scientific Grant Agency of the Ministry of Education of the Slovak Republic and the Slovak Academy of Sciences (VEGA) - grant No. VG-1/1163/12 and by the Slovak Research and Development Agency (APVV) under the contract No. APVV-0062-11.

REFERENCES

1. Noble I. E.: Electron. Commun. Eng. J. *4*, 263 (1992).
2. Dosoudil R., Ušáková M., Franek J., Sláma J., Gruskova A.: IEEE Trans. Magn. *46*, 436 (2010).
3. Dosoudil R., Franek J., Sláma J., Ušáková M., Gruskova A.: IEEE Trans. Magn. *48*, 1524 (2012).
4. Dosoudil R., Ušák E., Olah V.: J. Electric. Eng. *61*, 111 (2010).
5. Dosoudil R.: J. Electric. Eng. *63*, 97 (2012).

P-08
CARBON FIBRE COMPOSITES. PART I: FREQUENCY DEPENDENCE OF THE ELECTRICAL CONDUCTIVITY

LADISLAV FOJTL, SOŇA RUSNÁKOVÁ, MILAN ŽALUDEK, MARIAN KUBLIHA, and ONDREJ BOŠÁK

[a] *Department of Production Engineering, Faculty of Technology, Tomas Bata University in Zlín, Nad Stráněmi 4511, 760 05 Zlín, Czech Republic,* [b] *Department of Physics, Institute of Materials Science, Faculty of Material Science and Technology, Slovak University of Technology, Paulínska 16, 917 24 Trnava, Slovak Republic*
fojtl@ft.utb.cz

Introduction

Most polymeric materials belong to the group of electric insulators. However, the addition of a portion of conductive material in the form of powder or fibers enables to create conductive paths and increases the electrical conductivity of these materials[1]. The most frequently used electrical conductive fillers in polymer composite materials include metal particles, carbon powder, carbon black and carbon nanotubes, which have been examined from the viewpoint of the influence of the percentage on the conductivity of the composite[2,3]. However, little interest has been given so far to the carbon pre-impregnated materials (prepregs) and to the effect of the final part thickness on the conductivity. The use of prepreg materials with precisely defined share of fibers in the layer (generally about 57 %) limits problems with a weighing the right portion of conductive fillers and their mixing into the matrix or problems with perfect impregnation through fibrous materials without formation of bubbles and dry places[4].

The reinforcement in the form of woven fabric ensures a sufficient strength and stiffness in two directions and increases the visual quality of the final product. The fabric used prepregs can consist of various weave style (plain, satin, or twill). Furthermore, the type of the resin within the prepreg affects resistance to the environment and increased temperature and also influences the difficulty of processing[6]. Nevertheless, the influence of the prepreg thickness on the frequency-dependent electrical conductivity has not been examined by previous studies.

The aim of the present paper is to examine the frequency-dependent electrical conductivity of carbon polymer composites depending on the thickness of the material, made from continuous carbon fiber prepreg impregnated by the epoxy matrix.

Experimental

The samples were prepared from carbon prepreg HexPly® M49 from the Hexcel Composites company[5,6]. In total, three series of samples were prepared with different thicknesses. The first one with the thickness of 1 mm (A) was constituted by four layers of prepreg, the samples of the second series consisted of six layers, corresponding to the thickness of 1.4 mm (B) and the last series was comprised of 8 prepreg layers with the total thickness of 2 mm (C).

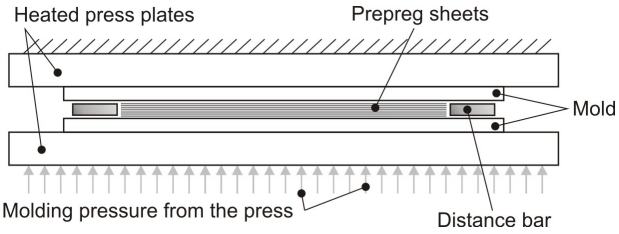

Fig. 1. **Scheme of the production of tested panels**

Composite panels were produced in a laboratory press with heated plates (Fig. 1). The temperature of plates was set to 140 °C and the curing time was 10 minutes. The values of the above parameters were chosen according to the material data sheet from the manufacturer[9]. Constant thickness of the panels was ensured by steel distance bars of appropriate size.

Electric and dielectric parameters were measured on LCR meter Goodwill 819. Totally, fifty frequencies in the range from 15 Hz to 100 kHz were used for measuring in alternating electric field (AC). The measuring apparatus for experiments was completely software controlled and adapted for monitoring of the changes in the polymer systems[7–9].

For the measurements, compression molded composite panels were cut for measurement into a shape of block with dimensions of base 30 × 30 mm, and the electrode was not applied directly on the sample. The measurements were conducted without protective atmosphere with the access of air.

Results

The frequency dependence of the AC conductivity of prepared composite samples measured at 100 °C is shown in Fig. 2. As can be seen, the sample with the lowest thickness (1 mm) shows almost unchanged value of conductivity with increasing frequency. This suggests that the electric charge is transported between composite surfaces through the conductive carbon reinforcement. On the other hand, the conductivity of thicker composite samples (B and C) was recorded only at frequencies above 1000 Hz, and 10 kHz respectively. AC conductivity for these thicknesses has an increasing trend with growing frequency. This dependence can be explained by the occurrence of a certain volume fraction of phases characteristic by polarization mechanisms with a short relaxation time. It is probable that the less conductive polymer matrix interrupts conductive pathways of carbon reinforcement with increasing thickness.

In the research we also followed changes in loss factor in dependence of frequency (Fig. 3) for all 3 samples. The shape of the curve in the case of sample A indicates that the transport of electric charge is achieved by particular conductive connection through fibers of woven fabric. The decline of loss factor for samples B and C indicates little influence of electrically low-conductive phase – the polymer matrix, which interrupts the pathways ensured by conductive fabric.

The shape of frequency dependence of samples B and C is also influenced by the occurrence of another phase in the form of conductive particles in the volume of the composite. Their presence affects the frequency dependence of loss fac-

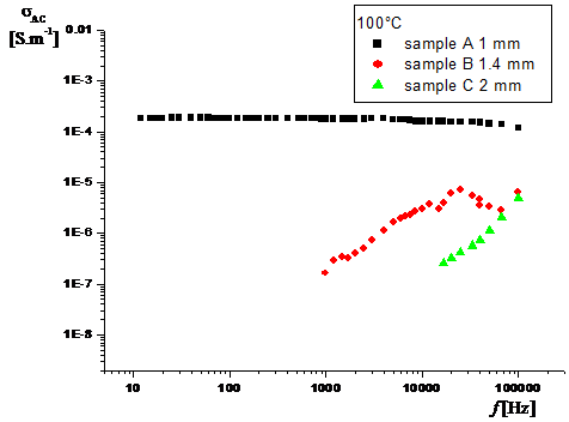

Fig. 2. **The frequency dependence of the AC conductivity (samples A, B, C) measured at 100 °C**

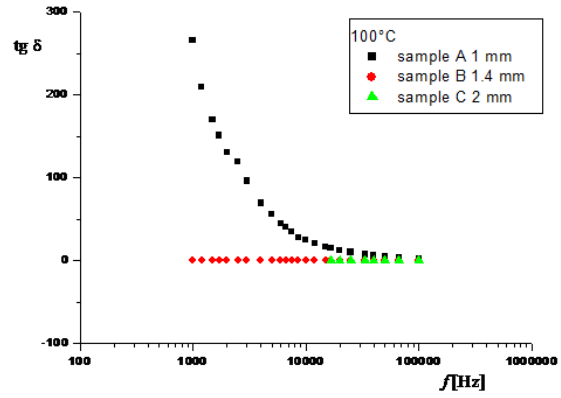

Fig. 3. **The frequency dependence of the loss factor (samples A, B, C) measured at 100 °C**

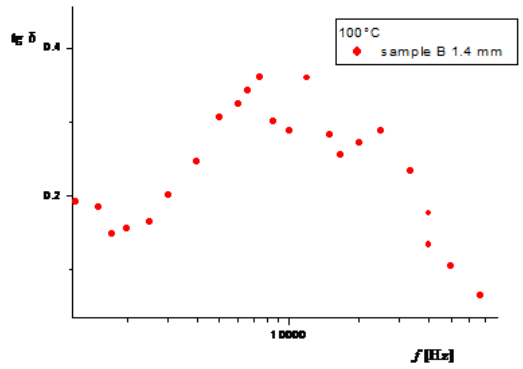

Fig. 4. **Detail of the frequency dependence of the loss factor (samples A, B, C) measured at 100 °C**

tor and showed an increase of this factor in the narrow value interval of frequencies (Fig. 4). This frequency interval is dependent on the temperature.

Conclusion

The results of the study show that the thickness of the carbon fabric/epoxy composite affects the frequency-dependent electrical conductivity. In the case of thin material (sample A), the amount of carbon fabric reinforcement is sufficient to ensure the required high values of electrical conductivity. Conversely, samples with a higher thickness (B, C) show that the polymer matrix has a significant influence on the values of the frequency-dependent conductivity.

Due to required use (facing parts in automotive) in order to achieve higher electrical conductivity it is necessary to use conductive fillers into these prepreg materials[3]. In this case, it is necessary to monitor the preparation technology of composite to ensure good dispersion of conductive particles in the volume of the polymer matrix reinforced with carbon fabric.

This work was supported by the Ministry of Education and Youth of the Czech Republic under project APVV CZ–0168-11,7AMB12SK109 and by Slovak National Science Foundation under grant VEGA No. 1/0356/13 and by internal grant of TBU in Zlín No.IGA/FT/2013/022 funded from the resources of specific university research.

REFERENCES

1. Harold Johnson J., Kiepura R., Humphries D.: *Engineered Materials Handbook*, Volume 1, p.983, Composites. ASM International, Ohio 1998.
2. Lonjon A., Demont P., Dantras E., Lacabanne C.: J. Non-Crystalline Solids *358*, 1859 (2012).
3. Jin J., Lin Y., Song M., Gui Ch., Leesirisan S.: Eur. Polymer J. , Available online 2013-1-31, ISSN 0014-3057.
4. Dorworth L., Gardiner G., Mellema G.: *Essentials of Advanced Composite Fabrication & Repair*, p. 304. Aviation Supplies & Academics, Newcastle 2010.
5. HexPly® M49, Datasheet, Hexcel Corporation.
6. HexPly® Prepreg Technology. http://www.hexcel.com [online]. c2013. [cit. 2013-2-27]. Available at WWW: <http://www.hexcel.com/resources/technology-manuals>
7. Minárik S., Labaš V., Berka M.: J. Optoelectronics Adv. Mater. 9, 1592 (2007).
8. Minárik S., Kubliha M., Labaš V., Kalužný J.: J. Optoelectronics Adv. Mater. 8, 1524 (2006).
9. Bošák O., Tóth M., Minárik S., Psota J.: Equipments for investigation of non-metallic materials. XXIV Didmattech 2011: Problems in teachers education, p. 63-68. Instytut Techniki UP, Kraków 2011.

P-09
CARBON FIBRE COMPOSITES. PART II: TEMPERATURE DEPENDENCE OF THE ELECTRICAL CONDUCTIVITY

LADISLAV FOJTL, SOŇA RUSNÁKOVÁ, MILAN ŽALUDEK, MINÁRIK STANISLAV, and ONDREJ BOŠÁK

[a] Department of production engineering, Faculty of technology, Thomas Bata University in Zlin, Nad Stráněmi 4511, 760 05 Zlín, Czech Republic, [b] Department of Physics, Institute of Materials Science, Faculty of Material Science and Technology, Slovak University of Technology, Paulínska 16,917 24 Trnava, Slovak Republic
fojtl.utb.cz

Introduction

Temperature dependent electrical conductivity of polymer composites has been subject of many former studies[1–3]. It was proved that the increased operating temperature may cause chemical changes in the composite and thereby changes of electrical or mechanical properties[4,5].

Research in this paper continues the previous part (Part I) and examines the changes of the electrical conductivity of carbon polymer composites in dependence on the thickness of the sample at various measuring temperatures. The conductivity is measured for various settings of measuring frequencies for different temperature conditions. The internal arrangement of reinforcement in the composite resulting from given production technology is observed.

Experimental

As was mentioned before, research extends the findings from the first part. Due to this, similar material was used for the production of the samples (HexPly® M49, Hexcel Composites)[6,7]. Layers of pre-impregnated material were placed in configuration 0 °/ 90 °. Description of the samples is shown in following table.

The samples were compression molded in a laboratory press at the temperature of 140 °C for 10 minutes according to the recommendations in the material sheet. Scheme of production is shown in the previous part (Part I).

LCR meter Goodwill 819 was used for measuring of electric conductivity at elevated temperature. The measuring apparatus was completely software controlled and the measurement itself was conducted with the access of air. The measurement was performed in one cycle for 6 measuring frequencies in alternating electric field (AC), successively at 20 °C, 30 °C, 40 °C, 50 °C, 60 °C, 70 °C, 80 °C, 90 °C, 100 °C, 110 °C, 120 °C, 130 ° C, 140 °C and 150 °C. The electrode was not applied directly on the samples and the samples were conditioned on measuring temperature before every measurement. The measurement was conducted in the cycle continuously without interruption (without removing from the electrode system)[8,9].

Table I
Samples for temperature-dependent AC conductivity

Sample	Thickness	Layers of M49	Dimensions
A	1 mm	4	30×30 mm
B	1.4 mm	6	30×30 mm
C	2 mm	8	30×30 mm

Results

Structure formed inside the composite due to the production technology is shown in Fig. 1. As can be seen, the layers in the view of microscope (50× magnification) are disordered and separate by differently wide layer of the polymer matrix. This fact is especially visible for samples A (1 mm) and B (1.4 mm).

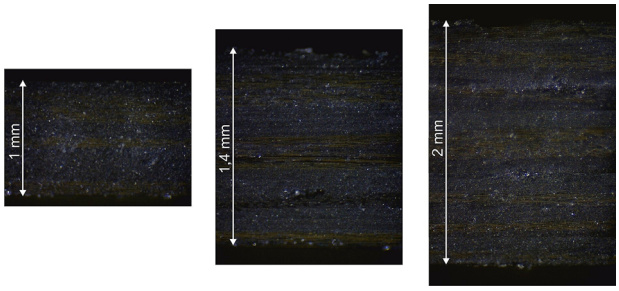

Fig. 1. **Structure inside the samples**

Temperature dependence of electrical conductivity for various measuring frequencies for differently wide samples is shown in following figures (Fig. 2, Fig. 3, Fig. 4).

As can be seen in Fig. 2, the temperature-dependent electrical conductivity of the sample A is stable to 90 °C, whereas is not practically influenced by the measurement frequency. This frequency independence and low temperature sensitivity refers to the dominant influence of the carbon reinforcement.

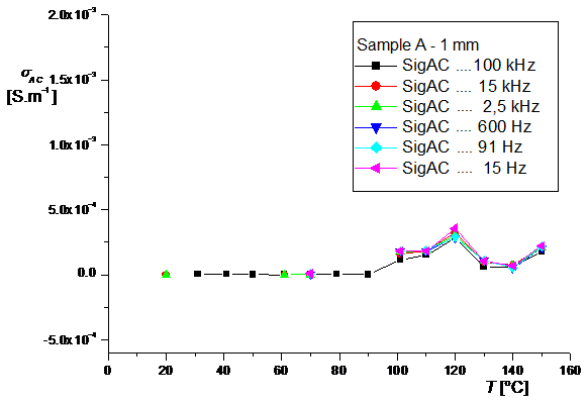

Fig. 2. **Temperature dependence of the AC conductivity (sample A) measured for different frequencies**

The part of the measurement course above the temperature of 90 °C is probably connected with additional changes in the polymer matrix of the composite. These changes are apparently continuing chemical reactions, namely curing of epoxy matrix.

The values measured for sample B (Fig. 3) are burdened with the high variance. This high variance could be caused by impurities, which could fell into the interlayer of materials during the preparation. The significant decrease of conductivity for highest measuring frequency (100 kHz) at the temperature of 90 °C is observed. The electrical conductivity for lower measuring frequencies was not almost recorded for this sample with rising temperature.

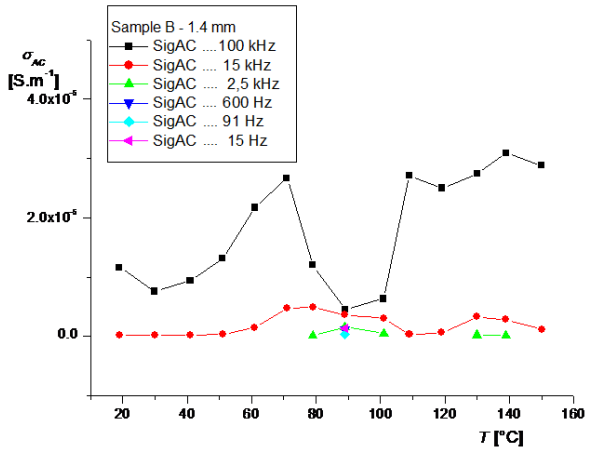

Fig. 3. **Temperature dependence of the AC conductivity (sample B) measured for different frequencies**

The course of the temperature-dependent electrical conductivity for the sample with the highest thickness C is shown in Fig. 4. This sample showed nearly constant course of conductivity up to the temperature of 110 °C. After this value of temperature the course firstly showed upward trend and then a sharp rise of electrical conductivity. The fact that there is a displacement of this increase compared to the sample A can be explained by the occurrence of greater amount of the polymer matrix in the structure of composite. Thus the additional curing occurs at a higher temperature than that of sample A.

Conclusion

The obtained results confirmed the dependence of electrical conductivity on the temperature. The increase of conductivity at temperatures above 100 °C for the samples A and C is observed. This increase is apparently caused by the completion of the chemical reactions of the polymer matrix. The measurement for sample B should be conducted again for eventual confirmation or refutation of the measured dependence. The significant change of the electrical conductivity observed for the sample C has no longer exponential character of increase, which is typical for filled polymeric systems according to the Arrhenius relations. The subsequent drop of electric conductivity, despite the rising temperature,

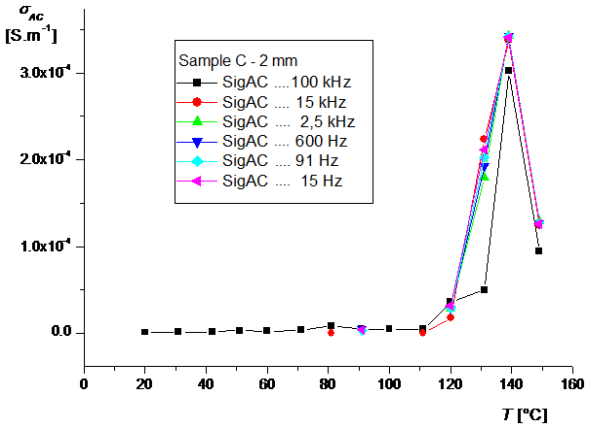

Fig. 4. **Temperature dependence of the AC conductivity (sample C) measured for different frequencies**

indicates that the values of conductivity in the temperature range above 120 °C are increasing as a result to significant changes in the structure of the reference composite.

This work was supported by the Ministry of Education and Youth of the Czech Republic under project APVV CZ–0168-11,7AMB12SK109 and by Slovak National Science Foundation under grant VEGA No. 1/0356/13 and by internal grant of TBU in Zlín No.IGA/FT/2013/022 funded from the resources of specific university research.

REFERENCES

1. Lonjon A., Demont P., Dantras E., Lacabanne C.: J. Non-Crystalline Solids *358*, 1895 (2012).
2. Mohiuddin M., Hoa S.V.: Compos. Sci. Technol. *72*, 21 (2011).
3. Jin J., Lin Y., Song M., Gui Ch., Leesirisan S.: Eur. Polymer J., Available online 2013-1-31, ISSN 0014-3057.
4. Harold Johnson J., Kiepura R., Humphries D.: *Engineered Materials Handbook*, Volume 1, Composites, p. 983, ASM International, Ohio 1998.
5. Dorworth L., Gardiner G., Mellema G.: *Essentials of Advanced Composite Fabrication & Repair*, p. 304. Aviation Supplies & Academics, Newcastle 2010.
6. HexPly® M49, Datasheet, Hexcel Corporation.
7. HexPly® Prepreg Technology. http://www.hexcel.com [online]. c2013. [cit. 2013-2-27]. Available at WWW: <http://www.hexcel.com/resources/technology-manuals>
8. Labaš V., Minárik S., Trnovcová V.: Eng. Mechanics 5, 399 (1998).
9. Berka M., Labaš V., Kubliha M: Acta Mechanica Slovaca 10, č. 2-B / konf. PRO-TECH-MA '06, Herľany, ISSN 1335-2393.

P-10

EFFICIENCY OF FULLY SCREEN PRINTED DYE SENSITIZED SOLAR CELLS WITH CONDUCTIVE POLYMER PEDOT:PSS COUNTER ELECTRODE

PAVOL GEMEINER and MILAN MIKULA

Department of Printing Arts Technology and Photochemistry IPM, Faculty of Chemical and Food Technology SUT, Radlinského 9, 812 37 Bratislava, Slovak Republic pavol.gemeiner@gmail.com

Abstract

Dye sensitized solar cells (DSSC), the special group of photovoltaic cells, are standardly composed of TiO_2 photoactive electrode and counter electrode (CE) with catalytic platinum (Pt) layer on the glass substrate. However, the effort is put to the replacement of Pt with low cost conductive polymers which may be used and printed on flexible polymer foils instead of rigid glass substrate. The most widely used conductive polymer poly (3,4-ethylendioxythiofene) – poly (styrenesulphonate) (PEDOT:PSS) was used as a catalytic layer for DSSC counter electrode and screen printed on the glass substrate with fluorine doped tin oxide (FTO). Screen printed counter electrodes of PEDOT:PSS were compared to layers deposit with doctor blade technique. The results have shown that the DSSC based on counter electrode with double printed PEDOT:PSS layer reached promising 0.79 % and layer deposited with doctor blade reached 1.1 % efficiency compared to 1.09 % efficiency of DSSC with standard Pt counter electrode.

Introduction

Dye sensitized solar cells are possible replacement for conventional silicon based solar cells thanks to their promising photon to electron conversion efficiency, possibility to use low cost and environmentally friendly printing technologies (screen printing, roll-to-roll, doctor blade) and used materials (TiO_2, carbon nanoparticles, conductive polymers). The DSSC standard structure contains five components, *1*) glass substrate coated with transparent conductive oxides, *2*) the semiconductor nonporous photoactive layer based on TiO_2, *3*) a dye used as sensitizer, *4*) an electrolyte containing redox mediator, *5*) and Pt counter electrode which has the crucial role in regenerating redox mediator and is responsible for the electron transport[1].

The conductive polymer PEDOT:PSS is very well known for its high conductivity, good catalytic activity, high transparency, possibility to be used for different printing technologies and printed on flexible substrates. Due to these properties PEDOT:PSS is used and studied as a CE in DSSC. The DSSCs based only on one layer PEDOT:PSS counter electrode generate significantly lower efficiencies then those with Pt based CE[2–5]. Therefore, most researchers are focusing on the study of composites of PEDOT:PSS and carbon nanotubes which achieved 16 % lower efficiencies compared to Pt CE and about 30 % higher efficiencies compared to only one pure PEDOT:PSS counter electrode layer[6]. Disadvantages of composite materials based on PEDOT:PSS/CNTs are difficult and long homogenization process and a significant decline of CE transparency which decrease cell efficiency illuminated from the back – CE side.

The aim of this paper was to prepare fully printed dye sensitized solar cell with screen printed photoactive TiO_2 electrode and polymer PEDOT:PSS multi-layered counter electrode. Properties as efficiency, transmittance of CE, volt-ampere characteristics and topography of DSSC using the counter electrodes with different numbers of screen printed or doctor bladed PEDOT:PSS layers on glass/FTO substrates were analyzed and compared with the standard DSSC containing Pt counter electrode.

Experimental

Preparation of nanoporous TiO_2 photoactive anode

TiO_2 paste for screen printing was prepared via homogenization process as mixture of 4.5 wt.% of TiO_2 nanopowder (Evonik, Aeroxide P25, ~ 22 nm), 1,5 wt.% of ethyl cellulose (Aldrich, viscosity 22 cp in toluene:ethanol 80:20), 70 wt.% of ethanol (>96,6 %), 20 wt.% of deionized water and 4 wt.% of acetic acid (>99,7). The TiO_2 nanopowder was added to mortar and stirred with gradual addition of acetic acid, deionized water and ethanol. The TiO_2 dispersion was transferred with excess of ethanol and 10 wt. % of ethyl cellulose to a beaker and stirred with magnetic stirrer for 24 hours and then homogenized by ultrasonic bath for 20 min. The prepared TiO_2 paste was screen printed (manual screen printer, polyester screen – 140 mesh, with mesh opening 64 μm, polyurethane squeegee and photosensitive emulsion Kasi, Fotecoat 1970), on the fluorine doped tin oxide coated glass (FTO glass, Aldrich, ~ 7 Ω/sq., 2×3 cm). After screen printing, the TiO_2 electrodes with size 1×1,5 cm were sintered at 450–460 °C for 30 min to remove residual organic compounds and to improve interconnection between nanoparticles.

Preparation of PEDOT:PSS and Pt counter electrodes

Catalytic layer of PEDOT:PSS (Orgacon Type P 3042, transparent screen printing ink) with size 1x1.5 cm was screen printed (305 mesh, with mesh opening 34 μm) onto the FTO glass (2×3 cm). Samples with one, two and three printed PEDOT:PSS layers were prepared. Each layer was dried at 120 °C for 40 min before printing additional layer. Pt catalytic layer 1×1.5 cm (Solaronix, Platisol T/SP) was screen printed onto the FTO glass and then sintered at 450 °C for 15 min. Un the case of doctor blade technique (DB), the FTO glasses with sticked scotch tapes (thickness 40 μm) on three sides were used. The movement of the blade created defined layer of 1×1.5 cm.

DSSC assembling

Prepared TiO_2 photoactive electrodes were sensitized in 0,4 mM solution of N3 dye in ethanol (Aldrich, cis-[(2,2´-bipyridyl-4,4´-karboxylát)$_2$(NCS)$_2$] ruténium(II)) for 24 hours. 18 μl of electrolyte (Solaronix, Iodolyte AN50) was added directly on the sensitized TiO_2 electrodes which were then assembled with Pt or PEDOT:PSS counter electrodes

into a sandwich type cell and caught with two binder clips. The photoactive TiO_2 layer has 1.5 cm^2.

DSSC and screen printed electrodes measurements

Transmittance of printed layers was measured with UV-Vis spectrophotometer Cecil CE 3055. 3D topography images, layer thickness and roughness were analyzed by atomic force microscope (Veeco microscope, 5 and 100 μm scanner, non-contact mode). I–V characteristic of DSSC were measured using day-light source with the power of 880 W/m and by the loading circuit containing two multimeters (Keithley 2000).

Results and discussions

The thickness, roughness and topography of screen printed and DB coated PEDOT:PSS layers were evaluated by AFM. The single screen printed and DB coated PEDOT:PSS layer have similar thickness of 0.7 μm and 0.8 μm respectively. Double and triple screen printed layers have thickness of 1.4 and 2.1 μm. As shown in Fig. 1, the topography of DB coated layer was more flat with roughness Rq = 24 nm compared to screen printed layer with Rq = 28 nm. The roughness of screen printed layers decreased with the number of printed layers, for double printed layer to Rq = 23 nm and for triple printed layer to Rq = 21 nm. It indicates the filling of free spaces and the higher homogeneity of double and triple screen printed PEDOT:PSS layers.

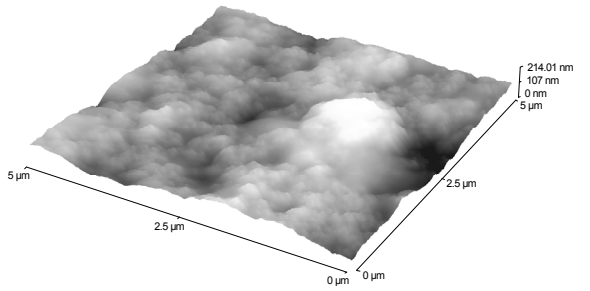

PEDOT:PSS screen printed on FTO glass

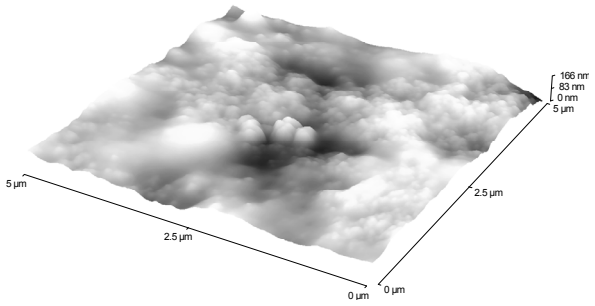

PEDOT:PSS coated on FTO glass with DB

Fig. 1. **Topoghraphy of screen printed and DB coated PEDOT:PSS**

The images of printed PEDOT:PSS layers taken from optical microscopy at 250× magnification (Fig. 2) shown that screen printed layers have surfaces marked by periodic structure of mesh fibers in positions where fibers cross each other. This inhomogeneity increased with number of printed layers.

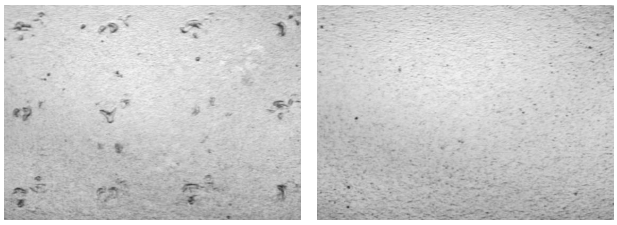

Fig. 2. **Optical images of screen printed PEDOT:PSS on left side shown periodic inhomogeneities caused by mesh; on the right side is flat surface of DB coated PEDOT:PSS layer**

Transmittance of printed CE layers, as an important factor for determination amount of accessible light to a dye, was evaluated at the wavelength of maximal absorbance of N3 dye λ_{max} = 534 nm. As shown in Fig. 3, highest transparency 75 % at wavelength 534 nm was reached by FTO glasses with Pt catalytic layer, values for single screen printed PEDOT:PSS layer and PEDOT:PSS coated with doctor blade are very similar 70 % and 69 %. It is obvious that the increasing of number of screen printed PEDOT:PSS layers decreased CE transparency in whole UV-Vis spectrum.

The I–V characteristics of prepared DSSC were measured at front side (FS – the TiO_2 electrode) and back side (CE – the counter electrode) illumination. The Fig. 4 shows the I–V characteristics of prepared DSSC with screen printed and DB coated PEDOT:PSS counter electrodes measured from front side. The highest value of photocurrent density J_{SC} = 2.59 mA cm^{-2} (BS, J_{SC} = 1.94 mA cm^{-2}) reached CE with double screen printed PEDOT:PSS layers with the open circuit potential V_{OC} = 0.68 V (BS, V_{OC} = 0.67 V) with η =

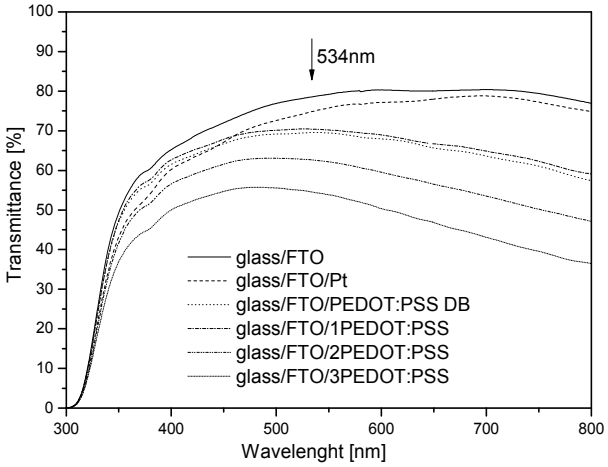

Fig. 3. **UV-Vis transmittance spectra of prepared PEDOT:PSS and Pt CE on glass/FTO subtrates**

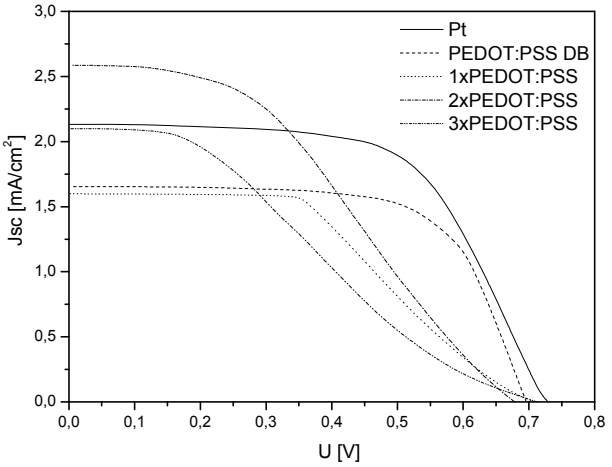

Fig. 4. **I-V characteristics of DSSC with screen printed and DB coated PEDOT:PSS counter electrodes measured from front side**

0.79 % (BS, η = 0.64 %). Higher J_{SC} value means better electron transfer to the redox mediator. Highest efficiency η = 1.1 % (BS, η = 0.88 %) was reached by DB coated PEDOT:PSS CE and Pt CE with similar η = 1.09 % (BS, η = 0.9 %). The highest efficiency of screen printed PEDOT:PSS CE was reached by double printed layer η = 0.79 % (BS, η = 0.64 %) followed single printed η = 0.63 % (η = 1.1 %) and triple printed layer η = 0.53 % (η = 1.1 %).

Conclusions

The efficiencies of fully printed dye sensitized solar cells onto glass/FTO substrates with photoactive TiO_2 electrode and conductive polymer PEDOT:PSS counter electrode were compared to standard DSSC based on Pt counter electrode. The DSSC with CE based on PEDOT:PSS double screen printed layers reached 0.79 % efficiency compared to η = 1.1 % doctor blade coated PEDOT:PSS layer and η = 1,09 % of screen printed Pt CE. The AFM and optical microscopy have shown that DB coated layers of PEDOT:PSS compared to screen printed have more flat surface without defects caused by screen printing mesh.

This work was supported by the Slovak Research and Development Agency under the contract No. APVV-0324-10, by the Slovak Grant Agency (project VEGA 1/0818/13) and by the OP Research and Development of the project National Centrum of Research and Application of Renewable Sources of Energy, ITMS 26240120016, co-financed by the Fund of European Regional Development.

REFERENCES

1. Nazeerudin Md. K., Baranoff E., Grätzel M.: Solar Energy *85*, 1172 (2011).
2. Fan B., Mei X., Sun K., Ouyang J.: Appl. Phys. Lett. *93*, (2008).
3. Muto T., Ikegami M., Miyasaka T.: J. Electrochem. Soc. *157*, (2010).
4. Hong W., Xu Y., Lu G., Li C., Shi G.: Electrochem. Commun. *10*, 1555 (2008).
5. Thompson S. J., Pringle J. M., Zhang X. L., Cheng Y. B.: J. Phys. D.: Appl. Phys. *46*, (2013).
6. Yun D. J., Ra H., Rhee S. W.: Renewable Energy *50*, 692 (2013).

P-11
INFLUENCE OF FIBER PARAMETERS ON THERMOMECHANICAL AND MECHANICAL PROPERTIES OF MODIFIED PP FIBERS

ĽUBA HORBANOVÁ[a], ANNA UJHELYIOVÁ[a], PETRONELA VENCELOVÁ[a], PETER MICHLÍK[b], and JOZEF RYBA[a]

[a] Department of Fibers and Textile Chemistry, Institute of Polymer Materials, Faculty of Chemical and Foot Technology, Slovak University of Technology in Bratislava, Radlinského 9, 812 37 Bratislava, [b] Research Institute for Man-Made Fibers, a.s., Štúrova 2, 059 21 Svit, Slovakia luba.horbanova@stuba.sk

Introduction

High compressive strength, long service life, and low cost are properties insuring concrete to be the most commonly used construction material. Disadvantages of concrete as low tensile strength and crack resistance may be improved by reinforcing of concrete, what was investigated in numerous studies[1].

Fiber-reinforced concrete is concrete containing dispersed randomly oriented fibers. Fibers primarily control the propagation of cracks and limit the crack width. Concrete reinforced with short discontinuous fibers considerably improves the performance of concrete and negates its disadvantages such as poor toughness, a serious shortcoming of high strength concrete, low ductility, and low energy absorption capacity[1–3].

There are many kinds of metallic or polymeric fibers are used in concrete for their advantages. Polypropylene (PP) fibers are one of the most widely used for construction applications such as in shotcrete tunnel linings, blast resistant concrete, overlays, and pavements. PP fibers are commercially utilized at relatively low volume fractions to control plastic shrinkage cracking of concrete and they are expected to improve concrete ductility, toughness, and impact resistance[1,4,5].

However, addition of sufficient additive to PP fibers may provide further improvements in this field. Physical and chemical modification induces more intense adhesion of PP fibers to concrete matrix[6]. Change of cross section of modified PP fibers from circle to star-shaped profile increases contact surface between fiber and concrete. This leads to expressive improve of functional of PP fibers in relation to transmission and absorption of deformation energy.

This article is focused on the structure and properties changes of polypropylene fibers after their modification by addition of inorganic filler with different cross section. Thermomechanical and mechanical properties of standard PP

fibers and PP fibers modified by inorganic additives with content 6.4 wt.% and 16.8 wt.%, with circle and star-shaped cross section were studied. Information about fiber structure was obtained from TMA scans. Tenacity at the break, Young's module and elongation of PP fibers were obtained at determination of mechanical properties.

Experimental

Material used

In this study the specimens were prepared using PP TATREN HT 1810 with MFI = 20.6 g/10 min produced by Slovnaft a.s., Bratislava (SK). Using the two screw extruder has been PP and PP with different content of inorganic filler mechanically mixed and melted. Obtained concentrates have been subsequently used for preparation of fibers with circuit and star-shaped cross section by continual technology. Prepared PP standard fibers (PPS) and composite PP fibers with content of inorganic filler 6.4 %wt. (PPC1) and 16,8 % wt. (PPC2) has been drawn in the range of drawing ratios 2–4.

Methods used

The evaluation of thermomechanical properties has been performed using Shimadzu Thermomechanical Analyzer TMA–50. Temperature (T_D) at which the fibers are deformed at a constant load and shrinkage (l_D) of fiber at 90 °C were determined using the TMA scans showing shrinkage behavior before melting. Conditions of measurement were following: heat from room temperature to 90 °C at the heating rate 5 ° C min^{-1}, and fiber length 9.8 mm.

Mechanical properties were measured by Instron 3343 device and evaluated using Instron program. Measuring conditions were: fixture length of fiber 125 mm, rate of clamp shifting 500 mm min^{-1}. Tensile test was done in order to measure the tension of fiber to tensile stress until the interruption of fiber. Fibers are straining continuously. Maximum tensile tenacity at the break and corresponding extension is measured at the rupture of fiber.

Results and discussion

Analysis of thermomechanical properties of PP fibers modified by various contents of inorganic additives was realized by TMA. Fiber prepared with both, circuit and star-shaped cross section, drawn to drawing ratio 2–4, were expose to temperature growth from room temperature to 90 ° C at rate 5 °C min^{-1}. Obtained experimental dependencies are used for determination of dimensional stability of samples, specifically by deformation temperatures and total shrinkages. Dimensional stability depends on the orientation and crystallinity of the samples.

From results shown in Tabs I, II it is obvious that addition of inorganic additives does not lead to considerable decrease of deformation temperatures. PP fibers samples with circuit cross section actually indicate higher temperature resistance, which is growing with higher fiber orientation. Temperature growth with higher drawn ratio did not occur only at PPC samples with star-shaped cross section. Deformation temperatures of PP fibers with 6.4 wt.% content of inorganic additives reached highest values.

Table I
Temperature (T_D) of standard PP fibers and composite PP fibers with 6.4 wt.% and 16.8 wt.% contents of inorganic additives with circle (o) and star-shaped (*) cross section

	T_D[°C]		
λ	PPS o	PPC1 o	PPC2 o
2.0	53.2	52.9	57.2
3.0	56.3	59.8	58.1
4.0	55.3	62.4	58.9
λ	PPS *	PPC1 *	PPC2 *
2.0	55.5	59.1	58.0
3.0	57.1	56.0	57.2
4.0	58.4	58.9	56.8

Table II
Shrinkage (l_D) of standard PP fibers and composite PP fibers with 6.4 wt.% and 16.8 wt.% contents of inorganic additives with circle (o) and star-shaped (*) cross section

	l_D[%]		
λ	PPS o	PPC1 o	PPC2 o
2.0	-1,9	-1,0	-0,8
3.0	-2,5	-1,8	-1,2
4.0	-3,8	-2,2	-1,8
λ	PPS *	PPC1 *	PPC2 *
2.0	-1.5	-0,1	-1.2
3.0	-1.9	-2,0	-1.2
4.0	-2.9	-2,1	-1.7

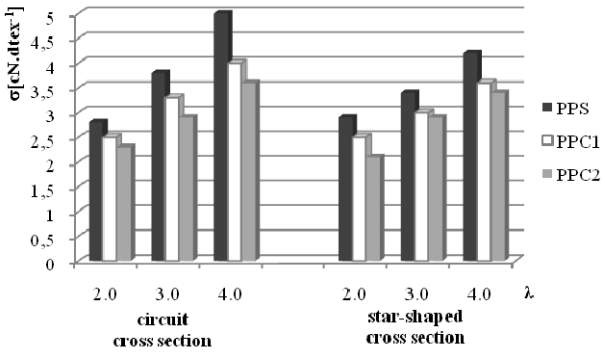

Fig. 1. **Tenacity at the break (σ) of standard PP fibers and composite PP fibers with 6.4 wt.% and 16.8 wt.% contents of inorganic additives with circle (o) and star-shaped (*) cross section**

Measuring of dimensional stability of fibers proves shrinkage at all samples. In consequence of drawing samples the shrinkage grows, while addition of inorganic additive improves dimensional stability of PP fibers with circuit as

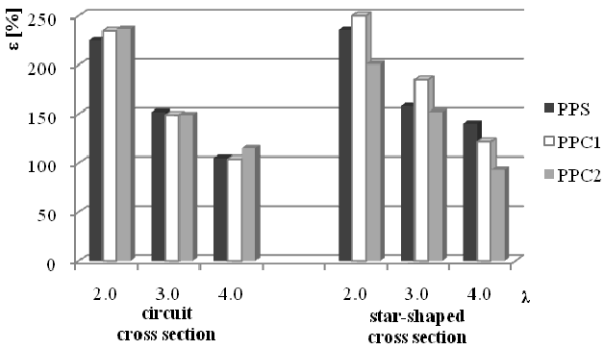

Fig. 2. **Elongation (ε) of standard PP fibers and composite PP fibers with 6.4 wt.% and 16.8 wt.% contents of inorganic additives with circle (o) and star-shaped (*) cross section**

well as with star-shaped cross section. In addition, fibers with circuit cross section achieved higher shrinkage than it was at PP fibers with star-shaped cross section, whereby differences decrease with increase of content of inorganic additives.

Evaluation of mechanical properties has shown dependency of tenacity at the brake of PP fibers on content of inorganic filler as well as on drawing ratio (Fig. 1). With increasing content of inorganic additives there is tenacity of PP fibers slightly lower, while orientation of fibers increases their tenacity. Tenacity at the brake of PP fibers with star-shaped cross section was lower than at samples with circuit cross section. Young's module of star-shaped cross section of PP fibers was similar to fibers with circuit cross section. The highest values of Young's module of modified PP fibers were measured at PPC1 fibers with star-shaped cross section.

Elongation (Fig. 2) decreases with fiber orientation. At PP fibers with circuit cross section there is observed increase of elongation at higher content of inorganic additives, while at PP fiber with star-shaped cross section there is higher elongation at 6.4 wt.% content of inorganic additives at lower drawing ratios.

Conclusions

Higher dimensional stability in dependence on temperature is achieved by PP fibers with 6.4 %wt. of inorganic additives, what is confirmed by higher deformation temperatures at PP fibers with circuit as well as with star-shaped cross section. PP fibers with star-shaped cross section have better dimensional stability at higher content of additives at circuit and star-shaped cross section. Dimensional stability increases with drawing ratio at all fibers as a result of higher input strain at fiber orientation. Modification of PP fibers with inorganic additives decreases their mechanical properties.

This work was supported by the Slovak Research and Development Agency under the contract VMSP-P-0007-09 and VEGA 1/0444/09.

REFERENCES

1. Kim S. B., Yi N. H., Kim H. Y., Kim J. J., Song Y.: Cem. Concr. Compos. *32*, 232 (2010).
2. Zollo R. F.: Cem. Concr. Compos. *19*, 107 (1997).
3. Sivakumar A.: Cem. Concr. Compos. *29*, 603 (2007).
4. Hsie M.: Mater. Sci. Eng., A *494*, 153 (2008).
5. Alhozaimy A. M.: Cem. Concr. Compos. *18*, 85 (1996).
6. Ujhelyiová A., et al.: *6th International Textile, Clothing & Design Conference*, 122–127 (2012).

P-12
SOLID PARTICLES - THEIR EFFECT ON PROPERTIES OF COMPOSITE FIBRES

MARCELA HRICOVA and ANTON MARCINCIN

Department of Fibres and Textile Chemistry, FCHPT, STU in Bratislava, Radlinskeho 9, 812 37 Bratislava, Slovakia
marcela.hricova@stuba.sk

Abstract

In this paper the effect of inorganic nanofillers, such as organoclays, boehmites and carbon nanotubes on spinning, drawing and mechanical properties of PP composite fibres was studied. The dependence between filler content, processing conditions and tensile properties of PP composite fibres are discussed.

Introduction

Oriented polymer nanocomposites such as nanocomposite fibres represent a special group of the polymer materials from the point of view of arrangement of nanofiller particles in polymer matrix.

Solid particles play an important role in modification the desirable properties of polymers. Compounding of polymers with suitable fillers is an effective way to improve the properties of composites, mainly mechanical, thermal, electrical as well as UV barrier and light stability[1–7].

The montmorillonite (MMT) is one of the most commonly used organically layered silicates. Organically treated layered silicates are organoclays suitable for preparation of polymer nanocomposites with polar functional groups such as polyester (PES) and polyamide (PA). For polyolefin nanocomposites such as polypropylene (PP) and polyethylene (PE) it is necessary to use the convenient compatibiliser in addition[8].

Boehmites are hydrophilic inorganic aluminium oxides based on γ-AlO(OH). With regard to hydrophilic nature the boehmites can be used also in latex and water solutions of polymers[9]. After suitable surface treatment they are dispersible in the organic solvents and become interesting inorganic nanofillers for polymers[10].

The carbon nanotubes (CNT) represent an unique nanofibrous materials for polymer composites because of their shape, morphology, electrical and mechanical properties. The high variability in morphology of CNT as well as the lack of precise knowledge regarding to structure and properties of CNT prevent their more widely application in thermoplastic composites. The chemical modification e.g. surface functionalization of CNT and suitable compatibiliser may improve their disintegration and distribution in polymer[11].

Experimental part

Polymers: Polypropylene (*PP*): PP HF 500R, MFR 25 g/10 min, flakes; PP Moplen HP561N, MFR 11 g/10 min, and PP Moplen HP561R, MFI 25 g/10 min.
Fillers: Disperal 40 (*D40*), Disperal 60 (*D60*), Disperal modified with undecylenic acid (*DUN*) and Disperal modified by 3-aminopropyltriethoxiloxane (*DAM*).
Cloisite 15A (*C15A*), and Cloisite 30B (*C30B*),
Multi-Wall Carbon Nanotubes – Nanocyl® 7000 (*CNT*).
Compatibilisers: Slovacid 44P and Tegopren 6875.

Preparation of PP composite fibres

The conventional concentrate technology was used for preparation of PP nanocomposite fibres. The method consists of two steps: preparation of PP/filler concentrate dispersions using the twin-screw extruder (f=28 mm) and spinning of mixture of the PP and PP concentrate dispersions to obtain the final concentration of filler in the fibres.

Method used

The Instron (Type 3343) was used for the measurements of the mechanical properties of fibres (according to ISO 2062:1993). Coefficients of variation of tensile strength and elongation at break were used as measure of internal (structural) non-uniformity of fibres.

Results and discussion

The effect of solid particles on parameters of the supermolecular structure of both spun and drawn fibres is very important for assessment of processing of polymer composite in spinning and drawing at conventional sinning speed. Especially, inconvenient supermolecular structure of PP spun fibres and non-uniform distribution of solid particles can negatively affect the drawing process and mechanical properties of fibres.

The results on the Fig. 1 reveal the effect of filler content on mechanical properties of PP composite fibres. The results obtained indicate that the tenacity of the fibres increase with content of nanofillers pass through maximum and above 0.3 wt.% decrease gradually with higher concentration of nanofillers. Maximum tenacity and modulus of the PP composite fibres were obtained at low concentration up to 0.2 wt.% for all kinds of Disperals and Cloisites.

Tenacity and Young's modulus of PP/MWCNT composite fibres decrease gradually with content of the fibrous particles in PP fibres. The tensile strength of fibres unambiguous decreased for fibres containing more than 0.1 wt.% of MWCNT (Fig. 2). The low elongation at break and high non-uniformity of the mechanical properties are characteristic for the fibres with content of MWCNT higher then 0.1 wt.%.

Higher concentration of MWCNT affects negatively processing of composites at spinning and drawing. Therefore, the combination of MWCNT with other additives such as organoclays, boehmites, and compatibilisers-dispersants based on derivatives of polyglycols and polysiloxanes, was used to obtain required processing, structure and properties of fibres.

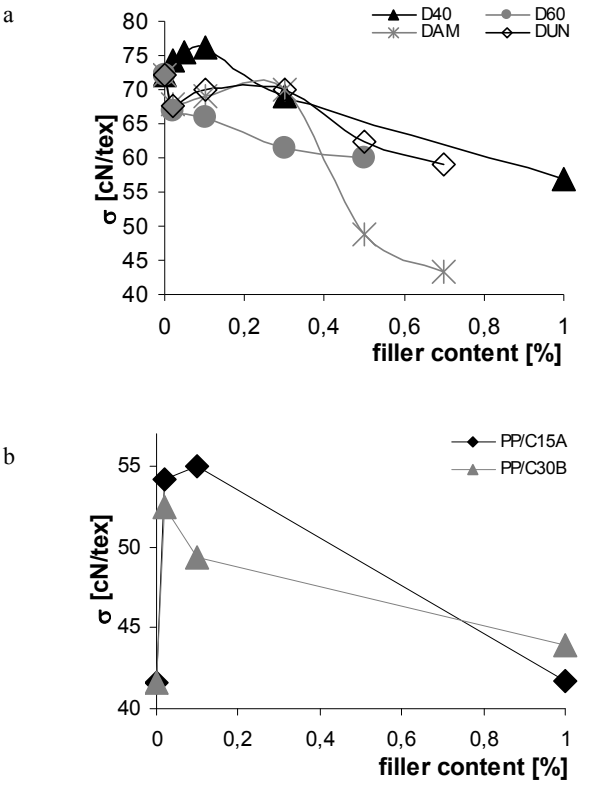

Fig. 1. **Dependence of tenacity σ on content of filler Disperal (a) and Cloisite (b) in PP composite fibers**

Analysis of these results leads to conclusions that higher mechanical properties including positive effect of nanofillers in PP matrix can be obtained only at optimized composition of the composites and spinning as well as drawing conditions.

Conclusions

The results show that the processing of the PP composites strongly dependences on concentration of solid particles (fillers) and spinning conditions. Spinnability

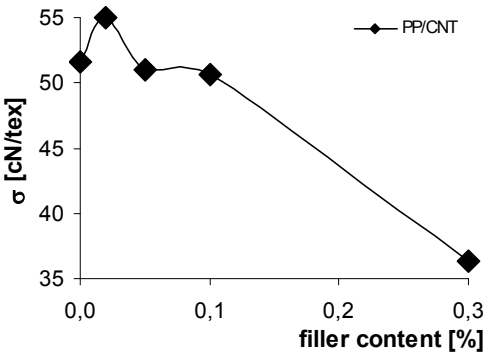

Fig. 2. **Dependence of tenacity σ on content of filler MWCNT in PP composite fibers**

decreases with content of the fillers in PP matrix. The effect of spinning temperature, take-up velocity as well as drawing temperature is very important and influences the structure and mechanical properties of final PP composite fibres.

The tenacity and Young modulus of PP composite fibres containing up to 1.0 wt.% of solid particles (boehmite, CNT) were significantly increased (up to 20 %) in comparison with PP standard fibres. Some selected compatibilisers also contribute to mechanical properties of composite fibres.

This work was supported by the Slovak Research and Development Agency under contract No. VMSP-P-0007-09.

REFERENCES

1. M. Alexandre, P. Dubois: Mater. Sci. Eng. *28*, 1 (2000).
2. L. Razafimahefa, S. Clebicki, I. Wroman, E. Devaux: Dyes and Pigments *66*, 55 (2005).
3. J. Ma, S. Zhang, Z. Qi, G. Li, Y. Hu: J. Appl. Polym. Sci. *83*, 1978 (2002).
4. L. Vaisman, B. Larin, I. Davidi, E. Wachtel, G. Marom, H. D. Wagner: Composites, Part A *38*, 1354 (2007).
5. Z. Li, G. Luo, F. Wei, Y. Huang: Compos. Sci. Technol. *66*, 1022 (2006).
6. P. B. Messersmith, E. P. Giannelis: J. Polym. Sci., A: Polym. Chem *33*, 1047 (1995).
7. D. Hanke, K. Hoffman, A. Altmeyer, G. Schindler, U. Schon, Wirppertal, M. L. Klotz: Chemical Fiber Int. *47*, 130 (1997).
8. W. Lertwimolnun, B. Vergnes: Polymer *46*, 3462 (2005).
9. K. G. Gatos, J. G. Martinez Alcazar, G. C. Psarras, R. Thomann, J. Karger-Kocsis: Compos. Sci. Technol. *67*, 157 (2007).
10. V. V. Ginzburg, Ch. Singh, A. C. Balazs: Macromolecules *33*, 1089 (2000).
11. E. T. Thostenson, Ch. Li, T. W. Chou: Compos. Sci. Technol. *65*, 491 (2005).

P-13
INFLUENCE OF FLAME-RETARDANTS ON MECHANICAL PROPERTIES AND THERMAL STABILITY OF EPOXY RESIN COATINGS

DANUTA CHMIELEWSKA*, MATEUSZ BARCZEWSKI, and TOMASZ STERZYŃSKI

Poznan University of Technology, Institute of Materials Technology, Piotrowo 3, 61-138 Poznan,Poland
danuta.chmielewska@doctorate.put.poznan.pl

Abstract

The modified epoxy resin coating were prepared by adding flame-retardant to commercial epoxy prime coat. The aluminum trihydroxide (ATH), nano size magnesium hydroxide (MH) and aluminum-layered double hydroxides (LDH) have been used as flame-retardants. The mechanical and thermal properties of the epoxy coating have been investigated. The aim of this paper has been determined by the optimal content of flame-retardant in coating compositions based on epoxy resin.

Introduction

The fire protection of metallic elements with use of polymer materials have become an important issue in the automotive, construction and marine industry. The coating systems have been applied to improve the appearance, adhesion, toughness, corrosion resistance and durability of products[1]. Epoxy resins have good mechanical properties, chemical resistance as well as low shrinkage on cure and superior adhesion to many substrate[2,3]. Nevertheless, the main problem during epoxy resins processing is their flammability. Materials coated by systems based on epoxy resins with flame retardants have gained fire penetration and flame spread resistance[4,5]. The recent investigation into the application of nano-size flame retardants to coating has indicated that nano-fillers can improve both the physical and chemical properties of polymer materials[6,7]. Interesting are also the layer double hydroxides LDH which are new inorganic materials made of magnesium and aluminum nanoparticles[8]. However, significant improvement of fire resistance efficiency in LDH composites is depending on homogeneous dispersion of nanofillers in the polymer matrix. The widely used flame retardants are magnesium hydroxide (MH) and aluminum trihydrate (ATH), which are economic, but their efficiency requires higher content than nano fillers[9].

In this paper the optimal content of flame-retardant in epoxy composition as well as mechanical properties of the coating have been investigated. The aluminum trihydroxide (ATH), nano size magnesium hydroxide (MH) and aluminum magnesium layered double hydroxides (LDH) were used as flame-retardants.

Experimental

The studied formulation was the commercial epoxy prime coat PROTECT 360 (Industrial coating system Novol) cured with hardener H 5960 (Novol). Aluminum hydroxide (Sigma-Aldrich), nano-Magnesium hydroxide (nanopowder, <100 nm Sigma-Aldrich), aluminum magnesium layered double hydroxides (Perkalite LD, Akzo Nobel) were used as flame-retardants. The epoxy prime coat, flame-retardants and hardener were mixed together using a mechanical stirrer. The weight ratio of epoxy to hardener was 4:1. The amounts of flame-retardants used in this study range from 5 to 30 weight percentage. The names of samples are listed in Table I. The

Table I
Compositions of the epoxy system

Content wt.%	Type of flame retardants/names of samples		
	ATH	MH	LDH
0	C	C	C
5	C5ATH	C5MH	C5LDH
10	C10ATH	C10MH	C10LDH
15	C15ATH		C15LDH
20	C20ATH		C20LDH
25	C25ATH		C25LDH
30	C30ATH		C30LDH

final compositions were spread to steel plates with a low pressure HVLP spray gun (diameter of nozzle 1,7). The average layer thickness was 80 µm. Samples were cured at ambient temperature during 24 h.

Test methods

The investigation of the coatings impact resistance was carried out in accordance with PN EN ISO 6272/1i.e one kilo spherical indenter was dropped down onto the coated sample. The drop height was adjusted to 25–100 cm to achieve property impact energy. The cross-cut adhesion tests of the coating samples were carried out as per ISO 2409. The six lines on the coatings were cut with a cutting blade. Then a cutting tool was rotated by 90° and next six lines were mark through the coating. The adherence of the coating was determined by using adhesive tape[10]. The thermal property of the coatings was determined by thermogravimetric analyses (TGA) with a temperature range between 30 and 900 °C at a heating rate of 10 °C min^{-1} under nitrogen atmosphere using a TG 209 F1 Netzsch. About 10 mg of powder was taken from the steel plates' coating for measurement. The initial decomposition temperature Ti was determined as the temperature at which the weight loss was 5 %. The residual mass (ΔW%) was defined at 900 °C.

Results and discussion

The results of the mechanical tests of epoxy coating are presented in Table II. The effects of impact tests indicated better performance of the modified coating compared with the commercial epoxy prime coat-C. For samples C10MH, C15ATH, C15LDH, C20LDH, C25LDH, C30LDH a 95 cm drop heights and for samples C and C5MH 80 cm drop heights were observed.

All the coating compositions filled with LDH as well as four types of samples with ATH show the highest cross-cut adhesion value (0°; Table II). These types of coatings exhibit good properties during the adhesion tests, smoothness of the cut edges as well as no detachment of any layer parts. On the contrary, compositions filled with MH and commercial compositions exhibit worse adhesive properties (Fig. 1).

The differences observed in mechanical properties of the samples are most likely influenced by different dispersions and characteristics of metal hydroxides particles.

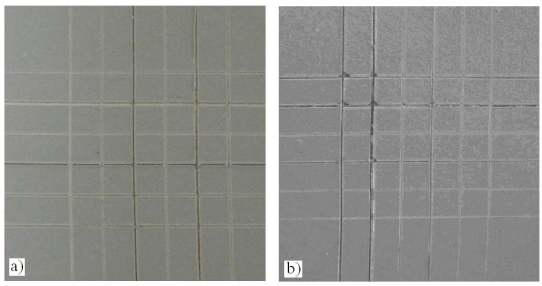

Fig. 1. **Surface appearance of a) C sample and b) C30ATH sample coatings after cross-cut adhesion tests**

Table II
Results of the mechanical tests of epoxy coating

Name of sample	Impact resistance height [cm]	Cross-cut adhesion tests [°]
C	80	1
C5MH	80	1
C10MH	95	1
C5ATH	90	0
C10ATH	90	0
C15ATH	95	0
C20ATH	85	0
C25ATH	85	1
C30ATH	90	1
C5LDH	85	0
C10LDH	90	0
C15LDH	95	0
C20LDH	95	0
C25LDH	95	0
C30LDH	95	0

Thermal stability of epoxy coating is presented in Table III. The Ti of commercial compositions was 337,2 °C. Nevertheless, the modified coating has indicated lower values of thermal stability. The samples with MH began to decompose at 333–334 °C. The Ti of coating with ATH and LDH decrease slightly with a growing flame retardant content. The difference in degradation behavior of these epoxy coatings took place probably due to the fact that ATH, MH and LDH have begun to decompose at lower temperatures than components of commercial epoxy coat. For

Table III
Thermal stability of epoxy coating

Name of sample	Ti [C°]	ΔW[%], 900 °C
C	337,2	56,87
C5MH	334,6	58,79
C10MH	333,6	61,56
C5ATH	335,4	58,79
C10ATH	321,7	61,80
C15ATH	314,5	58,67
C20ATH	294,5	57,36
C25ATH	296,7	57,47
C30ATH	296,9	58,16
C5LDH	335,8	56,18
C10LDH	315,6	53,22
C15LDH	327,4	58,02
C20LDH	312,3	57,78
C25LDH	319,2	59,89
C30LDH	301,0	56,76

all composites coatings the residual mass of was about 56 to 60 %.

The thermal stability gives indirect information about the potential flame retardancy of the polymer modified materials[11]. The mechanisms of flame retardancy will vary depending on the used flame retardant type. The metal hydroxides absorb the heat during fire and send out H_2O, CO_2, which lowers temperature of polymeric materials[5]. The initial decomposition temperature indicates the thermal stability of the epoxy coating, i.e., the failure temperatures of the resins in processing and moulding[12].

Conclusion

The aluminum trihydroxide (ATH), nano size magnesium hydroxide (MH) and aluminum magnesium layered double hydroxides (LDH) was introduced into the commercial epoxy prime coat. It have been found that the modified coatings have better mechanical and adhesion properties than the commercial epoxy prime coat. The thermal gravimetric analyses have indicated that flame retardants decrease the thermal stability of the coating, thus it is difficult to determine the optimal content of flame-retardant in coating compositions. Besides, the application of the flame retardants, for commercial epoxy prime coat is not recommended in case of thin layer coatings.

The authors would like to thank NOVOL Sp. z o.o for their help and support.

REFERENCES

1. Seubert C., Nietering K., Nichols M., Wykoff R., Bollin S.: Coatings *2*, 221 (2012).
2. Shieh J. Y., Wang C. S.: Polymer *42*, 7617 (2001).
3. Chmielewska D., Barczewski M., Sterzyński T.: Polimery *58*, 270 (2013).
4. Gu J., Zhang G., Dong S., Zhang Q., Kong J.: Surf. Coat. Technol. 7835-7841.
5. Wang Z., Han E., Ke W.: Prog. Org. Coat. *53*, 29 (2005).
6. Kelar K., Mencel K., Jurkowski B.: Archives of Mechanical Technology and Automation *32*, 2 (2012).
7. Półłka M.: Polimery *56*, 10 (2011).
8. C. M., Gabbardo A. D., Wypych F., Amico S. C., Composites: Part A *42*, 196 (2011).
9. Rakotomalala M., Wagner S., Döring M.: Materials *3*, 4300 (2010).
10. Kowalczyk K., Spychaj T.: Surf. Coat. Technol. *206*, 4692 (2012).
11. Prządka D., Jęczalik J., Andrzejewska E., Marciniec B., Dutkiewicz M., Szłapka M.: React. Funct. Polym. *73*, 114 (2013).
12. C. S. Wu, Y. L. Liu, Y. C. Chiu, Y. S. Chiu: Polym. Degrad. Stab. *78*, 41 (2002).

P-14

THE INFLUENCE OF MULTIPROCESSING ON MECHANICAL PROPERTIES OF POLYPROPYLENE/ POLYSTYRENE BLENDS OBTAINED FROM CARS

PAULINA JAKUBOWSKA and ARKADIUSZ KLOZIŃSKI

Poznan University of Technology, Institute of Technology and Chemical Engineering, Polymer Division, PL. M. Sklodowskiej-Curie 2, 60965 Poznan, Poland
Paulina.Jakubowska@put.poznan.pl

Abstract

Nowadays about 12 % of materials used in automotive industry are polymers. The most commonly used ones are PP, PVC, PE, polyurethanes, rubber and styrene polymers (PS, SAN, ABS). Post-consumer polymers are generally not easy to separate, and therefore, an interesting suggestion is non-separated processing. This paper presents the investigations of mechanical properties of repeatedly recycled (5 times) PP/ PS blends (100/0, 75/25, 50/50, 25/75, 0/100). Both materials used came from the body kit.

Introduction

Considering protection of the environment, a fundamental subject in recent years is recycling of waste plastics. The main problem encountered in the preparation of waste for recycling plastics is their segregation. Industrial waste is relatively easy to process as the content of impurities is usually small, therefore, re-processing of municipal plastic waste is more complicated[1,2]. Therefore, in recent years has become an important problem of the recovery of polymers in the form of mixed waste, which allows to avoid, in the recycling process, the troublesome operation of the waste sorting.

The influence of multiprocessing on the mechanical properties of polymers processed several times was a subject of many publications[3–6]. The authors found that the modulus of elasticity, stress and elongation at break depend on the re-processing times. In the literature there is no data on the mechanical recycling of PP/PS polymer blends. Therefore, this is the subject of our research.

In presented investigations the most important was to conclude whether mechanical recycling of mixed body kit (PP, PS) is possible and also to determine the properties of recycled materials.

Experimental

Materials

Two types of body car kits were used in our investigations consisting of polypropylene and polystyrene. Both of these materials were reprocessed in a coarse mill (Shini Plastics Technologies, model SG-1417) and then homogenized by means of one-screw extruder equipped with cylindrical die (Fairex, Mc Akron Repiquet, France). The

weight ratios of PP/PS were equal to 100/0, 75/25, 50/50, 25/75 and 0/100. This mixing process was repeated five times.

After each recycling process a part of every material was injected on the injection molding machine (Battenfeld Plus 35/75). As a result the samples required for further tests on mechanical properties (type 1A according to PN- EN ISO 527-2, ref.[7]) were produced.

Methods

In order to execute the mechanical tests a Zwick Roell Z020 testing machine, conjugated with a computer, and with a tensile strength measurement head in the range between 0–20 kN was used. For all the samples tensile and flexural strengths were determined and for all types of recycled materials this test was repeated five times.

For hardness determination the Brinell hardness tester (KB Prüftechnik GmbH, KB150R model) was used. Each sample was subjected to deformation during the time of 30 s with different loads – 132 N for polypropylene and polymer blends, and 358 N for polystyrene.

The temperature during all measurements was 21°C.

Results and discussion

Strength tests provide valuable information about the mechanical properties of the tested materials and determine potential applications for the finished product. Obtained results for recycled body kits from polypropylene, polystyrene and their blends are presented in Fig. 1–3.

The reported values of Young's modulus (E) as a function of the processing times and the composition of polymer blends are presented in Fig. 1. After analyzing the test results, it is clear that the properties of the polymer mixture are similar to the properties of the polymer, which forms the continuous phase of the mixture[8].

Considering the processing times it was noted that in case of polypropylene and a blend containing 25 wt.% of polystyrene the Young's modulus increases with the processing times up until the third cycle and then becomes constant. This suggests that in case of these materials three-times reprocessing causes the improvement of the mixture's homogeneity. In case of PP/PS blends with a weight ratio equal to 50/50 and 25/75 and polystyrene, the determined modulus of elasticity was at a constant level (within the limits of statistical error for consecutive measurements). Obtained results confirmed the rightness for common mechanical recycling of car spoilers made of PP and PS. The fact worth emphasizing was that similar dependence was also obtained for the designated true tensile stress and elongation at break.

The above conclusions also confirmed the results of flexural tests, as shown in Fig. 2. After analyzing the results it can be stated that with the increasing re-processing times the flexural modulus (E_t) in bending for polystyrene does not change – five times processing does not deteriorate PS stiffness. It was observed that in case of polypropylene, up until the second recycling time, the flexural modulus increased from 1.42 GPa (0x) to 1.55 GPa (2x) and then begun to decrease. However, the fifth processing does not result in lower rigidity in comparison to the input material. In case of PP/PS mixture (50/50) the value of the modulus oscillated at 1.85 GPa. The same was observed for PP/ PS (25/75) where the value was 2.40 GPa. Significant differences were noted only for PP/PS (75/25) – the value of the second reprocessing was maintained at a constant level and then started to decrease rapidly.

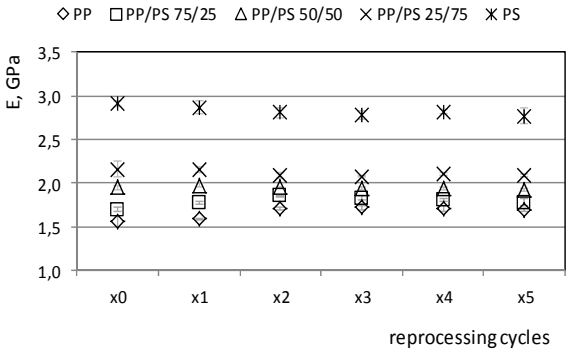

Fig. 1. **Young's modulus as a funtion of multiprocessing and the PP/PS weight ratio**

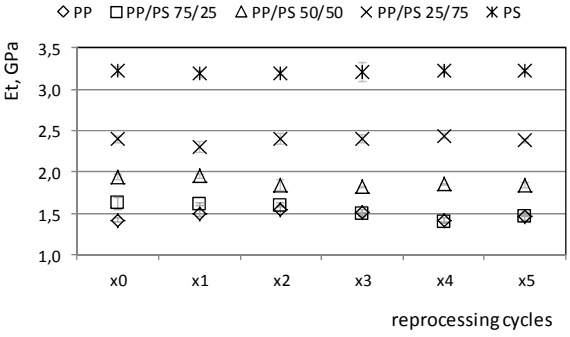

Fig. 2. **Flexual modulus as a funtion of multiprocessing and the PP/PS weight ratio**

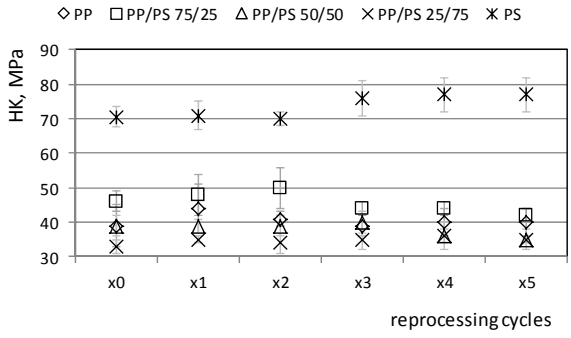

Fig. 3. **Brinell hardness as a funtion of multiprocessing and the PP/PS weight ratio**

The results of hardness tests (HK) are presented in Fig. 3. After analyzing the mechanical properties resulting from static stretching and bending, it might be assumed that the hardness of the mixture will increase with an increasing amount of polystyrene in the mixture. In Fig. 3 it can be seen that in case of five-times processing of polypropylene and all of polypropylene/polystyrene blends similar hardness values are observed. They begin to stabilize at the same level. The hardness of polystyrene revealed a growing trend in multiple processing.

Conclusion

Summarizing the results of the research it was found that the mechanical recycling of mixed (immiscible) plastic materials (like a PP and PS) is justified. The mechanical properties of input materials (PP, PS) and their blends expectancy are changed as a function of the composition structure – all mechanical properties of PP/PS blends are mainly determined by the material forming the continuous phase of the mixture (the phase inversion phenomenon).

Moreover, it was found that multiprocessing (five times) of polymer blends (PP/PS) (non-separated processing) has an insignificant influence on mechanical properties of recycled products. Polymer blends produced from re-granulate have good tensile strength, flexural and hardness, so they can be successfully used in many industries as well as in automotive.

This work was supported by grant 32-379/2013 DS-PB.

REFERENCES

1. Jakubowska P., Sterzyński T., Królikowski B.: Inż. Ap. Chem. *3*, 33 (2005).
2. Kloziński A., Jakubowska P., Sterzyński T.: Inż. Ap. Chem. *5*, 15 (2008).
3. Perez J. M., Vilas J. L., Laza J. M., Arnaiz S., Mijangos F., Bilbao E., Leon L. M.: J. Polym. Enviro *18*, 71 (2010).
4. Incarnato L., Scarfato P., Acierno D., Milana M. R., Feliciani R.: J. Appl. Polym. Sci. *89*, 1768 (2003).
5. Bai X., Isaac D. H., Smith K.: Polym. Eng. Sci. *47*, 120 (2007).
6. Elmaghor F., Zhang L., Li H.: J. Appl. Polym. Sci. *88*, 2756 (2003).
7. PN–EN ISO 527-2 Tworzywa sztuczne: Oznaczanie właściwości mechanicznych przy statycznym rozciąganiu
8. Kruszelnicka I., Sterzyński T.: Polimery *50*, 358 (2005).

P-15
SYNTHESIS AND UV CURING OF UNSATURATED POLY(VINYL ALCOHOL) DERIVATIVES

VIERA JANČOVIČOVÁ, PAVOL GEMEINER, and BOHUSLAVA HAVLÍNOVÁ

Department of Printing Arts Technology and Photochemistry IPM, Faculty of Chemical and Food Technology SUT, Radlinského 9, 812 37 Bratislava, Slovak Republic viera.jancovicova@stuba.sk

Abstract

Unsaturated derivatives of poly(vinyl alcohol) were synthesized by reactions of terminated poly(vinyl alcohol) macromolecule with glycidylmethacrylate and malein-anhydride. The extend of modification was monitored by acidobasic titration and spectroscopic techniques. The kinetics of radical crosslinking polymerization of layers coated on aluminium plates initiated by [4-(2-hydroxyethoxy) phenyl-(2-propyl) ketone] upon the irradiation by medium-pressure mercury vapour lamp was followed by monitoring the decrease of FTIR absorption band at 1630–1640 cm^{-1}. The results showed that the unsaturated moiety type, reaction mixture composition and external physical conditions were the significant factors affecting the polymerization course of UV-cured films.

Introduction

Poly(vinyl alcohol), PVA, is a water soluble polymer with a molecular weight between 30000 and 200000 Daltons. Due to its excellent biocompatibility and biodegradability, it has been widely used in medicine, cosmetic and packaging industries. It has been used for the development of new materials for various areas (intelligent polymers, sensors, drug release carriers and encapsulation). Many of these applications utilize the excellent hydrogel forming properties of PVA[1]. PVA hydrogel represents one of the most frequently studied polymeric systems. PVA has notable film-forming properties, it has been massively employed for the formulation of inkjet receiving layers or printed electronics substrate coatings.

The modification of polymers either synthetic or natural, by the addition of groups containing unsaturations, has been the objective of researches. The addition of unsaturations allows the reticulation of these polymers without the addition of a cross-linking agent[2,3]. This reaction can be carried out by radical addition of initiators or by UV light. PVA have been modified with acrylates, methacrylates and other unsaturated compounds by different means[2,4].

The goal of this study was to synthetise two unsaturated photoactive derivatives of poly(vinyl alcohol) and to investigate the UV curing process of a simple varnish model system composed of prepared derivatives and photoinitiator Irgacure®2959.

Experimental

Materials

Poly(vinyl alcohol) Poval 205 (degree of hydrolysis 88 %, Kuraray Japan), glycidylmethacrylate (GMA; Merck), maleic anhydride (MA; Aldrich), dimethylaminopyridine (DMAP, Aldrich), N,N-dimethylformamid (DMFA, Lachema, Czech Republic), dimethyl sulfoxide (DMSO, Merck), ethanol (Merck), acetone (Merck) and Irgacure®2959 (Ciba, Switzerland) were used as received.

Preparation of poly(vinyl alcohol) derivatives

In this work two types of poly(vinyl alcohol) derivatives containing polymerisable groups (MA PVA, GMA PVA) were synthesized.

Preparation of MA PVA and MA PVA 1 (PVA modified by maleic anhydride): 8.8 g PVA was dissolved in 50 ml water and 50 ml DMFA at 90–100 °C. After dissolution of PVA, the temperature was dropped to 60 °C and 9.3 g of maleic anhydride was added and let to dissolve. After its dissolution, 0.098 g of the catalyst (DMAP) was added, but only at the preparation of MA PVA 1. After 5 hours the mixture was let to cool down to room temperature, then precipitated in acetone and washed twice with ethanol and acetone. Washed product was dried at 37 °C till constant weight and ground into fine yellow powder.

Preparation of GMA PVA (PVA modified by glycidyl methacrylate): 10 g PVA was dissolved in 50 ml DMFA and 25 ml DMSO at 90 °C. After complete dissolution, the mixture was cooled down to 70 °C and 2.5 ml of GMA and 5 ml of 5 wt.% ethanolic solution of KOH was added dropwise. Mixture was kept at 70 °C for one hour and constantly agitated. Then it was cooled to ambient temperature, diluted with 25 ml of water and the product was precipitated into an excess of acetone. The precipitate (GMA PVA) was collected, washed in acetone and dried to constant weight at room temperature[5,6].

Preparation of samples and UV curing of coatings

The samples were prepared by mixing the aqueous solution of modified PVA (MA PVA, MA PVA 1 and GMA PVA,) with photoinitiator Irgacure®2959 (3 wt.%). These compositions coated on the aluminum plates were irradiated by a medium pressure mercury lamp 250W (RVC, Czech Republic). The curing process was evaluated by IR spectroscopy (FTIR spectrophotometer EXCALIBUR SERIES Digilab FTS 3000 NX, USA).

The degree of conversion in the cured film was determined according to the amount of double bond (twisting vibration at 810 cm^{-1}, stretching vibration at 1610–1640 cm^{-1}) by a baseline method. The degree of conversion X was calculated from well-known equations[6,7]

$$X = 1 - \frac{[A_\lambda]_0}{[A_\lambda]_t} \qquad (1)$$

where $[A_\lambda]_0$ and $[A_\lambda]_t$ is the absorbance measured at the chosen wavelength before and after the exposure to UV light for the time *t*, respectively. The values of maximum conversion X_{max} were obtained from the plots of *X vs.* time.

Results

The hydroxyl groups of the PVA were esterified by introduction of groups with unsaturated photochemically active bond. In order to prepare the modified poly(vinyl alcohol) with defined concentration of ester groups, we optimized the preparation of maleinated PVA (MA PVA). For derivatives preparation we used various amount of malein anhydride, to some samples we added catalyst (pyridine, DMAP, *p*-toluenesulfonic acid) and we changed the esterification time too. The conversion degree, i.e. extend of modification expressed as a molar fraction of modified monomeric units of the PVA macromolecular backbone, was quantified by acidobasic titration. In this work we used two prepared derivatives of PVA achieved at modification described in experimental part: MA PVA (without catalyst, esterification time 5 h, esterification degree 10 %) and MA PVA 1 (1 %wt. DMAP according to the mass malein anhydride, esterification time 5 h, esterification degree 16 %). FTIR spectroscopy was used to examine the modification and structural changes between original PVA and prepared modified PVA. By comparing of the spectra in Fig. 1, we observed that new peaks at 1638 a 815 cm^{-1} have emerged. These are due to C=C stretching and twisting vibrations. We also observed the extension of C=O peak at 1730 cm^{-1}, what confirms the inclusion of ester group into the molecule of PVA.

GMA PVA was prepared according to recipe described in experimental part. The modification reaction performed on PVA lead to the epoxide ring opening and the attachment of hydroxypropyl methacrylate moieties onto the PVA macromolecular backbone. The successfulness of modification was confirmed by FTIR spectroscopy (Fig. 2),

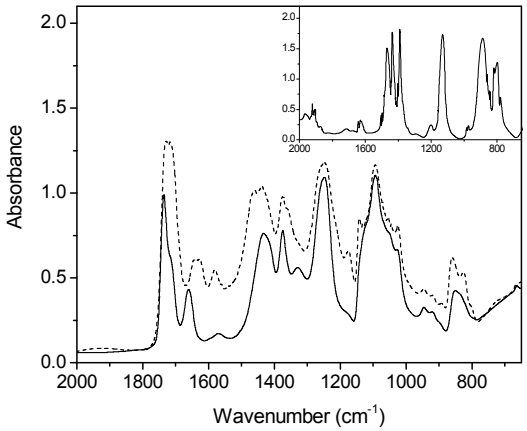

Fig. 1. **FTIR spectra of poly(vinyl alcohol) POVAL 205 (full line), modified poly(vinyl alcohol) MA PVA 1 (dash line). Inset FTIR spectrum of maleic anhydride**

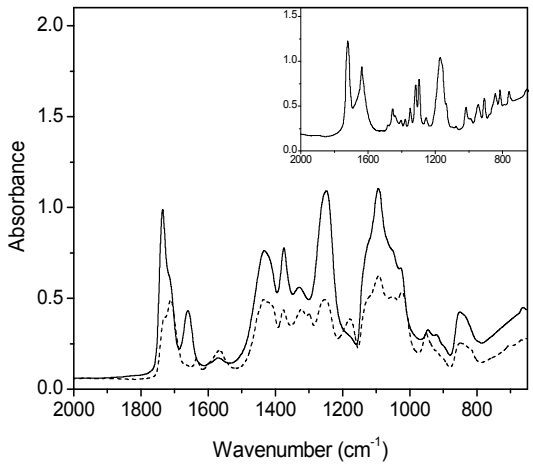

Fig. 2. **FTIR spectra of poly(vinyl alcohol) POVAL 205 (full line), modified poly(vinyl alcohol) GMA PVA (dash line). Inset FTIR spectrum of glycidyl methacrylate**

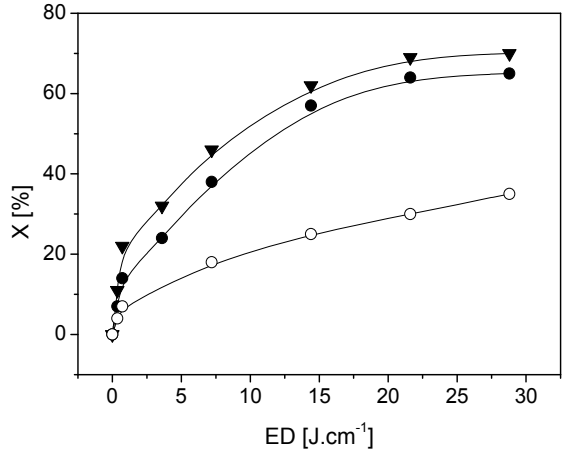

Fig. 3. **Influence of exposition dosage (ED) on the UV curing of MA PVA (○), MA PVA 1 (●) and GMA PVA (▼) in the presence of 3 wt% of Irgacure®2959 at the light intensity 12 mW cm^{-1}**

new peaks at 1634 and 810 cm^{-1} and the shift of peak at 1730 cm^{-1} were observed, peak at 1660 cm^{-1} has disappeared.

The UV curing process will be performed through radical polymerization of unsaturated groups in the lateral moieties. For the preparation of photochemicaly cured compositions a photoinitiator Irgacure®2959 ([4-(2-hydroxyethoxy) phenyl-(2-propyl) ketone]) was added to both prepared PVA derivates. It is a radical photoinitiator of 1st type, where radicals are created due to cleavage Norrish I (ref.[8]). The exposure by medium pressure mercury lamp caused the photopolymerisation, which shows as a decrease in the absorbance bands in the C = C bond in the FTIR spectrum. We observed spectrum decrease in range of 1630–1640 cm^{-1} and the change of conversion depending on exposition dose (exposition dose = light intensity x time). The absorbance was recalculated by the equation (*1*) to the conversion. The curing occurred at the intensity of incident light 12 mW cm^{-2}. The maximal conversion degree was reached at the initiator concentration of 3 wt.% (Fig. 3). Probably the higher initiator concentration exhibits high absorption at its absorptions maximum at 280 nm, and the initiator acts as internal filter. The maximal conversion degree reached at exposition dosage 29 mW cm^{-1} was 65 % for MA PVAl and 70 % for GMA PVA. The both compositions were good curred. For composition with MA PVA (prepared without catalyst) the maximal conversion was only 38 %. The composition was uncured in fact and tacky. However, in the case of MA PVA sufficient conversion can not be reached even after substantial extension of curing time.

Conclusions

Two types of modified photopolymerizable derivatives of PVA (MA PVA, GMA PVA) were synthesized. Reaction conditions were optimized in order to obtain such extend of modification (i.e. conversion degree) which would ensure efficient crosslinking.

The UV curable polymer films were prepared by addition of radical type photoinitiator Irgacure®2959 (1 wt.%) to both modified PVA. According to spectroscopic monitoring of the curing process we can say, that the curing was more effective for PVA GMA (higher conversion of double bond was reached).

The authors thank the Slovak Grant Agencies APVV (Project No. 0324-10) and VEGA (Project No.1/0811/11 and 1/0818/13) for their financial support.

This publication is the result of the project implementation: ITMS: 26240120016 supported by the Research & Development Operational Programme funded by the ERDF.

REFERENCES

1. Patachia S., Valente A. J. M., Baciu C.: Eur. Polymer J. *43*, 460 (2007).
2. Černá M., Dzik P., Veselý M.: J. Photopolymer Sci. Technol. *25*, 415 (2012).
3. Crispim E. G., Pii J. F., Rubira, A. F., Muniz E. C.: Polymer Testing *25*, 377 (2006).
4. Giménez V., Reina J. A., Mantecón A., Cádiz V.: Polymer *40*, 2759 (1999).
5. Dzik P, Veselý M.: Chem. Listy *99*, 376 (2005).
6. Jančovičová V., Amberg-Schwaab S., Dzik P., Mikula M.:. Chem. Listy *102*, 1051 (2008).
7. Müller U.: J. Photochem. Photobiol. A: Chem. *239*, 237 (1997).
8. Šima J., Čeppan M. Jančovičová V., Prousek J., Velič D.: *Fotochémia. Princípy a aplikácie.* p. 337. Nakladateľstvo STU, Bratislava 2011.

P-16

THE SORPTION AND BARRIER PROPERTIES OF POLYMER LAYERS BASED ON UNSATURATED POLY(VINYL ALCOHOL) DERIVATIVES

VIERA JANČOVIČOVÁ*, MILAN MIKULA, and ZUZANA BEKOVÁ

Department of Printing Arts Technology and Photochemistry IPM, Faculty of Chemical and Food Technology SUT, Radlinského 9, 812 37 Bratislava, Slovak Republic viera.jancovicova@stuba.sk

Abstract

Poly(vinyl alcohol) (PVA) is a water soluble, film-forming, biodegradable polymer. It unfortunately has insufficient resistance to water and water vapour. It is believed that modification of PVA by various organic moieties can significantly improve the barrier properties of coatings prepared from these modified grades of PVA thus widening the application possibilities in the industry. Selected UV cured formulations were coated on four types of paper and the influence of coatings on paper properties (swelling, water vapour sorption and permeability) was studied.

Introduction

Barrier materials has many packaging and protective applications. As barriers, they separate a system, such as article of food or electronic component, from outer environment. Paper, cardboard and other materials based on cellulose fibres are widely used in printing and packaging. Their porous structures make these materials highly permeable to gases and water vapour, which is unwelcome. One of the recent tendencies in packaging and printing papers is the improvement of their physical-mechanical and barrier properties, recycling and secondary use. Today, the barrier properties of standard packaging materials are commonly achieved by lamination. An additional polymer layer is used to prevent water sorption. For this purpose polyolefins are often chosen. Unfortunately, due to the addition of this synthetic layer, the material loses its natural and biodegradable properties as well as its recyclability[1]. An alternative to the lamination can be an introduction of the biodegradable polymer coating for the paper surface in order to enhance protective properties of printing or packaging materials.

To protect prints or paper substrates from the influence of the atmospheric humidity and the oxygen it is possible to use the hydrophobic protective coatings. On the other hand, the hydrophilicity of printing media is required in the case of widely used water-based inks. The possible solution is resulting from the introduction of the coating with the switchable properties, meaning that it shows both hydrophilic character before the printing process to ensure printability and required final quality of print, and the hydrophobic character induced after printing to improve weather fastness. The suitable solution can be presented by introduction of the hydrophilic waterbased systems and their finishing modification by UV-curing technology in order to achieve the hydrophobic surface of a print by a exposure to the UV-light after the printing[2].

The poly(vinyl alcohol) (PVA) is a water soluble polymer with applications in paper coating, textile sizing and packing. It is the only polyvinyl-type synthetic polymer that has been confirmed to be biodegradable[3]. This polymer fills the paper pores and forms a dense layer at the paper surface. Hydrogen bonds between the polar groups of PVA mainly explain the high cohesive energy density of this film and its good gas barrier properties in the anhydrous state[2]. PVA high barrier properties to gases are depend on low humidity. Moreover, its barrier properties to water vapour is not good. The modification of PVA by organic compounds such as acrylates, or carboxylic acids anhydrides can improve barrier properties of PVA coatings, that allows their application in the food packaging industry. In the case of application of inorganic-organic hybrid polymers (ORMOCER®s) as barrier coating, the modified PVA can be used also as coating primer[4,5].

The objective of our work was to investigate the influence of photochemically cured layers prepared from PVA GMA (PVA modified by glycidyl methacrylate) and photoinitiator Irgacure®2959 on the sorption and barrier properties of four kinds of paper with various grammages. The water diffusion of papers and cured coatings was determined by swelling measurement, the water vapour adsorption and permeability were investigated gravimetrically.

Experimental

Materials

Poly(vinyl alcohol) Sloviol 10-98 (NCHZ, Slovakia) of a degree of hydrolysis of 98.6 %, glycidylmethacrylate (Merck, Germany), dimethylformamid (DMF, Lachema, Czech Republic), dimethyl sulfoxide (DMSO, Merck, Germany), Irgacure®2959 (Ciba SC, Switzerland), and Acetone (Merck, Germany) were used.

Four types of paper were chosen to perform the tests: office paper **A** (grammage 80 g m^{-2}), packaging paper **B** (90 g m^{-2}, Mondi SCP), Arctic volume white paper **C** (100 g m^{-2}, Polo Sinak) and Arctic volume paper **D** (115 g m^{-2}, Polo Sinak).

Preparation of samples

10 g PVA was dissolved in 50 ml DMFA and 50 ml DMSO at 90 °C. After complete dissolution, the mixture was cooled down to 70 °C and 4.2 ml of GMA and 2.5 ml of 5 wt.% ethanolic solution of KOH was added dropwise. Mixture was kept at 70 °C for one hour. Then it was cooled to ambient temperature, diluted with 25 ml of deionized water and the product was precipitated into an excess of acetone. The precipitate (PVA GMA) was collected, washed in acetone and dried to constant weight at room temperature.

The water solution containing PVA GMA (5 wt.%) and photoinitiator Irgacure®2959 (0.1 wt.%) was prepared and applied onto the paper sheets from both sides. The samples containing 2 wt.% of photoinitiator in regards to PVA GMA were cured by a medium pressure mercury lamp (exposition dose 10 J cm^{-2}).

Measurements

The water diffusion to the UV-cured polymer coatings was investigated through swelling measurements by a Dogatkin device, thus allowing measuring a volume of water absorbed by a coating *Q*.

The water vapour permeability (WVP) was quantified according to a German norm DIN 53122 and determined as an amount of the water vapour in grams passed through paper coated with UV-curable coating of a certain thickness within 24 hours at the temperature of 20–23 °C and relative humidity of 85 % provided by saturated KCl solution. Water vapour was quantitatively absorbed on silicagel.

Water vapour sorption was measured by a gravimetric method[6], using classical McBain balances with a fine quartz spiral (diameter = 0.2 mm, coil diameter = 25 mm, number of turns = 50). The accuracy of the McBain balances was $5 \cdot 10^{-6}$ g.

The colorimetric coordinates of samples (*L*, a*, b**) were obtained by means of spectrophotometer Spectrodens (Techkon, illumination D50, standard observer 2°). The total color difference ΔE_{ab}* was calculated from the Eq. (*1*)[7]

$$\Delta E^*_{ab} = \sqrt{(\Delta L^*)^2 + (\Delta a^*)^2 + (\Delta b^*)^2} \qquad (1)$$

where values ΔL^*, Δa^* *and* Δb^* are the differences between relevant values attributed to coated and non-coated samples.

Results and discussion

The surface treatment of papers leads to change of their sorption and barrier properties. We measured water penetration, water vapour sorption and permeability for non-coated papers and papers coated with photochemically active polymer layers (uncured, cured). As the mentioned layers have potential to be used in packaging and printing industry, we also measured the colorimetric coordinates of samples (*L**, *a**, *b**). The calculated ΔE_{ab}* between coated and non-coated paper hasn't exceeded value 1.1 in any case, hence the used coatings didn´t significantly influence the optical properties of paper.

The time dependence of water penetration were fitted by exponential function $Q = Q_{max}(1-e^{-kt})$. The swelling degree for uncoated papers varied between 0.34–0,6 ml g^{-1}. The values of swelling degree for papers coated with uncured layers were similar (0.32–0.58 ml g^{-1}). It is evident, that the swelling degree of paper coated with modified poly(vinyl alcohol) PVA GMA with 2 wt.% of initiator Irgacure®2959 decreased with the UV exposition (Tab. I). The exposure reduced water diffusion into polymer layers, the lowest swelling values were achieved by the exposure dose 12 J cm^{-2} (0.26–0.28 ml g^{-1}) which are lower about 25–30 % than that for unexposed layer. The additional extension of exposure increased water diffusion into polymer layers, causing the deterioration of their barrier properties.

Adsorption properties of all samples were measured, each test lasted for 2 hours. The coating and even more significantly the curing of the coat layers influenced the resulting decrease of sorption of water vapour (Fig. 1). Measured curves are not equilibrium sorption isotherms because the data were gathered by non-equilibrium measurement. The water retention of layers was calculated from the measured weight changes as $\Delta m / m_{layer}$ in percentage (Δm relates just to the weight increase of the layers). The retention should be independent on the layer thickness and used substrate; however, it is problematic because of active interface absorption and condensation of water in pores as well as possible cracks due to surface roughness of used paper (according to AFM). The values of sorption of water vapour at 60 % relative humidity are in the Table I. For non-coated papers, the values varied between 5.0–6.9 %, but they tend to decrease with increasing grammage. Application of barrier layers and their subsequent

Table I
Maximal swelling degree (Q_{max}), water vapour sorption at RH 60 % $(\Delta m/m_{layer})_{60}$ and water vapour permeability (WVP) for non-coated papers (n) and papers coated with photochemically active layers (uncured u, cured c)

Paper	Q_{max} [ml g^{-1}]	$(\Delta m/m_{layer})_{60}$ [%]	WVP [g m^{-2} day^{-1}]
A (n)	0.60	6.9	1200
A (u)	0.48	6.0	1150
A (c)	0,26	2.8	750
B (n)	0.47	6.4	1130
B (u)	0.37	5.4	1100
B (c)	0.28	2.7	850
C (n)	0.35	5.9	1020
C (u)	0.32	5.5	970
C (c)	0.25	2.6	730
D (n)	0.34	5.0	1030
D (u)	0.32	5.3	1010
D (c)	0.27	2.7	820

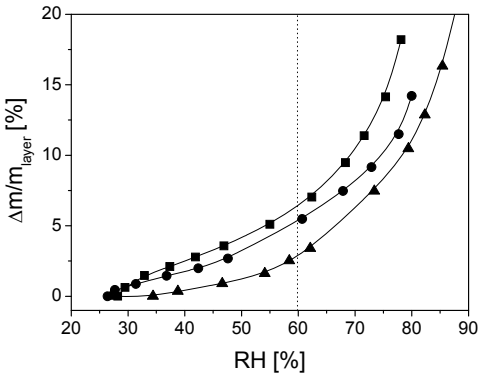

Fig. 1. **The dependency of the water retention of layers on relative humidity for paper B non coated (■), coated (●) and coated and cured (▲)**

curing led to decrease of sorption values down to 2.6–2.8 % in all samples.

Water vapour permeability (WVP) is a very important property of packaging materials. WVP was measured as described in experimental part. The above results showed, that all samples sorb water vapuor. Presence of water in the coating of the paper was detected by FTIR spectroscopy. Water vapour vibrational bands at 3400 cm^{-1} a 1600 cm^{-1} showed higher values for WVP tested samples (24 hours) compared to untested samples. In order to eliminate the influence of absorbed water in the layer, we subtracted weight of water sorbed in the paper from total weight change in sample covered by tested paper.

We observed the changes in WVP after coating with photochemically active layer. WVP was determined gravimetrically and the results are summarised in Table I. The WVP was basically not altered by coating with PVA-GMA, after curing of these coatings, the WVP decreased by 20–35 %.

Conclusions

The photochemically active polymer films were prepared by addition of the radical type photoinitiator to synthesized unsatured derivatives of poly(vinyl alcohol). The changes of barrier properties of coatings during curing were observed by swelling, water vapour sorption and permeability measurements. The optimal UV exposure leads to lowering all three measured parameters. The studied layers can be used as a planarizing primers for other types of overcoats, the result will be more pronounced barrier effect of multilayer systems.

The authors thank the Slovak Grant Agencies APVV (Project No. 0324-10) and VEGA (Project No.1/0811/11 and 1/0818/13) for their financial support.

This publication is the result of the project implementation: ITMS: 26240120016 supported by the Research & Development Operational Programme funded by the ERDF.

REFERENCES

1. Despond S., Espuche E., Cartier N., Domard A.: J. Appl. Polym. Sci. *98*, 704 (2005).
2. Jančovičová V,. Lörinczová I., Mrlláková .I, Iždinská Z.: Chem. Listy *99*, s522 (2005).
3. Alexy P., Bakoš D., Crkoňová G., Kramárová Z., Hoffmann J., Julinová M., Chiellini E2005., Cinnel P.: Polymer Testing *22*, 811(2003).
4. Jančovičová V., Amberg-Schwab S., Dzik P., Mikula M.: Chem. Listy *102*, s1051 (2008).
5. Jančovičová V., Gemeiner P., Havlínová B.: Chem. Listy *105*, s332 (2011).
6. Vaško K., Noller K., Mikula M., Amberg-Schwab S., Weber U.: Cent Eur. J. Phys. *7*, 371 (2009).
7. Hunt R. W. G.: *Measuring Colour*. Ellis Horwood Limited, London 1995.

P-17
NUMERICAL ANALYSIS AND SHAPE OPTIMIZATION OF RUBBER DIAPHRAGMS

JAKUB JAVORIK

Tomas Bata University in Zlin, nám. T.G. Masaryka 5555, 760 01 Zlin, Czech Republic
javorik@ft.utb.cz

1. Abstract

Shape optimization of rubber diaphragms for a pneumatic regulation valves is the subject of this article. Numerical analyses (by FEM system) of initial shapes of the diaphragms were made and their results were used for the shape optimization of diaphragms. Then new numerical analyses of optimized diaphragms were made and the fulfillment of the initial requirements was approved.

2. Introduction

Using finite element method (FEM) analysis leads to significant reduction of cost of design and moreover we can analyze deformation and stress of FEM model in more details then deformation of prototype.

We need to know how the rubber diaphragm will behave in real conditions in valve. If we would made and test a number of prototypes during design procedure it would be very time and money consuming. The monitoring of the diaphragm behavior in real valve would be next problem and in a many industrial applications it is absolutely impossible to study behavior of the material in real situations[1].

The diaphragm is made from silicone rubber. The large elastic strain is characteristic for behavior of rubber. The stress-strain relation of elastomers is strongly nonlinear. Such materials are called hyperelastic and we can use a number of hyperelastic material models to simulate this nonlinear behavior today[2,3]. We have to measure properties of every particular material for FEM analysis in laboratory tests.

The diaphragm is used as a component of pneumatic regulatory valve and it will be loaded by compressed air. The movable rod is fixed in the center of the diaphragm. Different pressure on inner and outer side of the diaphragm moves the rod to its upper or lower position and thus some parameters can be regulated by the rod position.

3. Material and methods

3.1. Material Characterization

For the exact evaluation of hyperelastic material constants, the test data obtained from the uniaxial and equibiaxial tension tests are suitable[4–6]. The uniaxial tension test was performed on standard testing machine in accordance with ISO 37 standard.

There are not currently ISO standard methods for equibiaxial tension test and such tests are rarely performed in industrial laboratories. Thus the bubble inflation technique was used for equibiaxial characterization of diaphragms[5–7]. In this

method a uniform circular specimen of elastomer is clamped at the rim and inflated using compressed air to one side. The specimen is deformed to the shape of bubble. The inflation of the specimen results in an equibiaxial stretching near the pole of the bubble and in the planar tension near the rim. The inflation of the specimen and current value of pressure is recorded in short time intervals using a high resolution digital camera. We are measuring stress/strain relation during the entire test.

3.2. Material model

The James-Green-Simpson (by another name 3rd order deformation) hyperelastic model was able to fit experimental data most closely and was chosen for analysis. The strain energy density function W for this model is in the following form:

$$W = c_{10}(J_1 - 3) + c_{01}(J_2 - 3) + c_{11}(J_1 - 3)(J_2 - 3) + c_{20}(J_1 - 3)^2 + c_{30}(J_1 - 3)^3 \quad (1)$$

Measured coefficients (in Pa) for this model are: $c_{10} = 510140$; $c_{01} = 70468.1$; $c_{11} = -946.852$; $c_{20} = 36418.3$; $c_{30} = -234.302$, error of model is 1.822.

3.3. Shape and function of the diaphragm

Initial shape of the diaphragm is shown in Fig. 1. Radius of the diaphragm is 35 mm, height is 12 mm and diaphragm thickness is 0.3 mm. Maximum stress value in the diaphragm must not exceed 2.5 Mpa.

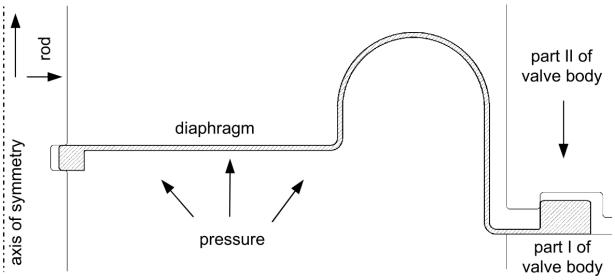

Fig. 1. **Initial shape of the diaphragm, its boundary conditions and loading**

3.4. Numerical model

Due to the fact that the diaphragm has axisymmetric shape it is very useful to create 2D axisymmetric FEM model. The diaphragm is mounted on the rod in center of valve and the outer rim of the diaphragm is clamped between two parts of valve body (Fig. 1).

Both parts of the valve body and the rod are modeled as absolutely rigid. The diaphragm is modeled as hyperelastic using material model (*1*) described above. Analysis consists of four steps (Fig. 1). The rod moves right in first step. In other words the diaphragm is mounted on the rod. Part II of valve body moves down in second step – the diaphragm is fixed in basic position in the valve now. The rod is moved to its upper position in third step and pressure is applied in last step because maximum of pressure can occur only when the rod is up.

4. Results

Two criteria were used for results evaluation: maximum stress in the diaphragm (2.5 MPa) and functionality of the diaphragm. It means that the diaphragm must stay fixed in all other parts (the rod and the body of valve) during maximal loading and it must remain hermetic.

First critical point of initial design is located at the rim of diaphragm. Critical situation occurred at the end of second step. Due to the fact that there was not enough space in the groove of valve body for proper deformation of the diaphragm rim, the stress increased to high. Thus the enlargement of this groove was the first modification of design.

Then the next analysis of the modified model was made. Problem at the outer rim was solved and the maximum stress in this area is 1.5 MPa.

The most critical point in the second version is near the central rim of the diaphragm. Its position is pointed as A in Fig. 2 and stress maximum (4.5 MPa) is located here. We can also see that the rim of the diaphragm is almost pulled out from the rod groove. But we can find others points where stress values are locally much higher than stress in their vicinity (points B and C in Fig. 2). Although stress does not exceed 2.5 MPa in these points we can reduce stress values by next modification of shape of the diaphragm. The two corners of the initial shape are reason of stress concentration in these areas.

With consideration of these results the final shape modifications were done: for point A – widening diaphragm thickness close to central rim and increasing the depth of rod groove; for point B – elimination of corner; and for point C – increasing corner radius (Fig. 3).

The shape shown in Fig. 3 was taken as the final design because its analysis did not reveal any critical points. The stress maximum of this shape is located in the same point as in previous version, but its value was significantly reduced to 2.3 MPa. Also the central rim is much steadier in the rod

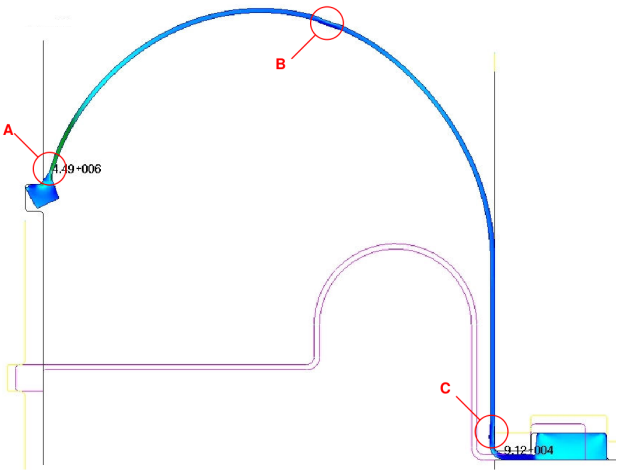

Fig. 2. **Results of second version of design (after 4th step)**

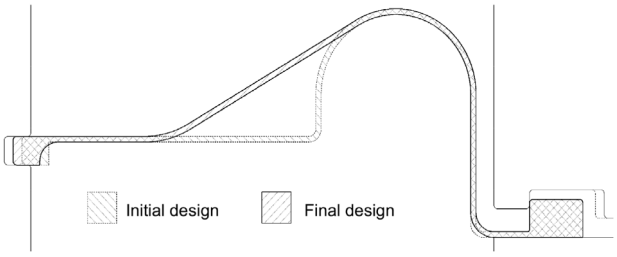

Fig. 3. **Final shape of the diaphragm**

groove. Reduction of stress in points B and C was reached too. Nevertheless it is not as significant as in case of the central rim (point A).

5. Conclusion

All criteria for the diaphragm were fulfilled and the final design of the diaphragm was created. Three versions of the diaphragm were analyzed – initial, second and final version. The enlargement of groove in valve body was necessary after analysis of the initial version. The next model (second version) with this modification was created and analyzed. With consideration of results of second version the rod groove was deepened and the shape of diaphragm was changed (final version – Fig. 3). The analysis of this modified shape proved that there are not exceeded stress/strain limits in the final version of diaphragm. Deformation does not exceed limit even in the initial model. But high stress was the reason of shape modification for the final version. The point where stress maximum is reached in diaphragm is near to the central rim (Fig. 2A).

REFERENCES

1. Manas D., Manas M., Stanek M., Zaludek M., Sanda S., Javorik J., Pata V.: Chem. Listy *103*, s72 (2009).
2. Boukamel A., Laiarinandrasana L., Méo s., Verron E.: *Constitutive Models for Rubber V*. Taylor & Francis, London 2008.
3. Ogden R.W.: *Non-linear Elastic Deformations*. Dover Publications, New York 1997.
4. Smith L. P.: *The language of Rubber*. Butterworth-Heinemann, Oxford 1993.
5. Reuge N., Schmidt F.M., Le Maoult Y., Rachik M., Abbé F.: Polym. Eng. Sci. *41*, 522 (2001).
6. Javorik J., Dvorak Z.: KGK, Kautsch. Gummi Kunstst. *60*, 608 (2007).
7. Javorik J., Dvorak Z.: Chem. Listy. *105*, s273 (2011).

P-18
EVALUATION OF 6PPD PREPARED BY A NEW TECHNOLOGY (BEING TESTED IN VUCHT a.s.)

K. KOSÁR, M. KRÁLIK, J. UHLÁR, ZS. VÉGH, M. NOVÁKOVÁ, and P. MAJOR

VUCHT a.s. (Research Institute of Chemical Technology), Nobel Str. 34, SK-83603 Bratislava, Slovakia
kkosar@vucht.sk, mkralik@vucht.sk

Abstract

This contribution compares 2 samples of 6PPD (*N*-1,3-dimethylbutyl-*N′*-phenyl-para-phenylenediamine) prepared by two different technologies:
– 6PPD prepared by "traditional" technology
– 6PPD prepared by a new, simplified technology (NASH) being tested in VUCHT a.s.

Introduction

In spite of their colouring and staining effects, derivatives of para-phenylenediamine (PPD) are the most efficient (and most widely used) antidegradants in rubber (tyre) industry. They protect the vulcanizates not only against oxidative heat aging, but show anti-flex cracking and antiozonant effects as well. As they are produced in huge quantities (hundred thousands tons per year all over the world[1]) the economical and ecological aspects of their production are not negligible. Because of these reasons VUCHT a.s. is working on an innovated technology for preparation of PPD derivatives.

Experimental

Fig. 1 shows the schematic steps of preparation technology of 4-aminodiphenylamine (ADPA), from which PPD derivatives are prepared by alkylation. The steps of traditional technology of ADPA (the so called Ouchi technology) are shown on the left side, while the method using reduced number of steps and the nucleophilic aromatic substitution of hydrogen (NASH)[2] can be seen on the right side. We have prepared samples of ADPA by both procedures shown on Fig. 1. Then we have used these samples of ADPA for the preparation of 6PPD marked 6PPD-Ouchi, and 6PPD-NASH, respectively. Though both samples of prepared 6PPD's were of high purity (6PPD NASH superior, Tab. I), we wanted to follow their behavior in rubber compounds and vulcanizates as well.

Table I
Analytical parameters of prepared 6PPD samples

	6PPD content [%]	Melting point [°C]	Volatile content [%]	Ash [%]
6PPD-Ouchi	99.3	48.5	0.08	0.014
6PPD-NASH	99.7	48.4	0.09	0.012

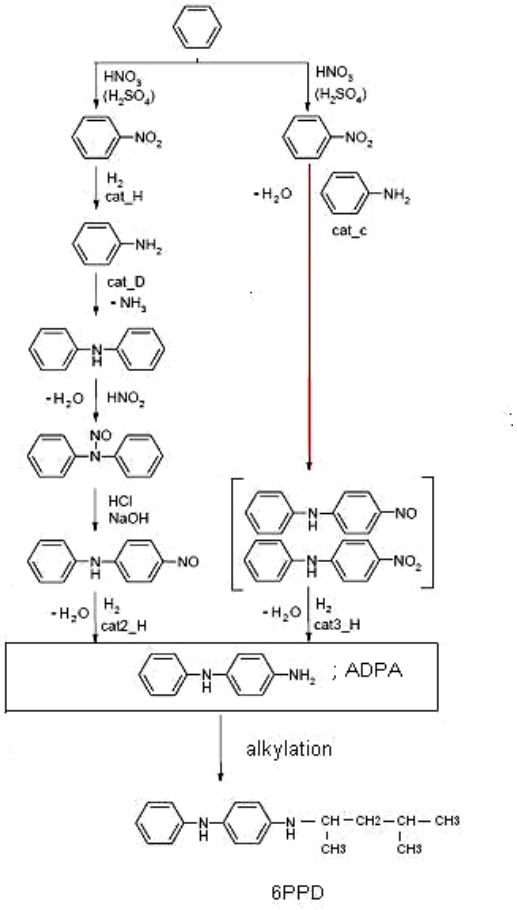

Fig. 1. **The preparation of ADPA;** traditional (Ouchi technology- left side) and the simplified (NASH) technology - right side

Results and discussion

It is known, that the insufficiently distilled PPD derivatives tend to shorten the scorch safety (initiation period, ts_1) and optimal cure time (tc_{90}) of rubber compounds. Fig. 2 shows, that neither the 6PPD-Ouchi nor the 6PPD- NASH samples influence these parameters of the test compound.

As it has been mentioned, a negative property of PPD derivatives is their colouring effect. Fig. 3 demonstrates, that though the 6PPD prepared by NASH technology is colouring the white vulcanizate, its colouring is not more intensive than the effect of 6PPD –Ouchi sample.

The sample of 6PPD prepared by the NASH technology also showed at least the same (or slightly better) protective efficiency as 6PPD-Ouchi during the thermo-oxidative aging (Fig. 4), the ozone test (Fig. 5) and the dynamic fatigue–to-failer De Mattia test (Fig. 6).

Conclusions

The above results demonstrate, that we have managed to prepare by an economically advantageous and ecologically

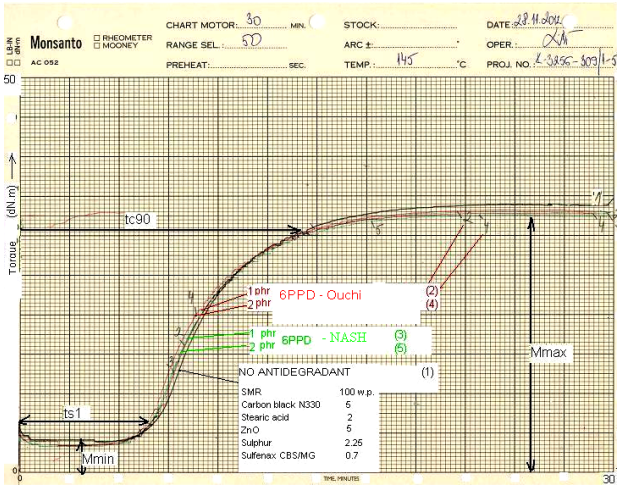

Fig. 2. **Rheometer cure curves [3] of compounds containing the tested 6PPDs** (natural rubber -SMR 5)

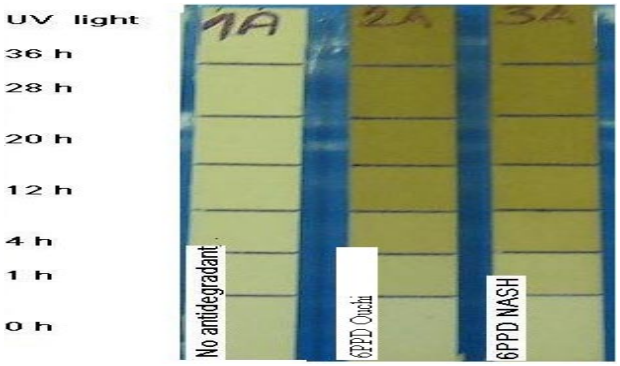

Fig. 3. **The effect of 6PPDs in a white vulcanizate exposed to UV light** (NR, TiO2,ZnO,Stearic acid, S, Sulfenax CBS)

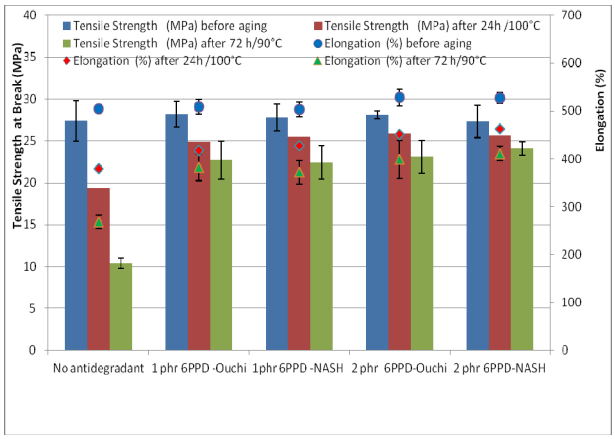

Fig. 4. **The tensile properties[4] of vulcanizates before and after thermo-oxidative aging** (composition of vulcanizates see on Fig. 2)

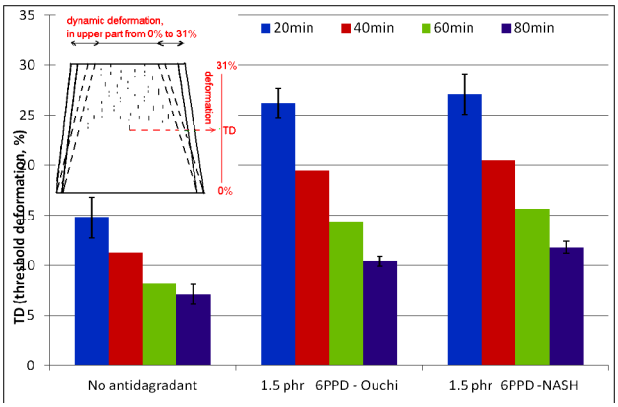

Fig. 5. **Development of cracks by time (threshold deformation - TD) on vulcanizates in ozone chamber (40 °C, 150 pphm O3, dynamic conditions ;** composition of vulcanizates see on Fig. 2)

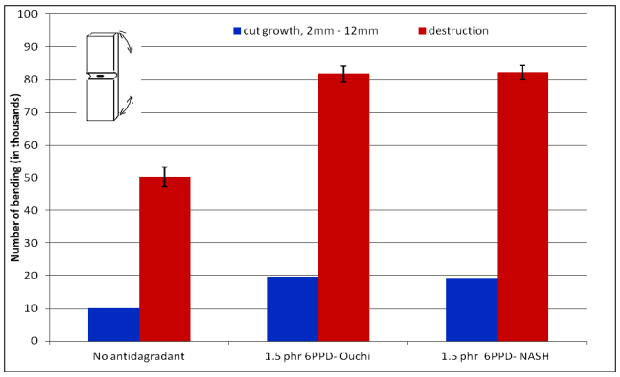

Fig. 6. **The dynamic properties of vulcanizates tested by DeMattia method**[5] (Kralex SBR 1500, Carbon Black N330, ZnO, Stearic acid, S, Sulfenax CBS/MG)

more friendly technology a sample of "6PPD- NASH" , which in its properties and efficiency in vulcanizates equals or prevails 6PPD prepared by "traditional" technology.

This publication is part of the results of the project implementation: Hydrogenation in the liquid phase, ITMS: 26220220144, supported by the Research & Development Operational Program funded by the ERDF.

REFERENCES

1. Freedonia 2002, Notch 2004 and SRI Consulting 2006.
2. SK Patent 171498A3.
3. ISO 3417.
4. ISO 37.
5. ISO 132.

P-19
SIMPLE METHOD FOR CHARACTERIZATION OF RUBBER FRACTURE IN PRACTICE

ONDŘEJ KRATINA*[a], MARTINA POLÁŠKOVÁ[a], RADEK STOČEK[b,c], and ROMAN ČERMÁK[a]

[a] Department of Polymer Engeneering, Faculty of Technology, Thomas Bata University in Zlín, náměstí T. G. Masaryka 275, 762 72 Zlín, [b] PRL Polymer Research Lab., Nad Ovčírnou 3685, 760 01 Zlín, [c] Centre of Polymer Systems, University Institute, Tomas Bata University in Zlín, Nad Ovčírnou 3685, 760 01 Zlín, Czech Republic
okratina@ft.utb.cz

Abstract

The fracture of rubber-like materials is mostly an undesirable process that reduces the service life of rubber components dramatically, whereas the fracture behaviour and durability of rubber are determined by its structure. The aim of this work was to study the fracture behaviour of standardized rubber compounds with different fracture toughness based on natural rubber (NR) and styrene butadiene rubber (SBR) realized due to various concentrations of carbon black and sulphur. The fracture behaviour has been analysed using different testing methods. Influence of this structure on fracture phenomena has been determined due to description of fracture surfaces by optical microscopy. As application, we introduce a simple method for characterization of the fracture in dependence on rubber compound's composition for efficient using in practice.

Introduction

Rubbers are elastomeric nanocomposites that have long been used in industry and are of great practical importance[1]. Rubber compounds are composed on a number of ingredients which have effect on quality of material. One of the characteristic which can be influenced by composition of compound is resistance to mechanical fatigue.
Mechanical fatigue is demonstrated in rubbery materials by a progressive weakening of physical properties as a result of slow crack growth during application of dynamic loads or deformations[2].

In addition to the compound affects the crack growth rate as well as the related loading speed ripping. Slow crack growth leads to a stable distribution, where individual small cracks merge into the main crack visible to the naked eye. During rapid tearing occurs surplus energy and material obtained is then unstable crack spreads, already without additional power supply. Fracture surface of the unstable distribution is smooth, without macroscopically visible major cracks[3].

Experimental

Materials

Used rubber compounds were based on NR and SBR. As filler was used carbon black with designation N220. Other used ingredients were sulphur, zinc oxide, stearin and MBTS

Table I
Recipe of standard compound

Ingredients	phr
Rubber	100,0
Stearin	3,0
Zinc Oxide	5,0
Carbon Black	50,0
MBTS	0,6
Sulphur	2,5
Total	161,1

80 as accelerator. Recipe of standard compound is presented in the Table I.

Prepared rubber compounds

For each type of rubber were prepared seven compounds with different composition. One of them was a standard compound prepared according ASTM D3192. Another three compounds were prepared with different concentration of carbon black and three with different sulphur content. The formulations of compounds are given in Tables II to III.

Testing

Mechanical properties were measured by tensile test on Alpha Technologies T2000 machine. For tensile test were used micro tensile dumb-bell shaped specimens. Dimensions of workspace were 10 × 2 × 2 millimetres and speeds of moving jaws were 5, 50 and 500 mm min^{-1}. Formed crack surfaces were analysed by optical microscopy with light polarizing filter. For determine of phenomena ware used samples with defined crack. For these samples were used tensile dumb-bell shapes specimens with dimensions of workspaces 40 × 6 × 2 millimetres. The following procedures were same as the first case.

Table II
Concentration of sulphur content

Compound no.	phr
XS01	1,0
Standard compound	2,5
XS05	5,0
XS10	10,0

Table III
Concentration of carbon black content

Compound no.	phr
XC00	0
XC20	20
Standard compound	50
XC70	70

Results and discussion

The tensile test showed that with increasing sulphur and carbon black content material becomes less pliable and modulus value in tensile elongation grow up. This is due to increased cross-linking density in the case of increasing the concentration of sulphur and bracing material in case of increasing carbon black additive.

By optical microscopy can see influence of value of modulus on appearance of fracture surface. For material with higher value of modulus is fracture surface with smoother surface than for material with lower value of modulus. This phenomenon is shown in Fig. 1 to 2.

For samples with defined length of crack was analysed influence of speed of feed rate of jaws. On created fracture surfaces were observed two phenomena accompanying fracture of rubber parts.

In the first case it was change of ratio of area of stable and unstable crack propagation. As shown in Fig. 3, increasing area of unstable crack propagation with increasing feed rate.

Another phenomenon which was observed was stick-slip effect. This effect represents jamming during crack growth. This means that the crack extends in differential gain and then growth stops until the accumulated enough energy needed to grow the crack. Stick-slip effect is visible in particular for compounds with a low content of carbon black for the 500 and 50 mm min^{-1}. This phenomenon is shown in Fig. 4.

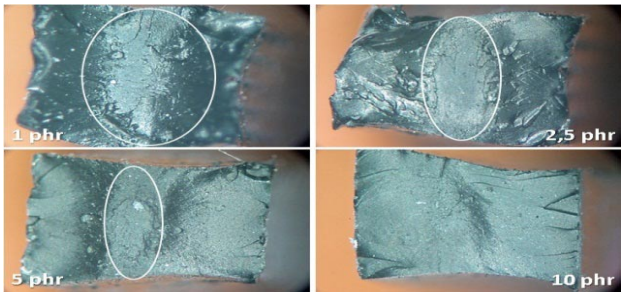

Fig. 1. **Influence of sulphur content on the** fracture surface

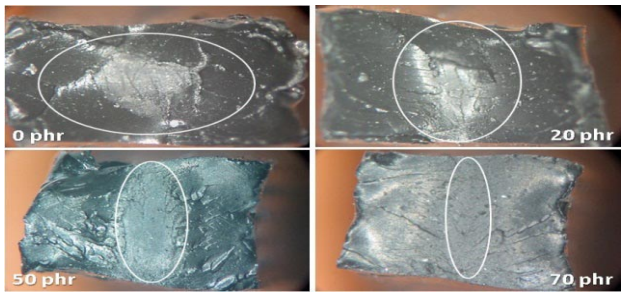

Fig. 2. **Influence of carbon black content on** the fracture surface

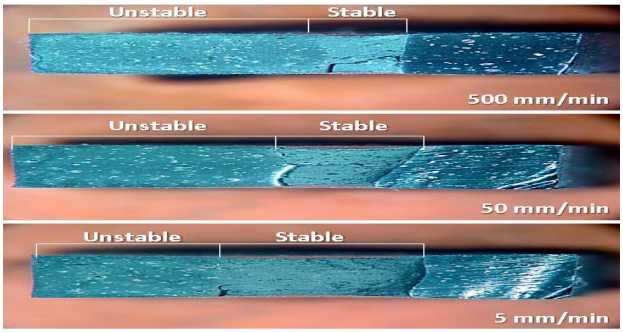

Fig. 3. **Stable and unstable area of crack** propagation

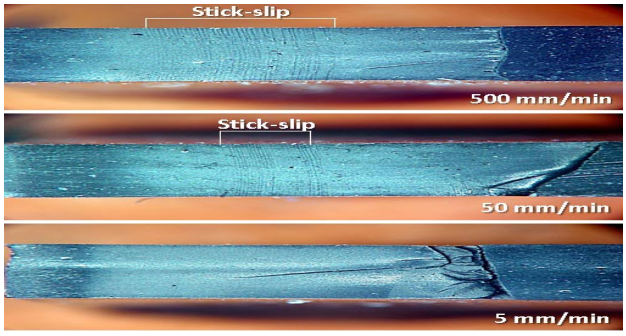

Fig. 4. **Stick slip effect**

Conclusion

Optical microscopy in conjunction with the basic knowledge of the mechanisms of crack propagation in the rubber used to the fundamental description of fracture surfaces, depending on the composition of the rubber compound and rubber loading mechanism. This basic method is the first practical approach describing a fracture behaviour of rubber. For a more thorough description is needed another research by using of quantitative analyses, this could be for example based on measurement of surface roughness.

This contribution was written with support of Operational Program Education for Competitiveness co-funded by the European Social Fund (ESF) and national budget of Czech Republic, within the framework of project Advanced Theoretical and Experimental Studies of Polymer Systems (reg. number: CZ.1.07/2.3.00/20.0104).

REFERENCES

1. A. L. Svistkov, A. G. Pelevin, A. A. Adamov, A. Lauke, G. Heinrich: *Constitutive Models for Rubber VI*, p. 85–89. CRC Press, London 2010.
2. A. N. Gent: *Engineering with Rubber – How to Design Rubber Components*, Hanser Publishers, Munich 2001.
3. T. Horst, G. Heinrich: *Constitutive Models for Rubber VI*, p. 331–336. CRC Press, London 2010.

P-20

NANOHARDNESS OF POLYMERS (POLY PROPYLENE)

PETR KRATKY, DAVID MANAS, MIROSLAV MANAS, MICHAL STANEK, MARTIN OVSIK, JAKUB JAVORIK, and MARTIN BEDNARIK

Tomas Bata University in Zlin, Faculty of technology, Department of Production Engineering, nam. T.G. Masaryka 275, 762 72 Zlin, Czech Republic
dmanas@ft.utb.cz

Abstract

Hard surface layers of polymer materials, especially polypropylene, can be formed by chemical or physical process. One of the physical methods modifying the surface layer is radiation cross-linking. Radiation doses used were 0, 33, 66 and 99 kGy for unfilled polypropylene with the 5% cross-linking agent (triallyl isocyanurate). The improvement of nanomechanical properties was measured by an instrumented nanohardness test.

1. Introduction

Isotactic polypropylene (iPP) is a commodity polymer with the semi-crystalline structure which is very complex and depends strongly on thermal history and processing conditions. Isotactic polypropylene can crystallize in to 3 phases: α-phase is the most stable and the most known. The crystals are monoclinic. Beta phase is metastable and the crystals are hexagonal β-phase is mainly found in block PP copolymers and can be generated by addition of specific nucleating agents. This phase was discovered by Padden and Keith in 1953 and can be improved by crystallization between 130 and 132 °C or by orientation with high shear or through addition of specific nucleating agents. Presence of β-phase in PP homopolymer generally increase ductility in the finished parts. Maximum effect is observed at 65 % of beta-phase. Gamma phase – this phase is also metastable with triclinic crystals. This form is not very familiar but appears mainly in low molecular weight polypropylene by crystallization at very high pressure and very low cooling rate[1,2].

The irradiation cross-linking of thermoplastic materials via electron beam or cobalt 60 (gamma rays) proceeds is proceeding separately after the processing. The cross-linking level can be adjusted by the irradiation dosage and often by means of a cross-linking booster[1–4].

The main deference between β- and γ-rays is in their different abilities of penetrating the irradiated material. γ-rays have a high penetration capacity (Fig. 1). The penetration capacity of electron rays depends on the energy of the accelerated electrons.

The thermoplastics which are used for production of various types of products have very different properties. Standard polymers which are easy obtainable with favourable price conditions belong to the main class. The disadvantage of standard polymers is limited both by mechanical and thermal properties. The group of standard polymers is the most con-

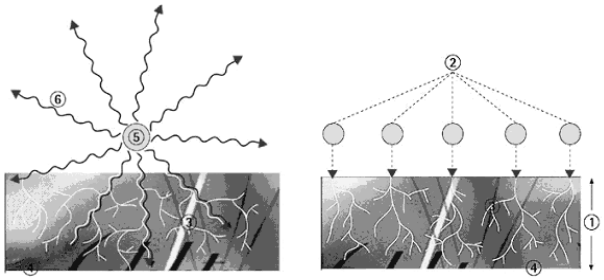

a b

Fig. 1. **Design of Gamma rays (a) and Electron rays (b);** a) 3 – secondary electrons, 4 – irradiated material, 5 – encapsulated Co – 60 radiation source, 6 – Gamma rays, b) 1 – penetration depth of electron, 2 – primary electron, 3 – secondary electron, 4 – irradiated material

siderable one and its share in the production of all polymers is as high as 90 %.

The engineering polymers are a very important group of polymers which offer much better properties in comparison to those of standard polymers. Both mechanical and thermal properties are much better than in case of standard polymers. The production of these types of polymers takes less than 1 % of all polymers[1–4].

High performance polymers have the best mechanical and thermal properties but the share in production and use of all polymers is less than 1 %.

The present work deals with the influence of irradiation doses on the nanohardness polypropylene. Nanohardness testing was chosen for one reason. Small, thin layers of the PP specimens, which can be produced by irradiation crosslinking, can be characterized by this method.

2. Experimental part

For this experiment isotactic polypropylene iPP PTS – Crealen EP-2300L1-M800; PTS Plastics Technologie Service, Germany (unfilled, iPP+TAIC, MFR – 230 °C/2.16 kg – 6 g/10 min) was used. The material already contained a special cross-linking agent TAIC – triallylisocyanurate (5 vol.%), which should enable subsequent cross-linking by ionizing β-radiation. The prepared specimens were irradiated with doses of 33.66 and 99 kGy at BGS Beta-Gamma Service GmbH & Co. KG, Germany[1–4].

The samples were made using the injection molding technology on the injection molding machine Arburg Allrounder 420C. Processing temperature 240–260 °C, mold temperature 75 °C, injection pressure 80 MPa, injection rate 65 mm s^{-1}.

Instrumented nanohardness tests were done using a Nanoindentation Tester (NHT2) – Opx/Cpx, CSM Instruments (Switzerland) according to the CSN EN ISO 650-1. Load and unload speed was 100 mN min^{-1}. After a holding time of 90 s at maximum load 50 mN the specimens were unloaded. The indentation hardness H_{IT} was calculated as maximum load to the projected area of the hardness impression according to:

$$H_{IT} = \frac{F_{max}}{A_p} \qquad \text{with} \qquad h_c = h_{max} - \varepsilon \frac{F_{max}}{S} \qquad (1)$$

Where h_{max} is the indentation depth at F_{max}, h_c is contact depth. In this study the Oliver and Pharr method was used calculate the initial stiffness (S), contact depth (h_c). The specimens were glued on metallic sample holders[1–5].

3. Results and discussion

The values measured during the nanohardness test showed that the lowest values of indentation hardness were found for the non-irradiated PP. On the contrary, the highest values of indentation hardness were obtained for PP irradiated by a dose of 99 kGy (by 14 % higher in comparison with the non-irradiated PP), as can be seen at Fig. 2.

According to the results of measurements of nanohardness, it was found that the highest values of indentation modulus of elasticity were achieved at the PP irradiated with dose of 66 kGy (by 24 % higher than compared with non-irradiated PP). On the contrary, the lowest values of the indentation modulus of elasticity were found for non-irradiated PP as is seen at Fig. 2.

Material deformation in time under constant stress (indentation creep) measured by instrumented test of nanohardness showed (Fig. 3) that the highest creep values were measured on non-irradiated PP (13,14 %), while the lowest creep value was found in PP irradiated by 66 kGy dose (11,48 %). The creep dropped by 13 % as a result of radiation, which represents a considerable increase of surface layer resistance.

The highest values of plastic and elastic deformation work were obtained for non-irradiated PP. The lowest values of both elastic and plastic deformation work were obtained for PP irradiated with a dose of 66 kGy. Radiation of specimens caused lower values of elastic as well as plastic deformation work which is apparent in Fig. 4. This drop corresponds to the macro tests of impact strength conducted. The non-irradiated specimen did not break during impact test. However, the irradiated specimen broke during the impact test.

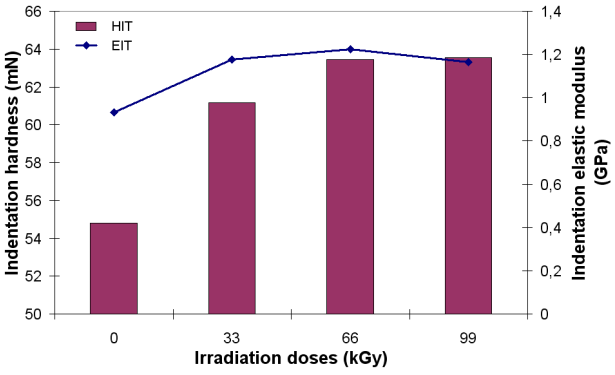

Fig. 2. **Hardness and elastic modulus of polypropylene**

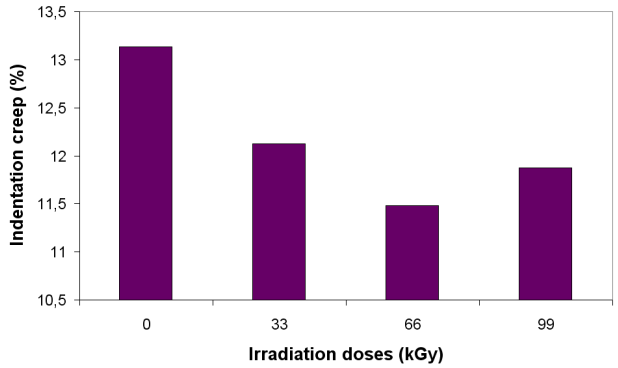

Fig. 3. **Indentation creep of polypropylene**

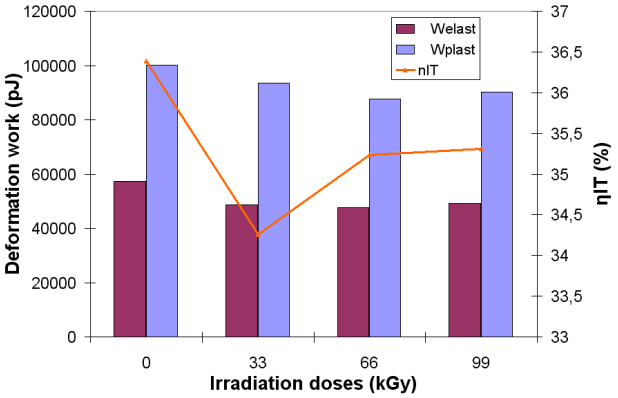

Fig. 4. **Elastic and plastic deformation work of polypropylene**

4. Conclusion

Very interesting results were obtained for irradiation modified PP. When comparing the irradiated and non-irradiated PP it was apparent that the values of indentation hardness and the indentation modulus considerably increased, in some cases even by 24 % at the irradiation dose of 66 kGy.

This paper is supported by the internal grant of TBU in Zlin No. IGA/FT/2013/020 funded from the resources of specific university research and by the European Regional Development Fund under the project CEBIA-Tech No. CZ.1.05/2.1.00/03.0089.

REFERENCES

1. Manas D., Manas M., Stanek M., Danek M.: Arch. Mater. Sci. Eng. *32*, 69 (2008).
2. Oliver W. C., G. M. Pharr: J. Mater. Res. *7*, 1564 (1992).
3. Chvatalova L., Navratilova J., Cermak R., Raab M., Obadal M.: Macromolecules *42*, 7413 (2009).
4. Manas D., et al.: Thin Solid Films *530*, 49 (2013).
5. Gilbert M., Hybart F.: J. Polymer *13*, 327 (1972).

P-21

RHEOLOGICAL AND ELECTRICAL PROPERTIES OF COMPOSITES BASED ON LOW DENSITY POLYETHYLENE AND EXPANDED GRAPHITE

JÁN KRATOCHVÍLA[a], ZDENKO ŠPITÁLSKÝ[a], and IGOR KRUPA[a,b]

[a] Polymer Institute, Slovak Academy of Sciences, Dúbravská cesta 9, 84541 Bratislava, Slovakia, [b] QAPCO Polymer Chair, Center of Advanced Materials, Qatar University, P.O. Box 2713, Doha, Qatar
jan.kratochvila@savba.sk

Investigation of the rheological and electrical behavior of polymer/graphite composites have attracted considerable interests because of their practical use for industry. Polymer micro and nanocomposites filled with expanded graphite have shown notable improvements of mechanical, thermal, electrical and barrier properties at very low filler concentrations[1], compared to conventional composites.

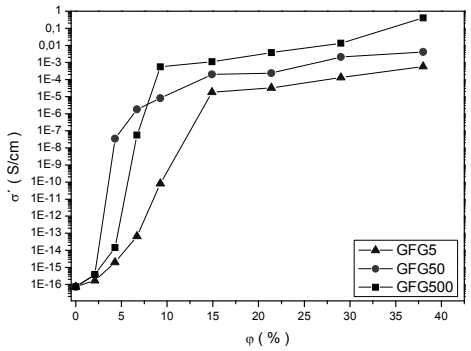

Fig. 1. **The dependence of the electrical conducitivity of composites on the filler content for different parcticle sizes**

In this work we refer the viscoelastic properties of composites and their relation to the electrical behavior. The composites under study were formed from low density polyethylene matrix filled with various grades of expanded graphite having an average size 5, 50 and 500 μm. Electrical conductivity compared at the same filler content increases with an average size of the graphite. The highest value of electrical conducitivity of $4{,}14 \cdot 10^{-1}$ S cm^{-1} was found for the mixture LDPE/GFG 500 at 38 vol.% of the filler. The percolation treshold ranged between 4,3 and 6,7 vol.% . The study of rheological properties shows that the reinforcement effect depends on the concentration of graphite in the LDPE matrix. Complex viscosity of composites increases with fillers content and complex viscosity decreases with increasing frequency.

The research was supported by the Scientific Grant Agency of the Ministry of Education of Slovak Republic and the Slovak Academy of Sciences (project No. 2/0119/12) and by grant NMT-ERANET "APGRAPHEL" No. ID 794.

REFERENCE

1. Kratochvíla J., Boudenne A., Krupa I.: Polymer Composites *34*, 149 (2013).

P-22
MAGNETIC AND MECHANICAL PROPERTIES OF MAGNETOACTIVE COMPOSITES BASED ON BR

JÁN KRUŽELÁK[a], RICHARD SÝKORA[a]*, DENISA BELLUŠOVÁ[c], RASTISLAV DOSOUDIL[b], and IVAN HUDEC[a]

[a] Faculty of Chemical and Food Technology, Institute of Polymer Materials, Department of Plastics and Rubber, Radlinského 9, 812 37 Bratislava, Slovakia, [b] Faculty of Electrical Engineering and Information Technology, Ilkovičova 3, 812 19 Bratislava, Slovakia, [c] Deutsches Institut für Kautschuktechnologie e.V., Eupener Strasse 33, D-30519 Hannover, Germany
richard.sykora@gmail.com

Introduction

Rubber magnetic composites are group of smart materials consisting of magnetically polarizable particles incorporated in soft elastomeric matrix[1,2]. In rubber magnetic composites, magnetic particles are randomly distributed inside the matrix (Fig. 1a). Those of which mechanical and rheogical properties can be controlled by external magnetic field are often called magnetorheological elastomers[3,4]]. When rubber compounds with magnetic fillers are exposed to external magnetic field, the field induced interactions between particles lead to the formation of particles chains within the structure of elastomeric matrix. In the process of vulcanization, the chain-like structure of magnetic particles can be permanently fixed in the rubber matrix (Fig. 1b). The results showed that such structure inside the rubber matrix leads to a strong anisotropic behavior of prepared composites. In dependence on the concentration of magnetic filler or applied magnetic field, the chain-like structure of magnetic particles may vary in wide range. Particles anisotropy affects magnetic as well as mechanical properties of prepared composites.

The scope of the work was to evaluate the influence of strontium ferrite content on physical-mechanical properties of prepared composites. Magnetic characteristics of these materials were investigated in absence or presence of an external magnetic field.

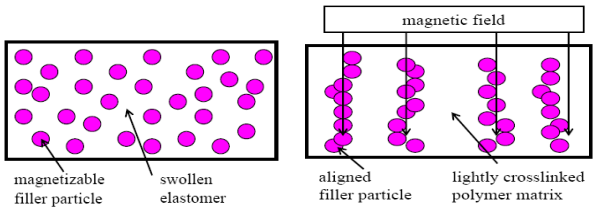

Fig. 1. **Particles alignment in rubber matrix in absence of magnetic field-isotropic state (a) and in presence of applied magnetic field-anisotropic state (b)**

Experimental

1,4-cis butadiene rubber (Buna CB 24, BR, Lanxess, Leverkusen, Germany) was chosen as soft elastomeric matrix. Strontium anisotropic hexaferrite $SrFe_{12}O_{19}$, type FD8/24 (Magnety a.s., Světlá Hora, Czech Republic) was applied as magnetic filler. It is product surface-modified by polyvinylalcohol (PVAL). Ferrite powder was dosed in several concentrations, varied from 0 to 100 phr. Besides rubber and filler, the rubber compounds contained only additives, which support curing process.

Ingredients of rubber compounds were mixed in the laboratory mixer Brabender in two mixing steps. The curing process was performed at 150 °C for the optimum cure time under a pressure of 15 MPa without or with external magnetic field of 0.35 T. The physical-mechanical properties were determined in accordance with the valid technical standards. The magnetic measurements of composites using magnetometer TVM-1 at room temperature were evaluated.

Results and discussion

The values of physical-mechanical properties of prepared rubber composites are graphically illustrated in Fig. 2–4. From Fig. 2 it becomes evident that the presence of magnetic filler leads to the increase of modulus M100. At maximum ferrite loading there was spotted more than 55 % increase of observed property in comparison with the ferrite free vulcanizate. The increasing tendency on magnetic filler content was recorded also in case of tensile strength at break (Fig. 3). From the dependence of elongation at break on magnetic filer content (Fig. 4) it was possible to see that the highest value of elongation at break reached the sample with 80 phr of ferrite.

The achieved results revealed that ferrite incorporated in rubber matrix exhibit slight reinforcing effect, although the degree of reinforcement is not as significant as in comparison with traditional fillers used in rubber technology (e.g. carbon black). The improvement of physical-mechanical properties by incorporation of ferrite can be attributed to the surface

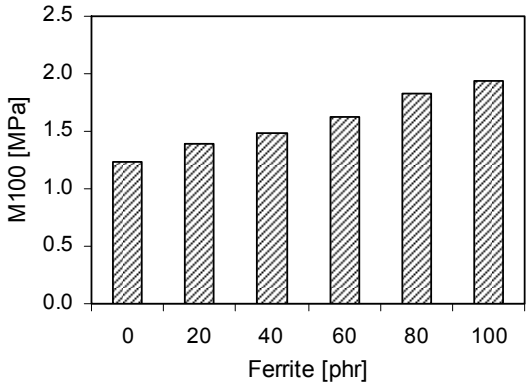

Fig. 2. **Influence of ferrite content on modulus M100 of composites**

modification of ferrite particles. Although PVAL is polar polymer, it is supposed that it is able to form interfacial layer between the magnetic filler and the non-polar butadiene rubber due to polymer physical entanglements between PVAL and the rubber matrix. The enhancement of adhesion between the rubber and ferrite subsequently leads to the improvement of observed properties of tested systems.

In order to investigate magnetic characteristics in absence and presence of magnetic field, the samples were cured with or without external magnetic field applied. Subsequently, the remanent Br and maximum Bm magnetic induction were determined (Fig. 5, 6). As seen in Fig. 5, the remanent magnetic induction was found to significantly increase with increasing content of magnetic filler. The values of both Br and Bm were spotted to be higher, when prepared samples were cured in presence of magnetic field. Based upon the obtained results, it can be stated, that during vulcanization process particles are aligned to the direction of applied magnetic field. It should be also mentioned, that alignment of the particles must be reached before the critical cross-linking plateau is finished. Otherwise the viscosity of mixtures increases and movement of magnetic particles is not possible anymore. After the curing process, the columnar structure of magnetic particles is permanently fixed in the rubber matrix. Such columnar structure within the rubber matrix leads to anisotropic behavior of prepared composites, what subsequently contributes to the enhanced values of observed magnetic characteristics.

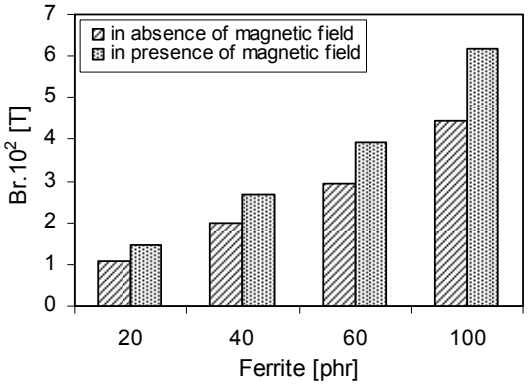

Fig. 5. **Influence of ferrite content on remanent magnetic induction Br of composites**

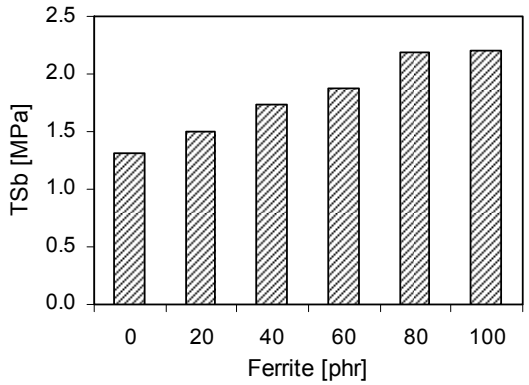

Fig. 3. **Influence of ferrite content on tensile strength at break TSb of composites**

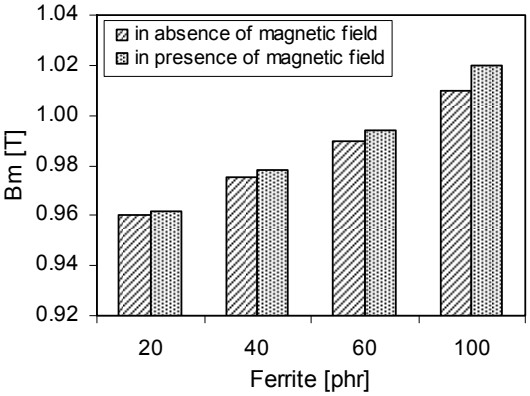

Fig. 6. **Influence of ferrite content on maximum magnetic induction Bm of composites**

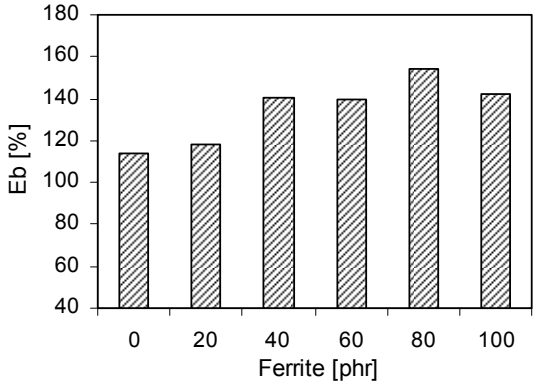

Fig. 4. **Influence of ferrite content on elongation at break Eb of composites**

This work was supported by the Slovak Research and Development Agency under the contract No. APVV-0062-11 and by grant agency VEGA, project No. 1/1163/12.

REFERENCES

1. Sun T. L, Gong X. L., Jiang W. Q., Li J. F., Xu Z. B., Li W. H.: Polym. Test. *27*, 520 (2008).
2. Kruželák J., Hudec I., Dosoudil R.: Polym. Deg. Stab. *97*, 921 (2012).

3. Varga Z., Filipcsei G., Zrínyi M.: Polymer *46*, 7779 (2005).
4. Bellušova D., Alshuth T., Schuster R. H., Myndyk M., Šepelak V., Hudec I.: KGK, Kautsch. Gummi Kunstst. *61*, 118 (2008).

P-23
NATURAL RUBBER/ORGANOMODIFIED KAOLIN COMPOSITES: THERMAL STUDIES AND FUTURE APPLICATIONS

CH. MGBEMENA, A. R. R. MENON, and N. O. IBEKWE

Nigerian Society of Engineers, National Engineering Design Development Institute, Nnewi, Anambra St., Nigeria
edumgbemena@yahoo.com

P-24
THE INFLUENCE OF PLASTICIZERS ON MECHANICAL PROPERTIES OF POLYLACTID ACID

MICHAL MIHALÍK*, PAVOL ALEXY, MIROSLAVA MIKUŠOVÁ, KATARÍNA TOMANOVÁ, RODERIK PLAVEC, JÁN BOČKAJ, and ZUZANA VANOVČANOVÁ

Slovak University of Technology in Bratislava, Faculty of Chemical and Food Technology, Institute of Polymer Materials, Radlinského 9, 812 37 Bratislava, Slovakia
michal.mihalik@stuba.sk

Introduction

A wide range of petroleum-based plastics are produced worldwide. In 2010 the global production of plastics increased to 265 million tonnes, European production increased to 57 million tonnes. The most produced plastics like PE, PP, PVC, PS, PET are used in various sectors of industry – automotive, building and construction, electrical and electronic equipments and packaging – due to good mechanical and processing properties, including the low cost[1]. The big amount of these plastics is exploited as packaging materials for food and beverages – for one-use applications. These materials represent the largest amount of plastic waste, simultaneously plastic waste represents growing global task to solve.

The biodegradable polymers offer acceptable solution. There are many known types of biodegradable polymers with various characteristic properties. Materials like polylactid acid, polyhydroxybutyrate are independent on crude oil , but on the other hand they have some disadvantages. These materials have often low thermal stability and specific mechanical properties – brittleness and low thoughness because of high crystallinity content[2].

The possibilities how to solve mentioned problems can be found in modification of biodegradable polymers by addition of modifiers, plasticizers or by blending of two or more polymers together. In present work, the influence of various types of plasticizers for PLA on mechanical properties was studied.

Materials and methods

Materials

PLA 4042D from NatureWorks, LLC, USA was used as polylactide acid, triacetine (TAC) and polyethylene glycol (PEG) with various molecular weight (600, 1500, 6000) were used as plasticizers.

Preparation of blends

The blends of polylactide acid/plasticizer with content of plasticizer 5, 10, 15 and 20 %wt. were prepared using twin screw extruder with screw diameter 16 mm, L/D = 40 equipped with four kneading zones. Liquid plasticizers were added by plunger-pump.

Preparation of films

The films were prepared using single-screw extruder with screw diameter 19 mm, L/D = 25, in combination with chill-roll technology.

Mechanical properties measurement

For tensile test according to ISO 527 the Zwick machine was used at cross-head speed 1mm/min while deformation range was of 0–3 % and after this value of deformation the speed increased up to 50 mm/min. The tensile strength at break (s_B), elongation at break (e_B), tensile strength at yield (s_Y) and Young´s modulus (E) were determined based on recorded tensile curves.

Results and discussion

The dependencies of mechanical properties on plasticizer content in the PLA are shown in Fig. 1–4.

Tensile strength at yield (Fig. 1) of pure PLA is near to 70 MPa. After addition of PEG 600 yield point disappear from tensile curve, as well as after addition of PEG 1500 in

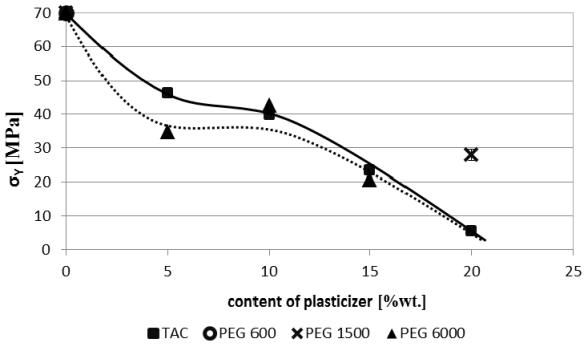

Fig. 1. **The dependency of tensile strength at yield on plasticizer content**

*Some blends exhibit no yield point (e.g. PLA/PEG 600). No values mean that samples exhibit no yield points.

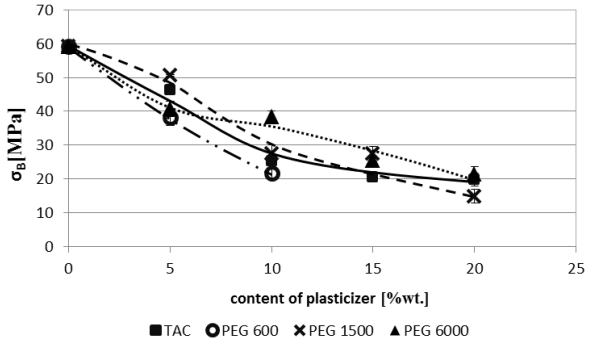

Fig. 2. **The dependency of tensile strength at break on plasticizer content**

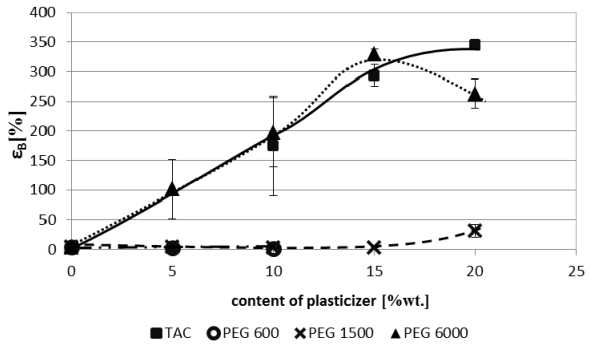

Fig. 3. **The dependency of elongation at break on plasticizer content**

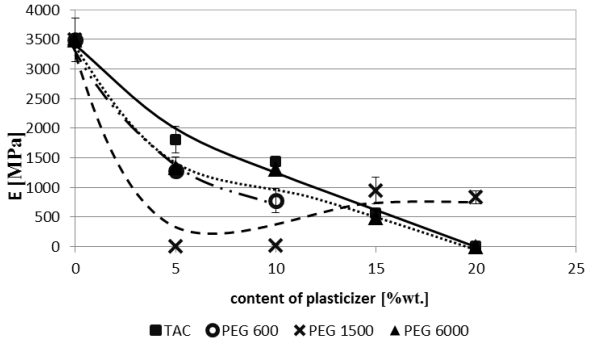

Fig. 4. **The dependency of Young´s modulus on plasticizer content**

*It was not possible to prepare film of blend PLA/PEG 600 with plasticizer content more than 10%wt. because of very low viscosity of blends.

concentration range 5–15 %wt. Values of tensile strength at yield decreased with increasing concentration of both plasticizers – TAC and PEG 6000. At the highest concentration (20 %wt.) of these plasticizers, the significant decreasing of evaluated property (s_Y) was achieved.

Tensile strength at break (Fig. 2) of pure PLA is near to 60 MPa. Addition of plasticizer results in the decreasing of tensile strength at break. Similar dependencies were observed in cases of all plasticizers. If the content of plasticizer was more than 15 %wt., significant decline of values of σ_B was observed in comparison with pure PLA.

In the Fig. 3 elongation at break is shown. Considerable improvement of ε_B was obtained after application of TAC and PEG 6000. Application of PEG 600 and PEG 1500 does not effect elongation at break if content of plasticizers is lower than 15 %wt. In the case of 20 %wt. of PEG 1500 ε_B slight increased near to 30 %. If 20 %wt. TAC or 15 %wt. PEG 6000 was applied in the blend, most significant improvement of elongation at break was observed. In the both cases more than 300 % elongation at break was achieved. By addition of PEG 6000, maximal value of elongation at break was achieved at concentration 15 %wt. Another increasing of plasticizer concentration caused decline of evaluated property (ε_B). If the content of PEG 6000 or TAC was 10 %wt., reasonable improvement of elongation at break was achieved, whereas from 30 to 40 MPa of tensile strength at break was observed. Maximal value of ε_B was observed at concentration 20 %wt. of TAC. On the other hand, at this content of TAC very low values of tensile strength and Young´s modulus was observed.

In the Fig. 4 it is seen, that even at low concentration (5 %wt.) of PEG 1500, the E is significantly decreasing. Addition of plasticizer causes lower values of Young´s modulus in comparison with pure PLA. Addition of TAC or PEG 6000 in concentration range 5–10 %wt. causes decreasing of Yong´s modulus near to 1500 MPa, that is reasonable value for application of packaging films.

Conclusion

Polyethylene glycol with various molecular weight and triacetine as plasticizers for polylactid acid were tested in present work. In case of PEG 600 and PEG 1500 no or only slight increasing of elongation at break were observed. Tensile strength at yield decreases with increasing content of plasticizer, as well as tensile strength at break. Even at small addition PEG 1500 (5 %wt.) decrease of Young´s modulus was significant. Using PEG with molecular weight 600 and 1500 as plasticizers for PLA does not improve mechanical properties in comparison to pure PLA.

Addition of PEG 6000 and TAC causes significant improvement of elongation at break (more than 300 %) while reasonable values of tensile strength and Young´s modulus were obtained. Increasing concentration of TAC results in increasing of elongation at break, on the other hand results in decrease of tensile strength and Young´s modulus. The similar influence of PEG 6000 on properties of PLA was observed. The optimal content of both plasticizers seems to be in the concentration range between 10 and 15 %wt.

Using TAC or PEG 6000 gives a good chance to prepare PLA/plasticizer blends with properties suitable for practical use of such materials for example in packaging.

REFERENCES

1. *Plastics – the Facts 2011*; An analysis of European plastics production, demand and recovery for 2010.
2. Nampoothiri K. M., Nair N. R., John R. P.: Bioresource Technology *101*, 8493 (2010).

P-25
PHOTOACTIVITY OF NANOPARTICLE OXIDE LAYERS OF DSSC ON PET FOILS

MILAN MIKULA*, PAVOL GEMEINER, VLADIMÍR DVONKA, and ZUZANA BEKOVÁ

Department of Printing Arts Technology and Photochemistry IPM, Faculty of Chemical and Food Technology SUT, Radlinského 9, 812 37 Bratislava, Slovak Republic milan.mikula@stuba.sk

Abstract

Polyethylene-terephthalate (PET) foils and glass slides coated with thin conductive layers were used as substrates for TiO_2 or ZnO based photoactive electrodes of dye-sensitized solar cells (DSSC) finalized using standard iodine electrolyte and counter electrode of Pt coated glass. The nanoparticle oxides were applied onto the substrates in a form of alcohol pastes by screen printing or by doctor blade technique. Photocurrents and I–V load characteristics were measured depending on the solar cell composition and preparation. To block the shot circuit current a 20 nm thin dip coated TiO_2 sol-gel layer was deposited onto substrates before metal oxides application. The influence of the blocking layer (as prepared or modified) in the presence of TiO_2 or ZnO active layer is discussed.

Introduction

Polyethylene-terephthalate plastic foil is a promising support and encapsulating material in organic and printed electronics, including photovoltaic applications. In the case of Dye Sensitized Solar Cells (DSSC) the standard photoactive layers based usually on TiO_2 nanoparticles on glass substrates involve sintering at 450 °C. In order to prepare a flexible solar cell on polymer plastic substrates (PET, PEN,...) low temperature processes (below 150 °C) of the coating of all functional layers ought to be discovered. To keep a low cost production the roll-to-roll processes are preferred, including screen printing, and all printing techniques[1,2].

The nano and microstructure of the active oxide layer (TiO_2) is critical to DSSC performance. In a low T process TiO_2 film has the tendency to crack, which resulted in the shunt of the device and reduction of solar cell efficiency. An alternative ZnO films on the other hand have better morphology tolerance and the interparticle contacts keep uninterupted[3].

To prevent the internal shortening of the cells fabricated from a binder-free nanoparticle-oxide pastes at low T a thin blocking layer, usually of an amorphous TiO_2, is deposited onto the substrate (ITO/PET) before photoactive oxide layer deposition. This hole blocking layer (BL) also avoids direct contact of the dye with the ITO surface. The electron conductive BL can be created chemically[4], physically by atomic layer deposition[5] or by sol-gel (SG) process[6].

The SG process is based on chemical reactions of hydrolysis and polycondensation of titania alcoxides, with formation of oxopolymers. These are transformed into oxide network. Condensation continues with gel formation. After evaporation of solution the xerogel is built and usually the calcination step continues at temperatures above 300 °C to make it more dense, ideally to anatase structure for application in photocatalysis or photovoltaics. To keep the low T technology, recently plasma treatments have been used as a calcination step for removal of organic additives and generation of mesoporous films with sol–gel precursors[7].

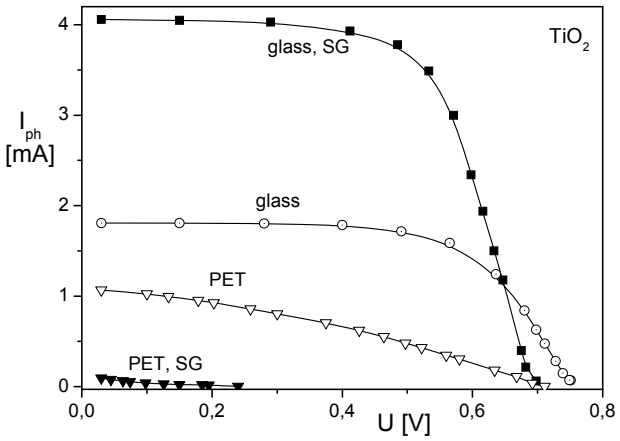

Fig. 1. **I-V loading curves of standard and low temperature TiO_2 DSSC on glass and on PET,** resp. (SG denotes sol-gel layer)

In this paper, physical and photoelectric properties of printed photoactive oxide layers and DSSC structures on PET and glass substrates with the codeposited BL layers were measured and correlated with overall cell structure and UV/ plasma pretreatment of BLs.

Experimental

Two electrically conductive substrates, PET foils (120 μm) and glass slides (3 mm) coated by thin indium or fluorine dopped tin oxide layer (ITO or FTO, 100 Ω/sq. or 7 Ω/sq., resp., Aldrich) were coated by nanoparticle metal oxides TiO_2 (20 nm, Degussa P25, Evonik) or ZnO (100 nm, Aldrich) and used as bases for solar cell (dye-sensitized, DSSC) preparation.

Two different types of nanopastes were prepared for both oxides. One, standard type for the screen printing application onto a glass substrates including sintering at 450 °C (metal-oxide, ethanol, water, acetylic acid, ethylcellulose[8]) and another paste type for low temperature application onto the plastic substrates (PET, with the curing temperature below 120 °C). In the latter case the powder nano-oxides were first homogenized in ethanol solution of Ru-dye (0.4 mM of standard dye-sensitizer, N3, Aldrich) and later, after oxide colorization and ethanol evaporation, in butanol (1 g of oxide into 1 ml).

The prepared standard pastes were applied by screen printing onto the FTO-glass and sintered (450 °C, 30 min, resulting in thickness of 1.5 μm). The Ru-dye was adsorbed into the sintered mesoporous structure of oxide layers from dye-ethanol solution. Low temperature pastes (already

colored) were applied onto ITO/PET substrate by doctor blade in thickness of about 50 μm and cured 30 min at 120 °C.

To prevent the internal short currents[1,3] of final solar cells, onto some substrates the very thin blocking (barrier) layer was deposited before oxide layers application described above. The blocking layers were deposited by sol-gel technique, e.g. by the simple dip coating applying the sol of 1 % TiO_2 (Ti-tetrabutoxide in ethanol, stabilized by HNO_3, the draw up rate was 10 cm min^{-1})[6]. To increase the electric conductivity without sintering, the sol-gel (SG) layers were treated by UV light (250 W Hg lamp) or by dielectric barrier discharge plasma (10 kHz, 2 W cm^{-2}) at atmospheric pressure in air.

The solar cells were finalized by contacting (face to face) the prepared oxide electrode on PET (or glass) and the Pt counterelectrode on FTO/glass substrate after dropping an iodine electrolyte into the oxide layer between. (Pt layer was created by doctor blading of nano-Pt paste, Solaronix, and sintering at 450 °C). The active area of the cells was 1.5 cm^2.

Afterwards, the solar cells were characterized measuring the photocurrent and cell voltage depending on the circuit loading (I–V loading curve[1]) under the standard day-light illumination (1 sun) 100 mW cm^{-2} (AM1.5, metal halide lamp box) by multimeters Keithley 2000 and Metex M-3650D.

UV-Vis absorption and AC conductivities (10 kHz) of sol-gel layers were measured by spectrometer CECIL 3055 and by LCR Digibridge Quadtech 1715, respectively. The surface nano-texture of the layers were studied by atomic force microscopy, Veeco, CP II.

Results and discussion

The photocurrent – voltage dependence of the standard composition of screen printed DSSC (sintered TiO_2 on FTO-glass, Fig. 1) had a standard shape and the photocurrent was significantly increased after incorporating the sol-gel (SG) layer. The solar cell efficiency had increased 2 times (from 0.7 to 1.4 %). However, when applying the oxide layers onto PET substrates, the photocurrents strongly decrease due to the worse contacts between nonsintered nanoparticles and more due to the low conductivity of sol-gel layers. The thickness and the specific resistivity of the coated non-treated SG layers were 20 nm and 20 kΩm. So the resistivity of active area, 1.5 cm^2, of the SG layer was just 3 Ω. (The specific resistivity of the crystalline anatase phase of TiO_2 is referred to round 0.1 Ωm.)

The plasma or UV treatment of the SG layers had practically no effect on the solar cell performance, while the resistivity of the treated layers decreased to 85 % 75 % of the nontreated values, respectively.

Consequently, supposing the better interparticle contacts and lower sensitivity to thermic treatment in ZnO systems[3] the ZnO pastes were applied onto PET without and including TiO_2 sol-gel blocking layer (Fig. 2). The shape of I–V characteristic was similar for both ZnO and TiO_2 cells. However, the effect of SG layer presence was different. The plasma and UV treatment increased the photocurrents, especially in the UV case. The absorption of SG layers in UV-C region (Fig. 3) is very high, so some reconstruction of the amorphous and free volume rich SG layer can occur after strong exposition.

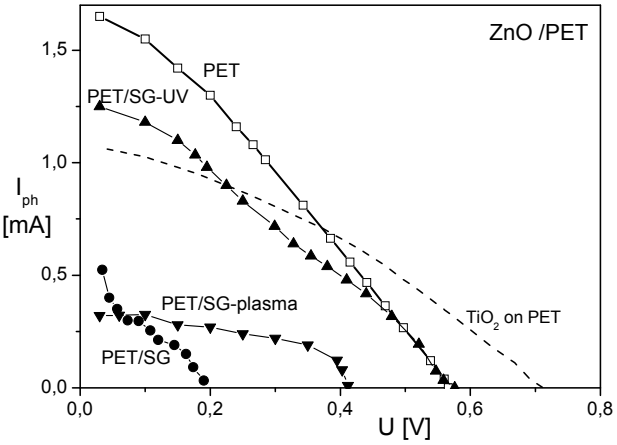

Fig. 2. **I-V loading curves of low temperature ZnO DSSC on PET substrates.** (TiO_2 for comparison.) SG denotes the presence of sol-gel layer, plasma (20 sec) and UV the treatment (10 min) manner of the SG layers

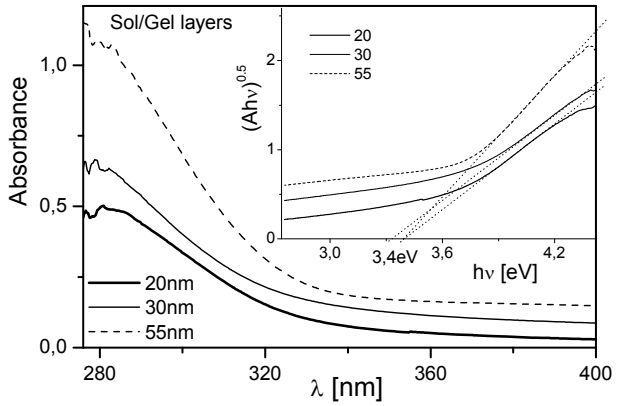

Fig. 3. **Absorption spectra and optical gap (inlet) of sol-gel layers with different thickness.** Optical gap is higher than the gap of anatase (3.2 eV). The thinnest (20 nm) SG layer was chosen for all experiments above

There is a chance that in the case of compact but much thinner SG layers the photocurrent would increases. The compactness and the texture on nano-level can be seen in AFM images (Fig. 4). The root mean square roughness of the base ITO layer (1.3 nm) is similar to that of SG layers (1.1 nm), but the texture is different. Above the microscale, the prepared xerogel layers were free of cracks and precipitates.

Conclusions

Mesoporous TiO_2 and ZnO photoactive electrodes of DSSC solar cells were prepared on PET and glass substrates by screen printing and doctor blade technique. Considerable enhancement of solar cell efficiency by sol gel blocking sublayer found in the case of sintered oxide photolayers did not occur in the case of low temperature process on PET substrates. The better performance of ZnO layers in

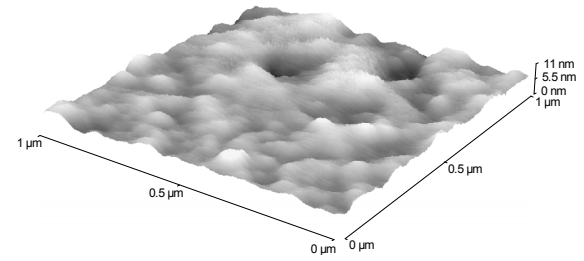

ITO on PET

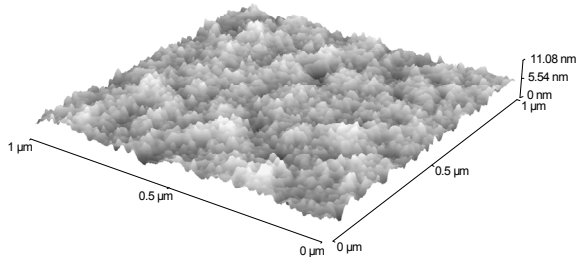

SG (20nm) on ITO

Fig. 4. **Surface topography of ITO and sol-gel/ITO layers on PET.** (AFM microscopy, tapping mode)

coincidence with TiO_2 sol-gel layers were confirmed, namely in cooperation with some reconstruction of a very thin sol-gel layer by UV light.

This work was supported by the Slovak Research and Development Agency under the contract No. APVV-0324-10", by the Slovak Grant Agency (project VEGA 1/0818/13) and by the OP Research and Development of the project National Centrum of Research and Application of Renewable Sources of Energy, ITMS 26240120016, co-financed by the Fund of European Regional Development

REFERENCES

1. Pagliaro M., Palmisano G., Ciriminna R.: *Flexible solar cells*, Wiley-VCH, Weinheim 2008.
2. Wei D.: Int. J. Mol. Sci. *11*, 1103 (2010).
3. Wang B., Kerr L. L.: Solar Energy Materials and Solar Cells *95*, 2531 (2011).
4. Mane R. S., Lee W. J., Pathan H. M., Han S. H.: J. Phys. Chem. B *109*, 24254 (2005).
5. Jiang C. Y., Koh W. L., Leung M. Y., Chyam S. Y., Wu J. S., Zhang J.: Appl. Phys. Lett. *100*, 113901 (2012).
6. Šandrej M., Mikula M., Gemeiner P.: Chem. Listy *105*, s334 (2011).
7. Huang J., Ichinose I., Kunitake T., Nakao A.: Langmuir *18*, 9048 (2002).
8. Fan K., Liu M., Peng T., Ma L., Dai K.: Renewable Energy *35*, 555 (2010).

P-26
EFFECT OF SELECTED MODIFIERS ON PROCESSING STABILITY OF BIODEGRADABLE POLYMERS

MIROSLAVA MIKUŠOVÁ, PAVOL ALEXY, KATARÍNA TOMANOVÁ, RODERIK PLAVEC, MICHAL MIHALÍK, JÁN BOČKAJ, and ZUZANA VANOVČANOVÁ

Institute of Polymer Materials, Faculty of Chemical and Food Technology, Slovak University of Technology, Radlinského 9, 812 37 Bratislava, Slovak Republic
miroslava.mikusova@stuba.sk

Introduction

Polymer materials with a range of excellent mechanical properties, low density, durability and low cost, are widely used in the daily needs of contemporary society, ranging from simple packaging to heavy construction, and play important role in the improvement and quality of life. However, due to their persistence in the environment, polymer materials represent a danger to our ecosystems. However, economic growth results in an increase in the amount of waste generated over the past decades. Plastic waste has become an environmental problem of growing concern in the world. It is expected that during the beginning of the 21 st century there will be two-to three-fold increases in plastics consumption, particularly due to growth in developing countries[1]. There are several manners how to solve problems with polymeric waste, including material recycling as well as energetic recycling. In the modern age, only reduction or elimination of plastic waste is not sufficient way to solve the ecological problems connected with production, processing and application of polymeric materials. Sources of raw materials for polymer production represent separate problem[2].

One possibility how to solve these problems can be production of biodegradable polymers. On the basis of origin, biodegradable polymers are derived from renewable and petrochemical resources. There are three principal ways to produce polymers from renewable resources, i.e. bio-based polymers, i.e.: (1) to make use of natural polymers which may be modified but remain intact to a large extent (e.g. starch polymers), (2) to produce bio-based monomers by fermentation which are then polymerized (e.g. polylactic acid), (3) to produce bio-based polymers directly in microorganisms or in genetically modified crops (polyhydroxyalkanoates, bacterial cellulose)[3]. Biodegradable polymers from petroleum sources comprise: (1) aliphatic polyesters and copolyesters (e.g. poly(butylenes succinate), poly(butylenes succinate adipate), (2) aromatic copolyesters (e.g. poly(butylenes adipate terephthalate), (3) poly(ε-caprolactone), (4) polyesteramides, (5) polyvinyl alcohol)[1].

On the other hand, these materials usually caused problems during processing, because of their partial sensitivity to thermal degradation which leads to lower mechanical properties. The possibilities how to solve mentioned problems can be found in modification of these polymers by addition of large variety of modifiers, plasticizers or by blending of two or more polymers together.

In this work modification of PLA, PHB and PCL was studied. Two types of styrene-acrylate copolymers containing epoxy groups were used as modifiers. The aim of our work was to study the influence of modifier on the processing stability of biodegradable polymers.

Materials and methods

Polylactic acid (PLA 4042D) from NatureWorks, LLC, USA was used as a biodegradable polymer produced by chemical synthesis from monomers of native renewable resources, Polyhydroxybutyrate (PHB) from Biomer, Germany was used as biodegradable polymer which is produced directly in microorganisms or in genetically modified crops, Poly(ε-caprolactone) (PCL) was used as synthetic biodegradable polymer and Joncryl ADR-4368 and Joncryl ADR-4300S from BASF, Asia were used as modifiers (styrene-acrylate copolymers containing epoxy groups).

Preparation of blends

The blends of biodegradable polymers and modifier with content of 2 %wt. were prepared using twin screw extruder with screw diameter 16 mm, L/D = 40 with three kneading zones, Labtech, Thailand.

Evaluation of processing stability of polymers

Processing stability of biodegradable polymers/modifier blends was measured by using oscillation rheometer RPA 2000 from Alpha Technologies. For this purpose, the timed test at constant strain 30° and constant frequency 60 cpm was used. Time periods of test was 20 min. Processing stability was evaluated from the dependency of relative values of complex viscosity vs. time. Relative values of complex viscosity were calculated according to the Eq. (*1*):

$$\eta^*_{rel(t)} = (\eta^* / \eta_0^*) - 1 \qquad (1)$$

where $\eta^*_{rel(t)}$ is relative value of complex viscosity, η^* is complex viscosity at time t, and η_0^* is complex viscosity at the start of test. Temperature of measurements for all tested polymers was kept constant at 210 °C.

Results and discussion

Processing stability of PLA, PHB and PCL was studied in oscillation rheometer RPA 2000. Possible stabilization effect of biodegradable polymers modified with styrene-acrylate copolymer containing epoxy groups (Joncryl ADR-4368 and Joncryl ADR-4300S) during melt processing was studied. The dependencies of relative values of complex viscosity vs time during the timed test for PLA/modifiers, PHB/modifiers and PCL/modifiers are shown in Fig. 1–3.

From Fig. 1 it can be seen, that addition of Joncryls does not influence the viscosity of PCL because PCL has good thermal stability at tested temperature.

In case of polylactic acid (Fig. 2), it is possible to observe, that Joncryls are able to significantly improve processing stability of PLA during its melt processing. From the curves of relative values of complex viscosity vs. time the maximums can be clearly observed. Effectiveness of Joncryls as modifiers depends on concentration of epoxy groups on polymer chain (in case of Joncryl ADR-4368 it is higher). Observed maximums can be apparently related with two

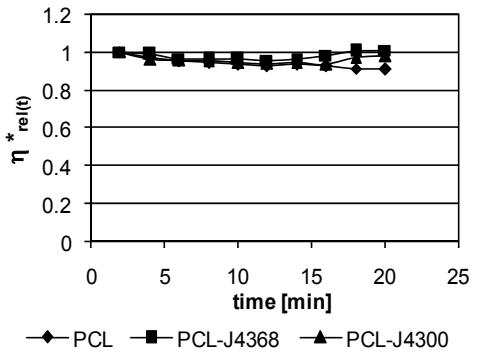

Fig. 1. **Effect of Joncryls on thermal degradation of PCL during the timed test at 210 °C**

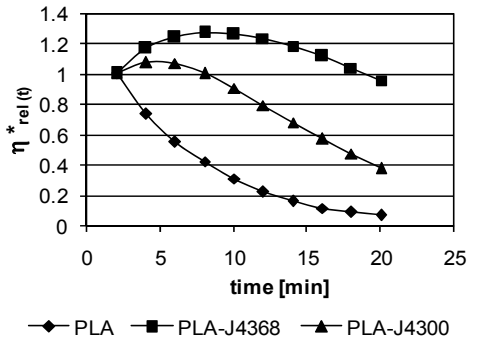

Fig. 2. **Effect of Joncryls on thermal degradation of PLA during the timed test at 210 °C**

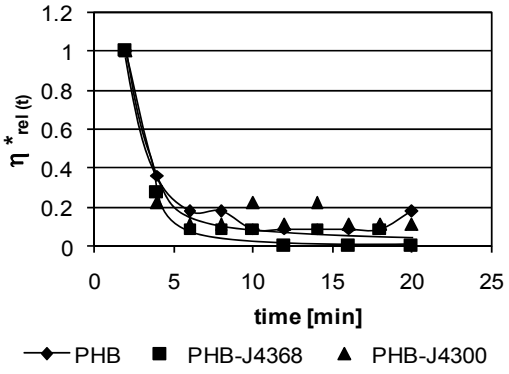

Fig. 3. **Effect of Joncryls on thermal degradation of PHB during the timed test at 210 °C**

contrary actions – degradation of PLA which leads to decreasing of molecular weight and subsequent reaction of polyester fragments with epoxy groups of modifier which leads to increasing of molecular weight. Viscosity of PLA melt is increased if there is sufficient number of epoxy groups able to react with final groups of degraded polyesters in system. Influence of degradation on increasing molecular weight is eliminated and in case of connecting several fragments through one ´s molecule of modifier is possible increasing molecular weight above original value of polyester. Increasing viscosity is connected with increasing molecular weight. This was confirmed by determination of intrinsic viscosity of prepared samples of PLA without and with addition of modifiers by using Ubbelohde capillary viscometer. Viscosity of polyester was decreasing as a function of decreasing concentration of epoxy groups of modifiers in studied systems during degradation.

From Fig. 3 it can be seen, that from tested biodegradable polymers, PHB is the most sensitive to thermal degradation. Effect of Joncryls on PHB is not strong enough, probably due to much higher rate of degradation of PHB. It is possible to suppose that rate of PHB degradation is such high because epoxy groups of modifiers are spent in first stages of thermal loading. From obtained results, it can concluded that Joncryls can eliminate negative effect of degradation, i.e. decreasing values of viscosity of melt as well as drop of molecular weight of polyesters.

Conclusion

Results obtained in this work show how to improve processing stability of biodegradable polymers. From the results it is obvious that epoxided styrene-acrylate copolymers improve processing stability of biodegradable polymers. The effectiveness of Joncryls depends on concentration of epoxy groups on polymer chain.

This work is supported by Norwegian Financial Mechanism, Financial Mechanism of EEA and State budget of Slovakia.

REFERENCES

1. Rudnik E.: Compostable polymer material (2008).
2. Alexy P., Bugaj P., Feranc J., Pavlačková M., Tomanová K., Benovič F., Plavec R., Mihalík M., Botošová M.: Chem. Listy *105*, s241 (2011).
3. Yu L., Dean K., Li L.: Prog. Polym. Sci. *31*, 576 (2006).

P-27
PROPERTIES OF LDPE AFTER RADIATION CROSS-LINKING

ALES MIZERA, MIROSLAV MANAS, DAVID MANAS, MICHAL DANEK, JAN NAVRATIL, and MARTIN BEDNARIK

Tomas Bata University in Zlín, nám. TGM 5555, 760 01 Zlín, Czech Republic
mizera@ft.utb.cz

Abstract

Radiation processing involves the use of natural or manmade sources of high energy radiation on an industrial scale. The principle of radiation processing is the ability of high energy radiation to produce reactive cations, anions and free radicals in materials. The industrial applications of the radiation processing of plastics and composites include polymerization, cross-linking, degradation and grafting. Radiation processing mainly involves the use of either electron beams from electron accelerators or gamma radiation from Cobalt-60 sources. The low density polyethylene (LDPE) tested showed significant changes of temperature stability and mechanical properties after irradiation. From this point-of-view, new applications could also be seen in areas with service temperatures higher than their former melting point. The comparison of the temperature stability and mechanical properties of irradiated and non irradiated LDPE is presented in this paper.

Introduction

Polymers belong to constructive materials which find use at the most industry branches. The advantage is a low weight together with the excellent mechanical properties, very good chemical resistance and other properties, which assign them for various applications. Disadvantage is mainly low temperature stability which significantly reduces usage of these polymers.

Every properties improvement especially temperature stability helps to increase application possibilities. In addition, properties modification of standard polymers, which are relatively cheap products, gives them advantage for another usage. One of the possibilities of polymers properties improvement is their radiation cross-linking.

The irradiation cross-linking of thermoplastic materials via electron beam or cobalt 60 (gamma rays) is performed separately, after processing. Generally, ionizing radiation includes accelerated electrons, gamma rays and X-rays. Radiation processing with an electron beam offers several distinct advantages when compared with other radiation sources, particularly γ-rays and x-rays. The process is very fast, clean and can be controlled with much precision. There is no permanent radioactivity since the machine can be switched off. In contrast to γ-rays and x-rays, the electron beam can be steered relatively easily, thus allowing irradiation of a variety of physical shapes. The electron beam radiation process is practically free of waste products and therefore is no serious environmental hazard. The main

difference between beta and gamma rays is in their different abilities to penetrate the irradiated material. Gamma rays have a high penetration capacity. The penetration capacity of electron rays depends on the energy of the accelerated electrons. Due to electron accelerators, the required dosage can be applied within seconds, whereas several hours are required in the gamma radiation plant[1,2].

Irradiation of polyolefins, particularly the family of polyethylenes, represents an important segment of the radiation processing. Polyolefins can be irradiated in many forms, such as pellets and powder, films, extruded and molded parts or as wire and cable insulation[1].

Radiation cross-linking usually improves strength, reduces creep, contributes to chemical resistance improvement and in many cases improves tribological properties. Effect of radiation cross-linking significantly improves temperature stability. Because of that, materials which belong to group of standard polymers can be used in applications, which would be in term of temperature stability intended only to constructive thermoplastic polymers.

Material

As the basic polymer material was used Low Density Polyethylene (LDPE 780E) made in DOW Chemical Company. An ARBURG Allrounder 420C Advance Injection molding machine was used for sample preparation, with the processing conditional to comply with the LDPE producer's recommendations. Irradiation of tested LDPE polymer was performed with the kind help of BGS Germany, in the BGS Wiehl plant using accelerated electrons with a dosage range of 0 to 198 kGy. The mechanical properties and the thermal stability of non-irradiated and irradiated low density polyethylene were tested after irradiation.

Methods

Firstly, was determined the degree of cross-linking by gel measurements (gel content), according to the standard EN ISO 579. Then the mechanical properties were measured. Tensile test was carried out on tensile machine ZWICK 1456, according to standard CSN EN ISO 527-1, 527-2. Used rate: 50mm/min. Test data was processed by Test Expert Standard software and modulus (E [MPa]) and tensile stress (σ_t [MPa]) were determined. The shape and the dimensions of the testing samples were in accord with the CSN 621431 standard. Lastly were measured the thermo-mechanical properties and the temperature stability. Perkin – Elmer Thermal Analyser TMA7 was used for the thermo-mechanical analysis; heated from 50 °C to 250 °C at 20 °C min^{-1}, hold for 1 min at 50 °C. The temperature stability was determined by visual observation in the temperature chamber.

Results and discussion

The gel content, mechanical and thermal behaviour of low density polyethylene (LDPE), before and after irradiation, was studied. For easy of evaluation of the measured data reasons, and the comparison of the irradiated polymer with a non-irradiated one, dimensionless values (–) were used in some cases. The property of the non-irradiated polymer had the dimensionless value of 1, while others were expressed as the ratio of measured property of irradiated polymers to the same property of non-irradiated polymer.

After performing the tensile test at ambient (23 °C) and elevated (100 °C) temperature the observed parameters (tensile strength and E-modulus) were compared. As can be seen from Fig. 1, there was a significant growth of the tensile strength with increasing doses of irradiation for both temperatures. At 23 °C it was just a steady increase, but at 100 °C it was a dramatic one. At 23 °C the tensile strength rises by 10% after irradiation with a dosage of 198 kGy, but at 100 °C the tensile strength rises by 60 % after the same irradiation.

In the Fig. 2 it is possible to see comparison of LDPE E-modulus in percentage at the ambient temperature and 100 °C.

The E-modulus rises more than 20 % after irradiation with a dosage of 198 kGy at 23 °C but at 100 °C the E-modulus rises only by 8 % after the same irradiation.

Fig. 3 shows effect of LDPE irradiation on the thermo-mechanical properties. As can be seen already small dose of radiation (up to 33 kGy) move the softening point up to 140 °C. LDPE irradiated by the dose of 198 kGy evince the significant improvement of the temperature stability. There is 20 % spike

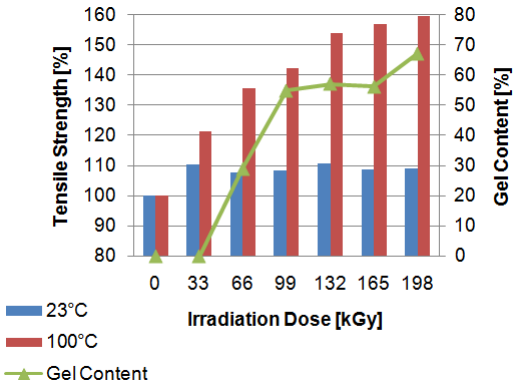

Fig. 1. **Comparison of LDPE Tensile Strength**

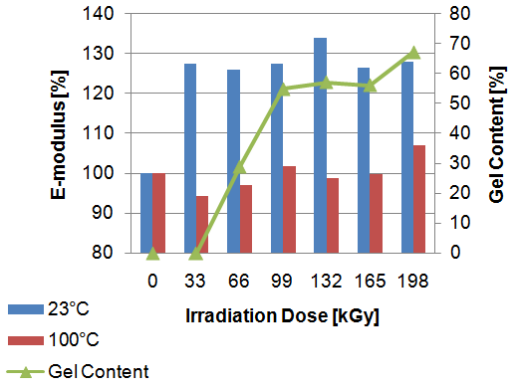

Fig. 2. **Comparison of LDPE E-modulus**

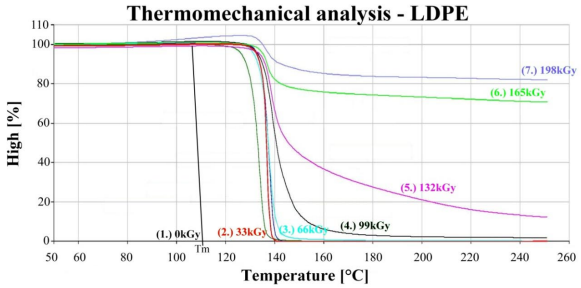

Fig. 3. **LDPE Thermo-mechanical Analysis**

penetration into LDPE radiated by dose of 198 kGy at 220 °C.

The visual observation of sample behavior at the temperature is given in Fig. 4. Specimens are fitted horizontally in the temperature chamber and loaded by the bending moment both form its own weight and the weight on the end of specimen. As can be seen the higher irradiation dosage, the better temperature stability of these polymers is. The tested specimens remained without dimensional changes at the higher temperatures after irradiation. The same specimen, at higher temperatures, creates changes of colour and surface due to thermal oxidation – but its dimension/ cross-section remains without change. Their better temperature stability make possible to use the studied selected polymers even at service temperatures higher than their former melting point.

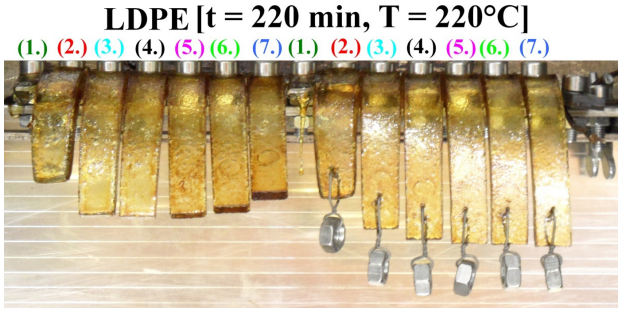

Fig. 4. **LDPE Specimen Deformation at 220 °C** (1. non-irradiated, 2. 33 kGy, 3. 66 kGy, 4. 99 kGy, 5. 132 kGy, 6. 165 kGy and 7. 198 kGy)

Conclusion

As can be seen from the tests results, the irradiation cross-linking improves the LDPE mechanical properties. The improvement is more considerable in case of higher temperature (100 °C), as a consequence of creation of cross-link (during irradiation cross-linking) resulting in protraction of macromolecular chain, which is thus more flexible during thermal load than individual shorter macromolecular chains.

Irradiation improves the thermal properties of polymer. Tested polymer (LDPE) shows better temperature stability after irradiation. Irradiation significantly extends the application area of polymers. The service temperature can be higher than the melting point of not irradiated polymers.

This paper is supported by the internal grant of TBU in Zlin No. IGA/FT/2013/020 funded from the resources of specific university research and by the European Regional Development Fund under the project CEBIA-Tech No. CZ.1.05/2.1.00/03.0089.

REFERENCES

1. Drobny J. G.: *Radiation Technology for Polymers*, Boca Raton, CRC Press 2003.
2. BGS – Beta Gama Service. [online]. www: <http://bgs.eu>.
3. Brocka Z., *Werkstoff- und Einsatzpotential strahlenvernetzter Thermoplaste,* Lehrsthul für Kunststofftechnik (LKT), Nürnberg 2008.
4. Woods R. J.: *Applied radiation chemistry: radiation processing,* A Wiley-Interscience publication, New York, 1994.
5. Manas M., Stanek M., Manas D., at all: Chem. Listy *105*, s254 (2011).
6. M. Manas, et al.: Chem. Listy *103*, s24, (2009).
7. A. Mizera, et al.: International Journal of Mathematics and Computers in Simulation *6*, 584 (2012).
8. A. Mizera, et al.: International Journal of Mathematics and Computers in Simulation *6*, 592 (2012).
9. Navratil J. et al.: Recent Researches in Circuits and Systems – *Proceedings of the 16th WSEAS International Conference on Circuits/Systems*, pp. 273–278 (2012).
10. Navratil J. et al.: Plasty a Kaučuk – Special 49, pp. 24–26 (2012).

P-28
TEMPERATURE STABILITY OF MODIFIED TPE-E BY RADIATION CROSS-LINKING

ALES MIZERA, MIROSLAV MANAS, DAVID MANAS, KAMIL KYAS, JAN NAVRATIL, and MARTIN BEDNARIK

Tomas Bata University in Zlín, nám. TGM 5555, 760 01 Zlín, Czech Republic
mizera@ft.utb.cz

Abstract

Radiation processing involves the use of natural or manmade sources of high energy radiation on an industrial scale. The principle of radiation processing is the ability of high energy radiation to produce reactive cations, anions and free radicals in materials. The industrial applications of the radiation processing of plastics and composites include polymerization, cross-linking, degradation and grafting. Radiation processing mainly involves the use of either electron beams from electron accelerators or gamma radiation from Cobalt-60 sources. The thermo-plastic elastomer (TPE-E) tested showed significant changes of temperature stability and mechanical properties after irradiation. From this point-of-view, new applications could also be seen in areas with service temperatures higher than their former melting point. The comparison of the temperature stability and mechanical

properties of irradiated and non irradiated TPE-E is presented in this paper.

Introduction

The cross-linking of rubbers and thermoplastic polymers is a well-proven process for the improvement of thermal properties. The chemical cross-linking or rubber vulcanization is normally induced by the effect of heating after processing with the presence of a curing agent. The cross-linking process for thermosets is very similar. In thermosets, the polymer molecules are also chemically linked due to heat after processing. Cross-linked rubbers have a wide-meshed molecular network that keeps them soft and their properties change only slightly on a wide temperature scale. On the other hand, thermosets are characterized by a very narrow-meshed network. Due to this fact, they hardly change their high level of stiffness on a wide temperature scale at all. The irradiation cross-linking of thermoplastic materials via electron beam or cobalt 60 (gamma rays) is performed separately, after processing. Generally, ionizing radiation includes accelerated electrons, gamma rays and X-rays[1].

Radiation processing with an electron beam offers several distinct advantages when compared with other radiation sources, particularly γ-rays and x-rays. The process is very fast, clean and can be controlled with much precision. There is no permanent radioactivity since the machine can be switched off. In contrast to γ-rays and x-rays, the electron beam can be steered relatively easily, thus allowing irradiation of a variety of physical shapes. The electron beam radiation process is practically free of waste products and therefore is no serious environmental hazard. The main difference between beta and gamma rays is in their different abilities to penetrate the irradiated material. Gamma rays have a high penetration capacity. The penetration capacity of electron rays depends on the energy of the accelerated electrons. Due to electron accelerators, the required dosage can be applied within seconds, whereas several hours are required in the gamma radiation plant[1,2].

The thermoplastics which are used for the production of various types of products have very different properties. The special group of polymers which exhibit elastic behaviour similar to that of a vulcanised conventional elastomer and which can be processed as thermoplastics (i.e. by melt processing) are called Thermo-Plastic Elastomers (TPEs). Most thermoplastic elastomers are essentially phase-separated systems. Usually, one phase is hard and solid at ambient temperature, whereas the other is an elastomer. Often, the phases are bonded chemically by block or graft polymerisation. In other cases, a fine dispersion of the phases is apparently sufficient. The hard phase gives these TPEs their strength and represents physical crosslinking. Without it, the elastomer phase would be free to flow under stress and the polymer would be practically unusable. On the other hand, the elastomer phase provides flexibility and elasticity to the system. When the hard phase is melted, the material can flow and be processed by the usual processing methods. Upon cooling, the hard phase solidifies and the material regains its strength and elasticity[3].

Radiation cross-linking usually improves strength, reduces creep, contributes to chemical resistance improvement and in many cases improves tribological properties. Effect of radiation cross-linking significantly improves temperature stability. Because of that, materials which belong to group of standard polymers can be used in applications, which would be in term of temperature stability intended only to constructive thermoplastic polymers.

Material

As the basic polymer material was used thermo-plastic elastomer (V-PTS-UNIFLEX-E25D/M*M800/20 natur) made in PTS Company. An ARBURG Allrounder 420C Advance Injection molding machine was used for sample preparation, with the processing conditional to comply with the TPE-E producer's recommendations. Irradiation of tested TPE-E polymer was performed with the kind help of BGS Germany, in the BGS Wiehl plant using accelerated electrons with a dosage range of 0 to 198 kGy. The mechanical properties and the thermal stability of non-irradiated and irradiated TPE-E were tested after irradiation.

Methods

Firstly, was determined the degree of cross-linking by gel measurements (gel content), according to the standard EN ISO 579. Then the mechanical properties were measured. Tensile test was carried out on tensile machine T 2000 Alpha Technologies, according to standard CSN ISO 37. Used rate: 500mm/min. Test data was processed by Test Expert Standard software and modulus (E [MPa]) and tensile stress (σ_t [MPa]) were determined. The shape and the dimensions of the testing samples were in accord with the CSN 621431 standard. Lastly were measured the thermo-mechanical properties, the temperature stability and 3D surface scan. Perkin – Elmer Thermal Analyser TMA7 was used for the thermo-mechanical analysis; heated from 50 °C to 400 °C at 20 °C min^{-1}, hold for 1 min at 50 °C. The temperature stability was determined by visual observation in the temperature chamber. 3D surface scan was obtained by Taylor Hobson Talysurf CLI 500.

Results and discussion

The gel content, mechanical and thermal behaviour of thermo-plastic elastomer (TPE-E), before and after irradiation, was studied. For easy of evaluation of the measured data reasons, and the comparison of the irradiated polymer with a non-irradiated one, dimensionless values (–) were used in some cases. The property of the non-irradiated polymer had the dimensionless value of 1, while others were expressed as the ratio of measured property of irradiated polymers to the same property of non-irradiated polymer.

After performing the tensile test at ambient (23 °C) temperature the observed parameters (tensile strength and elongation) were compared. As can be seen from Fig. 1, the tensile strength rises more than 35 % after irradiation with a dosage of 66 kGy. Although the gel content rises with the dose of irradiation, the tensile strength goes down with dosages higher than 66 kGy. Then, with a dosage of 132 kGy and higher, the value of the tensile strength oscillates around the value of the non-irradiated polymer. Elongation of the

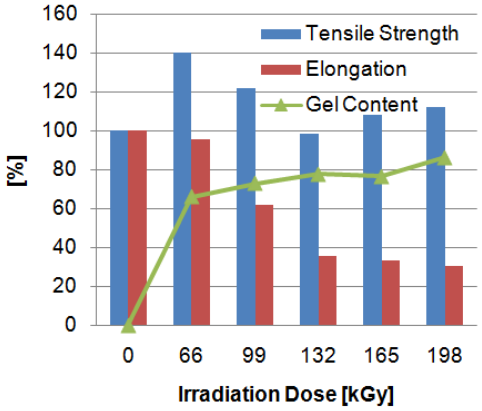

Fig. 1. **Comparison of TPE-E Mechanical Properties with Gel Content**

TPE-E goes down continually in line with the irradiation dosage. At the highest applied dosage of irradiation (i.e. 198 kGy), the elongation is only 25 % of the former (non-irradiated) polymer. Due to irradiation, the TPE-E studied significantly loses its flexibility.

Fig. 2 shows effect of TPE-E irradiation on the thermo-mechanical properties. As can be seen already small dose of radiation (up to 33 kGy) move the softening point up to 210 °C. TPE-E irradiated by the dose of 198 kGy evinces the significant improvement of the temperature stability. Irradiation TPE-E with the dose 198 kGy holds temperature stability up to 360 °C for short time.

The visual observation of sample behavior at the temperature is given in Fig. 3. Specimens are fitted horizontally in the temperature chamber and loaded by the bending moment both form its own weight and the weight on the end of specimen. As can be seen the higher irradiation dosage, the better temperature stability of these polymers is. The tested specimens remained without dimensional changes at the higher temperatures after irradiation. The same specimen, at higher temperatures, creates changes of colour and surface due to thermal oxidation – but its dimension/ cross-section remains without change. Their better temperature stability make possible to use the studied selected polymers even at service temperatures higher than their former melting point.

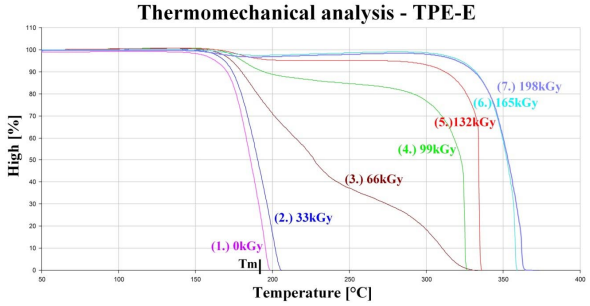

Fig. 2. **TPE-E Thermo-mechanical Analysis**

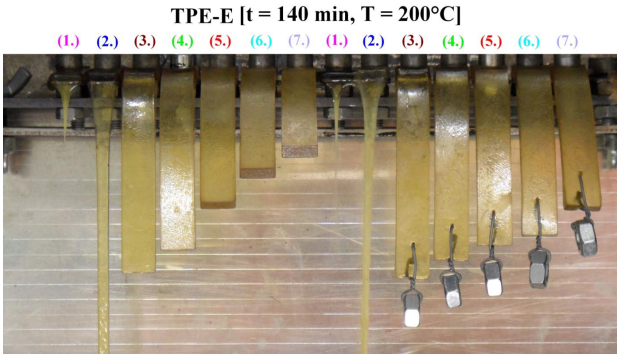

Fig. 3. **TPE-E Specimen Deformation at 200 °C** (1. non-irradiated, 2. 33 kGy, 3. 66 kGy, 4. 99 kGy, 5. 132 kGy, 6. 165 kGy and 7. 198 kGy)

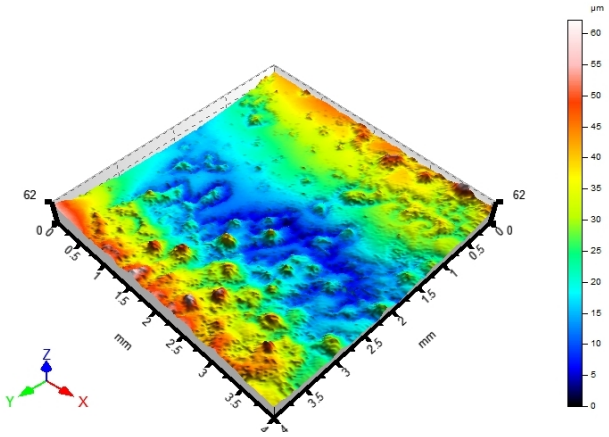

Fig. 4. **TPE-E 3D Surface Scan after 60 minutes at 200 °C**

In the Fig. 4 as can be seen 3D surface scan of irradiated TPE-E specimen with the dosage of 66 kGy after sixty minutes at 200 °C.

Conclusion

The results of the measurements of TPE-E after irradiation showed significant changes of its mechanical and thermo-mechanical properties. The tensile strength rises by 35 %, after irradiation with a dosage of 66 kGy. Elongation decreases gradually, with the dosage of irradiation. The lowest value of elongation was registred after irradiation by a dose of 198 kGy and reached only 25 % of elongation of a non-irradiated polymer.

Irradiation improves the thermal properties of polymer. Tested polymer (TPE-E) shows better temperature stability after irradiation. Irradiation significantly extends the application area of polymers. The service temperature can be higher than the melting point of not irradiated polymers.

This paper is supported by the internal grant of TBU in Zlin No. IGA/FT/2013/020 funded from the resources of specific university research and by the European Regional

Development Fund under the project CEBIA-Tech No. CZ.1.05/2.1.00/03.0089.

REFERENCES

1. Drobny J. G., *Radiation Technology for Polymers*, CRC Press, Boca Raton 2003.
2. BGS – Beta Gama Service. [online]. www: <http://bgs.eu>.
3. Drobny J. G.: *Handbook of Thermoplastic Elastomers*, William Andrew Publishing, Norwich 2007.
4. Brocka Z.: *Werkstoff- und Einsatzpotential strahlenvernetzter Thermoplaste,* Lehrsthul für Kunststofftechnik (LKT), Nürnberg 2008.
5. Woods R. J.: *Applied radiation chemistry: radiation processing,* A Wiley-Interscience publication, New York 1994.
6. Manas M., Stanek M., Manas D., at all: Chem. Listy *105*, 254 (2011).
7. M. Manas, et al.: Chem. Listy *103*, 24 (2009).
8. A. Mizera, et al.: International Journal of Mathematics and Computers in Simulation *6*, 584 (2012).
9. A. Mizera, et al.: International Journal of Mathematics and Computers in Simulation *6*, 592 (2012).
10. Navratil J., et al.: Recent Researches in Circuits and Systems – *Proceedings of the 16th WSEAS International Conference on Circuits/Systems*, pp. 273–278 (2012).
11. Navratil J., et al.: Plasty a Kaučuk – Special 49, pp24–26 (2012).

P-29
RECYCLATION OF IRRADIATED HDPE – INFLUENCE ON MATERIAL HARDNESS

JAN NAVRATIL, MIROSLAV MANAS, MICHAL STANEK, MARTIN BEDNARIK, ALES MIZERA, and KAMIL KYAS

Tomas Bata University in Zlin, Department of Production Engineering, nam. T.G. Masaryka 275, 762 72 Zlin, Czech Republic
j1navratil@ft.utb.cz

Abstract

Main purpose of this paper is to investigate possible utilization of irradiated materials (products) after their service life. This paper deals with an idea of using them as fillers into non-irradiated ones, therefore a grit of irradiated high-density polyethylene (HDPE) pipes was used as filler into a non-irradiated low-density polyethylene (LDPE). Influence of this filler on resulting material hardness was investigated.

Introduction

Radiation technology related to polymer modification has been successfully implemented in industrial applications for more than 50 years[1–6,11–14]. It is well known that polymers which undergo radiation either degrade or crosslink[1–7]. Those which crosslink rather than degrade show significant improvement mainly in mechanical, thermal and chemical properties. Among these belongs polyethylene[11–15].

Materials

HDPE pipes were made of TIPELIN PS 380-30/302 which was supplied by Slovnaft Petrochemicals, Inc. These were furthermore irradiated by ionizing beta radiation (dose 165kGy, energy 10MeV) in BGS Beta-Gamma-Service GmbH & Co. KG and provided for recyclation after their service life. Supplier of pure LDPE was The Dow Chemical Company, type 780E.

Properties of these materials guaranteed by manufacturer are shown in Table I.

Methods

Experiment was carried out in several steps. Firstly supplied pipes had to be crushed into the grit (Fig. 1) in rotary cutter mill RAPID SK 2218, resulting particle size oscillated between 3 and 5 mm.

Next step was to mix these materials and create compounds. Those were mixed in several concentrations (from 10 to 60 % of filler) and injection molded in Arburg Allrounder 420C injection molding machine under same process parameters (only for the concentrations of 50 and 60 % had to be injection and holding pressure slightly increased due to worse flow properties). For comparison purposes only additional specimens were prepared. Those were made of the same HDPE as filler/pipes and half of them irradiated by the same radiation; however, they were made of raw non-recycled material. Specimens´ shape is shown in Fig. 2.

Table I
Basic material properties[8,9]

	HDPE	LDPE
MFR (190°C/5kg)	0.95 g/10 min	–
MFR (190°C/2.16kg)	–	20 g/10 min
Density	0.948 g/cm^3	0.923 g/cm^3
Tensile strength at yield	19 MPa	8.2 MPa
Shore D hardness	65	49

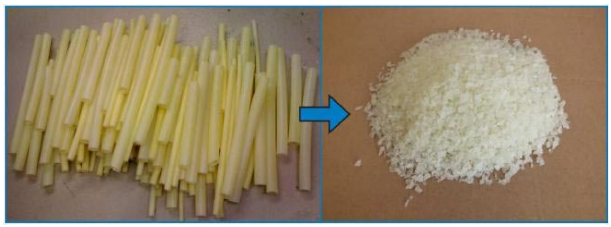

Fig. 1. **Crushed pipes**

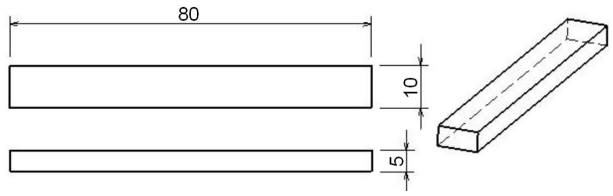

Fig. 2. **Shape and dimension of specimen**

Fig. 3. **AFFRI ART 13** (ref.[10])

Hardness of thus prepared specimens was measured on Shore D hardness tester OMAG AFFRI ART 13 (Fig. 3) according to ČSN EN ISO 868 standard at ambient conditions.

Results and discussion

Four types of materials were compared in this study (pure LDPE, LDPE with different filler concentration, pure HDPE and pure irradiated HDPE). Hardness of pure LDPE and HDPE is according to material datasheets; therefore chosen test method is satisfactory.

As can be seen from Fig. 4 irradiation has very limited influence on material hardness comparing non-irradiated and irradiated pure HDPE where it grown only by 2 %. However the most important finding is significant improvement in hardness when using recyclate of irradiated pipes as filler. This improvement grows gradually with increasing amount of filler up to 15 % (LDPE with 60 % of filler) comparing to pure LDPE. It might be caused by relatively high hardness of this filler which most probably remained unchanged even after service life; nevertheless, hardness of non-recycled HDPE was not achieved.

Conclusion

Possible method of recycling irradiated products after their service life was investigated in this paper. Irradiated HDPE pipes were crushed to grit and used as filler into pure LDPE. Results show that there is considerable increase in material hardness with raising amount of filler. Even though

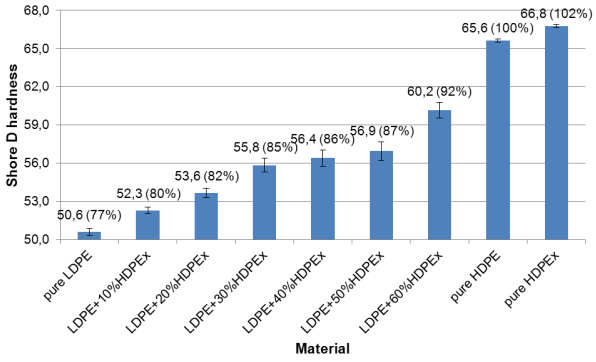

Fig. 4. **Shore D hardness comparison**

the hardness of original non-recycled HDPE was not achieved, positive effect on cheaper materials such as LDPE can be seen.

This finding might suggest possible utilization of irradiated products after their lifetime; however, further research is necessary.

This research paper is supported by the internal grant of TBU in Zlin No. IGA/FT/2013/020 funded from the resources of specific university research and by the European Regional Development Fund under the project CEBIA-Tech No. CZ.1.05/2.1.00/03.0089.

REFERENCES

1. Zimek Z., Przybytniak G., Nowicki A.: Radiat. Phys. Chem. *81*, 1398 (2012).
2. Bhatt S., Hoffman R.: *Antec Conference Proceedings* 2006 3, pp. 1540–1543 (2006).
3. Kerluke D. R., Cheng S.: *Antec Conference Proceedings* 2004 3, pp. 3738–3739 (2004).
4. Clough R. L.: Nucl. Instrum. Methods Phys. Res., Sect. B *185*, 8 (2001).
5. Mizera A., Manas M., Holik Z., Manas D., Stanek M., Cerny J., Bednarik M., Ovsik M.: Int. J. Math. Comput. Simulation *6*, 584 (2012).
6. Mizera A., Manas M., Holik Z., Manas D., Stanek M., Cerny J., Bednarik M., Ovsik M.: Int. J. Math. Comput. Simulation *6*, 592 (2012).
7. Gehring J., Zyball A.: Radiat. Phys. Chem. *46*, 931 (1995).
8. HDPE TIPELIN PS 380-30/302 Datasheet, Slovnaft.
9. LDPE DOW 780E Datasheet, Dow.
10. ART 13 [online], [cit. 2013-02-21], Available from http://www.affri.com/hardness_testers/plastic_materials.asp?id=73
11. Manas D., et al.: Thin Solid Films *530*, 49 (2013).
12. Manas D., Manas M., Stanek M., Danek M.: Arch. Mater. Sci. Eng. *32*, 69 (2008).
13. Ovsik M., Manas D., Manas M., Stanek M., Hribova M., Kocman K., Samek D.: Chem. Listy *106*, 507 (2012).
14. Navratil J., Stanek M., Sanda S., Manas M., Manas D.,

Mizera A., Bednarik M.: Recent Researches in Circuits and Systems – *Proceedings oft he 16th WSEAS International Conference on Circuits/Systems*, pp. 273–278 (2012).
15. Navratil J., Stanek M., Sanda S., Mizera A., Bednarik M., Kyas K., Cerny J.: Plasty a Kaučuk – Speciál *49*, pp. 24–26 (2012).

P-30
NEW POLYMER NANOFILLERS BASED ON MODIFIED FORMS OF ZEOLITE

DARINA ONDRUŠOVÁ, LENKA ŠPÁNIKOVÁ, SLÁVKA DOMČEKOVÁ, MARIANA PAJTÁŠOVÁ, MICHAELA ĎURČEKOVÁ, and EUGEN JÓNA

Faculty of Industrial Technologies in Puchov, TnUAD, I. Krasku 491/30, 020 01 Púchov, Slovakia
darina.ondrusova@fpt.tnuni.sk

The application of inorganic materials into organic polymers is one of the usual ways to improve up of physical and mechanical properties of polymers specifically hardness, tensile straight, module. Composite materials show generally better properties than pure and homogeneous materials. The positive changes have been observed at very low concentration of inorganic mineral component in polymers[1].

Natural zeolites form a group of aluminosilicate nanoporous materials with the special porous structure allowing lots of practical applications as an ion-exchange, adsorbent, material for reversible hydratation and dehydratation and also as ecological nanofiller in polymeric materials[1,2]. The best know type of zeolite is clinoptilolite. Its structure (Fig. 1) is based on treedimensional frameworks composed of tetrahedral SiO_4 and AlO_4 units, which are connected by shared oxygen atoms[2].

Porous structure of zeolites includes loosely bonded cations, often called exchangeable cations in the zeolite structure. The loosely bounded cations are easily replaceable in the contact of zeolites with solutions of ions. The exchange reaction between the zeolite and the ion solution is described as:

$$M_1(Z) + M_2(S) \leftrightarrow M_2(Z) + M_1(S) \quad (1)$$

where M_1 is an exchangeable cation present in zeolite and the M_2 is a saturated ion in solution S (ref.[3]).

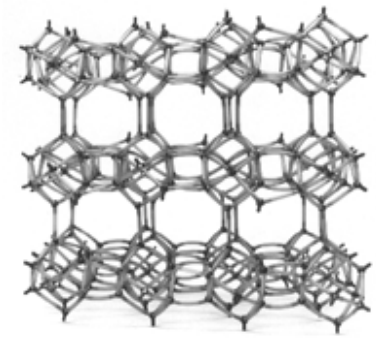

Fig. 1. **Structure of Zeolite - Clinoptilolite**

According to Grace M. Haggerty et al. organo-zeolites (Fig. 2) are zeolites, whose surface was modified with organic surface-active agents. These authors also propose to use that name for crystal materials, which have the inorganic skeleton of original zeolite and the covalent bounded organic part in the skeleton[4].

The present paper deals with the preparation of new mineral nanofillers on the base of monoionic and organic forms of natural zeolite – clinoptilolite and their utilization in the function of alternative mineral nanofillers in the rubber compounds. The modified forms of zeolite prepared have been added into rubber compounds to substitute the standard filler – carbon black[5]. The monoionic Co(II) form of zeolite has been prepared by the exchange reaction between natural zeolite – clinoptilolite and the Co(II) ion solution. In the preparation of organo-zeolite the powdered natural clinoptilolite has been saturated with the vapors of organic dithiophosphate accelerator. The prepared modified forms of zeolite were used in a function of mineral nanofillers in rubber compounds and commercially used filler – carbon black (N660) was used as a standard filler. The found values were compared to the values of standard rubber compounds containing the commercial filler – carbon black. Prepared mineral fillers have been applied into rubber compounds and the rheology, vulcanization performance and physical and mechanical properties of new prepared modified rubber compounds have been studied. The found values have been compared with the values of commercially used rubber compounds with the original composition. According to the obtained results it can be assumed that monoionic form Co(II) zeolite can be applied as environmentally friendly filler and organo-zeolite can be used as a filler with an additional accelerating effect for the application in the rubber compounds with the improving of physical and mechanical properties.

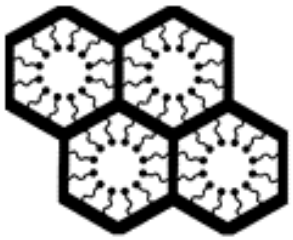

Fig. 2. **Schematic model of Organo-zeolite[5]**

The authors are grateful to the Slovak Grant Agency VEGA 1/0530/11 for financial support.

REFERENCES

1. Jesenák K.: Chem. Listy *101*, 657 (2007).
2. Šamajová E.: Z histórie výskumu zeolitových surovín Slovenska, *Seminár Prírodné a syntetické zeolity*, FCHPT STU, Bratislava 2003.
3. Ćurković L, Cerjan-Stefanović Š.: Water Res. *31*, 1379 (1997).

4. Maeda K, Mizukami F.: *Organozeolite materials and their properties.* In: Catalysis Surveys from Japan *3*, 119 (1999).
5. Ondrušová D., et al.: Hutnické Listy *2011*, 7.

P-31
IMPACT OF TECHNOLOGICAL ASPECTS ON EXTRUSION WIRE RUBBERISING QUALITY

LUBOSLAV TOMEK, PAVOL MELUS, and JAN ORAVEC

VIPO a.s., Gen. Svobodu 1069/4, 958 01 Partizánske, Slovak Republic
joravec@vipo.sk

Abstract

The influence of varying technological factors on the quality of wire rubberising were studied by technological trials carried out on a line for simultaneous winding of four rectangular multiwire (weft-less) beads for passenger cars. The bead winding line was equipped with rubberising extruder for 20 wires. During the trials various qualitative parameters of bead were recorded with respect to altering technological parameters, which were: rubber compounds (2 types), rubberising die-baffles (2 types), extrusion head pressure (2 levels), extrusion head temperature (2 levels) and line speed (four levels). The analyses of results suggest that the factor most significantly influencing the overall quality of bead wire rubberising is the rubberising die-baffle, or the geometrical design of extrusion head, respectively. The impacts of other technological factor considered seem to be far less important. This finding can be interpreted in such a way, that the rubber compounds and the range of extruder head pressures, extruder head temperatures and bead winding speeds used in the trials cover the area of optimum conditions of wire rubberising and the resulting bead quality strongly depends on the design of rubberising head.

Introduction

Tyre beads are rings of rubberised wire which hold the tyre on wheel rims[1]. In the manufacturing process the wire is rubberised in an extruder and then wound on a suitable former to form a ring of required dimension and cross-section. Two principal types of beads are used in tyres – single wire beads and multi-wire beads. A single-wire bead is made by winding a single wire on the former one turn next to the other until the bottom layer is wound. Then the winding continues with the next layer until the required number of layers is reached. A multi-wire bead is made of layers formed by several wires which are wound one on the top of the other until the required height of the wire is reached.

For the bead quality the process of wire rubberising is critical and to achieve satisfactory results requires the tuning of the composition of the rubber compound, wire coating, extruder head geometry and the temperature and pressure in the extruding head. This tuning is usually the most difficult part of putting a bead winding line to operation.

Having a possibility to carry out large-scale pre-production tests on a newly-built line for simultaneous winding of up to five rectangular multi-wire beads for passenger cars, an experiment was set up to identify relative importance of factors influencing the quality of produced beads.

Experimental

The bead winding line used was capable of producing beads with diameters 12–25 inches (330–610 mm) at the productivity of up to 5 beads with the diameter of 14 inches in 3.6 s. The wire rubberising extruder had the screw with the diameter 90 mm, pressure-regulated head with 20 inputs and a thermal control system.

During the trials four beads of were wound simultaneously at the following settings of technological parameters:

– line speed: 4 levels – 20 m min^{-1}, 40 m min^{-1}, 60 m min^{-1}, 80 m min^{-1}
– extrusion head pressure: 2 levels – 10 MPa, 20 MPa
– temperature: 2 levels – 80 °C, 100 °C
– rubber compounds: 2 levels – 1, 2
– rubberising die-baffles: 2 levels – 1, 2

Trials were carried out with bead diameters of 15, 16 and 17 inches. For each combination of technological parameters the production cycle was repeated five times. Altogether 3 840 beads were produced, 1 280 in each diameter. As the results found at different bead diameters were very similar, we will demonstrate general findings on 16-inch beads.

Of various quantitative and qualitative parameters of produced beads, the following set relates directly to the quality of wire rubberising:

– flawed rubber coat (Coat)
– burnt rubber (Burnt)
– dimensions out of tolerations (Dimensions)
– low weight (Weight)
– loose wires (Loose)

The presence or absence of respective bead fault was quantified by assigning the value of 1 if the fault was present and the value of 0 if the fault was not present.

Results and discussion

The quality of wire rubberising can be assessed according to the uniformity of bead weight – the more uniform bead weights are achieved, the better the rubberising quality, as the same amount of rubber was applied (the weight of wire itself remaining constant). The distribution of wire mass with respect to the numerical order in which respective beads were produced is illustrated in Fig. 1. Horizontal lines represent lower and upper toleration limits

As it follows from Fig. 1, the bead mass distribution became more uniform in the second half of the experiment, indicating that significant change in technological conditions then occurred, which was due to die-baffles alteration.

Fig. 2 illustrates the occurrence of faults with respect to the numerical order in which respective beads were produced.

As it follows from Fig. 2, beads with numerical orders in intervals 641–800, 921–1 120 and 1 161–1 280 were free of

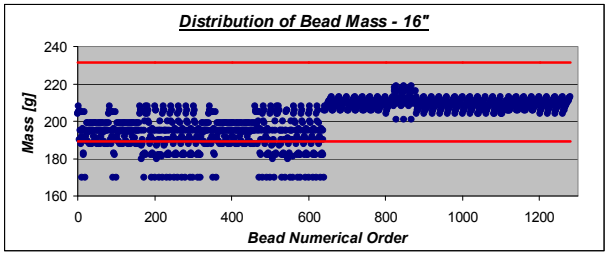

Fig. 1. **Distribution of bead mass with** respect to beads numerical order

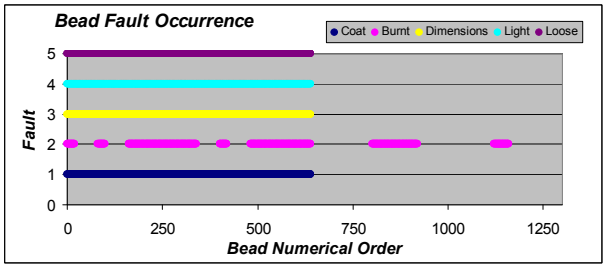

Fig. 2. **Occurrence of faults with respect to beads numerical order**

flaws. Fig. 2 also indicates that though the alteration of rubberising die-baffles in the second half of the experiment has a significant impact on bead quality, there are also other factors influencing the process of wire rubberising, as faulty beads occur even if the die-baffle has been altered.

To assess the importance of the impact of studied technological factors of the occurrence of bead flaws the method of Multiple Analysis of Variance was used[2]. The dependent variable was the sum of individual flaws occurred in a bead, i.e. Sum = 5 if all flaws are present, Sum = 0 if none flaw occurs, and the factors were line speed, extrusion head pressure, temperature, rubber compound and rubberising die-baffle. The respective ANOVA table is given in Tab. I.

The ANOVA analysis showed that all studied technological factors – line speed, extrusion head pressure, temperature, rubber compound and rubberising die-baffle – statistically significantly influence the quality of wire rubberising, though in widely varying extends. The extent of relative influence of studied technological factors on the quality of extrusion wire rubberising in bead winding is illustrated in Fig. 3

The most influential factor seems to be the type of rubberising die-baffle followed by extrusion temperature and line speed, while extrusion pressure and the type of rubber compound seem to have the least importance. A practical conclusion following from this finding is that it may be easier to improve the wire rubberising quality by experimenting with die baffles than by trying to develop a special coating rubber compound.

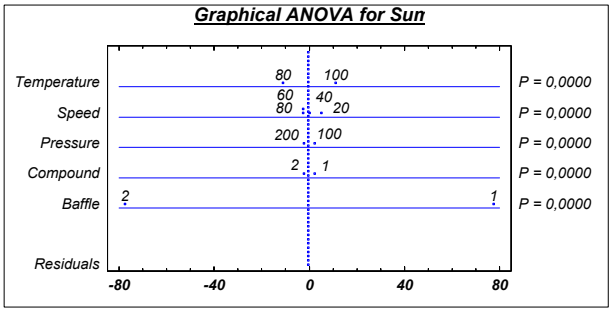

Fig. 3. **Relative influence of technological factors on the quality of wire rubberising**

Table I
ANOVA table for dependent variable Sum

Source	*Sum of Squares*	*Df*	*Mean Square*	*F-Ratio*	*P-Value*
MAIN EFFECTS					
A:Baffle	6125,0	1	6125,00	74 200,00	0,0000
B:Compound	5,0	1	5,00	60,57	0,0000
C:Pressure	5,0	1	5,00	60,57	0,0000
D:Speed	30,0	3	10,00	121,14	0,0000
E:Temperature	125,0	1	125,00	1 514,29	0,0000
RESIDUAL	105,0	1272	0,08		
TOTAL (CORRECTED)	6395,0	1279			

Conclusions

The analyses of results suggest that the factor most significantly influencing the overall quality of bead wire rubberising is the rubberising die-baffle, or the geometrical design of extrusion head, respectively.

The impacts of other technological factors considered seem to be less important. This finding can be interpreted, that the rubber compounds and the range of extruder head pressures, extruder head temperatures and bead winding speeds used in the trials cover the area of optimum conditions of wire rubberising and the resulting bead quality strongly depends on the design of rubberising head.

This publication was prepared as part of the project MŠSR-3933/2010-11 „Application of Knowledge-based Methods in Designing Manufacturing Systems and Materials – MANUSMAT" co-funded by the Ministry of Education, Science, Research and Sport of the Slovak Republic within the scheme constituted by Act No. 185/2009 Coll. "Research and Development Incentives".

REFERENCES

1. Mark J. E., Erman B., Eirich F. R.: *Science and Technology of Rubber*, Third Ed., Elsevier, Academic Press, London 2005.
2. Montgomery D. C., Runger G. C., Hubele N. F.: *Engineering Statistics*, Fifth Ed., J. Wiley, Hoboken 2011.

P-32
THE INFLUENCE OF ORGANOMODIFIED CLAY FILLERS AND COTTON WASTE ON PROPERTIES OF RUBBER COMPOUNDS

MARIANA PAJTÁŠOVÁ, DARINA ONDRUŠOVÁ, EUGEN JÓNA, ZUZANA JANKUROVÁ, KATARÍNA HOLCOVÁ, and SLÁVKA ĽALÍKOVÁ

Faculty of Industrial Technologies in Puchov, TnUAD, I. Krasku 491/30, 020 01 Púchov, Slovakia mariana.pajtasova@fpt.tnuni.sk

The organo-clays produced by treatment of clay minerals, (montmorillonite (Fig. 1)) with organics have a lot of applications in many fields of industry due to their high surface area, specific active sites and attractive adsorptive properties. Isomorphous substitutions of Si^{4+} cation by Al^{3+} cation in the tetrahedral layer and those of Al^{3+} cations by Mg^{2+}, Fe^{2+} etc. cations in the octahedral layer of the aluminosilicate structured clay minerals result in a negative charge which is balanced by the cations such as Na^{+}, K^{+}, Ca^{2+} etc. These substitutions and hydrated cations strongly give rise to hydrophilic nature of the clay surface. The surface modification is necessary for making natural clays suitable for specific adsorption and catalysis since they are not very effective by themselves in removal of hazardous compounds from water and soil environments. One of these modification processes is to insert the organic compound into the interlayer space of the clay minerals as a cationic species or a neutral molecule under certain conditions[1,2].

The different types of fillers were examined. These investigated non-conventional fillers included dry matter from fabric from waste recycling of tire (cotton waste), monoionic Ca^{2+} and Co^{2+} forms of clay mineral – montmorillonite and organo-modified clay fillers on the base thiazole accelerator of cure. The study of structural, spectral and thermal properties of organomodified clay products has shown, that studied organic adsorbat enter into interlayer spaces of initial clay materials by ion exchange mechanism[4]. The modified forms of montmorillonite prepared have been added into rubber compounds to substitute the standard filler – carbon black. The main aim of the study was closely connected with application of monoionic and organomodified clay materials on the basis of thiazole in function of fillers at

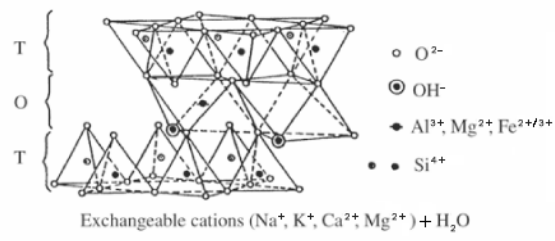

Fig. 1. **Montmorillonite structure, T - tetrahedral sheet, O - octahedral sheet[3]**

preparation of polymer/clay (organoclay) composite materials and the use of cotton waste to rubber to improve the properties of vulcanizates. The present paper is closely connected with measurement of vulcanization characteristics (minimum torque M_L, maximum torque M_H, time of start of vulcanization ts, optimum time of vulcanization t_{c90}, rate coefficient of vulcanization R_v) and evaluation of the measured data in relation to non-vulcanized model rubber compounds. Moreover, the physical and mechanical properties (tensile strength, modulus 300, tensibility) of resulting vulcanizates were investigated. All these properties were compared to properties of standard filler used in the rubber industry while this standard filler was highly reinforcing carbon black of type N660.

According to the obtained results it can be assumed that the cotton waste added to the model rubber compounds has a positive impact on the properties of the resulting vulcanizates and prepared monoionic forms montmorillonite can be applied as fillers and organo- montmorillonite can be used as a filler with an additional accelerating effect for the application in the rubber compounds with the improving of physical and mechanical properties.

The authors are grateful to the Slovak Grant Agency VEGA 1/0530/11 and VEGA 1/0185/12 for financial support.

REFERENCES

1. Khaorapapong N.: Appl. Clay Sci. *50*, 414 (2010).
2. Koksal E.: J. Therm. Anal. Calorim. *87*, 375 (2007).
3. Volzone C., Rinaldi J. O., Ortiga J.: Mat. Res. *5*, ISSN 1516–1439. 2002.
4. Ľalíková S., Pajtášová M., Ondrušová D., Bazyláková T., Olšovský M., Jóna E., Mojumdar S. C.: J. Therm. Anal. Calorim. *100*, 745 (2010).

P-33
INFLUENCE OF MODIFIERS ON POLYLACTID ACID/ THERMOPLASTIC STARCH BIODEGRADABLE POLYMER BLENDS

RODERIK PLAVEC, MIROSLAVA MIKUŠOVÁ, KATARÍNA TOMANOVÁ, MICHAL MIHALÍK, JÁN BOČKAJ, ZUZANA VANOVČANOVÁ, and PAVOL ALEXY

Institute of Polymer Materials, Faculty of Chemical and Food Technology, Slovak University of Technology, Radlinského 9, 812 37 Bratislava, Slovak Republic roderik.plavec@stuba.sk

Introduction

The current global consumption of plastics is more than 280 million tonnes. It represents the largest field of application for crude oil. It emphasises how dependent the plastic industry on oil and consequently how the increasing crude oil and natural gas price can have an economical influence on the plastic market. It is becoming increasingly important to utilize alternative raw materials. Until now petrochemical-based plastics have been increasingly used as packaging materials because of their large availability at

relatively low cost and because of their good mechanical performance. But nowadays their use has to be restricted because they are not completely recyclable and/or biodegradable so they pose serious ecological problems. Plastic packaging materials are also often contaminated by foodstuff and biological substance, so recycling these material is impracticable and most of the times economically not convenient. The growing environmental awareness imposes to packaging films and process both user-friendly and eco-friendly attributes[1,2]. One possibility how to solve this problem can be production of biodegradable polymers On the other hand, biodegradable polymers have often some disadvantages, such as low flexibility and degradation during processing. These disadvantages can be reduced by blending of two or more polymers as well as by addition of modifiers.

In this work polylactid acid / thermoplastic starch (PLA/ TPS) blends were studied. We used three types of modifiers – M1, M2, M3. The aim of our work was to study the influence of modifiers on rheological and mechanical properties of PLA/TPS blends.

Materials and methods

Polylactid acid – PLA 4042D from NatureWorks, LLC, USA and corn starch from Amylum, Slovakia were used as biodegradable polymers, Glycerine and Water were used as plasticizers. Labeling of used modifiers is: M1, M2, M3.

Preparation of blends

The blends of polylactide acid/thermoplastic starch with content of thermoplastic starch 35,4 %wt. were prepared using twin screw extruder with screw diameter 16 mm, L/D = 40 with four kneading zones. The content of glycerol was 16,5 %wt. and content of water was 3,1 %wt. These blends were modified by addition of modifiers in content 0,1; 0,2 and 0,4 %wt.

Rheological measurements

Rheological parameters of blends were measured using capillary rheometer Rheograph 20 from Göttfert, Germany. Diameter of capillary was 1 mm and length of capillary was 30 mm. Timed test was done on oscillation rheometer RPA 2000 from Alpha Technologies at constant angle of strain 30° and constant frequency 60 cpm. Time period of test was 9 min. Temperature of measurement for both methods and for all prepared blends was 170 °C.

Mechanical properties measurement

For tensile test according to ISO 527 the Zwick machine was used at cross-head speed 1mm/min while deformation range was of 0–3 % and after this value of deformation the speed increased up to 50 mm min^{-1}. The tensile strength of break (σb), elongation at break (εb) and tensile strength at yield (σy) were determined based on recorded tensile curves.

Results and discussion

The dependencies of mechanical properties on rest time after preparation of sample of the blends of PLA/TPS are shown in Fig. 1 and Fig. 2. Content of modifiers was 0,4 %wt.

In terms of stability of mechanical properties, modifier M3 gives the most stable sample. Although the film with modifiers M1 and M2 achieved higher value of tensile strength at break (Fig. 1), in terms of their change over time is much more advantageous stability of these properties, although at a lower level. In addition, the flexibility of foil derived from the relative elongation at break reached the highest values in the applications with modifier M3 (Fig. 2). The highest value of elongation at break of polymer blends was measured immediately after preparation of films. Flexibility of polymer blends with modifiers M1 and M2 decreased after one day on almost zero value. But flexibility of polymer blend with modifier M3 increased after one day from value 80 % to value 180 % after three days of sample preparation. Differences of tensile strength at break were minimal. Due to the good mechanical properties of biodegradable polymer blends with modifier M3, we examined the rheological properties and thermal stability of these polymer blends.

The dependency of viscosity on shear rate for polymer blends with modifier M3 is on Fig. 3. The graph shows that

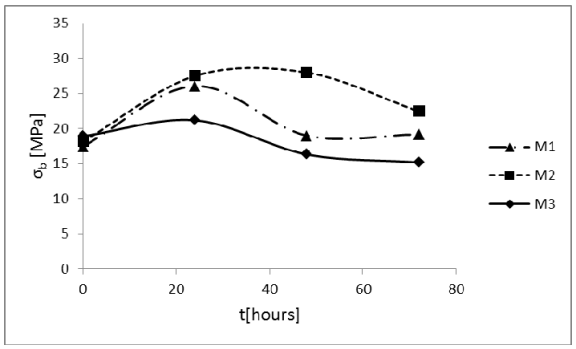

Fig. 1. **The dependency of tensile strength at break on rest time after preparation of sample**

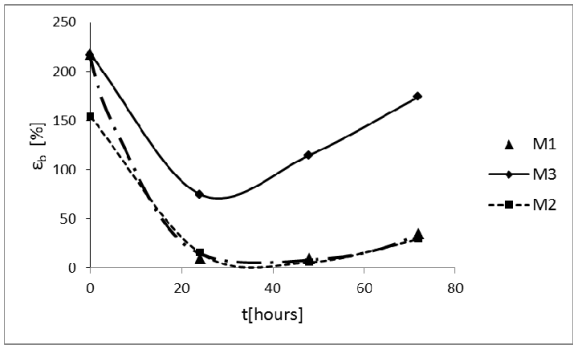

Fig. 2. **The dependency of elongation at break on break on rest time after preparation of sample**

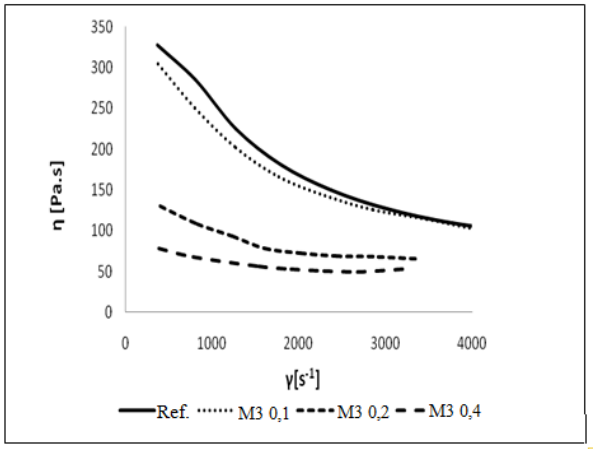

Fig. 3. **The dependency of viscosity on shear rate for polymer blends with modifier M3**

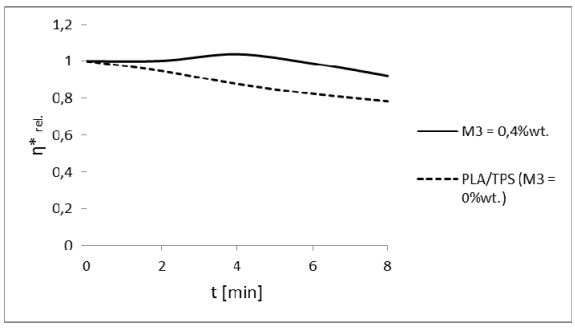

Fig. 4. **The dependency of relative complex viscosity on time during oscillation test**

the higher modifier content reduces the viscosity of the polymer blend PLA/TPS. Therefore, we conclude that the appropriate choice of content modifier M3 can adjust the rheological parameters of the blends as needed for different processing methods of polymers.

Thermal stability of polymer blend was measured as dependence of relative complex viscosity on time during oscillation test. Relative complex viscosity is the ratio of complex viscosity in real time t and the complex viscosity in time t = 0. We can say that modifier M3 affects decrease viscosity of polymer blend PLA / TPS during thermal loading. It can be seen that the dependence of η * rel (t) in case of blend PLA / TPS (without modifier) decreases with time, indicating degradation (decreasing in molecular weight). The presence of modifier considerably reduced the decreasing, and the modifier can be considered effective processing stabilizer for biodegradable polymer blend PLA – TPS.

Conclusion

The results obtained in the work showed that the application of appropriate modifiers to polymer blends PLA / TPS can inhibit degradation processes during processing in the form of melt and also improves the mechanical properties of these materials. All the tested modifiers exhibit positive effects on melt viscosity of PLA and TPS themselves as well as of their binary blends. Tested modifier also inhibit degradation process of these blends. Tested modifiers act as effective processing stabilizers. All tested modifiers have a positive influence on the mechanical properties of PLA / TPS films. Most stable strength values, but also the relative elongation at break is achieved when modifier M3 is applied. Combination of PLA/TPS biodegradable polymer blend with suitable modifiers (M1-M3) give a good chance for application of this material in packaging industry.

REFERENCES

1. Siracusa V., Rocculi P., Romani S., Dala Rosa M., Trends Food Sci. Technol. *19*, 634 (2008).
2. *Plastics – the Facts 2011*; An analysis of European plastics production,demand and recovery for 2010; www.plasticseurope.org

P-34
POLYETHYLENE ANTIBACTERIAL MODIFIED BY POLYSACCHARIDES VIA COLD PLASMA

ANTON POPELKA[a], IGOR NOVÁK[a], IVAN CHODÁK[a], MARIÁN LEHOCKÝ[b], ANGELA KLEINOVÁ[a], and VLADIMÍR VANKO[c]

[a] Polymer Institute, Slovak Academy of Sciences, Dúbravská cesta 9, 845 41 Bratislava 45, Slovakia, [b] Centre of Polymer Systems, University Institute, Tomas Bata University in Zlín, Nam. T.G.M. 5555, 76001 Zlín, Czech Republic, [c] VIPO, a.s., Partizánske, Slovakia
anton.popelka@savba.sk

Abstract

Low-density polyethylene (LDPE) belongs to commodity polymer materials applied in many applications due to its favorable mechanical and chemical properties. Its main disadvantage is low resistance to bacterial infections in biomedical applications. Antibacterial modification of LDPE appears to be a solution to this problem. In this paper, chitosan and chitosan/pectin multilayer was immobilized via polyacrylic acid (PAA) brushes grafted on LDPE surface using low-temperature plasma treatment. The surface and adhesive properties of thus prepared LDPE samples were investigated by surface analysis techniques. The antibacterial effect was confirmed by inhibition zone measurements of Escherichia coli and Staphylococcus aureus.

Introduction

Polyethylene (PE) belongs among the most used polymers in many industrial applications[1]. PE has hydrophobic a chemical inert surface as follows from theirs chemical composition[2]. Its bulk properties exhibit appropriate tensile and barrier characteristics. However, the many of their surface and adhesion properties such as adhesion, wettability,

biocompatibility, printability and friction do not achieve required values for the purpose of some applications. Therefore the additional surface modification of these polymers is necessary. The surface treatment is being increasingly used modification methods based on the plasma effect, which is environmentally friendly, clean and dry process[3]. The uniform layer and high surface power density of plasma can be generated by diffuse coplanar surface barrier discharge (DCSBD) plasma generator. This equipment is working at atmospheric pressure and therefore it is suitable for continual industry applications[4]. On plasma treated surface polyacrylic acid (PAA) can be easily grafted that can to create an effective interfacial layer for antibacterial immobilization. The PAA brushes can be used as an interfacial layer that may bind antibacterial agents by effective way[5]. The polysaccharides excel appropriate properties for antibacterial immobilization. These substances are formed from large number of molecules of simple sugars and contain characteristic groups, by which they should be firmly anchored at the created brushes. Polysaccharide based on chitosan is representing significant compound that can be immobilized on pre-treated PE surface via plasma and PAA grafting. Chitosan is a linear cationic polysaccharide derived from deacetylation of chitin and used in pharmaceutical, cosmetic, and food industry applications[6]. It is composed from randomly distributed β-(1-4)-linked D-glucosamine and *N*-acetyl-D-glucosamine, which in contact with bacterial cell wall disrupts the cell metabolism and kills the bacteria. Pectin, a structural heteropolysaccharide is one of the most widely investigated polysaccharides in the field of colon-specific drug delivery. The characteristic structure of pectin is a linear chain of α-(1-4)-linked D-galacturonic acid that forms the backbone. Pectin has been well-tried as an effective gelling and thickening agent, as well as stabilizer for foods. Very interesting possibility of the polysaccharides effective immobilization is the creation of multilayer layers between polyelectrolytes of opposite charges of structures. Chitosan and pectin multilayer using layer-by-layer assembly excels in their surface, adhesive and antibacterial properties[7].

Experimental

Following materials and treatment conditions were used in our experiment. LDPE BRALEN FB 2-17 (Slovnaft MOL, Slovakia) foils with thickness 20 μm containing no additives were used. The LDPE foil modification were carried out by DCSBD equipment produced by Comenius University (Department of Experimental Physics, Faculty of Mathematics, Physics and Informatics) in Bratislava under dynamic conditions in air atmosphere: power supply was 200 W, treatment time was 20 sec. The surface properties of antibacterial modified LDPE were carried out by the measurements of contact angle of water by Surface Energy Evaluation System (See system, Advex Instruments, Czech Republic).

The adhesive properties represented by peel strength (force per unit width) of adhesive joint of LDPE samples to poly(2-ethylhexyl acrylate) deposited on polypropylene foil (with 15 mm width), were carried out by measurements of 90° peel test using Instron 4301 (England).

The Fourier Transformed Infrared Spectroscopy with Attenuated Total Reflectance (FTIR-ATR) was used for investigation of the surface chemical composition. The spectra were recorded by FTIR NICOLET 8700 spectrometer (Thermo Scientific, (USA) through the single ATR Ge crystal at 45° incident angle. The spectral resolution and the number of scans were 2 cm^{-1} and 64, respectively for each measurement. A pressure clamp was used to obtain highest quality of the spectra. The acquired spectra were analyzed using OMNIC ™, v8.1 software.

Antibacterial activity of prepared samples was tested against *Staphylococcus aureus* (CCM 4516) and *Escherichia coli* (CCM 4517) by inhibition zone method (diffusion test) on agar. A nutrient agar No.2 M1269 – 500 g from HiMedia Laboratories PII.Ltc. was used for our experiments. Tested samples were cut in a circular shape (d = 8 mm), washed in ethanol, dried and placed on agar plate inoculated by bacterial suspension (volume: 100 μl, concentration: 10^7 units/ml). The samples were incubated for 24 hours at 37 °C and diameters of inhibition zone were measured in 5 directions to obtain an average values for inhibition zone calculations. The test with each sample was triplicate.

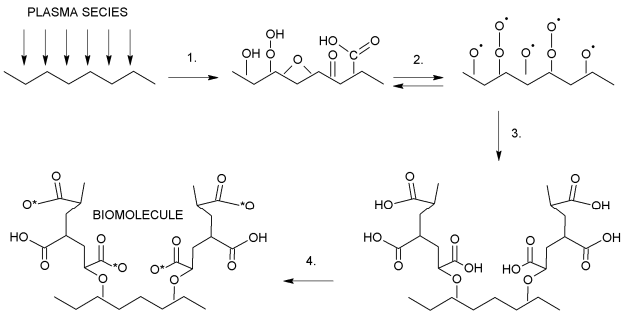

Scheme 1. **Multistep approach of polysaccharides binding:** (1) plasma treatment, (2) radical generation, (3) AA radical graft polymerization, and (4) polysaccharides immobilization

Results and discussion

The hydrophobic and chemical inert surface nature of untreated LDPE is the reason for high values of contact angle of water due to a low surface wettability. A significant decrease of contact angle of water was observed after plasma treatment as result of an introduction of polar functional groups on the LDPE surface. The PAA grafting led to the further decrease of contact angle of water due to polar character of PAA. The creation of chitosan and chitosan/ pectin multilayer led to the significant decrease of contact angle of water due to the presence of polar functional groups.

An adhesion of two materials in contact can be expressed by force per width (peel strength). The peel strength relates to the roughness and wettability of investigated materials forming an adhesive joint. Therefore, the decrease of contact angle of water results in the peel strength increase of adhesive joint to more polar polyacrylate deposited on polypropylene foil. The adhesion is thus a complex of the several related chemical and physicochemical properties. The peel strength of untreated LDPE achieved very low values. The plasma treatment

resulted in an increase of the peel strength caused by the changes in the polarity and surface roughness. The PAA grafting, chitosan and chitosan/pectin multilayer coating led to further increase of the peel strength of LDPE.

The FTIR-ATR measurements provide mostly semi-quantitative information about chemical changes in a near-surface region. The spectrum of untreated LDPE is a characteristic spectrum of PE with only few characteristic peaks. The plasma exposure of the LDPE sample led to significant changes in the measured spectrum. An incorporation of oxygen containing groups was observed, i.e. hydroperoxides (region 3700–3080 cm^{-1}) and/or other oxygen containing products at the surface of LDPE (region 1845–1510 cm^{-1}, 1280 cm^{-1}, 1126 cm^{-1}, 1150 cm^{-1}, carboxyl, carbonyl or aldehydic moieties). Other significant changes in the spectra were observed for LDPE modified by the PAA grafting and also after subsequent treatment by chitosan/pectin, respectively. The spectrum of grafted LDPE contains several characteristic peaks of PAA, i.e. the most intense peak at 1712 cm^{-1} (carbonyl band, C=O stretching) and also some unresolved peaks in the fingerprint region (1300–1100 cm^{-1}, C-O stretching and CH_2 bending). The presence of chitosan in samples was confirmed by a presence of the band at 1653 cm^{-1} in corresponding spectra (amide band arising from chitosan). After chitosan/pectin treatment the shape of the spectrum is changing. Spectra of these samples indicate also the presence of acrylic acid (carbonyl band, 1712 cm^{-1}), pectin – 1734 cm^{-1} (C=O band arising from pectin). The changes in spectra are significant almost in a whole mid-infrared region, especially in the fingerprint region and they confirm the incorporation of the chemicals used for the surface treatment of LDPE.

Chitosan/pectin coated LDPE samples showed minor activity only against *Staphylococcus aureus,* their inhibition zone move around 70 mm^2. The highest and most clear inhibition zones were given by samples grafted by PAA and coated by chitosan. Their levels were on average 35 mm^2 for *Escherichia coli* and 275 mm^2 for *Staphylococcus aureus*.

Conclusions

This work has given important information in a field of the biocide properties study of polysaccharides coatings on LDPE. The multistep physicochemical approach was shown to be effective for binding the polysaccharides, namely chitosan and chitosan/pectin multilayer on the LDPE surface. DCSBD plasma treatment results in the increase of the LDPE surface roughness as well as the wettability. PAA brushes synthesized via plasma-initiated graft polymerization of AA led to the increase of the wettability representing a stable base for the polysaccharides binding. The most effective bacterial inhibition zone was observed for LDPE coated by chitosan. Chitosan/pectin coated LDPE sample showed minor antibacterial activity only against *S. aureus*.

Authors are grateful to financial supports by the Ministry of Education of the Slovak Republic project No. 26220220091 by Research & Development Operational Program funded by ERDF, as well as „Application of Knowledge-based Methods in Designing Manufacturing Systems and Materials" the project No. MESRSSR 3933/2010 -11, and the project of the Ministry of Education, Youth, and Sports of the Czech Republic (CZ.1.05/2.1.00/03.0111), Czech Science Foundation (project 104/09/H080)).

REFERENCES

1. Sanchis R., Fenollar O., García D., Sánchez L., Balart R.: Inter. J. Adh. & Adh. *28*, 445 (2008).
2. Drnovská H., Lapčík L. Jr., Buršíková V., Zemek J., Barros-Timmons A. M.: Coll. Polym. Sci. *281*, 1025 (2003).
3. Kale K. H., Desai A. N.: Indian J. Fiber. Textil. Res. *36*, 289 (2011).
4. Černák M., Černáková Ľ., Hudec I., Kováčik D., Zahoranová A.: Eur. Phys. J. Appl. Phys. *47*, 22806 (2009).
5. Bazaka K., Jacob M. V., Crawford R. J., Ivanova E. P.: Acta Biomater. *7*, 2015 (2011).
6. Renault F., Sancey B., Badot P. M., Crini G.: Eur. Polym. J. *45*, 1337 (2009).
7. Elsabee M. Z., Abdou E. S., Nagy K. S. A., Eweis M.: Carbohydr. Polym. *71*, 187 (2008).

P-35
APPLICATION OF LIGNOSULFONATE AS A COMPONENT OF RUBBER BLENDS FOR TIRE INDUSTRY

JOZEF PREŤO*[a], JÁN HRONKOVIČ[a], IVAN HUDEC[b], VLADIMÍR VANKO[a], and JÁN ORAVEC[a]

[a] Vipo a.s., Gen. Svobodu 1069/4, 95801 Partizánske, [b] Slovak University of Technology in Bratislava, Faculty of Chemical and Food Technology, Institute of Polymer Materials, Department of Plastics and Rubber, Radlinského 9, 812 37 Bratislava, Slovakia
jpreto@stonline.sk

Abstract

The goal of the work was the study of influence of calcium lignosulfonate as a component of rubber compositions with fiber reinforcements. The fiber reinforcements are based on synthetic polymers, such as polyester. The experimental work was examined the effects of calcium lignosulfonate on the vulcanization characteristics, physical-mechanical and adhesive properties of rubber blends based on natural rubber. It was found, that the addition of lignosulfonate has a positive influence on the adhesive properties rubber composition for coating to a polyester textile cord. The rubber composition was consisted from 5 to 20 phr calcium lignosulfonate.

Introduction

Utilization of certain types of lignin for preparation of crosslinked resins is described in these publications[1,2]. Application of lignin or lignosulfonate as a filler, antidegradant or promoter of adhesion in rubber blends was investigated in some earlier papers[3,4].

Calcium lignosulfonate is an amorphous light-yellow-brown powder obtained from the sulfite pulping of softwood.

Calcium lignosulfonate is an amorphous material derived from lignin, is soluble in water, but practically insoluble in organic solvents. Lignosulfonates are commercially available as sodium and calcium salts and have been used by industry in a wide variety of applications. The usefulness of commercial lignosulfonate products comes from their dispersing, binding, complexing, and emulsifying properties. The structure of the polymeric fraction of calcium and sodium lignosulfonate is presented in Scheme 1 (ref.[5]).

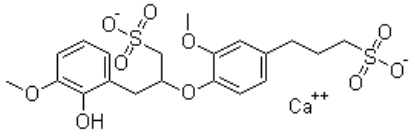

Scheme 1. **Structure of the polymeric fraction of calcium lignosulfonate**

Our contribution deals with the study of effect of biopolymers as a component or fillers on the selected properties of rubber blends. The experimental work is oriented on the evaluation of calcium lignosulfonate utility as fillers in rubber blends.

Experimental

On the basis the results obtained in our previous work[6] there was decided to examine the influence of calcium lignosulfonate as a replacement for carbon black on selected properties of rubber composition for coating. Details of the calcium lignosulfonate (Borrement CA 120) used in the present study are listed in Table I.

Calcium lignosulfonate can be used in rubber processing as additive, as a partial replacement of filler. The effect of calcium lignosulfonate was investigated by vulcanization characteristics, physical-mechanical, and adhesive properties. The composition was prepared with calcium lignosulfonate as a replacement for carbon black in interval 0–20 phr as shown in Tab. II. In the first step the compounds were mixed in a Banbury mixer at mixing temperature 120 °C and rotor speed 60 rpm. In the second step the curing additives were added in calendar at mixing temperature 60 °C.

The continuous measurements of vulcanization were carried out in a rheometer MDR 2000 E at 150 °C. The vulcanizates sample physical-mechanical properties were determined according to STN ISO 37. The adhesive properties were measured according to ASTM D4393/D4393-M. The selected vulcanization characteristics of the blends are displayed in Table II.

Table I
List of the applied calcium lignosulfonate properties

Product	Calcium content [%]	Sulfur content [%]	pH (10% solution)	Mw [g mol^{-1}]	Specific Surface [m^2 g^{-1}]
Borrement CA 120	5	7	4,5	24000	3,9

Table II
Formulations and rheological properties of compounds with calcium lignosulfonate as a replacement for carbon black

Compound (phr)	L0	L5	L10	L15	L20
SMR 5	80	80	80	80	80
SBR 1500	20	20	20	20	20
Borrement CA120	0	5	10	15	20
Carbon black N550	50	45	40	35	30
Other ingredients	26	26	26	26	26
Rheological properties					
ML (dNm)	1,94	1,87	1,83	1,78	1,72
MH (dNm)	15,86	13,32	12,55	11,41	10,65
TS2 (min)	6,01	6,43	6,30	6,82	6,67
TC90 (min)	16,14	15,67	16,73	18,32	18,89
Peak Rate (dNm/min)	2,49	1,92	1,52	1,19	1,04

Results and discussion

As specified in Tab. II the ability to crosslinking (expressed in the difference MH and ML values) of all rubber compounds with increasing quantity of calcium lignosulfonate are decreased in comparison with reference compound L0. The peak rate acquires the similar characteristic. There is the insignificant effect of lignosulfonate on the scorch time (TS2) and optimum cure time (TC90).

The physical-mechanical properties of the prepared vulcanizates are shown in Fig. 1–3. It is evident that lignosulfonate replacements for carbon black causes significant decrease of tensile strength and contrast to it the elongation at break are increased. It was investigated the effect after ageing what describes the parameter "change after ageing" displayed in Fig. 1–3. The decrease of this parameter indicates the improvement of measured properties after ageing, specifically tensile strength (Fig. 1) and elongation at break (Fig. 2), what pointed to the antidegradable effect of

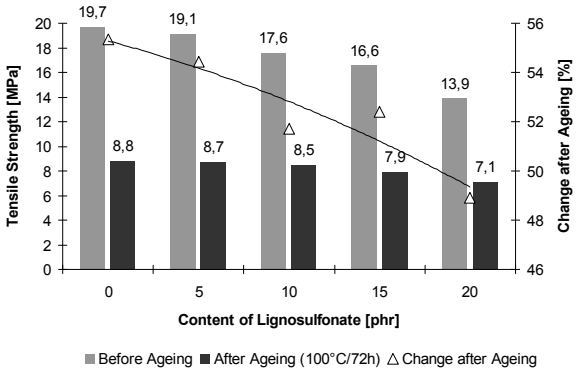

Fig. 1. **Dependence of tensile strength at break of vulcanizates on lignosulfonate content before and after ageing and on change after ageing**

investigated calcium lignosulfonate. Similarly, as shown on Fig. 3, the structural strength values decrease with higher content of calcium lignosulfonate except for 20 phr concentration.

Influence of calcium lignosulfonate to adhesive properties of tested compounds was evaluated by obtained values of peel strength and degree of coverage as shown in Fig. 4. It is seen the increase of lignosulfonate content causes the increase of degree of coverage, what points to increasing adhesion to textile cords. On other side the peel strength growths to the content 10 phr of lignosulfonate only. Consequently this concentration would be the optimum that takes into account the values of the tensile and adhesion tests.

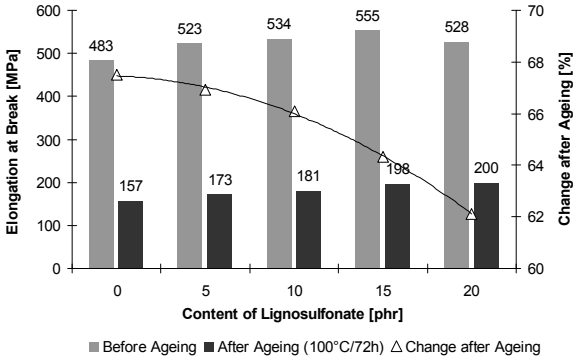

Fig. 2. **Influence of content of lignosulfonate on elongation at break of vulcanizates before and after ageing and on change after ageing**

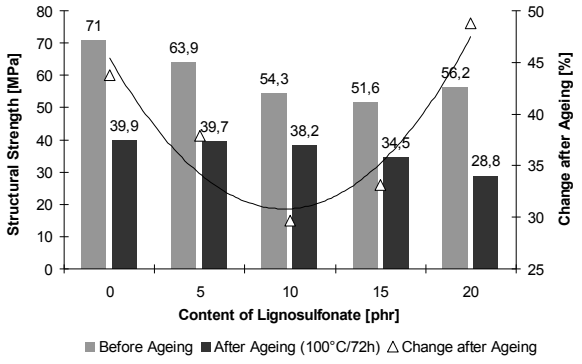

Fig. 3. **Dependence of structural strength of vulcanizates on lignosulfonate content before and after ageing and on change after ageing**

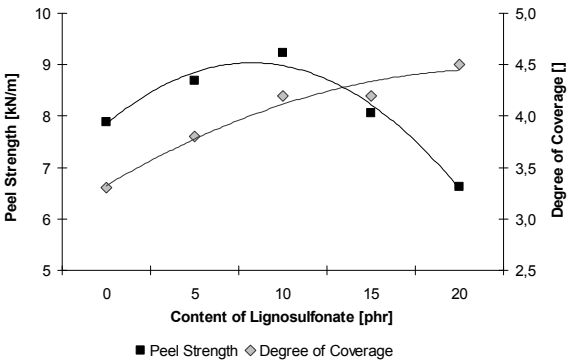

Fig. 4. **Influence of content of lignosulfonate on peel strength and on degree of coverage of rubber blends for coating vulcanizates**

Conclusions

From results of used measurements is evident that calcium lignosulfonate has the significant effect to the process of vulcanization, tensile and adhesion properties.

The increasing amount of lignosulfonate reduces the crosslinking effect as shown at values of torque, peak rate and optimum cure time. The tensile tests revealed the increase of elasticity with gradually increasing amount of lignosulfonate in examined compounds. It was observed the improvement of measured tensile properties after ageing, what pointed to the antidegradable effect of investigated calcium lignosulfonate. The adhesive properties of lignosulfonate were confirmed and determined the optimum concentration for investigated composition.

This work was supported by Ministry of Education of Slovak Republic project No.26220220091 by the Research & Development Operational Program funded by the ERDF.
The project „Application of Knowledge-based Methods in Designing Manufacturing Systems and Materials“, No. MESRSSR 3933/2010-11.

REFERENCES

1. Glasse W. G., Barnett Ch. A., Sano Y. J.: J. Appl. Polym. Sci.: Appl. Polymer Symp. *37*, 441 (1983).
2. Kuom M., Hse CH. Y., Huang D. H.: Holzforschung *45*, 47 (1991).
3. Gregorová A., Košíková B., Moravčík R.: Polym. Degrad. Stab. *91*, 229 (2006).
4. Kramárová Z., at all: Polym. Adv. Technol. *18*, 135 (2007).
5. http://www.chemicalbook.com
6. Preťo J., Hronkovič J., Oravec J., Vanko V., Hudec I.: *IRC2012*, Jeju, Korea, P04024.

P-36

THE APPLICATION OF THERMAL DESORPTION AND REACTIVE PYROLYSIS – GAS CHROMATOGRAPHY – MASS SPECTROMETRY FOR THE IDENTIFICATION OF END CAPPED BROMINATED EPOXY POLYMERS BASED ON TETRABROMOBISPHENOL A DIGLYCIDYL ETHER IN PBT

FRANKY PUYPE and JIRI SAMSONEK

Institute for Testing and Certification – Zlín, analytical division – separation science, Třida T. Bati 299, 764 21 Zlín-Louky, Czech Republic
fpuype@itczlin.cz

Introduction

A new trend in polymer additive chemistry is the increasing use of polymeric additives. Mainly in the field of polymeric antioxidants, stabilizers or polymeric flame retardants new polymeric additives are coming up. Polymeric additives have the big advantage to make the final product blooming free and the additives are available all over the polymer. Polymeric additives give nearly no emissions, no migration loss and allow higher application temperatures. For analysis by gas chromatography, the main focus stays on difficulties concerning volatility, separation and detection, therefore thermal desorption and pyrolysis as a sample introduction system were evaluated for characterization of some polymeric additives.

Thermal desorption (TD-GC-MS) is the sample injection system which is able to separate volatiles from a solid matrix by heat and sweep them with the carrier gas stream towards the GC. The operating temperature is approximately 250–300 °C and generally, the molecular weight of the analytes ranges from very volatiles to additives of about 1000 Da.

Pyrolysis as an injection technique coupled to classical gas chromatography with mass detection (PY-GC-MS) makes firstly fragments from the polymer and the polymeric additive fraction. Then these fragments are separated by classical gas chromatography and easily detectable by mass spectrometry. This method can be applied if there is interest into the structure of compounds and not primary in the molecular weight. According to thermal gravimetric analysis, carbon covalent bounds cut from 450 °C. For polymers and additives based on ethers and ester functions, there is the option to perform reactive pyrolysis. The reagent tetramethylammonium hydroxide (TMAH) in methanol is the only derivatization reaction which is able to cut ether bounds resulting in methyl ethers. The carboxyl groups of polyesters results in methyl ester groups. This reaction takes place at a temperature of 400 °C.

Analytical laboratories are sometimes asked to identify the presented brominated flame retardant (BFR) which is not requested or supported by any law. Therefore this case study for explaining some possibilities by thermal desorption and reactive pyrolysis – gas chromatography – mass spectrometry.

Material and methods

Sample and first screening

A black housing sample of polybutylene terephthalate (PBT) from an electric fan for automotive applications was measured by X-ray fluorescence analysis (XRF) for the bromine content. This analysis was performed with an Oxford Instruments ED 2000 Ag instrument under the conditions for measuring of medium elements in air. The tube voltage was 45 kV and the current to the tube was set at 50 mA with a time of measuring of 30 seconds. The sample preparation for XRF analysis requires only cutting the samples in a size they fit in the XRF module (optimal 22 mm diameter). The bromine content gives an indication for the possible BFR presence and semi-quantitative concentration value. The sample of interest contained more than 1,0 weight % of bromine.

Thermal desorption and reactive pyrolysis GC-MS method for BFR identification

All experiments were carried out with a thermal desorption and pyrolysis unit PY-2020iD (Frontier Laboratories Ltd., Japan) with a 48 position auto sampler connected to a GC/MS QP2010plus (Shimadzu, Japan). A special metal capillary separation column (Ultra ALLOY-PBDE; 0.25 mm i.d. × 15 m, Frontier Laboratories Ltd., Japan) coated with a very thin (0,05 um) film of immobilized-polydimethylsiloxane is used for separation of the thermal desorption products. The ionisation mode was electron impact with ionisation at 70 eV. Thermal desorption was done at 300 °C for 2 minutes and reactive pyrolysis at 400 °C for 2 minutes.

Sample preparation for TD-GC-MS and reactive pyrolysis-GC-MS

Thermal desorption: The sample preparation was done by a static extraction of the polymer additives in toluene for 24 hours at ambient temperature. Toluene as extraction solvent was chosen due to the fact that most BFRs are soluble in toluene. The extract is spiked (approximately 5 ul) into a stainless steel sample cup which is inside covered with a thin layer (< 1 um) of fused silica. This sample cup is placed into an auto-sampler and during thermal desorption heated in the furnace of the pyrolyzer.

Reactive pyrolysis: The sample preparation was done by a static extraction of the polymer additives in toluene for 24 hours at ambient temperature. The toluene was evaporated and TMAH/MeOH reagent was added, after shaking, the extract was spiked (approximately 2 ul) into a stainless steel sample cup which contains a small disc made of high quality glass fibres (Auto-Rx Disc, frontier laboratories, Japan). This disc adsorbs the liquid and so avoids ``creeping`` of the mobile TMAH/MeOH from the inner of the cup towards the outer side[1].

Results and discussion

Thermal desorption-GC-MS

The sample extract was measured by TD-GC-MS (Fig. 1). Three bromine containing peaks were identified. 2,4,6-tribromophenol (t_R at 12,25 min), tetrabromobisphenol A (TBBPA, t_R at 20,4 min) and an unknown higher molecular weight brominated molecule at 21,6 min.

The mass spectrum of the peak in at 21,6 min is shown in Fig. 2. It presents the typical electron impact fragmentation ions from a group based on 2,4,6-bromophenol (M/z 62,0 ; M/z 140,95 ; M/z 233,85 ; M/z 327 as M-1). Intense peaks are seen at M/z 312,75 and M/z 356,8 which are the result of electron impact fragmentation of a 2,4,6-tribromophenol glycidyl ether. Moreover the peaks at M/z 402,85 and M/z 483,70 confirm this. The peaks at M/z 584,80; M/z 608,60 and M/z 687,55 are the fragmentation ions of tetrabromobisphenol A diglycidyl ether with 2,4,6-tribromophenol on one side.

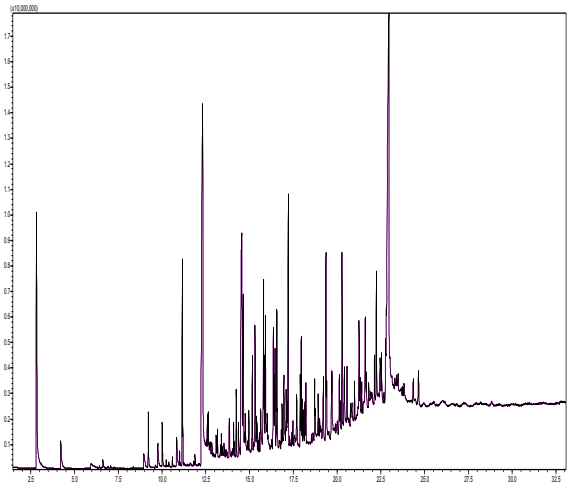

Fig. 1. **TD-GC-MS chromatogram of PBT sample extract**

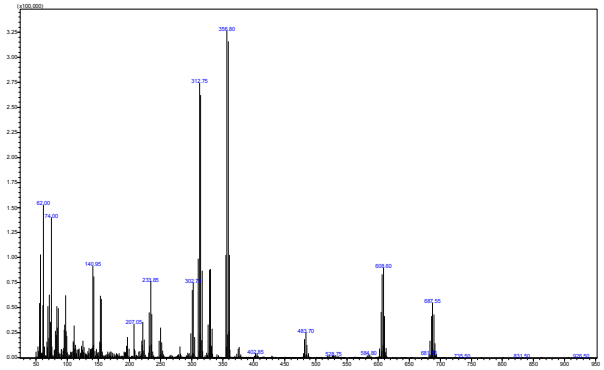

Fig. 2. **Electron impact mass spectrum of unknown peak at t_R 21,6 minutes**

Reactive pyrolysis-GC-MS

The pyrogram after reactive pyrolysis looks cleaner than the thermal desorption chromatogram and allows the analyst to detect methylether and methylester derivates (Fig. 3). At retention time 4,7 min a peak of trimethylglcerol was detected, coming from bounded glycerol (glycidyl ether). The presence of this glycerol derivate after reactive pyrolysis and the missing of free glycerol after thermal desorption, confirms the presence of bounded glycidylether in the original substance.

The other brominated substances are identified and given according to retention time in Table I. Many of these compounds are de-brominated due to the higher operation temperature of the pyrolysis process, but the main structures of the hydrocarbons stays and can be used for structural analysis.

There has been detected at 18,3 min a peak of dibromobisphenolA-4-monomethylether-4`ethyleneglycol-ether which indicates again the suspected presence of an end

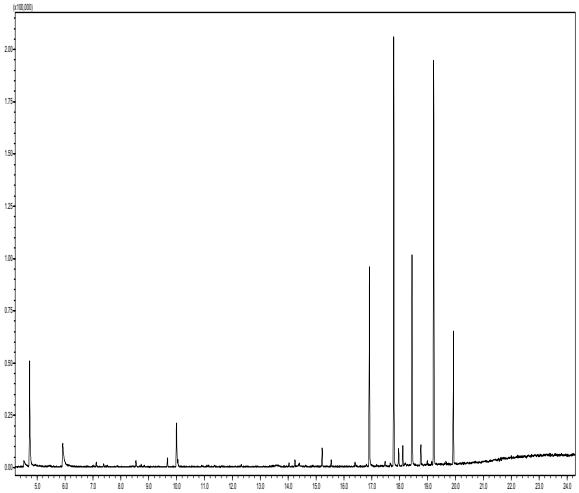

Fig. 3. **Pyrogram of the sample extract after reactive pyrolysis**

Table I
Identification of compounds shown in Fig. 3

Retention time t_R [minutes]	Identified compound
4,7	Glycerol trimethylether
10,0	Di-bromoanisole (from dibromophenol)
17,0	Monobromobisphenol A dimethylether
17,7	Dibromobisphenol A dimethylether
18,3	Dibromobisphenol A 4- monomethylether--4`-ethyleneglycolether
19.2	Tribromobisphenol A dimethylether
19,8	Tetrabromobisphenol A dimethylether

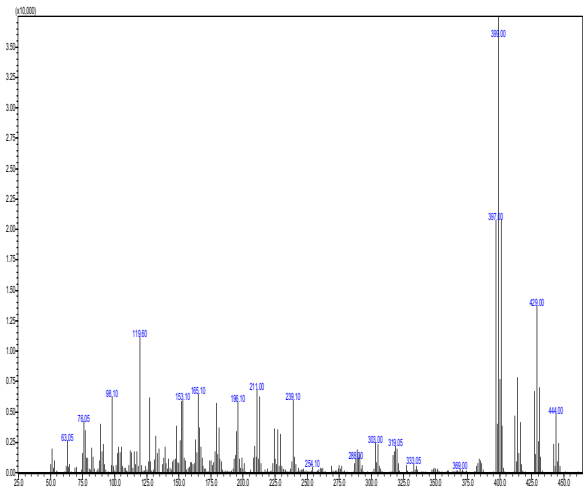

Fig. 4. **Mass spectrum of one of the peaks detected at 18,3 minutes** (dibromobisphenol A-4- monomethylether-4`-ethyleneglycolether)

capped brominated epoxy oligomer of tetrabromobisphenol A.

Figures of merit

A real overview of detection limits for chemicals measured by reactive pyrolysis-GC-MS cannot precisely been given due to variations depending on the complexity of the matrix, extraction step and efficiency of the reaction. However, a 100 ng spike of tetrabromobisphenol A into the cup gives a sufficient sensitivity (S/N >6).

The use of the Auto-Rx discs by reactive pyrolysis was evaluated by relative standard deviation (RSD) measurement; 3 times a sample extract of the PBT sample was measured by reactive pyrolysis. The RSD for reacted tetrabromobisphenol A came towards 6,2 %. This result is far better than the classical in-cup spiking which gave far worse results (overall RSD > 10 %)! The auto-RX discs are innovative due to the fact that no internal standard was used to obtain the presented data.

Summarizing data

The end capped brominated epoxy oligomer of tetrabromobisphenol A and 2,4,6-tribromophenol in plastics (PBT) can be determined by the combination of XRF (quantitative), thermal desorption-GC-MS and reactive pyrolysis (qualitative). For bromine positive samples toluene extracts are a clean approach to significantly decrease oligomer contamination into the instrumentation and so reduce the background signal. In this case firstly thermal desorption screening is needed to find the main identity of the BFR. In case of suspected presence of polymeric flame retardants, reactive pyrolysis can be applied (Fig. 5).

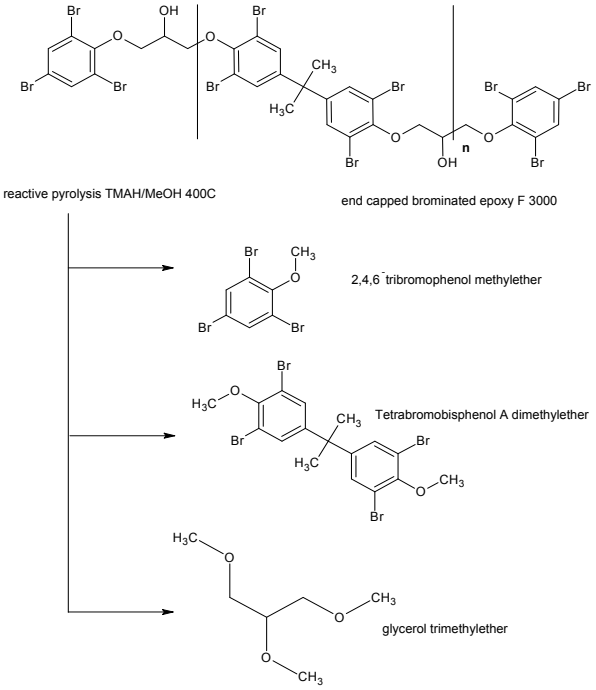

Fig. 5. **Schematic fragmentation guide of end capped brominated epoxy oligomer of tetrabromobisphenol A and 2,4,6-tribromophenol** (CAS No. 135229-48-0) by reactive pyrolysis.

REFERENCE

1. Frontier Lab application note – SK1108401 (ver1.07), http://www.frontier-lab.com

P-37

IDENTIFICATION AND SCREENING OF DIELS-ALDER CYCLOADDITION REACTION PRODUCTS FROM ACRYLONITRILE-(BUTADIENE)-STYRENE BASED COPOLYMERS BY MASS SPECTROMETRY AND THEIR IMPACT ON THE CAR INDOOR ENVIRONMENT

FRANKY PUYPE and JIRI SAMSONEK

Institute for Testing and Certification – Zlín, analytical division – separation science, Třida T. Bati 299, 764 21 Zlín-Louky, Czech Republic
fpuype@itczlin.cz

Introduction

Acrylonitrile-(butadiene)-styrene (ABS) resins are a very important group of engineering thermoplastics for automotive. Many engineering applications for the car indoor environment like panels, consoles, grilles and housings are made of this copolymer. ABS is mostly synthesized by grafting styrene-acrylonitrile copolymer (SAN) with polybutadiene rubber.

Physically, ABS has an improved toughness and a significantly better impact and heat resistance than polypropylene or polyethylene. Acrylonitrile is responsible for the chemical resistance and heat stability while styrene is achieving rigidity and processibility. The dispersed softer butadiene rubber is fully compatible with the continuous phase of the rigid SAN by grafting.

Beside the production of the macromolecule there are always side-reactions and oligomer formations appearing. Oligomers are the result of the initial polymer formation and are categorized under the so called non-intentionally added substances (NIAS) due to the fact their formation cannot be avoided[1]. Due to their low molecular weight and volatility, monomers and oligomers can migrate through the polymer matrix and create defects like smelling, blooming and fogging. Oligomers can appear linear and cyclic (ring-closed) and are the fingerprint of the polymer. From the analytical point of view, by screening the oligomer structures, batch-to-batch differences can be detected. Additionally the presence of a recycled fraction can be seen by oligomer identification in some cases.

Therefore as an analytical approach in modern separation science, a thermal desorbing unit as injector is able to deliver quick and reproducible results. Thermal desorption uses heat for the extraction of non-covalent bounded volatile organic molecules from the polymer matrix. This device is mostly coupled to a gas chromatograph for separation of the emissions and mass spectrometry is used for the identification (TD-GC-MS). Thermal desorption allows analysis of almost all sorts of materials including insoluble and complex materials. No solvent extraction or other pretreatment is needed and small amount of sample is required (approx. 20 mg).

The analytes/emissions are trapped in the GC injector on an electrically-cooled sorbent trap (Tenax TA). After trapping the obtained emissions (concentrating), analytes are transfered from the injector towards the analytical column of the gas chromatograph by quickly heating of this cooled sorbent trap. After chromatographic separation mass spectrometry detects the compounds and helps the scientist to identify the emissions[4,5].

Typical emissions from automotive parts are firstly the oligomers or matrix related compounds and secondarily the additives and their degradation products.

Diels-Alder cycloaddition reaction

The production of SAN starts always with the heat induced mixing of two monomers, styrene (after dehydrogenation of ethylbenzene) and acrylonitrile (mixed propylene with ammonia). During the SAN production there is formation of a complex series of Diels-Alder adducts. The Diels-Alder reaction is a one step [4+2] cyclic addition reaction between 4 π orbitals (a diene) and 2 π orbitals (a dienophile). For SAN this reaction is the most probable between styrene (as the diene) and acrylonitrile (as the dienophile). This probability is not only caused by abundance of the acrylonitrile monomer but also due to the polarized (more positive) carbon atom next to the alkene bound. This electron delocalization effect induced by the nitrile-group (arbitrary group) explains the high yield of this combination (Fig. 1a).

Moreover, there is another reason for the high Diels-Alder coupling between acrylonitrile with styrene explained by the 1,3-diene structure from the styrene which is mostly in the s-cis conformation. Never there will happen spontaneous a Diels-Alder reaction with a 1,3-diene in the s-trans conformation due to the spatial distance. This explains also the possibility to have a Diels-Alder reaction between 2 styrene monomers where the ethene-group from styrene acts as a dienophile (Fig. 1b).

The Diels-Alder reaction gives some structural possibilities. This question of regioselectivity arises when the diene and alkene are un-symmetrically substituted. The preference can be understood from the frontier orbital theory where for styrene/acrylonitryle and styrene/styrene Diels-Alder reaction the region of chemical preference is observed in the ``para/meta``-like form. Moreover, regarding the geometric isomerism, cis and trans isomers are existing.

The Diels-Alder dimers allow another second addition reaction with an available monomer which is able to make a stable group of Diels-Alder trimers[2,3]. During the addition reaction the initial benzene structure receives again its` aromaticity. After this reaction there are a few enantiomers possible due to the fact that the stereospecificity and regiochemistry of the addition is respected. This explains that in some additions R or S chirality is appearing due to the formation of chirality centers (Fig. 2).

The second addition reaction result in a group of stable Diels-Alder trimers which can be categorized in three classes (Fig. 3). The most abundant Diels-Alder trimer from (styrene + acrylonitrile + acrylonitrile) is 4-cyano-1,2,3,4-tetrahydro--1-naphthaleneacetonitrile (THAN) with 4 structural possibilities (cis-S-THAN, cis-R-THAN, trans-S-THAN and trans-R-THAN).

A less abundant Diels-Alder trimer from (styrene + acrylonitrile + acrylonitrile) is the 4-cyano-1,2,3,4-tetrahydro-1-naphthalenepropanenitrile (THNP) with 2 structural possibilities (cis-THNP and trans-THNP). The THAN and

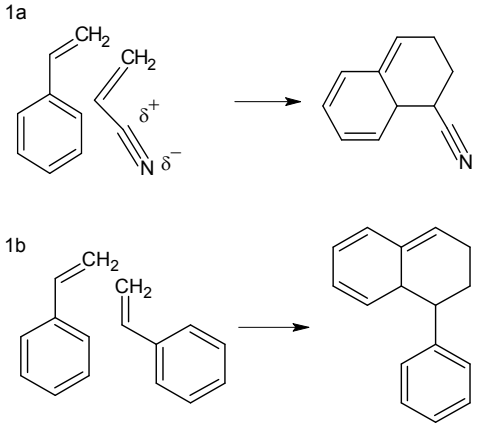

Fig. 1. **Diels-Alder reaction between styrene and acrylonitrile (1a) and between 2 styrene monomers (1b).** Both are shown in the ``para``-like form. The nitrile –and phenyl-group can appear in cis or trans

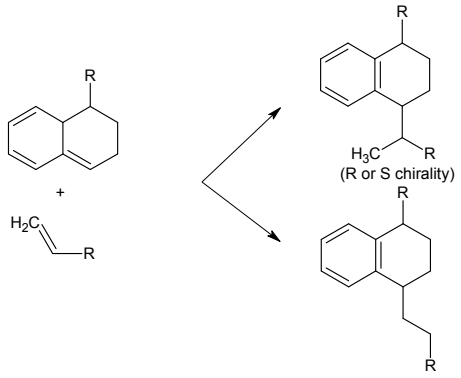

Fig. 2. **Second addition step to the Diels-Alder dimer with 2 addition possibilities and creating R or S chirality centers.** R, as substituent, represents the phenyl or nitrile-group.

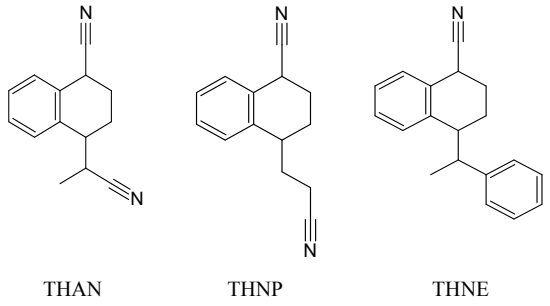

Fig. 3. **Overview of the main abundant Diels-Alder trimers from SAN/ABS**

THNP are quite common in SAN due to the fact they are the result of the Diels-Alder reaction between acrylonitrile and styrene.

Another abundant Diels-Alder trimer based on 3 styrene monomer units is the 4-cyano-1,2,3,4-tetrahydro-phenyl-1--naphthalene-ethane (THNE) which has again chiral and cis/ trans conformation possibilities.

Identification of emissions

In order to get introduced with potential emissions from ABS/SAN, a sample of ABS was thermally desorbed at 250 ° C for 2 minutes. The evolved emissions were separated by gas chromatography and identified by mass spectrometry under electron impact ionization (70 eV). The results are shown in Fig. 4 and explained in Tab. I.

Despite the fact that ABS contains a big part of polybutadiene, most of the emissions are related to the styrene acrylonitrile combinations. Therefore the oligomers are already formed during the SAN chemistry process.

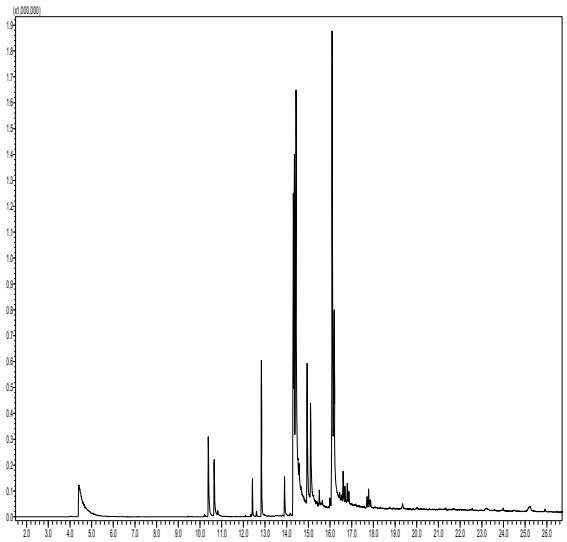

Fig. 4. **Thermal desorption GC-MS chromatogram of ABS**

Table I
Identification of emissions in a sample of ABS

t_R [minutes]	Identification
4,5	Free styrene
10,1-11,1	Styrene dimers (linear combinations: head-tail, head-head, tail-tail)
12,2-13,2	(2-Phenylcyclobutyl)benzene with cyclic combinations in trans and cis
13,8	4-Phenylcyclohexene
14,2-14,8	THAN (group of 4 isomers)
14,8-15,4	THNP (group of 2 isomers)
16,0-16,5	THNE (group of 4 isomers)
17,0-19,0	Styrene trimers (linear combinations)
others	All other peaks were identified as linear combinations of styrene and acrylonitrile

Influence on the car indoor environment according to VDA 278

In total 5 ABS samples from car interior parts were selected for this study. The emissions were quantified and evaluated according to the non-metallic emission testing procedure of VDA (Verband der Automobilindustrie) number 278. VDA is the German quality management system for the automobile industry which is concerned about the passengers` health, comfort and protection. The standard VDA 278 requires emission testing of non-metal materials intended for use in automotive industry and is based on analytical thermal desorption by a semi-quantitative method. This test method requires dynamic desorption of analytes from the solid phase (sample) to a vapour phase (emissions). The VDA 278 is for

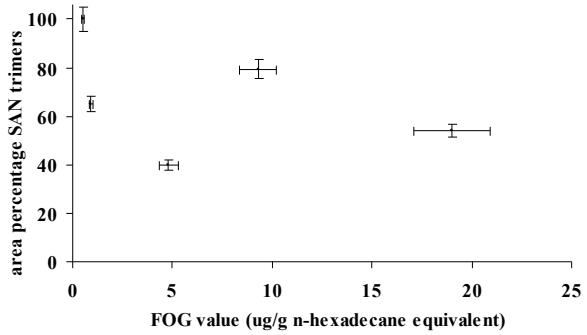

Fig. 5. **Test results from FOG measurement of 5 ABS samples**

many years already a reference for the European automotive industry.

The samples were cut into small pieces and thermally desorbed at a temperature of 90 °C for 30 minutes. The emission area was compared according to a toluene standard and is expressed as a volatile organic carbon value (VOC) or toluene equivalent emission in ug g^{-1}. The limit of detection is 0,2 ug g^{-1} toluene equivalent.

The same sample is once more thermally desorbed at a temperature of 120 °C for 60 minutes. The emission area was compared according to a *n*-hexadecane standard and is expressed as a fogging value (FOG) or *n*-hexadecane equivalent emission in ug g^{-1}. The limit of detection is 0,2 ug g^{-1} *n*-hexadecane equivalent.

The main emissions from ABS after VOC testing are ethylbenzene and styrene. Free styrene will be ever presented in VOC tests due to the availability in the polymer and volatility. In the VOC fraction no Diels-Alder trimers were detected. The limit of detection is 0,2 ug g^{-1}.

The Diels-Alder trimers are more a concern for the fogging results. In each ABS sample they are appearing and are responsible for an additional FOG value ranging from 0,5 till 19,2 ug g^{-1} *n*-hexadecane equivalent. Depending on the quality and composition of the polymer, the area percent of the emissions coming from the Diels-Alder trimers is ranging between 40 and 100 area percent from the total emission peak area. Fig. 5 compares the total FOG value from the Diels-Alder trimers (sum of THAN, THNP and THNE) with the area percentage of the Diels-Alder trimers relative to the total emission area.

Conclusion

Diels-Alder trimers are always presented in SAN/ABS as they are created during the SAN production. As ABS is used as a car indoor material, the influence of the car indoor quality from the SAN Diels-Alder trimers was investigated according the principle of the VDA 278 emission analysis. In the VOC fraction traces of free styrene or ethylbenzene were detected. However in the FOG fraction, the higher amount of emissions is related to the presence of stable Diels-Alder trimers from the SAN production. Always very abundant were seen THAN, THNP and THNE in all measured samples. No emissions from the butadiene rubber were detected.

REFERENCES

1. Commision regulation (EU) No 10/2011 on plastic materials and articles intended to come into contact with food of 14 January 2011.
2. Michael L. Gargas: Toxicology Letters, 178, 1–8 (2008) DOI: 10.1016/j.toxlet.2008.01.016
3. A. Ferrando.: Eur. Polym. J. *32*, 899 (1996).
4. Baier HU: Shimadzu news 2 (2007).
5. VDA 278 (2000).

P-38
THE STUDY OF INFLUENCE OF METAL POWDER FILLERS ON THE PROPERTIES OF COMPOSITE MATERIALS

JANA REKOŠOVÁ[a], ZUZANA NÓGELLOVÁ[b], IVAN HUDEC[a], and IVAN CHODÁK[b]

[a] Slovak University of Technology in Bratislava, Faculty of Chemical and Food Technology, Institute of Polymer Materials, Department of Plastics and Rubber, Radlinského 9, 812 37 Bratislava, [b] Slovak Academy of Sciences, Polymer Institute, Dúbravská cesta 9, 845 41 Bratislava 45, Slovak Republic
jana.rekosova@stuba.sk

Introduction

Among the advanced engineering materials and different of applications, metal matrix composites (MMC) are of great interest owing to their remarkable mechanical properties, including low density, strength etc. The driving force behind the development of MMC is the possibility to tailor their properties to meet specific requirements, which renders this type of material unique in comparison with conventional unreinforced materials[1].

In this work mechanical properties and the impact resistance of composite materials based on polyamide and metal powder fillers were studied.

Experimental

For the preparation of polymer composite materials commercially available ferrosilicium powder (Kovohuty, Dolný Kubín, Slovak Republic), aluminium powder (ALBO SCHLENK, a.s., Czech Republic) and magnesium powder filler (Ing. Jozef Vrba – Práškové Kovy, Czech Republic) were applied. As a matrix for the preparation of composite materials the polyamide (PA 12) Vestamid®, as a modifier NBR – Europrene N 3345, (Polimeri, Italy) and compatibilizer Joncryl® ADR 4300 S (BASF, Ludwigshafen, Germany) were used.

The particle size distribution of metal powder fillers were confirmed by laser analyser Cilas 1064L and pore size of metal fillers on the device Porosimeter Series 2000, Fisons Instruments, were measured.

The composite materials filled with metal powder fillers were prepared by melt mixing in 30 cm^3 mixing chamber of Plasticorder Brabender PLE 331 at the temperature 190 °C, speed 35 rpm min^{-1} and time of mixing 8 minutes. The modified composite materials were prepared by two – stage mixing. In the first stage the batch of metal powder fillers and NBR was prepared. In the second stage this batch was inserted to the polyamide matrix followed by addition of compatibilizer Joncryl. The composite materials with different content of powder fillers in the range from 0 to 30 wt.% were prepared.

The prepared compounds were moulded in the laboratory press Fontijne Holland Model TP 50. The physical-mechanical properties of prepared composites were performed using testing instrument Instron 3365. The impact resistance was measured by Charpy notch impact test. The tests were performed at room temperature and at 0 °C.

Results and discussion

The study of structural characteristics showed that the particle size distribution diameters at 50 % of ferrosilicium powder filler was 42,99 μm (Fig. 1), of aluminium powder filler 19 μm (Fig. 2) and of magnesium powder filler 71,72 μm (Fig. 3). The distribution curve of aluminium powder filler has three fraction of filler contrary to aluminium and magnesium powder filler.

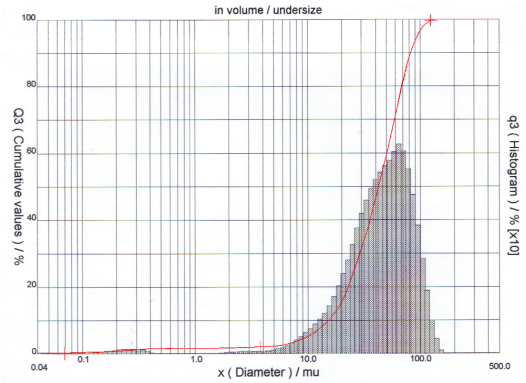

Fig. 1. **Particle size distribution of ferrosilicium powder filler**

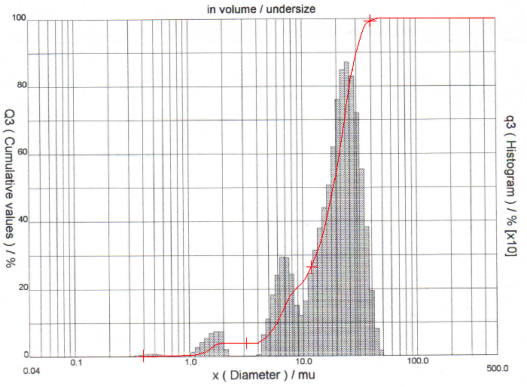

Fig. 2. **Particle size distribution of aluminium powder filler**

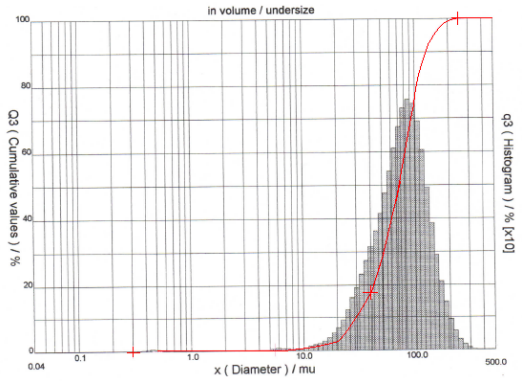

Fig. 3. **Particle size distribution of magnesium powder filler**

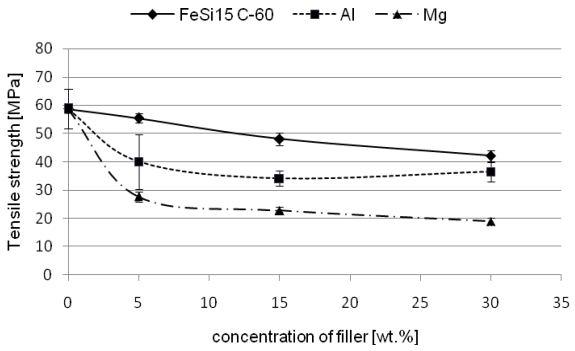

Fig. 4. **Influence of metal fillers content on tensile strength of composites based on polyamide**

The mechanical properties of composite materials as the tensile strength, elongation at break and Young's modulus were evaluated. The influence of metal powder fillers content on tensile strength of composite materials is shown in Fig. 4. With increasing of amount of the metal powder the tensile strength decreases. The minimum decrease of tensile strength was obtained in composites filled with ferrosilicium filler.

In the case of elongation at break, which dependence on the metal fillers content is showed in Fig. 5, it is clear that with increasing of concentration of metal fillers the elongation at break slightly decreased in composites with ferrosilicium but in the case of the composites filled with aluminium and magnesium metal power marked decreasing of elongation at break were obtained.

The dependence of the Young's modulus on the concentration of the metal powder fillers is shown in the Fig. 6. The Young's modulus using aluminium powder is increased, but using of magnesium and ferrosilicium powder had practically identical character as virgin polyamide.

In Tab. I the results of mechanical properties and notch impact resistance of NBR modified composite materials with

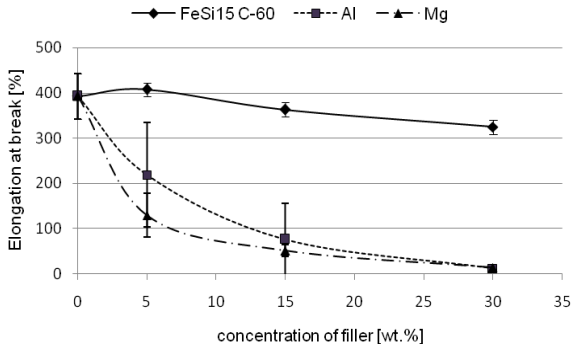

Fig. 5. **Influence of content of metal fillers on elongation at break of composites based on polyamide**

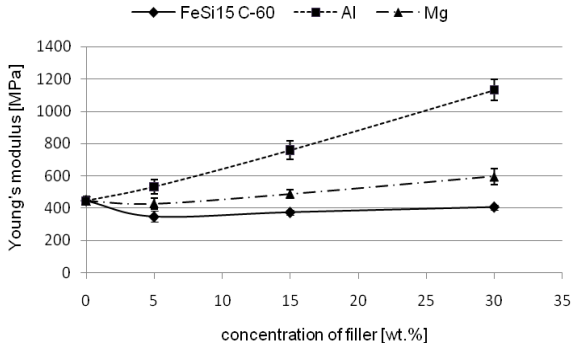

Fig. 6. **Influence of content of metal fillers on Young's modulus of composites based on polyamide**

Table I
Mechanical properties and notch impact resistance of NBR modified composite materials

Type of filler	PA virg.		Mg		Al		FeSi15 C-60	
	value	st. dev	value	st. dev	value	st. dev	value	st. dev
Tensile strength [MPa]	**60,59**	2,47	**28,53**	1,54	**38,68**	2,92	**31,85**	4,94
Elongation at break [%]	**408,34**	23,56	**264,45**	17,08	**324,97**	21,07	**265,30**	61,22
Young's modulus [MPa]	**383,44**	35,43	**430,10**	7,03	**574,52**	32,76	**326,04**	8,77
Notch impact resistance [kj/m*m]	**8,99**	0,55	**9,68**	0,45	**5,88**	0,42	**13,15**	1,41

20 % of metal powder fillers are shown. For some type of modified composite on mechanical properties was change. The values of notch impact in composite with magnesium and ferrosilicium were increased in comparison with virgin polyamide.

Conclusion

On the basis of experiments the polymer composite materials filled with metal powder fillers it is obvious that various different metal fillers incorporated to the polyamide matrix have different effect on mechanical properties. It is caused by various density of the filler, the shape of the filler and its dispergation in the polymer matrix etc. The results of NBR modified composite materials showed that the tensile strength and elongation at break increased by composites with magnesium and aluminium powder in comparison with composites without modifiers. On the contrary, the mechanical properties of NBR modified composite with ferrosilicium decrease compared with unmodified composite material filled with ferrosilicium powder.

On the other hand from results of testing of the notch impact resistance of modified composite materials the best results were achieved in composite with ferrosilicium metal powder filler.

This work was supported by the Slovak Research and Development Agency under the contract No. APVV-0062-11 and by the Scientific Grant Agency of the Ministry of Education, Science, Research and Sport of the Slovak Republic and the Slovak Academy of Sciences (VEGA), projects No. VG-1/1163/12 and VG-1/1325/12.

REFERENCE

1. Scudino S., Liu G., Prashanth K. G., Bartusch B., Surreddi K. B., Murty B. S., Eckert J.: Acta Materialia *57*, 2029 (2009).

P-39
MECHANICAL PROPERTIES OF MODIFIED POLYPROPYLENE FIBRES FOR REINFORCED CONCRETE

JOZEF RYBA[a], ANNA UJHELYIOVÁ[a], ĽUBA HORBANOVÁ, and PETER MICHLÍK[b]

[a] Department of Fibres and Textile Chemistry, Institute of Polymer Materials, Faculty of Chemical and Food Technology, Slovak University of Technology in Bratislava, Radlinského 9, 812 37 Bratislava, [b] Research Institute for Man-Made Fibres, a.s., Štúrova 2, 059 21 Svit, Slovakia
jozef.ryba@stuba.sk

Abstract

Polypropylene (PP) fibres are chemically inert, sufficiently thermally stable, extremely strong, and the lightest from the textile fibres. In recent years they have become more attractive as the reinforcing additives for concrete matrices. Some properties, such as tensile strength, durability, shrinkage and permeability resistance of the concrete matrices, have been greatly improved after the concrete matrices were reinforced by PP fibres. However, the ordered chemical structure and lack of polar functionalities, as well as surface smoothness of PP fibres, result in poor adhesion characteristics between fibres and cement matrix. Before fibre reaches its best tensile strength, fibres and cement matrices have already separated from each other, therefore the poor bonding characteristic is a limitation to the effective use of PP fibres in high performance concrete

matrices. During recent years modification procedures in preparation of new types of PP fibres are used. This leads to improvement of interfacial strength between PP fibres and cement matrices. Reinforced concrete modified by PP fibres is a novel concrete material, and will be more and more widely used in modern buildings.

Introduction

Synthetic fibers which are based on fiber-forming polymer blends belong to a special fiber group. A variability of properties in fibers and their fuctionality can be reached using two or more components in the fiber –forming blend[1].

Polypropylene (PP) is one of the most extensively used plastics both in developed and developing countries. It provides advantages in regard to economy (price), ecological (recycling

behavior) and technical requirements (higher thermal stability).

Today synthetic polymers are combined with various fillers in order to improve the mechanical properties and obtain the characteristics demanded in actual applications[2–4].

This article deals about influence of inorganic nano filler on the mechanical properties of modified polypropylene fibres.

Experimental

Materials used

The isotactic Ziegler-Natta polypropylene TATREN HT 1810 (PP), Slovnaft Petrochemicals Co., Slovakia, MFI = 20,9 g/10 min and masterbatch (MB) (inorganic nano filler (INF)) and PP were used for the preparation of modified PP fibres.

Preparation of modified PP fibres

The undrawn PP/MB fibres were prepared by conventional procedure of spinning from mechanical mixture using semi-industrial plant Fleissner with the extruder 2× Φ = 16 mm. It was equipped with side filling, temperature profile of 270 °C and 280 °C at branch with the take-up speed 120 m min^{-1} at the spinning. The prepared undrawn fibres were drawn in range of drawing ratios from 2.0 to 4.0.

Method used

Mechanical properties were measured and evaluated according to STN EN ISO 139, 2060, 2062 – standard methods for evaluation of mechanical parameters.

Results

Mechanical properties of non-modified and modified PP fibres for both profiles type are shown in Table I and Table II.

Fineness of modified fibres is slightly higher in consequence of addition of inorganic nano filler (2 % or 4 %) in comparison with nonmodified PP fibres.

Table I
Drawing ratio λ, Fineness (T_d), tenacity (σ) and elongation (ε) at the break, Young's modulus (E) of the non-modified and modified PP fibres with circle profile

Sample	λ	T_d [dtex]	σ [cN/dtex]	ε [%]	E [cN/dtex]
PP	2.0	5.7	2.8	225	17.0
PP	2.5	5.7	3.5	194	25.4
PP	3.0	5.8	3.8	152	31.2
PP	3.5	5.7	4.7	136	34.5
PP	4.0	5.7	5.0	105	39.3
2 wt.% INF	2.0	5.8	2.3	325	17.2
2 wt.% INF	2.5	6	2.9	210	19.4
2 wt.% INF	3.0	5.9	3.3	192	26.2
2 wt.% INF	3.5	5.9	3.5	167	29.6
2 wt.% INF	4.0	5.9	3.9	127	33.9
4 wt.% INF	2.0	5.8	2.0	283	15.3
4 wt.% INF	2.5	6.1	2.5	195	18.4
4 wt.% INF	3.0	6.1	2.9	184	20.0
4 wt.% INF	3.5	6,0	3.3	156	25.6
4 wt.% INF	4.0	6.1	3.4	127	30.2

Tenacity at the break of nonmodified PP fibres is higher with increase of drawing ratio. Tenacity at break of modified PP fibres is 20 % or 30 % lower in comparison with non-modified PP fibres at all drawing ratios. Similar situation occurs in case of Young's modulus.

Tenacity at break of modified PP fibres with circle profile is higher in comparison with modified PP fibres with star profile is higher. This is related with probability of inperfection in supramolecular structure for star profile.

These observations relate with lower amount of polypropylene in matrix of composite fibres and also with amount and influence of particles of nano filler onto supramolecular structure of modified PP fibres.

Elongation at break of nonmodified and modified PP fibres markedly decrease with higher drawing ration. Differences are lower with increase of drawing ratio. Evenness of mechanical properties is comparable.

For modified PP fibres was proofed influence of content of nano filler and degree of uniaxial orientation onto internal and surface supramolecular structure of fibres

Higher content of nano filler in matrix of modified PP fibres cause higher probability of creation of cavities that surround particles of nano filler.

Conclusion

On the backround of experimentally obtained results it can be concluded that:

– fineness of modified PP fibres is higher in comparison with fineness nonmodified PP fibres of due to content of nano filler.

Table II
Drawing ratio λ, Fineness (T_d), tenacity (σ) and elongation (ε) at the break, Young's modulus (E) of the non-modified and modified PP fibres with star profile

Sample	λ	T_d [dtex]	σ [cN/dtex]	ε [%]	E [cN/dtex]
PP	2.0	5.7	2.9	236	18.5
PP	2.5	5.7	3.2	178	22.2
PP	3.0	5.8	3.4	158	26.2
PP	3.5	5.7	3.9	142	29.0
PP	4.0	5.7	4.2	140	35.0
2 wt.% INF	2.0	5.8	2.1	321	17.8
2 wt.% INF	2.5	6.0	2.5	194	18.4
2 wt.% INF	3.0	5.9	3.3	169	24.7
2 wt.% INF	3.5	5.9	3.6	155	32.7
2 wt.% INF	4.0	5.9	3.9	97	40.3
4 wt.% INF	2.0	6.1	2.0	224	15.5
4 wt.% INF	2.5	6.1	2.2	161	18.1
4 wt.% INF	3.0	6.0	2.4	156	18.9
4 wt.% INF	3.5	6.1	2.6	118	28.6
4 wt.% INF	4.0	6.1	3.1	96	32.0

- change of cross-section geometry from circle to star has negative influence onto tenacity at break of modified PP fibres with star profile.
- Young's modulus of the modified PP fibres with star profile is slightly higher in comparison with modified PP fibres with circle profile.

Changes in supramolecular structure are caused by presence of nano filler in polymer matrix. This inperfection can cause better interphase interactions.Modified fibres like these are applicable for technical fabric and for improving of the other types of materials like concrete for example.

This work was supported by the VMSP-P-0007-09 and VEGA 1/0444/09.

REFERENCES

1. Ryba J., Ujhelyiová A., Horbanová Ľ., Michlík P.: *ITC&DC Book of Proceedings* – Dubrovnik Croatia, 93 (2012).
2. Yang H. S., Kim H. J., Park H. J., Lee B. J., Hwang T. S.: Comp. Struct. *72*, 429 (2006).
3. Yang H. S., Kim H. J., Park H. J., Lee B. J., Hwang T. S.: Comp. Struct. *77*, 45 (2007).
4. Choi N. W., Mori I., Ohama Y.: Waste Manage *26*, 189 (2006).

P-40

EFFECT OF COOLING SYSTEM ON DEFORMATION AND PRODUCTION TIME OF THE PRODUCT

VOJTECH SENKERIK*, MICHAL STANEK, MIROSLAV MANAS, DAVID MANAS, and ADAM SKROBAK

Tomas Bata University in Zlin, nam. T. G. Masaryka 5555, 760 01 Zlin, Czech Republic
vsenkerik@ft.tub.cz

Abstract

This research paper deals with construction solution of an injection mold for specific product in automotive industry. Differences in deformations and production time between individual versions are rather significant. There are different layouts of drilled cooling channels and their influence on deformation compared. Analysis results show that it influence mainly on manufacturing production and also deformation. Eligible usage of these parameters can improve quality – lower product deformation.

1. Introduction

Injection molding is the most commonly used manufacturing process for the fabrication of plastic parts. It is suitable for mass production of consumer articles, since raw material can be converted into inject by a single procedure. An important advantage of injection molding is that with it we can make complex geometries in one production step in an automated process. The injection molding technique has to meet the ever increasing demand for a high quality product (in terms of both consumption properties and geometry) that is still economically priced.

This is feasible only if the molder can adequately control the whole molding process, if the configuration of the molded part is adapted to the characteristics of the molding polymer material and the respective conversion technique. Typical injection moldings can be found everywhere in daily life; examples include toys, automotive parts, micro parts, household articles and consumer electronic goods. For plastic injection molding, gate location has a significant effect on part quality and can determine if the part can be molded successfully. Some of the effects attributable to cooling system are: warpage, shrinkage. In addition, as cooling system has an effect on the cooling processing history and cooling time.

2. Experiment

Attention is focused on the cooling system. Several injection molds were designed with different variants of the cooling system, which were subsequently analyzed. The aim was to design the simplest mold in terms of functionality and price and also maintaining acceptable quality.

Water was chosen for cooling because of its high cooling effect. It is cheap and environmentally friendly, unlike oil. The channels have a diameter of 10 mm, only

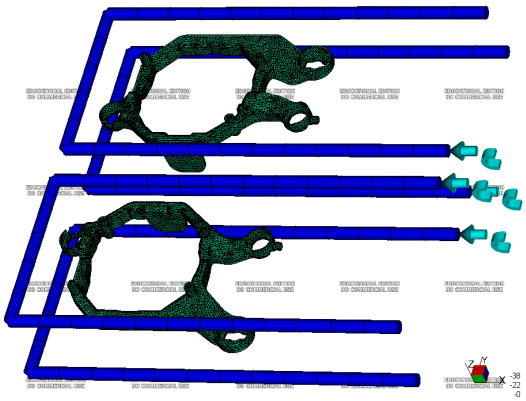

Fig. 1. **Cooling system version 1**

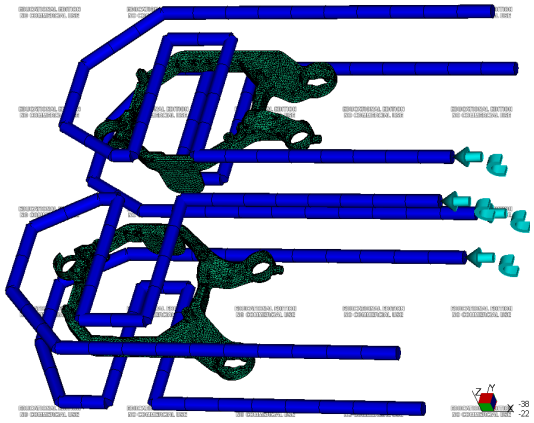

Fig. 2. **Cooling system version 2**

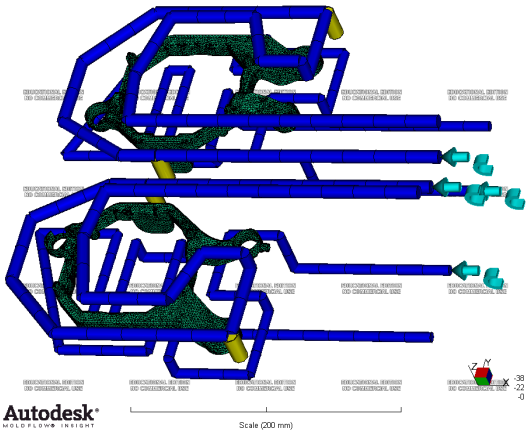

Fig. 3. **Cooling system version 3**

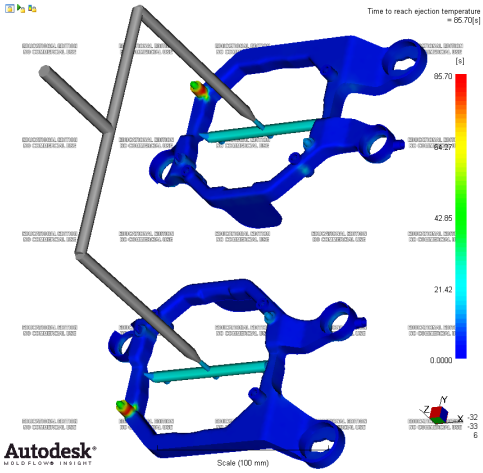

Fig. 4. **Time to reach ejection temperature, cooling system version 1**

cooling system version 3 uses diameter 8mm in the cavity because of better intertwine between the shape cavity, ejectors and replaceable inserts.

Cooling system version 1 (Fig. 1) has the simplest shape and a large distance between the cooling channels and sprue channels.

Cooling system version 2 (Fig. 2) has a more complex shape which partially copies the shape of the product and it cools the area around the sprue channels.

Cooling system version 3 (Fig. 3) has a very difficult storied shape that best copies the shape of the product and which contains two buffle elements for one cavity for cooling further parts of the inserts and cooling channels. Better heat distribution is achieved.

3. Results

Analysis of time to reach the ejection temperature is very important. It displays the time needed for ejection of the product, measured since the beginning of injection molding process.

The longest time for cooling down to the ejection temperature is at protrusion because there is quite a thick wall. It would be appropriate to modify this part of the product so that there was less material and thus also reduce the ejection time and material consumption.

One way to speed up cooling would be to insert another baffle element next to protrusion. The cooling system version

Table I
Time to reach ejection temperature

Version of cooling system	Time to eject [s]	Difference [%]
Version1	85.70	100.00
Version 2	79.66	92.95
Version 3	77.98	90.99

Table II
Total deformation

Version of cooling system	Deformation [mm]	Difference [%]
Version1	1.477	98.66
Version 2	1.497	100.00
Version 3	1.441	96.26

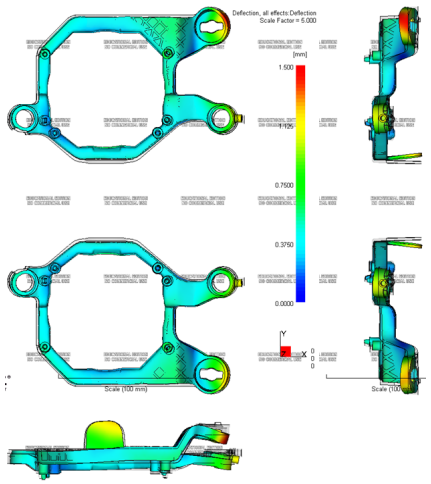

Fig. 5. **Total deformation for the cooling system version 3**

3 already has two baffles and adding another baffle would raise the pressure loss in cooling medium. Higher number of baffles means greater loss of pressure in cooling system.

The cooling system version 1 takes the longest time to reach the ejection temperature. The version 2 cools the examined product by nearly 7 % faster than the version 1. The version 3 cools the product the fastest, by 2 % faster than cooling 2 and up to 9 % faster than cooling 1.

Fig. 5 shows that the product made using cooling system version 3 has the smallest deformation. Overall, the product is not too deformed in middle part, but side construction lug is twisted to main lengthwise plane of product, scale is 5:1. The total deformation is affected by shrinkage, orientation, cooling system, and also mentioned the gate position.

In Table II can be seen difference deformations. These deformations are very similar, because each deformation has the same design molds that differ only by cooling system. Thus, differences between the deformations are only a cooling effect on the product. The difference of the influence between cooling systems versions 1 and 2 is nearly 1.5 %, which is relatively insignificant size and between 2 and 3 is nearly 4 %. The cooling system version 3 has the most optimal cooling temperature field distribution and thus the product deforms the least.

4. Conclusion

The objective of this research is to study the influence of cooling system. Filling and deformation analysis of the specific real plastic product, which is support frame for light module to front headlight of car, was performed.

Several variants of cooling systems were designed with varied shape, complexity and usage baffle elements. They were analyzed and compared with each other. Complete analysis of filling, including runner and cooling system was performed. Analysis revealed differences between the designed cooling systems versions. By appropriate usage of these proposals a smaller deformation and increased productivity of the product can be achieved.

This paper is supported by the internal grant of TBU in Zlin No. IGA/FT/2013/020 funded from the resources of specific university research and by the European Regional Development Fund under the project CEBIA-Tech No. CZ.1.05/2.1.00/03.0089.

REFERENCES

1. Manas D., Manas M., Stanek M., Danek M.: Arch. Mater. Sci. Eng. *32*, 69 (2008).
2. K. Kyas, M. Stanek, Manas, M. Stanek, M. Krumal, Z. Holik: Chem. Listy *105*, s354 (2011).
3. D. Manas, et al.: Thin Solid Films *530*, 49 (2013).

P-41
INFLUENCE OF PRODUCTION PROCESS ON MECHANICAL PROPERTIES OF RUBBER SAMPLES

ADAM SKROBAK*, MICHAL STANEK, DAVID MANAS, MIROSLAV MANAS, VOJTECH SENKERIK, and KAMIL KYAS

Tomas Bata University in Zlin, nam. T. G. Masaryka 5555, 760 01 Zlin, Czech Republic
skrobak@ft.tub.cz

Abstract

This paper shows how is changed the mechanical properties of rubber products based on changes in the technological process of production. It compares two basic production methods, such as compression molding and injection molding of rubber components.

1. Introduction

In the compression molding process, a sample is preweighed and pre-formed so as to fill the mold cavity quickly and easily when the mold is closed. The mold is held closed with the sample under pressure until sufficient time has elapsed for vulcanization. The mold is then opened, the sample removed and the mold cleaned and reloaded for the next cure. Cavity pressure is maintained by slightly

overfilling the mold and by forcing the mold components together, usually with a hydraulic press. The heat for curing is provided by electric heaters.

Injection molding of vulcanizing rubber compounds combines components of simpler forming and molding processes into an integrated feed and mold system. The most basic component of this process is similar to compression molding. In recent years, technology of injection molding has led to a very productive manufacturing process.

The injection molding process consists of an injection machine, mold and a rubber compound. Each component influences the success of every molding cycle. Batch variation of a rubber compound particularly affects the success of each molding cycle. Rubber compounds contain many ingredients and require a complex mixing and preparation process that can cause significant variation from batch to batch.

Rubber compounds can – like any other – undergo a series of tests (tensile properties, structural strength). Test samples are used for these tests, their shape and dimensions are prescribed by the standards. All materials and products covered by these test methods must withstand tensile forces for adequate performance in certain applications. These test methods cover procedures used to evaluate the tensile (tension) properties of vulcanized thermoset rubbers and thermoplastic elastomers.

No studies with this research have, to our best knowledge, been published, this area is still unexplored.

In order to conduct such research, in the first step, the injection mold had to be designed (Fig. 2).

It is a well-known fact that elastomeric mixture consists of various ingredients of different quantities; each mixture is the original with different flow properties. This rheological behavior of each elastomeric compound inside the mold during filling and subsequent vulcanization must be known beforehand. In the second step, software Cadmould 3D-F was used for these analyses and subsequent optimization of the processes (Fig. 3).

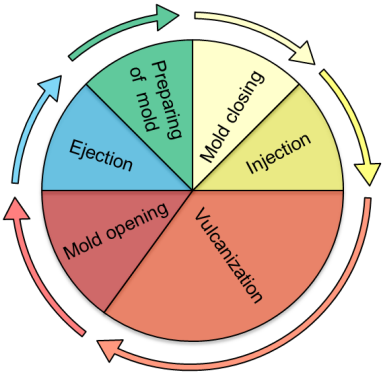

Fig. 1. **Assembly of injection mold**

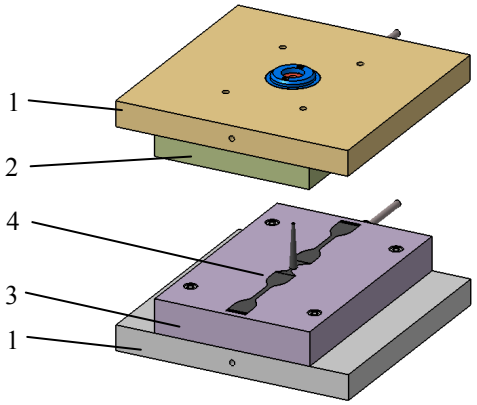

Fig. 2. **Assembly of injection mold;** 1 – frame, 2 – upper plate, 3 – lower plate, 4 – testing samples

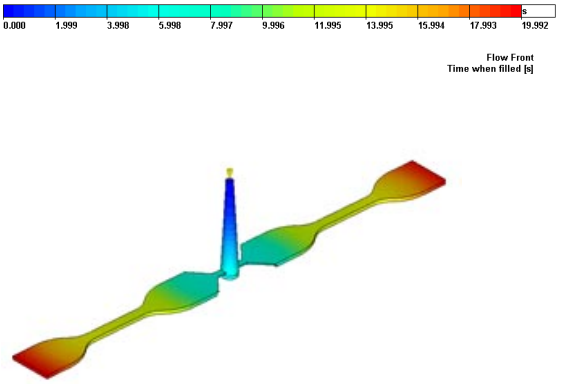

Fig. 3. **Injection molding analysis**

2. Measurement method

This paper deals with the preparation of rubber samples to determine their tensile properties and tear strength. Tread rubber compound was used as material of samples.

A standard test sample the shape of dumbbell is used for the test of tensile strength. The sample has the norm prescribed dimensions and shape, which must be preserved.

Firstly, test sample was produced both compression molding and injection molding. Secondly, the test samples were stretched at a standard constant rate 500 mm min^{-1} using the special clamping jaws at each end of the sample in the tensile stress machine Tensometer 2000 Alpha Technologies. The tensometer can automatically evaluate the measured data, such as Tensile stress, stress at given elongation (100 %, 200 %, 300 %) were evaluated of tensile test.

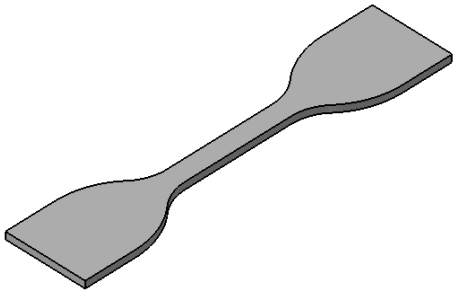

Fig. 4. **Dumbbell test sample for determination of tensile stress-strain properties (ISO 37)**

3. Results

Fig. 5 shows tensile curves for test samples made by compression molding technology.

Fig. 6 shows tensile curves for test samples made by injection molding technology.

Table I compares the results, specifically the tensile stress, tread rubber compound of the processed compression molding and injection molding. As shown in Table, injected samples have higher values of tensile stress than pressed samples.

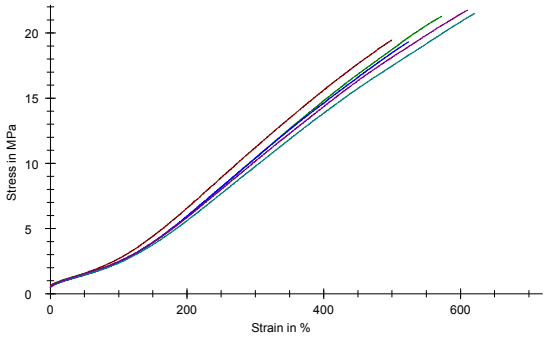

Fig. 5. **Tensile test of test samples made by compression molding**

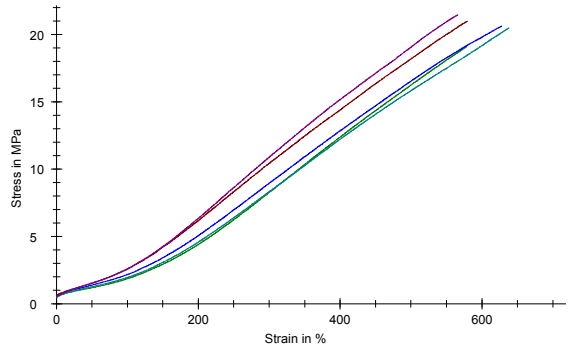

Fig. 6. **Tensile test of test samples made by injection molding**

Table I
Comparison of tensile tests

	Break stress [MPa]	Break strain [%]	Mod. 100% [MPa]	Mod. 200% [MPa]	Mod. 300% [MPa]
Compression molding	20,54	598,3	2,22	5,30	9,36
Injection molding	22,67	620,8	2,65	5,97	10,58

4. Conclusion

The results indicate, overall, that injected samples have better tensile and tear properties than the compressed samples. The samples produced by injection molding exhibit improved properties, thanks to a more regular arrangement of macromolecular chains, which are aligned linear flow during the filling of the mold cavity. The other way around, samples made by cutting from the pre-compressed plates are negatively affected by transverse micro-cracks, which arise after cutting knives and just in these micro-cracks under load concentrated stress which adversely effects the elongation and strength of the sample. In this paper was shown that the technological process of manufacturing rubber products cannot be selected at random, but must be considered what function the product will perform and how the product will be loaded.

This paper is supported by the internal grant of TBU in Zlin No. IGA/FT/2013/020 funded from the resources of specific university research and by the European Regional Development Fund under the project CEBIA-Tech No. CZ.1.05/2.1.00/03.0089.

REFERENCES

1. Sezna J. A.: Rubber World *207*, 12 (1993).
2. Kyas K, et al.: Int. J. Math. Comput. Simulation *6*, 600 (2013).

P-42
PLASTIC WASTE AS A GOOD RAW MATERIAL FOR DESIGN MODULAR FLOOD BARRIER

ĽUBOMÍR ŠOOŠ, JURAJ ONDRUŠKA, PETER BIATH, VILIAM ČAČKO, MILOŠ MATÚŠ, MICHAL ČEKAN, PETER KRIZAN, and JURAJ BENIAK

Faculty of mechanical engineering STU in Bratislava, Nám. Slobody 17, 812 31 Bratislava, Slovakia
lubomir.soos@stuba.sk

The Slovak university of technology in Bratislava is currently involved in the project "Research of progressive technologies for the recovery of waste from scrap automobiles"[1] , in harmony with the priorities of the Slovak ministry of environment (SME). The principal coordinator of the project is the faculty of mechanical engineering, and the project is financed by the Recycling fund in Slovakia. SME has stated in a press release that: "foremost, the effective protection against flooding, and the reduction of environmental burdens in sensitive and national park zones remain our priority". (SME, Ing. Peter Žiga, PhD., press release ME SR, 1.7.2012.)."

Design of flood barrier

The basic requirements for the new barrier were that it would be: produced from recycled materials, self-anchoring but not permanently anchored to the ground, could be used on firm and soft ground, allow for convex and concave configurations, can copy rough terrain, can be easily deployed and removed, and can adjust the barriers height. The investigators filed a utility model application no. SK 5847 Y12 entitled "Modular flood barrier structure"[2].

If the barriers are installed on firm ground, then a rubber seal, designed from waste rubber, is placed below the horizontal parts of both water barriers. Connecting the vertical parts is done by using attachment bars. To obtain greater stability, the vertical parts are mounted to each other in a pattern. In the case that the barriers are located on uneven or soft ground, then anchoring pikes are used on the horizontal parts.

Before the development of the prototype, it was necessary to define the conditions under which the development team could determine appropriate solutions. In terms of innovative structural design, it was necessary to take into consideration some important factors: cost of production, assembly and disassembly, internal and external stability, flexibility, storage, and risk and safety. These factors have been attributed in the development process according to the importance of each one. Based on the comprehensive assessment of the whole structure the final design of the structure was proposed.

For a better understanding of the system, some important structural characteristics are considered. In order to maximize the strength of the barrier wall with a sloping height of 2 m, a pattern arrangement of two different block sizes is proposed (0,5 and 1 m blocks). The plastic half blocks are made by dividing larger 1×1 m blocks. In order to connect the blocks together in the vertical direction, a figure-eight connection concept is adopted (Fig. 2). In this way, a connection is created which ensures adequate strength, flexibility, and ease of connection in even the toughest of conditions. It also allows for a large difference (vertical movement – adaptability to varying terrain) between each individual block. In order to reduce excessive leaks between the blocks, terrain, and walls, a UV resistant sleeve made of sufficiently strong sheets was designed. These sheets are a cost effective solution

Anchoring the support rods (Fig. 5) to the plastic blocks is designed to be relatively simple, but also sufficient in distributing load onto the double rib section of the blocks. The

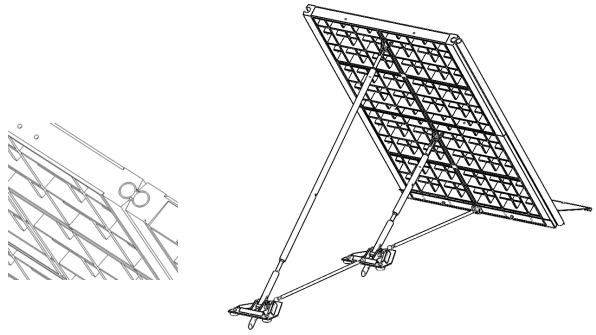

Fig. 2. **Modular structure of flood barrier, "figure-eight" connection**

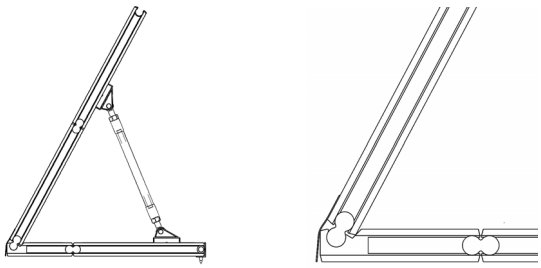

Fig. 1. **First virtual concept made from plastic**

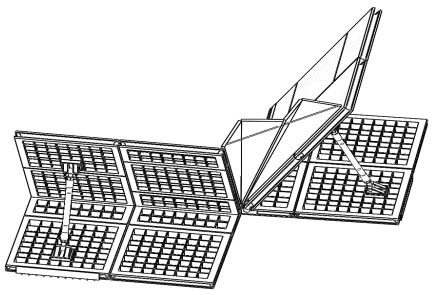

Fig. 3. **First virtual concept made from plastic**

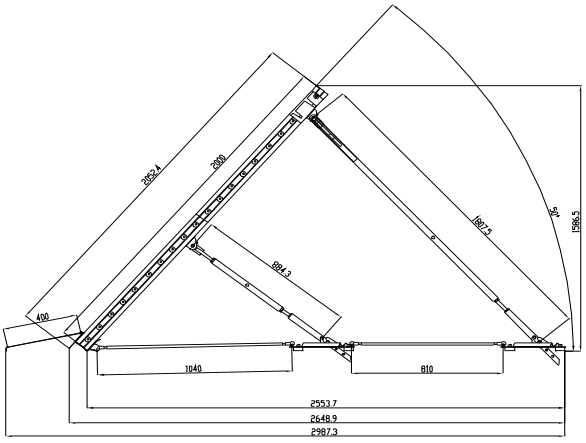

Fig. 4. **Dimensions of the modular flood barrier "side-view"**

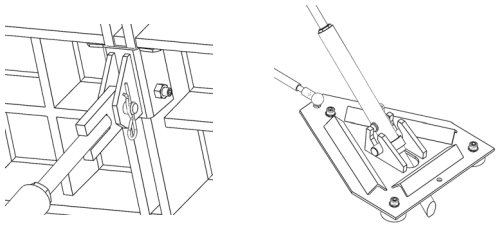

Fig. 5. **Structural nodes for support anchorage**

Fig. 6. **Static test under real conditions of hydrostatic loading in canal**

Fig. 7. **"Pool" test for the verification of maximum hydrostatic load**

length of the bracings can be adjusted in operation or in flooded conditions. Based on the calculations of internal and external stability, a flap is incorporated at the point of highest hydrostatic pressure which greatly increases safety. The FEA analysis of the structure and its individual parts allowed for calculating the optimal compromise between weight, strength, and geometry. The pattern structure of the plastic blocks connected by figure eight bars was structurally assessed. Based on the results, a simplification was designed for the length of the figure eight bars which were reduced to 700 mm which significantly simplifies the assembly and disassembly of the system.

An extendable tip provides versatility in anchoring in different types of terrain (Fig. 5).

After processing the necessary drawings and verifying the analysis results, a test sample for field testing of the flood protection system was produced.

Flood test by hydrostatic pressure

In the first stage of the projects realization, the investigators were able to develop a modular structure for flood barriers made from difficult to recover recycled materials. This is important, mainly in the recovery of composite materials from scrap automobiles. Parts of the prototype structure have been made at Chemosvit Environchem, a.s. and at the centre of innovation at STU. The investigators, in the first stage, decided to test the flood barriers with hydrostatic pressure to verify the theoretical basis of the design.

The flood test itself underwent a comprehensive analysis for determining where these tests would be performed. It was necessary to have a test site which encompassed the shape of the canal, its surface, water source, and above all, its safety and elimination of possible damage if the structure suddenly failed. As a result of the search for a suitable location to test the systems ability to withstand real conditions of water pressure and verify the stability of the individual modules, two tests were carried out at the water dam in Vištuk by Pezinok, Slovakia.

The first test was to erect a 3.6 m wide barrier on a rocky base with relatively perpendicular walls (Fig. 6). This test required that barrier to be assembled in one of the overflow canals by the dam. The second test involved constructing a square pool with the dimensions 3 × 3 meters entirely with the developed water barrier units (Fig. 7). Water was then pumped into the pool from a nearby source and filled to the intended max height of 160 cm. This test verified the integrity of the designed flood barrier at maximum water level for all criteria mentioned above. The ground consisted of a wet grass field which verified the ability of the barrier to be deployed in uneven terrain. The third, dry test was realized at a conference "Technology for environmental protection" – TOP2012.

Conclusion

Both verification tests obtained very positive results which complimented the designed structure and indicated that the flood barrier which was developed behaved very well under its intended operation.

This contribution/publication is the result of the project implementation: National Center for Research and Application of Renewable Energy Sources, ITMS 26240120016 supported by the Research & Development Operational Programme funded by the ERDF.

REFERENCES

1. Šooš Ľubomír, a kol.: Research of progressive waste recovery technologies for scrap vehicles, Project Recycling fund, April 2011.
2. Šooš Ľ., Prikkel K., Ondruška J., Olekšák J.: Modular structure of flood barrier. 16 s. : No. *Utility model: 5847 SK*, Effective as of: 19.8. 2011 (2011).

P-43
PRACTICAL USE OF LASER TECHNOLOGIES IN FIELD OF PLASTICS

LIBUŠE SÝKOROVÁ*, OLDŘICH ŠUBA, and JANA KNEDLOVÁ

Tomas Bata University in Zlin, Faculty of Technology, Department of Production Engineering, T. G. Masaryka 275, 762 72 Zlín, Czech Republic
sykorova@ft.utb.cz

Abstract

The paper deals with optimal adjust parameters of laser beam for laser marking of polymers. Commercial CO2 laser Mercury L-30 by firm LaserPro, USA was used for experimental describing. It was selected 5 basic of sorts covering materials, which was performed laser marking of text. The specimens were inspected and their characteristics were investigated. At last economic comparison of laser technologies and gold stamping no manual press was performed.

Introduction

Engraving belongs among non-conventional method of laser scribing that are based mainly on the physical or the physic-chemical principle of stock removal without the action of force on the machined material. This study deals with optimal setting of parameters of laser beam for booking scribing.

Experiment

Commercial CO2 laser Mercury L-30 by firm LaserPro, USA was used for experiment. It is possible to change power and feed rate of laser system. Ray of laser could be focused on mark diameter d = 185 μm. The maximum value of power is 30 W and maximum value of feed is 1066 mm s^{-1}. Laser is machining with the software help of Corel Draw. Wide spectrum of different materials (ceramic, quartz, plastic, rubber, wood and certain composite structures) can be scribed and machined by laser MERCURY L-30. This laser type is used mainly for commercial engraving.

Table I
Covering materials used for experiments

N.	Material title	Colour	Surface	Description
1	BALADEK	dark-blue	roughened of slight grooves	leather imitation
2	BALADEK	vinous	smooth without visible defects	leather imitation
3	IMPERIAL	green	visible cross and lengthwise fibrous structure	natural buckram
4	IMPERIAL	red	visible cross and lengthwise fibrous structure	natural buckram
5	COVERING PAPER	blue	rough, visible relief	properties like hard paper
6	NATURAL	white-grey	markedly visible structure fibrous	tow-cloth

5 basic types of covering materials were selected for experiment. These samples were scribed by laser. Each material differed from others by its colour, surface and structure – see Table I.

Experimental text was scribed with parameters combination of laser system – maximum feed 100% (1066 mm/s) and power was being changed – see Table II (ref.[1,4]).

Due to space limit is in paper showed only one described material IMPERIAL green – see Fig. 1.

Optimal parameters combination of laser system

Value of input characteristics are stated as a percents from maximal power (pmax=30W) and maximal feed (fmax=1066mm/s) – see table III.

Table II
Selected technological parameters for the experiment

Feed f [%]	Feed f [mm/s]	Power [%]	Power P [W]
100	1066	10	3
100	1066	7	2,1
100	1066	20	6
100	1066	40	12
100	1066	60	18
100	1066	80	24

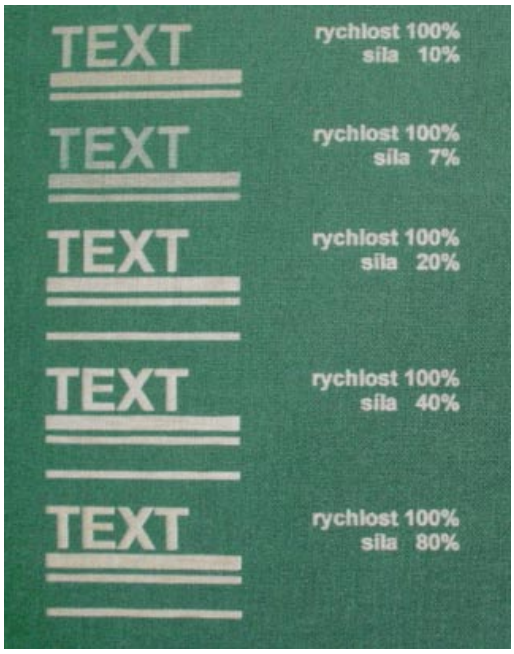

Fig. 1. **IMPERIAL (green)**

Table III
Optimal parameters combination of laser system for used materials

N.	Material title	Optimal feed	Optimal power	Annotation
1	BALADEK	100%	40-50%	Narrow interval of power is caused especially by properties of material surface layer
2	BALADEK	100%	40-80%	Power range mainly depends on required text colour
3	IMPERIAL	100%	20-80%	Text is even legible with power value under 20%
4	IMPERIAL	100%	20-80%	Text parameters are same as for the previous material
5	COVERING PAPER	100%	5-20%	Suitable for lower power value. The material began burn at power over 40%
6	NATURAL	100%	40-50%	Suitable for higher power - over 40%

Economic evaluation of laser scribing usage

The laser technology is usually used everywhere cannot be using conventional method of machining. The fast changes of working cycle can be applied with advantage by the laser system. It is possible to achieve high level of productivity with rapid symbol change in program Corel Draw[1,4].
Advantages of usage of laser system:
– good working conditions for machine operator
– silent running
– higher safety of work than conventional machining
– reduction man power and production place
– stock removal without the action of force on the machined material
– nearly maintenance-free
Disadvantages of usage of laser system:
– too high actual price of laser system
– necessity of the evaporated material exhaust
– difficult reparation in case of laser machine damage
– colour of the text is affected only by the character of some layers of used material

Economic comparison of laser technologies and manual gold stamping of a thesis title part

From experimental results it is possible to state the laser scribing of title part of thesis took about 4 minutes – attributable costs are about 0,5 EU.

It was also observed that the scribing time with common technology of manual gold stamping would take about 60 minutes – attributable costs are about 5 EU (ref.[1,4]).

Conclusion

From table is evident it is not necessary used lower feed than maximal for bookbinding laser scribing. Laser is capable to create desired text on the material surface even by low power value. Hence, it is not necessary to lower laser feed from the point of view productivity.

It is necessary to know suitable output parameters setting of specific laser system and properties of machined materials for obtaining good results of scribing by laser.

Furthermore, it was observed the laser power and properties of particular material layers have biggest influence on properties and appearance of scribing text. The optimal setting laser power in interval 40–50 % from maximal power of the laser machine was possible to use for almost all covering materials. Only covering paper was different because its properties are rather similar to normal paper than textile or imitation of leather.

Influence of the covering material colour was last factor which was evaluated. It was observed the colour does not influence properties and appearance of scribing text.

It stands to reason that technologies utilizing of laser beam are severalfold faster than gold stamping on manual press. Long adjustment and composing of single letters into desired text have biggest participation on long working time at gold stamping usage. While at laser scribing is this time shorter thanks to the work in Corel Draw software.

At the conclusion, it is possible to state that increasing of quality of scribing and machined surface, increasing of productivity and economic profit are main priority targets of laser scribing and machining[1–4].

REFERENCES

1. Žídek D.: *Diplomová práce*. FT VUT ve Zlíně, 2005.
2. Halaška P., Manas M.: Laser Cutting Optimization of the Polymeric Plates and Films. In: *42nd Sciece Week Laser Science and Applications*, 2.–4.11.2002, s. 80, University of Aleppo, Syria 2002.
3. Maňková I.: *Progresívné technologie*, Vienala, Košice 2000.
4. Sýkorová L.: *Výzkum mikroobrábění polymerních materialů laserem*. Ediční středisko VŠB-TU, Ostrava 2009.

P-44
FEM MODELLING OF MECHANICAL PROPERTIES OF INJECTION-MOULDED CYLINDRICAL PARTS REINFORCED WITH SHORT FIBRES

OLDŘICH ŠUBA, LIBUŠE SÝKOROVÁ, and ONDŘEJ BÍLEK

Tomas Bata University in Zlín, Faculty of Technology, Department of Production Engineering, T.G.Masaryka 275, 762 72 Zlín, Czech Republic
suba@ft.utb.cz

Abstract

An investigation was carried out through a study of the influence of material anisotropy of the cylindrical plastic parts reinforced by short-fibres, on the stress and deformation. It has been shown that the result of such injection-moulded processes is an anisotropic product, whose mechanical behaviour differs considerably for that of isotropic solids. Some unusual effects of their mechanical properties need to be considered in the course of designing of reinforced plastic parts.

Introduction

Plastic composite parts reinforced by short-fibres are, with increasing frequency, being applied to cases where an emphasis is placed on the level of the utility characteristics value of finished products. The outcome of the resultant distribution and orientation of such short-fibres is, generally speaking, an anisotropic and heterogeneous body whose mechanical behaviour may well be significantly different to that of a conventional understanding of the behaviour of isotropic and homogeneous bodies. A certain weak below of point from the perspective of a potential impairment is represented by thick cylindrical injection-moulded components. With isotropic and unreinforced plastic parts the reason lies in the geometric factor. For anisotropic and heterogeneous structures of injection moulded walls the resultant stress and deformation state due to curving are further affected by material factors.

Problem of layered orthotropic thick cylinder under internal pressure

Let us consider a basic case of a thick cylinder exposed to radial stress. As it is shown in Fig. 1, this can be considered to be a rotationally symmetrical problem. During the moulding process, the fibres may become oriented in a complex manner[1,2]. In the component itself, a characteristic quasi-layered structure is frequently observed. The fibres are oriented in quite different ways according to their location through the thickness of the wall. The polymer melt viscosity and flow rate significantly alter the proportions of the oriented regions. Obviously, for cases of fast injection speeds, the core of the moulding contains fibres mainly aligned perpendicular to the flow direction. Above and below this are regions with the predominant fibre orientation in the flow direction and most of the fibres are lying in planes parallel with the reference plane of the wall.

Selected types of idealized wall structures are shown in Fig. 2. The wall is divided into three layers of identical thicknesses, with different orientation of short fibres 0°, 90°. Case A – in this case it is considered that the short-fibres in skin layers are totally oriented in the direction of the periphery. Vice versa, in case B the fibres in core are totally oriented in the axial direction. The direction of orientation of the short-fibres in a totally oriented structure gives the axis of a monotropic material in given area. The material characteristics in case of linear elasticity are given by the set of elastic constants, making up the appropriate matrix of compliance.

Making up the set of effective elastic constants of a 3D monotropic structure on the basis of experimental measurement is virtually impossible. For this reason, the

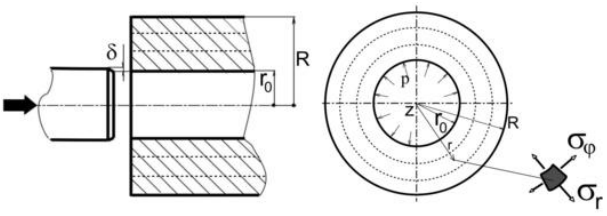

Fig. 1. **Cylindrically symmetric problem of cylindrical thick part**

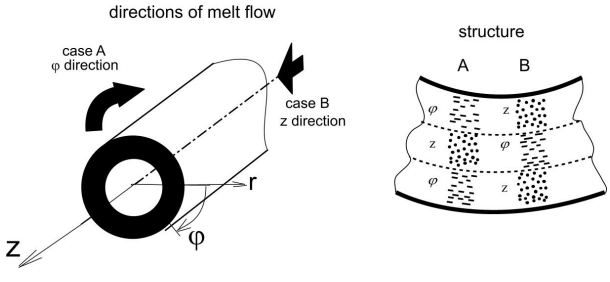

Fig. 2. **Idealized model structures of an injection-moulded cylindrical part**

theoretical prediction of these elastic constants is irreplaceable. We have already mentioned the outcomes of the modelling of the elastic behaviour of short-fibre plastic composites at the micro-mechanical level[2]. Here, we used the results achieved to establish the macro-mechanical model of the cylindrical injection moulded part.

For the purpose of studying the behaviour of highly orthotropic rounded plastic components, we selected an orthotropic case with following values of elastic constants: Modules of the elasticity: E_L = 10560 MPa, E_T = 2340 MPa, Poisson ratios: n_{LT} = 0.367, n_{TT} = 0.576, shear modulus: G_{LT} = 1000 MPa.

Stress state under radial loading

Distributions of stress components of idealised structures of injection wall are compared with stresses of unreinforced polymer, i.e. of isotropic and homogeneous case.

The FEM results are shown in the Fig. 3. Radial displacement of relative value $\delta / r_0 = 0{,}01$ is considered in the inner radius r_0. The values of the maximal peripheral and radial stresses are depicted for cases of structures A, B, and nonfilled that is isotropic and homogenous case. As it follows from the obtained results, peripheral stresses σ_φ reach diverse values dependently on resultant short-fibre structure. These values considerably differ from isotropic and homogenous – nonreinforced case.

In case of structure A, the core – transversal material direction T is strained slightly. However, extensive values of peripheral stress in material direction L imply significant disadvantage of this case. Vice versa, structure B shows low values of peripheral stress σ_φ in the direction L, but levels of stress in material direction T must be taken in account, because the transversal strength of fibrous structures is generally low, obviously at levels of unreinforced polymer.

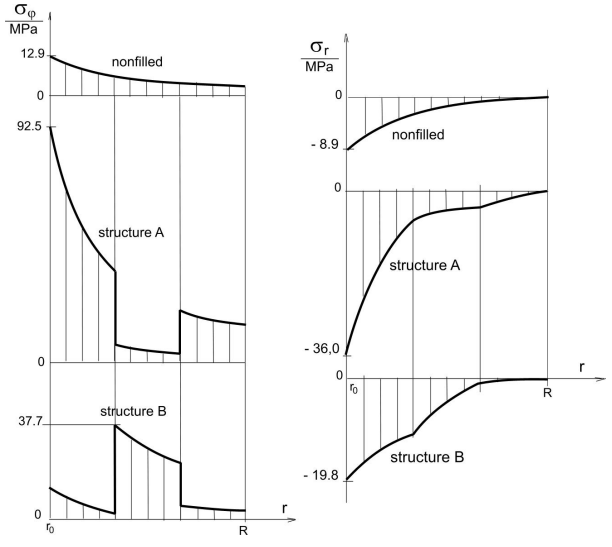

Fig. 3. **Distribution of peripheral stress σ_φ and radial stress σ_r for unreinforced and short-fibre reinforced injection-moulded cylindrical unit.** Curvature ratio R / r_0 =2,5 , relative radial displacement $d / r_0 = 0{,}01$

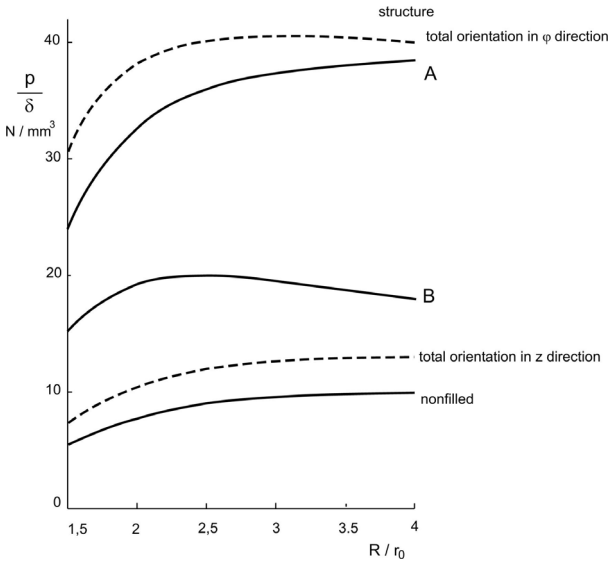

Fig. 4. **Values of radial stiffness versus curvature ratio R / r_0 for unreinforced and short-fibre reinforced injection-moulded cylindrical part.** Relative radial displacement $\delta / r_0 = 0{,}01$.

Similarly, the values of the maximal radial stresses σr are shown in Fig. 3. As has been demonstrated, there is substantial difference in the values of radial stress. However, in both case A and B, stress components σ_r in r_0 fall into the material direction T and thus it is necessary to consider these values of stresses when considering the mechanical behaviour in view of the generally low levels for transverse strength of fibrous materials.

Radial stiffness under radial loading

In order to illustrate the role of the injection-moulded structure in the thick rounded walls like cylindrical bosses, values of radial stiffness of idealised structures of injection wall are compared with unreinforced polymer, i.e. of isotropic and homogeneous case. The results are shown in the Fig. 4. As it follows from the obtained results, radial stiffness reach diverse values dependently on resultant short-fibre structure. These values considerably differ from isotropic and homogenous – nonreinforced case. Further it follows, that values of radial stiffness of cylindrical parts practically do not depend on curvature ratio in ranges of extensive values of R/ r_0.

Conclusions

Load capacity and stiffness of short fibre structures substantially differs from a nonfilled case and thus it is necessary to consider these values when considering the mechanical behaviour of injection moulded parts. The anisotropy and the heterogenity of mechanical properties caused by short-fibre orientation and distribution in melt flow can influence the macromechanical behaviour of injection

moulded parts. Therefore, it is necessary to pay attention to the design of products exposed to higher mechanical loadings. In such a way failures can be reduced at least.

REFERENCES

1. Matsuoka T., Takabatake J.-I., Inoue Y., Takahashi H.: Polym. Eng. Sci. *30*, 957 (1990).
2. Gupta K., Wang K. K.: Polym. Compos. *14*, 367 (1993).
3. Suba O.: In: *Proc. of PPS-16 The Polymer Processing Society, Shanghai, China*. p. 299–300, 2000.

P-45
EFFECT OF PLASTICEZER ON PROPERTIES OF PVA/SO BLENDS

STANISLAVA UHERKOVÁ[a], P. SKALKOVÁ[a], E. JÓNA[a], V. PAVLÍK[b], and I. KOVÁROVÁ[a]

[a] *Faculty of Industrial Technologies, Trenčín University of A. Dubček, I. Krasku 491/30, 020 01 Púchov,* [b] *Institute of Inorganic Chemistry, Slovak Academy of Sciences, Department Of Molten Systems, Dúbravská cesta 9, 945 36 Bratislava 45, Slovak Republic*
uherkova.stanka.u@gmail.com

In recent years, the increasing demand for eco-friendliness packaging and the emphasis of growing environmental awareness stimulated the search for alternative products obtained from renewable sources. One of the many approaches to produce eco-friendly material was to blend biodegradable plastics with natural polymers as reinforcement agent[1]. Polyvinyl alcohol (PVA) is a highly used thermoplastic material that assembles good biocompatible properties and excellent film forming capacity. Due to the characteristics such as easy preparation, chemical resistance, and mechanical properties, the PVA has been used combined with natural polymers in many biomaterial applications[2]. This work deals with preparation of PVA/SO (starch oleate) blends in five different amounts of SO (10, 20, 30, 40, 50 wt.%). As plasticizers was used citric acid (CA) in amounts 10, 25, 35, 50 wt.% in respect of starch oleate. Prepared PVA/SO blends with and without of CA were characterized by FTIR. On prepared blends were studied thermal properties by TG and mechanical properties such as tensile strength, elongation of break.

Experimental part

Materials

Potato starch (approximately 22 % amylose and 80 % amylopectin) was supplied by Spolana Neratovice. The water content was determined by drying the potato starch in a oven at 105 °C until its constant weight and was found to be 10,62 % (w/w). The oleoyl chloride and pyridine were obtained from Aldrich Chemie (Germany). Polyvinyl alcohol – Slovio R16 (16 % – aqueous solution) (PVA) was supplied Fichema Moravians, Czech Republic. Citric acid (CA) (Mw = 192,13 g mol^{-1}) was supplied by Chemapol Praha, Czech Republic.

Esterification of potato starch

Starch oleate (SO, DS = 2,69) was prepared by esterification of starch with oleoyl chloride in the analogous method used to modification of native starch with oleoyl chloride , in pyridine at constant weight ratio 1:3 and at temperature 100 °C and at time 3 h (ref.[3]).

FT-IR spectroscopy

The FT-IR spectra of PVA/SO, PVA/SO/CA films were measured on a FTIR NICOLET 5700 the number of scans 64 cm^{-1} by Company Thermo Electron Corporation.

TG measurements

TG measurements were performed on a Digitalized Derivatograph-Q 1500-D, under air atmosphere, at a heating rate of 10 °C min^{-1} up to 800 °C. The mass loss permits to estimate all the films content and the thermal stability.

Mechanical properties

The mechanical properties were examined according to EN ISO 527-3, 1995 on the unit Hounsfield H20K-W at a speed 5 mm min^{-1}. Five measurements of each samples were tested at 21 °C and the average value of each quantity was reported.

Results and discussion

The spectra of PVA, PVA/SO and PVA/SO/CA films were studied and some spectra are presented in Fig. 1. For each of the films, the spectra of the both sides had the same number of peaks and the positions and relative intensities of these peaks were identicated. In all spectra a peak at 2027, 2160 and 2361 cm^{-1} is due assigned to carbon dioxide in the PVA absorbed from the atmosphere. Peaks due to water in the films occur at 1633 cm^{-1}. The later peak overlaps the peak due to the O–H stretching of hydroxyl groups[4]. Peak at 2922 cm^{-1} it attributes for the CH_2 group, and 1371, 843 and 1084 cm^{-1} are attributed to the C–H stretching, C–H bending and C–O stretching of PVA, respectively. The broad high absorption peak at 3317 cm^{-1} is assumed to arise from the O–H stretching frequencies of PVA and water hydroxyl groups. The band at 1708 cm^{-1} was attributed to the carbonyl functional groups due to residual acetate groups remaining after the manufacture of PVA from hydrolysis of polyvinyl acetate or oxidation during manufacturing and processing[4]. In the spectrum PVA and PVA/SO films there are new band peaks at 1636 cm^{-1}, which are attributed to C=C band stretching groups of oleate. FT-IR spectra of PVA/SO films show characteristic band at 1738 cm^{-1} where their intensity increases with increasing content of SO than the through conjugation C=C bonds. Peaks at the value 2922 cm^{-1} and 2871 cm^{-1} are characteristic for CH_2 groups and their intensity increases with increasing content SO.

The FT-IR spectrum of prepared PVA/SO/CA films

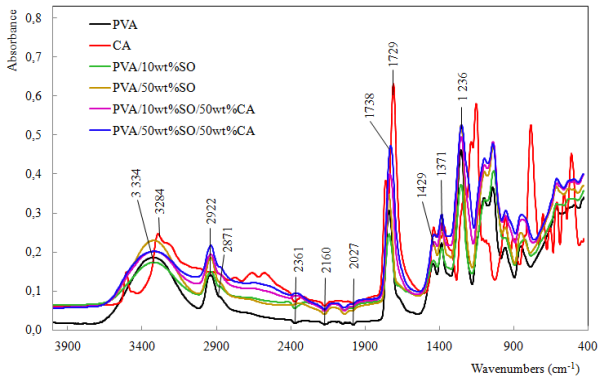

Fig. 1. **FT-IR spectra of PVA and PVA/SO films with different amounts of SO and plasticizer CA**

(Fig. 1) shows bands at the value 2922 cm^{-1} and 2871 cm^{-1} are characteristic for CH_2 groups and their intensity increases with increasing content SO and CA. In spektra of citric acid band around 3284 cm^{-1} is assigned to the stretching vibration of the hydroxyl groups.

The intensity band OH groups of prepared films increased and the maximum shifts to higher wave numbers. The effects of CA on the FT-IR spectra of PVA, PVA/SO and PVA/SO/CA films are shown in Fig. 1. In the spectrum citric acid band at 1729 cm^{-1} it atributed C=C group. By increasing the amount of citric acid in PVA/SO films increases the intensity of this band. Probably this phenomenon illustrates that the esterification occurred more easily between the SO and CA than that between PVA and SO acordink as in the work[5].

TG curves pure PVA showed a two-step decomposition. The first step began around 80 °C, and the second one began around 225 °C. The final temperature of the decomposition was around 565 °C. TG profile of the PVA/SO films presents three degrading areas. The first in the range from 80 °C to 225 °C is related to desorption of water, resulting in 12 % of mass loss in this interval. The second mass loss, observed from 320 °C to 427 °C, is probably associated to degrading of PVA chains, representing 66 % of mass loss. In the last degrading areas, from 510 °C to 552 °C, a mass loss of 12 % was observed is related to SO. Important observation can be extracted from TG analysis and increasing the SO content in the PVA/SO film will increase thermal stability of the blended film. The addition of CA obviously reduced the mass loss rate and increased the residual mass percentage at 600 ° C. After of CA content was added, the shape of the TG curve of PVA/SO/CA changed as compared to that of CA. The films showed a three-step of decomposition. The first step was attributed to the elimination of water from films. The second step was same as that of PVA. The third step was attributed to the SO and cross-linked CA component. The TG curves of PVA/SO/CA films showed a three-step decomposition: 80–165 °C, 318–427 °C, 492–552 °C, which is similar to the classical TG curve of the PVA and to the PVA/SO films.

Tensile strength of PVA/10 wt.% SO film compared to tensile strength of pure PVA. With increasing content of SO in PVA films, tensile strength increases. The tensile strength of plasticized PVA films with amounts of SO out of 30 wt.% increases. In addition, PVA film plasticized with 10 wt.% CA, where the tensile strength decreases with increasing amount of SO. CA has a negative effect on the tensile strength of prepared PVA/SO films. The mechanical properties are not only related with the cross linker but are also related with the plasticizer. The cross linker and the plasticizer always have the contrary effects on the tensile properties. Generally, the tensile strength increased and the elongation at break decreased as the percentage of cross linker increased. The results are opposite when the plasticizers increased. The CA acted both as the cross linker and the plasticizer in composites. So that different functions of CA would be exhibited when different amounts of CA were added[6]. The residual CA in the blends played a role as the plasticizer, which reduced the interactions among the macromolecules, which resulted in the decrease of the tensile strength and increase of the elongation at break. Elongation at break of PVA films without plasticizer (CA) with increasing amount of SO slightly increasing. Elongation at break of PVA films containing CA (10, 25 wt.%) is about the same course as the elongation at break unplasticized films. Elongation at break of PVA film with 50 wt.% CA with amount of SO out of 30 wt.% increased. It reaches a maximum value of 31 wt.%. It can be concluded that the high content of plasticizer (50 wt.% CA) has a positive effect on the elongation break.

Conclusion

The PVA/SO films were prepared with and without of plasticizer citric acid. Evidence for the modification of the films has been obtained from by means several techniques including FT-IR, TGA and mechanical properties. In the structural changes gave rise to a series of property changes. The thermal stability improved as function of cross-linking and it improved molecular interactions. The mass loss is improved compared with pure PVA. The tensile strength in the majority of samples reduced but sampling PVA/40 wt.% SO (85,7 MPa) and PVA/40 wt.% SO/25 wt.% CA (92,5 MPa) in comparison with the pure PVA (84,9 MPa). Elongation at break is reduced most samples except samples PVA/10 wt.% SO/35 wt.% CA (21,23 %), PVA/10 wt.% SO/50 wt.% CA% (50,4 %), PVA/40 wt.% SO SO/50 wt.% (11,6 %) and % PVA/50 wt.% SO/50 wt.% CA (31 %) in comparison with the pure PVA (3,6 %). This was caused by the plasticizing effect of the CA in the blend.

REFERENCES

1. Lopez-Rubio A., Gavara R., Lagaron J. M.: Trends Food Sci. Technol. *17*, 567 (2006).
2. Srinivasa P. C., Ramesh M. N., Kumar K. R., Tharanathan R. N.: Carbohydr. Polym. *53*, 431 (2003).
3. Abburto J., Thiebaud S., Alric I., Borredon E., Bikiaris D., Prinos J., Panayiotou C.: Carbohydr. Polym. *34*, 101 (1997).
4. Jayasekara R., Harding I., Bowater I., Christie G. B. Y., Lonergan G. T.: Palymer Testing *23*, 17 (2004).
5. Rui S., Jingliang B., Zizheng Z., Aichen Z., Dafu C., Xinhua Z., Liqun Z., Wei T.: Carbohydr. Polym. *74*, 763

(2008).
6. Sreedhar B., Sairam M., Chattopadhyay D. K., Syamala Rathnam P. A., Mohan Rao D. V.: J. Appl. Polymer Sci. *96*, 1313 (2005).

P-46
CONDUCTIVE MAGNETOPOLYMER COMPOSITES WITH FERROSILICON FILLER

MARIANA UŠÁKOVÁ*[a], JANA REKOŠOVÁ[b], ELEMÍR UŠÁK[a], RASTISLAV DOSOUDIL[a], and IVAN HUDEC[b]

[a] *Slovak University of Technology in Bratislava, Faculty of Electrical Engineering and Information Technology Ilkovičova 3, 812 19 Bratislava,* [b] *Slovak University of Technology in Bratislava, Faculty of Chemical and Food Technology, Department of Plastic and Rubber, Radlinského 9, 812 37, Bratislava, Slovak Republic*
mariana.usakova@stuba.sk

The magneto-polymer composites comprise the magnetic fillers incorporated into the non-magnetic polymer matrix. These materials attract increasing interest in electrical engineering applications especially thanks to the simplicity of fabrication process. The polymer magnetic composites with conductive magnetic filler are also characterised by good electromagnetic properties. In comparison to spinel ferrite/ polymer absorbers, the composites with conductive magnetic filler exhibit better electromagnetic wave (EM-wave) absorbing properties, such as lower matching thickness and wider EM-wave absorbing bandwidth[1,2].

The purpose of this work was the study of magnetic and physical-mechanical properties of magneto-polymer composite materials. Vestamid® L2122 polyamide was used in the investigated materials as the non-magnetic polymer matrix. Commercially manufactured ferrosilicon powder FeSi15 C-60 was used as the magnetic filler. The magneto-polymer composite samples with filler contents varied from 0 to 60 vol.% were prepared by mixing the magnetic filler and polymer matrix in the laboratory mixer at 190 °C.

Structural characteristics, such as size, shape and distribution of used filler were investigated by means of laser particle distribution analyser. Physical-mechanical properties of prepared composites were measured in accordance with valid technical standards on the double side blade specimens (width 6.4 mm, length 100 mm, thickness 2 mm). Static magnetic properties of prepared samples represented by initial permeability were measured by means of customised software-controlled experimental equipment built-up from commercially available instruments. Dynamic magnetic properties, such as e.g. the frequency dependencies of real (μ') and imaginary (μ'') parts of the complex permeability of the composites were obtained by means of impedance spectroscopy (coaxial S-parameter method) in the frequency range from 10 MHz to 6.5 GHz. The measured composite samples were prepared in the form of toroids with an outer diameter of 8 mm, an inner diameter of 3.5 mm and a height of 2 mm. The conductive magnetic ferrosilicon filler with the content of 82.5 % Fe, 15.0 % Si and small amounts of C, Al, Mn and Cr (≤ 1 %) consists of randomly shaped particles with diameter less than 100 μm. The size of FeSi particles was verified by laser particle size distribution (Fig. 1)[2].

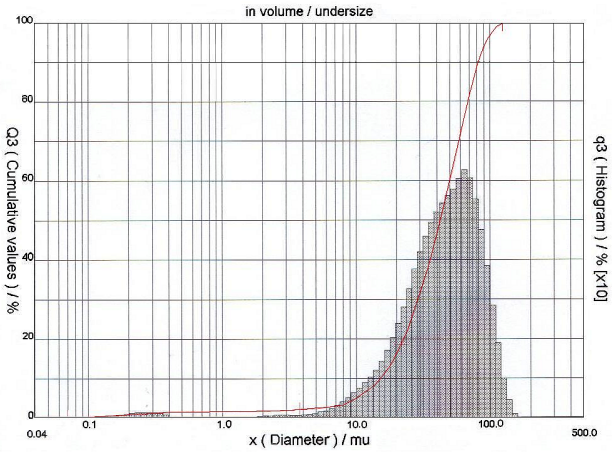

Fig. 1. **Particle size distribution of ferrosilicon filler**

The magnetic filler in polymer matrix clearly influences physical-mechanical and magnetic properties of composite samples. The dependence of the tensile strength value as a function of ferrosilicon contents in prepared magneto-polymers initially shows rapid fall - the tensile strength value decreased about 48 % for the sample with ferrosilicon concentration 10 vol.% in comparison with tensile strength value of pure polymer sample. Further increasing of magnetic filler content caused only slight decrease of tensile strength value oscillating about 20 MPa (Fig. 2, solid line, open circles). The influence of ferrosilicon filler on the Young's modulus of composite samples is even more significant (see Fig. 2, dashed line, closed circles), The values of Young's modulus increase with magnetic filler content; for the maximum concentration (60 vol.%) it was about 7 times higher than for pure polymer.

The dependencies of initial permeability (μ_i) upon filler concentration measured at the frequency of 50 Hz (quasi-

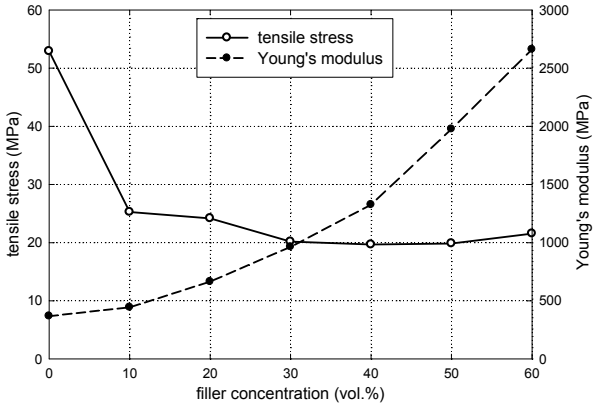

Fig. 2. **Dependence of the tensile strength and the Young's modulus value on ferrosilicon content of magneto-composites**

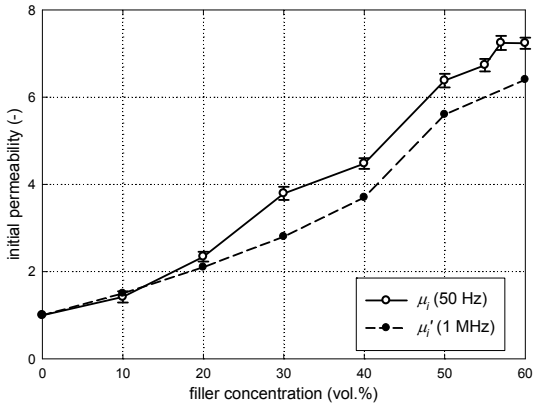

Fig. 3. **Dependence of initial permeability on ferrosilicon content of magneto-composites**

static for these materials) as well as the real component of complex permeability at constant frequency of 1 MHz (μ_i') are displayed in Fig. 3. One can see almost linear increase of the permeability values with the increase of ferrosilicon amount.

Note that the real part μ_i' (Fig. 3; dashed line, closed circles) gives slightly less values than quasi-static (50 Hz) initial permeability μ_i (Fig. 3; solid line, open circles). This can easily be explained by the influence of the eddy currents, since FeSi is a metallic (thus, electrically conductive) alloy.

The frequency dependencies of real and imaginary parts of complex permeability for the prepared composite samples are shown in Fig. 4. The values of μ_i' shown in Fig. 3 originate from Fig. 4a. We can observe the typical relaxation type of frequency dispersion of permeability with only one dispersion range. The real component of permeability for all the composites nearly monotonically decreased meanwhile the imaginary part of permeability increased with frequency and reached the maximum value at the resonant frequency f_r, (see also Table I). On the other hand, the resonant frequency f_r, raises from 0.32 GHz for 60 vol.% composite sample to over 3 GHz for 10 vol.% one. This behaviour is the direct consequence of two phenomena, namely the domain wall resonance and the natural ferromagnetic resonance[3,4]. The domain walls follow the high-frequency ac electromagnetic field up to about 10^8 Hz, over this value they cannot follow the changes of exciting field and their contribution to permeability starts to decrease. As a result, the measured

Table I
Real component of complex permeability at the lowest frequency μ_i' and resonant frequency f_r, for FeSi-PAD composites

Filler content (vol.%)	10	20	30	40	50	60
μ_i' (–)	1.5	2.1	2.8	3.7	5.6	6.4
f_r (GHz)	>3	2.83	1.27	0.72	0.38	0.32

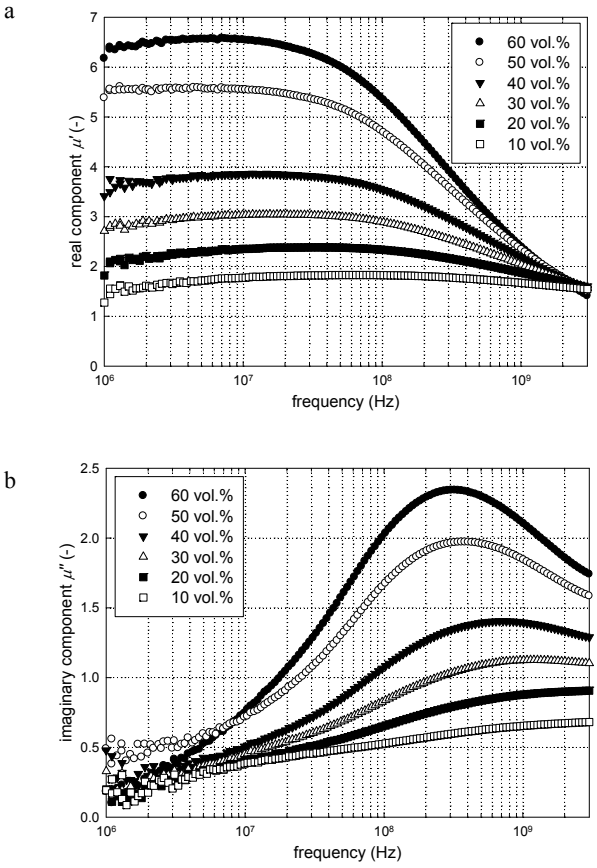

Fig. 4. **Frequency dependences of a) real and b) imaginary parts of complex permeability for FeSi-PAD composites with various filler contents**

dispersion of permeability is mainly caused by the natural ferromagnetic resonance. The decrease of μ_i' and increase of f_r with reduced FeSi filler content in composite materials is associated with the origin of the demagnetising field formed in filler particles dispersed in polymer matrix[3].

The experiments confirmed the impact of ferrosilicon FeSi15 C-60 powder filler content on both the physical-mechanical properties as well as magnetic properties of the composites.

This work was supported by the Slovak Research and Development Agency under the contract No. APVV-0062-11 and by the Scientific Grant Agency of the Ministry of Education, Science, Research and Sport of the Slovak Republic and the Slovak Academy of Sciences (VEGA), projects No. VG-1/1163/12 and VG-1/1325/12.

REFERENCES

1. Yi Z., Shuhua Q., Fan Z., Yongqing Y., Guochen D.: Appl. Surf. Sci. *258*, 732 (2011).
2. Dosoudil R., Ušáková M., Sláma J.: Chem. Listy *105*, 429 (2011).

3. Dosoudil R., Ušáková M., Franek J., Sláma J., Grusková A.: IEEE Trans. Magn. *46*, 436 (2010).
4. Dosoudil R., Franek J., Sláma J., Ušáková M., Grusková A.: IEEE Trans. Magn. *48*, 1524 (2012).

P-47
MODIFICATION OF PUR DISPERSIONS IN THE ADHESIVES FOR 3D BONDING IN THE FURNITURE INDUSTRY

VLADIMÍR VANKO[a], IGOR NOVÁK[b], JOZEF PREŤO[a], and JÁN HRONKOVIČ[a]

[a] Vipo Partizanske, [b] Polymer Institute of the Slovak Academy of Sciences, Dúbravská cesta 9, 845 41 Bratislava 45, Slovakia
vvanko@stonline.sk

Abstract

The aim of the work was the study of modification PUR dispersions used in adhesives for 3D bonding of high glossy foils in the furniture industry. The hydrophobization additives were used in order to improve the wetting of bonding substrate – middle density fiberboard (MDF). The influence of additives was examined by the measurement of contact angle, shear strength of adhesive joint, tensile strength at break of adhesives films and surface quality of adhesive joint. In relation to modification of PUR dispersion was examined also the influence of modification MDF surface by the barrier plasma. The experiment showed that the addition of hydrophobization additives improves the wetting properties of PUR dispersions and has positive effect on surface quality of adhesive joint.

Introduction

Polyurethane dispersions generally consist of urethane urea polymers dispersed in water in preference based on aliphatic polyisocyanates and therefore offer good resistance to discoloration[1]. Heat-activated adhesives based on polyurethane dispersions have become established for joining processes in which synthetic materials need to be adhesively bonded and are gradually displacing conventional solvent-based adhesives[2]. Examples include laminating PVC foils on MDF sheets. Usually polyester PUR dispersions are preferred for bonding soft PVC due to their good plasticizer resistance. For 3-D laminating PVC foils on MDF sheets the polyurethane dispersion adhesives can be applied either as two-component materials, i.e. in combination with a hydrophilically modified isocyanate, or in the form of a latent-reactive dispersion with a surface-deactivated solid isocyanate which are applied by spraying on the surface of profiled MDF[3] .When high glossy foils are used the problem of rough surface is observed, caused by poor quality adhesive spread or eventually by next processes of his drying, pressing and curing. In generally the right formulated PUR dispersion adhesive suitable for the bonding of high glossy foils should meet two basic requirements of good wetting and flowing properties as well as the lower reactivation temperature of 50–55 °C. The lower the press reactivation temperature, the less the elasticity of the foil and hence the less risk of the soft foil telegraphing an uneven surface of the adhesive coated MDF. The wetting properties of examined system are possible to change not only by the modification of adhesive but also by the treatment of bonded substrates. When the plasma treatment is used the significant changes on the surface are observed[4]. Among numerous kinds of electric discharge plasmas, coplanar surface barrier plasma at atmospheric pressure and/or radio-frequency volume plasma at reduced pressure are currently the most promising methods of surface modification, and are considered as the 'green' ecologically friendly modification method[5].

Because the surface of evaluated MDF is non-polar – hydrophobic, when the polar component of surface energy MDF is significantly lower than polar component of surface energy of films prepared from Dispercoll U 53 (ref.[6]), we studied in our work two kinds of modifications: The addition of oleic acid which is non-polar to polyurethane dispersion in order to reach the better wetting properties on the MDF as a basic presumption for smoother surfaces of adhesive joints and also was studied the treatment of MDF sheets by the coplanar barrier plasma and its influence on wetting and bonding characteristics.

Experimental

In this study was used the commercial polyurethane dispersion Dispercoll U 53 produced by Bayer, Germany. The properties of Dispercoll U 53 are described in the Table I. As a hydrophobization additive was used oleic acid in pure quality. The content of oleic acid in PUR dispersion was given as weight % calculated on polymer content of PUR dispersion. MDF was type Antine, density 800 kg m^{-3}, produced by Bipan, Italy, PVC foil was Darkar HG, thickness 0, 5 mm produced by Riken Technos, Japan.

The wetting properties were evaluated by measurement of contact angles with selected testing liquids set using SEE (Surface Energy Evaluation) device completed with a web camera (Advex, Czech Republic) and necessary PC software. The adhesive joints for measurement of shear strength were prepared by pressing at the temperature 60 °C on the hydraulic press Fontijne SR 100 and evaluated by Instron 4301. The dispersion spread was done by brush only on MDF, 30 minutes drying. Adhesives films for the measurement of tensile strength were prepared by spraying in several layers on inert board. The adhesive joints for evaluation of surface

Table I
The basic properties of used polyurethane dispersion

Product	Polymer content [%]	Viscosity [mPa s]	pH	Density [g cm^{-3}]	Minimum activation temperature [°C]
Disper-coll U 53	40±1	50–600	7.5	approx. 1.07	45–55

quality were prepared by spraying dispersions on MDF; adhesive coating was approx. 40 g m^{-2}, dried 30 minutes and pressed on vacuum membrane press in the Decodom Ltd. Topoľčany in standard technology conditions. The surface quality of adhesive joints was evaluated using Wave scan II device from BYK Instruments, as a value of waviness with the length 2–15 mm referred to as longwave. They were evaluated in horizontal and vertical direction respective the direction of spraying. The content of longwave is decisive factor for evaluation of surface quality regarding to sensitivity of human eye from the observing distance over 50 cm (ref.[7]).

Plasma modification was implemented in static conditions by diffuse coplanar barrier surface discharge (DCSBD) plasma technology of laboratory scale at atmospheric pressure and room temperature.

Results and discussion

The contact angles of modified Dispercoll U 53 by the adittion of oleic acid on MDF, tensile strength of adhesive films and shear strength of adhesive joints are shown in Table I. The addition of oleic acid causes changes in wetting properties of Dispercoll U 53.The contact angles of modified Dispercoll U 53 were significantly decreased.As beter is wetting the higher shear strength of adhesive joint was expected. The higher shear strength was reached only up to addition of 2 weight % oleic acid and next addition of oleic acid caused the decrease of shear strength. It can be related to potential incompatibility of oleic acid in Dispercoll at higher concentrations resulting in worse adhesion and cohesion properties. The cohesion of PUR films was decreased and the shear strength well correlates to tensile strength of adhesive films.

Table II
Shear strength of adhesive joints, contact angles and tensile strength of films modified Dispercoll U 53

Content of oleic acid [%]	Shear strength of adhesive joint [MPa]	Contact angle [deg]	Tensile strength at break [MPa]
0	12,0	101,4	19,6
1	12,3	91,9	19,6
2	12,5	86,3	19,5
3	10,9	83,6	19,0
4	8,5	80,7	17,2
5	7,9	77,1	12,0

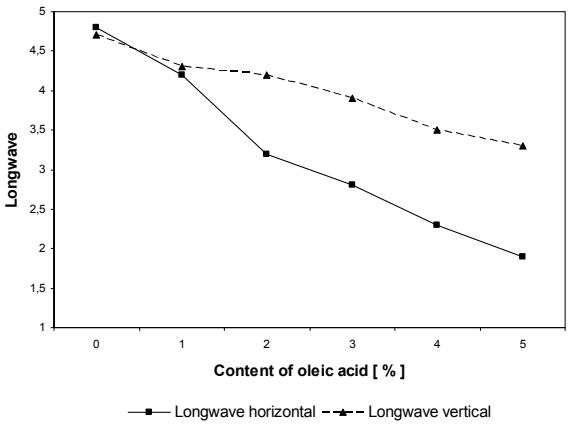

Fig. 1. **Dependency of longwave surface of adhesive joints on content of oleic acid**

The influence of addition of oleic acid on the surface quality of adhesive joints is shown in Fig. 1.The higher is content of oleic acid the lower value of longwave in both direction we reached. The lower value of longwave means the smoother surface of adhesive joints.

The contact angles modified Dispercoll U 53 with oleic acid on treated surface MDF by plasma are shown in the Fig. 2. After treatment of surface MDF by plasma the contact angles modified Dispercoll U 53 were significantly decreased. The addition of non-polar oleic acid causes better wetting although the treatment by plasma causes higher polarity of surface MDF[6].

The shear strengths of adhesive joints given in Fig. 3 are significantly affected by the exposure time of treatment surface MDF by plasma and addition of oleic acid. The values of shear strengths increase with the exposure time only when unmodified Dispercoll U 53 is used. The addition of oleic acid causes the decrease of shear strengths. It can be explained by different effect both types of modifications. With longer exposure time of plasma treatment is surface of MDF more polar and with higher content of oleic acid is dried PUR film more non-polar.

Conclusion

The addition of oleic acid to polyurethane dispersion improves the wetting properties of PUR dispersion and has

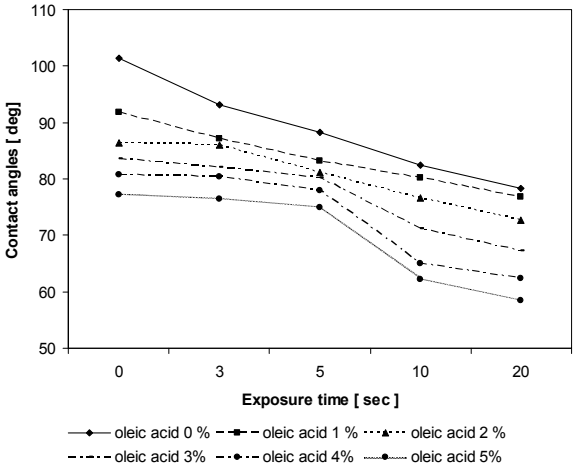

Fig. 2. **The contact angles modified Dispercoll U 53 by oleic acid as function of exposure time of plasma treatment surface MDF**

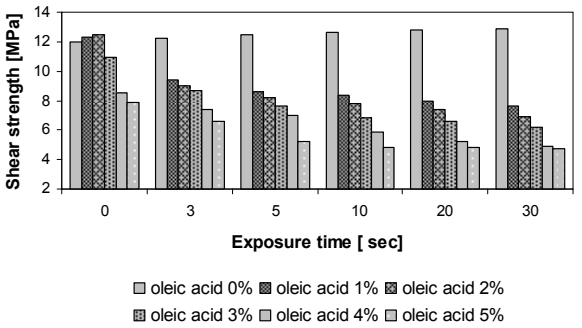

Fig. 3. **Dependency of shear strength of adhesive joint on the content added oleic acid and exposure time of plasma treatment surface of MDF**

positive effect on surface quality of adhesive joint and also improves the shear strengths up to 2 weight % of oleic acid. The modification of PUR dispersion by oleic acid is the potential way how to formulate the adhesives for 3-D bonding of glossy foils in furniture industry.

When the plasma treatment of surface MDF was applied the significant decrease of contact angles and shear strengths were observed when the oleic acid was added to PUR dispersion. Using the both kind of modifications together is not the right way how to modify and apply the PUR dispersions.

This work was prepared as part of the project „Application of Knowledge-based Methods in Designing Manufacturing Systems and Materials“, project No. MESRSSR 3933/2010-11.

REFERENCES

1. Bodo Müller, Walter Rath: „Formulating adhesives a sealants“, 2010, p. 67 – 71.
2. D. Dieterich: Angewandte Makromolekulare Chemie *98*, 133 (1981).
3. Jörg Büchner, Wolfgang Henning: “Latent – reactive and storable“, adhesion ADHESIVES & SEALANTS 9/2007, p. 4–8.
4. Novák I., Popelka A., Vanko V., Chodák I., Preťo J.: “Modification of wood by low-temperature atmospheric discharge plasma”, Annals of Warsaw University of Life Sciences – SGGW Forestry and Wood Technology No 75, 2011: 135–141
5. Kiguchi M.: Surface modification and activation of wood. In: Hon D. N. (ed.), *Chemical modification of lignocellulosic materials*. Marcel Dekker, New York 1996.
6. Novák I., Vanko V., Preťo J, Chodák I.: ”Povrchové a adhézne vlastnosti substrátov v spoji drevotriesková doska –PVC fólia lepenom polyuretánovým adhezívom”, *63. Zjazd chemikov,5.–9.9.2011,Tatranske Matliare*
7. Catalogue of BYK products for 2010 – 2011. p 33–47.

P-48
APPLICATION OF CORN STARCH AS A FILLER IN RUBBER BLENDS

PETRA VÁŇOVÁ[a], IVAN HUDEC[a]*, and ALENA KŇAZEOVÁ[b]

[a] Slovak University of Bratislava, Faculty of Chemical and Food Technology, Radlinského 9, 812 37 Bratislava,
[b] VEGUM a.s., Gumárenská 337, 972 23 Dolné Vestenice, Slovakia
petra.vanova@stuba.sk

In the last periods, the major environmental problem relating to increasing amount of waste rubber production has become still more actual. The rubber waste remains in landfills many years without a change of its volume. Sources of rubber compounds are often non-renewable and their exhaustion loses the ability to manufacture these products. Therefore, in the recent years, the producers of rubber have been searching for new renewable sources, environmentally safe that might be able to support decomposition of rubber products, and thus they could contribute to reducing of waste rubber.

This work is focused on the application of corn starch as a filler for elastomeric composites based on EPDM. There was observed the influence of natural filler on the curing process and physical-mechanical properties of EPDM blends. The main goal was to find suitable amount of used corn starch in combinations with other additives of rubber compounds in order to support biodegrability and to reduce the cost of the final products. The corn starch was applied in natural form, and also after subsequent drying. The results indicate the possibility of application of corn starch in rubber blends, but in many cases it is necessary to modify corn starch before it is used.

Introduction

Starch is a dominant carbohydrate that represents reserve material of higher plants. Starch consists of two basic types of α-D-glucose homopolymers, namely amylose and amylopectin. Amylose is a linear molecule composed of anhydroglucose units connected through (1/4)-α-linkages and with a few (1/6)-α-linkages, too. Amylopectin is a much larger molecule with very branched structure built from about 95% (1/4)-α- and 5 % (1/6)-α-linkages[1]. The ratio between amylose and amylopectin varies depending on the starch source. In normal starches, amylose constitutes about 15–30 % of total starch.

The size and shape of starch granules vary in different plant species. Starch granules have a semi-crystalline structure with a typical crystallinity around 15–45 % (ref.[1]). Starch is a plentiful, biodegradable, naturally renewable, environmentally friendly, and inexpensive nature polymer[2]. Starch characteristics have an influence on the properties of final products, into which they are added, such as viscosity, moisture retention, gel formation and product homogeneity.

A considerable interest has been focused on finding new applications for this biopolymer in food and also non-food industry, for instance as low-calorie substituent,

biodegradable packaging materials, thin films and thermoplastic materials with improved thermal and mechanical properties[3]. Native starch does not have high thermal stability and tends to form agglomerates and that's the reason why it often undergoes the surface modification.

Experimental

Ethylene propylene diene rubber EPDM (DUTRAL TER 4049 Polimeri, Italy), was compounded with various amount of corn starch (in native and dried form) in order to prepare rubber composites. The content of processing additives, fillers (carbon black N550 and kaolin) and components of sulfur curing system was kept constant in all experiments. Corn starch (the trade name Meritena 100) with moisture content 11 % and pH 6.7 was supplied by AMYLUM SLOVAKIA, Boleráz. The content of corn starch in rubber blends varied from 0 to 40 phr.

The methods and procedures

The rubber compounds were prepared in laboratory mixer Brabender in two mixing steps. In the first step, the rubber, the processing additives and the fillers were mixed together. In the second step, the curing system was introduced.

The curing characteristics of prepared materials were determined from the corresponding curing isotherms measured by rheometer Monsanto R100 at 150 °C. The curing process of rubber compounds was performed in hydraulic press at 150 °C under a pressure of 15–17 MPa for the optimum cure time.

The tensile properties of cured rubber compounds were measured by using ZWICK ROELL/Z 2.5 appliance at cross-head speed of 500 mm min^{-1} at laboratory temperature in accordance with the valid technical standards. The hardness Shore A of vulcanizates was measured.

Results and discussion

As seen in Fig. 1, by incorporation of 10, 20 and 30 phr corn starch in native form into rubber compounds the optimum cure time t_{c90} decreased in comparison with t_{c90} of the sample which content only carbon black and kaolin, used as reference. The sample with 40 phr of applied filler required the longest time essential for curing process. The optimum cure time of rubber compounds filled with dried corn starch was found to be much longer in comparison with the previous systems.

The values of physical-mechanical properties of prepared composites are illustrated in Figs. 2–4. The tensile strength at break of vulcanizates showed the decreasing tendency with increasing amount of applied corn starch as shown in Fig. 2.

The differences in the values of tensile strength at break of vulcanizates in dependence on the type of filler were different. At lower filler contents (10, 20 phr), higher values of tensile strength at break were spotted in case of vulcanizates with corn starch applied in native form. Higher values of tensile strength at break of samples with higher filler contents (30, 40 phr) were reached by incorporation of corn starch in dried form.

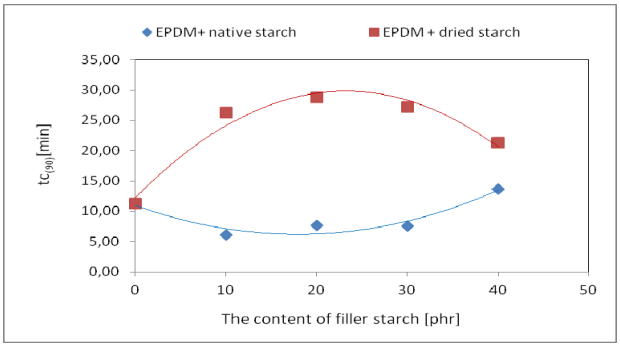

Fig. 1. **Influence of corn starch content on optimum cure time $t_{c(90)}$ of rubber blends based on EPDM**

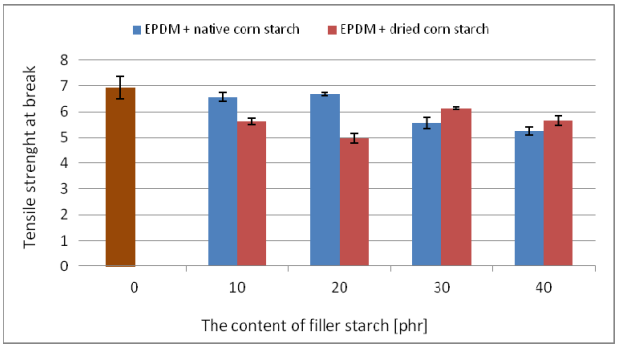

Fig. 2. **Influence of corn starch content on tensile strength at break of vulcanizates based on EPDM**

From Fig. 3 it evident, that the elongation at break of vulcanizates with corn starch in native form was kept almost unchanged up to 20 phr of filler incorporated. Then sharp decrease of elongation at break values was recorded at higher corn starch contents. In case of samples with dried corn starch, rapid decrease of elonagtion at break was possible to see by application of 10 phr filler. The elongation at break values of samples with higher filler contents were similar to those of equivalent samples with corn starch in native form.

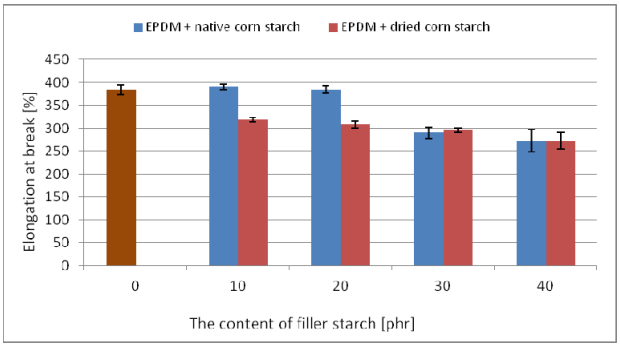

Fig. 3. **Influence of corn starch content on elongation at break of vulcanizates based on EPDM**

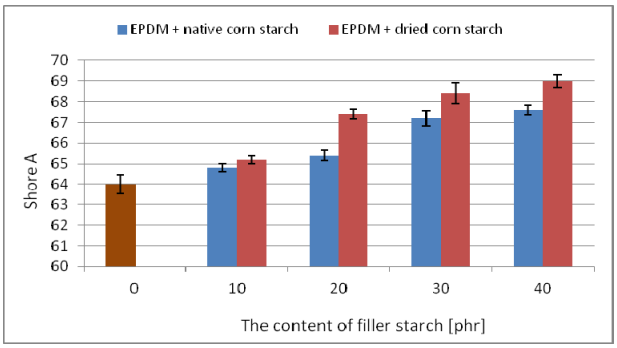

Fig. 4. **Influence of corn starch content on hardness of vulcanizates based on EPDM**

The hardness of vulcanizates (Fig. 4) increased with increasing amount of corn starch, as the hardness of corn starch particles is higher than the hardness of the rubber matrix. The highest values of hardness were reached by applying of corn starch in dried form.

Conclusion

The results achieved by the study revealed that the presence of corn starch in rubber compounds influences the curing process and also the physical-mechanical properties of rubber compounds. The decrease of tensile strength at break and elongation at break with increasing content of corn starch was recorded. The reason might be attributed to the structure of natural filler and the presence of hydroxyl groups on the surface of corn starch particles, which tend to form intra- and intermolecular hydrogen bonds. This leads to the forming of aggregates and agglomerates of filler particles in the rubber matrix, what to a large extent contribute to the deterioration of observed properties. Weak mutual interactions and adhesion between the particles of corn starch and the rubber matrix could be the next reason why corn starch does not act as a reinforcing filler in rubber matrix. Seeing that the incorporation of examined type of corn starch into the rubber compounds caused the decrease of observed properties of equivalent vulcanizates, the utilization of such materials is so far estimated for applications, which are not subjected to the excessive dynamic-mechanical strain. On the other hand, the increase of hardness of prepared systems in dependence of corn starch contents suggest that such materials could be possibly used in applications required higher hardness and stiffness of final products. For broader utilization of such systems, the efficient methods of corn starch modifications should be developed, in order to improve the compatibility and adhesion between the rubber matrix and the particles of corn starch.

REFERENCES

1. Chung Y.-L., Lai H.-M.: Carbohydr. Polym. *63*, 527 (2006).
2. Ren L.-L., Jiang M., Wang L., Zhou J., Tonga J.: Carbohydr. Polym. *87*, 1874 (2012).
3. Kaur B., Ariffin F., Bhat R., Karim A. A.: Food Hydrocolloids *26*, 398 (2012).

P-49

THE INFLUENCE OF DYEING TIME AND TEMPERATURE FOR THE DYEABILITY OF UNTREATED AND PLASMA TREATED COTTON FABRICS

PETRONELA VENCELOVÁ*, ANNA UJHELYIOVÁ, MONIKA BOTOŠOVÁ, MILAN MIKULA, ĽUBA HORBANOVÁ, and MARCELA HRICOVÁ

Slovak University of Technology in Bratislava, FCHFT, Institute of Polymer Materials, Radlinského 9, 812 37 Bratislava, Slovak Republic
petronela.vencelova@stuba.sk

Introduction

Plasma is a partially ionized gas, containing a mixture of electrons, positive and negative ions, radicals, and various excited molecules. It might be regarded as a "fourth state of matter"[1,2]. Historically, plasmas could be produced only at high temperatures or in vacuums; however, recent breakthroughs, in plasma physics have allowed development of plasma at room temperature and atmospheric pressure, so-called non-thermal or (cold or low temperature) atmospheric plasma[1].

Atmospheric plasma has many advantages. It can be generated under atmospheric conditions and requires no vacuum systems and therefore can be applied on-line for textiles[3,4]. The species that participate in plasma reactions (excited atoms, free radicals and metastable particles, electrons and ions) can interact either physically or chemically with the substrate[3]. Exposure of natural fabrics to a plasma environment can produce more reactive surfaces.

This type of plasma is used in surface modification. It is a very helpful technique where surface chemical modification is required. Plasma treatment modifies surfaces without affecting the characteristics of the bulk. Consequently, plasma processes have found a wide range of very important technological applications of surface energetic to improve adhesion strength cleaning, coating[2]. Plasma surface modification does not require the use of water and chemicals, resulting in a more economical and ecological process[4].

In this paper the influence of dyeing time and temperature for dyeing of untreated and plasma treated cotton fabrics was investigated. There was evaluated % of exhaustion after dyeing. FTIR was used for analysing the cotton fabrics after dyeing and after dyeing the values of rubbing fastness were determined.

Experimental

Material used

The woven textile fabrics from cotton were used as a substrate for the treatment of low temperature plasma and subsequently were dyed.

Methods used

The surface of cotton textiles were activated by low temperature plasma generated discharged at the atmospheric

pressure at 350 W for 3 seconds. There was used different ageing time (AT) 10, 20 and 30 minutes.

Then there was measured % of exhaustion dyeing (ED) of cotton untreated and treated fabrics. Samples were dyed by classical exhaustion dyeing from bath.

The equipment AHIBA ↑↓ AG CH 4127 Bisfelden (Switzerland), type G6 RTC (4.4 kW) was used for the dyeing of cotton materials by classical exhaustion method from bath. Conditions for dyeing were followed:
As the dye was used – Bezaktiv Rot, concentration of dye – 2 % o.w.f., concentration of auxiliary agents – 20 g l^{-1} Na_2CO_3 and 75 g l^{-1} NaCl, dyeing time was 30 and 60 minutes, dyeing temperatures were 60 and 70 °C. After the dyeing the fabrics were washed for 30 minutes, by 70–80 °C and dried.

The Bruker (Vektor 22) FTIR spectrometer with the ATR attachment with a ZnSe crystal was used for the FTIR analysis of cotton fabrics.

The values of dry and wet rubbing fastness of cotton fabrics were measured by using the Stainingtester FD 17 equipment. The measuring was doing according to the Standard STN EN 20105-A03 and STN EN ISO 105-X12.
The cotton samples were submitted to abrasion by dry and wet cotton woven fabrics. Degree of bleeding colour from dyed cotton fabrics to the white cotton fabrics were specified by using grey scale.

Results and discussion

The results of % of exhaustion dyeing of plasma treated and untreated cotton fabrics are shown in Fig. 1.

At the dyeing temperature 60 °C and dyeing time 30 minutes the percentage of exhaustion dyeing are lower for plasma treated samples. On the other hand at higher dyeing time the percentage of exhaustion dyeing is decreasing for 10 and 20 minutes ageing time in comparison to untreated sample. But at the dyeing of cotton fabrics after 30 mins since plasma treatment the percentage of exhaustion dyeing is better than untreated fabric.

At the dyeing temperature 70 °C and dyeing times 30 minutes and 60 minutes there can observe the improving of dyeing cotton fabrics by using plasma treatment. The deyability is better for dyeing time 60 mins and ageing time 30 mins.

From results of dyeing cotton fabrics is obvious that increasing dyeing temperature decrease the dyeability of

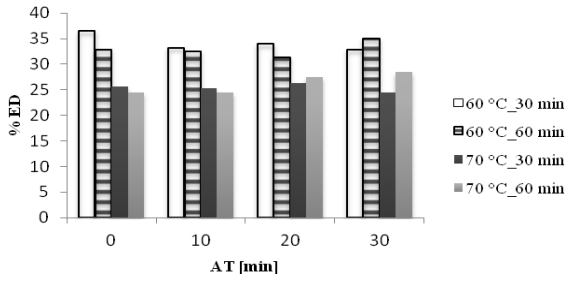

Fig. 1. **Exhaustion dyeing of untreated and plasma treated cotton fabrics after various ageing time**

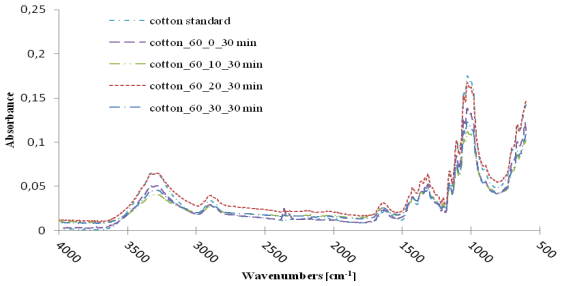

Fig. 2. **FTIR spectrum of untreated and treated cotton fabric, dyeing for 30 min by 60 °C**

Table I
The dry and wet rubbing fastness of cotton fabrics. Dyeing time 30 min and dyeing temperature 60 °C

AT [min]	Rubbing fastness			
	Dry		Wet	
	Before cleaning	After cleaning	Before cleaning	After cleaning
0	4-5	5	1-2	3-4
10	5	5	2-3	3-4
20	5	5	2	3-4
30	5	5	3-4	3

Table II
The dry and wet rubbing fastness of cotton fabrics. Dyeing time 60 min and dyeing temperature 60 °C

AT [min]	Rubbing fastness			
	Dry		Wet	
	Before cleaning	Before cleaning	Before cleaning	Before cleaning
0	5	5	2	3
10	5	5	3	3
20	5	5	2-3	3
30	5	5	2-3	3-4

Table III
The dry and wet rubbing fastness of cotton fabrics. Dyeing time 30 min and dyeing temperature 70 °C

AT [min]	Rubbing fastness			
	Dry		Wet	
	Before cleaning	Before cleaning	Before cleaning	Before cleaning
0	5	5	3	4-5
10	5	5	3	5
20	5	5	3-4	5
30	5	5	3	5

Table IV
The dry and wet rubbing fastness of cotton fabrics. Dyeing time 60 min and dyeing temperature 70 °C

AT [min]	Rubbing fastness			
	Dry		Wet	
	Before cleaning	Before cleaning	Before cleaning	Before cleaning
0	5	5	3	4
10	5	5	3-4	3-4
20	5	5	3-4	4-5
30	5	5	3-4	4-5

untreated as well as plasma treated samples.

Plasma treating is the most efficient at 30 mins of ageing time for dyeing temperatures 60 and 70 °C.

FTIR spectrum shows that plasma treatment did not lead to greater changes in functional groups between untreated cotton fabrics before dyeing and treated cotton fabrics after dyeing.

The dry and wet rubbing fastness of cotton fabrics before and after cleaning which were dyed after various ageing time are in the Tables I–IV.

The obtained results have shown that the dry rubbing fastness for all samples before and after cleaning is 5 which means that colour was not bleeding from dyed cotton fabrics to the white cotton fabric.

The wet rubbing fastness before and after cleaning is lower compare to dry rubbing fastness. It means that unbounded dye molecules diffused from cotton to cleaning bath.

The rubbing fastness improves for treated fabrics after cleaning and it improves with increasing ageing time.

Results confirm that rubbing fastness of cotton fabrics which were dyed 30 and 60 minutes at 70 °C temperature is higher than at 60 °C. The cleaning improves the quality of dyeability of cotton fabrics what is confirmed by higher rubbing fastness at longer dyeing time.

Conclusions

The plasma treatment has positively effect to dyeability of cotton fabrics for both dyeing temperatures and at the higher dyeing time.

Dry rubbing fastnesses do not depend on the type of plasma ageing time before and after cleaning.

The plasma surface modification and higher dyeing temperatures improve the wet rubbing fastness.

ITMS 262202220134 VY-INTECH-TEX.

REFERENCES

1. Walk R. M., et al: Journal of Pediatric Surgery *48*, 67 (2013).
2. Kizling M. B., et al: Appl. Catal. A: General *147*, 1 (1996).
3. Karahan H. A., et al: Coloration Technol. *124*, 106 (2008).
4. Wang C. X., et al: Surf. Coat. Technol. *201*, 6273 (2007).

P-50
DETERMINATION OF POLYOLEFINS' ODOUR PROPERTIES IN CONNECTION WITH C-EMISSIONS

ANITA VÍGHOVÁ, EVA LUKÁČOVÁ*, ZUZANA WETTEROVÁ, and RÓBERT POLNIŠER

SLOVNAFT, a.s., Quality Control Petchem, Vlčie Hrdlo 1, 824 12 Bratislava, Slovakia
anita. vighova@slovnaft.sk

One of the most important characteristics in vehicle interior is polymer´s parts smell. It is the main criterion during the selection of polymers suitable for using in automotive industry, as far as the polymers comprise more than 50 % of cars' construction. Subject is focused on the sensory testing by human and determining the C-emissions by GC-Headspace[1].

Volatiles may contain residual monomers, additives, moisture, solvents, residual catalysts, decomposition products of resins and their additives and can be associated with odour and off-taste in packaging foodstuffs[2].

Determination of polyolefin's odor properties is based on assessing the sensory characteristics of pellets/ films/ other forms of plastic materials or additives by mean of the increased or in special case room temperature, from which the released volatile substances may show detectable odour. Samples are tested in the 1 litre test bottle (glass and perfectly odour neutral). The intensity of odour is marked by at least 3 trained and verified workers according to established "intensity scale from 1 to 6" (ref.[3]). For polyolefin used in automotive industry is the maximum allowed intensity scale mark for pellets 3 and for films or the other forms 3.5.

The identifications of emitted substances generated during polymer production or processing is critical for material safety, health and environmental aspects. A wide range of polyolefin was studied, because the automobile indoor air quality influences comfort, interior microenvironment, safety and health. Whilst by the sensory testing we can detect just smelly odours the others (from time to time much more interesting) are hardly detected and therefore the analytical method – determining of C-emissions was developed.

C – emissions are evaluated from final pellets by method designed for GC/Static Headspace with Flame Ionization Detector (FID). Exact amount of sample is preheated in glass vials for specific time and temperature. Organic compounds are evaporated from the heated sample and released into the space above pellets. When equilibrium is reached, the concentration of the volatiles in the headspace is at its maximum and it is injected onto the analytical column for separation Then the C – emissions potential is measured on the basis of the sum of all values provided by the emitted substances after gas chromatography analysis and flame ionization detection.

Still we can say that polymers vary their composition like their chemical structure and could emit chemical

substances, compounds into the air inside the car. The concentration of emitted volatile compounds is influenced by the individual sources in the interior equipment, outdoor and indoor air contaminants, and interior sources, internal parts exposed to the heat and ventilation conditions. Significant concentration of volatile organic compounds can be present in the interior of vehicles due to emissions from materials which are part of the interior fittings[2].

REFERENCES

1. VDA 277, *Determination of emission of organic compounds*, 1995.
2. C. Henneuse-Boxus, T. Pacary: *Rapra Review Reports*, Volume 14, Number 5, 2003.
3. VDA 270, *Determination of the odour characteristics of trim materials in motor vehicles*, 1992.

P-51
MODIFICATION OF BIODEGRADABLE CHITOSAN SCAFFOLD

MIROSLAVA VITTEKOVÁ, MÁRIA HNÁTOVÁ, KATARÍNA KOMAROVÁ, and DUŠAN BAKOŠ

Institute of Polymer Materials, Faculty of Chemical and Food Technology, Slovak University of Technology, Radlinského 9, 812 37 Bratislava, Slovak Republic
miroslava.vittekova@stuba.sk

Introduction

Chitosan is interesting biopolymer predestined for biomedical applications due to its properties (easy to fabricate, film and fiber-forming, excellent biological properties – biocompatibility, bioresorption, antimicrobial properties). Cationic character of chitosan is used for complex formation with anionic polymers, as well as amino-groups on chain can be used for chemical modification and crosslinking, e.g with dialdehydes, through the formation of Schiff base[1].

Cyclodextrins have been studied intensively as carriers of bioactive substances. Cyclodextrins are natural, from starch derived oligosaccharides. They are composed of α-1,4-linked D-glucose units with arrangements containing a hydrophobic internal cavity that can act as a host for various, generally lipophilic, guest molecules[2]. Salicylic acid has favorable pharmacological effects and also is able to create a cyclodextrin inclusion complex[3].

The work is focused on the study of biodegradable chitosan scaffold modified by molecules of *β*-cyclodextrin and cross-linked with poly-dialdehyde of starch. One of the aims of this work has been to study the influence of added components on surface energy and properties of scaffolds. UV/VIS spectrophotometry was used in order to determine quantitatively sorption of salicylic acid on the lyophilized matrixes or on nonwoven layers from nano-fibres of poly (vinyl) alcohol (PVA) and poly(glycolic-lactic) acid (PLGA) prepared by electrospinning and coated with the film of *β*-cyclodextrin and chitosan.

Materials and methods

High molecular chitosan (Shanghai Hong Yea Food Co., Ltd.), *β*-cyclodextrin (*β*-CD) (Sigma-Aldrich Co., USA) and starch poly-dialdehyde (DS) (FCHPT STU BA) were used. Salicylic acid (SA) was supplied by Mikrochem s.r.o., Pezinok, Slovakia. Non-woven fabric – polymeric carrier consisted of two parts – the non-woven liner (PP), on which two types of polymer nanofibers were applied (PVA and PLGA), made in SPUR a.s. Zlín, Czech Republic.

Chitosan scaffolds and films preparation

Chitosan solution (2 wt.%) was prepared by dissolving of polymer in 0.5 M acetic acid at the laboratory temperature. *β*-CD solution in deionized water at the concentrations 6, 9 and 18 g l^{-1} was added to chitosan solution and mixed together. 1.3 wt.% DS solution was used as crosslinking agent of scaffolds and films at the content gradually increased from 1 to 4 wt. % in regard to the total amount of polymer and CD. Films from such mixture were dried at 37 °C and scaffolds were prepared after freezing the mixture by lyophilizing in JOUAN LP3 equipment at –47 °C for 19–24 hours. The surface of nano-fibres layers was covered by film soaking them in 0.5 wt.% solution of chitosan with *β*-CD of concentration 18 g l^{-1} and drying at 37 °C.

Measurement of surface energy

Surface energy was measured on chitosan-CD films on both sides using the drops method. The samples were prepared by chitosan film cutting into thin strips. Drops with volume of 5 μl were applied on samples. Each measurement was repeated five times. Photos of all samples were taken with a CCD camera with SEE System. Surface energy of the solid test samples was calculated according to the Owens-Wendt method.

Swelling

The measurements were performed on lyophilized scaffolds. Deionized water was used as swelling medium. Samples were swelled in medium at room temperature for 30 seconds. Comparing to dry sample, the water content was recalculated to 1 g of sample.

UV/VIS spectrophotometry

Absorption spectra of all samples were recorded by UV/VIS spectrophotometer CECIL CE 7450 in the wavelength range 220–360 nm in *n*-hexane.

SA sorption measurements

Two solutions of SA (1.0 mM and 0.5 mM) were used for sorption measurements. Scaffolds with crosslinked agent (1 wt.%) and different *β*-CD concentrations (6, 9 and 18 g l^{-1}) were evaluated after their dipping during 24 hours at the room temperature.

Nanofiber layers were soaked in the solution of 0.5 mM SA for 5 hours. Decrease of solution concentration after

sorption was monitored after 1, 2, 3, 4 and 5 hours using UV/VIS spectrophotometry.

Results and discussion

16 lyophilized chitosan scaffolds and chitosan model films modified with *β*-CD and crosslinked with DS were examined to evaluate DS and CD concentrations influence on surface energy.

From measurements of the surface energy of solid films at different concentrations of both DS and CD, it can be seen in Fig. 1 that increasing concentration of *β*-CD at all concentrations of crosslinking agent DS increase surface energy measured on front sides. From this, probably *β*-CD presence on the film surface can change a surface structure and with increasing amount of *β*-CD molecules the surface is more hydrophilic.

Results obtained from swelling measurements of lyophilized scaffolds showed that to be able to express an influence of *β*-cyclodextrin on swelling, scaffolds should be sufficiently crosslinked (higher amounts of DS) as can be seen from Fig. 2. It was confirmed that higher concentration of *β*-CD in the scaffold composition, the higher amount of water accepts.

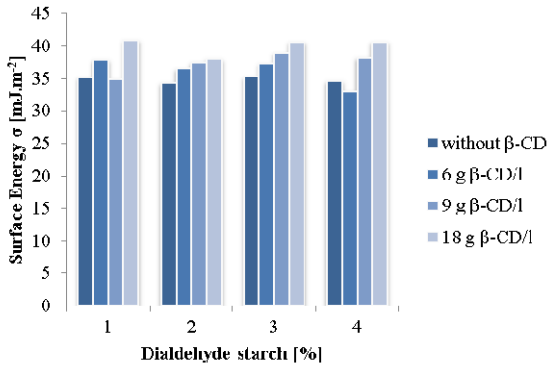

Fig. 1. **The dependence of surface energy of films measured on the front side at different concentrations of DS and *β*-CD**

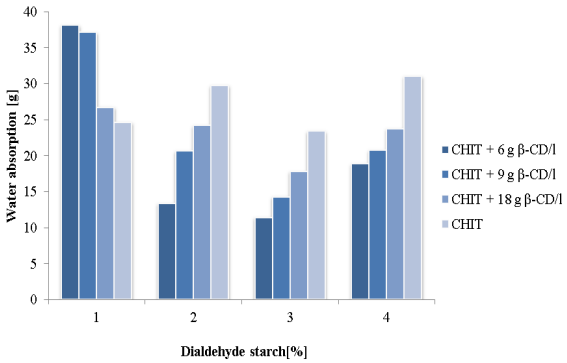

Fig. 2. **The dependency of accepted water on scaffold composition**

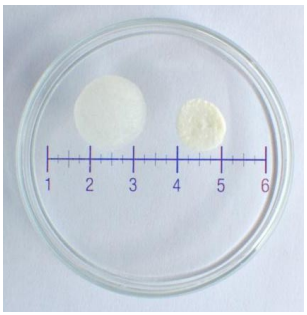

Fig. 3. **The comparison of the sample volume before and after swelling**

During swelling chitosan scaffold samples the volume increased very quickly and swelled samples were twice larger (Fig. 3).

The sorption experiments of chitosan scaffolds of different composition from SA solutions showed that the concentration of SA in the solution after long time (at least 24 hours) decreased. The results of sorption measurements were obtained comparing values on constructed calibration curve of reference solutions (Fig. 4).

Increased soaking time led to absorbance decreasing with a reduction of SA concentration in solution. Probably, there is an inclusion of SA into the *β*-CD hydrophobic cavity on the scaffold surface. On the other hand, adsorption on the chitosan molecule is not avoided.

The results of sorption measurements on nano-fibres layer showed an importance of chitosan film deposition with *β*-CD on the nano-fibres (sorption on this film). It can be assumed that the sorption, as is documented in Fig. 5 and 6, is connected with inclusion of SA molecules into the *β*-CD cavity. These results were compared to unmodified nano-fibres layers where sorption of SA did not observed.

Conclusion

The results show that scaffolds must be sufficiently crosslinked and the active substances which contents must be well dispersed to reach a positive influence on required scaffolds properties. The concentration range of solutions

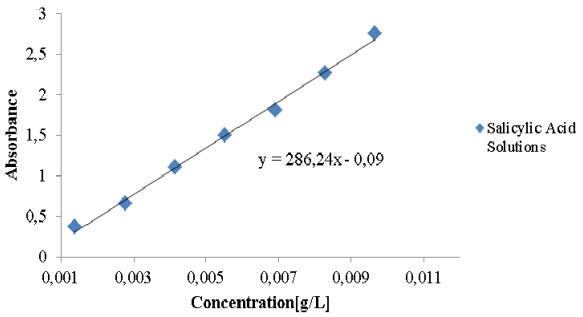

Fig. 4. **The calibration curve of SA solutions**

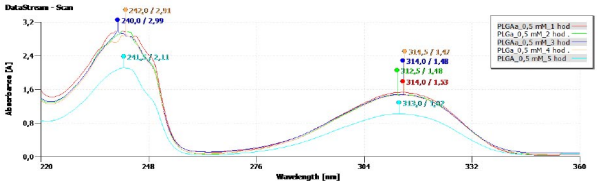

Fig. 5. **The changes in UV spectrum after SA sorption from 0.5 mM solution on PLGA layer**

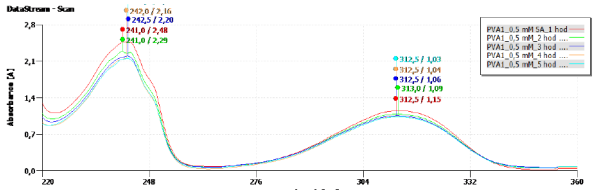

Fig. 6. **The changes in UV spectrum after SA sorption from 0.5 mM solution on PVA layer**

used was sufficient for sorption of the active substance SA on scaffolds or nano-fibres layers connected with inclusion to *β*-CD cavity. Environment of *n*-hexane as a solvent in this case was the model as experiments were focused on characterization of materials in solid form. Results showed the importance of modifications of chitosan with CDs and further study to clarify sorption of other bioactive substances in such systems will be valuable.

REFERENCES

1. Rinaudo M.: Progress Polym. Sci. *31*, 603 (2006).
2. Manakker F., Vermonden T., Nostrum C. F., Hennink W. E.: Biomacromolecules *10*, 3157 (2009).
3. Mahdí J. G.: J. Saudi Chem. Soc. 14 (2010).

P-52
MODIFICATION OF ACRYLONITRILE-BUTADIENE RUBBER COMPOUND BY NANOCLAY AND SILICA

ZDENĚK ZÁVORKA[a] and JIŘÍ MALÁČ [b]

[a] Department of Polymer Engineering, Faculty of Technology, Tomas Bata University in Zlin, 762 72 Zlin, [b] Centre of Polymer Systems, University Institute, Tomas Bata University in Zlin, Nad Ovcirnou 3685, 760 01 Zlin, Czech Republic z.zavorka@seznam.cz

Introduction

The cooling effect of air conditioning (A/C) systems is typically achieved by a hydro-fluorocarbon refrigerant such as 1,1,1,2-Tetrafluoroethane (R-134a). However, R-134a has a very high relative global warming potential (GWP) and will be restricted after 2016 (ref.[1]). One of the proposed replacements is 2,3,3,3-Tetrafluoropropene (HFO-1234yf) developed by E.I. duPont deNemours and Honeywell International.

Due to differences in molecular composition and size permeation through rubber sealing components increases by about 30% when compared to the current R-134a (ref.[2]). This demonstrates the challenges and importance of improving permeation behavior of rubber compounds for future use with low GWP refrigerants without sacrificing mechanical properties necessary for sealing performance.

Improving permeation resistance of these rubber materials can be achieved by proper selection of the "white fillers" added to the rubber compound. Specially, permeation resistance can be improved by utilizing common fillers with plate-like structure such as kaolin, clay and talc. While these fillers tend to be cost effective, they may cause unacceptable deterioration of the mechanical properties of the rubber compound[3]. Addition of nanoclay fillers appears to offer both reduced permeation rates for refrigerant and improvement of mechanical properties.

Combination of silica and nanoclay was subject of our study and our effort to identify the most cost effective A/C rubber compounds which optimize both mechanical properties and permeation resistance. Combinations of silica, kaolin and talc were investigated in parallel as low cost solutions and compared with silica and nanoclay combinations in their effect on property modification.

Experimental

Mineral materials used:

– Nanoclays Cloisite® 15A, 20A, 25A, 93A, Na+
– Nanofil® 5 (Sud-Chemie)
– Kaolin – type KKAKA (LB Minerals Kaznejov)
– Calcinated kaolin PO5 + (Ceske lupkove zavody)
– Talc – type 1.A (Demerska Hnusta)

Formulations of rubber compounds are shown in Table I.

Table I
NBR compound formulations

Chemical	No. 1 [phr]	No. 2 to 10 [phr]
NBR Krynac® 33.45	100	100
Silica Perkasil® KS 300	30	30
Oil	20	20
Nanoclay, kaolin or talc	–	10
Norperox BIBP 40	7	7
Rhenofit TAC/GR 70	2	2
Total	159	169

Measurements

Vulcanization characteristics were determined by a RPA 2000 at temperature 175 °C. Dynamic-mechanical properties were consequently tested at temperatures 40, 70 and 120 °C in constant strain amplitude of 1 % with constant oscillation frequency 0.3 Hz

Tensile strength and elongation were determined according to ISO 37 on an Alpha Technologies Tensometer 2000 test machine at 23 °C. Hardness durometer (Shore "A scale) was measured according to standard ISO 7619-1.

Permeation of refrigerant R-134a through samples of vulcanized rubber was measured utilizing a photoacoustic spectrometer (Innova model 1314) at a pressure 2 MPa and temperature 70 °C. The test was done according to European Union Commission Regulation (EC) No 706/2007 (ref.[4]).

Results and discussion

As it is shown in Fig. 1 and 2, the addition of all types of tested nanoclay fillers resulted in significant increase in hardness, tensile strength and elongation except nanoclay Cloisite Na+.

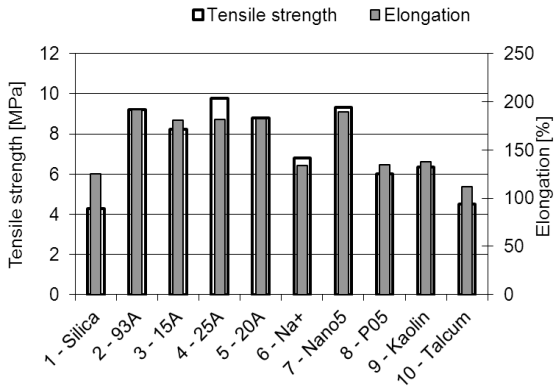

Fig. 1. **Comparison of tensile strength and elongation**

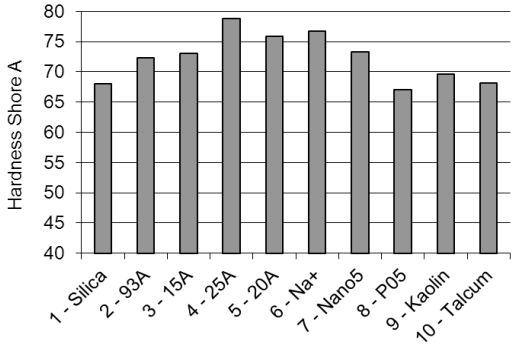

Fig. 2. **Comparison of hardness**

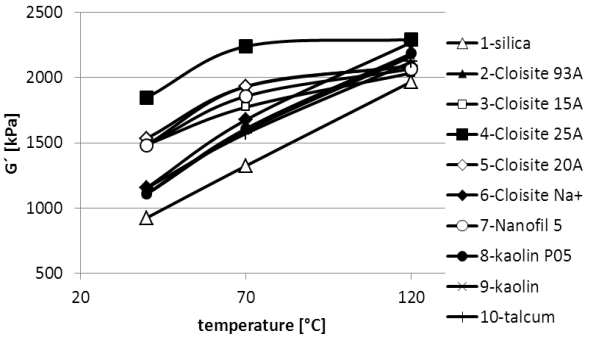

Fig. 3. **Dependence of dynamic storage shear modulus G' on temperature**

The improvement could be caused by the higher aspect ratio of exfoliated nanoclays compared to silica or common white fillers.

The results in Fig. 3 reveal that dynamic storage modulus in shear (G') for compounds with nanoclays increases to temperature of approximately 70 °C, where G' begins to level off. It is possible that NBR chains are intercalated into the structure of the nanoclay filler and as the temperature increases above 70 °C, the chains are released. This figure shows a linear increase of dynamic modulus G´ with temperature for compounds with silica, kaolin and talc, due to the different particle structure of the fillers.

Fig. 4 reveals that the addition of nanoclay significantly improves gas barrier properties, which manifests itself through a reduction in permeation. As can be seen, the permeation of refrigerant R-134a decreased by 15–30 % after addition of nanoclays into compound of NBR and silica. The reduction is probably caused by plate-like shape of exfoliated nanoclays created more tortuous pathways which the refrigerant molecules must travel to diffuse through the

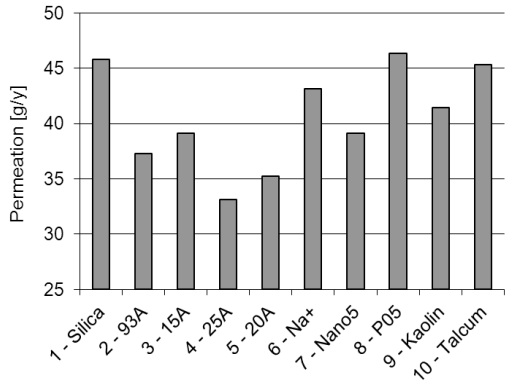

Fig. 4. **Comparison of refrigerant R-134a permeation**

material. Exfoliated nanoclays should also reduce the diffusion coefficient by restriction of motion of NBR chains[5]. The recent research has shown that the higher aspect ratio fillers are the key factor to reduce gas permeation through nanocomposites[6,7] and the results presented in this paper agree with this conclusion.

Conclusion

The objective of this study was to reduce permeation of refrigerant R-134a through NBR rubber by using suitable combination of fillers in NBR compounds, without significantly degrading mechanical properties. Nanoclay fillers demonstrated the ability to provide a 30 % reduction in permeation and achieving improved mechanical properties. The key to obtaining these enhancements was adequate level of exfoliation and polymer-filler interaction of the nanoclay fillers, confirmed by dynamic-mechanical measurements.

This exfoliation and interaction was dependent on the type and amount of the nanofiller modifier. Cloisite Na+ is the unmodified nanoclay and in the NBR compound gives properties similar to common white fillers as talc and kaolin. On the other hand, Cloisite 20A and 25A contain the same modifier at different levels. The good performance of the Closite 25A with a higher modifier level led to the best results seen in this study. Combinations of nanoclay with silica enhanced exfoliation during mixing of the compounds due to the increase of viscosity caused by presence of silica.

Application of nanoclay Cloiste 25A with silica has shown to be a combination that results in a compound with higher permeation resistance to R-134a and improvement in tensile strength, elongation and dynamic modulus of rubber compound for sealing applications in the automotive A/C systems.

REFERENCES

1. Directive 2006/40/ec of the european parliament and of the council relating to emissions from air-conditioning systems in motor vehicles and amending Council Directive 70/156/EEC, 17 May 2006
2. Sae cooperative research program 1234-2: Material compatibility of HFO-R1234yf (final report), 2008
3. Ducháček V.: *Světlá plniva*, Česká společnost průmyslové chemie, Praha 2010.
4. Commission regulation (EC) No 706/2007 – laying down, pursuant to Directive 2006/40/EC of the European Parliament and of the Council, administrative provisions for the EC type-approval of vehicles, and a harmonised test for measuring leakages from certain air conditioning systems, 21 June 2007
5. Yurong Liang, Yiqing Wang, Youping Wu, Yonglai Lu, Huifeng Zhang, Liqun Zhang: Polymer Testing *24*, 12 (2005).
6. K. Ynao, A. Usuki, A. Okada, T. Kurauchi, O. Kamigatio: J. Polymer Sci.: Part A: Polymer Chemistry *35*, 2289 (1997).
7. T. Lan, P. D. Kavirtana, T. J. Pinnavaia: Chem. Mater. *6*, 573 (1994).

CONTENTS

Main Lectures

Key Lectures

Contributed Lectures

Posters

AUTHOR INDEX

CONTENTS

CHEMICKÉ LISTY • ročník/volume 107 (2013), čís./no. S • LISTY CHEMICKÉ, roč./vol. 137, ČASOPIS PRO PRŮMYSL CHEMICKÝ, roč./vol. 123 • ISSN 0009-2770, ISSN 1213-7103 (e-verze) • evidenční číslo MK ČR E 321 • Vydává Česká společnost chemická jako časopis Asociace českých chemických společností ve spolupráci s VŠCHT Praha, s ČSPCH a ÚOCHB AV ČR za finanční podpory Nadace Český literární fond a kolektivních členů ČSCH • IČO 444715 • Published by the Czech Chemical Society • VEDOUCÍ REDAKTOR/EDITOR-IN-CHIEF: P. Chuchvalec • REDAKTOŘI/ EDITORS: J. Barek, Z. Bělohlav, P. Drašar, J. Hetflejš, P. Holý, J. Horák, B. Kratochvíl, J. Podešva, P. Rauch; Bulletin: P. Drašar; Webové stránky: R. Liboska, P. Zámostný • ZAHRANIČNÍ A OBLASTNÍ REDAKTOŘI/ FOREIGN AND REGIONAL EDITORS: F. Švec (USA), Z. Kolská (Ústí nad Labem) • KONZULTANT/CONSULTANT: J. Kahovec • TECHNICKÁ REDAKTORKA/EDITORIAL ASSISTANT: R. Řápková • REDAKČNÍ RADA/ADVISORY BOARD: K. Bláha, L. Červený, E. Dibuszová, J. Hanika, Z. Havlas, J. Káš, M. Koman, J. Koubek, K. Melzoch, T. Míšek, V. Pačes, O. Paleta, V. Růžička, I. Stibor, V. Šimánek, R. Zahradník • ADRESA PRO ZASÍLÁNÍ PŘÍSPĚVKŮ/ MANUSCRIPTS IN CZECH, SLOVAK OR ENGLISH CAN BE SENT TO: Chemické listy, Novotného lávka 5, 116 68 Praha 1; tel./phone +420 221 082 370, +420 222 220 184, e-mail: chem.listy@csvts.cz • INFORMACE O PŘEDPLATNÉM, OBJEDNÁVKY, PRODEJ JEDNOTLIVÝCH ČÍSEL A INZERCE/ INFORMATION ADS: Sekretariát ČSCH, Novotného lávka 5, 116 68 Praha 1; tel. +420 222 220 184, e-mail: chem.spol@csvts.cz, chem.ekonom@csvts.cz • PLNÁ VERZE NA INTERNETU/FULL VERSION ON URL: http://www.chemicke-listy.cz • TISK: Rodomax s.r.o., Rezecká 1164, 549 01 Nové Město nad Metují • Redakce čísla Symposia (ISSUE EDITOR) Ľ. Černáková • SAZBA, ZLOM: ČSCH, Chemické listy • Copyright © 2013 Chemické listy/Česká společnost chemická • Cena výtisku 177 Kč, roční plné předplatné 2013 (12 čísel) 1793 Kč, individuální členské předplatné pro členy ČSCH 897 Kč. Roční předplatné ve Slovenské republice 96 EUR (doručování via SCHS), individuální členské předplatné pro členy ČSCH 73 EUR (doručování via SCHS), 268 EUR (individuální doručování), ceny jsou uvedeny včetně DPH • DISTRIBUTION ABROAD: KUBON & SAGNER, POB 34 01 08, D-80328 Munich, FRG • This journal has been registered with the Copyright Clearance Center, 2322 Rosewood Drive, Danvers, MA 01923, USA, where the consent and conditions can be obtained for copying the articles for personal or internal use • Pokyny pro autory najdete na http://www.chemicke-listy.cz , zkratky časopisů podle Chemical Abstract Service Source Index (viz http://cassi.cas.org/search.jsp) • Chemické listy obsahující Bulletin jsou zasílány zdarma všem individuálním a kolektivním členům ČSCH a ČSPCH v ČR i zahraničí, do všech relevantních knihoven v ČR a významným představitelům české chemie a chemického průmyslu; v rámci dohod o spolupráci i členům dalších odborných společností • Molekulární námět na obálce: P. Drašar • Dáno do tisku 8.4.2013.